

Seagate Pretrial Exhibit D REDACTED

**IN THE UNITED STATES DISTRICT COURT
FOR THE WESTERN DISTRICT OF PENNSYLVANIA**

LAMBETH MAGNETIC STRUCTURES,)	
LLC,)	
)	
Plaintiff,)	
)	Case No. 2:16-cv-00538-CB
v.)	
)	
SEAGATE TECHNOLOGY (US))	
HOLDINGS, INC. and SEAGATE)	
TECHNOLOGY LLC,)	
)	
Defendants.)	

EXPERT REPORT OF DR. ERIC STACH

CONFIDENTIAL ATTORNEY EYES ONLY

TABLE OF CONTENTS

I.	INTRODUCTION	1
II.	PROFESSIONAL BACKGROUND AND QUALIFICATIONS	2
III.	MATERIALS CONSIDERED	3
IV.	SUMMARY OF OPINIONS	4
V.	LEGAL ISSUES	5
VI.	TECHNOLOGY BACKGROUND	7
	A. Crystal Structures, Orientations, and Variants	7
	1. Unit Cells	7
	2. Orientations of Crystals Relative to a Substrate	8
	3. In-Plane Orientations of Crystals	12
	4. Crystal Growth and Variants	12
	5. Crystals and Variants in the '988 Patent	13
	B. Measuring Crystal Structures	16
	1. X-Ray Measurements	16
	2. TEM Imaging	18
	a. Diffraction mode	19
	b. Image mode and related measurements	30
VII.	BRIEF OVERVIEW OF SEAGATE'S WRITE HEADS	32
	A. Material Structure of [REDACTED] Write Head Designs	32
	B. Samples Analyzed	33
VIII.	OPINIONS	34
	A. Dr. Clark's Conclusions Relating to the Crystalline Structure and Texture of the NiFe Layers in Samples S0GPPC, S2MMMC, and SBRD8K Are Based on a Misapplication of Scientific Principles and Methods, Are Unreliable, and Do Not Have a Reliable and Sufficient Factual and Scientific Basis	34
	1. Sample S0GPPC ([REDACTED] Design)	34
	a. Lower NiFe Layer	35
	b. Upper NiFe Layer	47
	c. Other Data Not Considered by Dr. Clark	61
	d. Conclusion Regarding NiFe Layers	62
	2. Sample S2MMMC ([REDACTED] Design)	62
	a. Lower NiFe Layer	63
	b. Upper NiFe Layer	74

c.	Other Data Not Considered by Dr. Clark.....	84
d.	Conclusion Regarding NiFe Layers.....	85
3.	Sample SBRD8K ([REDACTED] Design)	86
a.	Lower NiFe Layer.....	86
b.	Upper NiFe Layer	96
c.	Other Data Not Considered by Dr. Clark.....	104
d.	Conclusion Regarding NiFe Layers.....	105
B.	Dr. Clark's Conclusions Relating to the Crystalline Structure, Texture, Variants, and Symmetry Broken Structures in Certain FeCo Layers in Samples S0GPPC, S2MMMC, and SBRD8K Are Based on a Misapplication of Scientific Principles and Methods, Are Unreliable, and Do Not Have a Reliable and Sufficient Factual and Scientific Basis	105
1.	Sample S0GPPC ([REDACTED] Design)	105
a.	Flawed and Unsupported Conclusions Based on Microbeam Diffraction Data	106
b.	Flawed and Unsupported Conclusions Based on Dark Field Images	119
c.	Other Data Not Considered by Dr. Clark.....	128
d.	Conclusion Regarding FeCo Layers	128
2.	Sample S2MMMC ([REDACTED] Design).....	128
a.	Flawed and Unsupported Conclusions Based on Microbeam Diffraction Data	130
b.	Flawed and Unsupported Conclusions Based on Dark Field Images	139
c.	Other Data Not Considered by Dr. Clark.....	146
d.	Conclusion Regarding FeCo Layers	146
3.	Sample SBRD8K ([REDACTED] Design)	146
a.	Flawed and Unsupported Conclusions Based on Microbeam Diffraction Data	148
b.	Other Data Not Considered by Dr. Clark.....	165
c.	Conclusion Regarding FeCo Layers	166
IX.	SUMMARY	166
A.	No Evidence of (111) Textured Hexagonal Atomic Template	166
B.	No Evidence of Six-Variant System and Symmetry Broken Structure	168

I. INTRODUCTION

1. I have been retained by Seagate Technology (US) Holdings, Inc. and Seagate Technology, LLC (“Seagate”) as an independent expert witness in connection with the patent litigation brought by Lambeth Magnetic Structures, LLC (“LMS”) against Seagate. In particular, I have been asked to provide a report and to testify in the case on certain topics relating to testing performed on certain write heads that have been accused of infringing claims in U.S. Patent No. 7,128,988 (“the ’988 Patent” or the “Asserted Patent”) and the crystallographic properties of those write heads.

2. My opinions and the bases for my opinions are contained in the remainder of this report. If Seagate calls me as a witness in this matter, I currently expect that my testimony will relate to the issues described above and elsewhere in this report.

3. I am being compensated for my work on this matter at the rate of \$300 per hour, with reimbursement for actual reasonable expenses. I have no other interest in this matter, and my compensation does not depend on the outcome of this case.

4. I have not provided any expert testimony at a deposition or trial in the last four years.

5. If I am called to testify in this matter, I may use as exhibits various documents produced in this case that refer or relate to the matters discussed in this report. I may also use as exhibits photos, videos, models, or other graphical or multimedia presentations depicting or illustrating the matters discussed in my report. I may also use as exhibits physical samples of materials referred to in this report. I have not yet selected the particular exhibits that might be used. In addition, I reserve the right to and may create or assist in the creation of certain demonstrative exhibits or summaries of my findings and opinions to assist me in testifying.

6. I may testify as an expert regarding additional matters, including (i) to rebut positions that LMS takes, including opinions of its experts and materials they discuss or rely upon, (ii) based on any Orders from the Court, (iii) based on documents or other discovery that LMS or other parties have not yet produced or that were produced too late to be fully considered before my report was due, or (iv) based on deposition or witness testimony which has not yet been given. I reserve the right to supplement or amend this report based on such materials and information.

II. PROFESSIONAL BACKGROUND AND QUALIFICATIONS

7. I am a Professor at the University of Pennsylvania in the Department of Materials Science and Engineering. In particular, I am part of the Laboratory for Research on the Structure of Matter and the Singh Center for Nanotechnology. I direct the research of three graduate students who focus on the characterization of materials using transmission electron microscopy. My research has focused generally on the development and application of electron microscopy techniques to solve a wide range of materials problems in the areas of nanotechnology, materials characterization, crystallography and crystal growth, and crystalline dislocations and defects.

8. I earned a Bachelor of Science degree (1992) in Mechanical Engineering and Materials Science at Duke University. I earned a Master of Science degree (1994) in Materials Science and Engineering from the University of Washington in Seattle, and a Ph.D. in Materials Science and Engineering (1998) from the University of Virginia in Charlottesville. My Ph.D. thesis related to the characterization, via transmission electron microscopy, of dislocations and defects in the crystalline lattice of SiGe/Si heterostructures.

9. Before joining the University of Pennsylvania, I held a variety of professional and academic positions. I was a Materials Staff Scientist from 1998 to 2002 at the National Center for Electron Microscopy at the Lawrence Berkeley National Laboratory, before being promoted to Program Leader of the Metals Program in 2003. As Program Leader, I directed research on the mechanisms of mechanical deformation using transmission electron microscopy methods. I then joined the School of Materials Engineering at Purdue University in 2005 as an Associate Professor and was appointed to Full Professor in 2010. At Purdue, I taught undergraduate and graduate classes in optical and magnetic properties of materials, materials processing and advanced materials characterization. I also managed the research of graduate and post-graduate students with a budget of approximately \$1 million a year.

10. In 2010, I joined the Electron Microscopy Group at the Center for Functional Nanomaterials at Brookhaven National Laboratory as a Group Leader. I managed a \$2.25 million annual research effort at a Department of Energy National User Facility, including overseeing a staff of 10 permanent staff, post-doctoral and student researchers and over 100 external users. My research was directed toward catalytic nanomaterials for energy conversion, solid-state materials for energy storage, earth-abundant materials for solar energy, the

fundamentals of nanoscale crystal growth, and the development of novel experimental methods for *in situ* and *operando* characterization.

11. I am a member of numerous professional societies and organizations, including the Materials Research Society, of which I am the Secretary for the Board of Directors. I also am a Fellow of the Microscopy Society of America and the American Physical Society. I have received several awards, including the Microscopy Society of America's Eli F. Burton (Young Scientist) Award and Purdue University's Faculty Scholar and Early Career Research Excellence Awards.

12. I have published over 250 papers in the fields of materials science, nanotechnology, condensed matter physics, and organic chemistry. This includes papers published in *Science*, *Nature*, *Nature Materials*, *Physical Review Letters*, *Nano Letters*, and *Applied Physical Letters*. I also have edited books and contributed chapters to books in several of these areas. These include "*Current Issues in Heteroepitaxial Growth – Stress Relaxation and Self Assembly*," edited by E.A. Stach, E. Chason, R. Hull and S.M. Bader, Proceedings of the Materials Research Society, Volume 696, 2002; "*Strain accommodation and relief in SiGe / Si heteroepitaxy*," a book chapter by R. Hull and E.A. Stach in Thin Films: Heteroepitaxial Systems volume 15 of Directions in Condensed Matter Physics, edited by A. W. Liu and M. B. Santo, World Scientific Publishing Co., Inc., Rivers Edge, NJ, 1999.

13. Exhibit A is a copy of my curriculum vitae, which includes a list of all publications that I have authored, including my time as a graduate student.

III. MATERIALS CONSIDERED

14. In preparing to write this report and forming my opinions in this matter, I have reviewed the '988 Patent, including the '988 Patent's claims, specification, and drawings. I also have reviewed a number of materials produced by LMS and Seagate in this case, together with the Court's Claim Construction Order, among other things.

15. I have extensively reviewed the expert report of Dr. William Clark, dated May 2, 2018, along with portions of the data and other materials produced with his report. I also have reviewed the expert report of Dr. Kevin Coffey, also dated May 2, 2018.

16. I also have considered the results of testing and measurements I performed on two samples relating to two designs for Seagate's write heads used in various hard disk drives. These samples are described more specifically in Exhibits C and D of my report.

17. A summary of materials I considered in connection with this report are set forth in Exhibit B. I may rely on those materials, in addition to the materials specifically cited as supportive examples in particular sections of this report, as additional support for my analysis and opinions. In addition, I may rely on my own experience and professional and academic background in electron diffraction and microscopy techniques, materials characterization, crystallography and crystal growth. I reserve the right to supplement and amend my opinions as more information or documents are received.

IV. SUMMARY OF OPINIONS

18. I expect to testify on issues relating to the '988 Patent and the testing conducted by Dr. William Clark and the conclusions described in his expert report relating to the crystal structures of the [REDACTED] write-head designs used by Seagate in its hard disk drives. In particular, I expect to testify regarding the testing conducted by Dr. Clark on the samples described in his report and the opinions expressed in that report. For example, I expect to testify regarding the reliability of certain testing methods and measurements that Dr. Clark relied on to form his opinions, whether he applied those methods and measurement in a scientifically valid and reliable way, and whether the conclusions drawn by Dr. Clark have a factual basis supported by sufficient and scientifically reliable data.

19. Based on all of the materials I have considered, it is my opinion that the test methods and measurements relied on by Dr. Clark to form his opinions are not reliable and have been applied in a flawed, unscientific, and unreliable manner, and that the majority of the conclusions he draws from his tests are not supported by sufficient and scientifically reliable data. Based on the test methods and measurements described in Dr. Clark's report and his application of those methods and measurements, no reasonable scientist in my opinion would agree with the conclusions expressed in Dr. Clark's report regarding the crystallographic properties of the NiFe and FeCo layers in Seagate's [REDACTED] write-head designs.

20. In my opinion, the testing results and data from Dr. Clark's report do not show either the presence of a "layer providing a (111) textured hexagonal atomic template" or a layer forming a "symmetry broken structure."

21. I also provide opinions relating to testing that I performed on samples from two Seagate write heads (one from the [REDACTED] design and one from the [REDACTED] design), and the results of that testing, as described in this report.

22. In addition, I express further opinions in the remainder of my report.

23. All of my opinions, and the bases of those opinions, are true and correct to the best of my knowledge and belief, including those related to scientific issues, which I believe are true and correct to a reasonable degree of scientific certainty.

V. LEGAL ISSUES

24. I understand that LMS is contending that Seagate's hard disk drive products containing write heads with an [REDACTED] design infringe independent claims 1 and 27 of the '988 Patent and dependent claims 3, 6, 7, 9, 17, 19, 27, 28 and 29. I understand that these contentions are based in part on testing performed by Dr. Clark and certain conclusions drawn by Dr. Clark based on that testing relating to "the composition of certain layers; the crystal structure and texture for certain FeCo and NiFe layers; whether the NiFe layers directed the growth of the FeCo layers deposited directly on top of the respective NiFe layers; the presence of crystallographic orientational variants; whether there is an unequal amount of variants in a six-variant system in the lower FeCo layer of the write pole; and the fractional distribution of the different orientations of the crystallites in the lower FeCo layer." (*See* Clark at ¶ 14.) I understand that his testing relates to particular elements of the asserted claims, including (i) a "layer providing a (111) textured hexagonal atomic template" and (ii) a "symmetry broken structure."

25. I have been asked to provide opinions regarding the testing methods and measurements conducted by Dr. Clark relating to the samples described in his report, whether he applied those methods and measurement in a scientifically valid and reliable way, and whether the conclusions drawn by Dr. Clark have a factual basis supported by sufficient and scientifically reliable data and, in particular, whether they show the presence of a "layer providing a (111) textured hexagonal atomic template" and (ii) a "symmetry broken structure" as those terms have been construed by the Court.

26. Counsel for Seagate has informed me of general guidelines and rules for examining the claims of an issued patent to determine whether or not a claim is infringed by an accused device. I understand that to show that an accused device or product literally infringes a claim, the party claiming infringement must show that it meets all of the limitations of the claim. If a device does not contain one or more limitations of a claim, I understand that device does not

literally infringe the claim. I understand infringement is determined by comparing what is accused of infringement to the claims as construed by the Court.

27. I understand that, for this case, the Court issued an order dated October 18, 2017 in which the Court construed certain terms in the limitations of the asserted claims.

28. I have applied these claim constructions in forming my opinions in this case. I have listed the claim constructions from the Court's order relevant to my report below:

Term	Construction
"[Layer] providing a (111) textured hexagonal atomic template"	Layer that is predominately (111) hexagonal and that provides an atomic template
"atomic template"	An atomic pattern upon which material is grown and which is used to direct the growth of an overlying layer
"symmetry broken structure"	A structure consisting of unequal volumes or unequal amounts of the bcc-d variants of a six variant system
"variant" / "orientational variant"	One of a set of possible crystal orientations
"variants" / "orientational variants"	Two or more of a set of possible crystal orientations

29. Counsel for Seagate also has informed me of the standard for providing expert testimony under Rule 702 of the Federal Rules of Evidence.

30. I understand that an expert may testify in the form of an opinion or otherwise if: (a) the expert's scientific, technical, or other specialized knowledge will help the trier of fact to understand the evidence or to determine a fact in issue; (b) the testimony is based on sufficient facts or data; (c) the testimony is the product of reliable principles and methods; and (d) the expert has reliably applied the principles and methods to the facts of the case. I understand that

other relevant factors mentioned in the comments to Rule 702 and referred to as *Daubert* factors are (1) whether the expert's technique or theory can be or has been tested—that is, whether the expert's theory can be challenged in some objective sense, or whether it is instead simply a subjective, conclusory approach that cannot reasonably be assessed for reliability; (2) whether the technique or theory has been subject to peer review and publication; (3) the known or potential rate of error of the technique or theory when applied; (4) the existence and maintenance of standards and controls; and (5) whether the technique or theory has been generally accepted in the scientific community.

VI. TECHNOLOGY BACKGROUND

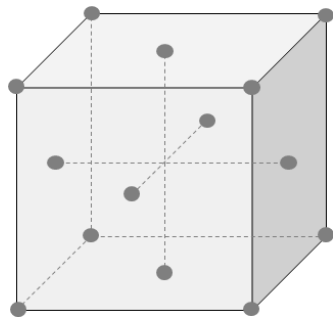
31. In this section, I provide a description of some of the technology related to the '988 Patent and the opinions I express in this case. In addition, I have reviewed the "Technology Background" of the expert report being submitted by Dr. Eric Fullerton and believe that it contains an accurate description of the relevant technology relating to issues that I address in this case. My discussion here focuses principally on particular concepts relating to the testing, measurements, principles, and methods used by Dr. Clark, and Dr. Clark's conclusions relating to the crystal structure and orientation of the NiFe and FeCo layers in the samples that he tested relating to Seagate's [REDACTED] write-head designs.

A. Crystal Structures, Orientations, and Variants

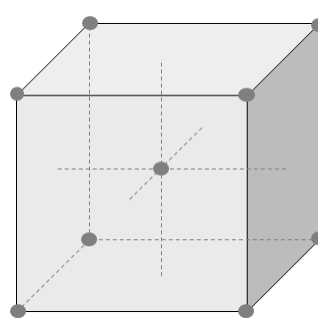
32. Crystal structures are characterized by long-range geometric order on the atomic scale. In general, this highly-ordered geometry takes the shape of a three-dimensional repeating pattern of atoms that is called a *crystal lattice*.

1. Unit Cells

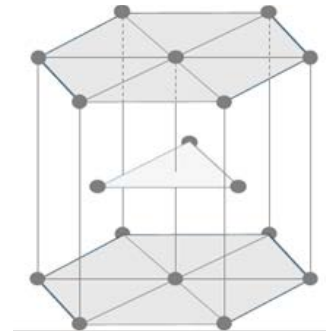
33. A *unit cell* represents the smallest basic building block of a crystal lattice and repeats itself via simple unit translations along the primary axes of the overall structure. Among the types of crystal lattices discussed in the '988 Patent are bcc (body-centered cubic), fcc (face-centered cubic), and hcp (hexagonal close-packed) lattices. I reproduce below examples of each of these structures as unit cells showing the locations of the atoms for each:



Face-Centered Cubic (FCC)

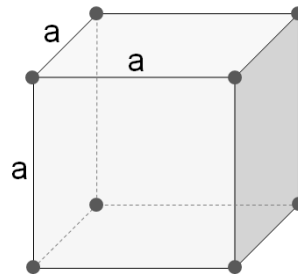


Body-Centered cubic (BCC)



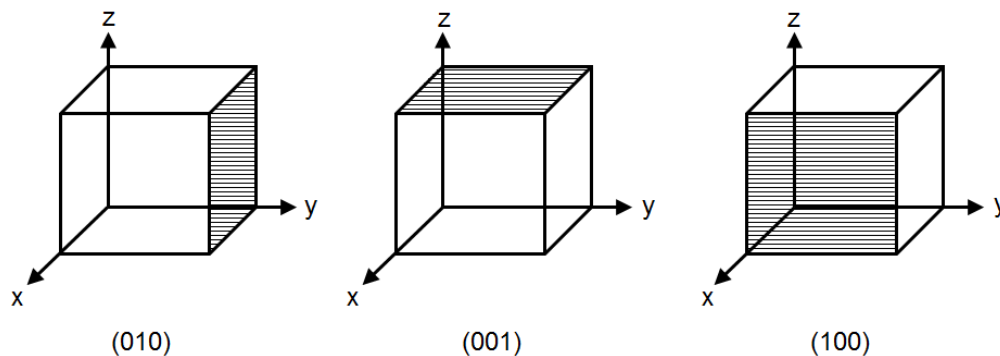
Hexagonal Close-Packed (HCP)

34. A *lattice parameter* refers to the dimension of the unit cell in a particular direction. Lattices generally will have three lattice constants—one for each dimension—although sometimes the constants will be the same. For example, as shown below, the distance between the atoms shown in adjacent corners of a cubic unit cell will have the same dimension “a,” and thus the same lattice parameter:



2. Orientations of Crystals Relative to a Substrate

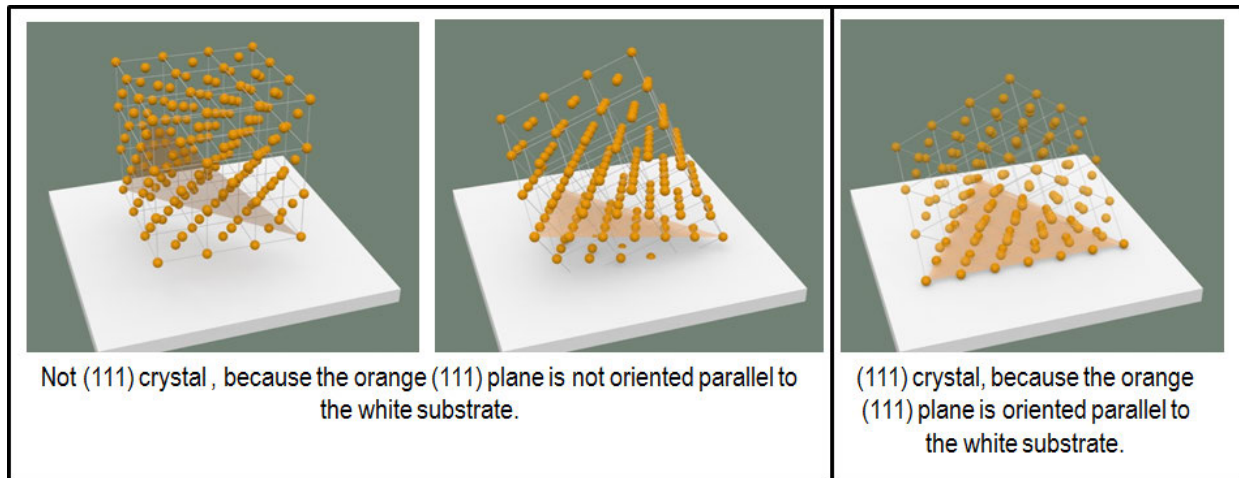
35. Planes and directions in a crystal can be described using a coordinate system known as the Miller Index. It is worth noting here that in addition to using the Miller Index to identify a particular plane, we can also identify a family of planes that are related by the symmetry of the lattice. For example, the faces of a cubic unit cell, which are (010), (001), and (100), are all part of the same {100} family of planes, as shown below:



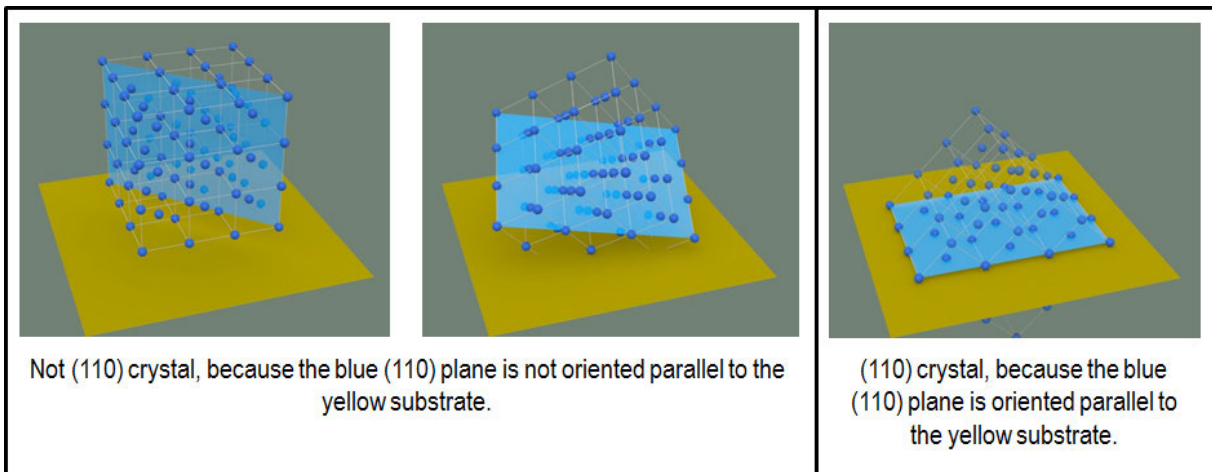
36. In general, in a cubic system, the three Miller Index digits are interchangeable within the same family. For example, as long as you have two “zeroes” and one “one,” you are in the $\{100\}$ family of planes. Likewise, as long as you have two “ones” and one “zero,” you are in the $\{110\}$ family of planes. Thus, (110) , (101) , and (011) are all in the same family of planes, and are related via symmetry. In other words, there is no physical difference between the members of these family of planes, and the digits can be exchanged because in a cubic structure their order is based on a wholly arbitrary choice of the initial unit axes, a , b and c .

37. We also can characterize a crystal not only by its *crystal structure* (e.g., bcc, fcc, hcp), but by its *orientation* relative to another surface using Miller indices. For the purposes of this report, these indices are used most often to describe the orientation of the crystal with respect to the substrate (the underlying layer of material on which the crystal lattice is grown).

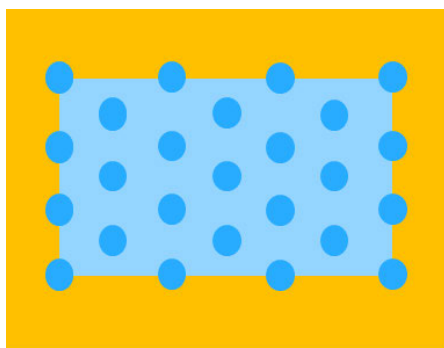
38. For example, I will use the description of an fcc(111) crystal to describe a crystal with an fcc crystal structure and whose (111) plane lies parallel to the substrate. The picture below depicts three crystal lattices. All have an fcc crystal structure, but only the right-most crystal has its (111) plane (shaded in orange) parallel to the substrate (the surface shown in white). The right-most crystal is therefore described as an fcc(111) crystal:



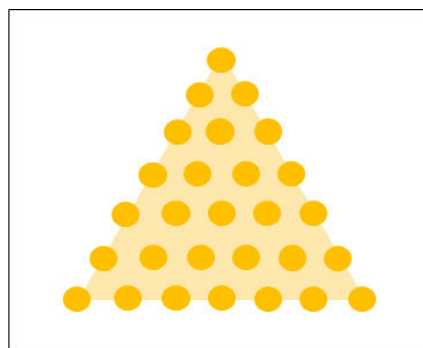
39. Similarly, a bcc(110) crystal describes a crystal with a bcc crystal structure and whose (110) plane lies parallel to the substrate. The picture below depicts three crystal lattices. All have a bcc crystal structure, but only the right-most crystal has its (110) plane (shaded in blue) parallel to the substrate (the surface shown in yellow). The right-most crystal is therefore described as a bcc(110) crystal:



40. When rotated and viewed from the top down (in a plan view), the planes from the right-most fcc and bcc figures would look like this (shown schematically below):

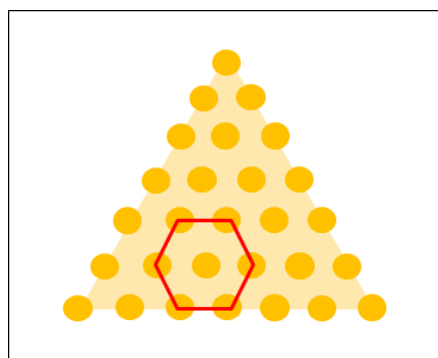


BCC – Plan View



FCC – Plan View

41. Note that a plan view for an fcc(111) crystal that has formed a lattice will have a hexagonal structure, as shown below in red (shown schematically below):



FCC – Plan View

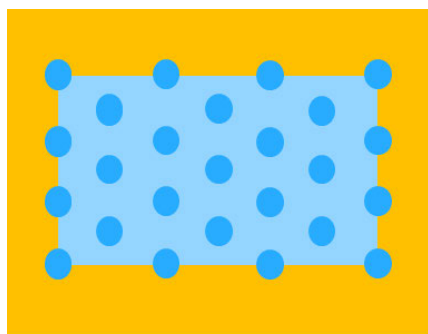
42. As I explain below, each of these plan views showing these orientations for a bcc(110) crystal lattice and an fcc(111) crystal lattice can be used to compare the orientations of each crystal relative to a common substrate and to one another.

43. Sometimes a structure comprises more than a single crystal. If so, the individual crystals comprising the overall structure are referred to as *grains*. If a structure's grains are predominantly oriented with a particular plane parallel to the substrate, the structure is said to be *textured*. For example, if a structure's crystals are predominantly oriented with their (111) plane parallel to the substrate, the structure is said to be "(111) textured." If a structure's crystals are predominantly oriented with their (110) plane parallel to the substrate, the structure is said to be "(110) textured." In general, "crystallographic texture," or just "texture," describes the predominant orientation of the crystals in a structure relative to the substrate. If there is no predominant orientation among the crystals in a structure relative to the substrate, the structure is not textured (and can be described as "randomly oriented").

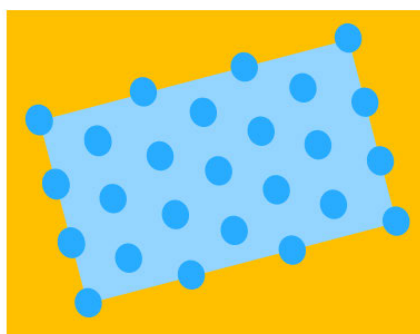
44. To summarize, crystals can be characterized by their crystal structure (*e.g.*, fcc, bcc, hcp) as well as their orientation relative to a substrate. An fcc(111) crystal refers to an fcc crystal whose (111) plane is parallel to the substrate. A bcc(110) crystal refers to a bcc crystal whose (110) plane is parallel to the substrate.

3. In-Plane Orientations of Crystals

45. There is another dimension along which we characterize crystals: their in-plane orientation. Shown schematically below in a plan view, for example, are two bcc(110) crystals with different in-plane orientations:



Bcc(110)



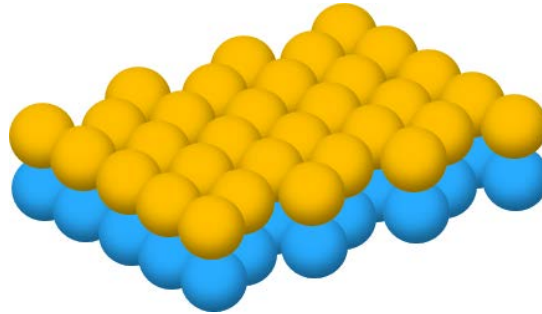
Bcc(110) – rotated in-plane 15 degrees

46. Both crystals shown in the above illustration are bcc (because their atoms are arranged at the center and eight corners of the cubic unit cell). Both crystals are also (110) (because their (110) plane is parallel to the substrate). But the crystals are rotated in different directions relative to one another within the (110) plane. Therefore, we say that they have different “in-plane orientations.”

4. Crystal Growth and Variants

47. *Crystal growth* refers generally to the process of depositing, or “growing,” an overlayer of one crystalline material on another, such as a crystal substrate. Depending on the nature of the crystal structure of each material, the material being deposited may attempt to arrange itself to align with the atoms in the structure of the underlying material. If it is able to do so, we refer to this process as *epitaxial growth*, and the overlayer is referred to as an *epitaxial layer*. This growth is more likely to happen if the lattice parameters of the crystal structure of the overlayer are in a position to align themselves with the location of atoms in the underlying crystal structure, and if there is a small difference in lattice parameter (generally less than 1%).

In general, epitaxial growth requires some degree of mobility of the atoms of the surface of the overlying material during deposition and results because, in general, the overlayer will seek to minimize the energy between it and the material of the underlying crystal. Shown schematically below is an example of alignment of two bcc(110) crystals from epitaxial growth. The upper bcc(110) layer (in orange) is directly aligned with the lower bcc(110) layer (in blue):



48. We use the term *homoepitaxy* to refer to the epitaxial growth of an overlying material made of the same material as the underlying material on which it is grown. We use the term *heteroepitaxy* to refer to such growth when the overlying material and the underlying material are different.

49. When the overlying crystalline lattice grows in an epitaxial manner, the possible arrangements for the overlying crystal relative to the underlying crystal is sometimes called *variants*. Each variant represents one of the possible ways in which a single overlying crystal can grow and arrange itself over the underlying crystalline lattice on which it is grown while maintaining a specific orientation between the two layers.

5. Crystals and Variants in the '988 Patent

50. Using the principles described above, the focus of the '988 Patent is the growth of bcc(110) crystals so that they have one of six particular in-plane orientations—each a “variant”—relative to an underlying (111) textured hexagonal crystalline lattice on which they are epitaxially grown. The patent refers to this underlying layer as an “atomic template.” As noted above, I understand that the Court in this case has construed the term “[layer] providing a (111) textured hexagonal atomic template” as a “layer that is predominately (111) hexagonal and that provides an atomic template,” and that it has construed the term “variant” to mean “one of a set of possible crystal orientations.”

51. There are six variants in the claimed invention of the '988 Patent because the invention calls for six different in-plane orientations—six possible and specific ways for the bcc(110) crystals to orient themselves relative to an underlying (111) textured hexagonal crystal template. (*See, e.g.*, '988 Patent 18:33-45.)

52. The concept of variants is also relevant to the “symmetry broken structure” claim limitation of the '988 Patent. As noted above, I understand that the Court has construed “symmetry broken structure” to mean “a structure consisting of unequal volumes or unequal amounts of the bcc-d variants of a six variant system.”

53. In particular, the '988 Patent states that growing a bcc-d magnetic layer over a (111) textured hexagonal atomic template will, under certain conditions, result in six and only six possible variants. The '988 Patent theorizes that if one can induce specific combinations of these six variants to grow in unequal amounts or volumes, “a symmetry broken uniaxial magnetic thin film is obtained”:

By carefully controlling the epitaxial growth conditions of (110) crystalline textured bcc or bcc derivative thin film materials on highly oriented (111) hexagonal atomic templates the applicant has invented a new set of six crystalline variants with special orientational relationships. By the selection and growth of a very special exchange coupled subset of these six orientational variants a symmetry broken uniaxial magnetic thin film is obtained.

(*Id.* at 14:48-55.)

54. The '988 Patent defines each of the six variants based on the orientation of the bcc(110) crystal in the magnetic layer relative to the underlying (111) textured hexagonal crystals that directed its growth. For example, Figure 5 of the '988 Patent depicts two of the six variants—which it refers to as “a1” and “c2”—based on their orientational relationship relative to the underlying (111) hexagonal crystal. The '988 Patent describes Figure 5 as “an illustration of two of the six possible orientational variants of the (110) crystal plane of a bcc-d crystal in comparison to the atomic arrangement of the (111) crystal plane of a hexagonal lattice template crystal.” (*Id.* at 13:39-42.)

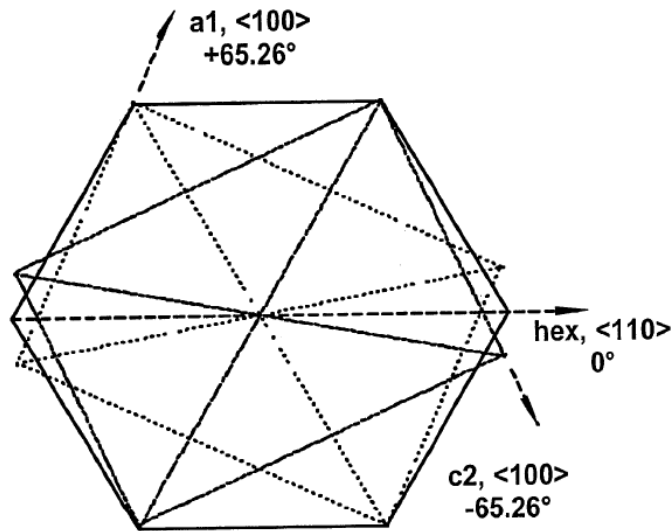
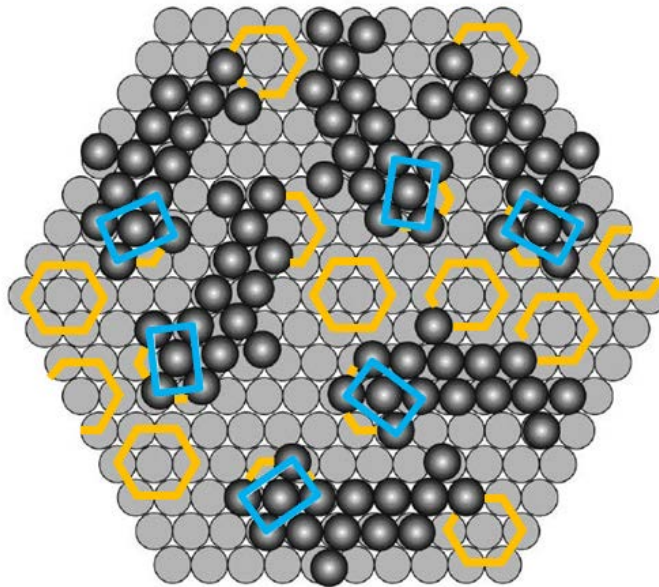


Fig. 5, '988 Patent

55. The '988 Patent contemplates six specific possible variants, and defines them based on their angle to the underlying (111) hexagonal atomic template. ('988 Patent at 18:33-45.) As shown below, there are six—and only six—possible bcc(110) variants (the blue rectangles) that can form in a six-variant system over the (111) hexagonal crystals in the underlying layer (shown as the gray textured template, with representative individual crystals from the template shown by yellow hexagons). Each of the six blue rectangles has a specific, different in-plane orientation relative to the underlying hexagonal crystalline template:



56. I note that, in his report, Dr. Clark sometimes refers to these six possible relationships as the Kurdjumov-Sachs (“KS”) orientational relationships. (*E.g.*, Clark at ¶ 33.)

B. Measuring Crystal Structures

57. There are a number of methods that can be used to probe a layer’s crystallographic properties, including its texture (if any). I describe several of these methods below.

1. X-Ray Measurements

58. One method used to test for crystallographic properties is x-ray diffraction (XRD). X-rays with a specific, fixed wavelength interact with the atoms in the material. Because the atoms of a crystal are arranged in a long-range order (translational periodicity), this causes x-rays shot into a crystal to diffract at specific angles and intensities, according to Bragg’s law. Bragg’s law states a specific relationship between the spacing between lattice planes (d), the wavelength of the x-ray radiation (λ), and the incident angle of the illumination (θ), such that $2d\sin\theta = n\lambda$ where n is an integer. Constructive interference between the waves occurs when Bragg’s Law is satisfied, leading to measurable intensity. The diffracted beams are recorded in a *diffraction pattern*, which when analyzed may provide information about the arrangement of the atoms via Bragg’s Law, and therefore the crystal structure and texture (if any) in the material. Bragg’s Law is a universally established scientific principle, and Sir Lawrence Bragg was awarded the Nobel Prize in Physics in 1915 for his elucidation of this phenomena.

59. XRD can be used to create *diffraction patterns* that show the out-of-plane orientation of crystals over a range of angles, sometimes referred to as a powder pattern or a Bragg-Brentano pattern. In order to create a diffraction powder pattern, the crystalline sample is rotated on one axis over a range of angles, and the resulting diffracted x-rays are plotted on a graph with x-ray intensity on the y-axis and angle (called “2 theta”) on the x-axis, as shown below:

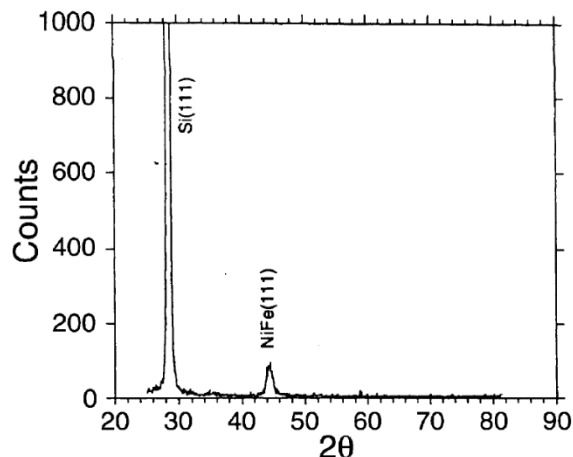


FIG. 27(a)

U.S. Patent No. 6,248,416

60. As can be seen in the example above, each peak is labeled with the crystal planes that produced the peak. The intensity of the peak is not necessarily an indication of the prevalence of a particular texture, but can be related to it with proper analysis. The particular peaks that appear and the intensity of each peak can be matched to a database of reference XRD spectra, which include the expected intensities for a randomly-oriented set of crystals. The intensities that appear in the database result from the relative strength of x-ray scattering from the atoms in the crystal, as well as the “multiplicity” of a given set of planes. The multiplicity refers to the number of different planar variants that occur for the given crystal structure.

61. XRD also may be used to create another type of plot called a *pole figure*. A pole figure also involves rotating a crystalline sample, typically a full 360-degree rotation, and measuring the intensity of the diffracted x-rays. However, in contrast to XRD spectra—which involve a rotation about a single axis—pole figures are created using rotations about two different axes. A typical pole figure is shown in the '988 Patent in Figure 14:

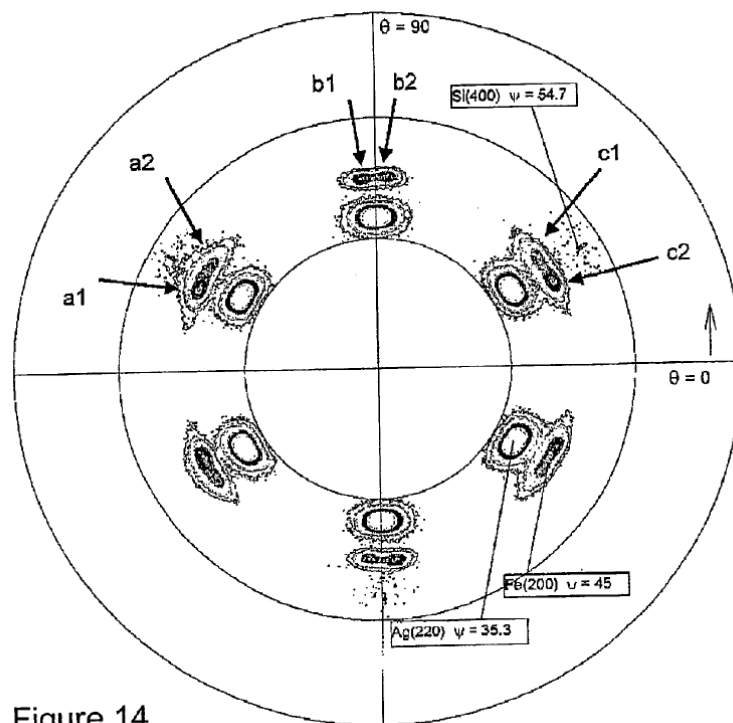


Figure 14

Fig. 14, '988 Patent

62. The above pole figure has a polar coordinate system, meaning that each point on the pole figure can be located using two coordinates, theta and phi. Theta is a measure of the rotational angle, with zero degrees at the horizontal line on the right side of the figure, and 90 degrees at the upper portion of the vertical line. Phi is a measure of the distance of a peak from the center of the figure. There are roughly twelve peaks, which represent peaks of diffracted x-ray intensity passed through the sample. For example, in the pole figure shown above, there are two peaks at a theta of 90 degrees. The lower (or inner) peak is the result of diffraction from a thin film of Ag(220). The upper peak is the result of diffraction from Fe(110). Because the bcc(110) crystal structure of the Fe forms multiple variants, this particular peak is split into two peaks, with each variant forming a peak (labeled b1 and b2 in the pole figure shown above).

2. TEM Imaging

63. Another method used to test for a texture is transmission electron microscopy, or TEM. TEM uses high energy electrons of short wavelength to interact with the sample.

64. Two basic modes of TEM operation include *diffraction mode* and *image mode*. As with x-ray diffraction, electron diffraction follows the same principles of Bragg's Law.

65. Diffraction mode produces a diffraction pattern in the back focal plane of the primary imaging (objective) lens. Image mode produces a black and white image, much like the image produced by a light microscope, which provides information in real space. An advantage of TEM is that it is capable of providing both kinds of information for the same region. I address both of these modes, and some of their associated properties, below.

a. Diffraction mode

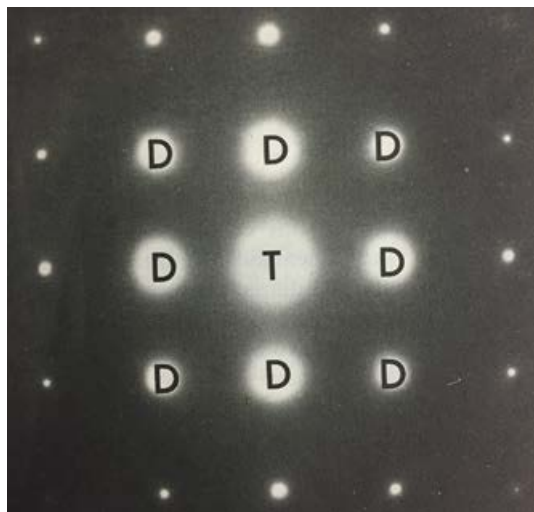
66. The concept of electron diffraction using TEM is similar to that of x-ray diffraction. Because the atoms of a crystal are arranged in a long-range order, electrons transmitted into the crystal will diffract at specific angles and intensities. The electrons diffracted from a specific set of planes—because they are parallel to each other—are recombined to form corresponding spots on the back focal plane of the objective lens of the microscope.

67. The resulting diffraction patterns provide information about the arrangement of atoms (and therefore the crystal structure and texture, if any) in the material. The distances between the individual spots and the central “undiffracted spot” are inversely related to the distance between planes, and the angles between different diffracted spots when measured with respect to the central spot also reflect the angles between the corresponding planes.

68. In addition, because there is a “reciprocal” relationship between the image and the diffraction pattern, there exists a “reciprocal space” in which the information about potential diffraction events is contained. This reciprocal space is sampled by the particular orientational relationship between the incident electron illumination and the crystal orientation: this orientation relationship thus determines the exact diffraction pattern that is formed.

69. As noted above, Bragg’s law is foundational in the field of crystallography, and the ability to measure distances and angles is routinely used to understand crystal structure. In particular, the angles between planes in real space and the measured angles in the diffraction pattern should be quite accurate—meaning that deviations of 0.5 degrees are significant from expected. Similarly, the ratio of measured distances is also something that should be quite accurate to be considered definitive (less than 3% error). (*See, e.g., B. Fultz and J. Howe, Transmission Electron Microscopy and Diffractometry of Materials* 290-292 (2013) (noting that accuracy should be within 3% for measuring the ratio of atomic distances).)

70. A typical electron diffraction spot pattern from a single crystalline material is shown below with annotations:

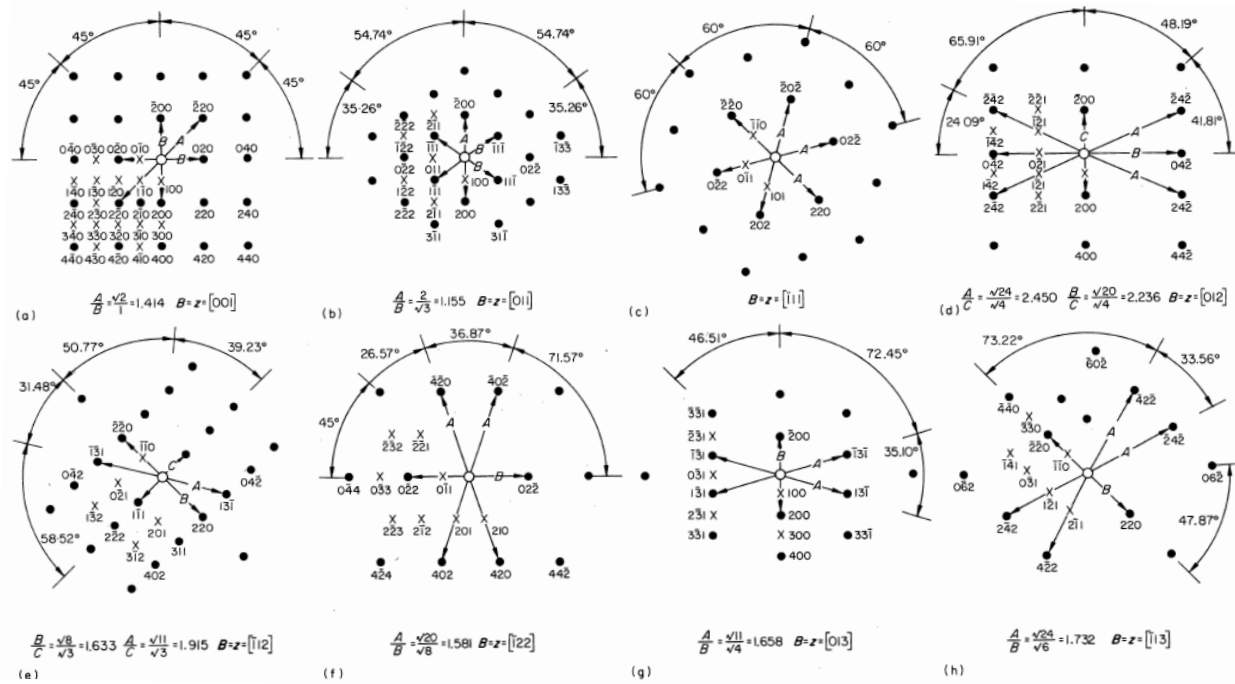


(J.W. Edington, *Practical Electron Microscopy in Materials Science* 32 (1976).)

71. In the image shown above, the TEM diffraction pattern has a bright spot in the center (labeled “T” for transmitted spot) that is the result of the TEM electron beam passing directly through the sample. The spots surrounding the center beam (labeled “D” for diffracted spot) each represents a series of planes. In this image, the square pattern of spots is formed because the electron beam impinges into the sample along the 001 orientation of the crystal.

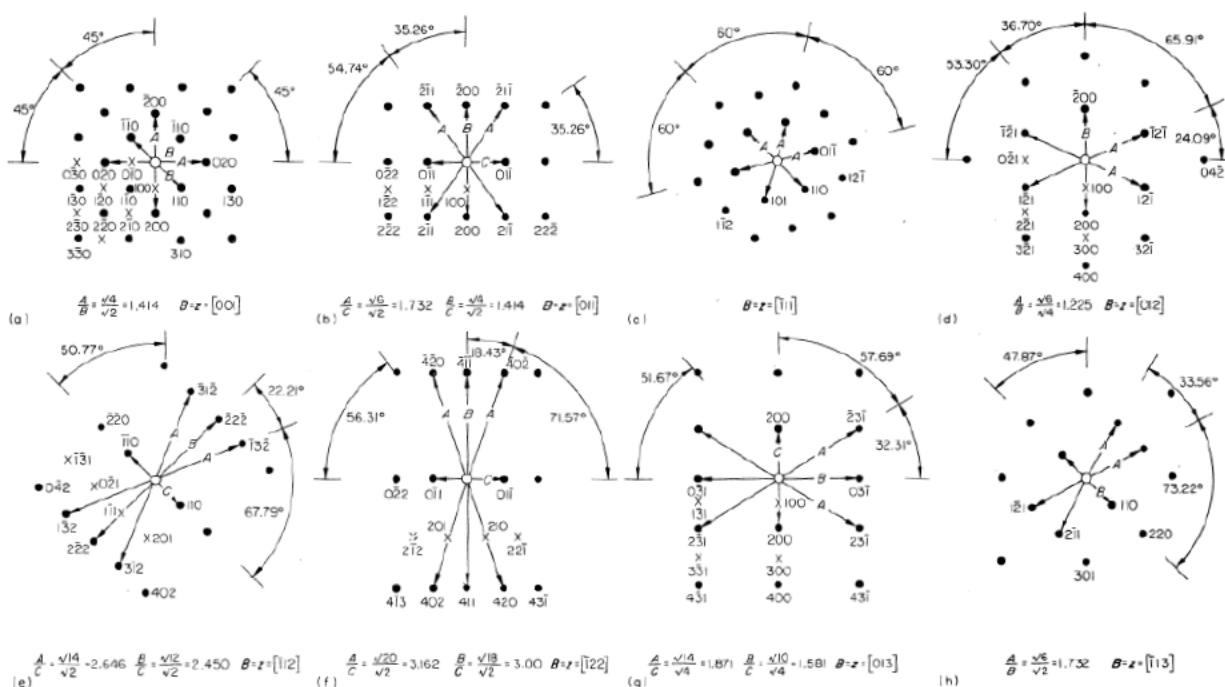
72. The same crystal may produce different diffraction patterns, depending on how the beam is aligned with the crystal. If the beam is aligned along what is known as a *zone axis*, it is aligned along a direction that has number of different planes that are diffracting at the same time. These are generally directions that have a high degree of symmetry.

73. The diffraction patterns obtained from a particular material can be compared to standard diffraction patterns to determine the crystal structure for the material. In comparing patterns, it is important to understand the direction that the electron beam has with respect to the sample that produces the particular diffraction pattern image that is being analyzed. Pertinent to this case, for example, are the standard zone axis diffraction patterns—with locations, distances, and angles—for an fcc crystal structure (such as NiFe) and for a bcc crystal structure (such as FeCo). The standard diffraction patterns for the eight most common zone axes for fcc crystals are shown below:



(J.W. Edington, *Practical Electron Microscopy in Materials Science* 32 (1976).) The dots indicate where – by Bragg’s Law – intensity should be expected. The “x” indicates locations where spots do not appear.

74. The standard diffraction patterns for the eight most common zone axes for bcc crystals are shown below:



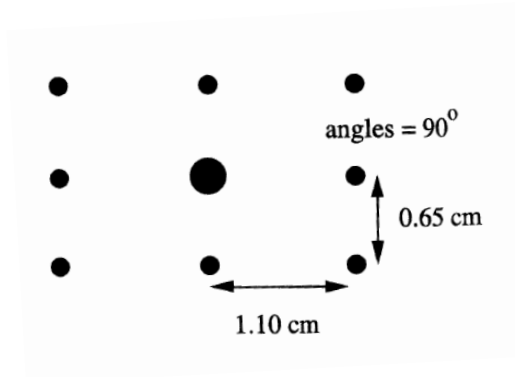
(J.W. Edington, *Practical Electron Microscopy in Materials Science* 304-306 (1976).)

75. In Exhibit E to this report, I have included enlargements of these standard patterns for fcc and bcc crystals, along with other relevant standard diffraction patterns.

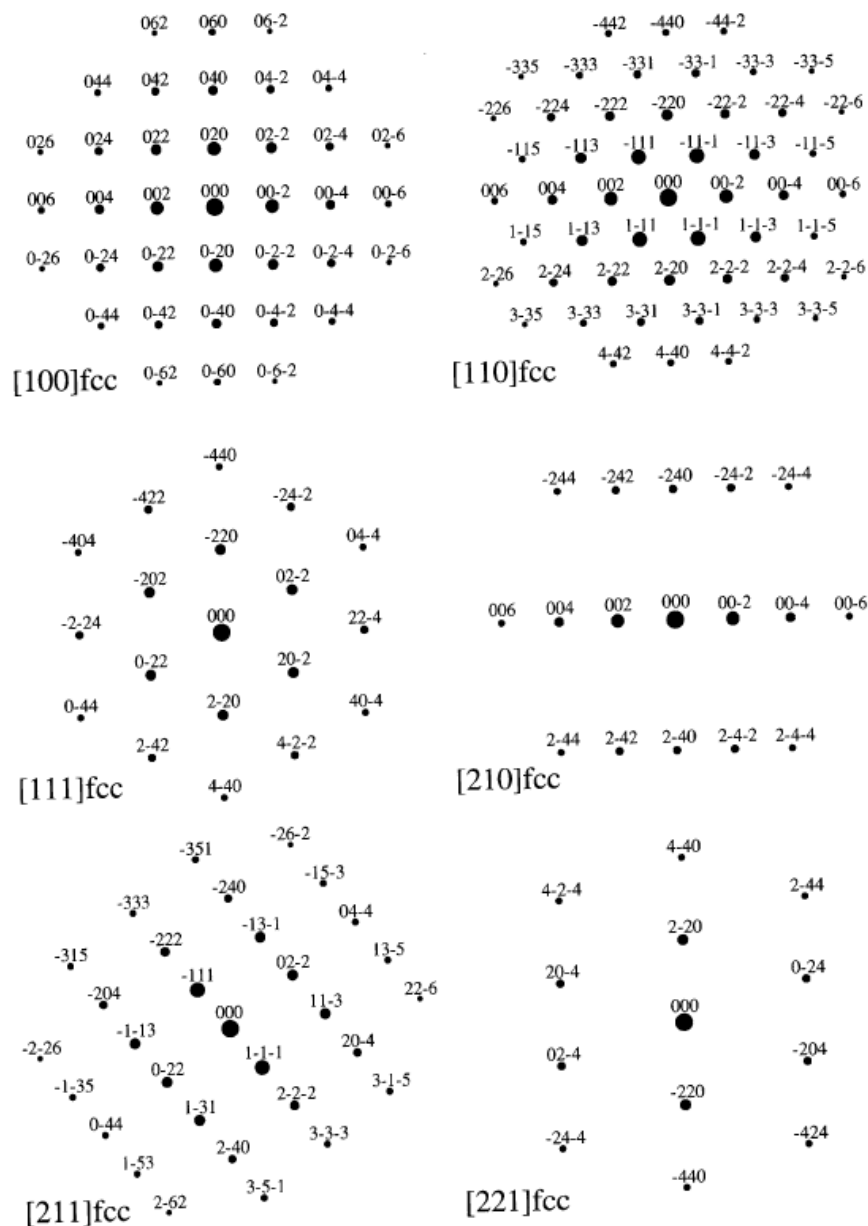
76. In the examples above, the zone axis for each standard pattern is noted below the pattern, and is indicated by $B = z = [hkl]$, where hkl is the particular zone axis orientation. For example, below the first pattern, in the upper left of both the fcc and bcc, the zone axis is $[001]$. The zone axis is parallel to the direction of the electron beam. For the standard patterns illustrated above, the primary zone axis for comparison would be the $[011]$ zone axis (which is the same as a $[110]$ or $[101]$ zone axis, *see supra* ¶¶ 35-36) if the beam was transmitted parallel to the $[011]$ direction for a bcc material such as FeCo (which would be the direction in a plan view looking top-down), whereas the $[111]$ zone axis would be used for comparison if the beam direction were aligned along the $[111]$ direction, such as occurs during a cross-sectional view of FeCo. (See generally (J.W. Edington, *Practical Electron Microscopy in Materials Science* 44-45, 283-84 (1976).)

77. There are standard methods scientists working in this field use for comparing diffraction patterns. One such method involves measuring the spacings and angles of the diffraction pattern being analyzed and then comparing those spacings and angles to the spacings

and angles listed for a standard diffraction pattern. In this method, the particular spacings and angles are noted and specifically compared using the center bright spot to orient the comparison. This can also sometimes be shown by overlaying the standard diffraction pattern onto the diffraction image and noting any differences in spacings and angles. (*See id.* at 47 (“In the case of cubic structures the symmetry of the pattern may be directly compared with those standard patterns shown in appendix 4, using the distances from the centre spot to diffracted spots and angles between g vectors as a check.”); B. Fultz and J. Howe, *Transmission Electron Microscopy and Diffractometry of Materials* 292 (2013) (“The easy way to index this diffraction pattern is to look it up in Appendix A.6 of this book.”).) An example of this is as follows. Assume we have the diffraction pattern shown below, and are able to measure the angles and distances between the spots:



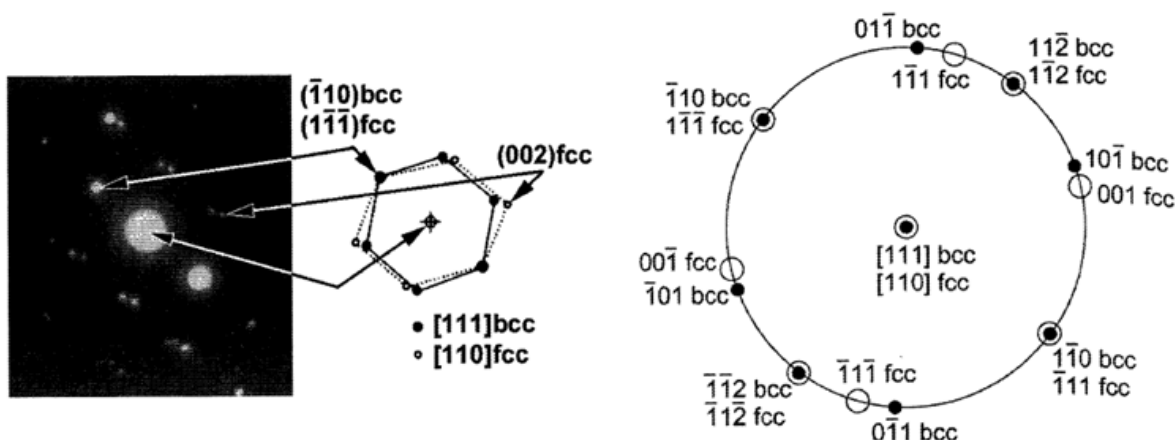
78. If we know this diffraction pattern is fcc, we can do a quick comparison of this rectangular pattern of spots to the most common fcc zone axes, shown below:



79. A quick visual comparison indicates that the rectangular pattern of spots matches the fcc[211] zone axis. We can reject the [100] zone axis because it is square, and the [110], [111], and [221] zone axes because they are all hexagonal. The [210] is rectangular, but the ratio of the sides of the rectangle is too large, at 2.236. Our data indicate a ratio of 1.10 cm / 0.65 cm, or about 1.69, which is within 2% of the 1.63 ratio listed for fcc[211].

80. TEM diffraction patterns also can be used to show the nature of an orientational relationship between crystals. For example, if a plan view (top-down view) is used for the electron beam direction, one can plot a bcc(110) crystal's orientation relative to an underlying

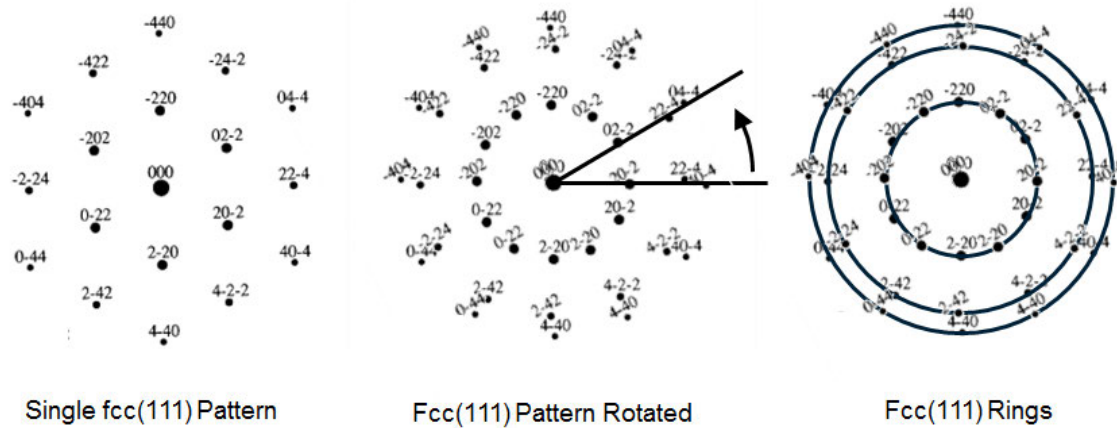
fcc(111) crystal using the resulting TEM diffraction patterns that should appear for both crystals. Shown below, for example, is a TEM diffraction pattern showing a bcc(110) crystal oriented over an fcc(111) hexagonal crystal like that shown in Figure 5 of the '988 Patent:



(B. Fultz and J. Howe, *Transmission Electron Microscopy and Diffractometry of Materials* 306 (2013).)

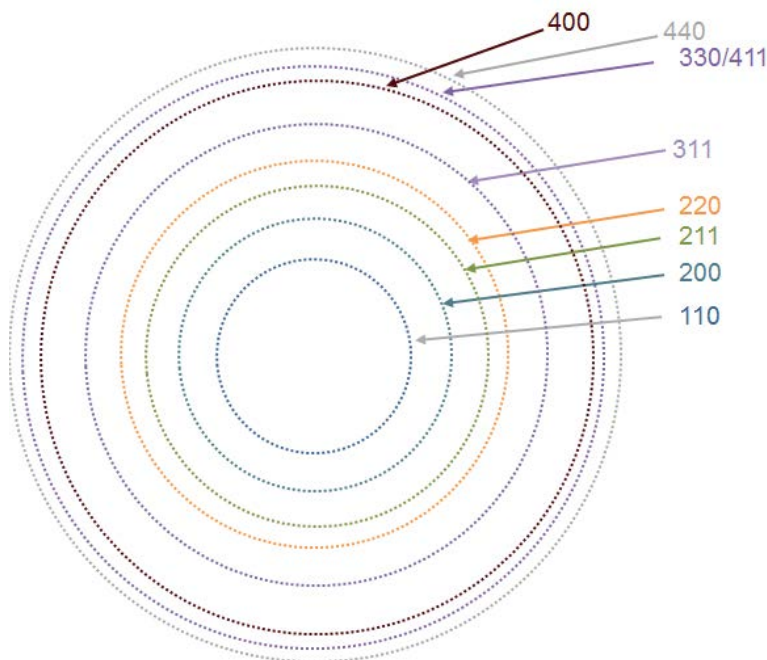
81. It is important to note that care must be taken when making comparisons using diffraction patterns to ensure that the ratios between diffraction spots and angles between diffraction spots are exactly as shown in the standard diffraction patterns. The failure to align the patterns with the correct atomic spacing will lead to inaccurate and unreliable results. (*Id.* at 290-292 (noting accuracy should be within 3% for measuring the ratio of atomic distances).)

82. Ring Patterns. If a sample is polycrystalline, the diffraction pattern will reflect the fact that the beam is likely intersecting multiple crystal grains, each with a different orientation within the plane. As a result of these different orientations, the ensuing diffraction pattern is not a series of repeating spots, but is instead a series of rings centered around the beam. This can be seen below, by rotating an example diffraction pattern of fcc(111):



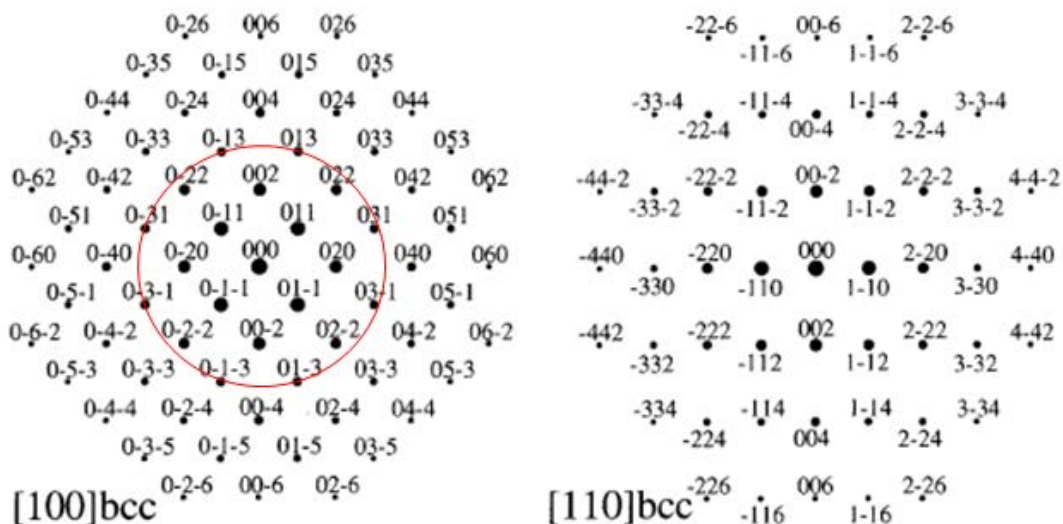
83. As is shown above, as the fcc(111) pattern is rotated about the center beam, the diffraction spots form a series of rings, each at a certain radius. The radius of each ring is related to the spacing between the planes forming each ring in the sample crystal. As shown in the example above, the innermost ring is formed from the {220} set of planes, the second ring is formed from the {422} set of planes, and the outermost ring is formed from the {440} set of planes.

84. Shown below is a simulated ring diffraction I created for a bcc material composed entirely of (110) crystals such as FeCo, randomly oriented about the electron beam direction:



85. Each of the rings in the above image is labeled with the crystalline orientation that contributed to that particular ring, and reflects a completely random distribution of rotations of bcc(110) grains within the plane of the crystal. It is important to note that a crystal with a single texture, in this case bcc(110), will have many rings in addition to the ring labeled 110 above, including the 200, 211, 220, 330/411 (which overlap as they have nearly the same d-spacing), 400, and 440 rings. This is because while the name “bcc(110) crystal” indicates that the (110) plane will be parallel to the substrate, other planes within a bcc crystal will also diffract the electron beam and produce spots in the diffraction pattern. Each of these spots then forms a ring when the sample is a crystal with many in-plane orientations (*i.e.*, it is polycrystalline), as explained above.

86. Each ring in a given pattern can be indexed by its distance from the center beam spot. Once the rings have been indexed, it is possible to compare them to standard diffraction patterns and identify the crystals creating the rings. Although many different crystals may contribute to each ring, there are also rings that are only created by certain crystals, which allow us to identify the crystal. For example, while both a bcc(110) and a bcc(100) crystal will have a 110 ring, only the bcc(100) crystal will have an 013 ring. This is apparent by comparing the standard diffraction patterns for a bcc(100) crystal, shown below on the left, with a bcc(110) crystal, shown below on the right:



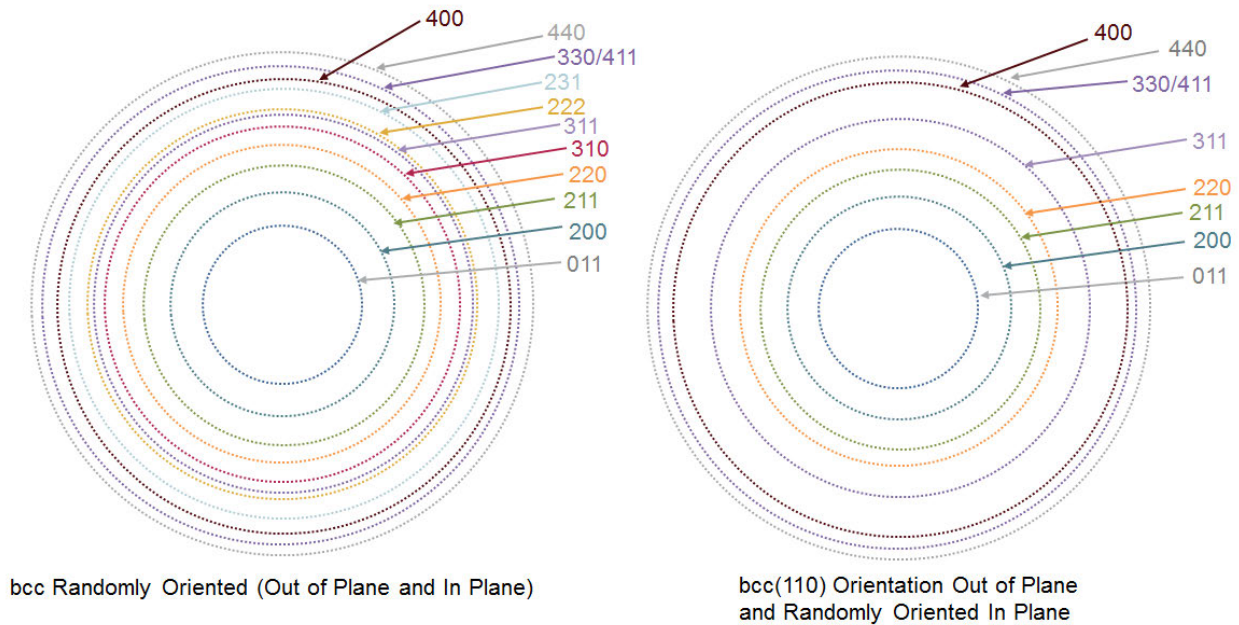
87. As can be seen from the comparison above, only the bcc(100) pattern contains 013 spots. All of the equivalent 013 spots form the red circle drawn above on the bcc(100)

pattern. Due to the symmetry of a cubic crystal, the following planes are all symmetrical: 013, $0\bar{1}3$, $0\bar{3}1$, $0\bar{3}\bar{1}$, $01\bar{3}$, $01\bar{3}$, $03\bar{1}$, and 031. (*See supra* ¶¶ 35-36.) Here the ‘bars’ over the top of the numbers are equivalent to negative numbers.

88. It is also important to note that if a diffraction pattern has rings that are not associated with the standard ring pattern for a particular crystal, we can conclude that the material does *not* have that crystal structure. For example, a crystal that has some 110 rings but also includes 310 and 213 rings means that the crystal is not solely a bcc(110) crystal but also has other crystals with different orientations. For example, if other rings were to appear in the pattern—*e.g.*, the 310, the 213, or the 222 ring—it would be conclusive proof that the given specimen contains grains oriented in directions other than 110.

89. Furthermore, it is possible for the presence of a given set of rings to be consistent with more than one crystal orientation. For example, in Dr. Clark’s expert report, he focuses on the 200 diffraction rings to conduct an analysis of the amount of bcc(110) crystals at certain angles in a sample. (*See, e.g.*, Clark at ¶ 117.) As discussed in more detail below, however, the 200 diffraction ring is consistent with a number of different possible grain orientations, including 110, but also 100, 012, 013, 023, and 014. To be succinct, diffraction from 200 rings does not indicate 110 texture.

90. I have created two sets of simulated diffraction rings below. The set of rings on the left reflects a randomly oriented bcc material (*e.g.*, FeCo), and the set of rings on the right reflects a perfectly bcc(110) oriented material (*e.g.*, FeCo):

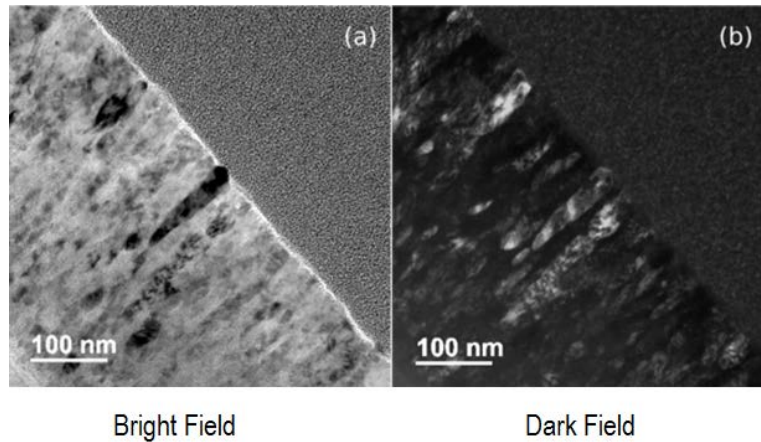


91. As can be seen above, the randomly oriented bcc material has 310, 222, and 231 rings, which are completely absent from the bcc(110) textured material's diffraction rings.

Larger versions of the above and other simulated diffraction patterns I have created can be seen in Exhibit H to my report.

92. Microbeam Diffraction. Microbeam diffraction is a variation of TEM imaging in the diffraction mode, where a finely-focused beam is used to provide greater sampling resolution in real space. The condenser lenses of the microscope are used to restrict the size of the electron beam that transmits through the sample. This limits the area from which the diffraction information will be obtained.

93. Bright and Dark Field Imaging. In addition, there are two modes of TEM diffraction known as "bright field" and "dark field" imaging. These methods use an aperture to select a single diffraction spot and block out others, so that the resulting image is based on the electrons in the beam that pass through the aperture. Shown below are examples of a bright field image and a dark field image:

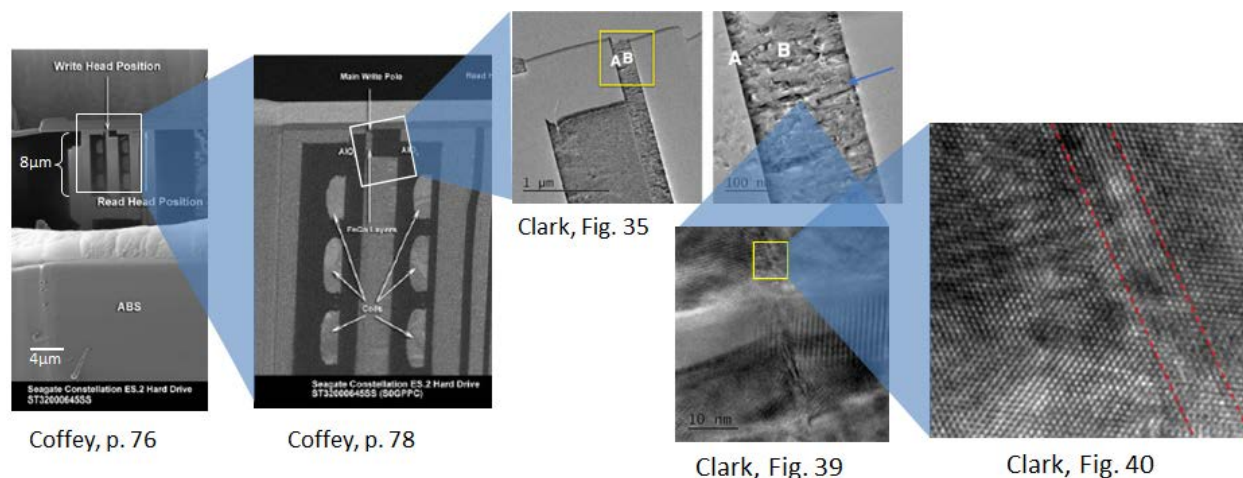


94. As can be seen above, the bright field image is lighter, as it is formed by placing an aperture in the TEM that allows the direct beam to pass through to the detector. The bright field image appears similar to a photonegative of the dark field image. The dark field image, as the name suggests, is darker as a result of an aperture blocking the direct TEM beam and only allowing beams that have been strongly scattered to particular distances and angles by the sample to pass through to the detector.

95. Most often, dark field images are taken using specific diffraction spots, leading to images that show bright in the image from regions that are diffracting to that specific crystallographic direction. Furthermore, because of the inverse relationship between real space and diffraction space, the planes that are diffracting in real space are absolutely perpendicular to the direction of a line drawn from the central spot to the given diffraction spot used to form the image.

b. Image mode and related measurements

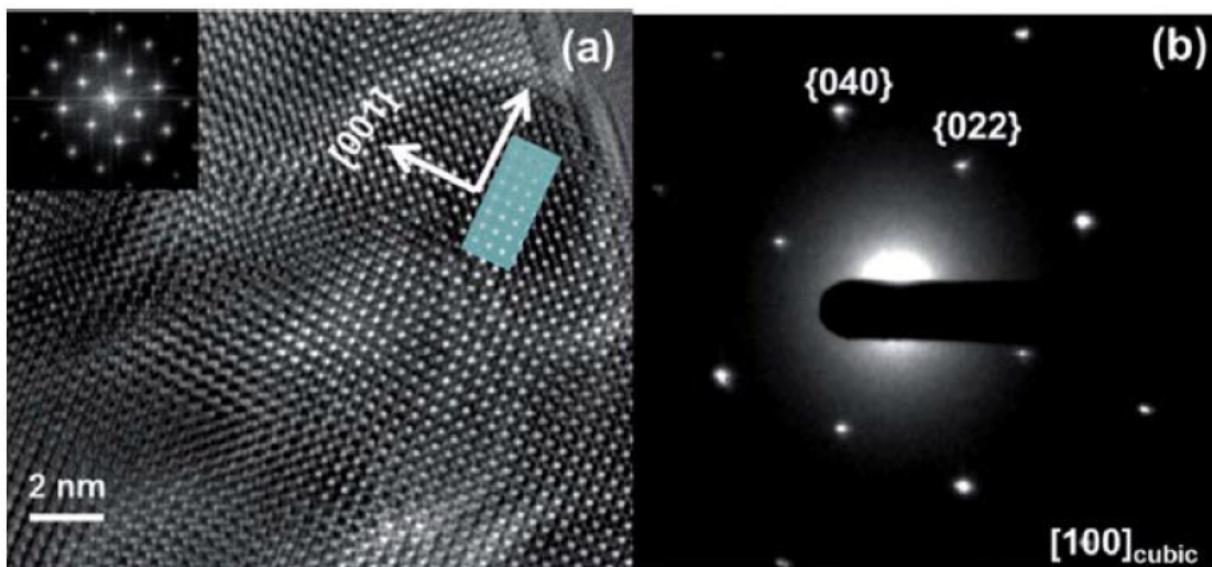
96. High-Resolution Phase-Contrast Images. High-resolution phase-contrast images are formed by using a TEM in image mode to create an image of a sample using the phase overlap of both the direct (transmitted) electron beam and one or more diffracted beams. An example of a series of TEM cross-section images from a Seagate HDD is shown below, compiled from Dr. Coffey and Dr. Clark's reports, that show a gradually increasing magnification:



97. These kinds of images can provide additional information about a structure, such as its scale. For example, as can be seen from the image and its scale on the far left, Seagate's write head is approximately 8 microns long in cross section. In contrast, the high-resolution cross-section image on the far right covers an area of about only 7 nanometers across. The individual dots that appear in this image are roughly at the scale of individual atoms, and to first order reflect the atom positions in the sample

98. FFTs. A Fast Fourier transform (FFT) is a computational method that can be used to reconstruct a diffraction pattern from a particular portion of a high-resolution image. In general, an FFT is a representation of some function in terms of a set of sine-waves. If there is a function that contains sets of many different waves, such as in the case of a diffraction pattern, an inverse FFT can be used to determine the individual frequencies of the diffracted waves and their relative strengths. Because different lattice spacings in a crystal will diffract differently, each decomposed sine-wave can provide information about the crystal structure.

99. FFTs can be used in certain cases to show the existence of particular crystalline orientations by matching the computed FFT of the image with a standard diffraction pattern in the same way as described above. For example, shown below on the left is a high-resolution TEM image for a crystal and the accompanying FFT generated from that crystal is shown in the far upper left. The TEM diffraction pattern for the same crystal is shown on the right:



100. In addition, FFTs for two separate crystals that are oriented parallel to one another and perpendicular to the substrate can be used to draw conclusions about the orientational direction of the overlying crystal relative to the underlying crystal, at least for the specific crystals being analyzed.

VII. BRIEF OVERVIEW OF SEAGATE'S WRITE HEADS

A. Material Structure of [REDACTED] Write Head Designs

101. I understand that LMS contends that Seagate's hard disk drives containing write heads that use one of the following Seagate designs infringe one or more claims of the '988 Patent: [REDACTED]. (*E.g.*, Clark at ¶ 76.) Because Dr. Clark did not describe any testing for the [REDACTED] design in his report (*see id.* at ¶ 76 n.12), I have focused only on the [REDACTED] [REDACTED] designs for purposes of my analysis and opinions in this report. I set forth below my understanding of the material structures of those two designs based on information provided by Seagate, which I understand Dr. Clark also used for purposes of his report. (*See id.* at ¶¶ 77-78.)

102. [REDACTED] Design. I understand that [REDACTED]
[REDACTED] According to
Seagate, these materials have the following characteristics:

[REDACTED]

[REDACTED]

(Seagate's First Supplemental Response to LMS's Interrogatory No. 10 at 14-15.) I further understand that Nanowebers of FeCo can be converted to Angstroms, with 1000 Angstroms of FeCo (2.4T) equal to 45.5 nanowebers. (*Id.*)

103. [REDACTED] Design. I understand that the write heads using the [REDACTED] design are made of thin films with a different material structure. In particular, I understand that [REDACTED]

[REDACTED] According to Seagate, these materials have the following characteristics:

[REDACTED]

(Seagate's First Supplemental Response to LMS's Interrogatory No. 10 at 14.)

B. Samples Analyzed

104. [REDACTED] Design. I understand that for purposes of analyzing the crystallographic properties of the materials in the [REDACTED], Dr. Clark used samples taken from the write heads of two different Seagate hard disk drives with the [REDACTED] write head design. In his report, Dr. Clark refers to these samples as S0GPPC and S2MMMC. Dr. Coffey explains the origins of samples S0GPPC and S2MMMC in his report. (*See, e.g.,* Coffey at ¶¶ 131-132.)

105. I also had a sample prepared at my direction of a portion of a Seagate write head utilizing the [REDACTED] design. This sample is described in more detail in Exhibit C of my report.

106. [REDACTED] Design. For the [REDACTED] design, I understand that Dr. Clark analyzed one sample—which he refers to as SBRD8K—that was taken from the write head of a Seagate hard disk drive with the [REDACTED] write head design. Dr. Coffey explains the origins of sample SBRD8K in his report. (*See, e.g.*, Coffey at ¶ 299.)

107. I also had a sample prepared at my direction of a portion of a Seagate write head utilizing the [REDACTED] design. This sample is described in more detail in Exhibit D of my report.

VIII. OPINIONS

A. Dr. Clark’s Conclusions Relating to the Crystalline Structure and Texture of the NiFe Layers in Samples S0GPPC, S2MMC, and SBRD8K Are Based on a Misapplication of Scientific Principles and Methods, Are Unreliable, and Do Not Have a Reliable and Sufficient Factual and Scientific Basis

1. Sample S0GPPC ([REDACTED] Design)

108. Dr. Clark’s report describes a number of TEM images and FFTs taken from these images that focus on the two NiFe layers he has identified in sample S0GPPC. In particular, Dr. Clark identifies two regions of sample S0GPPC where these images were taken, which he labels “A” and “B.” These are shown in Figure 35 of his report, which I have reproduced below:

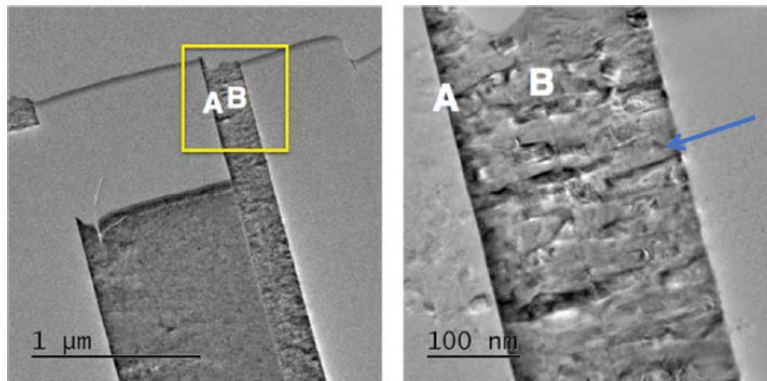


Figure 35 from Clark Report

109. Dr. Clark describes the area labeled “A” as the region “where the lower NiFe layer is” and the area labeled “B” as the region “where the upper NiFe layer is.” (Clark at ¶ 81.) As discussed below, Dr. Clark’s application of his methodology and test results from these regions are unreliable and do not provide a sufficient factual and valid scientific basis for concluding that either NiFe layer in sample S0GPPC provides a “(111) textured hexagonal

atomic template.” I address the testing performed by Dr. Clark and the conclusions he reaches for each of these regions below.

a. Lower NiFe Layer

110. Flawed Conclusions Regarding the Presence of fcc(111) Crystals. Dr. Clark relies on an FFT taken from a high-resolution cross-section at point 2 in region A of sample S0GPPC as the primary basis for his contention that the lower NiFe layer has an fcc crystal structure. (Clark at ¶ 88.) In my opinion, the methodology applied by Dr. Clark is flawed and unreliable, and his conclusions are not supported by the scientific data.

111. In particular, Dr. Clark shows FFTs in Figure 42 of his report derived from point 2 of the TEM image shown in Figure 41 of this report. Dr. Clark states that the FFT image shown on the left in Figure 42 relates to the lower NiFe layer, and the FFT image on the right relates to the adjacent FeCo layer. (*Id.* at ¶ 88 and Fig. 42.) Dr. Clark also provides under each FFT the “standard diffraction patterns” for single fcc(111) and bcc(110) crystals rotated into similar orientations for each FFT that he obtained from *Transmission Electron Microscopy*, D.B. Williams and C.B. Carter, Springer (2009) at pp. 299-301. (Clark at ¶ 88 n.16 and Figure 42.) I have reproduced Figure 42 from Dr. Clark’s report below, which on the left shows the FFT for the lower NiFe layer along with a standard diffraction pattern, and the FFT of the adjacent FeCo layer and standard diffraction pattern on the right:

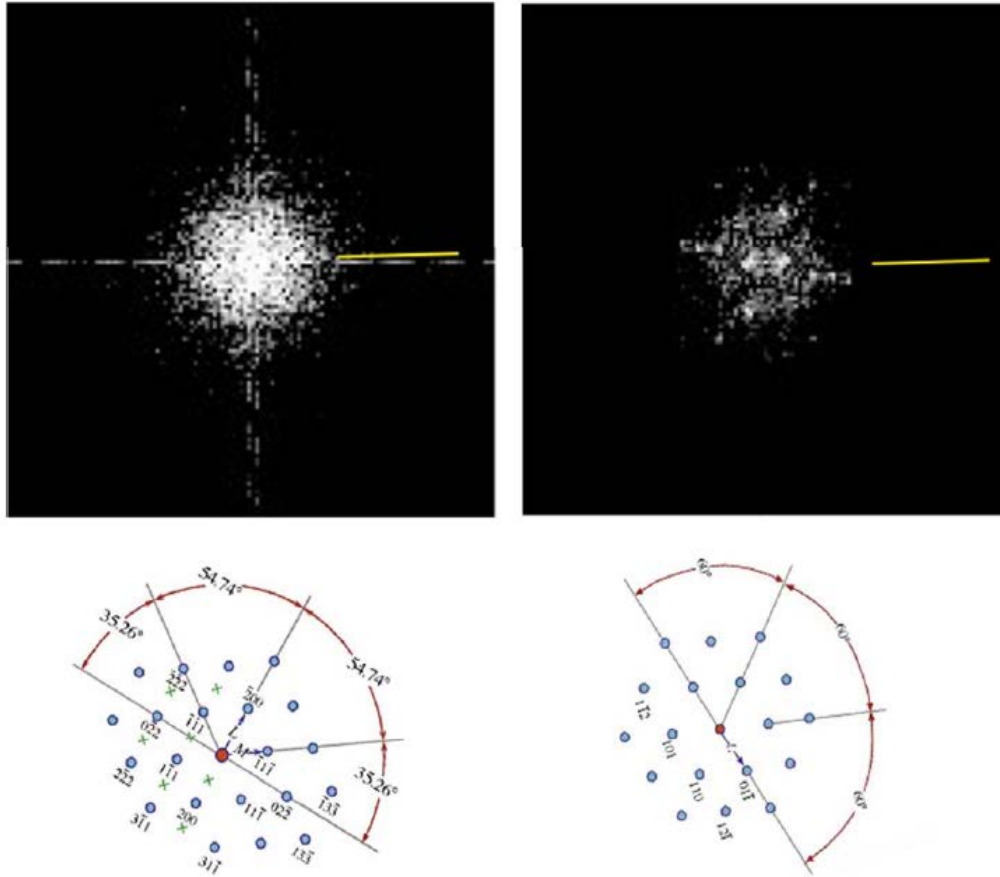


Figure 42: above: FFTs from the NiFe layer (left) and FeCo layer (right); below: standard diffraction patterns rotated into similar orientations as respective FFTs shown immediately above.

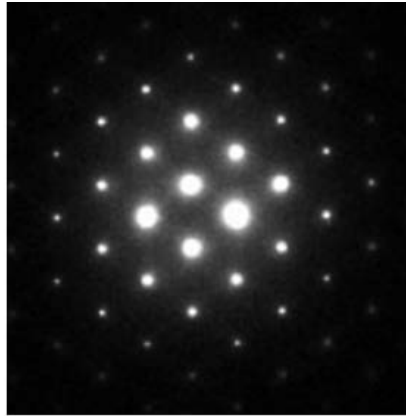
112. Dr. Clark states that “[a]nalysis of the FFTs was performed by measuring the diffraction spot spacings and the angles between rows of diffraction spots and comparing that information with standard diffraction patterns.” (*Id.* at ¶ 88.) Dr. Clark states that despite the existence of “a few overlapping spots from the lower FeCo layer,” a comparison between the FFT image for the lower NiFe layer and the standard pattern leads him to conclude that the diffraction pattern for the left-hand FFT is $\{110\}_{\text{FCC}}$ and that “the crystal structure of the NiFe layer is FCC.” (*Id.* at ¶ 89.)

113. The FFT image shown in Figure 42 that Dr. Clark relies on as evidence of the presence of an fcc crystal does not support his conclusion that the portion of the lower NiFe layer he analyzed has an fcc—much less an fcc(111)—crystal structure. Dr. Clark does not describe the particular methodology he applied for making his comparison. He does not, for example,

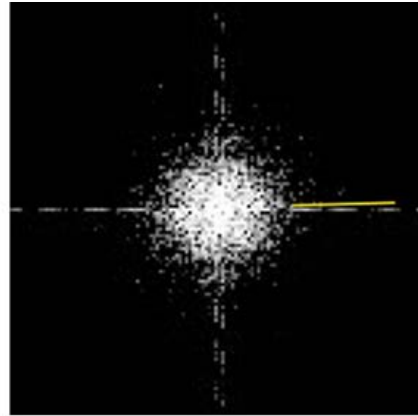
identify the location of the particular spots that he allegedly used to line up with the 111 spacings and directions of the standard diffraction pattern. Nor does he try to overlay the FFT image with the center spot in the standard diffraction pattern to show how all of the spots and angles are consistent with the standard diffraction pattern. The reason for this is clear: the image does not match the standard diffraction pattern. In fact, I do not see any particular diffraction spots in Dr. Clark's FFT at all. In my opinion, no reasonable scientist working in the field would agree with Dr. Clark's conclusion that this FFT shows an fcc crystal based on this data.

114. In order to show alignment with the standard pattern, the FFT image would need to have a clearly discernable center spot and other spots located at the same distances and angles from the center spot as shown in the standard diffraction pattern using the methodology I described earlier. Applying that methodology here, what is shown in the FFT pattern in Figure 42 is a splotch of white with virtually no discernable spots—much less distances or angles aligning with the fcc(111) standard diffraction pattern. In my opinion, this image does not show anything close to an fcc standard diffraction pattern for a (110) zone axis. One cannot even compare the FFT to the standard diffraction pattern because there are no discernable spots and spacings in the FFT image that can be aligned with the standard diffraction pattern. I am not aware of any published paper or study in this field that would support Dr. Clark's interpretation of this FFT image.

115. The fact that the FFT image shown in Figure 42 of Dr. Clark's report does not show an fcc structure—much less an fcc(111) structure—can be further illustrated by comparing it to the spot pattern of an actual fcc(111) crystal. Shown below on the left is the diffraction spot pattern for an actual fcc(111) crystal. (This is taken from KK Fung, *Identification and Determination of Crystal Structures and Orientations by Electron Diffraction* (Jan. 2001), available at: <http://personal.cityu.edu.hk/~appkchu/AP5301/Electron%20Diffraction%20-%20Paper.pdf>.) Shown below on the right is the FFT image for the lower NiFe layer from Figure 42 in Dr. Clark's report. As is evident from this side-by-side comparison, the FFT image from Dr. Clark on the right bears no resemblance to the pattern for an actual fcc(111) crystal shown on the left:

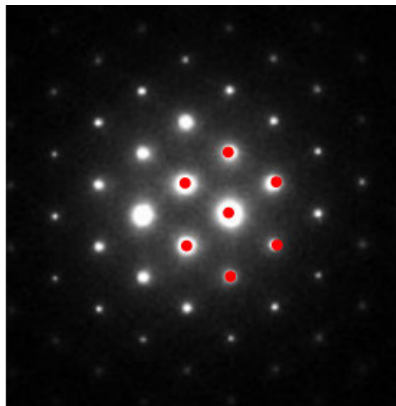


Measured Diffraction Pattern - fcc(110) zone axis

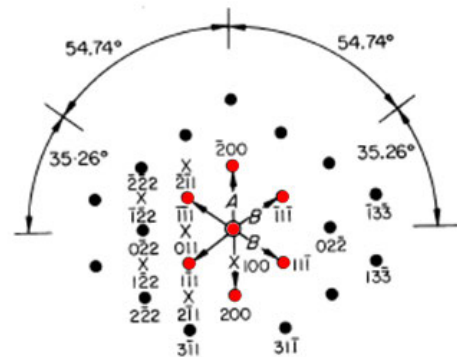


Clark FFT of NiFe, Figure 42

116. As a further illustration, in contrast to the lack of any discernable spots in Dr. Clark's FFT image that match the standard diffraction pattern, the image of the diffraction pattern for an actual fcc(111) crystal closely matches the standard pattern (fcc along a 110 zone axis), as shown in the annotated comparison below:



Measured Diffraction Pattern - fcc(110) zone axis



Standard Diffraction Pattern - fcc(110) zone axis

117. In my opinion, the FFT image shown in Figure 42 of Dr. Clark's report clearly does not show an fcc structure, much less an fcc(111) structure. Therefore, all of the conclusions drawn by Dr. Clark regarding the crystalline properties of the lower NiFe layer for sample S0GPPC lack any factual and scientific basis.

118. This problem is compounded to the extent Dr. Clark contends that other unidentified FFT images taken at points other than point 2 allegedly "showed similar results." (*Id.* at ¶ 94.) If these showed "similar results," then they are flawed for the same reason as the FFT for the single crystal that he does show in Figure 42.

119. Furthermore, to the extent Dr. Clark purports to rely on other FFTs, he does not specifically identify them and he does not provide the factual basis for his analysis. In fact, he does not provide any analysis. He does not show through overlays, spacing data, or any other methodology how he compared them, the basis for his comparison, or how any of them allegedly match the standard diffraction pattern.

120. To the extent one can speculate as to what these other FFTs might be based on Dr. Clark's naming convention for the images in Appendix C to his report (*see* Clark at ¶ 94 n. 17), there appear to be a total of 27 FFTs for individual crystals that purportedly relate to the lower NiFe layer. These are identified in a chart I have included in Exhibit F of my report under the filenames "Frameright1, Frameright2, Frameright3, Frameright4, and Frameright5."

121. I have reviewed each of these 27 FFT images (which include the one FFT image in Figure 42 of his report), and none of them is consistent with an fcc standard diffraction pattern along a 110 or 112 zone axis. In particular, none of the images provides a clearly discernable pattern that aligns with the standard spacings and angles for the fcc 110 or 112 zone axis patterns. My comparisons are contained in Exhibit F of my report.

122. I note that it is not surprising that the FFT data from Dr. Clark's report for the lower NiFe layer does not match an fcc standard diffraction pattern along a 110 or 112 zone axis in view of the thinness of the NiFe layer. Materials deposited [REDACTED]

[REDACTED]—are almost certainly too thin to have developed any significant crystal texture. (*See generally* M. Ohring, MATERIALS SCIENCE OF THIN FILMS 529, 562 ("[T]exture evolves from random in initial deposits, to strong orientation of low-energy planes parallel to the film surface, and finally, to changes in preferred texture as the film thickens further."); *see also* D. Lambeth et al., *Magnetic Media Performance: Control Methods for Crystalline Texture and Orientation*, Mat. Res. Soc. Symp. Proc., Vol. 517, p. 185 (1998) (noting that "below 5 nm the Cr is so thin that little or no crystalline texture has evolved as it could, perhaps, be thought of as amorphous").)

123. Flawed Conclusions Regarding (111) Orientation. Even if the specific crystals Dr. Clark purportedly analyzed using FFTs actually showed the presence of some individual fcc crystals (which they do not), they would not provide a reliable scientific basis for drawing any conclusions regarding the orientation of the crystals. As I explain above (*see supra* ¶ 37-39),

knowing that a crystal has an fcc structure does not tell you anything about its orientation relative to the substrate (such as whether it has a 111 orientation).

124. In his report, Dr. Clark attempts to draw conclusions about the orientation of all of the alleged fcc crystals in the lower NiFe layer by relying on the single FFT image in Figure 42 of his report for the lower NiFe layer. (For the other FFTs for the lower NiFe, Dr. Clark does not provide any information about their orientations relative to the substrate.) In my opinion, the methodology applied by Dr. Clark is flawed and unreliable, and his conclusions are not supported by the data.

125. As the basis for his conclusion, Dr. Clark states that the two FFT patterns in Figure 42 “show there are two parallel directions, one in the lower NiFe layer and one in the lower FeCo layer, pointing out of the page.” (*Id.* at ¶ 91.) He then contends that, “when analyzing the pattern from the spot spacing and distribution, it can be seen that a $\langle 111 \rangle_{\text{FCC}}$ direction in the NiFe is also parallel to a $\langle 110 \rangle_{\text{BCC}}$ in the FeCo, and lie in the plane of the page.” (*Id.*) He states that these are indicated in Figure 42 by the yellow lines marked on the FFT that he has added. (*Id.*) Dr. Clark then asserts that “[t]he directions are also perpendicular to the lower NiFe/lower FeCo interface, and so confirm the epitaxial growth in that direction and is evidence of epitaxial growth of the lower FeCo layer on the lower NiFe layer, which functions as an atomic template.” (*Id.*) Dr. Clark then concludes: “These two mutual relationships are also sufficient to determine the relative orientation of the lower NiFe Layer and the lower FeCo layer above it. Therefore, the lower NiFe layer exhibits (111) texture, and the lower FeCo layer exhibits (110) texture.” (*Id.*)

126. Dr. Clark’s assertion that the NiFe and FeCo crystals are parallel to one another and perpendicular to the substrate is not supported by his own data and is based on an unreliable methodology. In particular, neither of the yellow lines that Dr. Clark has drawn in Figure 42 for the two layers is perpendicular to the interface shown in Figure 41. This can be seen by comparing the angle between the substrate (the line along points 1, 2, 3 and 4) in Figure 41, which is shown in the annotated illustration below on the left, with the yellow lines from the FFTs in Figure 42, which are shown below on the right. Yellow lines have been added to show the relationship, with one yellow line drawn parallel to the substrate in Figure 41 on the left, and a second yellow line drawn perpendicular to the substrate, labeled as 90 degrees. Then, the yellow line from Figure 42 in Dr. Clark’s report has been extended to intersect with the substrate

in Figure 41 that is also shown in his report, and labeled to show that the intersection is at 76 degrees:

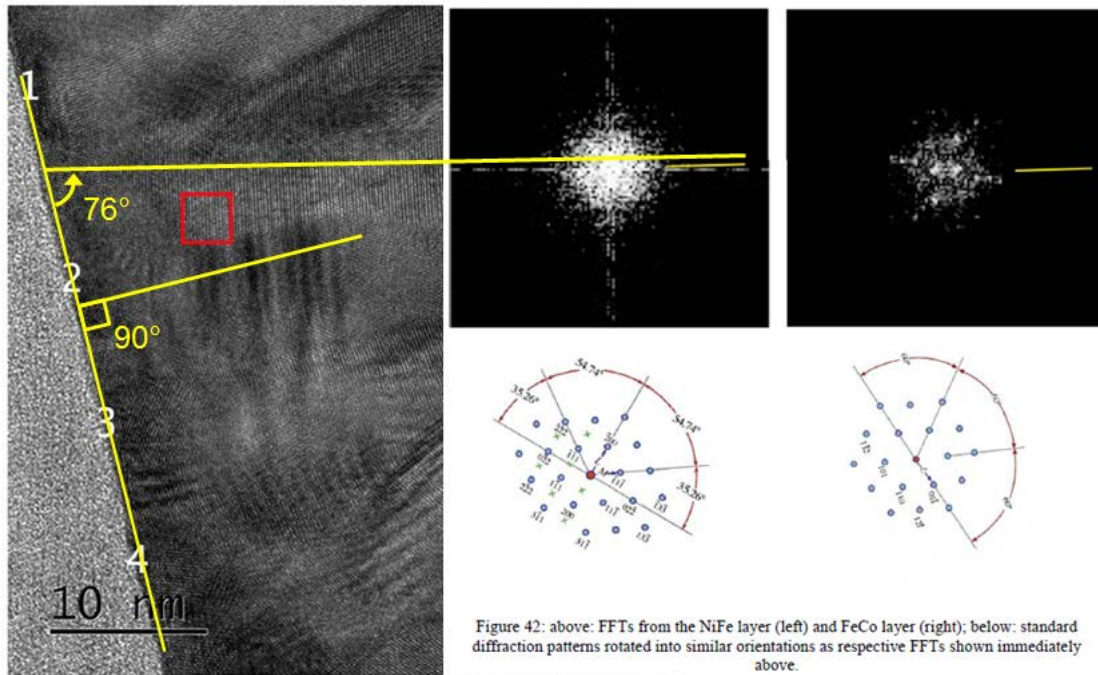


Figure 41: Example high resolution cross-section from region A. The numbered points indicate where FFTs were taken.

127. This comparison shows that the yellow lines relied on by Dr. Clark to show that the NiFe crystals are perpendicular to the substrate shown in Figure 41 are in fact *not* perpendicular, but instead are at approximately 76 degrees from the substrate – in other words, they are off by around 14 degrees from the substrate and therefore are not perpendicular to the substrate. This is a very significant deviation.

128. The fact that the FFT for the lower NiFe layer that Dr. Clark relies on is not perpendicular to the substrate means that it cannot have a (111) orientation parallel to the substrate, even if it had been shown to be an fcc crystal (which Dr. Clark has not done). This is because every fcc crystal contains a (111) plane, but only those fcc crystals in which the (111) plane is aligned parallel to the substrate are defined to have an fcc(111) orientation. Thus, for Dr. Clark to contend that the fcc crystal represented by the FFT in his Figure 42 has a (111) orientation, he would need to show that its (111) plane is oriented parallel to the substrate shown in Figure 41. Thus, a line drawn from the central spot in the diffraction pattern to the 111 diffraction spot would have to be exactly perpendicular to the interface (due to the reciprocal

relationship between real space and the diffraction space). It is not perpendicular, so Dr. Clark has failed to show an fcc(111) texture.

129. Accordingly, Dr. Clark's methodology for trying to show the orientation of the NiFe and FeCo crystals is flawed and unreliable and does not provide a factual basis and reliable scientific basis for his conclusion about the orientation of the single crystal he allegedly analyzed based on the FFTs discussed above.

130. Flawed Conclusions Regarding fcc(111) Texture. Even if Dr. Clark had been able to reliably discern the presence of some fcc(111) crystals in the lower NiFe layer of sample S0GPPC, there is no reliable or scientifically valid basis for his sweeping conclusion regarding the texture of the entire lower NiFe layer. This is an important point: just because *one* grain of hundreds is oriented in the 111 direction, does not in any way imply that *all* grains are oriented in the same direction. In my opinion, the methodology applied by Dr. Clark to reach his conclusions is flawed and unreliable, and his conclusions are not supported by the data.

131. For his broad pronouncements regarding the texture of the lower NiFe layer, Dr. Clark relies on the same flawed data mentioned above. For example, Dr. Clark's conclusion in paragraph 91 of his report regarding the texture of the lower NiFe layer apparently stems from his conclusion regarding the presence and alleged orientation of the single crystals he purported to identify. Yet, as shown above, there is no scientifically valid basis for this conclusion.

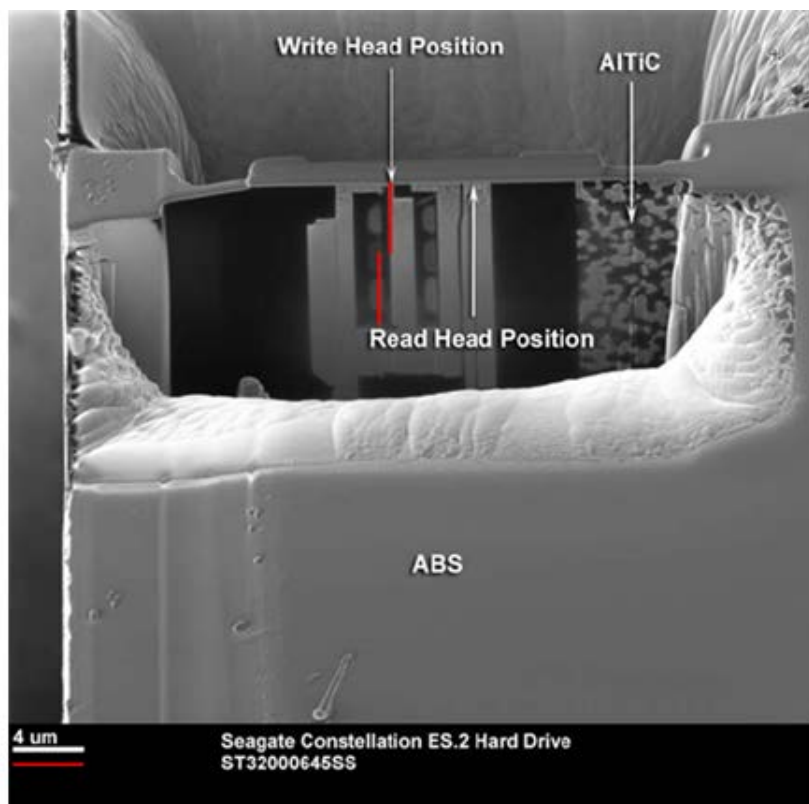
132. Dr. Clark asserts in another portion of his report that "[t]he parallel directions in the FCC and BCC layers normal to the interface show repeatedly <110> direction in the BCC layers and <111> direction in the FCC layers," which he contends "shows that the lower NiFe layer has a predominant (111) texture, and the lower FeCo layer has a predominant (110) texture." (*Id.* at ¶ 92.) But, once again, Dr. Clark does not provide any factual basis for his claim that there are "repeated[]" examples in the alleged fcc-bcc interface of the "<111> direction." To the extent his assertion that "the interface show repeatedly <110> direction in the BCC layers and <111> direction in the FCC layers" is based on the FFT images, these are flawed, as discussed above. He does not provide any other basis for his conclusion, and I have not seen any other basis for such a conclusion from the other materials provided in his report.

133. In fact, as I have explained, not only does the single FFT discussed by Dr. Clark in the body of his report not support the conclusion that this single grain has a (111) orientation relative to the substrate, but the other FFTs do not provide any information about the alleged 111

directions associated with each. Without such information, at most they represent many different orientations, which would be inconsistent with any predominate crystalline direction for any fcc crystals in the lower NiFe layer.

134. Furthermore, even if all of the FFTs from the lower NiFe layer that form the basis for Dr. Clark's analysis showed an fcc(111) crystal structure (which they do not), they would amount to a sample of approximately 1%, at best, of the lower NiFe layer, based on my calculation of the overall NiFe length dimension of approximately 8 micrometers (with 1 micrometer = 1,000 nanometers) and the aggregate length dimension for the FFTs being approximately 89.1 nanometers, or 1.1%.

135. My calculation for the overall length is based on the image of the write head in the device from which sample SOGPPC was taken as shown on page 76 of Dr. Coffey's report. That image shows an overall length dimension for the write head of approximately 8 micrometers, or 8,000 nanometers, as shown below in an annotated image from Dr. Coffey's report using the dimensions he provides (my annotations are in red to show the length dimension):



Annotated image of write head from Coffey Report at page 76

136. My calculation for the aggregate length dimension for the FFTs for the lower NiFe layer is based on the dimensions provided by Dr. Clark in Figure 41 of his report. Dr. Clark states that the FFTs for the lower NiFe layer were taken at points along the lower NiFe/lower FeCo interface marked with the numbers 1, 2, 3 and 4 as shown in Figure 41, with the area sampled for each FFT “confined to an area of the size indicated by the red square.” (Clark at ¶ 87 and Fig. 41.) I have reproduced this image from Dr. Clark’s report below:

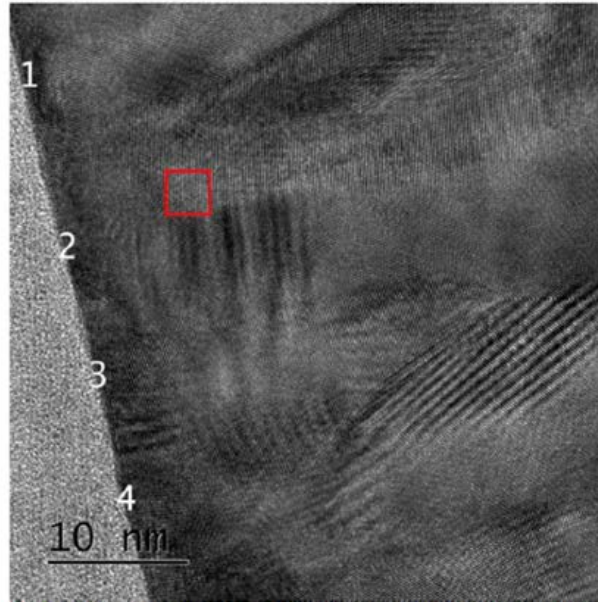


Figure 41: Example high resolution cross-section from region A. The numbered points indicate where FFTs were taken.

137. Based on the dimensions of the red box shown in Figure 41 of Dr. Clark’s report, the length dimension for each FFT taken by Dr. Clark at a particular location would be approximately 3.3 nanometers in length. As shown in Exhibit F of my report, a total of 54 FFTs were taken in this area based on Dr. Clark’s naming convention. While two FFTs were taken at each point, only one at each point was focused on the NiFe, so of the 54 total FFTs, only half (*i.e.*, 27) of them were focused on the NiFe layer. Therefore, 27 FFTs x 3.3 nm each = 89.1 nm. Taking the aggregate length dimensions of the areas from which the FFTs were taken of 89.1 nm, and dividing it by the overall length dimension of 8,000 nm results in 0.011, which is 1.1 percent. In other words, the sample size represented by Dr. Clark’s FFTs for the lower NiFe layer represents little more than 1 percent of the overall length of lower NiFe layer in the write head from which sample S0GPPC was taken.

138. Dr. Clark does not cite any source that has used his methodology of a 1 percent sample to draw conclusions about the alleged texture of an entire layer, and I am not aware of

any source that would provide a scientific basis for his approach. Accordingly, in my opinion, there is no scientific basis from which to draw a conclusion about the overall texture of the NiFe layer based on these images, even assuming Dr. Clark had been able to show the presence of some fcc(111) crystals at the locations of his images, and especially given all of the other flaws with his analysis as explained above.

139. Other Flaws. I also disagree with a number of Dr. Clark's other statements regarding the structure of the lower NiFe layer and the adjacent FeCo layer made in his report regarding sample S0GPPC. I address several of these below.

140. First, I note that Dr. Clark himself apparently has doubts about his conclusions for the lower NiFe layer. He states, for example, that "[t]o the extent that the FFT results for the lower NiFe layer are inconclusive, I conclude that the lower NiFe layer is FCC and exhibits a predominant (111) texture based further on the discussion of the upper NiFe / FeCo layers below." (Clark at ¶ 95.) For reasons I explain, however, Dr. Clark's data for the upper NiFe layer does not support any conclusion that the upper NiFe layer in sample S0GPPC is fcc(111) textured. Furthermore, there is no reliable scientific basis for Dr. Clark to make judgments about the lower NiFe based on data from the upper NiFe layer, especially where, as discussed below, there is no evidence to support a conclusion of (111) texture for the upper NiFe layer.

141. I also disagree with several observations or conclusions made by Dr. Clark based on the high-resolution images he took for portions of region A (shown originally in Figure 35 of Dr. Clark's report and which allegedly shows the region of the lower NiFe layer) that are shown in Figures 36 and 38 of his report. By way of example, I have reproduced the images from Figure 38 below:

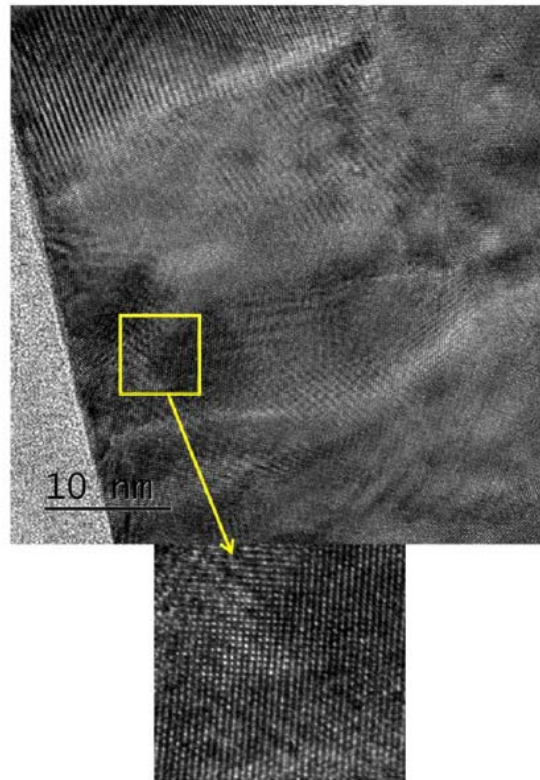


Figure 38: Example showing zoomed-in crossed lattice fringes from a high resolution cross-section from region A as discussed above.

142. Based on this and the other high-resolution images, Dr. Clark states that the grain structure shown in the image is “elongated perpendicular to the lower NiFe layer normal” and describes it as a “bamboo” structure consistent with epitaxial growth. (*Id.* at ¶ 82.) I disagree. While some grains in the FeCo layer shown in these images appear to be oriented approximately perpendicular to the substrate, others clearly are not.

143. To the extent Dr. Clark also suggests that his high-resolution images show evidence of epitaxial growth between the lower NiFe layer and the adjacent FeCo layer, I disagree. For example, as can be seen in Figures 38 and 41 from Dr. Clark’s report, the NiFe layer is not even clearly discernable. There also is no discernable relationship between the lower NiFe layer and any growth patterns of the FeCo grains, which grow in a variety of different directions. In my opinion, none of the images provided by Dr. Clark in his report for this region provides a factual basis for any conclusion about epitaxial growth.

144. Summary. In view of all of the flaws in Dr. Clark’s analysis that I have described above, it is my opinion that the conclusions drawn by Dr. Clark regarding the crystalline properties of the lower NiFe layer in sample S0GPPC lack a reliable factual and scientific basis

and are based on the application of flawed and unreliable methodologies. In my opinion, the testing data provided by Dr. Clark provides no evidence of the presence of an fcc(111) texture in the lower NiFe layer in sample S0GPPC.

b. Upper NiFe Layer

145. Flawed Conclusions Regarding the Presence of fcc(111) Crystals. Dr. Clark relies on an FFT taken from a high-resolution cross-section at points in region B of sample S0GPPC as the primary basis for his contention that the upper NiFe layer has an fcc crystal structure. (Clark at ¶¶ 97-98.) In my opinion, the methodology applied by Dr. Clark is flawed and unreliable, and his conclusions are not supported by the scientific data.

146. In particular, Dr. Clark shows FFTs in Figure 44 of his report derived from point 1 of the TEM image shown in Figure 41 of this report. Dr. Clark states that the FFT shown on the left in Figure 44 relates to the lower FeCo layer, the FFT in the middle relates to the upper NiFe layer, and the FFT on the right relates to the upper FeCo. (*Id.* at ¶ 97 and Fig. 44.). As before, Dr. Clark also provides under each FFT the “standard diffraction patterns” for fcc(110) and bcc(111) zone orientations, rotated into similar orientations for each FFT. (*Id.*) I have reproduced Figure 44 of Dr. Clark’s report below:

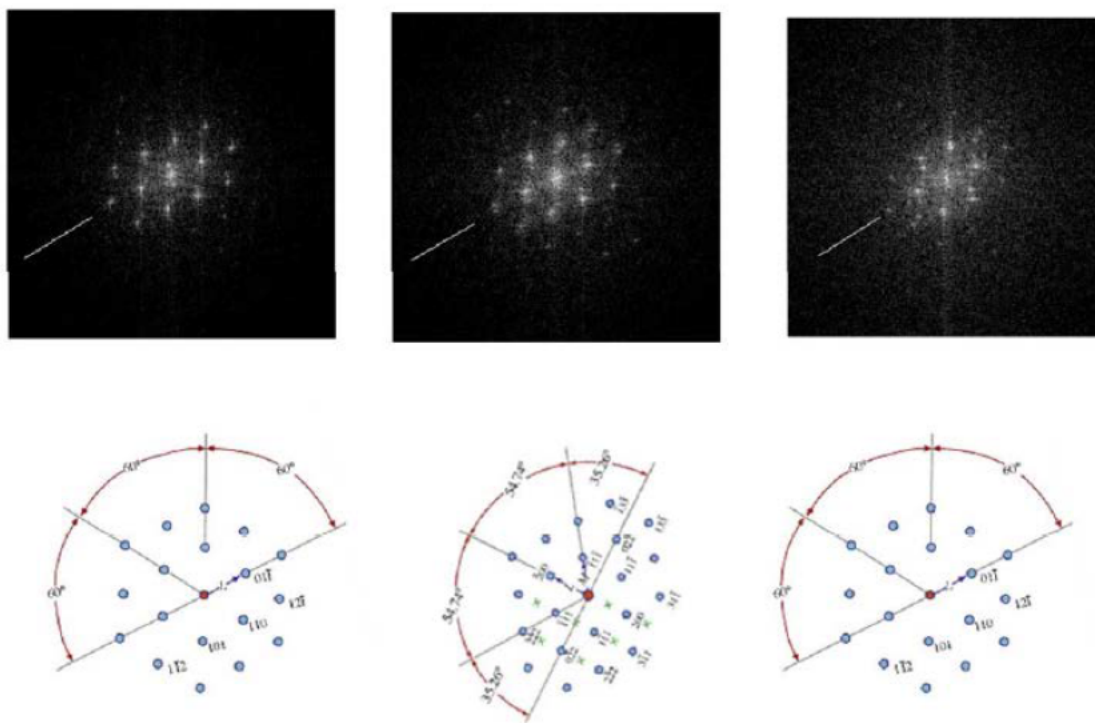


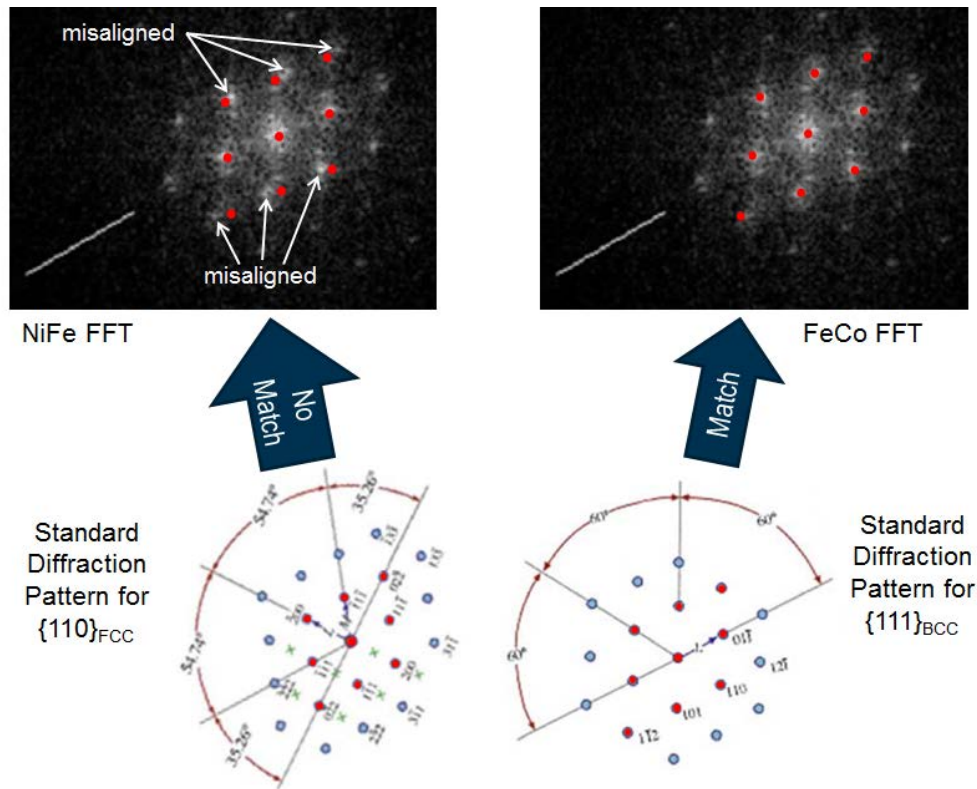
Figure 44: above: FFTs from: (a) the upper FeCo layer to the left of the upper NiFe layer (left); (b) in the upper NiFe layer (center); (c) the lower FeCo layer to the right of the NiFe layer (right); below: standard diffraction patterns rotated into similar orientations as respective FFTs shown immediately above.

147. Dr. Clark states that “following the procedures outlined for region A above, the two patterns in the upper and lower FeCo layers are identified as $\{111\}_{\text{BCC}}$, while the upper NiFe pattern is identified as $\{110\}_{\text{FCC}}$.” (*Id.* at ¶ 98.) He states that “[t]hese FFTs, like those analyzed above, indicate that “the crystal structure of the NiFe layer is FCC and the upper and lower FeCo layers is BCC.” (*Id.*)

148. The FFT image shown in Figure 44 that Dr. Clark relies on as evidence of the presence of an fcc crystal does not support the conclusion that the portion of the upper NiFe layer he analyzed has an fcc—much less an fcc(111)—crystal structure. Dr. Clark does not describe the particular methodology he applied for making his conclusions. He does not, for example, identify the rows of spots that allegedly line up with any 111 spacing and direction. Nor does he try to overlay the FFT image with the standard diffraction pattern to show how all of the spots and angles are consistent with the standard pattern. Once again, the reason for this is clear: the image does not match the standard diffraction pattern. In my opinion, no reasonable scientist working in the field would agree with Dr. Clark’s conclusion based on this data.

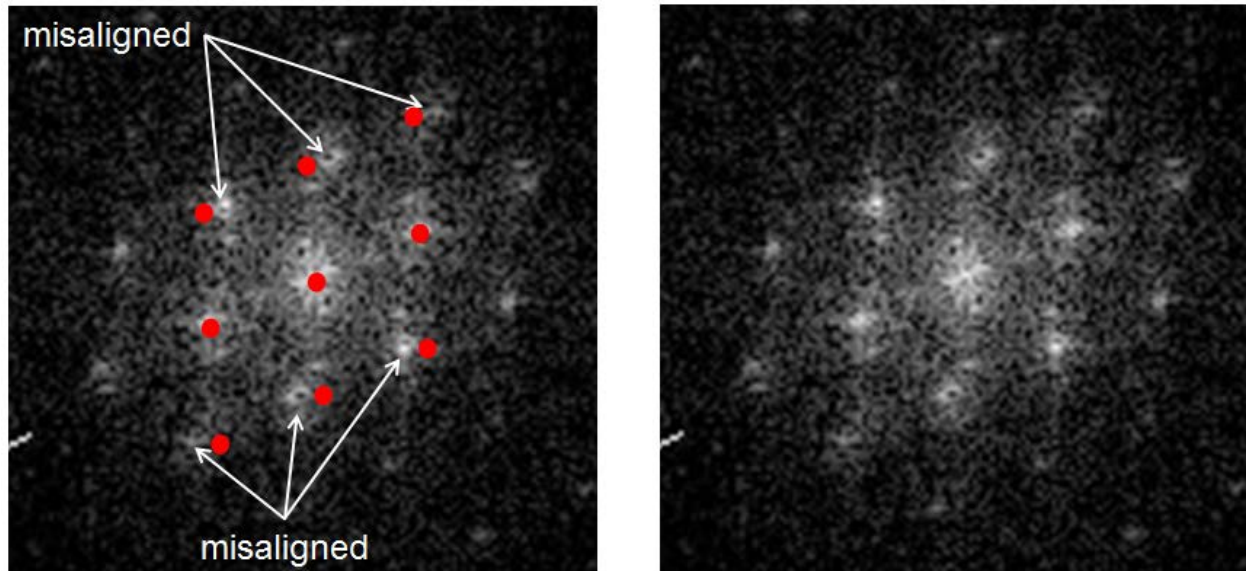
149. In order to show alignment with the standard pattern, the FFT image would need to have clearly discernable spots located at same locations, spacings, and angles as shown in the diffraction pattern using the methodology I described earlier. Applying that methodology here, what is shown in the FFT pattern in Figure 44 are spacings and angles that are inconsistent with the standard cross-section diffraction pattern for fcc(111).

150. To demonstrate this more clearly, I took the middle FFT image (which is for the upper NiFe layer) from Figure 44 and attempted to align the spots in this FFT with the $\{110\}_{\text{FCC}}$ diffraction pattern provided by Dr. Clark, using the 9 innermost spots of the template, which I have colored red. On the right, I attempted to align the purported upper FeCo FFT with the $\{111\}_{\text{BCC}}$ diffraction pattern, again using the 9 innermost spots of the template, which I have colored red. This is shown below:

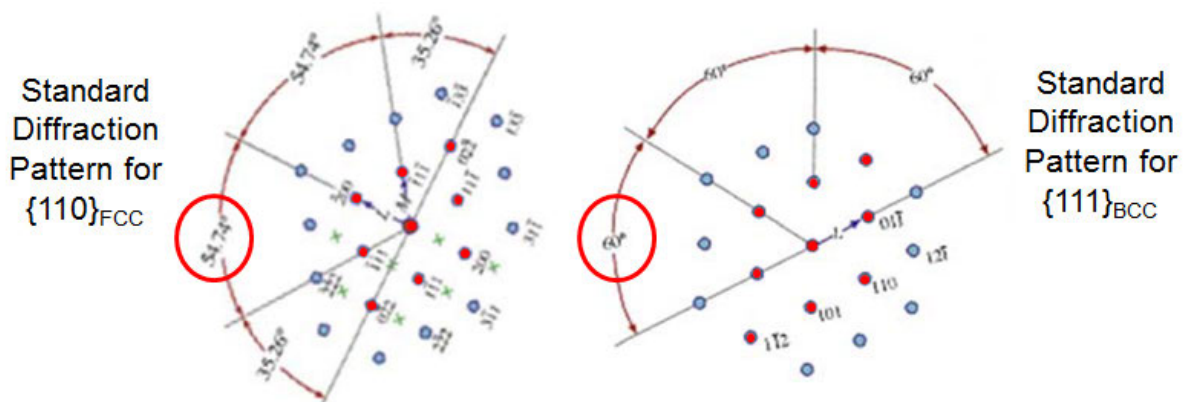


151. As can be seen, the spots for the NiFe FFT image do not align with the $\{110\}_{\text{FCC}}$ standard diffraction pattern. In contrast, there is actually a better match with the $\{111\}_{\text{BCC}}$ spots and the diffraction pattern for the FeCo layer, shown on the right.

152. To better see the extent of the mismatch between the NiFe FFT and the standard diffraction pattern, I have expanded the comparison shown above on the left, and reproduce that comparison showing the misalignment below (along with the same NiFe FFT without the spots):



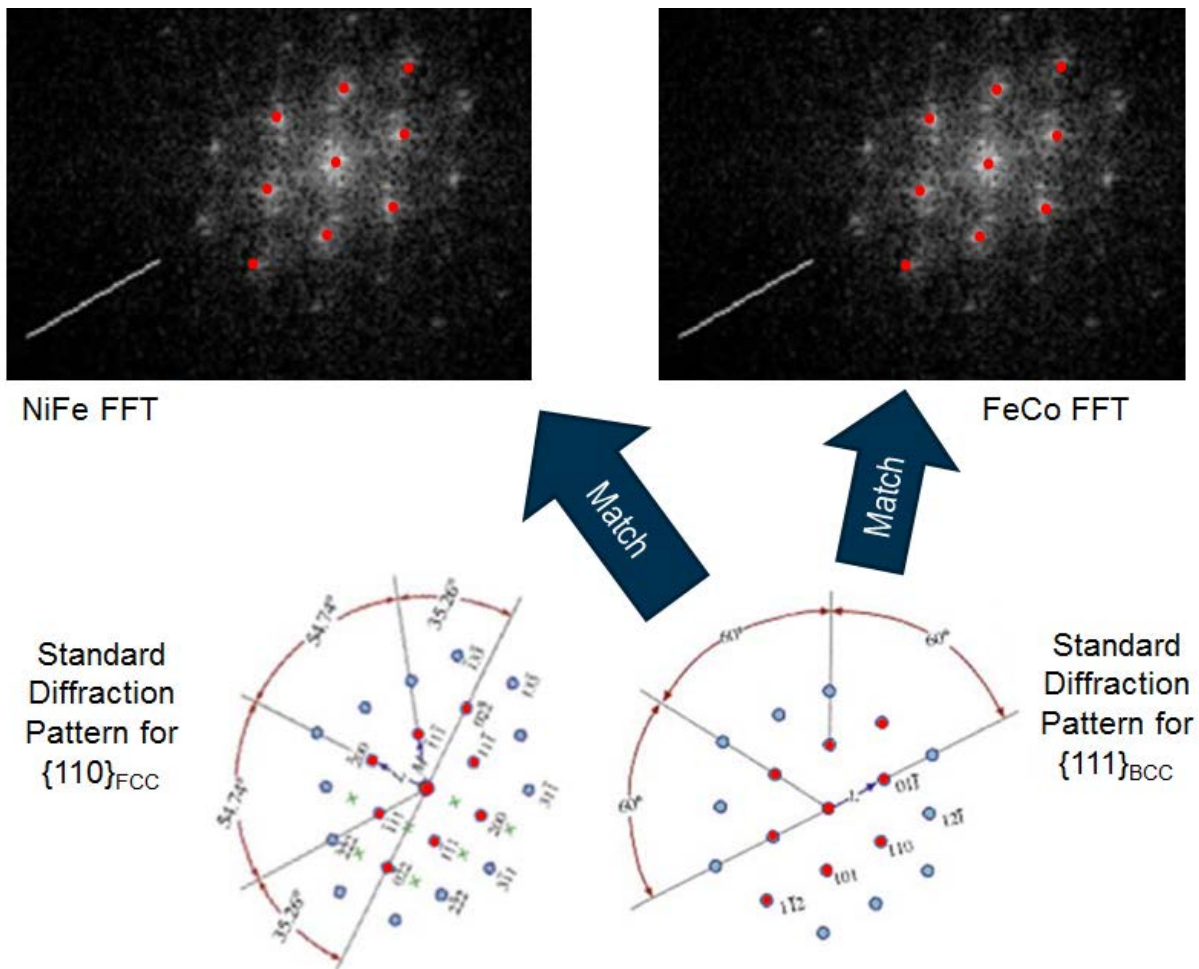
153. As can be seen, if the center row of three spots are aligned, the top three and bottom three spots are misaligned. Thus, the spacings and angles are misaligned. It is important to emphasize that the mismatch shown above is not just some “near miss.” The difference is illustrated, for example, in the angle from the center spot to two red spots left of the center spot: for $\{110\}_{\text{FCC}}$ that angle is labeled as 54.74 degrees, while for $\{111\}_{\text{BCC}}$ that angle is labeled as 60 degrees:



154. Thus, the misalignment of the top and bottom spots for NiFe is significant. This misalignment is critical, and makes all the difference between two completely very different crystalline textures. The alignment must be very close, typically within 0.5 degrees, before there

is any reasonable scientific basis to make a judgment about the crystal structure of the material, in this case NiFe. (See, e.g., B. Fultz and J. Howe, *Transmission Electron Microscopy and Diffractometry of Materials* 290-292 (2013) (noting accuracy should be within 3% for measuring the ratio of atomic distances).) That is not the case here.

155. Moreover, the fact that the FeCo and NiFe spot patterns look nearly the same suggests that Dr. Clark's FFT measurement actually is mostly of the FeCo layers on either side of the NiFe layer. In fact, I have overlaid the {111}Bcc pattern on Dr. Clark's NiFe FFT below, and it appears to be a close match:



156. This is not surprising, given that [REDACTED] —so that it would have been difficult to isolate the upper NiFe from the FeCo layers above and below it for purposes of an FFT measurement on the NiFe layer.

157. In my opinion, because the FFT image does not show an fcc structure, all of the conclusions drawn by Dr. Clark regarding the crystalline properties of the upper NiFe layer lack any factual and scientific basis.

158. This problem is compounded to the extent Dr. Clark contends that other unidentified FFT images taken at points other than point 1 allegedly “showed similar results.” (Clark at ¶ 104.) If these showed “similar results,” then they are flawed for the same reason as the FFT for the single crystal that he does show in Figure 44.

159. Furthermore, to the extent Dr. Clark purports to rely on other FFTs, he does not specifically identify them and he does not provide the factual basis for his analysis. In fact, he does not provide any analysis. He does not show through overlays, spacing data, or any other methodology how he compared them, the basis for his comparison, or how any of them allegedly match the standard diffraction pattern.

160. To the extent one can speculate as to what these other FFTs might be, based on Dr. Clark’s naming convention, there appear to be a total of 14 FFTs for individual crystals that purportedly related to the upper NiFe layer. These are identified in a chart I have included in Exhibit F of my report as those under the filenames “Middle1, Middle2, Middle3, Middle4, and Middle5.”

161. I have reviewed each of these 14 FFT images (which includes the FFT image in Figure 44 of his report), and none of them is consistent with an fcc standard diffraction pattern along a 110 or 112 zone axis. In particular, none of the images provides a clearly discernable pattern that aligns with the standard spacing and angles for the fcc 110 or 112 zone axis patterns. My comparisons are contained in Exhibit F of my report.

162. As I note above, none of this is surprising in view of the thinness of the layer. Materials deposited [REDACTED]
[REDACTED]—are almost certainly too thin to have developed any significant crystallographic texture, and may even be too thin to have a distinct crystalline structure.

163. Flawed Conclusions Regarding (111) Orientation. Even if the specific crystals Dr. Clark purportedly analyzed using FFTs actually showed the presence of some individual fcc crystals, they would not provide a reliable scientific basis for drawing any conclusions regarding the orientation of the crystal. As I explain above (*see supra* ¶ 37-39), knowing that a crystal has

an fcc structure does not tell you anything about its orientation relative to the substrate (such as a 111 direction).

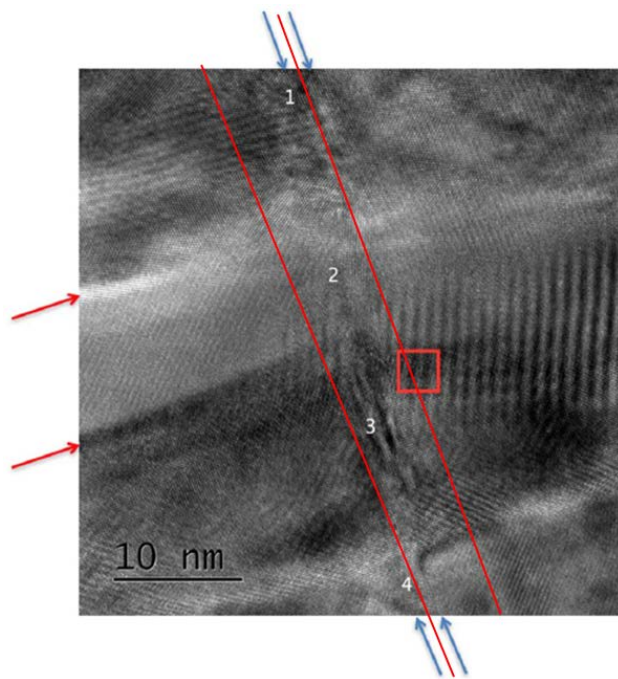
164. In his report, Dr. Clark apparently seeks to draw conclusions about the orientation of all of the alleged fcc crystals in the *lower* NiFe layer by relying on the single FFT image in Figure 44 of his report for the *upper* NiFe layer. (I am not sure whether Dr. Clark's reference to the *lower* NiFe layer here is an error in his report, but I will take his assertions at face value for purposes of my response here.) Once again, I note that for the other FFTs for the upper NiFe layer, Dr. Clark does not provide any information about their orientations relative to the substrate. In my opinion, the methodology applied by Dr. Clark is flawed and unreliable, and his conclusions are not supported by the data.

165. As the basis for his conclusions, Dr. Clark states that the FFT patterns in Figure 44 “show there are two parallel directions, one in the upper NiFe layer and one each of the adjacent FeCo layers, pointing out of the page.” (Clark at ¶ 101.) He then contends that, “when analyzing the pattern from the spot spacing and distribution, it can be seen that a $\langle 111 \rangle_{\text{FCC}}$ direction in the NiFe is also parallel to a $\langle 110 \rangle_{\text{BCC}}$ in the FeCo, and lie in the plane of the page.” (*Id.*) He states that these are indicated in Figure 44 by the yellow lines marked on the FFT that he has added. (*Id.*) Dr. Clark then asserts that “[t]he directions are also perpendicular to the upper NiFe/FeCo interfaces, and so confirm the epitaxial growth in that direction and is evidence of the epitaxial growth of the lower FeCo layer on the lower NiFe layer, which functions as an atomic template.” (*Id.*) Dr. Clark then concludes: “These two mutual relationships are also sufficient to determine the relative orientation of the lower NiFe Layer and the lower Fe Co layer above it. Therefore, the lower NiFe layer exhibits (111) texture, and the lower FeCo layer exhibits (110) texture.” (*Id.*)

166. Dr. Clark's assertion that the NiFe and FeCo crystals are parallel to one another and perpendicular to the interface of the NiFe and FeCo layers is not supported by his own data and is based on an unreliable methodology. Furthermore, even if true, it provides no evidence regarding the orientations of the FFTs relative to the substrate, which is necessary to show the orientation of the crystals and whether the FFT for the NiFe layer shows a 111 direction.

167. First, the three yellow lines (they actually appear to be gray in the image) inserted by Dr. Clark to show the orientation of the three FFTs in Figure 44 are *not* perpendicular to any clearly discernable NiFe/FeCo interface in Figure 43. In fact, it is somewhat unclear what

interface Dr. Clark is actually referring to in Figure 43. This is because while Dr. Clark apparently seeks to show the location and orientation of the interfaces of the FeCo with the upper NiFe layer with pairs of blue arrows at the top and bottom of the image in Figure 43 (*see id.* at ¶ 96 (“the two FeCo/NiFe interfaces are indicated by the blue arrows”)), those pairs of blue arrows are not themselves aligned. Below in an image annotated with red lines showing that if you extend the pair of parallel blue arrows at the top of Figure 43, they are not aligned with the lower pair of blue arrows:



168. Second, assuming that Dr. Clark is referring to this general region as the interface represented by the blue arrows in Figure 43 (as Dr. Clark implies), none of the lines that Dr. Clark has drawn in Figure 44 is perpendicular to this interface. For example, if you draw a line between the midpoints of the pairs of blue arrows, the resulting line, or interface, is not perpendicular to the lines drawn in Figure 44. This can be seen by comparing the angle between the alleged interface (the line established by the midpoint between the pair of top blue arrows and the bottom two arrows) in Figure 43, which is shown below on the left, with the lines from the FFTs in Figure 44, which is shown below on the right. This comparison shows that the lines in Figure 44 relied on by Dr. Clark to show that the FFTs are perpendicular to the interface shown in Figure 43 are in fact *not* perpendicular, but instead are off in the range of 16 degrees from perpendicular.

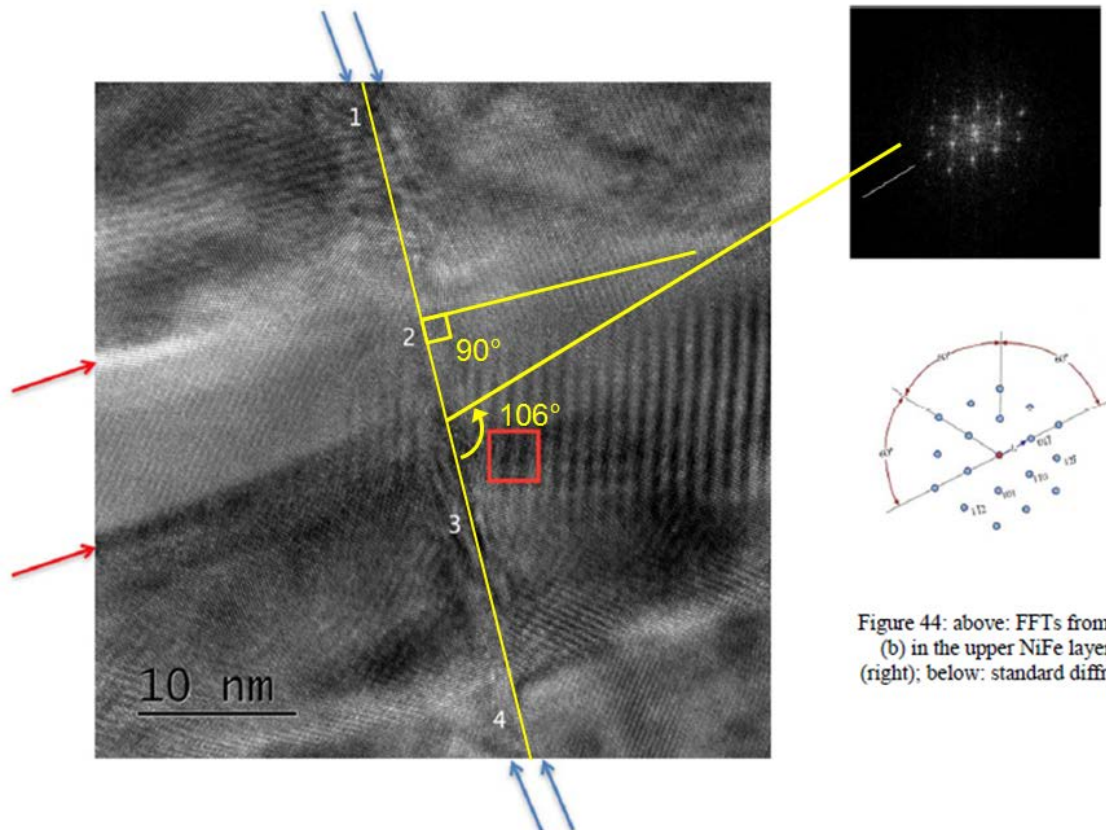


Figure 44: above: FFTs from: (b) in the upper NiFe layer (right); below: standard diffrac

169. Third, even if Dr. Clark had established a perpendicular orientation between the FFTs and the upper NiFe/FeCo interfaces, this would tell you nothing about the orientation of the upper NiFe layer relative to the substrate. Dr. Clark provides no location for the substrate relative to the FFT for the NiFe layer. Without this information, there is no way to assess the actual orientation of the NiFe crystal.

170. Finally, Dr. Clark's main point appears to be that a perpendicular orientation between the upper NiFe crystal and the upper NiFe/FeCo interfaces would tell you something about the orientation of the *lower* NiFe layer, but this clearly is not the case. Dr. Clark states that the two mutual orientations of upper NiFe crystal and the upper NiFe/FeCo interfaces "are also sufficient to determine the relative orientation of the *lower* NiFe layer and the lower FeCo layer above it." (*Id.* at ¶ 101 (emphasis added).) But what the orientation is of the upper NiFe layer relative to the interface tells you nothing about the orientation of the lower NiFe layer. There is no valid scientific basis for Dr. Clark to make such an assertion.

171. Because Dr. Clark provides no information about the angle of the NiFe crystal for the upper NiFe layer relative to the substrate, there is no evidence that any crystal in the upper

NiFe layer has a (111) orientation, even if he had been able to show that such a crystal had an fcc structure (which Dr. Clark also has not done).

172. Accordingly, Dr. Clark's methodology for trying to show the orientation of the upper NiFe and FeCo crystals, and to rely on them as evidence for the orientation of the lower NiFe layer, is flawed and unreliable and does not provide a factual basis and a reliable scientific basis for his conclusion about the orientation of the single crystals he allegedly analyzed based on the FFTs discussed above.

173. Flawed Conclusions Regarding fcc(111) Texture. Even if Dr. Clark had been able to reliably discern the presence of some fcc(111) crystals in the upper NiFe layer of sample S0GPPC, there is no reliable or scientifically valid basis for his sweeping conclusion regarding the texture of either the upper or lower NiFe layers. In my opinion, the methodology applied by Dr. Clark to reach his conclusions is flawed and unreliable, and his conclusions are not supported by the data.

174. For his broad pronouncements regarding the texture of the NiFe layers, Dr. Clark relies on the same flawed data mentioned above. For example, Dr. Clark's conclusion in paragraph 101 of his report regarding the texture of the *lower* NiFe layer apparently stems from his conclusion regarding the presence and alleged orientation of the single crystals he purported to identify in the upper NiFe layers. Yet, as explained above, there is no scientifically valid basis for this conclusion.

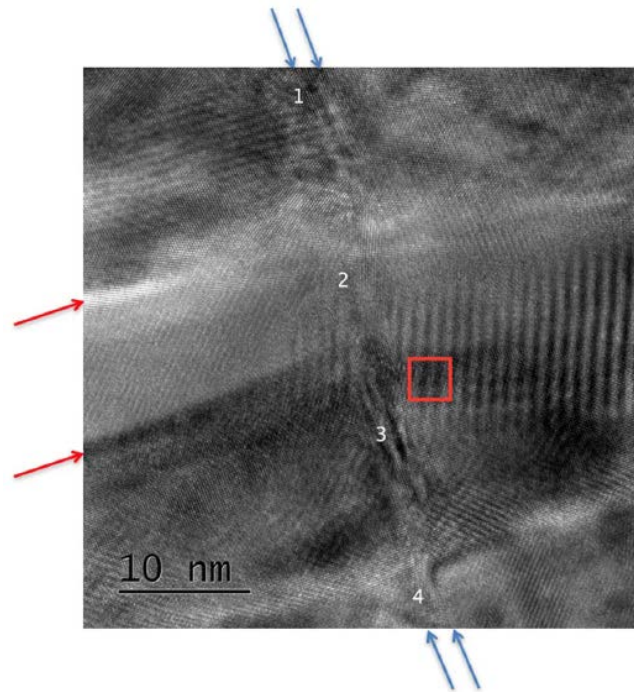
175. Dr. Clark asserts in another portion of his report that "[t]he parallel directions in the FCC and BCC layers normal to the interface show repeatedly <110> direction in the BCC layers and <111> direction in the FCC layers," which he contends "shows that the *lower* NiFe layer has a predominant (111) texture, and the *lower* FeCo layer has a predominant (110) texture." (*Id.* at ¶ 92 (emphasis added).) Once again, Dr. Clark does not provide any factual basis for his claim that there are "repeated[]" examples in the alleged fcc-bcc interface of the "<111> direction." To the extent his assertion that "the interface show repeatedly <110> direction in the BCC layers and <111> direction in the FCC layers" is based on the FFT images, these are flawed, as discussed above. He does not provide any other basis for his conclusion, and I have not seen any other basis for such a conclusion from the other materials provided in his report.

176. In fact, as I have explained, not only does the single FFT discussed by Dr. Clark in the body of his report not have a (111) orientation relative to the substrate, but the other FFTs do not provide any information about the alleged 111 directions associated with each. Without such information, at most they represent many different orientations, which would be inconsistent with any predominate crystalline direction for any fcc crystals in the lower NiFe layer.

177. Furthermore, even if all of the FFTs from the upper NiFe layer that form the basis for Dr. Clark's analysis showed an fcc(111) crystal structure (which they do not), they would amount to a sample of less than 0.8%, at best, of the upper NiFe layer, based on my calculation of the overall NiFe length dimension of approximately 8 micrometers (with 1 micrometer = 1,000 nanometers) and the aggregate length dimension for the FFTs being approximately 62.7 nanometers, or 0.78%.

178. My calculation for the overall length is based on the image of the write head in the device from which sample S0GPPC was taken is explained above. (*See supra* ¶ 135.) Once again, the overall length dimension for the write head is approximately 8,000 nanometers. (*Id.*)

179. My calculation for the aggregate length dimension for the FTTs for the upper NiFe layer is based on the dimensions provided by Dr. Clark in Figure 43 of his report. Dr. Clark states that the FFTs for the upper NiFe layer were taken at points along the upper NiFe/FeCo interfaces marked with the numbers 1, 2, 3 and 4 as shown in Figure 43, with the area sampled for each FFT "confined to an area of the size indicated by the red square." (Clark at ¶ 97 and Fig. 43.) I have reproduced this image from Dr. Clark's report below:



180. Based on the dimensions of the red box shown in Figure 43 of Dr. Clark's report, the length dimension for each FFT would be approximately 3.3 nanometers in length. As shown in Exhibit F of my report, a total of 42 FFTs were taken for this area based on Dr. Clark's naming convention, with three at each location. Only one of the three FFTs taken at each location was focused on the NiFe layer. Therefore, $17 \text{ FFTs} \times 3.3 \text{ nm each} = 62.7 \text{ nm}$. Taking the aggregate of the length dimensions of the areas from which the FFTs were taken of 62.7 nm, and dividing it by the overall length dimension of 8,000 nm results in 0.0078, which is 0.78 percent. In other words, the sample size represented by Dr. Clark's FFTs for the upper NiFe layer represents less than 0.8 percent of the overall length of upper NiFe layer in the write head from which sample S0GPPC was taken.

181. Dr. Clark does not cite to any source that has used this methodology of a 0.8% sample to draw conclusions about the alleged texture of an entire layer, and I am not aware of any source that would provide a scientific grounding for his approach. Accordingly, in my opinion, there is no scientific basis from which to draw a conclusion about the overall texture of the NiFe layer based on these images, even assuming Dr. Clark had been able to show the presence of some fcc(111) crystals at the locations of his images, and especially given all of the other flaws with his analysis as explained above.

182. Other Flaws. I also disagree with a number of Dr. Clark's other statements regarding the structure of the upper NiFe layer and the adjacent FeCo layers made in his report regarding sample S0GPPC. I address several of these below.

183. First, I disagree with several observations or conclusions made by Dr. Clark based on the high-resolution images he took for portions of region B (shown originally in Figure 35 and which allegedly is the region of the upper NiFe layer that are shown in Figures 39 and 40 of his report. By way of example, I have reproduced the images from Figure 39 and 40 below:

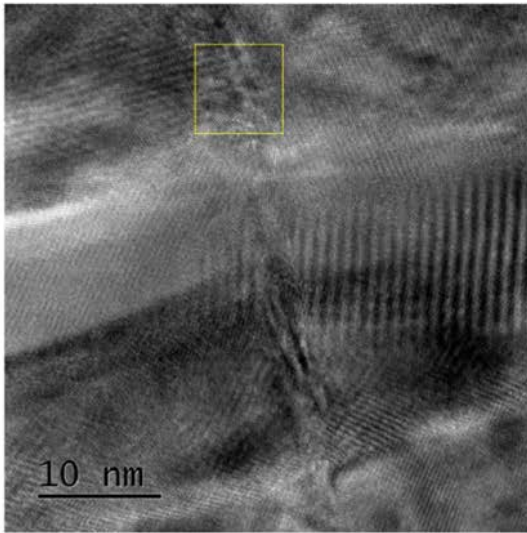


Figure 39: Example high resolution cross-section from region B. The area marked with the yellow square is shown zoomed-in in Figure 40 below.

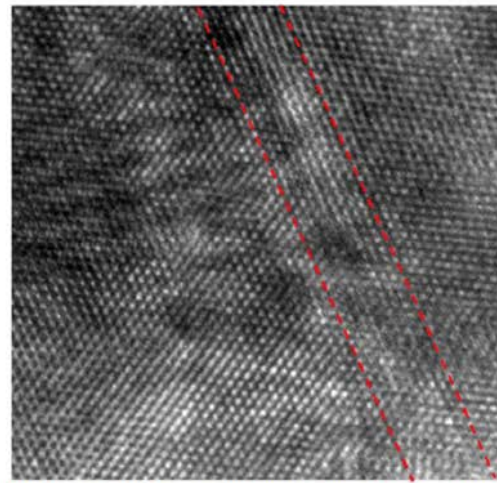


Figure 40: Zoomed-in area from Figure 39 above showing crossed lattice fringes.

184. Based on this and the other high-resolution images, Dr. Clark states that they show “crossed lattice fringes.” (*Id.* at ¶ 85.) He also says the zoomed-in area of Figure 39 shows “[s]everal sets of lattice fringes,” which he indicates with two red-dashed lines, and states that “[t]he fringes that run parallel to the red dashed line are present on both sides of the NiFe, and in the NiFe layer itself, indicating that the orientation of the FeCo is maintained on both sides of the NiFe.” (*Id.* at ¶ 86.) He goes on to say that “[t]he continuity of these fringes across all three layers show that there is an orientation relationship between the FeCo and the NiFe” and further concludes that there is a “hexagonal arrangement of spots in the FeCo lattice image” that “shows a $\{111\}_{\text{BCC}}$ plane, and a $\langle 110 \rangle_{\text{BCC}}$ direction” that “is normal to the interface.” (*Id.*) I disagree with Dr. Clark's analysis and his conclusions.

185. First, it is not apparent from the image that the area between the red-dashed lines clearly represents an area of NiFe material. But giving Dr. Clark the benefit of the doubt and

assuming that this is a region of NiFe, Dr. Clark's suggestion that this image can be used to determine that the FeCo is "normal to the interface" is incorrect. It provides no information about its orientational relationship to the substrate and therefore provides no data that can be relied on to determine whether the FeCo layer has a bcc(110) orientation with respect to the substrate.

186. Dr. Clark also states that "the FFTs taken from various points along the NiFe layers, while they maintain a common direction with the FeCo layers normal to the interface, change significantly with position along the interface." (*Id.* at ¶ 105). He goes on to say that these changes indicate differences in the grain size in the NiFe layer, and concludes that the "grain size in the NiFe template layers is comparable to the width of the FeCo grains" and that "there is ordinarily only one or two FeCo grains per NiFe template grain." (*Id.*) I disagree with Dr. Clark's analysis and his conclusions.

187. As an initial matter, Dr. Clark does not explain what "changes" with respect to "position along the interface" he is referring to. To the extent he is suggesting that these changes relate to grain size, or that there are clearly discernable grain sizes for the NiFe layer that can be determined from his images, I disagree. While these images provide some information about the grain sizes for portions of the FeCo layer, there is no clear evidence of NiFe grains or their sizes in these images. Therefore, in my opinion, there is no reliable factual and scientific basis for Dr. Clark to draw conclusions about the relative size of grains between the upper NiFe layer and the FeCo layers based on the data he has presented.

188. To the extent Dr. Clark also suggests that his high-resolution images show clear evidence of epitaxial growth between the upper NiFe layer and the upper FeCo layer, I disagree. For example, as can be seen in his Figures 39 and 40 from Dr. Clark's report, the FeCo grains appear to grow through the area of the alleged NiFe layer without significant change. Therefore, there is no clearly discernable relationship between the upper NiFe layer and any growth patterns of the FeCo grains from these images. In my opinion, these images do not provide a reliable basis for drawing any conclusions about whether the NiFe layer is directing the growth of the upper FeCo layer. An equally probable inference is that it has no effect on the growth of the upper FeCo layer.

189. Summary. In view of all of the flaws in Dr. Clark's analysis that I have described above, it is my opinion that the conclusions drawn by Dr. Clark regarding the crystalline

properties of the upper NiFe layer lack a reliable factual and scientific basis and are based on the application of flawed and unreliable methodologies. In my opinion, the testing data provided by Dr. Clark provides no evidence of the presence of an fcc(111) texture in the upper NiFe layer in sample S0GPPC.

c. Other Data Not Considered by Dr. Clark

190. In addition to the flaws in Dr. Clark's analysis and conclusions described above relating to the lower and upper NiFe layers in sample S0GPPC, I note that Dr. Clark did not consider other information and data that was or could have been available to him relating to the crystal structure of the NiFe layers in sample S0GPPC. I address these additional areas below.

191. No Consideration of Ring Patterns. Dr. Clark used TEM testing to produce a general diffraction pattern for the materials contained in sample S0GPPC. (Clark at ¶ 57 and Figure 19.) I note that Dr. Clark does not refer to this diffraction pattern, and he apparently did not consider it, in connection with his analysis of whether the NiFe layers in sample S0GPPC contain material with an fcc(111) texture. I have reviewed the ring pattern from Dr. Clark's report, and I agree that it provides no evidence that would support the conclusion that the NiFe layers in sample S0GPPC for the [REDACTED] write-head design are predominately (111) hexagonal. I also note that this is consistent with the ring diffraction pattern I obtained from my own sample of an [REDACTED] write-head design.

192. No Consideration of Microbeam Diffraction. For sample S0GPPC, Dr. Clark provides a number of plan-view TEM microbeam images. Dr. Clark contends that selected microbeam images show the existence of bcc(110) crystals for the FeCo layers. (*See, e.g.*, Clark at ¶ 108.) As I explain below (*see infra* ¶¶ 349-369), these images and Dr. Clark's methodology do not support his conclusions regarding the crystal structure of the bcc FeCo layers. I also note that they do not provide any evidence of the underlying NiFe layers having a (111) texture. One could seek to show the presence of a strongly-textured underlying layer by identifying such crystals in the microbeam images. The fact that Dr. Clark does not attempt to do so, and the fact that such images do not show the presence of any such crystals, is further support for the conclusion that the NiFe layers in sample S0GPPC do not have a (111) texture.

193. No XRD Testing. In his report, Dr. Clark does not refer to any XRD testing he conducted, and he apparently did not consider any XRD data from any source in connection with his analysis of whether the NiFe layers in sample S0GPPC contain material with a (111) texture.

Accordingly, I note that there is no XRD data that would support a conclusion that the NiFe layers in sample S0GPPC for the [REDACTED] write-head design are predominately (111) hexagonal.

d. Conclusion Regarding NiFe Layers

194. In view of the flaws in Dr. Clark's analysis that I have described above, and in view of all of the evidence, it is my opinion that the conclusions drawn by Dr. Clark regarding the crystalline properties of the NiFe layers in sample S0GPPC lack a reliable factual and scientific basis and are based on the application of flawed and unreliable methodologies. It is my opinion that none of the evidence I have seen supports the conclusion that either of the NiFe layers in sample S0GPPC has an fcc(111) texture.

2. Sample S2MMC ([REDACTED] Design)

195. Dr. Clark's report describes a number of high-resolution cross-section TEM images that he took of portions of sample S2MMC. In particular, Dr. Clark identifies a region where these images were taken shown by a red circle in Figure 67 of his report, with the image on the right of Figure 67 showing a zoomed-in image with the area of the red circle marked as "A." I have reproduced Figure 67 below:

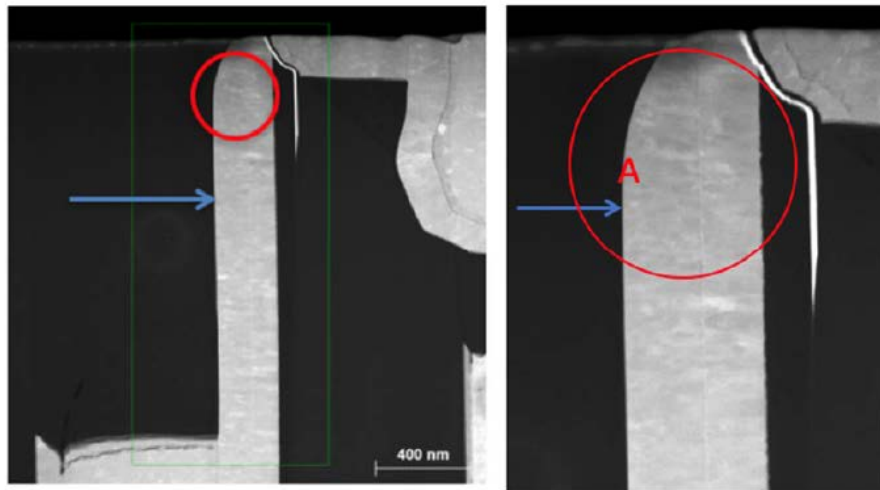


Figure 67: STEM overviews of S2MMC, with regions where high resolution cross-sections were taken shown in the red circle. The blue arrow indicates the growth direction, the letter indicates the NiFe/FeCo interface. Note the pronounced columnar growth seen in the FeCo region.

196. Dr. Clark describes the area labeled "A" as a region where the high-resolution cross-section TEM images were taken of the lower and upper NiFe layer in sample S2MMC. (Clark at ¶¶ 133, 143.) As discussed below, Dr. Clark's application of his methodology and test

results for these images is unreliable and does not provide a valid scientific basis for concluding that either NiFe layer in sample S2MMMC provides a “(111) textured hexagonal atomic template.” I address the testing performed by Dr. Clark and the conclusions he reaches for each of these regions below.

a. Lower NiFe Layer

197. Flawed Conclusions Regarding the Presence of fcc(111) Crystals. Dr. Clark relies on an FFT taken from a high-resolution cross-section of a portion of region A as the primary basis for his contention that the lower NiFe layer has an fcc crystal structure. (Clark at ¶¶ 133-135.) In my opinion, the methodology applied by Dr. Clark is flawed and unreliable, and his conclusions are not supported by the scientific data.

198. In particular, Dr. Clark shows FFTs in Figure 72 of his report derived from point 1 of the TEM image shown in Figure 71 of his report. Dr. Clark states that the FFT shown on the left in Figure 72 relates to the lower NiFe layer, and the image on the right relates to the adjacent FeCo. (*Id.* at ¶ 135 and Fig. 72.) Although Dr. Clark states that he performed comparisons of these FFTs with the standard diffraction patterns shown in Figure 72 (*id.* at ¶ 134), Dr. Clark does not provide any standard diffraction pattern for the FFT that relates to the lower NiFe layer. He does provide a “standard diffraction pattern” for single bcc(110) crystals that is allegedly rotated into a similar orientation for the FFT of the FeCo layer on the right. I have reproduced Figure 72 of Dr. Clark’s report below, which on the left shows the FFT for the lower NiFe layer with no standard diffraction pattern, and the FFT of the adjacent FeCo layer on the right with a standard diffraction pattern:

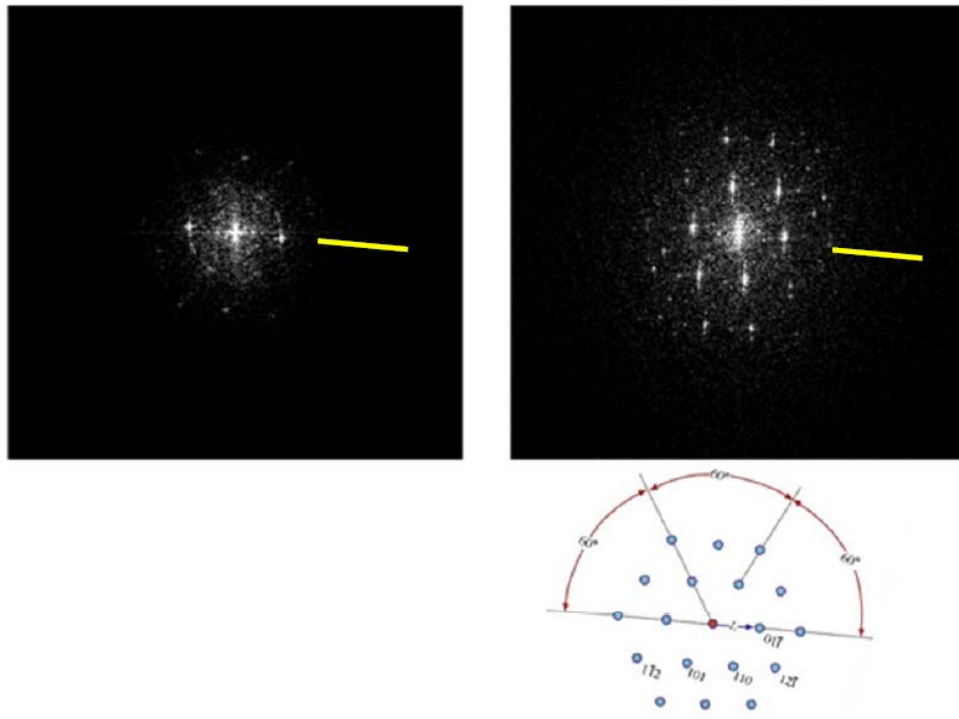


Figure 72: above: FFTs from the NiFe layer (left) and FeCo layer (right) – note that the NiFe pattern is indistinct; below: standard diffraction patterns rotated into similar orientations as respective FFTs shown immediately above.

199. Dr. Clark states that “[a]nalysis of the FFTs was performed by measuring the diffraction spot spacings and the angles between rows of diffraction spots and comparing that information with standard diffraction patterns.” (*Id.* at ¶ 134.) Dr. Clark states that “[a]lthough the left hand FFT from the NiFe template is not distinct enough to analyze with certainty, the arrangement of the faint diffraction spots that are visible most closely resemble the $\{110\}_{\text{FCC}}$ pattern.” (*Id.* at ¶ 136.) He goes on to state that “[g]iven the evidence for the $\{110\}$ orientation in the NiFe layer in the mid-region of the sample discussed further below, I conclude that this pattern is $\{110\}_{\text{FCC}}$.” (*Id.*) Unlike with his opinions for sample S0GPPC, Dr. Clark does not state that the crystal structure of the lower NiFe layer “is FCC.”

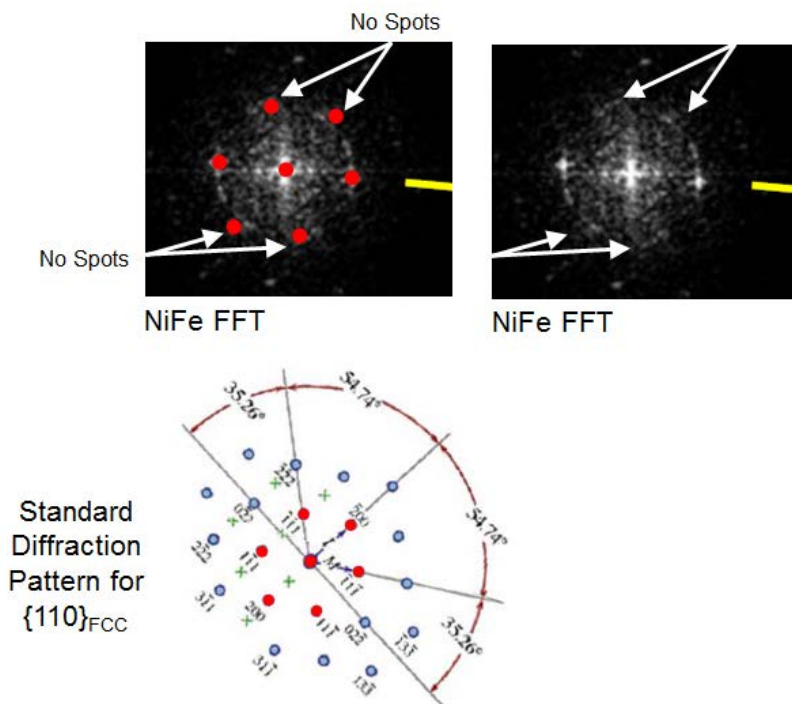
200. The FFT image shown in Figure 72 that Dr. Clark relies on as evidence of the presence of an fcc crystal does not support the conclusion that the portion of the lower NiFe layer he analyzed has an fcc—much less an fcc(111)—crystal structure. Dr. Clark himself acknowledges that the FFT is indistinct and does not provide a reliable basis “to analyze with certainty.” (*Id.*) I agree. Nonetheless, Dr. Clark opines that based on the arrangement of “faint

diffraction spots” he is able to conclude that they “most closely resemble the $\{110\}_{\text{FCC}}$ pattern.” (*Id.* at ¶ 136.) I disagree with his conclusion, which is based on speculation.

201. For example, Dr. Clark does not describe the particular methodology he applied or which “faint diffraction spots” in the FFT he has discerned that allegedly provide the basis for his comparison. Nor has he provided the diffraction pattern he is using for his comparison. Assuming it is the same as the one he used for sample S0GPPC, he does not provide the orientation he is using for this standard pattern. He also does not identify the location of the center spot he uses for his orientation or the particular spots and angles that he allegedly used to line up with the 111 spacings and directions of the standard diffraction pattern. Nor does he try to overlay the FFT image with the center spot in the standard diffraction pattern to show how all of the spots and angles are consistent with the standard pattern. There simply is no reliable factual and scientific basis for Dr. Clark to draw his conclusions. In my opinion, no reasonable scientist working in the field would agree with Dr. Clark’s conclusion based on this data.

202. In order to show alignment with the standard pattern, the FFT image would need to have clearly discernable spots located at same locations, spacings, and angles as shown in a diffraction pattern using the methodology I described earlier. Applying that methodology here with the standard diffraction pattern that Dr. Clark used for sample S0GPPC and assuming the orientation is consistent with that shown in the yellow line in Figure 72, what is shown in the FFT pattern in Figure 72 are spacings and angles that are inconsistent with the standard cross-section diffraction pattern for fcc(111).

203. To demonstrate this more clearly, I took the FFT image for the lower NiFe layer from Figure 72 and attempted to align the spots in this FFT with the $\{110\}_{\text{FCC}}$ diffraction pattern provided by Dr. Clark for sample S0GPPC, using the 9 innermost spots of the standard template, which I have colored red. This is shown below:



204. I included the same NiFe FFT twice, in order to show there are no spots under four of the red template dots. Thus, there are no distinct spots for the NiFe FFT image that align with the standard diffraction pattern. In my opinion, this FFT does not come close to demonstrating that the lower NiFe layer has an fcc or fcc(111) crystal.

205. Dr. Clark's suggestion that he can make judgments about the structure and orientation of the lower NiFe layer in sample S2MMMC based on his analysis of the upper NiFe layer has no valid scientific basis. As I explain below, the alleged "evidence" for the upper NiFe layer Dr. Clark analyzes from sample S2MMMC does not in any way support a conclusion that it has a {110}FCC pattern. In addition, Dr. Clark does not provide a valid and verifiable explanation for why the structure of one layer would necessarily be the same for a different layer with a different substrate. In fact, he does not provide any explanation. Accordingly, there is no factual predicate, much less a scientifically valid one, to draw a conclusion about the lower NiFe layer based on his analysis of the upper NiFe layer for sample S2MMMC.

206. In my opinion, because the FFT image relied on by Dr. Clark does not show an fcc structure, all of the conclusions drawn by Dr. Clark regarding the crystalline properties of the lower FeCo layer lack any factual and scientific basis.

207. This problem is compounded to the extent Dr. Clark contends that other unidentified FFT images taken at points other than point 1 allegedly “showed similar results.” (*Id.* at ¶ 140.) If these showed “similar results,” then they are flawed for the same reason as the FFT for the single crystal that he does show in Figure 72.

208. Furthermore, to the extent Dr. Clark purports to rely on other FFTs, he does not specifically identify them and he does not provide the factual basis for his analysis. In fact, he does not provide any analysis. He does not show through overlays, spacing data, or any other methodology how he compared them, the basis for his comparison, or how any of them allegedly match the standard diffraction pattern.

209. To the extent one can speculate as to what these other FFTs might be based on his naming convention, there appear to be a total of 12 FFTs for individual crystals that purportedly related to the lower NiFe layer. These are identified in a chart I have included in Exhibit F of my report as those under the filename “18.08.14 CCD Acquire.”

210. I have reviewed each of these 12 FFT images (which include the FFT image above), and none of them is consistent with an fcc standard diffraction pattern along a 110 or 112 zone axis. In particular, none of the images provides a clearly discernable pattern that aligns with the standard spacings and angles for the fcc 110 or 112 zone axis patterns. My comparisons are contained in Exhibit F of my report.

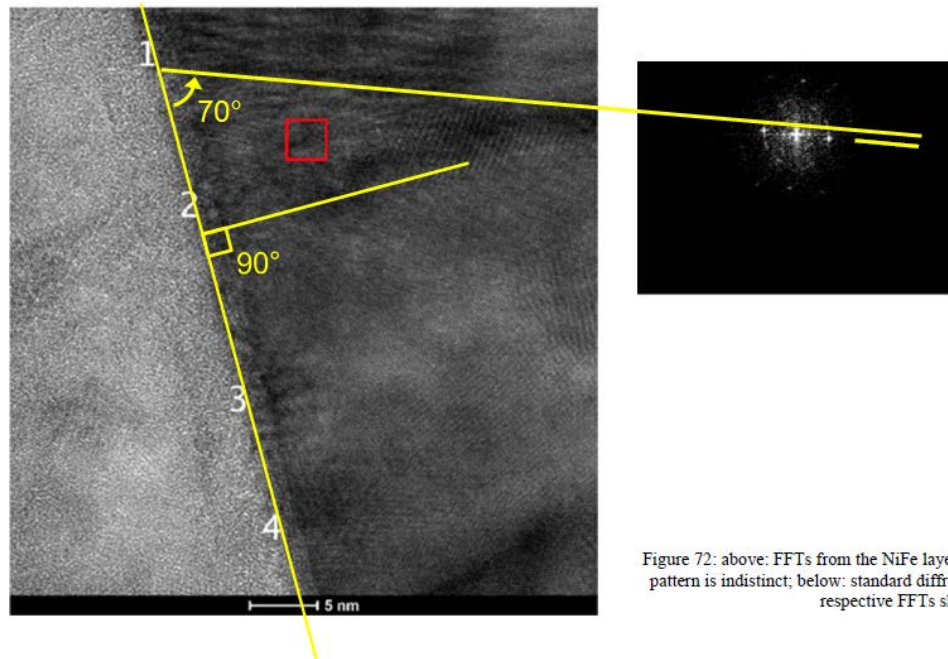
211. Once again, I note that it is not surprising that the FFT data from Dr. Clark’s report for the lower NiFe layer does not match an fcc(111) crystal pattern in view of the thinness of the layer. Materials deposited at a thickness of [REDACTED] [REDACTED]—are almost certainly too thin to have developed any significant crystallographic texture, and may even be too thin to have a distinct crystalline structure.

212. Flawed Conclusions Regarding (111) Orientation. Even if the specific crystals Dr. Clark purportedly analyzed using FFTs actually showed the presence of some individual fcc crystals, they would not provide a reliable scientific basis for drawing any conclusions regarding the orientation of the crystal. As I explain above (*see supra* ¶ 37-39), knowing that a crystal has an fcc structure does not tell you anything about its orientation relative to the substrate (such as a 111 direction).

213. In his report, Dr. Clark purports to draw conclusions about the orientation of all of the alleged fcc crystals in the lower NiFe layer by relying on the single FFT image in Figure 72 of his report for the lower NiFe layer. (For the other FFTs for the lower NiFe, Dr. Clark does not provide any information about their orientations relative to the substrate.) In my opinion, the methodology applied by Dr. Clark is flawed and unreliable, and his conclusions are not supported by the data.

214. As the basis for his conclusions, Dr. Clark states that the two FFT patterns in Figure 72 “show there are two parallel directions, one in the lower NiFe layer and one in the lower FeCo layer, pointing out of the page.” (*Id.* at ¶ 137.) He then contends that, “when analyzing the pattern from the spot spacing and distribution, it can be seen that a $\langle 111 \rangle_{\text{FCC}}$ direction in the NiFe is also parallel to a $\langle 110 \rangle_{\text{BCC}}$ in the FeCo, and lie in the plane of the page.” (*Id.*) He states that these are indicated in Figure 72 by the yellow lines marked on the FFTs that he has added. (*Id.*) Dr. Clark then asserts that “[t]he directions are also perpendicular to the lower NiFe/lower FeCo interface, and so confirm the epitaxial growth in that direction and is evidence of epitaxial growth of the lower FeCo layer on the lower NiFe layer, which functions as an atomic template.” (*Id.*) Dr. Clark then concludes: “These two mutual relationships are also sufficient to determine the relative orientation of the lower NiFe Layer and the lower Fe Co layer above it. Therefore, the lower NiFe layer exhibits (111) texture, and the lower FeCo layer exhibits (110) texture.” (*Id.*)

215. Dr. Clark’s assertion that the NiFe and FeCo crystals are parallel to one another and perpendicular to the substrate is not supported by his own data and is based on an unreliable methodology. In particular, neither of the yellow lines that Dr. Clark has drawn in Figure 72 for the two layers is perpendicular to the interface shown in Figure 71. This can be seen by comparing the angle between the substrate (the line along points 1, 2, 3 and 4) in Figure 71, which are shown below on the left, with the yellow lines from the FFTs in Figure 72, which are shown below on the right. This comparison shows that the yellow lines relied on by Dr. Clark to show that the NiFe crystals are perpendicular to the substrate shown in Figure 71 are in fact *not* perpendicular, but instead are off in the range of 20 degrees from perpendicular.



216. The fact that the FFT for the lower NiFe layer that Dr. Clark relies on is not perpendicular to the substrate means that it cannot have a (111) orientation, even if it had been shown to be an fcc crystal (which Dr. Clark has not done).

217. Accordingly, Dr. Clark's methodology for trying to show the orientation of the NiFe and FeCo crystals is flawed and unreliable and does not provide a factual basis and reliable scientific basis for his conclusion about the orientation of the single crystals he allegedly analyzed based on the FFTs discussed above.

218. Flawed Conclusions Regarding fcc(111) Texture. Even if Dr. Clark had been able to reliably discern the presence of some fcc(111) crystals in the lower NiFe layer of sample S2MMMC (which he has not), there is no reliable or scientifically valid basis for his sweeping conclusion regarding the texture of the entire lower NiFe layer. In my opinion, the methodology applied by Dr. Clark to reach his conclusions is flawed and unreliable, and his conclusions are not supported by the data.

219. For his broad pronouncements regarding the texture of the lower NiFe layer, Dr. Clark relies on the same flawed data mentioned above. For example, Dr. Clark's conclusion in paragraph 137 of his report regarding the texture of the lower NiFe layer apparently stems from his conclusion regarding the presence and alleged orientation of the single crystals he purported to identify. Yet, as shown above, there is no scientifically valid basis for this conclusion.

220. Dr. Clark asserts in another portion of his report that “[t]he parallel directions in the FCC and BCC layers normal to the interface show repeatedly $\langle 110 \rangle$ direction in the BCC layers and $\langle 111 \rangle$ direction in the FCC layers,” which he contends “shows that the lower NiFe layer has a predominant (111) texture, and the lower FeCo layer has a predominant (110) texture.” (*Id.* at ¶ 138.) But, once again, Dr. Clark does not provide any factual basis for his claim that there are “repeated[.]” examples in the alleged fcc-bcc interface of the “ $\langle 111 \rangle$ direction.” To the extent his assertion that “the interface show repeatedly $\langle 110 \rangle$ direction in the BCC layers and $\langle 111 \rangle$ direction in the FCC layers” is based on the FFT images, these are flawed, as discussed above. He does not provide any other basis for his conclusion, and I have not seen any other basis, for such a conclusion from the other materials provided in his report.

221. In fact, as I have explained, not only does the single FFT discussed by Dr. Clark in the body of his report not have a (111) orientation relative to the substrate, but the other FFTs do not provide any information about the alleged 111 directions associated with each. Without such information, at most they represent many different orientations, which would be inconsistent with any predominate crystalline direction for any fcc crystals in the lower NiFe layer.

222. Furthermore, even if all of the FFTs from the lower NiFe layer that form the basis for Dr. Clark’s analysis showed an fcc(111) crystal structure (which they do not), they would amount to a sample of approximately 0.165%, at best, of the lower NiFe layer, based on my calculation of the overall NiFe length dimension for the [REDACTED] design of approximately 8 micrometers (with 1 micrometer = 1,000 nanometers) and the aggregate length dimension for the FFTs being approximately 13.2 nanometers, or 0.165%.

223. My calculation for the overall length is based on the image of the write head in the device from which sample S0GPPC for the [REDACTED] design was taken. (*See supra* ¶ 135.) My calculation for the aggregate length dimension for the FFTs for the lower NiFe layer is based on the dimensions provided by Dr. Clark in Figure 71 of his report. Dr. Clark states that the FFTs for the lower NiFe layer were taken at points along the lower NiFe/lower FeCo interface marked with the numbers 1, 2, 3 and 4 as shown in Figure 71, with the area sampled for each FFT “confined to an area of the size indicated by the red square.” (Clark at ¶ 134 and Fig. 71.) I have reproduced this image from Dr. Clark’s report below:

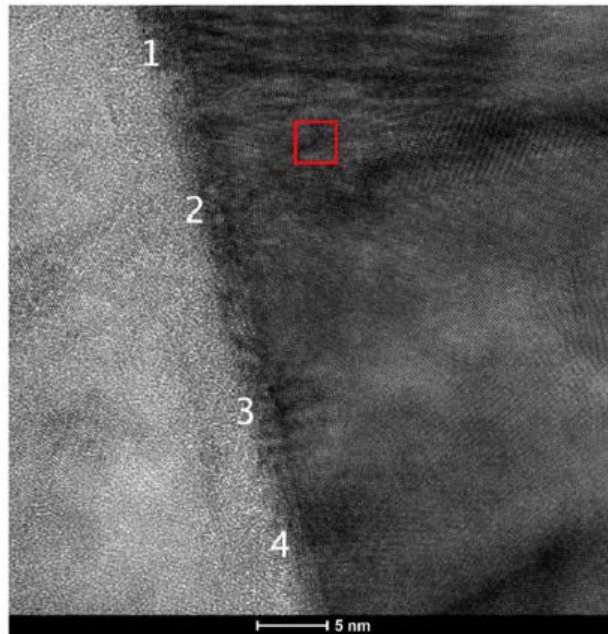


Figure 71: Example high resolution cross-section from circled region. The numbered points indicate where FFTs were taken.

224. Based on the dimensions of the red box shown in Figure 71 of Dr. Clark's report, the length dimension for each FFT at a particular location would be approximately 3.3 nanometers in length. As shown in Exhibit F of my report, a total of 12 FFTs were taken in total for this area based on Dr. Clark's naming convention, with three at each location, and a total of 4 focused on the NiFe layer. Therefore, 4 FFTs x 3.3 nm each = 13.2 nm. Taking the aggregate length dimensions of the areas from which the FFTs were taken of 13.2 nm, and dividing it by the overall length dimension of 8,000 nm results in 0.00165, which is 0.165 percent. In other words, the sample size represented by Dr. Clark's FFTs for the lower NiFe layer represents less than 0.165 percent of the overall length of lower NiFe layer in the write head from which sample S2MMMC was taken.

225. Dr. Clark does not cite to any source that has used this methodology of a 0.165 percent sample to draw conclusions about the alleged texture of an entire layer, and I am not aware of any source that would provide a scientific grounding for his approach. Accordingly, in my opinion, there is no scientific basis from which to draw a conclusion about the overall texture of the NiFe layer based on these images, even assuming Dr. Clark had been able to show the presence of some fcc(111) crystals at the locations of his images, and especially given all of the other flaws with his analysis as explained above.

226. Other Flaws. I also disagree with a number of Dr. Clark's other statements regarding the structure of the lower NiFe layer and the adjacent FeCo layer made in his report regarding sample S2MMMC. I address several of these below.

227. First, I note that Dr. Clark himself apparently has doubts about his conclusions for the lower NiFe layer. He states, for example that "[t]o the extent that the FFT results for the lower NiFe layer are inconclusive, I conclude that the lower NiFe layer is FCC and exhibits a predominant (111) texture based further on the discussion of the upper NiFe / FeCo layers herein." (Clark at ¶ 141.) For reasons I explain, however, Dr. Clark's data for the upper NiFe layer does not support any conclusion that the upper NiFe layer in sample S2MMMC is fcc(111) textured. Furthermore, there is no reliable scientific basis for Dr. Clark to make judgments about the lower NiFe based on data from the upper NiFe layer, especially where, as discussed below, there is no evidence to support a conclusion of (111) texture for the upper NiFe layer.

228. I also disagree with several observations or conclusions made by Dr. Clark based on the high-resolution images he took for portions of region A (shown originally in Figure 67 and which allegedly is the region of the lower NiFe layer) that are shown in Figures 68 and 69 of his report. By way of example, I have reproduced the images from Figure 69 below:

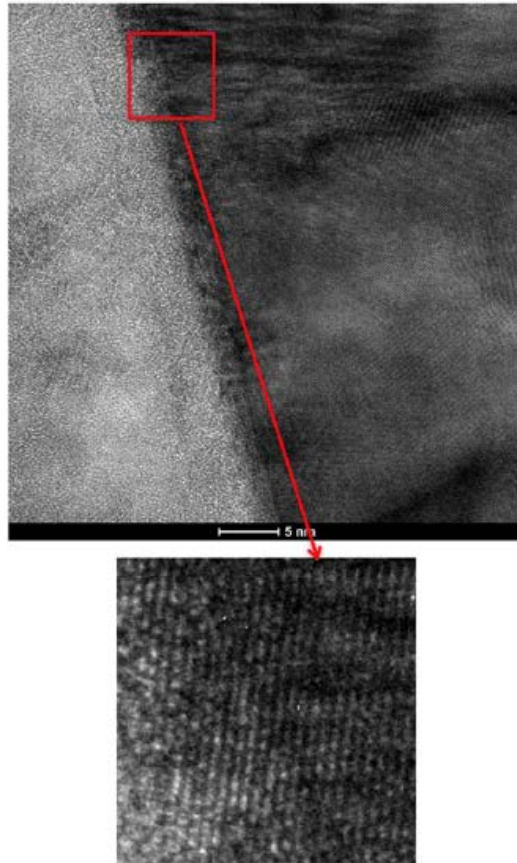


Figure 69: Example showing zoomed-in crossed lattice fringes from a high resolution cross-section from the NiFe/FeCo interface region.

229. To the extent Dr. Clark suggests that his high-resolution images show clear evidence of epitaxial growth between the lower NiFe layer and the adjacent FeCo layer, I disagree. For example, as can be seen in his Figure 69 from Dr. Clark's report, the lower NiFe layer is not even clearly discernable. There also is no discernable relationship between the lower NiFe layer and any growth patterns of the FeCo grains, which grow in a variety of different directions. In my opinion, these images provided by Dr. Clark in his report for this region do not provide a clear factual basis for any conclusion about epitaxial growth.

230. Finally, I strongly disagree with Dr. Clark's statements that "[s]ince the FFT analysis above shows that the lower NiFe / lower FeCo relationship is $\{111\}_{\text{FCC}} \parallel \{110\}_{\text{BCC}}$, as well as $\langle 110 \rangle_{\text{FCC}} \parallel \langle 111 \rangle_{\text{BCC}}$, this shows that the Kurdjumov-Sachs orientation relationship is present." (*Id.* at ¶ 139.) As discussed above, Dr. Clark's analysis does not establish any such orientations for these layers, much less a Kurdjumov-Sachs orientation relationship. There is absolutely no factual and scientific basis for such an assertion. Furthermore, as discussed more

fully below (*see infra* ¶¶ 404-427), Dr. Clark’s own microbeam diffraction images on plan-view samples further confirms the absence of such a relationship.

231. Summary. In view of all of the flaws in Dr. Clark’s analysis that I have described above, it is my opinion that the conclusions drawn by Dr. Clark regarding the crystalline properties of the lower NiFe layer lack a reliable factual and scientific basis and are based on the application of flawed and unreliable methodologies. In my opinion, the testing data provided by Dr. Clark provides no evidence of the presence of an fcc(111) texture in the lower NiFe layer in sample S2MMC.

b. Upper NiFe Layer

232. Flawed Conclusions Regarding the Presence of fcc(111) Crystals. Dr. Clark relies on an FFT taken from a high-resolution cross-section of sample S2MMC as the primary basis for his contention that the upper NiFe layer has an fcc crystal structure. (Clark at ¶¶ 143-144.) In my opinion, the methodology applied by Dr. Clark is flawed and unreliable, and his conclusions are not supported by the scientific data.

233. In particular, Dr. Clark shows FFTs in Figure 74 of his report apparently derived from point 1 of the TEM image shown in Figure 73 of this report. Dr. Clark states that the FFT shown on the left in Figure 74 relates to the lower FeCo layer, the FFT in the middle relates to the upper NiFe layer, and the FFT on the right relates to the upper FeCo. (*Id.* at ¶ 143 and Fig. 74.). Dr. Clark also provides under each FFT the “standard diffraction patterns” for single fcc(111) and bcc(110) crystals, as appropriate. (*Id.*) I have reproduced Figure 74 of Dr. Clark’s report below:

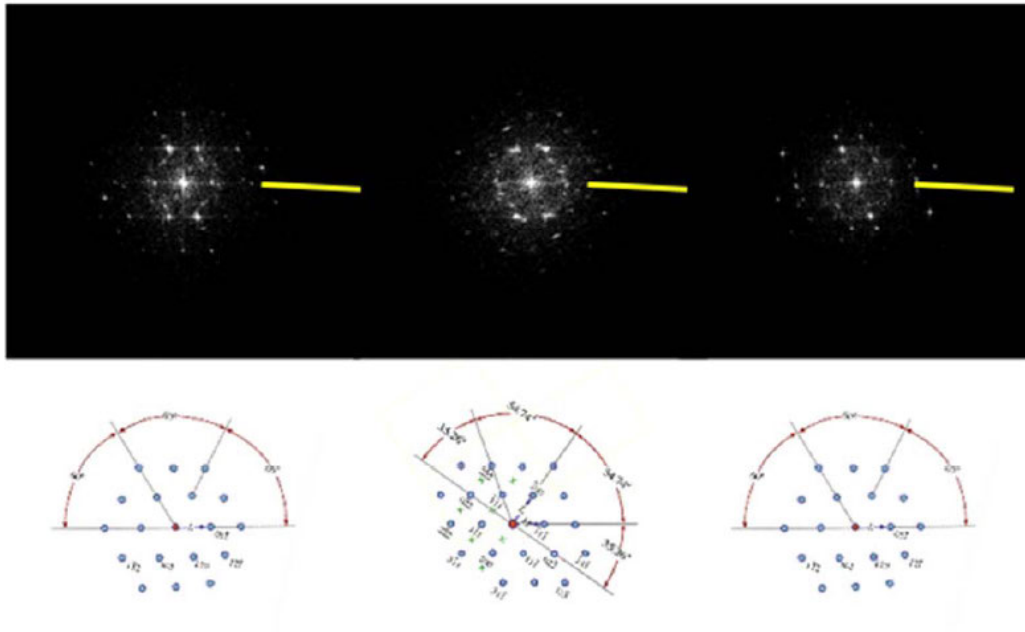


Figure 74: above: FFTs from point 1 from the FeCo layers (left and right) on either side of the upper NiFe layer (center). The FeCo patterns are $\{111\}_{BCC}$, as determined from the ratio of the lengths of the sides of the pattern motif, and the angles between directions, while the NiFe pattern is $\{111\}_{FCC}$.

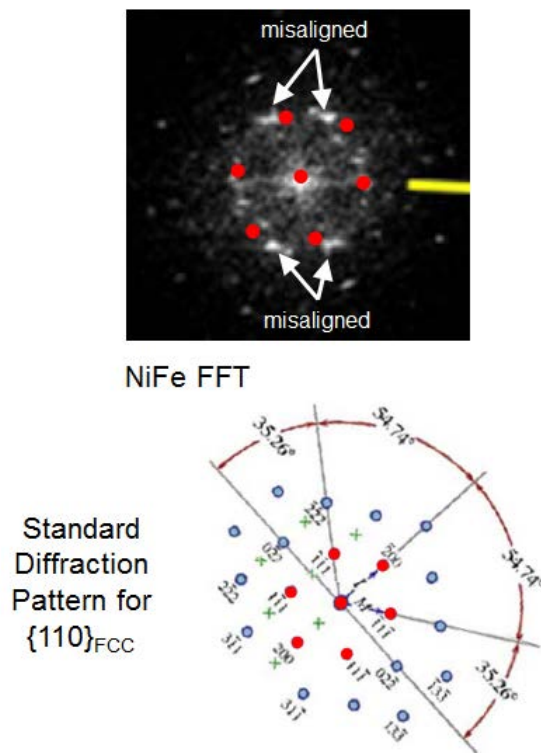
234. Dr. Clark states that “following the procedures outlined above, the two patterns in the upper and lower FeCo layers are identified at $\{111\}_{BCC}$, while the upper NiFe pattern is identified as $\{110\}_{FCC}$.” (*Id.* at ¶ 98.) He states that “[t]hese FFTs, like those analyzed above, indicate that “the crystal structure of the NiFe layer is FCC and the upper and lower FeCo layers is BCC.” (*Id.* at ¶ *Id.*)

235. The FFT image shown in Figure 74 that Dr. Clark relies on as evidence of the presence of an fcc crystal does not support the conclusion that the portion of the upper NiFe layer he analyzed has an fcc—much less an fcc(111)—crystal structure. Dr. Clark does not describe the particular methodology he applied or which diffraction spots in the FFT he has discerned that allegedly provide the basis for his comparison. He also does not identify the location of the center spot he uses for his orientation or the particular rows of spots that he allegedly used to line up with the 111 spacings and directions of the standard diffraction pattern. Nor does he try to overlay the FFT image with the center spot in the standard diffraction pattern to show how all of the spots and angles are consistent with the standard pattern. There simply is no reliable factual and scientific basis for Dr. Clark to draw his conclusions. In my opinion, no

reasonable scientist working in the field would agree with Dr. Clark's conclusion based on this data.

236. In order to show alignment with the standard pattern, the FFT image would need to have clearly discernable spots located at same locations, spacings, and angles as shown in the diffraction pattern using the methodology I described earlier. Applying that methodology here, what is shown in the FFT pattern in Figure 74 are spacings and angles that are inconsistent with the standard cross-section diffraction pattern for fcc(111).

237. To demonstrate this more clearly, I took the middle FFT image (which is for the upper NiFe layer) from Figure 74 and attempted to align the spots in this FFT with the $\{110\}_{\text{FCC}}$ diffraction pattern provided by Dr. Clark, using the 9 innermost spots of the template, which I have colored red. I attempted to align the purported lower NiFe FFT with the $\{110\}_{\text{FCC}}$ diffraction pattern, again using the 9 innermost spots of the template, which I have colored red. This is shown below:



238. As can be seen, the spots for NiFe FFT image do not align with the standard diffraction pattern.

239. As I noted above, it is important to emphasize that the mismatch shown above is not just some “near miss.” The alignment must be exact before there is any reasonable scientific basis to make a judgment about the crystal structure of the material, in this case NiFe. Moreover,

[REDACTED]

240. In my opinion, because the FFT image does not show an fcc structure, all of the conclusions drawn by Dr. Clark regarding the crystalline properties of the upper FeCo layer lack any factual and scientific basis. Furthermore, I note that for his analysis of the upper NiFe layer here for sample S2MMMC, Dr. Clark does not contend that any other FFT images support his conclusion other than the single FFT he is relying on in Figure 74.

241. As I note above, none of this is surprising in view of the thinness of the layer.

[REDACTED]
[REDACTED]—are almost certainly too thin to have developed any significant crystallographic texture, and may even be too thin to have a distinct crystalline structure.

242. Flawed Conclusions Regarding (111) Orientation. Even if the specific crystal Dr. Clark purportedly analyzed using the FFT in Figure 74 actually showed the presence of an individual fcc crystal, it would not provide a reliable scientific basis for drawing any conclusions regarding the orientation of the crystal. As I explain above (*see supra* ¶¶ 37-39), knowing that a crystal has an fcc structure does not tell you anything about its orientation relative to the substrate (such as a 111 direction).

243. In his report, Dr. Clark apparently seeks to draw conclusions about the orientation of all of the alleged fcc crystals in the upper NiFe layer by relying on the single FFT image in Figure 74 of his report. In my opinion, the methodology applied by Dr. Clark is flawed and unreliable, and his conclusions are not supported by the data.

244. As the grounds for his conclusions, Dr. Clark states that the FFT patterns in Figure 74 “show there are two parallel directions, one in the upper NiFe layer and one each of the adjacent FeCo layers, pointing out of the page.” (*Id.* at ¶ 147.) He then contends that, “when

analyzing the pattern from the spot spacing and distribution, it can be seen that a $\langle 111 \rangle_{\text{FCC}}$ direction in the NiFe is also parallel to a $\langle 110 \rangle_{\text{BCC}}$ in the FeCo, and lie in the plane of the page.” (*Id.*) He states that these are indicated in Figure 74 by the yellow lines marked on the FFT that he has added. (*Id.*) Dr. Clark then asserts that “[t]he directions are also perpendicular to the upper NiFe/FeCo interfaces, and so confirm the epitaxial growth in that direction and is evidence of the epitaxial growth of the lower FeCo layer on the lower NiFe layer, which functions as an atomic template.” (*Id.*) Dr. Clark then concludes: “These two mutual relationships are also sufficient to determine the relative orientation of the *lower* NiFe Layer and the *lower* Fe Co layer above it. Therefore, the *lower* NiFe layer exhibits (111) texture, and the *lower* FeCo layer exhibits (110) texture.” (*Id.*) (Once again, I am not sure whether Dr. Clark’s conclusions are meant to be directed to the *upper* NiFe layer, or whether he means to draw conclusions about the *lower* NiFe layer, as he suggests he is going to do based on his statements in paragraph 141 of his report. For purposes of my report, I am taking Dr. Clark’s assertions at face value and will take him to be referring to the crystal properties of the lower NiFe layer in sample S2MMC for purposes of his last statement in paragraph 147 of his report.)

245. Dr. Clark’s assertion that the upper NiFe and adjacent FeCo crystals are parallel to one another and perpendicular to the interface of the NiFe and FeCo layers is not supported by his own data and is based on an unreliable methodology. Furthermore, even if true, it provides no evidence regarding the orientations of the FFTs relative to the substrate, which is necessary to show the orientation of the crystals and whether the FFT for the NiFe layer shows a 111 direction.

246. First, if one were to accept Dr. Clark’s contention that there is an interface shown in the middle of Figure 73, none of the lines that Dr. Clark has drawn in Figure 74 would be perpendicular to that interface. For example, if you assume the interface to be represented by the lightest area shown in the red box drawn in Figure 73, that interface is not perpendicular to the lines drawn in Figure 74. This can be seen by comparing the angle between the alleged interface in Figure 73, shown below on the left, with the lines from the FFTs in Figure 74, shown below on the right. This comparison shows that the lines in Figure 74 relied on by Dr. Clark to show that the FFTs are perpendicular to the interface shown in Figure 73 are in fact *not* perpendicular, but instead are off in the range of 17 degrees from perpendicular.

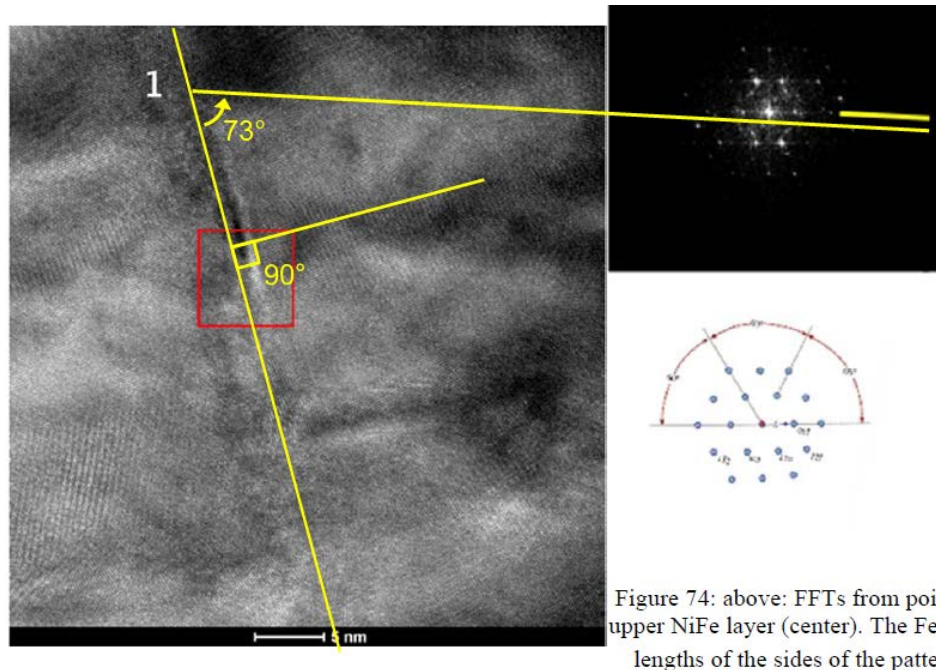


Figure 74: above: FFTs from point upper NiFe layer (center). The FeC lengths of the sides of the pattern

247. Second, even if Dr. Clark had established a perpendicular orientation between the FFTs and the upper NiFe/FeCo interfaces, this would tell you nothing about the orientation of the upper NiFe layer relative to the substrate. Dr. Clark provides no location for the substrate relative to the FFT for the NiFe layer. Without this information, there is no way to assess what the actual orientation of the NiFe crystal is that is purported to have a (111) orientation.

248. Finally, Dr. Clark's main point appears to be that a perpendicular orientation between the upper NiFe crystal and the upper NiFe/FeCo interfaces would tell you something about the orientation of the *lower* NiFe layer, but this clearly is not the case. As noted above, Dr. Clark states that the two mutual orientations of upper NiFe crystal and the upper NiFe/FeCo interfaces "are also sufficient to determine the relative orientation of the *lower* NiFe layer and the lower FeCo layer above it." (*Id.* at ¶ 101 (emphasis added).) But what the orientation is of the upper NiFe layer relative to the interface tells you nothing about the orientation of the lower NiFe layer. There is no valid scientific basis for Dr. Clark to make such an assertion.

249. Because Dr. Clark provides no information about the angle of the NiFe crystal for upper NiFe layer relative to the substrate, there is no evidence that any crystal in the upper NiFe layer has a (111) orientation, even if he had been able to show that such a crystal had an fcc structure (which Dr. Clark also has not done).

250. Accordingly, Dr. Clark's methodology for trying to show the orientation of the upper NiFe and FeCo crystals is flawed and unreliable and does not provide a factual and reliable scientific basis for his conclusion about the orientation of the single crystals he allegedly analyzed based on the FFTs discussed above.

251. Flawed Conclusions Regarding fcc(111) Texture. Even if Dr. Clark had been able to reliably discern the presence of an fcc(111) crystal in the upper NiFe layer of sample S2MMMC, there is no reliable or scientifically valid basis for his sweeping conclusion regarding the texture of either the upper or lower NiFe layers. In my opinion, the methodology applied by Dr. Clark to reach his conclusions is flawed and unreliable, and his conclusions are not supported by the data.

252. For his broad pronouncements regarding the texture of the NiFe layers, Dr. Clark relies on the same flawed data mentioned above. For example, Dr. Clark's conclusion in paragraph 147 of his report regarding the texture of the *lower* NiFe layer apparently stems from his conclusion regarding the presence and alleged orientation of the single crystal he purported to identify in the *upper* NiFe layers. Yet, as explained above, there is no scientifically valid basis for this conclusion.

253. Dr. Clark asserts in another portion of his report that "[t]he parallel directions in the FCC and BCC layers normal to the interface show repeatedly <110> direction in the BCC layers and <111> direction in the FCC layers," which he contends "shows that the *lower* NiFe layer has a predominant (111) texture, and the *lower* FeCo layer has a predominant (110) texture." (*Id.* at ¶ 147 (emphasis added).) Once again, Dr. Clark does not provide any factual basis for his claim that there are "repeated[]" examples in the alleged fcc-bcc interface of the "<111> direction." To the extent his assertion that "the interface show repeatedly <110> direction in the BCC layers and <111> direction in the FCC layers" is based on a single FFT image, it is flawed, as discussed above. He does not provide any other basis for his conclusion, and I have not seen any other basis for such a conclusion from the other materials provided in his report.

254. In fact, as I have explained, not only does the single FFT discussed by Dr. Clark in the body of his report not have a (111) orientation relative to the substrate, there are no other FFTs relied on by Dr. Clark that provide any information about the alleged 111 directions associated with each.

255. Furthermore, even if all of the single FFT from the upper NiFe layer that forms the basis for Dr. Clark's analysis showed an fcc(111) crystal structure (which it does not), it would amount to a sample of less than 0.0875%, at best, of the upper NiFe layer, based on my calculation of the overall NiFe length dimension of approximately 8 micrometers (with 1 micrometer = 1,000 nanometers) and the aggregate length dimension for the single FFT being approximately 7 nanometers.

256. My calculation for the overall length is based on the image of the write head in the device from which sample S0GPPC was taken is explained above. (*See supra* ¶ 135.) Once again, the overall length dimension for the write head is approximately 8,000 nanometers. (*Id.*)

257. My calculation for the aggregate length dimension for the FFTs for the upper NiFe layer is based on the dimensions provided by Dr. Clark in Figure 73 of his report. Dr. Clark states that the FFT for the upper NiFe layer was taken at point 1 in the alleged upper NiFe/FeCo interface marked with the number "1" as shown in Figure 73, with the area sampled for each FFT "confined to an area of the size indicated by the red square." (Clark at ¶ 143 and Fig. 73.) I have reproduced this image from Dr. Clark's report below:

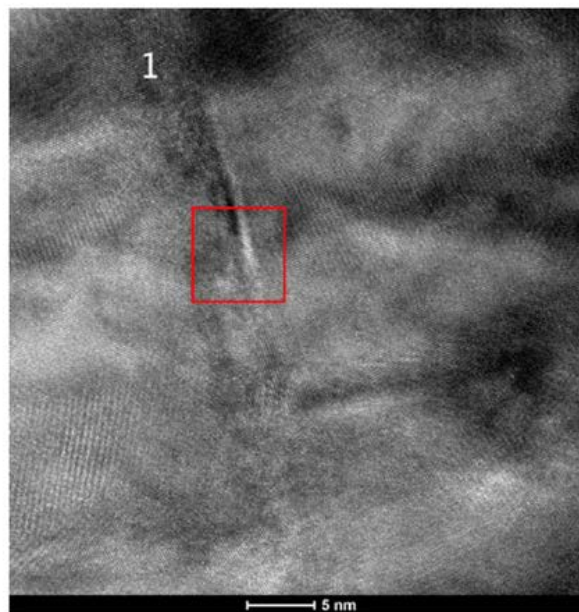


Figure 73: Example high resolution cross-section from the upper NiFe / upper FeCo region. The numbered point indicates where FFTs were taken.

258. Based on the dimensions of the red box shown in Figure 73 of Dr. Clark's report, the length dimension for the single FFT he relies on would be approximately 7 nanometers in length. Taking this length dimension and dividing it by the overall length dimension of 8,000

nm results in 0.000875, which is 0.0875 percent. In other words, the sample size represented by Dr. Clark's FFTs for the upper NiFe layer represents less than 0.0875 percent of the overall length of upper NiFe layer in the write head from which sample S2MMMC was taken.

259. Dr. Clark does not cite to any source that has used this methodology of a 0.0875 percent sample to draw conclusions about the alleged texture of an entire layer, and I am not aware of any source that would provide a scientific grounding for his approach. Accordingly, in my opinion, there is no scientific basis from which to draw a conclusion about the overall texture of the NiFe layer based on these images, even assuming Dr. Clark had been able to show the presence of some fcc(111) crystals at the locations of his images, and especially given all of the other flaws with his analysis as explained above.

260. Other Flaws. I also disagree with a number of Dr. Clark's other statements regarding the structure of the upper NiFe layer and the adjacent FeCo layers made in his report regarding sample S2MMMC. I address several of these below.

261. First, I disagree with several observations or conclusions made by Dr. Clark based on the high-resolution images shown in Figures 70 and 73, which allegedly is the region of the upper NiFe layer. By way of example, I have reproduced the images from Figure 70 and 73 below:

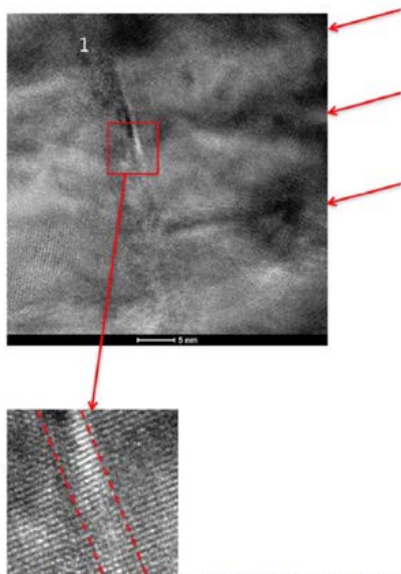


Figure 70: Example high resolution cross-section from NiFe layer in the center of the head (marked by the dashed red lines), with an enlargement showing the continuity of the lattice fringes across the interface.

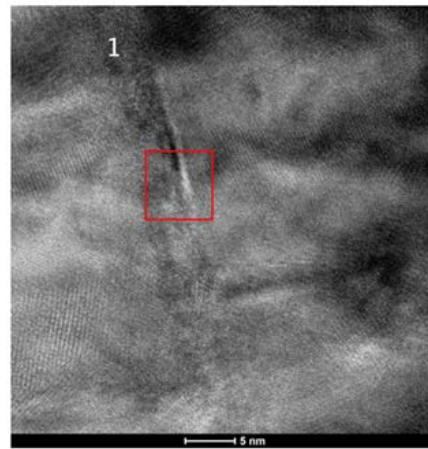


Figure 73: Example high resolution cross-section from the upper NiFe / upper FeCo region. The numbered point indicates where FFTs were taken.

262. Based on this and the other high-resolution images, Dr. Clark states that they show "crossed lattice fringes." (*Id.* at ¶ 131.) He also says the zoomed-in area of Figure 70

shows “[s]everal sets of lattice fringes,” which he indicates with two red-dashed lines, and states that “[t]he fringes that run parallel to the red dashed line are present on both sides of the NiFe, and in the NiFe layer itself, indicating that the orientation of the FeCo is maintained on both sides of the NiFe.” (*Id.* at ¶ 132.) He goes on to say that “[t]he continuity of these fringes across all three layers show that there is an orientation relationship between the FeCo and the NiFe” and further concludes that there is a “hexagonal arrangement of spots in the FeCo lattice image” that “shows a $\{111\}_{\text{BCC}}$ plane, and a $\langle 110 \rangle_{\text{BCC}}$ direction” that “is normal to the interface.” (*Id.*) I disagree with Dr. Clark’s analysis and his conclusions.

263. First, to the extent Dr. Clark suggests that his high-resolution images show clear evidence of epitaxial growth between the upper NiFe layer and the upper FeCo layer, I disagree. For example, the FeCo grains appear to grow through the area of the alleged upper NiFe layer without significant change. Therefore, there is no clearly discernable relationship between the upper NiFe layer and any growth patterns of the FeCo grains from these images. In my opinion, these images do not provide a reliable basis for drawing any conclusions about whether this portion of the NiFe layer is directing the growth of the upper FeCo layer directly above it. An equally probable inference is that it has no effect on the growth of the upper FeCo layer.

264. Second, Dr. Clark’s suggestion that the images can be used to determine that the FeCo is “normal to the interface” is incorrect. It provides no information about its orientational relationship to the substrate and therefore provides no data that can be relied on to determine whether the FeCo layer has a $\text{bcc}(110)$ orientation.

265. Dr. Clark also states that “the FFTs taken from various points along the NiFe layers, while they maintain a common direction with the FeCo layers normal to the interface, change significantly with position along the interface.” (*Id.* at ¶ 150.) He goes on to say that these changes indicate differences in the grain size in the NiFe layer, and concludes that the “grain size in the NiFe template layers is comparable to the width of the FeCo grains” and that “there is ordinarily only one or two FeCo grains per NiFe template grain.” (*Id.*) I disagree with Dr. Clark’s analysis and his conclusions.

266. As an initial matter, Dr. Clark does not at all explain what “changes” with respect to “position along the interface” he is referring to. To the extent he is suggesting that these changes relate to grain size, or that there are clearly discernable grain sizes for the NiFe layer that can be determined from his images, I disagree. While these images provide some

information about the grain sizes for portions of the FeCo layer in the portion of the layer that was imaged, there is no clear evidence of NiFe grains or their sizes in these images. Therefore, in my opinion, there is no reliable factual and scientific basis for Dr. Clark to draw conclusions about the relative size of grains between the upper NiFe layer and the FeCo layers based on the data he has presented.

267. Finally, I strongly disagree with Dr. Clark's statements that "[s]ince the FFT analysis above shows that the upper NiFe / FeCo relationship is $\{111\}_{\text{FCC}} \parallel \{110\}_{\text{BCC}}$, as well as $\langle 110 \rangle_{\text{FCC}} \parallel \langle 111 \rangle_{\text{BCC}}$, this shows that the Kurdjumov-Sachs orientation relationship is present with respect to both the lower NiFe / FeCo layers, and the upper NiFe / FeCo layers." (*Id.* at ¶ 149.) As discussed above, Dr. Clark's analysis does not establish any such orientations for these layers, much less a Kurdjumov-Sachs orientation relationship. There is absolutely no factual and scientific basis for such an assertion. Furthermore, as discussed more fully below (*see infra* ¶¶ 404-427), Dr. Clark's own microbeam diffraction images on plan-view samples further confirms the absence of such a relationship.

268. Summary. In view of all of the flaws in Dr. Clark's analysis that I have described above, it is my opinion that the conclusions drawn by Dr. Clark regarding the crystalline properties of the upper NiFe layer lack a reliable factual and scientific basis and are based on the application of flawed and unreliable methodologies. In my opinion, the testing data provided by Dr. Clark provides no evidence of the presence of an fcc(111) texture in the upper NiFe layer in sample S2MMMC.

c. Other Data Not Considered by Dr. Clark

269. In addition to the flaws in Dr. Clark's analysis and conclusions described above relating to the lower and upper NiFe layers in sample S2MMMC, I note that Dr. Clark did not consider other information and data that was or could have been available to him relating to the crystal structure of the NiFe layers in sample S2MMMC. I address these additional areas below.

270. No Consideration of Ring Patterns. Unlike for sample S0GPPC, Dr. Clark apparently did not produce a general diffraction ring pattern for the materials contained in sample S2MMMC. As noted above, Dr. Clark did use TEM testing to produce a general diffraction pattern for the materials contained in sample S0GPPC, which also is a sample taken from an [REDACTED] write-head design. (Clark at ¶ 57 and Figure 19.) I note that Dr. Clark does not refer to this diffraction pattern, and he apparently did not consider it, in connection with his

analysis of whether the NiFe layers in sample S2MMMC contain material with a (111) texture. As noted above, I have reviewed the ring pattern from Dr. Clark's report, and I agree that it provides no evidence that would support the conclusion that the NiFe layers for the [REDACTED] write-head design are predominately (111) hexagonal. I also note that this is consistent with the ring diffraction pattern I obtained from my own sample of an [REDACTED] write-head design.

271. No Consideration of Microbeam Diffractions. For sample S2MMMC, Dr. Clark provides a number of plan-view TEM microbeam images. Dr. Clark contends that selected microbeam images show the existence of bcc(110) crystals for the FeCo layers. (*See, e.g.*, Clark at ¶¶ 154-158.) As I explain below (*see infra* ¶¶ 404-427), these images and Dr. Clark's methodology do not support his conclusions regarding the crystal structure of the bcc FeCo layers. I also note that they are inconsistent with the underlying NiFe layers having a (111) texture. As I explain above (*see supra* ¶ 192), one could seek to show the presence of a strongly-textured underlying layer by identifying such crystals in the microbeam images. The fact that Dr. Clark does not attempt to do so, and the fact that such images do not show the presence of any such crystals, is further support for the conclusion that the NiFe layers in sample S2MMMC for the [REDACTED] write-head design do not have a (111) texture.

272. No XRD Testing. In his report, Dr. Clark does not refer to any XRD testing he conducted, and he apparently did not consider any XRD data from any source in connection with his analysis of whether the NiFe layers in sample S2MMMC contain material with a (111) texture. Accordingly, I note that there is no XRD data that would support a conclusion that the NiFe layers for sample S2MMMC from the [REDACTED] write-head design are predominately (111) hexagonal.

d. Conclusion Regarding NiFe Layers

273. In view of all of the flaws in Dr. Clark's analysis that I have described above, and in view of all of the evidence, it is my opinion that the conclusions drawn by Dr. Clark regarding the crystalline properties of the NiFe layers in sample S2MMMC lack a reliable factual and scientific basis and are based on the application of flawed and unreliable methodologies. It is my opinion that none of the evidence I have seen supports the conclusion that either of the NiFe layers in sample S2MMMC has an fcc(111) texture.

3. Sample SBRD8K ([REDACTED] Design)

274. Dr. Clark's report describes a number of high-resolution cross-section TEM images that he took of portions of sample SBRD8K. In particular, Dr. Clark identifies a region where these images were taken shown by a red circle in Figure 96 of his report, with the image on the right of Figure 96 showing a zoomed-in image with the area of the red circle marked as "A." I have reproduced Figure 96 below:

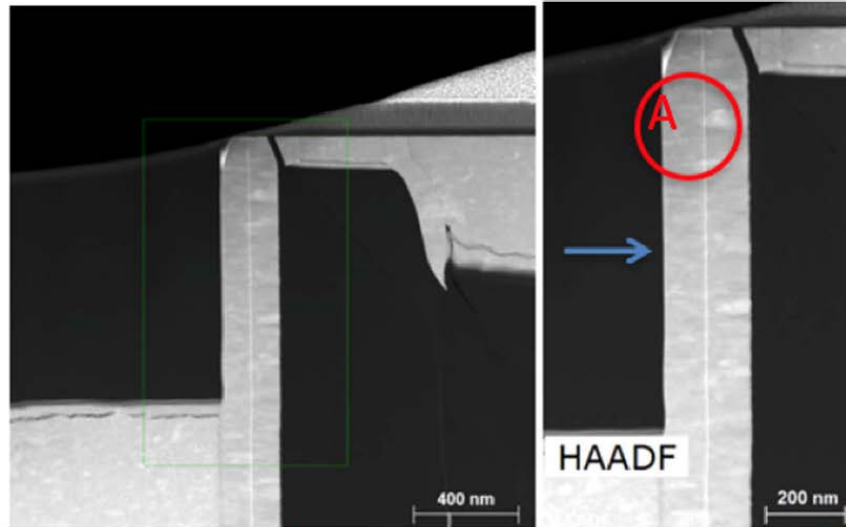


Figure 96: TEM overview of SBRD8K, with regions where high resolution cross-sections were taken shown in the red circle. The blue arrow indicates the growth direction, and A indicates the NiFe template/FeCo interface. Note the pronounced columnar growth seen in both images.

275. Dr. Clark describes the area labeled "A" as a region where high-resolution cross-section TEM images were taken of the lower and upper NiFe layer in sample SBRD8K. (Clark at ¶¶ 170 and Fig. 96.) As discussed below, Dr. Clark's application of his methodology and test results for these images is unreliable and does not provide a valid scientific basis for concluding that either NiFe layer in sample SBRD8K provides a "(111) textured hexagonal atomic template." I address the testing performed by Dr. Clark and the conclusions he reaches for each of these regions below.

a. Lower NiFe Layer

276. Flawed Conclusions Regarding the Presence of fcc(111) Crystals. Dr. Clark relies on an FFT taken from a high-resolution cross-section of a portion of region A as the primary basis for his contention that the lower NiFe layer has an fcc crystal structure. (Clark at

¶¶ 176-178.) In my opinion, the methodology applied by Dr. Clark is flawed and unreliable, and his conclusions are not supported by the scientific data.

277. In particular, Dr. Clark shows FFTs in Figure 102 of his report derived from point 2 of the TEM image shown in Figure 101 of his report. Dr. Clark states that the FFT shown on the left in Figure 102 relates to the lower NiFe layer, and the image on the right relates to the adjacent FeCo. (*Id.* at ¶ 177 and Fig. 102.). Dr. Clark also provides a “standard diffraction pattern” for each that is allegedly rotated into a similar orientations for the FFTs shown above them. (*Id.* at 177 and Fig. 102.) I have reproduced Figure 122 of Dr. Clark’s report below, which on the left shows the FFT for the lower NiFe layer with a standard diffraction pattern, and the FFT of the adjacent FeCo layer on the right with a standard diffraction pattern:

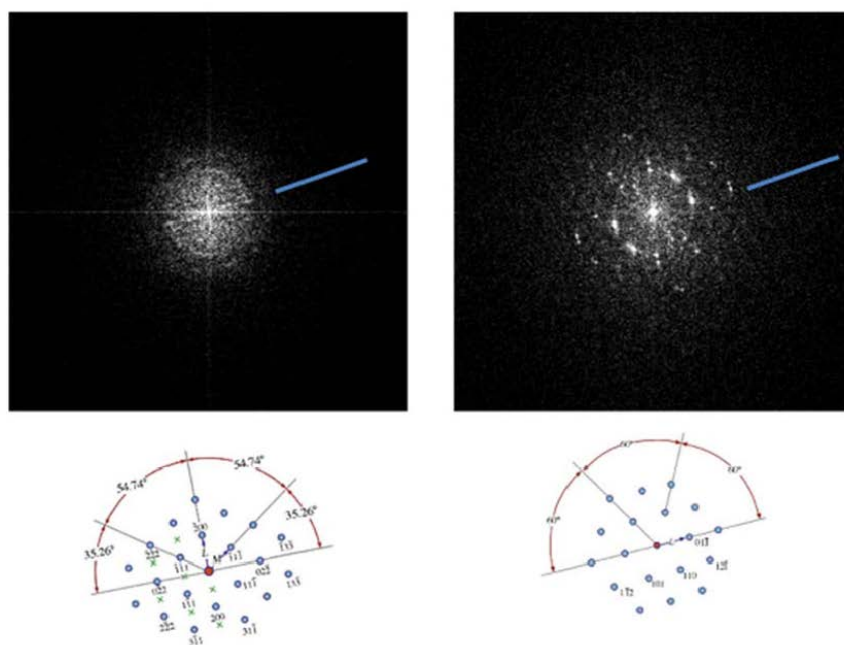


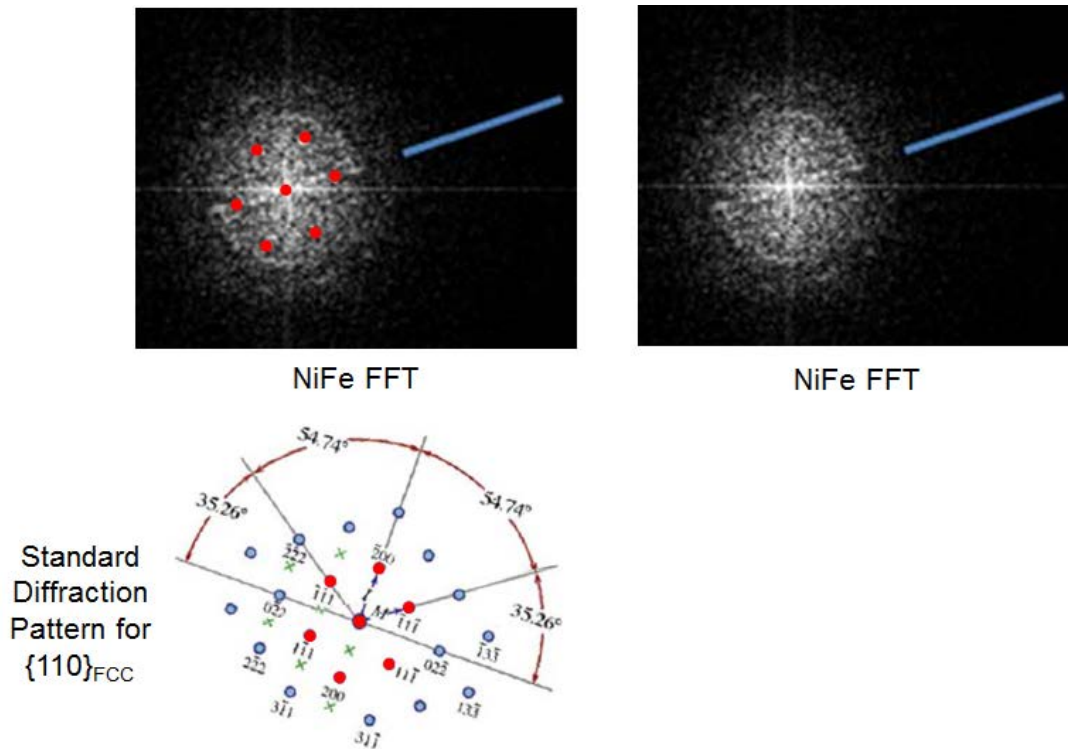
Figure 102: above: FFTs from the NiFe layer (left) and FeCo layer (right); below: standard diffraction patterns rotated into similar orientations as respective FFTs shown immediately above.

278. Dr. Clark states that “[a]nalysis of the FFTs was performed by measuring the diffraction spot spacings and the angles between rows of diffraction spots and comparing that information with standard diffraction patterns.” (*Id.* at ¶ 177.) Dr. Clark states that his analysis for the left-hand FFT from the lower NiFe layer “indicates that the diffraction pattern is {110}_{FCC}” and that “the crystal structure of the NiFe layer is FCC.” (*Id.* at ¶ 178.)

279. The FFT image shown in Figure 102 that Dr. Clark relies on as evidence of the presence of an fcc crystal does not support the conclusion that the portion of the upper NiFe layer he analyzed has an fcc—much less an fcc(111)—crystal structure. Dr. Clark does not describe the particular methodology he applied or which diffraction spots in the FFT he has discerned that allegedly provide the basis for his comparison. He also does not identify the location of the center spot he uses for his orientation or the particular rows of spots that he allegedly used to line up with the 111 spacings and directions of the standard diffraction pattern. Nor does he try to overlay the FFT image with the center spot in the standard diffraction pattern to show how all of the spots and angles are consistent with the standard pattern. There simply is no reliable factual and scientific basis for Dr. Clark to draw his conclusions. In my opinion, no reasonable scientist working in the field would agree with Dr. Clark's conclusion based on this data.

280. In order to show alignment with the standard pattern, the FFT image would need to have clearly discernable spots located at same locations, spacings, and angles as shown in the diffraction pattern using the methodology I described earlier. Applying that methodology here, one can see that the FFT image for the lower NiFe layer consists of a mishmash of spots with no discernable individual spots that can even provide a basis for comparison. There simply are no discernable spots with spacings and angles that are consistent with the standard cross-section diffraction pattern for fcc(111).

281. To demonstrate this more clearly, I took the FFT image for the upper NiFe layer from Figure 102 and attempted to align the spots in this FFT with the $\{110\}_{\text{FCC}}$ diffraction pattern provided by Dr. Clark, using the center spots and the 7 innermost spots of the template, which I have colored red. I repeated the same FFT on the right, but without the red template spots. This is shown below:



282. As can be seen, there are no discernable spots, other than the center spot, for NiFe FFT image that align with the standard diffraction pattern. The FFT image is a haphazard pattern of spots that do not clearly align with the standard diffraction pattern.

283. In my opinion, because the FFT image does not show an fcc structure, all of the conclusions drawn by Dr. Clark regarding the crystalline properties of the upper FeCo layer lack any factual and scientific basis.

284. This problem is compounded to the extent Dr. Clark contends that other unidentified FFT images taken at points other than point 1 allegedly “showed similar results.” (*Id.* at ¶ 183.) If these showed “similar results,” then they are flawed for the same reason as the FFT for the single crystal that he does show in Figure 102.

285. Furthermore, to the extent Dr. Clark purports to rely on other FFTs, he does not specifically identify them and he does not provide the factual basis for his analysis. In fact, he does not provide any analysis. He does not show through overlays, spacing data, or any other methodology how he compared them, the basis for his comparison, or how any of them allegedly match the standard diffraction pattern.

286. To the extent one can speculate as to what these other FFTs might be based on his naming convention, there appear to be a total of 12 FFTs for individual crystals that purportedly

related to the lower NiFe layer. These are identified in a chart I have included in Exhibit F of my report as those under the filename “18.21.37 CCD Acquire.”

287. I have reviewed each of these 12 FFT images (which includes the FFT image from Figure 102 of his report), and none of them is consistent with an fcc standard diffraction pattern along a 110 or 112 zone axis. In particular, none of the images provides a clearly discernable pattern that aligns with the standard spacing and angles for the fcc 110 or 112 zone axis patterns. My comparisons are contained in Exhibit F of my report

288. As I note above, none of this is surprising in view of the thinness of the layer.

—are almost certainly too thin to have developed any significant crystallographic texture, and may even be too thin to have a distinct crystalline structure.

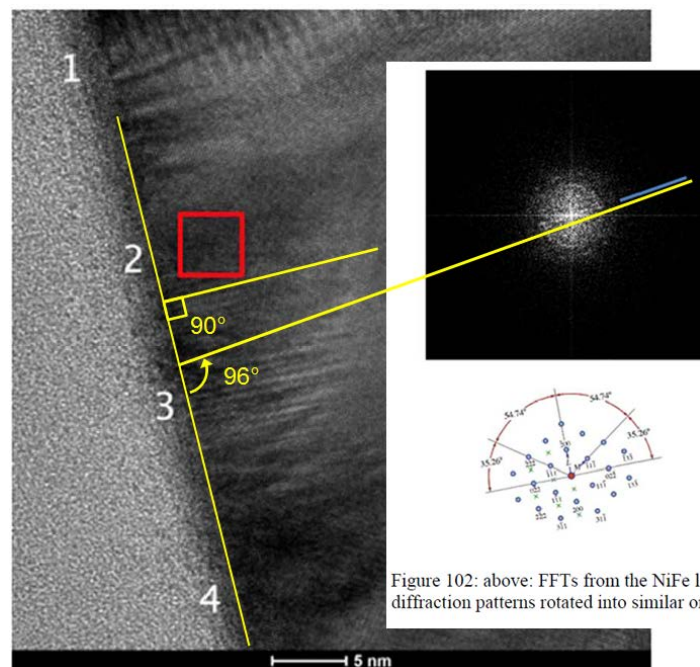
289. Flawed Conclusions Regarding (111) Orientation. Even if the specific crystals Dr. Clark purportedly analyzed using FFTs actually showed the presence of some individual fcc crystals, they would not provide a reliable scientific basis for drawing any conclusions regarding the orientation of the crystal. As I explain above (*see supra* ¶ 37-39), knowing that a crystal has an fcc structure does not tell you anything about its orientation relative to the substrate (such as a 111 direction).

290. In his report, Dr. Clark purports to draw conclusions about the orientation of all of the alleged fcc crystals in the lower NiFe layer by relying on the single FFT image in Figure 102 of his report for the lower NiFe layer. (For the other FFTs for the lower NiFe, Dr. Clark does not provide any information about their orientations relative to the substrate.) In my opinion, the methodology applied by Dr. Clark is flawed and unreliable, and his conclusions are not supported by the data.

291. As the grounds for his conclusions, Dr. Clark states that the two FFT patterns in Figure 102 “show there are two parallel directions, one in the lower NiFe layer and one in the lower FeCo layer, pointing out of the page.” (*Id.* at ¶ 180.) He then contends that, “when analyzing the pattern from the spot spacing and distribution, it can be seen that a $\langle 111 \rangle_{\text{FCC}}$ direction in the NiFe is also parallel to a $\langle 110 \rangle_{\text{BCC}}$ in the FeCo, and lie in the plane of the page.” (*Id.*) He states that these are indicated in Figure 72 by the lines marked on the FFT that he has added. (*Id.*) Dr. Clark then asserts that “[t]he directions are also perpendicular to the lower

NiFe/lower FeCo interface, and so confirm the epitaxial growth in that direction and is evidence of epitaxial growth of the lower FeCo layer on the lower NiFe layer, which functions as an atomic template.” (*Id.*) Dr. Clark then concludes: “These two mutual relationships are also sufficient to determine the relative orientation of the lower NiFe Layer and the lower Fe Co layer above it. Therefore, the lower NiFe layer exhibits (111) texture, and the lower FeCo layer exhibits (110) texture.” (*Id.*)

292. Dr. Clark’s assertion that the NiFe and FeCo crystals are parallel to one another and perpendicular to the substrate is not supported by his own data and is based on an unreliable methodology. In particular, neither of the blue lines that Dr. Clark has drawn in Figure 102 for the two layers is perpendicular to the interface shown in Figure 101. This can be seen by comparing the angle between the substrate (the line along points 1, 2, 3 and 4) in Figure 101, shown below on the left, with the blue lines from the FFTs in Figure 102, shown below on the right. This comparison shows that the blue lines relied on by Dr. Clark to show that the NiFe crystals are perpendicular to the substrate shown in Figure 101 are in fact *not* perpendicular, but instead are off in the range of 6 degrees from perpendicular.



293. The fact that the FFT for the lower NiFe layer that Dr. Clark relies on is not perpendicular to the substrate means that it cannot have a (111) orientation, even if it had been shown to be an fcc crystal (which Dr. Clark has not done).

294. Accordingly, Dr. Clark's methodology for trying to show the orientation of the NiFe and FeCo crystals is flawed and unreliable and does not provide a factual and reliable scientific basis for his conclusion about the orientation of the single crystals he allegedly analyzed based on the FFTs discussed above.

295. Flawed Conclusions Regarding fcc(111) Texture. Even if Dr. Clark had been able to reliably discern the presence of some fcc(111) crystals in the lower NiFe layer of sample SBRD8K, there is no reliable or scientifically valid basis for his sweeping conclusion regarding the texture of the entire lower NiFe layer. In my opinion, the methodology applied by Dr. Clark to reach his conclusions is flawed and unreliable, and his conclusions are not supported by the data.

296. For his broad pronouncements regarding the texture of the lower NiFe layer, Dr. Clark relies on the same flawed data mentioned above. For example, Dr. Clark's conclusion in paragraph 137 of his report regarding the texture of the lower NiFe layer apparently stems from his conclusion regarding the presence and alleged orientation of the single crystals he purported to identify. Yet, as shown above, there is no scientifically valid factual basis for this conclusion.

297. Dr. Clark asserts in another portion of his report that "[t]he parallel directions in the FCC and BCC layers normal to the interface show repeatedly <110> direction in the BCC layers and <111> direction in the FCC layers," which he contends "shows that the lower NiFe layer has a predominant (111) texture, and the lower FeCo layer has a predominant (110) texture." (*Id.* at ¶ 181.) But, once again, Dr. Clark does not provide any factual basis for his claim that there are "repeated[]" examples in the alleged fcc-bcc interface of the "<111> direction." To the extent his assertion that "the interface show repeatedly <110> direction in the BCC layers and <111> direction in the FCC layers" is based on the FFT images, these are flawed, as discussed above. He does not provide any other basis for his conclusion, and I have not seen any other basis for such a conclusion from the other materials provided in his report.

298. In fact, as I have explained, not only does the single FFT discussed by Dr. Clark in the body of his report not have a (111) orientation relative to the substrate, but the other FFTs do not provide any information about the alleged 111 directions associated with each. Without such information, at most they represent many different orientations, which would be inconsistent with any predominate crystalline direction for any fcc crystals in the lower NiFe layer.

299. Furthermore, even if all of the FFTs from the lower NiFe layer that form the basis for Dr. Clark's analysis showed an fcc(111) crystal structure (which they do not), they would amount to a sample of approximately 0.1467%, at best, of the lower NiFe layer, based on my calculation of the overall NiFe length dimension for the [REDACTED] design of approximately 3.3 micrometers (with 1 micrometer = 1,000 nanometers) and the aggregate length dimension for the FFTs being approximately 13.2 nanometers.

300. My calculation for the overall length is based on the image of the write head in the device from which sample SBRD8K was taken as shown on page 163 of Dr. Coffey's report. That image shows an overall length dimension for the write head of approximately 9 micrometers, or 9,000 nanometers, as shown below in an annotated image from Dr. Coffey's report using the dimensions he provides (my annotations are in red to show the length dimension):

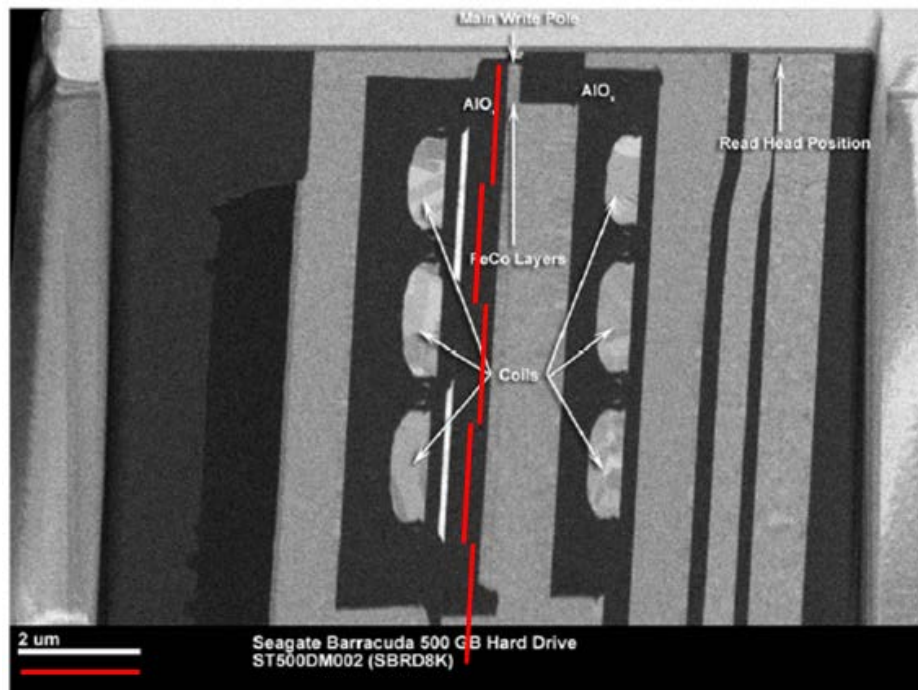


Image from Coffey Report at page 163

301. My calculation for the aggregate length dimension for the FFTs for the lower NiFe layer is based on the dimensions provided by Dr. Clark in Figure 101 of his report. Dr. Clark states that the FFTs for the lower NiFe layer were taken at points along the lower NiFe/lower FeCo interface marked with the numbers 1, 2, 3 and 4 as shown in Figure 101, with

the area sampled for each FFT “confined to an area of the size indicated by the red square.” (Clark at ¶ 176 and Fig. 101.) I have reproduced this image from Dr. Clark’s report below:

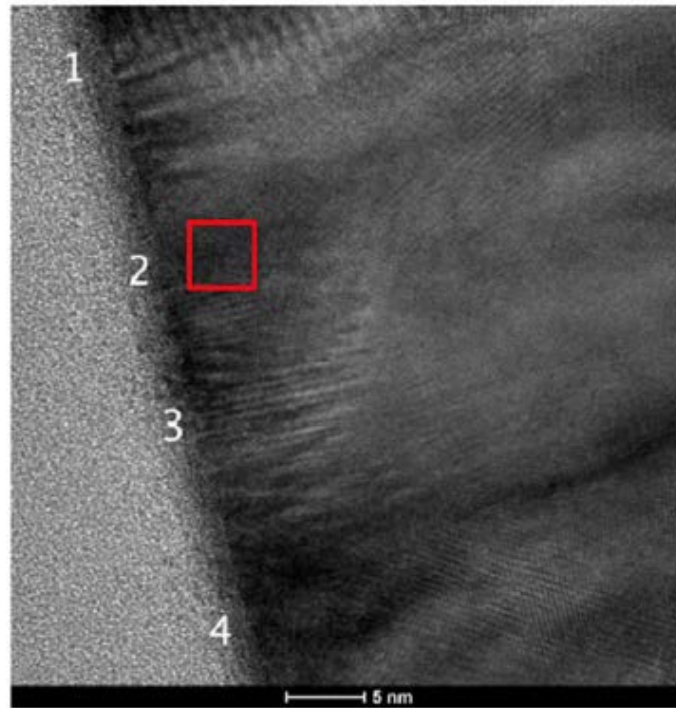


Figure 101: Example high resolution cross-section from the lower NiFe/FeCo interface region. The numbered points indicate where FFTs were taken.

302. Based on the dimensions of the red box shown in Figure 101 of Dr. Clark’s report, the length dimension for each FFT at a particular location would be approximately 3.3 nanometers in length. As shown in Exhibit F of my report, a total of 12 FFTs were taken in total for this area based on Dr. Clark’s naming convention, with three at each location, and only 1 taken of the NiFe layer. Therefore, 4 FFTs x 3.3 nm each = 13.2 nm. Taking the aggregate length dimensions of the areas from which the FFTs were taken of 13.2 nm, and dividing it by the overall length dimension of 9,000 nm results in 0.001467, which is 0.1467 percent. In other words, the sample size represented by Dr. Clark’s FFTs for the lower NiFe layer represents little more than approximately 0.1467 percent of the overall length of lower NiFe layer in the write head from which sample SBRD8K was taken.

303. Dr. Clark does not cite to any source that has used this methodology of a 0.1467 percent sample to draw conclusions about the alleged texture of an entire layer, and I am not aware of any source that would provide a scientific grounding for his approach. Accordingly, in my opinion, there is no scientific basis from which to draw a conclusion about the overall texture

of the NiFe layer based on these images, even assuming Dr. Clark had been able to show the presence of some fcc(111) crystals at the locations of his images, and especially given all of the other flaws with his analysis as explained above.

304. Other Flaws. I also disagree with a number of Dr. Clark's other statements regarding the structure of the lower NiFe layer and the adjacent FeCo layer made in his report regarding sample SBRD8K. I address several of these below.

305. First, I note that Dr. Clark himself apparently has doubts about his conclusions for the lower NiFe layer. He states, for example that "[t]o the extent that the FFT results for the lower NiFe layer are inconclusive, I conclude that the lower NiFe layer is FCC and exhibits a predominant (111) texture based further on the discussion of the upper NiFe / Fe Co layers herein." (Clark at ¶ 184.) For reasons I explain, however, Dr. Clark's data for the upper NiFe layer does not support any conclusion that the upper NiFe layer in sample SBRD8K is fcc(111) textured. Furthermore, there is no reliable scientific basis for Dr. Clark to make judgments about the lower NiFe based on data from the upper NiFe layer that—as discussed below—is also insufficient to support a conclusion of (111) texture.

306. I also disagree with several observations or conclusions made by Dr. Clark based on the high-resolution images shown in Figures 98 and 101, which allegedly is the region of the lower NiFe layer. By way of example, I have reproduced the images from Figure 98 and 101 below:

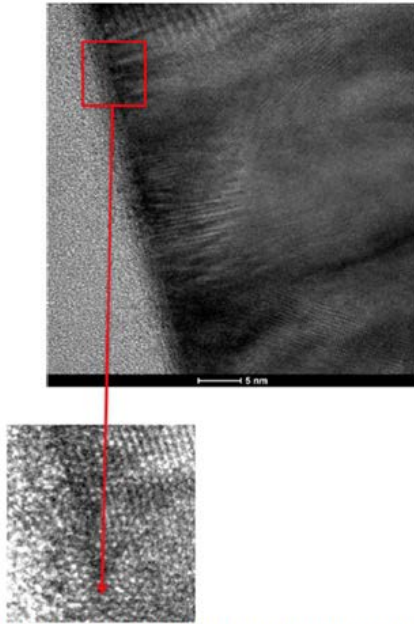


Figure 98: Example showing zoomed-in crossed lattice fringes from a high resolution cross-section from the lower NiFe/FeCo interface region as discussed above.

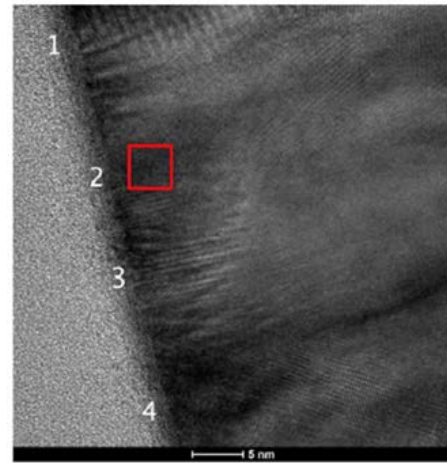


Figure 101: Example high resolution cross-section from the lower NiFe/FeCo interface region. The numbered points indicate where FFTs were taken.

307. To the extent Dr. Clark also suggests that his high-resolution images show evidence of epitaxial growth between the lower NiFe layer and the adjacent FeCo layer, I disagree. For example, as can be seen in his Figures 98 and 101 from Dr. Clark's report, the NiFe layer is not even clearly discernable. There also is no discernable relationship between the lower NiFe layer and any growth patterns of the FeCo grains, which grow in a variety of different directions. None of the images provided by Dr. Clark in his report for this region provide a clear factual basis for any conclusion about epitaxial growth.

308. Summary. In view of all of the flaws in Dr. Clark's analysis that I have described above, it is my opinion that the conclusions drawn by Dr. Clark regarding the crystalline properties of the lower FeCo layer lack a reliable factual and scientific basis and are based on the application of flawed and unreliable methodologies. In my opinion, the testing data provided by Dr. Clark provides no evidence of the presence of an fcc(111) texture in the lower NiFe layer in sample SBRD8K.

b. Upper NiFe Layer

309. Flawed Conclusions Regarding the Presence of fcc(111) Crystals. Dr. Clark refers to an FFT taken from a high-resolution cross-section at points in region A of sample SBRD8K as a basis for making assertions about the crystal structure of the upper NiFe layer of

the sample. (Clark at ¶¶ 186-187.) In my opinion, the methodology applied by Dr. Clark is flawed and unreliable, and his conclusions are not supported by the scientific data.

310. In particular, Dr. Clark shows FFTs in Figure 104 of his report apparently derived from area “A” of the TEM image shown in Figure 103 of this report. (*Id.* at ¶ 186.) Dr. Clark states that the FFT shown on the far left in Figure 104 relates to the lower FeCo layer, the FFT from the second to the left is an FFT of upper NiFe layer, the FFT in the middle relates to an FFT of the middle FeCo layer, the FFT from the second to the right relates to a Ru layer, and the FFT on the far right relates to the uppermost FeCo layer. (*Id.* at ¶ 186 and Fig. 104.). Dr. Clark does not provide any standard diffraction patterns for these images. (*Id.*) I have reproduced Figure 104 of Dr. Clark’s report below:

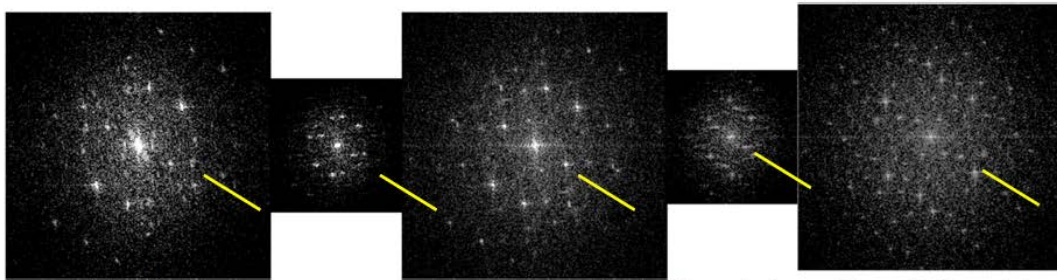


Figure 104: Diffraction patterns across the central region indicated above. From left to right they are: FeCo, NiFe, FeCo, Ru, FeCo. The continuity of the lattice fringes is reflected in common directions in all five patterns, indicated by the yellow lines.

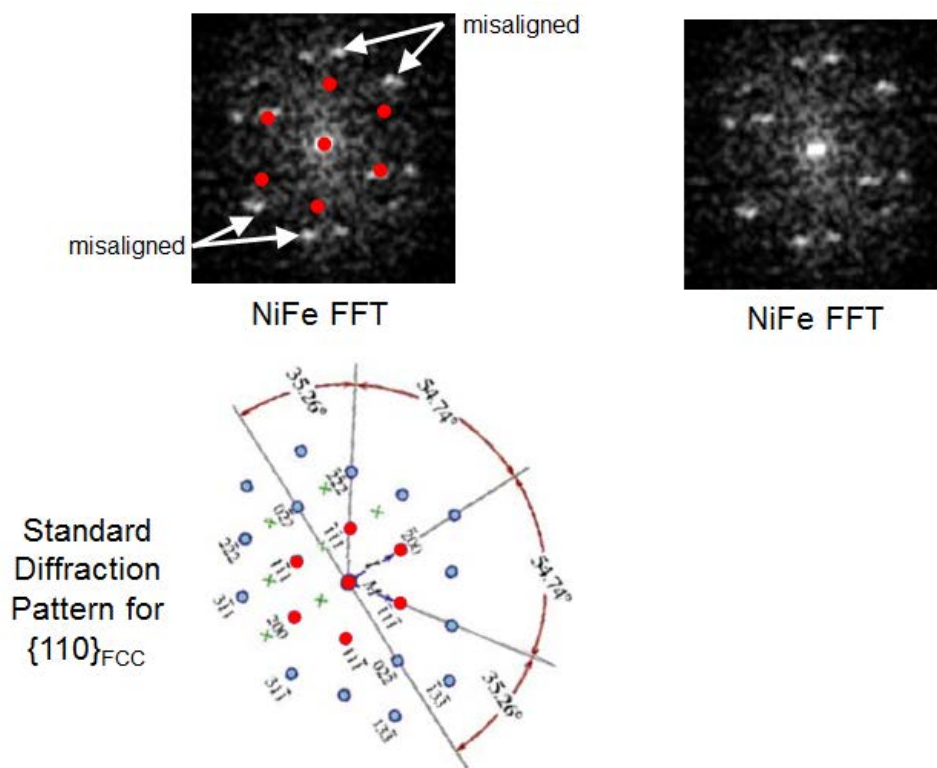
311. Unlike for the other NiFe layers analyzed by Dr. Clark in his report, Dr. Clark does not state that he undertook any analysis of the FFT for the NiFe layer by comparing it to a standard diffraction pattern. Instead, Dr. Clark states that “the FFTs as specific directions in the layers are not all readily ascertainable.” (*Id.* at ¶ 187.) He goes on to state, however, that “the three FeCo layers all exhibit a common pattern” and that “all five patterns share a common direction” which he has indicated through yellow lines. (*Id.*) Based on this observation, he makes the broad statement that these “[c]ommon directions in all three layers show the persistence of the epitaxial relationship between $\langle 111 \rangle_{\text{BCC}}$ and $\langle 110 \rangle_{\text{FCC}}$, as was found at the NiFe/FeCo interface of region A.” He further asserts that “this is indicative of the upper NiFe layer exhibiting (111) texture, and the FeCo layers exhibiting (110) texture.” (*Id.*) He then concludes that “[t]his also indicates the Kurdjumov-Sachs orientational relationship between the upper NiFe and upper FeCo layers.” (*Id.*)

312. Neither the FFT images shown in Figure 104 nor any other data supports Dr. Clark’s broad conclusions. First, it is worth noting that Dr. Clark does not purport to compare

the FFT for the upper NiFe layer to any standard diffraction pattern. The reason for this is clear. The image does not match the standard diffraction pattern.

313. In order to show alignment with the standard pattern, the FFT image would need to have clearly discernable spots located at same locations, spacings, and angles as shown in the diffraction pattern using the methodology I described earlier. Applying that methodology here, what is shown in the FFT pattern in Figure 104 are spacings and angles that are inconsistent with the standard cross-section diffraction pattern for fcc(111) used by Dr. Clark elsewhere in his report.

314. To demonstrate this more clearly, I took the FFT image for the upper NiFe layer from Figure 104 and attempted to align the spots in this FFT with the standard $\{110\}_{\text{FCC}}$ diffraction pattern provided by Dr. Clark elsewhere in his report, using the 9 innermost spots of the template, which I have colored red. I repeated the same NiFe FFT on the right, but without the red template spots. This is shown below:



315. As can be seen, the spots for NiFe FFT image do not align with the standard diffraction pattern. There is a complete mismatch, which demonstrates that the upper NiFe layer does *not* have fcc (111) crystals.

316. In my opinion, because the FFT image does not show an fcc structure, all of the conclusions drawn by Dr. Clark regarding the crystalline properties of the upper FeCo layer lack any factual and scientific basis.

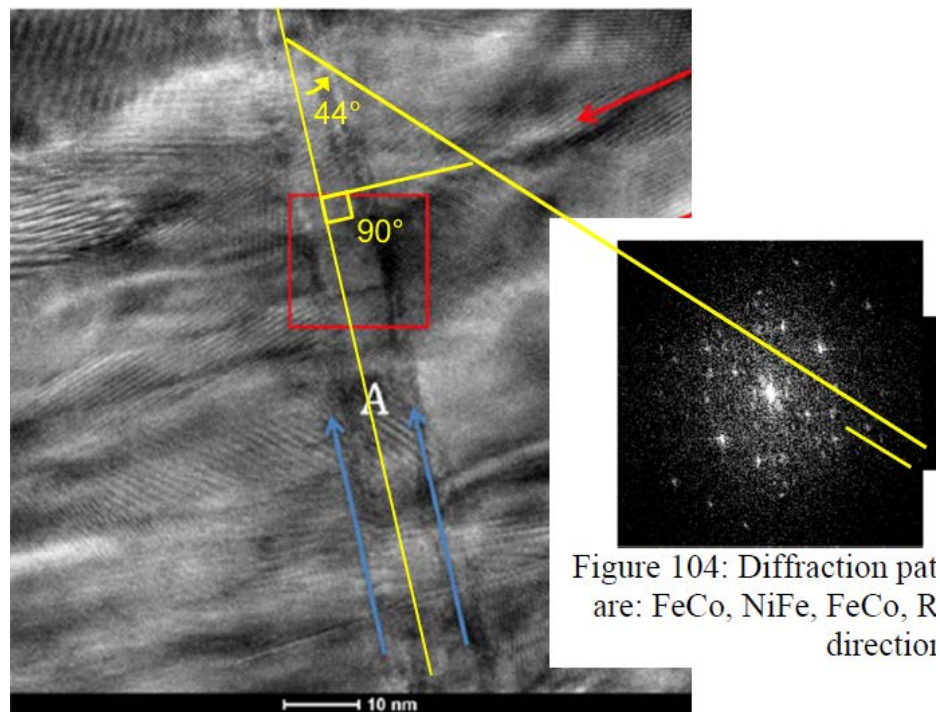
317. Dr. Clark does not provide any other viable scientific basis for his conclusion that the upper NiFe layer is fcc(111). He simply asserts that because he believes there is an epitaxial relationship at the NiFe/FeCo interface, and because there allegedly are common directions in the area where he gathered FFTs in Figure 104, the upper NiFe layer must be exhibiting (111) texture. As shown above, however, none of this is true. There is no epitaxial relationship shown by any of his images, and the lower NiFe layer does *not* have a (111) texture. Even Dr. Clark's own FFTs in Figure 104 belie this, as discussed below.

318. Flawed Conclusions Regarding (111) Orientation. Even though he does not seek to demonstrate, much less show, that the FFT for the specific NiFe crystal shown in Figure 104 actually has an fcc or fcc(111) crystal structure, Dr. Clark nonetheless proceeds to make broad pronouncements about the texture of the upper NiFe layer in sample SBRD8K.

319. Apparently as the basis for his conclusions, Dr. Clark states that the FFT patterns in Figure 104 “show there are two parallel directions, one in the upper NiFe layer and one each of the adjacent FeCo layers, pointing out of the page.” (*Id.* at ¶ 190.) He then contends that, “when analyzing the pattern from the spot spacing and distribution, it can be seen that a $\langle 111 \rangle_{\text{FCC}}$ direction in the NiFe is also parallel to a $\langle 110 \rangle_{\text{BCC}}$ in the FeCo, and lie in the plane of the page.” (*Id.*) He states that these are indicated in Figure 104 by the yellow lines marked on the FFT that he has added. (*Id.*) Dr. Clark then asserts that “[t]he directions are also perpendicular to the upper NiFe/FeCo interfaces, and so confirm the epitaxial growth in that direction and is evidence of the epitaxial growth of the *lower* FeCo layer on the *lower* NiFe layer above it.” (*Id.*) Dr. Clark then concludes: “These two mutual relationships are also sufficient to determine the relative orientation of the *lower* NiFe Layer and the *lower* Fe Co layer above it. Therefore, the *lower* NiFe layer exhibits (111) texture, and the *lower* FeCo layer exhibits (110) texture.” (*Id.*) (Once again, I am not sure whether Dr. Clark's conclusions are meant to be directed to the *upper* NiFe layer, or whether he means to draw conclusions about the *lower* NiFe layer. For purposes of my report, I am taking Dr. Clark's assertions at face value and will take him to be referring to the crystal properties of the lower NiFe layer in sample SBRD8K for purposes of his last statement in paragraph 190 of his report.)

320. Dr. Clark's assertion that the upper NiFe and adjacent FeCo crystals are parallel to one another and perpendicular to the interface of the upper NiFe/FeCo interfaces is not supported by his own data and is based on an unreliable methodology. Furthermore, even if true, it provides no evidence regarding the orientations of the FFTs relative to the substrate, which is necessary to show the orientation of the crystals and whether the FFT for the NiFe layer shows a 111 direction.

321. First, the five yellow lines drawn by Dr. Clark showing the orientation of the three FFTs in Figure 104 are *not* perpendicular to any discernable NiFe/FeCo interface in Figure 103. Dr. Clark apparently seeks to show the location and orientation of the interfaces of the FeCo with the upper NiFe layer with pairs of blue arrows at the bottom of the image. (*Id.* at ¶ 185 ("the two FeCo/NiFe interfaces are indicated by the blue arrows".) If you assume the interface to be represented by these blue lines, that interface is not perpendicular to the lines drawn in Figure 104. This can be seen by comparing the angle between the alleged interface in Figure 103, shown below on the left, with the lines from the FFTs in Figure 104, shown below on the right. This comparison shows that the lines in Figure 104 relied on by Dr. Clark to show that the FFTs are perpendicular to the interface shown in Figure 103 are in fact *not* perpendicular, but instead are off in the range of 46 degrees from perpendicular.



322. Moreover, even if Dr. Clark had established a perpendicular orientation between the FFTs and the upper NiFe/FeCo interfaces, this would tell you nothing about the orientation of the upper NiFe layer relative to the substrate. Dr. Clark provides no location for the substrate relative to the FFT for the upper NiFe layer. Without this information, there is no way to assess what the actual orientation of the upper NiFe crystal is that is purported to have a (111) orientation.

323. Finally, Dr. Clark's main point appears to be that a perpendicular orientation between the upper NiFe crystal and the upper NiFe/FeCo interfaces would tell you something about the orientation of the *lower* NiFe layer, but this clearly is not the case. As noted above, Dr. Clark states that the two mutual orientations of upper NiFe crystal and the upper NiFe/FeCo interfaces "are also sufficient to determine the relative orientation of the *lower* NiFe layer and the lower FeCo layer above it." (*Id.* at ¶ 190 (emphasis added).) But what the orientation is of the upper NiFe layer relative to the interface tells you nothing about the orientation of the lower NiFe layer. There is no valid scientific basis for Dr. Clark to make such an assertion.

324. Because Dr. Clark provides no information about the orientation of the NiFe crystal for the upper NiFe layer relative to the substrate, there is no evidence that any crystal in the upper NiFe layer has a (111) orientation, even if he had been able to show that such a crystal had an fcc structure (which Dr. Clark also has not done).

325. Accordingly, Dr. Clark's methodology for trying to show the orientation of the upper NiFe and FeCo crystals is flawed and unreliable and does not provide a factual and reliable scientific basis for his conclusion about the orientation of the upper NiFe layer discussed above.

326. Flawed Conclusions Regarding fcc(111) Texture. Even if Dr. Clark had been able to reliably discern the presence of an fcc(111) crystal in the upper NiFe layer of sample SBRD8K, there is no reliable or scientifically valid basis for his sweeping conclusion regarding the texture of either the upper or lower NiFe layers. In my opinion, the methodology applied by Dr. Clark to reach his conclusions is flawed and unreliable, and his conclusions are not supported by the data.

327. In this case, Dr. Clark does not even try to show any examples based on FFTs he allegedly took to show the presence of fcc(111) crystals. Instead, he simply asserts in another portion of his report that "[t]he parallel directions in the FCC and BCC layers normal to the interface show repeatedly <110> direction in the BCC layers and <111> direction in the FCC

layers,” which he contends “shows that the lower NiFe layer has a predominant (111) texture, and the lower FeCo layer has a predominant (110) texture.” (*Id.* at ¶ 181.) But, once again, Dr. Clark does not provide any factual basis for his claim that there are “repeated[]” examples in the alleged fcc-bcc interface of the “<111> direction.” To the extent his assertion that “the interface show repeatedly <110> direction in the BCC layers and <111> direction in the FCC layers” is based on the FFT image, this is flawed, as discussed above, because Dr. Clark does not even rely on that FFT to try to show that it aligns with a standard fcc(111) diffraction pattern. He does not provide any other basis for his conclusion, and I have not seen any other basis for such a conclusion from the other materials provided in his report. Accordingly, Dr. Clark’s assertions are unreliable and have no factual scientific basis.

328. Other Flaws. I also disagree with a number of Dr. Clark’s other statements regarding the structure of the upper NiFe layer and the adjacent FeCo layers made in his report regarding sample SBRD8K. I address several of these below.

329. I disagree with several observations or conclusions made by Dr. Clark based on the high-resolution images shown in Figures 99 and 100, which allegedly is the region of the upper NiFe layer. (*Id.* at ¶ 104.) By way of example, I have reproduced the image from Figures 99 and 100 below:

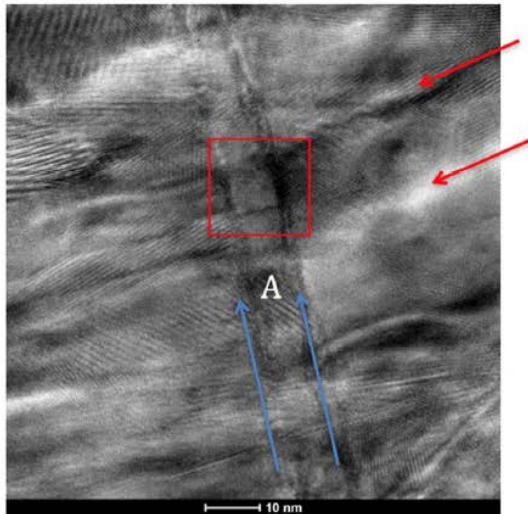


Figure 99: Example high resolution cross-section from the upper NiFe/FeCo/Ru interface area. Area highlighted in red is shown enlarged below.

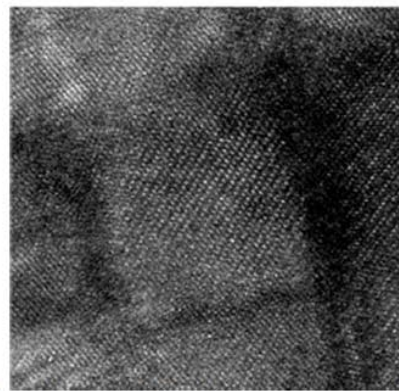


Figure 100: Zoomed-in area from Figure 99 above showing crossed lattice fringes.

330. Based on these and the other high-resolution images, Dr. Clark states that they show “crossed lattice fringes” in the area designated by the red box. (*Id.* at ¶ 174.) He also says the zoomed-in area in the red square of Figure 99 shows “prominent patterns of crossed fringes,”

along with the FeCo/NiFe/Ru interfaces. (*Id.*) He states that “[t]he fringes are present on both sides of the NiFe layer, in the NiFe layer itself, and on both sides of the Ru layer, indicating that the orientation of the FeCo is maintained on both sides of the NiFe.” (*Id.* at ¶ 175.) He goes on to say that “[t]he continuity of these fringes across all layers show that there is an orientation relationship between the FeCo and the NiFe” and further concludes that there is a “hexagonal arrangement of spots in the FeCo lattice image” that “shows a $\{111\}_{\text{BCC}}$ plane, and a $\langle 110 \rangle_{\text{BCC}}$ direction” that “is normal to the interface.” (*Id.*) I disagree with Dr. Clark’s analysis and his conclusions.

331. First, to the extent Dr. Clark also suggests that his high-resolution images show clear evidence of epitaxial growth between the upper NiFe layer and the upper FeCo layer, I disagree. For example, as can be seen in Figure 103 from Dr. Clark’s report, the FeCo grains appear to grow through the area of the alleged NiFe layer without significant change. Therefore, there is no clearly discernable relationship between the upper NiFe layer and any growth patterns of the FeCo grains from these images. In my opinion, these images do not provide a reliable basis for drawing any conclusions about whether the NiFe layer is directing the growth of the upper FeCo layer. An equally probable inference is that it has no effect on the growth of the upper FeCo layer.

332. Second, Dr. Clark’s suggestion that these images can be used to determine that the FeCo is “normal to the interface” is incorrect. The images provide no information about the orientational relationship of any NiFe layers relative to the substrate and therefore provide no data that can be relied on to determine whether the FeCo layer has a $\text{bcc}(1110)$ orientation.

333. Dr. Clark also states that “the FFTs taken from various points along the NiFe layers, while they maintain a common direction with the FeCo layers normal to the interface, change significantly with position along the interface.” (*Id.* at ¶ 193). He goes on to say that these changes indicate differences in the grain size in the NiFe layer, and concludes that the “grain size in the NiFe template layers is comparable to the width of the FeCo grains” and that “there is ordinarily only one or two FeCo grains per NiFe template grain.” (*Id.*) I disagree with Dr. Clark’s analysis and his conclusions.

334. As an initial matter, Dr. Clark does not explain what “change” with respect to “position along the interface” he is referring to. To the extent he is suggesting that these changes relate to grain size, or that there are clearly discernable grain sizes for the NiFe layer that can be

determined from his images, I disagree. While these images provide some information about the grain sizes for portions of the FeCo layer, there is no clear evidence of NiFe grains or their sizes in these images. Therefore, in my opinion, there is no reliable factual and scientific basis for Dr. Clark to draw conclusions about the relative size of grains between the upper NiFe layer and the FeCo layers based on the data he has presented.

335. Summary. In view of all of the flaws in Dr. Clark's analysis that I have described above, it is my opinion that the conclusions drawn by Dr. Clark regarding the crystalline properties of the upper FeCo layer lack a reliable factual and scientific basis and are based on the application of flawed and unreliable methodologies. In my opinion, the testing data provided by Dr. Clark provides no evidence of the presence of an fcc(111) texture in the upper NiFe layer in sample SBRD8K.

c. Other Data Not Considered by Dr. Clark

336. In addition to the flaws in Dr. Clark's analysis and conclusions described above relating to the lower and upper NiFe layers in sample SBRD8K. I note that Dr. Clark did not consider other information and data that was or could have been available to him relating to the crystal structure of the NiFe layers in sample SBRD8K. I address these additional areas below.

337. No Consideration of Ring Patterns. Unlike for sample S0GPPC, Dr. Clark apparently did not include a general diffraction ring pattern for the materials contained in sample SBRD8K in the body of his report. However, Dr. Clark apparently did use TEM testing to produce a general diffraction pattern for the materials contained in sample SBRD8K, which I found in Dr. Clark's Appendix C. I note that Dr. Clark does not refer to this diffraction pattern, and he apparently did not consider it, in connection with his analysis of whether the NiFe layers in sample SBRD8K contain material with a (111) texture. I have reviewed the ring pattern from Dr. Clark's report, and I agree that it provides no evidence that would support the conclusion that the NiFe layers in sample SBRD8K for the [REDACTED] write-head design are predominately (111) hexagonal. I also note that this is consistent with the ring diffraction pattern I obtained from my own sample of a [REDACTED] write-head design.

338. No Consideration of Microbeam Diffractions. For sample SBRD8K, Dr. Clark provides a number of plan-view TEM microbeam images. Dr. Clark contends that selected microbeam images show the existence of bcc(110) crystals for the FeCo layers. (*See, e.g.*, ¶¶ 196-201.) As I explain below (*see infra* ¶¶ 452-479), these images and Dr. Clark's methodology

do not support his conclusions regarding the crystal structure of the bcc FeCo layers. I also find that they are inconsistent with the underlying NiFe layers having a (111) texture. As I explain above (*see supra* ¶ 192), one could seek to show the presence of a strongly-textured underlying layer by identifying such crystals in the microbeam images. The fact that Dr. Clark does not attempt to do so, and the fact that such images do not show the presence of any such crystals, is further support for the conclusion that the NiFe layers in sample SBRD8K do not have a (111) texture.

339. No XRD Testing. In his report, Dr. Clark does not refer to any XRD testing he conducted, and he apparently did not consider any XRD data from any source in connection with his analysis of whether the NiFe layers in sample SBRD8K contain material with a (111) texture. Accordingly, I note that there is no XRD data that would support a conclusion that the NiFe layers in sample SBRD8K for the [REDACTED] write-design are predominately (111) hexagonal.

d. Conclusion Regarding NiFe Layers

340. In view of all of the flaws in Dr. Clark's analysis that I have described above, and in view of all of the evidence, it is my opinion that the conclusions drawn by Dr. Clark regarding the crystalline properties of the NiFe layers in sample SBRD8K lack a reliable factual and scientific basis and are based on the application of flawed and unreliable methodologies. It is my opinion that none of the evidence I have seen supports the conclusion that either of the NiFe layers in sample SBRD8K has an fcc(111) texture.

B. Dr. Clark's Conclusions Relating to the Crystalline Structure, Texture, Variants, and Symmetry Broken Structures in Certain FeCo Layers in Samples S0GPPC, S2MMC, and SBRD8K Are Based on a Misapplication of Scientific Principles and Methods, Are Unreliable, and Do Not Have a Reliable and Sufficient Factual and Scientific Basis

1. Sample S0GPPC ([REDACTED] Design)

341. In his report, Dr. Clark states that TEM microbeam diffraction was performed on a region of the lower FeCo layer of sample S0GPPC. In particular, Dr. Clark states that the microbeam diffraction was taken at the area shown by the red square in Figure 45 of his report from a sample that was prepared where the upper FeCo/NiFe layer was removed. (Clark at ¶ 106.) He states that from this area represented by the red square, "1,600 diffraction patterns were obtained by scanning the electron beam incrementally area in the box." (*Id.*) However, only a handful of these (eight, to be exact) are actually included and discussed in his report.

342. Dr. Clark goes on to state that “[b]y defocusing the diffraction pattern image slightly” (as shown in Figure 46), he was able to obtain an enlarged central spot that contains an image of the portion of the sample and that, from this, he was able to confirm that the plan view sample and diffraction pattern were within an alignment of ± 10 degrees. (*Id.* at ¶ 107 and Fig. 46.) In his report, Dr. Clark then provides examples of eight diffraction patterns (out of the 1,600 he took) that he says show the presence of bcc(110) crystals, which he indicates by drawing yellow rectangles onto the diffraction pattern. He then goes on to provide conclusions regarding another 100 patterns taken from this area that he purportedly analyzed, although he does not include these images in his report or include his specific analysis of any of them (such as trying to draw the crystals on these images that he does for the eight he actually discusses in his report).

343. In the remainder of this section of his report (*see* Clark at ¶¶ 116-124), Dr. Clark describes dark field images that he took from the plan view specimen for sample S0GPPC. He uses these images in an attempt to isolate crystals that have their $\langle 200 \rangle$ directions purportedly aligned perpendicular to the long axis of the write head sample. He then tries to calculate the area fraction of the crystals with these directions at 10-degree increments.

344. From this microbeam diffraction and dark-field testing, Dr. Clark purports to draw broad conclusions about the crystal properties of the lower FeCo layer in sample S0GPPC (he does not analyze the upper layer), the presence of bcc(110) crystals, the distribution of such crystals, their in-plane orientations, and whether they are part of a six-variant system. For the reasons I explain below, it is my opinion that the methodology applied by Dr. Clark to reach his conclusions about the presence of bcc(110) crystals, their relative amounts, and their orientations, and whether they are part of a six-variant system and a symmetry broken structure is flawed and unreliable, and that his conclusions are not supported by any valid scientific data. I address separately below the microbeam diffraction testing and the dark-field testing performed by Dr. Clark and the conclusions he reaches.

a. Flawed and Unsupported Conclusions Based on Microbeam Diffraction Data

345. Flawed and Unsupported Conclusions Regarding the Presence of bcc(110) Crystals. In paragraphs 108-113 and Figures 47-52 of his report, Dr. Clark explains that individual frames from the set of 1,600 microbeam diffraction images that he captured “may

contain diffraction patterns from one, two, or sometimes more separate FeCo crystallites.” (*Id.* at ¶ 108.) He then states that “[t]ypical single crystal patterns for this analysis” are shown in Figure 47 of his report, and that “[t]hese patterns are readily identified and indexed as patterns in the (110)_{BCC} direction.” (*Id.*) He states that this was confirmed by measurement of the ratio of the sides of the rectangles, which were “found to be $5.4:3.8 = 1:\sqrt{2}$, as required.” (*Id.*)

346. Dr. Clark provides a total of eight examples of diffraction patterns that allegedly show the presence of individual bcc(110) crystals from the lower FeCo layer of the plan view specimen from sample S0GPPC. For each of the eight images shown in his report, Dr. Clark draws yellow boxes (“annotated using Keynote” software from Apple (*see id.* at ¶ 106)) around the portions of the diffraction pattern that he contends show the presence of a bcc(110) crystal.

347. Apart from his statement noted above regarding the required ratio of the sides to establish the presence of a bcc(110) crystal, Dr. Clark does not explain or describe the particular methodology he used to draw his yellow boxes or to calculate the angles that he includes in the annotations in his report that form the basis for his conclusion. At most, he suggests that the microbeam diffraction patterns “visually identify as standard (110)_{BCC} patterns.” (*Id.* at caption to Fig. 47.) He does not show any indexing of these patterns, however, or describe the basis on which he selected certain spots for his annotations, how he calculated the ratios between the sides of the rectangles he drew, or the method by which he derived his angles (other than nominally for two of his examples). He frequently relies on alleged “spots” that are not clearly discernable, and ignores spots that are inconsistent with his conclusions.

348. In my opinion, Dr. Clark’s methodology for drawing the boxes and calculating the angles purporting to identify individual bcc(110) crystals from the red-box region does not support his conclusion that it shows the presence of a bcc(110) crystal for most of the examples he discusses in this section of his report. Furthermore, his eight examples provide no scientific basis for the broad conclusions he draws about the crystallographic structure of the lower FeCo layer in sample S0GPPC.

349. To accurately identify the presence of bcc(110) crystals in TEM microbeam diffraction patterns, one needs to clearly identify discernable spots (including the appropriate bright center spot), align those spots with those that are associated with bcc(110) crystals from standard ring diffraction patterns, determine whether there are other diffraction spots that are inconsistent with a bcc(110) crystal, and measure the ratio of the two sides of the rectangles to

confirm they match the ratio of $1:\sqrt{2}$ for a bcc(110) crystal. To accurately calculate the relative angle between two alleged crystals, one needs to extend either the two longer or two shorter sides of each of the crystals being compared and then accurately measure the angle between them. Because Dr. Clark does not clearly follow this approach, many of his results are flawed, as I explain below.

350. For example, for Figure 48 in his report, Dr. Clark acknowledges that “some spots in the motif are weak or barely detectable” (which he ascribes to distortions in the sample or tilting of the sample off the exact (110) orientation), and that “some diffraction spots do not make perfect intersection with the Ewald sphere, and so are faint or not visible at all.” (*Id.* at ¶ 109.) Despite these clear problems with his image, Dr. Clark nonetheless concludes that “it is readily ascertainable that this is a (110)_{BCC} diffraction pattern as no other orientation describes it.” (*Id.*) I have reproduced Figure 48 from Dr. Clark’s below:

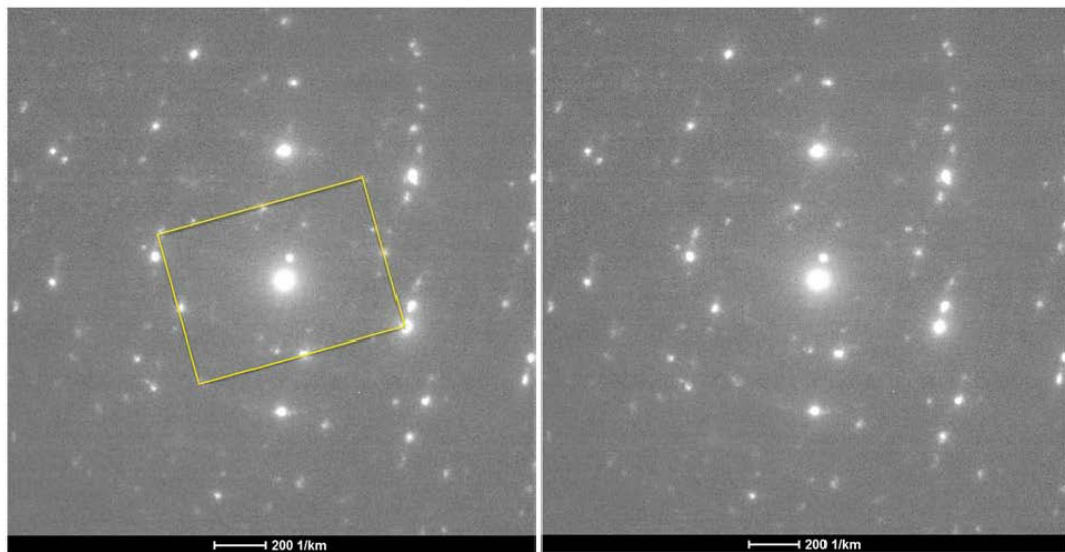
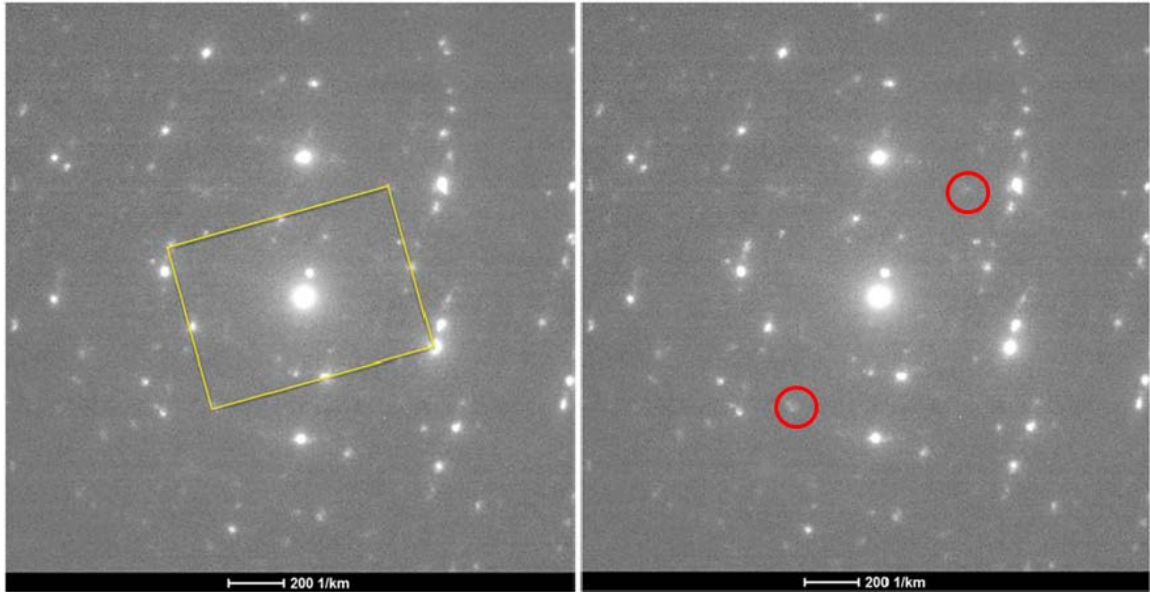
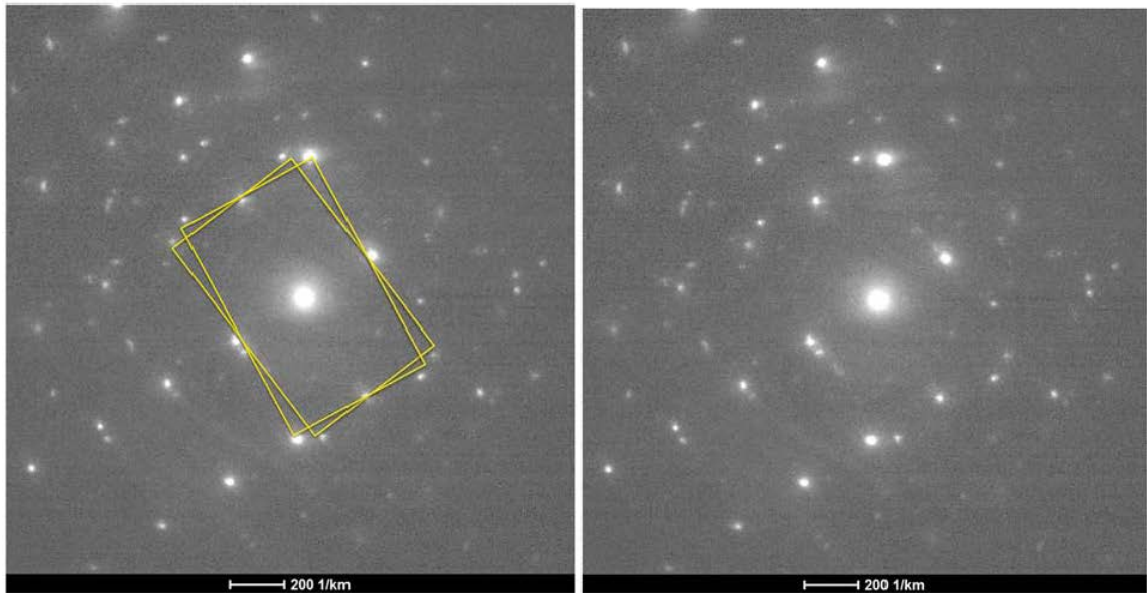


Figure 48: Single crystallite diffraction pattern, frame 837, in the (110) orientation. While there are additional or weak spots, this motif is readily identifiable as a (110)_{BCC} pattern.

351. In my opinion, Dr. Clark’s analysis of the pattern in Figure 48 (Frame 837) is flawed because several of the spots he has chosen as the basis for his drawing are not clearly discernable (*e.g.*, to use Dr. Clark’s words, “faint or not visible at all”). Therefore, in my opinion, this pattern does not provide a good basis for assessing whether it shows the presence of a bcc(110) crystal. I have noted examples of the spots that Dr. Clark purports to rely on that in my opinion are not clearly discernable with red circles below:

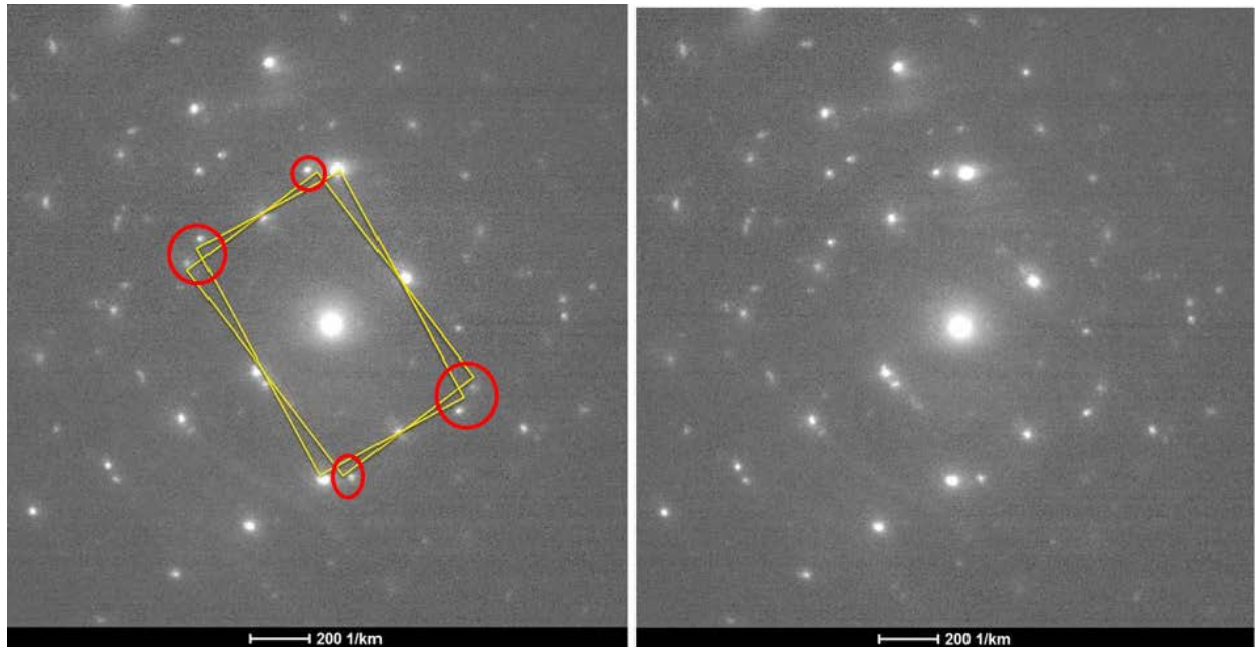


352. The microbeam diffraction pattern in Figure 49, which purports to show the presence of two bcc(110) crystals, has similar flaws. I have reproduced Figure 49 from Dr. Clark's report below:

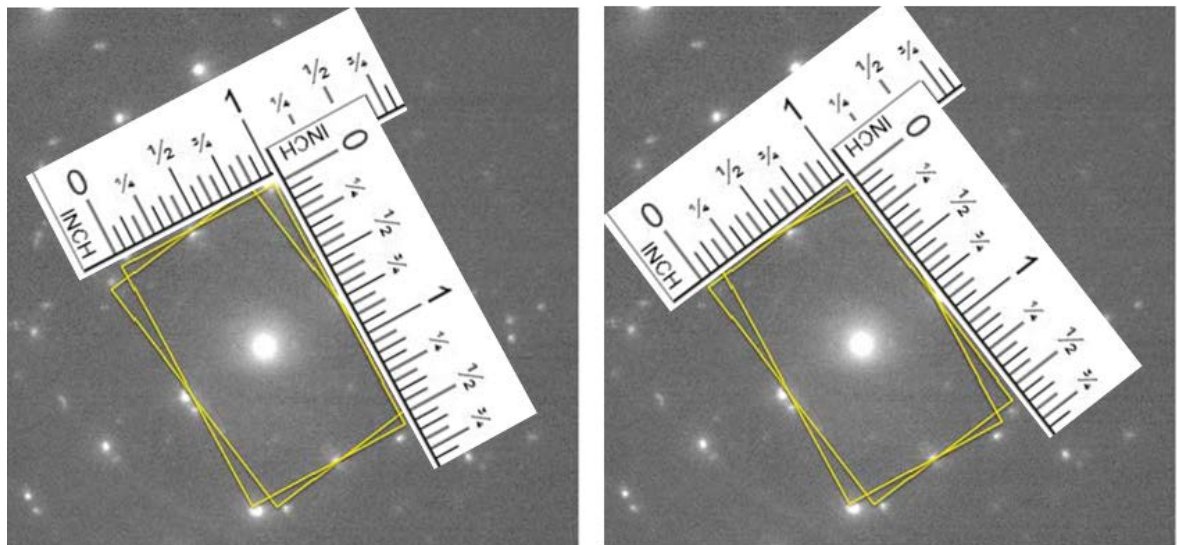


353. In my opinion, Dr. Clark's analysis of the patterns for the two alleged bcc(110) crystals he has drawn in Figure 49 (from Frame 721) does not allow for his conclusion that it shows the presence of a bcc(110) crystal. First, similar to Figure 48, there are some spots that Dr. Clark has chosen in Figure 49 as the basis for his drawings that are not clearly discernable, or his rectangles are misaligned. Therefore, in my opinion, these patterns do not provide a good

basis for assessing whether they show the presence of bcc(110) crystals. I have noted examples of the spots from Frame 721 that Dr. Clark purports to rely on to draw his two crystals that are not clearly discernable with red circles below:



354. Second, Dr. Clark is not correct when he says that “[t]he measured ratio of the sides of the motif are $1:\sqrt{2}$ as required.” Dr. Clark states that he measured the angles directly using Keynote, but according to my measurements, his conclusion about the ratio of the two sides is incorrect. Shown below are the measured distances for each of the alleged crystals in Figure 49:



355. Using these measurements, the ratio for one of the crystals is 1 inch to 1 and $9/16^{\text{th}}$ of an inch, or 1:1.56, and for the other it is the same. Neither of these ratios is equivalent to the required ratio of $1:\sqrt{2}$ (with $\sqrt{2}$ being equal to approximately 1.41). The ratio of 1:1.56 is more than 10% different than the required ratio of 1:1.41, much greater than the maximum 3% error typically allowed. Thus, these measurements do not support the conclusion that the crystals Dr. Clark has drawn in Figure 49 are bcc(110) crystals.

356. Finally, I note that that Dr. Clark uses this Figure 49 as a basis for making the sweeping statement that because the two crystals he has drawn allegedly are offset from one another by an angle of approximately 9 degrees (*i.e.*, they are rotated in the plane about 9 degrees relative to one another) this shows “the separation of two variants in the Kurdjumov-Sachs orientation.” (Clark at ¶ 110.) This is simply incorrect. As I explained above (*see supra* ¶¶ 50-55) and explain in more detail below (*see infra* ¶ 377), one cannot show the existence of a particular variant without showing the orientation of the overlying crystal *relative to* the underlying crystal on which it was grown. As the '988 Patent makes clear (and as Dr. Clark confirms elsewhere in his report, *see, e.g., id.* at ¶¶ 33-35)), a variant is defined based on the orientational relationship of the “the (110) crystal plane of a bcc-d crystal in comparison to the atomic arrangement of the (111) crystal plane of a hexagonal lattice template crystal.” ('988 Patent, 13:40-43.) Therefore, the relative orientation of the two alleged bcc(110) crystals in the plane cannot be used as a basis for making judgments about whether they are part of the six-variant system required by the '988 Patent without first showing the orientation of each relative to an underlying (111) hexagonal crystal, which may have a different in-plane orientations from another. Dr. Clark does not do this. In fact, as I note below, Dr. Clark has not shown the presence of any underlying (111) hexagonal crystals through his microbeam diffractions patterns.

357. I have analyzed the patterns in the other figures and provided a table below summarizing my analysis of the eight examples of microbeam diffraction patterns for the lower FeCo layer in sample S0GPPC included in Dr. Clark's report:

Figure and Frames	Analysis
Figure 47 Frame 722 (upper) Frame 417 (lower)	Rectangles do not have the expected ratio of $1:\sqrt{2}$ for bcc(110) crystals
Figure 48 Frame 837	Some diffraction spots not clearly discernable or are not present at the expected location
Figure 49 Frame 721	Some diffraction spots not clearly discernable or are not present at the expected location; rectangles do not have the expected ratio of $1:\sqrt{2}$ for bcc(110); the lack of alignment of the rectangle corners with nearby spots is significant enough to indicate that Dr. Stack's interpretation is incorrect
Figure 50 Frame 817	Some diffraction spots not clearly discernable or are not present at the expected location; rectangles do not have the expected ratio of $1:\sqrt{2}$ for bcc(110) crystals; the lack of alignment of the rectangle corners with nearby spots is significant enough to indicate that Dr. Stack's interpretation is incorrect
Figure 51 Frame 726 (upper) Frame 802 (lower)	Upper image: some diffraction spots are not clearly discernable or are not present at the expected location; rectangles do not have the expected ratio of $1:\sqrt{2}$ for bcc(110) crystals; the lack of alignment of the rectangle corners with nearby spots is significant enough to indicate that Dr. Stack's interpretation is incorrect Lower image: some diffraction spots are not clearly discernable or are not present at the expected location; rectangles do not have the expected ratio of $1:\sqrt{2}$ for bcc(110) crystals; the lack of alignment of the rectangle corners with nearby spots is significant enough to indicate that Dr. Stack's interpretation is incorrect
Figure 52 Frame 1487	Some diffraction spots not clearly discernable or are not present at the expected location; rectangles do not have the expected ratio of $1:\sqrt{2}$ for bcc(110) crystals; blue lines labeled 71 degrees actually have an angle of 66 degrees; no scale bars; the lack of alignment of the rectangle corners with nearby spots is significant enough to indicate that Dr. Stack's interpretation is incorrect

358. My analysis for these eight examples is contained in Exhibit G of my report.

359. Presumably, Dr. Clark chose what he considered to be the best eight examples out of the 1,600 images available to him to try to show the presence of bcc(110) crystals in the lower FeCo layer of sample S0GPPC. Yet, as demonstrated above, most of his examples are flawed.

360. In addition to these examples, Dr. Clark states that he analyzed another 100 diffraction patterns taken from this area that were randomly selected out of the 1,600 total diffraction patterns. (Clark at ¶ 114.) He states that he categorized these diffraction patterns into four categories as follows:

Category	Results
a) Showed no recognizable pattern	27
b) Showed a single {110} pattern	30
c) Showed two or three {110} patterns	44 (including twins)
d) Showed {110} twins	included in (c)
e) Showed a pattern other than {110}	apparently none

361. Dr. Clark does not provide his analysis for any of these other 100 microbeam diffraction patterns that he mentions in his report, and he did not include any of the actual images in Appendix C of his report. Dr. Clark's failure to include these images is inconsistent with the basic scientific practice of showing the data on which you are basing your conclusions. Because Dr. Clark has not provided any of the data on which he allegedly basis his analysis for these 100 other diffraction patterns, it is not possible to assess whether Dr. Clark's categorization of these other 100 images is accurate. To the extent Dr. Clark used the same approach that he did for the eight examples for the categorization of the patterns that he does provide in his report, then they will be flawed to the same extent as discussed above.

362. I note, however, that according to Dr. Clark, 27 percent of these additional 100 crystals did not have a recognizable pattern. The alleged presence of these other unrecognizable crystals is inconsistent with the bcc(110) crystals predominating in the FeCo layer and with the lower FeCo layer forming a symmetry broken structure, because it means that the lower FeCo layer has crystals that are not bcc(110) and therefore not part of a six-variant system. (*E.g.*, '988 Patent at 12:66-13:2 ("this invention deals with a structure to achieve uniaxial magnetocrystalline orientation via the use of the (110) texture of body centered cubic (BCC) or body centered cubic derivative crystal thin film structures.").)

363. Furthermore, there is other clear evidence in the microbeam diffraction patterns that Dr. Clark provides for orientations other than bcc 110. For example, taking the diffraction pattern shown by Dr. Clark on the right-hand side of Figure 48 of his report, in order for the pattern to show only (110) crystals, all of the spots would have to lie upon the yellow rings that I have added in the image shown below on the right. Specifically, I added the set of rings that would appear from a bcc(110) textured sample, and I aligned the innermost yellow ring, which is 110, with the spots lying in the middle of the long side of Dr. Clark's yellow rectangle. As

shown below, many of the spots do not lie on the yellow rings I have added. Thus, there must be grain orientations that are not associated with a 110 texture in the layer. I have performed similar analyses (shown in Exhibit G), and other of Dr. Clark's examples also have numerous spots inconsistent with a bcc 110 texture.

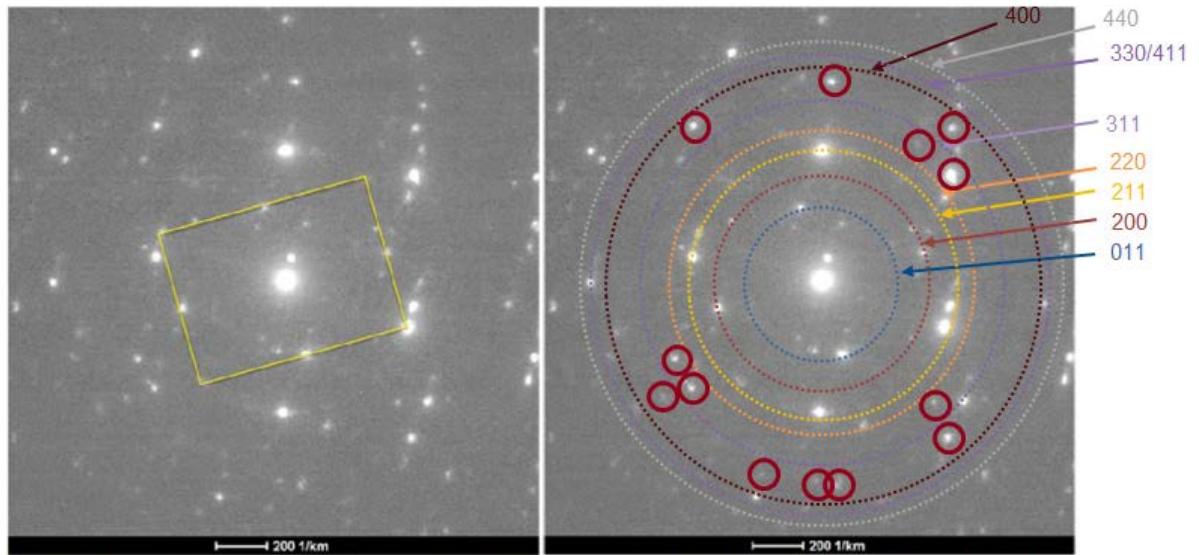


Figure 48: Single crystallite diffraction pattern, frame 837, in the (110) orientation. While there are additional or weak spots, this motif is readily identifiable as a (110)_{BCC} pattern.

Circled spots are at locations not consistent with a 110_{BCC} orientation

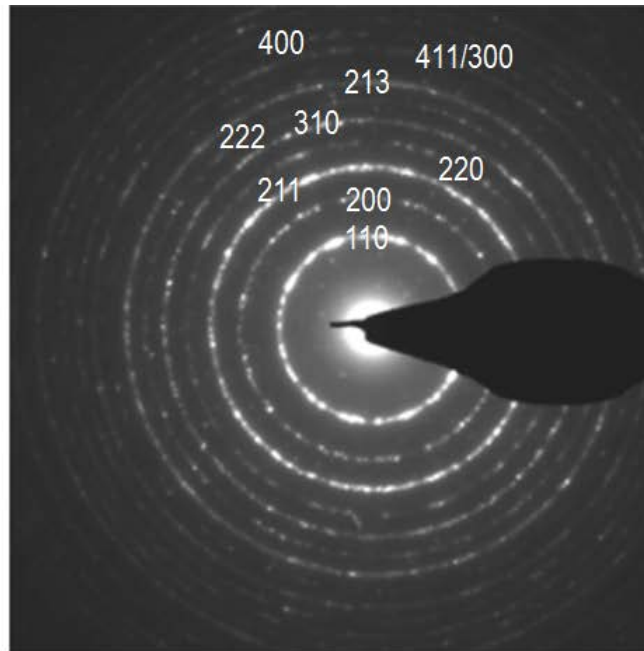
364. Flawed and Unsupported Conclusions on Texture, Variants, and Symmetry Broken Structure. Based on the eight examples Dr. Clark provides, and apparently also based on his summary of the other 100 diffraction patterns that he does not show, Dr. Clark makes the sweeping statement that “[t]hese patterns are further confirmation that the FeCo layer is BCC with (110) texture.” (*Id.* at ¶ 108.) He also states that the “microbeam diffraction imaging results confirm that the lower FeCo layer is BCC and contains variants with the expected orientation relationship for the Kurdjumov-Sachs six variant system.” (*Id.* at 115.) I disagree with both of these statements, which are not supported by Dr. Clark’s microbeam diffraction data, or any other scientifically valid data in his report.

365. In my opinion, Dr. Clark’s assertion that the lower FeCo layer in sample S0GPPC has a bcc(110) texture is not supported by his microbeam diffraction patterns and any valid and reliable scientific analysis. As explained above, most of the eight microbeam diffraction examples do not support the presence of even individual bcc(110) crystals. In addition, these eight examples provide no basis for a conclusion that bcc(110) crystals predominate throughout

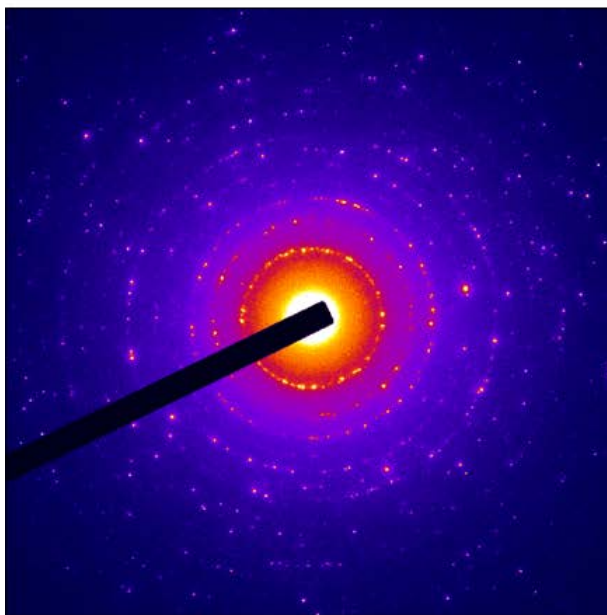
the lower FeCo layer. For example, Dr. Clark says that he took 1,600 images from this region of the sample, yet he provides images for only eight of them. Even if every one of the eight samples hand-picked by Dr. Clark was an individual bcc(110) crystal (which is not the case), there is no valid scientific basis for drawing a conclusion about the texture for this entire layer from a sample comprising no more than 0.5 percent of the layer.

366. In addition, as noted above, the presence of crystals with orientations other than (110) shown by Dr. Clark's purported analysis of the 100 other microbeam diffraction images that he apparently took of the lower FeCo layer of sample S0GPPC is inconsistent with the bcc(110) crystals predominating in the FeCo layer and with the lower FeCo layer forming a symmetry broken structure, because it means that the lower FeCo layer has crystals that are not bcc(110) and therefore not part of a six-variant system.

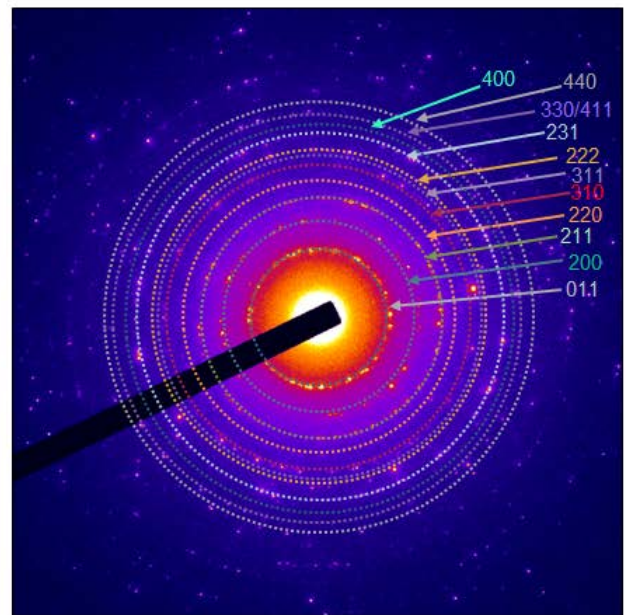
367. Other data, including Dr. Clark's diffraction pattern testing and my own testing, also show that the magnetic layers in Seagate's [REDACTED] write heads contain bcc crystals other than (110). In particular, both Dr. Clark and I took diffraction ring patterns of samples of Seagate's [REDACTED] write heads. (*See, e.g.*, Clark at ¶ 57 and Fig. 19.) I indexed the rings for both Dr. Clark's and my ring patterns, which I have reproduced below, with Dr. Clark's ring diffraction pattern shown and indexed above, and mine shown below left and indexed on the below right:



Clark, Figure 19



Dr. Stach Measurement

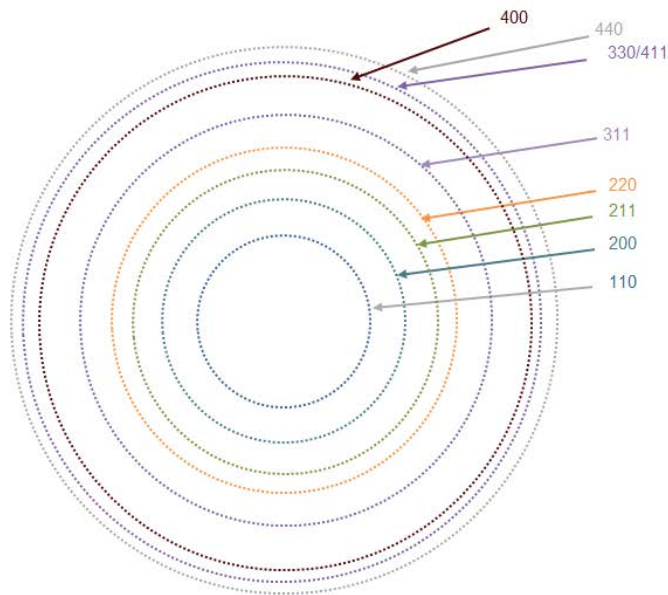


Dr. Stach Measurement and Indexing

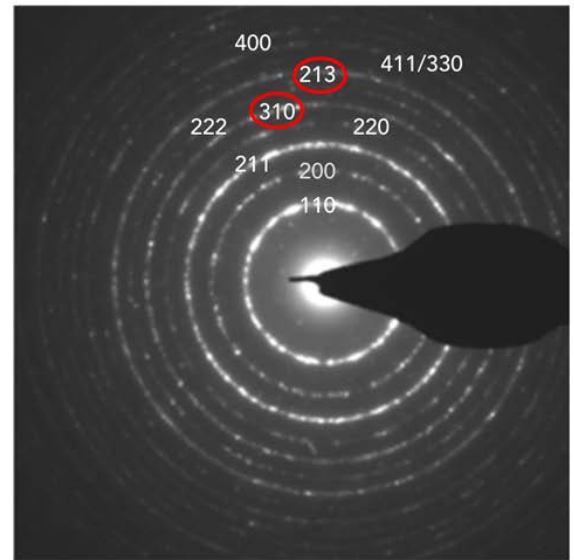
368. This data shows that there are orientations other than (110). In particular, there is strong intensity from the 310 ring, and weaker 222 and 213 rings are also present. The fact that there is strong diffraction from the {310} family of planes means that there are grains oriented along the $\langle 100 \rangle$, $\langle 013 \rangle$, and/or $\langle 113 \rangle$ orientations. This can be shown by the fact that the 310 spot appears in the bcc standard diffraction patterns for the $\langle 100 \rangle$, $\langle 013 \rangle$, and $\langle 113 \rangle$ zone axes.

Most likely, these additional grains are $\langle 100 \rangle$ oriented, as that orientation has a relatively low energy surface, second only to $\{110\}$. (See, e.g., L. Vitos, A.V. Ruban, H.L. Skriver, and J. Kollár, “The Surface Energy of Metals,” *Surface Science* 411 (1998), Table 5.)

369. To demonstrate this more clearly, I have set forth below on the left a simulated diffraction ring pattern that would appear for a material that had only (110) grains, and on the right the actual diffraction pattern for the sample from Dr. Clark’s report. As can be seen below, the 310 and 213 rings are present in the data in the ring pattern on the right, which should *not* be the case if the material had only (110) grains (which is the ring pattern shown on the left):

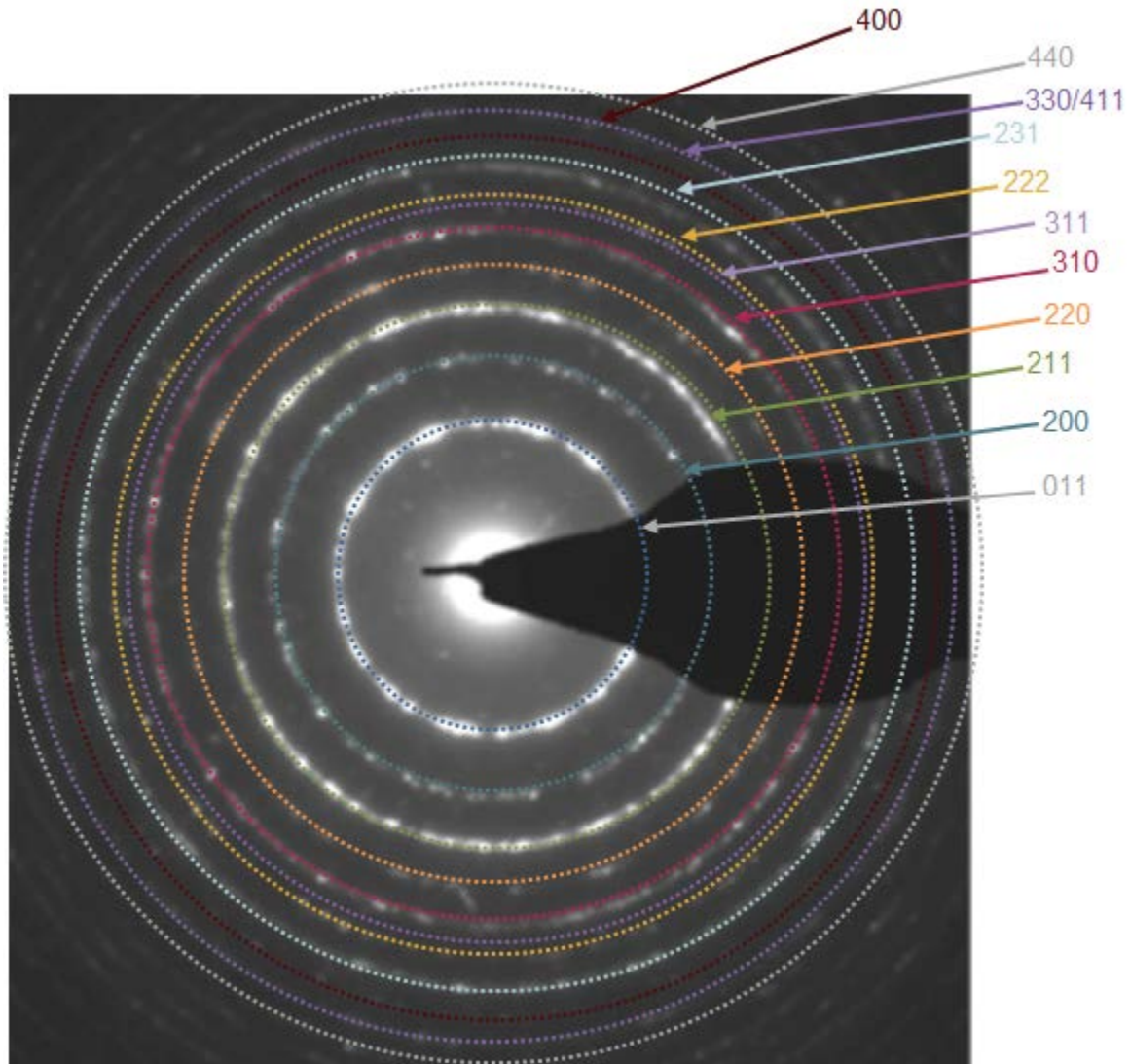


bcc(110) Out of Plane Orientation
and Randomly Oriented In Plane



Clark, Figure 19

370. Next, I provide an overlay of a bcc pattern that is randomly oriented out of plane – *i.e.* one that does not have bcc(110) texture – on Dr. Clark’s from Figure 19 of his report:



371. From this image, it is clear that the 310 and 213 reflections are present, explaining the additional rings. I note that the actual data does not present perfectly round rings, indicative of an astigmatism in the intermediate / projector lens system of the microscope that was not properly corrected prior to the image acquisition. The presence of these two rings indicates the significant presence of directions other than bcc(110), and is inconsistent with Dr. Clark's contention that the FeCo layer is bcc(110) textured. It also is inconsistent with the FeCo layer forming a symmetry broken structure, which requires a six-variant system where such variants can only be bcc(110) crystals.

372. Dr. Clark's opinion is further undercut by his dark-field area fraction analysis, which I discuss below. In particular, the data from Dr. Clark's area fraction analysis further

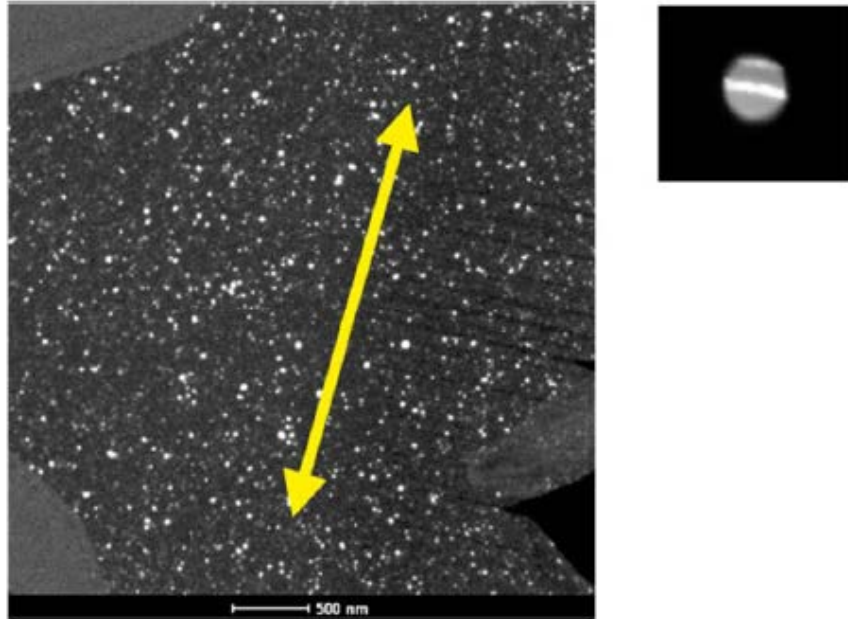
confirms that the FeCo layer contains a substantial portion of non-(110) crystals, which means that the layer is not part of a six-variant system and does not form a symmetry broken structure.

373. In my opinion, Dr. Clark's assertion that the lower FeCo layer in sample S0GPPC contains variants with the expected orientational relationship for the Kurdjumov-Sachs six-variant system is not supported by any scientifically valid and reliable data or analysis. As noted above, in order to form a six-variant system and a symmetry broken structure, the bcc(110) crystals in the overlying layer must be one of six possible variants with particular orientations *relative to* an underlying (111) hexagonal crystal from a (111) textured hexagonal atomic template. Therefore, in order to identify a variant, one must identify not only the overlying bcc(110) crystal, but the underlying (111) hexagonal crystal on which it was grown and determine the orientation of the overlying bcc(110) crystal relative to the underlying (111) hexagonal crystal. Dr. Clark has not shown, or even attempted to show, the presence of any such (111) hexagonal crystals from his microbeam diffraction analysis. None of the microbeam diffraction images he provides corresponds to a (111) hexagonal crystal. Accordingly, there is no data that remotely supports Dr. Clark's assertion that the bcc(110) crystals that he purports to identify for the lower FeCo layer of sample S0GPPC in his microbeam diffraction analysis are one of the six possible variants from a six-variant system and form the symmetry broken structure of the '988 Patent. In addition, because the evidence clearly establishes the presence of a substantial number of non-(110) crystals in the FeCo layer, it cannot possibly be part of a six-variant system and form a symmetry broken structure.

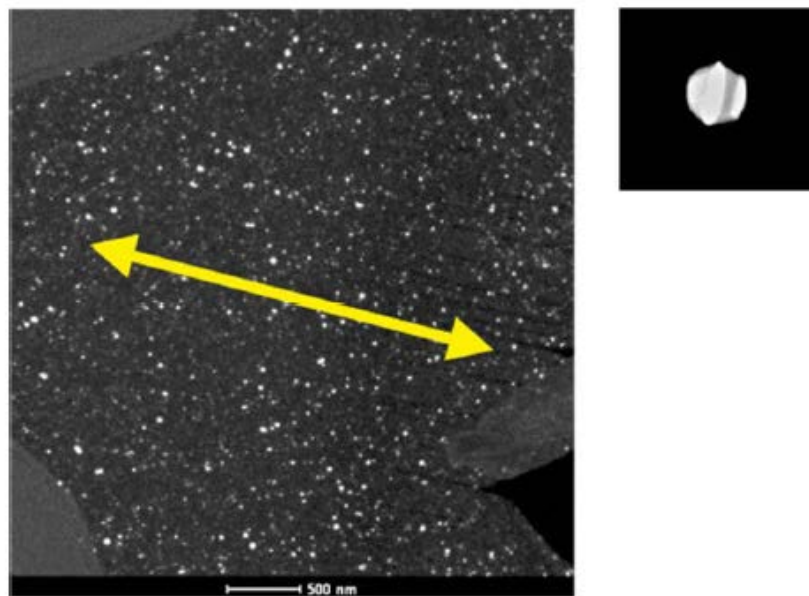
b. Flawed and Unsupported Conclusions Based on Dark Field Images

374. I next address Dr. Clark's dark field images. Dr. Clark apparently took these images from sample S0GPPC from the same area of the write head where the microbeam diffraction patterns were taken. (Clark at ¶ 116.)

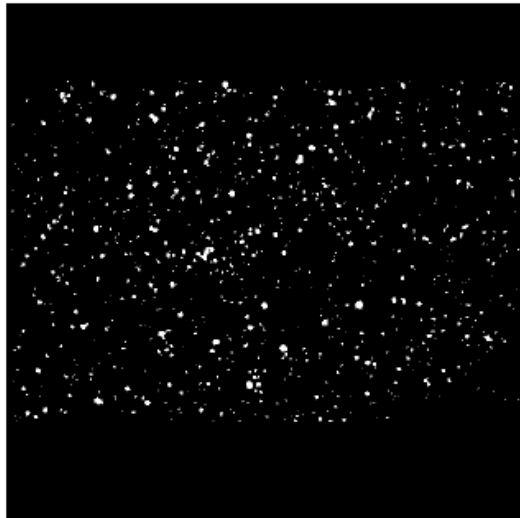
375. Dr. Clark states that in this area the sample was aligned so that the area in which the images were taken are parallel to the tip of the sample within a rotation of 10 degrees of one another. (*Id.*) Dr. Clark states that he then used a small objective aperture to enclose a segment of the {200} diffraction ring, from which a dark field image in the area of the lower FeCo layer was obtained. (*Id.* at ¶ 117.) He states that the crystallites from this segment of the {200} diffraction ring show up as the bright spots in Figure 54, which I have reproduced below:



376. Dr. Clark states that the yellow arrow in Figure 54 (shown above) allegedly points in the direction of the objective aperture from the center of the diffraction, so that the bright crystallites allegedly “have their $\langle 200 \rangle$ directions aligned parallel to the arrow,” which purportedly is “perpendicular to the long axis of the write head.” (*Id.*) Dr. Clark next states that, in contrast, an image taken at roughly 90 degrees to the position of the yellow arrow in Figure 54 produced an image with significantly fewer illuminated crystallites. (*Id.* at ¶ 118.) He shows this in Figure 55, which I have reproduced below from his report:

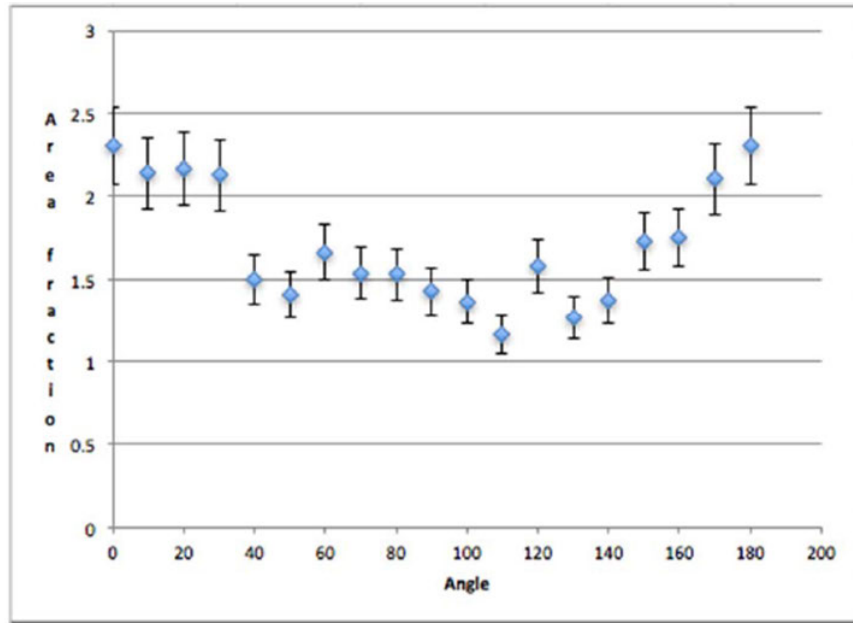


377. Dr. Clark then states that this procedure was repeated at 10-degree intervals around the {200} segment of the diffraction ring in at least a 180-degree rotation, which produced dark field images from this portion of the ring similar to those shown in Figures 54 and 55. (*Id.* at ¶ 119.) To analyze these images, Dr. Clark states that a large area of the dark field image was separated as shown in Figure 56 of his report. (*Id.*) He goes on to say that a “standard stereological computer program,” in this case ImageJ, was used to analyze these images. For each image, he states that a threshold was applied to the isolated area to produce a binary black and white image, as shown in Figure 57 of his report. (*Id.* at ¶ 120.) I have reproduced Figure 57 below:



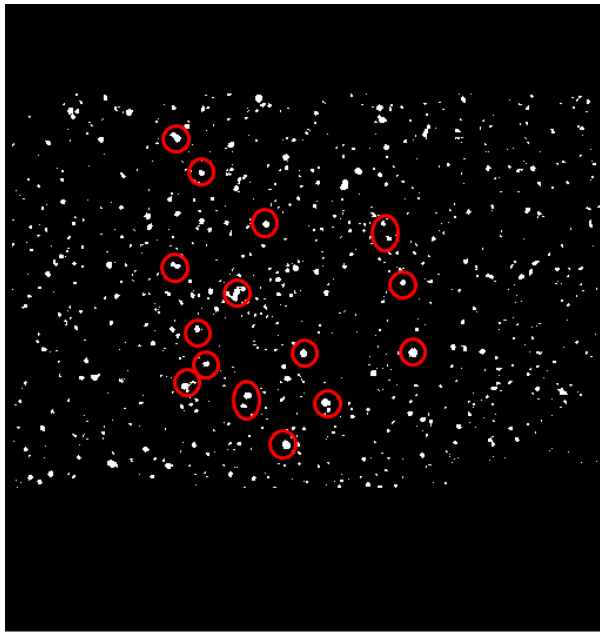
378. Using the ImageJ software, Dr. Clark states that he sought to measure the fraction of the crystallites that are white, namely, “the area fraction of crystallites that scatter into the objective aperture at that particular position.” (*Id.* at ¶ 121.) He then added the area fractions for each of the angles he analyzed at 10-degree increments and tabulated them in a table and graphed them in Figure 59. (*Id.* at ¶ 122.) I have reproduced both Table 1 and the graph from Figure 59 below—shown side-by-side:

Angle	%Area
0	2.3
10	2.137
20	2.163
30	2.129
40	1.501
50	1.404
60	1.661
70	1.533
80	1.527
90	1.421
100	1.362
110	1.156
120	1.576
130	1.269
140	1.372
150	1.724
160	1.748
170	2.103
180	2.306

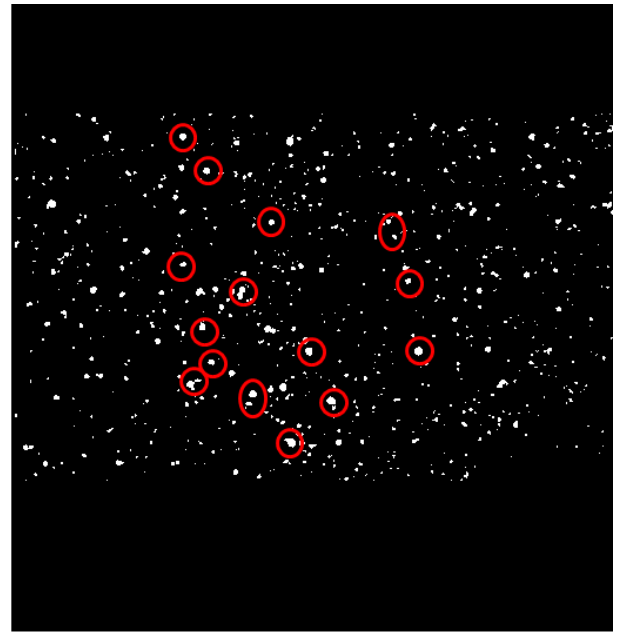


379. I note that Dr. Clark does not provide many details relating to how he conducted his dark field imaging arrived at the data he includes in Table 1 and Figure 59 of this report. In particular, Dr. Clark does not provide information about what settings and thresholds he chose to produce his binary black and white images, the specific aperture size he used, how he ensured the aperture was focused solely on the {200} segment, or how he chose his error range, which he has set at 10 percent for each measurement. The results may depend greatly on these parameters, yet no information is provided about them by Dr. Clark.

380. In addition, I note that there are serious issues with Dr. Clark's testing methodology that render his data inaccurate. For example, Dr. Clark counts some of the crystallites twice, which should not occur if the testing was performed correctly. An example of this can be seen below, where the same crystallites appear and are being counted at two different angles:



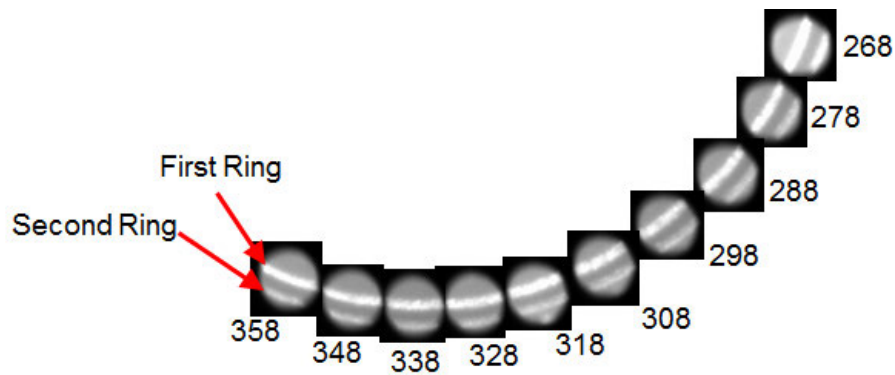
S0GPPC – 168-1



S0GPPC – 178-1

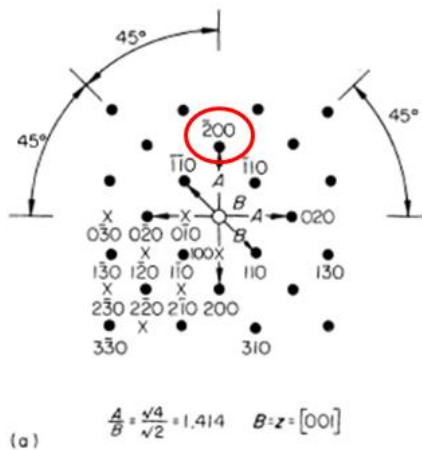
381. As can be seen above, all of the crystallites circled in red light up at both 168 degrees and 178 degrees. This double-counting, which is present in the majority of the images for each angle, means that Dr. Clark's data is inaccurate and overstates the population of crystallites at the angles where there is double-counting.

382. Similarly, I note that Dr. Clark includes both data for 0 degrees and data for 180 degrees, when one of those measurements should be excluded if he is purporting to show data across a 180-degree range. I also note that Dr. Clark appears to be capturing data from rings other than the 200 ring, as can be seen in Figures 54 and 55 of his report, both of which show multiple rings within the aperture. Examining all of the apertures from Dr. Clark's Appendix C clearly shows that two rings were captured within the aperture in all of Dr. Clark's dark field images. In the illustration shown below, I have arranged the apertures in order and next to each other to make it more apparent that they capture both a first ring (presumably {200}) and a second ring (presumably {211}):



383. All of these issues raise serious questions regarding the methodology used by Dr. Clark and renders the data unreliable.

384. The goal of Dr. Clark's analysis apparently was to show that there are different amounts of crystallites oriented with their $\langle 200 \rangle$ directions perpendicular to the long axis of the write head in the area of the sample where images were taken. (*Id.* at ¶ 123.) Dr. Clark does not explicitly state, however, why he chose to focus on these crystallites, as they would include crystals whose orientations are not only (110). This is because, for example, a bcc(100) crystal also will create a $\{200\}$ ring, as discussed above. This is apparent from noting that the 200 spot appears in the $\{001\}$ zone axis bcc standard diffraction pattern, indicating a bcc(100) crystal would create a 200 diffraction spot:



bcc{001} zone axis standard diffraction pattern

385. In addition, the 200 spot also shows up on the bcc $\{012\}$, $\{013\}$, $\{023\}$ and $\{014\}$ standard diffraction patterns, meaning that bcc(012), bcc(013), bcc(023), and bcc(014) textured crystals could also all be contributing to the $\{200\}$ ring in Clark's report.

386. Dr. Clark proceeds to make a number of broad and conclusory statements that are unsupported by his dark field image data and have no reliable scientific basis. Dr. Clark first repeats a statement from earlier in his report that is unrelated to his dark field image analysis. Dr. Clark simply reasserts that the grain sizes of each are roughly similar with only one or two FeCo grains per NiFe grain for the great majority of the NiFe grains. (*Id.* at ¶ 124.) As I discuss above, however, there is no reliable and valid scientific basis for Dr. Clark’s claim, which is not supported by any reliable and valid data. One cannot draw conclusions about the grain sizes of the entire lower FeCo and especially the NiFe below it from this sample based on any images provided by Dr. Clark (and certainly not from the microbeam diffraction or dark field images). Moreover, even if there were some evidence of grain sizes at particular locations, such incidental images would be insufficient to support broad generalizations about the grain sizes about the entire lower FeCo and adjacent NiFe layers.

387. Dr. Clark next makes the sweeping statement that his “dark field analysis, in conjunction with the microbeam diffraction analysis discussed above, shows that the various FeCo grains on top of the various NiFe template layer grains have members of the six-variant system preferentially aligned such that there is an unequal amount of the six variants in the FeCo layer.” (*Id.*) Once again, there is no reliable and valid scientific basis for this claim, which also is not supported by any reliable and valid data. Dr. Clark’s dark field analysis does not say anything about FeCo grains being “on top of” NiFe grains. Nor does his microbeam diffraction analysis, which does not even attempt to show the orientation of any bcc(110) crystals relative to an underlying NiFe crystal, as discussed above. In fact, as I already have noted, nowhere in Dr. Clark’s dark field image analysis, in his microbeam diffraction analysis, or anywhere else in his report does Dr. Clark show or even attempt to show the specific orientational relationships between any overlying bcc(110) FeCo grains relative to specific underlying (111) hexagonal NiFe grains (such as what is shown in Figure 5 of the ’988 Patent), which is required to determine whether a particular FeCo grain can be one of the six possible variants of the ’988 Patent. As noted above, in order to form a six-variant system, a bcc(110) crystal in the overlying FeCo layer must be one of six possible variants with a particular orientation *relative to* an underlying (111) hexagonal crystal from a (111) textured hexagonal atomic template. This means that one must identify not only the overlying bcc(110) crystal, but also the underlying (111) hexagonal crystal on which it was grown and the orientation of the overlying bcc(110)

crystal relative to the underlying (111) hexagonal crystal. Dr. Clark has not shown the presence of any such (111) hexagonal crystals from his microbeam diffraction or dark field analysis or otherwise. Therefore, in my opinion, his statement has no valid or reliable scientific basis.

388. Moreover, even if Dr. Clark had been able to show that there were bcc(110) crystals in the lower FeCo layer that were oriented over a (111) textured NiFe layer, his dark field data does not support any conclusions about the specific orientations of such crystals relative to the underlying NiFe crystals such that they are one of the only six possible variants allowed by the '988 Patent, or what the relative amounts of specific variants are. Dr. Clark simply shows relative amounts of crystals at particular angles in his sample from his dark field images that have a common $\langle 200 \rangle$ direction, but he has not shown what percentage of these for each angle is a bcc(110) crystal. As noted above, the crystals that will show up having a $\langle 200 \rangle$ direction include crystals not only with (110) orientations but also (100) and potentially other orientations. Therefore, because Dr. Clark has not determined the relative amounts of each, there is no way for him to draw a scientifically reliable and valid conclusion about what the amount of (110) crystals at each angle is, especially given the other flaws in his testing that I have noted above.

389. Furthermore, without showing the orientation of the bcc(110) crystals that are included in his measurements for each angle (of which there are 18 based on his sampling at each 10-degree interval, starting at 0 degrees), Dr. Clark at most has shown the existence of many orientations—many more than the six possible orientations allowed by the '988 Patent. If these were all “variants” within the meaning of the '988 Patent as Dr. Clark appears to incorrectly assume, this would mean that the lower FeCo layer is not a “symmetry broken structure,” because it would not consist of unequal amounts of the six variants required by the '988 Patent—it would have at least eighteen different “variants.”

390. Dr. Clark goes on to make yet another sweeping and unsupported statement by saying that, “[g]iven the relative grain sizes in the FeCo layer and NiFe template layer, there are no NiFe template grains that have six different overlying grains in the FeCo layer, let alone that each of the six different overlying grains would have equal area and each represent a different variant from the six-variant system present in the FeCo layer.” (Clark at ¶ 124.) This statement has no factual basis, much less any scientifically reliable and valid underpinnings. It is simply a conclusory assertion. As discussed above, Dr. Clark lacks valid data showing the relative grain

sizes for these layers across the entire layers, much less the specific relationship and orientation between any two layers, and certainly not anything that allows one to make assessments about variants. As I have noted, Dr. Clark has not shown, and never attempts to show, the orientation of any specific bcc(110) FeCo crystal from the lower FeCo layer of sample S0GPPC relative to an underlying (111) hexagonal crystal. Neither his FFT data nor his microbeam diffraction patterns show the presence of even a single NiFe fcc(111) crystal, much less how any such crystals are oriented with respect to any overlying FeCo bcc(110) crystals. In addition, there certainly is no valid scientific basis for drawing broad conclusions about the entire layer of each. As noted above, none of the data in Dr. Clark's report supports a finding regarding the crystal orientations within the NiFe layer as a whole, and certainly not the presence of a (111) texture. Similarly, none of the data in Dr. Clark's report shows the existence of any variant, much less the particular variants required by the '988 Patent, because Dr. Clark never provides data regarding the relative orientations of any overlying FeCo bcc(110) crystals relative to specific underlying NiFe (111) crystals from a textured atomic template. Accordingly, in my opinion, all of Dr. Clark's statements and conclusions in paragraph 124 of his report are unsupported by his data and have no reliable scientific basis.

391. Finally, the data from Dr. Clark's area fraction analysis further confirms in a dramatic way that the FeCo layer analyzed by Dr. Clark cannot possibly be part of a six-variant system and form a symmetry broken structure. Dr. Clark's analysis shows that in the 180-degree range he analyzes (which should be symmetrical for the remaining 180-degrees for the rest of the sampled area), *fewer than half* of the crystals in the FeCo layer can be bcc(110) crystals. Specifically, in Table 1 of paragraph 122 of his report, Dr. Clark calculates the percentage area of crystallites he has captured, which are from the <200> direction and purport to capture all of the bcc(110) crystals (as I have noted above, he actually is overstating this amount because there are other crystals with different orientations, namely bcc(100) crystals, that he is counting, but we will disregard that for the moment here). When these areas are totaled, they amount to 32.39% of the total area, meaning that the bcc(110) crystals comprise less than half of all of the crystals in the FeCo sample. Because the FeCo layer contains a substantial portion of non-(110) crystals, it cannot possibly be part of a six-variant system, which can consist only of bcc(110) crystals, and does not form a symmetry broken structure.

c. Other Data Not Considered by Dr. Clark

392. In addition to the flaws in Dr. Clark's analysis and conclusions described above relating to the lower FeCo layer in sample S0GPPC, I note that Dr. Clark did not consider other information and data that was or could have been available to him relating to the crystal structure of the lower FeCo layer in sample S0GPPC.

393. For example, in his report, Dr. Clark does not refer to any XRD testing he conducted, and he apparently did not consider any XRD data from any source in connection with his analysis of whether the lower FeCo layer in sample S0GPPC contains material with a (110) texture. Accordingly, I note that there is no XRD data that would support a conclusion that the lower FeCo layer in the S0GPPC sample has a bcc(110) texture.

394. I also note that, in an attempt to show the presence of bcc(110) crystals from a six-variant system in one of the samples discussed in the '988 Patent, the patent uses a pole figure measurement. (*See, e.g., '988 Patent, Fig. 14.*) Dr. Clark did not include any pole figure measurements in his report. Accordingly, I note that there is no pole figure data that would support a conclusion that the lower FeCo layer in the S0GPPC sample has only six variants.

d. Conclusion Regarding FeCo Layers

395. In view of all of the flaws in Dr. Clark's analysis that I have described above, and in view of all the evidence, it is my opinion that the conclusions drawn by Dr. Clark regarding the crystalline properties of the lower FeCo layer in sample S0GPPC lack a reliable factual and scientific basis and are based on the application of flawed and unreliable methodologies. It is also my opinion that none of the evidence I have seen supports the conclusion that the lower or upper FeCo layers in sample S0GPPC has a bcc(110) texture or forms a symmetry broken structure, and that in fact the evidence confirms that the lower FeCo layer in sample S0GPPC and the FeCo layers in general in Seagate's write-head [REDACTED] designs do *not* form a symmetry broken structure.

2. Sample S2MMMC ([REDACTED] Design)

396. In his report, Dr. Clark states that a similar TEM microbeam diffraction was performed on a region of the lower FeCo layer of sample S2MMMC as was done for sample S0GPPC. (Clark at ¶ 151.) In particular, Dr. Clark states that the microbeam diffraction was taken at the area shown by the red square in Figure 75 of his report from a sample that was

prepared where the upper FeCO/NiFe layer was removed. (*Id.*) He states that from this area represented by the red square, “1,600 diffraction patterns were obtained by scanning the electron beam incrementally area in the box.” (*Id.*) However, only a handful of these (six, to be exact) are actually included and discussed in his report.

397. Dr. Clark goes on to state that “[b]y defocusing the diffraction pattern image slightly” (as shown in Figure 76), he was able to obtain an enlarged central spot that contains an image of the portion of the sample and that, from this, he was able to confirm that the plan view sample and diffraction pattern were within an alignment of ± 10 degrees. (*Id.* at ¶ 152 and Fig. 76.) In his report, Dr. Clark then provides examples of six diffraction patterns (out of the 1,600 he took) that he says show the presence of bcc(110) crystals. He indicates these crystals by drawing yellow rectangles onto the diffraction pattern (for one example, he uses red, blue and green rectangles). Dr. Clark then goes on to provide conclusions regarding another 100 patterns taken from this area that he purportedly analyzed, although he does not include these images in his report or include his specific analysis of any of them (such as trying to draw the crystals on these images that he does for the six he actually discusses in his report).

398. In the remainder of this section of his report (*see* Clark at ¶¶ 159-167), Dr. Clark describes dark field images that he took from the plan view specimen for sample S2MMMC. He uses these images in an attempt to isolate crystals that have their $\langle 200 \rangle$ directions purportedly aligned perpendicular to the long axis of the write head sample. He then tries to calculate the area fraction of the crystals with these directions at 10-degree increments.

399. From this microbeam diffraction and dark-field testing, Dr. Clark purports to draw broad conclusions about the crystal properties of the lower FeCo layer in sample S2MMMC (he does not analyze the upper layer), the presence of bcc(110) crystals, the distribution of such crystals, their in-plane orientations, and whether they are part of a six-variant system. For the reasons I explain below, it is my opinion that the methodology applied by Dr. Clark to reach his conclusions about the presence of bcc(110) crystals, their relative amounts, and their orientations, and whether they are part of a six-variant system is flawed and unreliable, and that his conclusions are not supported by any valid scientific data. I address separately below the microbeam diffraction testing and the dark-field testing performed by Dr. Clark and the conclusions he reaches.

a. Flawed and Unsupported Conclusions Based on Microbeam Diffraction Data

400. Flawed and Unsupported Conclusions Regarding the Presence of bcc(110) Crystals. In paragraphs 153-158 and Figures 77-80 of his report, Dr. Clark explains that individual frames from the set of 1,600 microbeam diffraction images that he captured “may contain diffraction patterns from one, two, or sometimes more separate FeCo crystallites.” (*Id.* at ¶ 153.) He then states that “[t]ypical single crystal patterns for this analysis” are shown in Figure 77 of his report, and that “[t]hese patterns are readily identified and indexed as patterns in the (110)_{BCC} direction.” (*Id.*) He states that this was confirmed by measurement of the ratio of the sides of the rectangles, which were “found to be $5.4:3.8 = 1:\sqrt{2}$, as required.” (*Id.*)

401. Dr. Clark provides a total of six examples of diffraction patterns that allegedly show the presence of individual bcc(110) crystals from the lower FeCo layer of the plan view specimen from sample S2MMC. For each of the six images shown in his report, Dr. Clark draws yellow boxes (and in one case, red, blue and green boxes) (“measured directly in Keynote” software from Apple (*see id.* at ¶ 154)) around the portions of the diffraction pattern that he contends show the presence of a bcc(110) crystal.

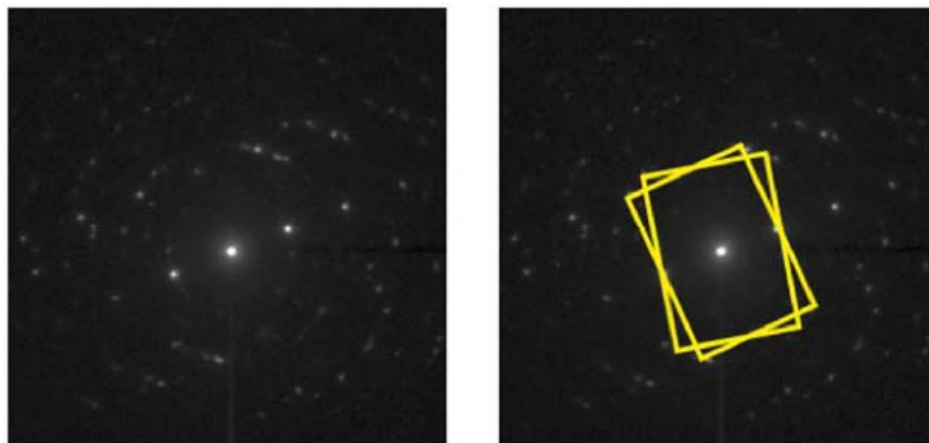
402. Apart from his statement noted above regarding the required ratio of the sides to establish the presence of a bcc(110) crystal, Dr. Clark does not explain or describe the particular methodology he used to draw his boxes or to calculate the angles that he includes in the annotations in his report that form the basis for his conclusion. At most, he suggests that the microbeam diffraction patterns “visually identify as standard (110)_{BCC} patterns.” (*Id.* at caption to Fig. 77.) He does not show any indexing of these patterns, however, or describe the basis on which he selected certain spots for his annotations, how he calculated the ratios between the sides of the rectangles he drew, or the method by which he derived his angles (other than nominally for two of his examples). He frequently relies on alleged “spots” that are not clearly discernable, and ignores spots that are inconsistent with his conclusions.

403. In my opinion, Dr. Clark’s methodology for drawing the boxes and calculating the angles purporting to identify individual bcc(110) crystals from the red-box region does not support his conclusion that it shows the presence of a bcc(110) crystal for most of the examples he discusses in this section of his report. Furthermore, his six examples provide no scientific

basis for the broad conclusions he draws about the crystallographic structure of the lower FeCo layer in sample S2MMMC.

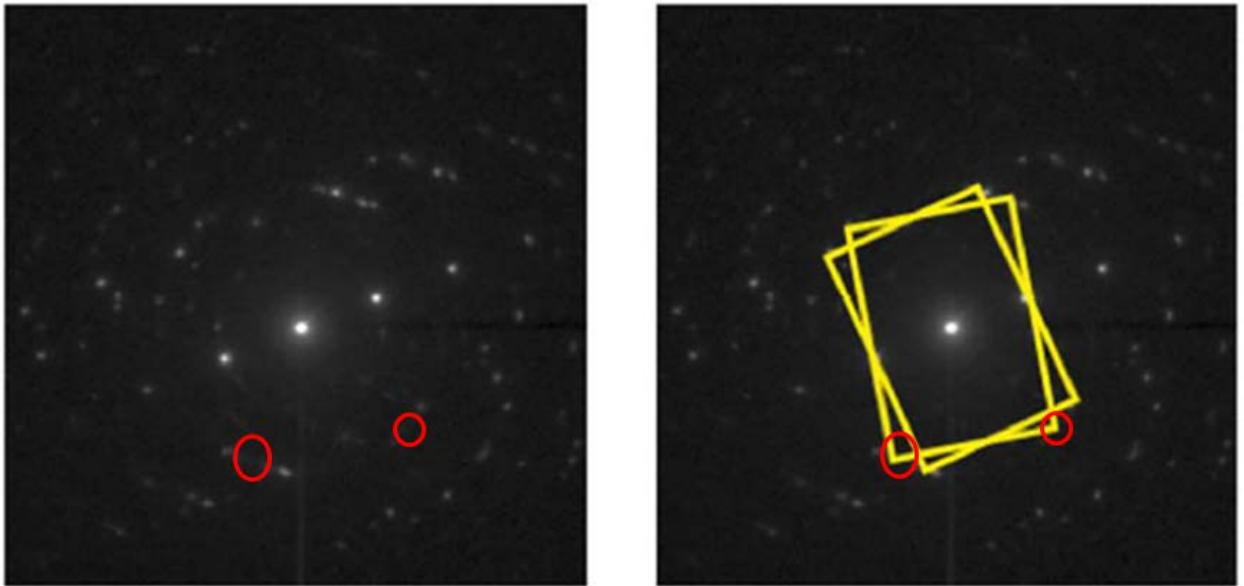
404. To accurately identify the presence of bcc(110) crystals in TEM microbeam diffraction patterns, one needs to clearly identify discernable spots (including the appropriate bright center spot), align those spots with those that are associated with bcc(110) crystals from standard ring diffraction ring patterns, determine whether there are other diffraction spots that are inconsistent with a bcc(110) crystal, and measure the ratio of the two sides of the rectangles to confirm they match the ratio of $1:\sqrt{2}$ for a bcc(110) crystal. To accurately calculate the relative angle between two alleged crystals, one needs to extend either the two longer or two shorter sides of each of the crystals being compared and then accurately measure the angle between them. Because Dr. Clark does not clearly follow this approach, many of his results are flawed, as I explain below.

405. For example, for Figure 78 in his report, Dr. Clark states that “it shows an example diffraction pattern with two crystallites, both in the $(110)_{\text{BCC}}$ orientation, but rotated by $\sim 12^\circ$ about their common $[110]_{\text{BCC}}$ direction.” (*Id.* at ¶154.) He goes on to say that “[t]his is the separation of two variants in the Kurdjumov-Sachs orientation,” and states that “[t]he measured ratio of the sides of the motif are $1:\sqrt{2}$ as required. (*Id.*) I have reproduced Figure 78 from Dr. Clark’s below:



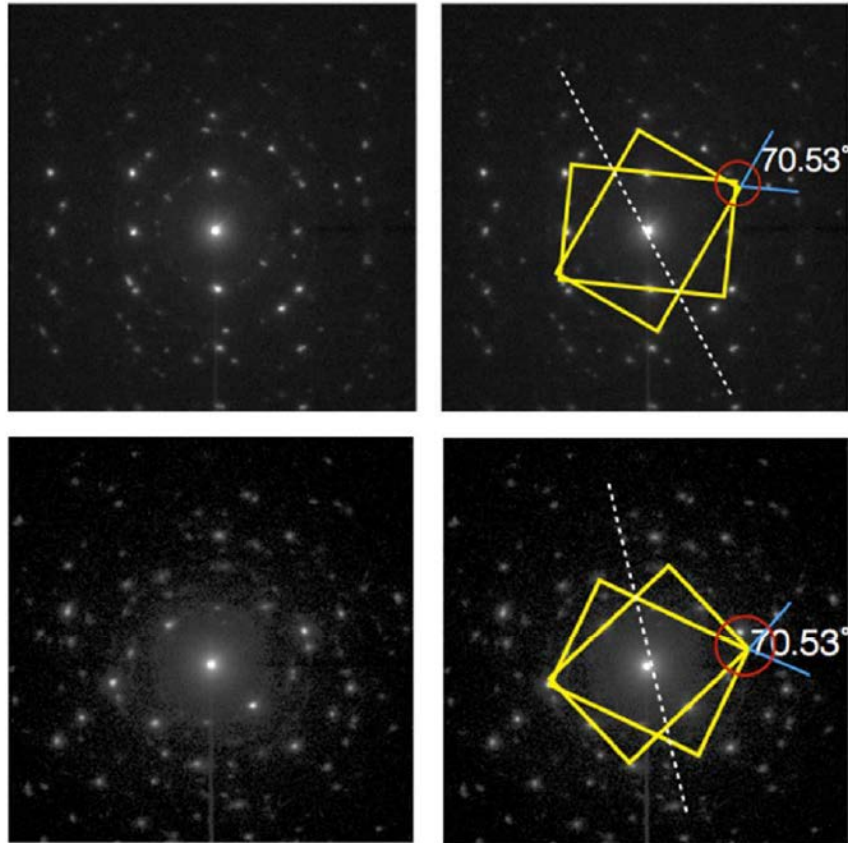
406. In my opinion, Dr. Clark’s analysis of the pattern in Figure 78 (Frame 137) is flawed because the spots he has chosen as the basis for his drawing are not discernable. Therefore, in my opinion, this pattern does not provide a reliable and valid basis for assessing

whether it shows the presence of a bcc(110) crystal. I have noted the spots that Dr. Clark purports to rely on that in my opinion are not clearly discernable with red circles below:

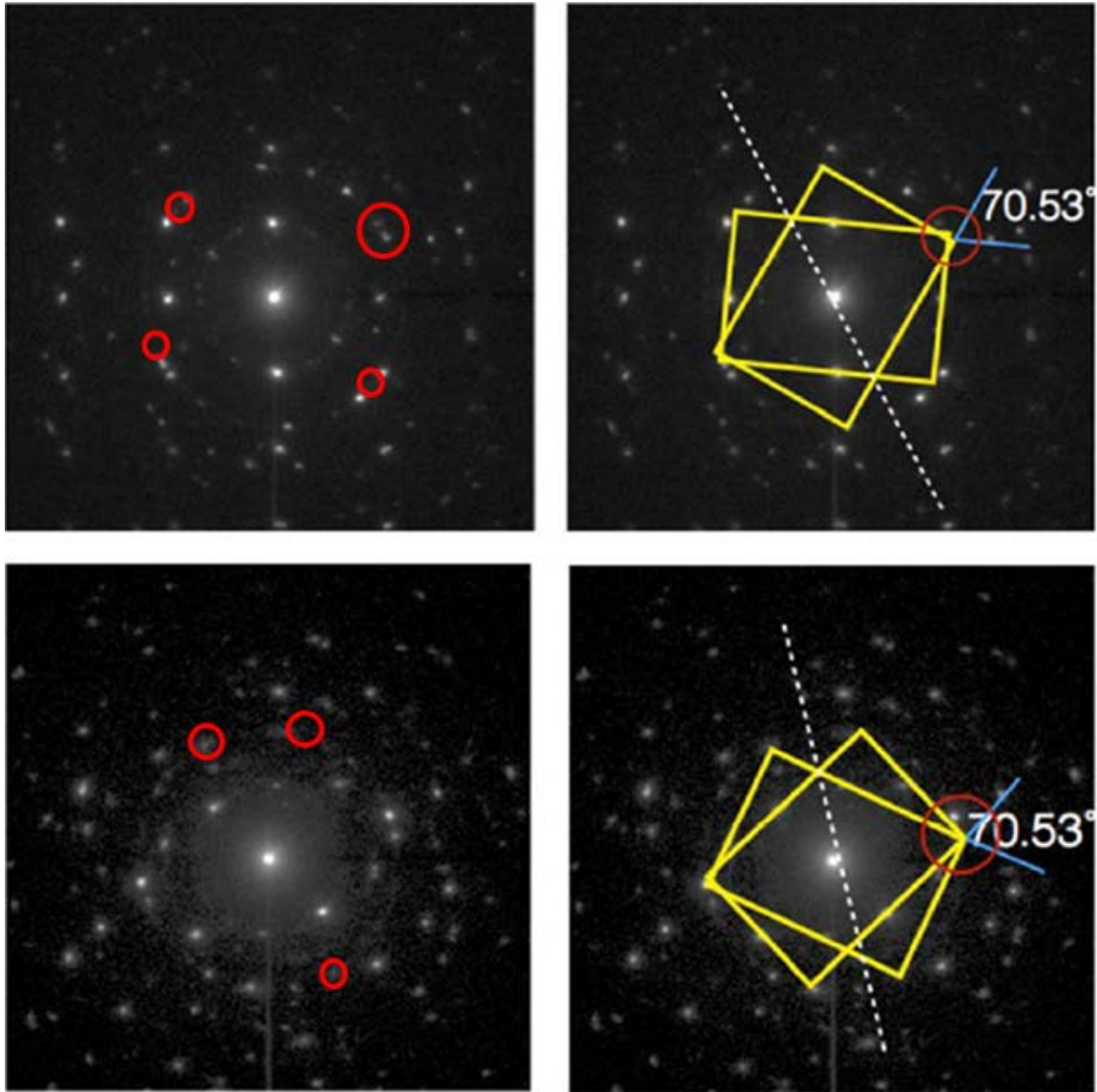


407. I also note that that Dr. Clark uses this Figure 78 as a basis for making the sweeping statement that because the two crystals he has drawn allegedly are offset from one another by an angle of approximately 9 degrees (*i.e.*, they are rotated in the plane about 12 degrees relative to one another) this shows “the separation of two variants in the Kurdjumov-Sachs orientation.” (Clark at ¶ 154.) This is simply incorrect. As I have explained above, one cannot show the existence of a particular variant without showing the orientation of the overlying crystal *relative to* the underlying crystal on which it was grown. As the ’988 Patent makes clear (and as Dr. Clark confirms elsewhere in his report, *see, e.g., id.* at ¶¶ 33-35), a variant is defined based on the orientational relationship of the “the (110) crystal plane of a bcc-d crystal in comparison to the atomic arrangement of the (111) crystal plane of a hexagonal lattice template crystal.” (’988 Patent, 13:40-43.) Therefore, the relative orientation of the two alleged bcc(110) crystals in the plane cannot be used as a basis for making judgments about whether they are part of the six-variant system required by the ’988 Patent without first showing the orientation of each relative to an underlying (111) hexagonal crystal, which may have a different in-plane orientations. Dr. Clark does not do this. In fact, as I note below, Dr. Clark has not shown the presence of any underlying (111) hexagonal crystals through his microbeam diffractions patterns.

408. The microbeam diffraction pattern in Figure 79, which purports to show the presence of two bcc(110) crystals in different frames, has similar flaws. I have reproduced Figure 79 from Dr. Clark's report below:



409. In my opinion, Dr. Clark's analysis of the patterns for the alleged bcc(110) crystals he has drawn in Figure 79 (two from Frame 120 and two from Fame 669) does not allow for his conclusion that it shows the presence of bcc(110) crystals. First, similar to Figure 78, numerous spots that Dr. Clark has chosen in Figure 79 as the basis for his drawings that are not clearly discernable. Therefore, in my opinion, these patterns do not provide a reliable and valid basis for assessing whether they show the presence of bcc(110) crystals. I have noted the spots from Frames 120 and 669 that Dr. Clark purports to rely on to draw his two crystals that are not clearly discernable with red circles below:



410. Finally, I note that that Dr. Clark once again uses this Figure 79 as a basis for making the sweeping statement that because the two crystals he has drawn allegedly are offset from one another by an angle of approximately 70.53 degrees, this shows “the separation of two variants in the Kurdjumov-Sachs orientation.” (Clark at ¶ 155.) This is simply incorrect. First, his angle is incorrect. As drawn, it is closer to 66 degrees. Second, for the same reasons I explained for Figure 78 above, one cannot show the existence of a particular variant without showing the orientation of the overlying crystal *relative to* the underlying crystal on which it was grown. Dr. Clark does not do this. In fact, as I note below, Dr. Clark has not shown the presence of any underlying (111) hexagonal crystals through his microbeam diffractions patterns.

411. I have analyzed the patterns in the other figures and provided a table below summarizing my analysis of the six examples of microbeam diffraction patterns for the lower FeCo layer in sample S2MMMC included in Dr. Clark's report:

Figure and Frames	Analysis
Figure 77 Frame 419 (upper) Frame 836 (lower)	Upper image: Some diffraction spots not clearly discernable or are not present at the expected location; no scale bars Lower image: Some diffraction spots not clearly discernable or are not present at the expected location; no scale bars
Figure 78 Frame 137	Some diffraction spots not clearly discernable or are not present at the expected location; rectangles don't actually have rotation of 12 degrees (they are 14 degrees as drawn); no scale bars; this interpretation is clearly incorrect
Figure 79 Frame 120 (upper) Frame 669 (lower)	Upper image: Some diffraction spots not clearly discernable or are not present at the expected location; angle labeled as 71.53 degrees is actually 66 degrees as drawn; no scale bars Lower image: Some diffraction spots not clearly discernable or are not present at the expected location; no scale bars
Figure 80 Frame 17	Some diffraction spots not clearly discernable or are not present at the expected location; no scale bars

412. My analysis for these six examples is contained in Exhibit G of my report.

413. Presumably, Dr. Clark chose what he considered to be the best six examples out of the 1,600 images available to him to try to show the presence of bcc(110) crystals in the lower FeCo layer of sample S2MMMC. Yet, as demonstrated above, most of his examples are flawed.

414. In addition to these examples, Dr. Clark states that he analyzed another 100 diffraction patterns taken from this area that were randomly selected out of the 1,600 total diffraction patterns. (Clark at ¶ 157.) He states that he categorized them into four categories as follows:

Category	Results
a) Showed no recognizable pattern	86
b) Showed a single {110} pattern	9
c) Showed multiple {110} patterns	0
d) Showed {110} twins	5
e) Showed a pattern other than {110}	0

415. Dr. Clark does not provide his analysis for any of these other 100 microbeam diffraction patterns that he mentions in his report, and he did not include any of the actual images in Appendix C of his report. Dr. Clark's failure to include these images is inconsistent with the basic scientific practice of showing the data on which you are basing your conclusions. Because Dr. Clark has not provided any of the data on which he allegedly basis his analysis for these 100 other diffraction patterns, it is not possible to assess whether Dr. Clark's categorization of these other 100 images is accurate. To the extent Dr. Clark used the same approach that he did for the six examples for the categorization of the patterns that he does provide in his report, then they will be flawed to the same extent as discussed above.

416. I note that Dr. Clark state in a footnote (*id.* at ¶ 157 n.23) that the numbers are influenced by the initial orientation of the sample in the microscope that may affect the number of {110}_{BCC} patterns that will be observed. He says, however, that this does not affect his opinions, including his view that "the FeCo layer is predominantly (110)_{BCC}." (*Id.*) Once again, Dr. Clark does not provide any details on how these images were created or provide the images themselves. Accordingly, it is not possible to assess his approach. However, to the extent he purports to rely on this data at all, as noted below, it is inconsistent with his conclusion about the texture of the lower FeCo layer in sample S2MMMC.

417. In particular, according to Dr. Clark, 86 percent of these additional 100 crystals did not have a recognizable pattern. The alleged presence of these other unrecognizable crystals is inconsistent with the bcc(110) crystals predominating in the FeCo layer and with the lower FeCo layer forming a symmetry broken structure, because it means that the lower FeCo layer has crystals that are not bcc(110) and therefore not part of a six-variant system. (*E.g.*, '988 Patent at 12:66-13:2 ("this invention deals with a structure to achieve uniaxial magnetocrystalline orientation via the use of the (110) texture of body centered cubic (BCC) or body centered cubic derivative crystal thin film structures.").)

418. Furthermore, there is clear evidence in the patterns that he does provide for orientations other than bcc 110, as shown below. In order for the pattern to show only (110) crystals, all of the spots would have to lie upon the yellow rings that I have added in the image shown below on the right. Specifically, I added the set of rings that would appear from a bcc(110) textured sample, and I aligned the innermost yellow ring, which is 110, with the spots lying in the middle of the long side of Dr. Clark's yellow rectangle. As shown below, many of

the spots do not lie on the yellow rings I have added. Thus, there must be grain orientations that are not associated with a 110 texture in the layer. I have performed similar analyses (shown in Exhibit G), and other of Dr. Clark's examples also have numerous spots inconsistent with a bcc 110 texture.

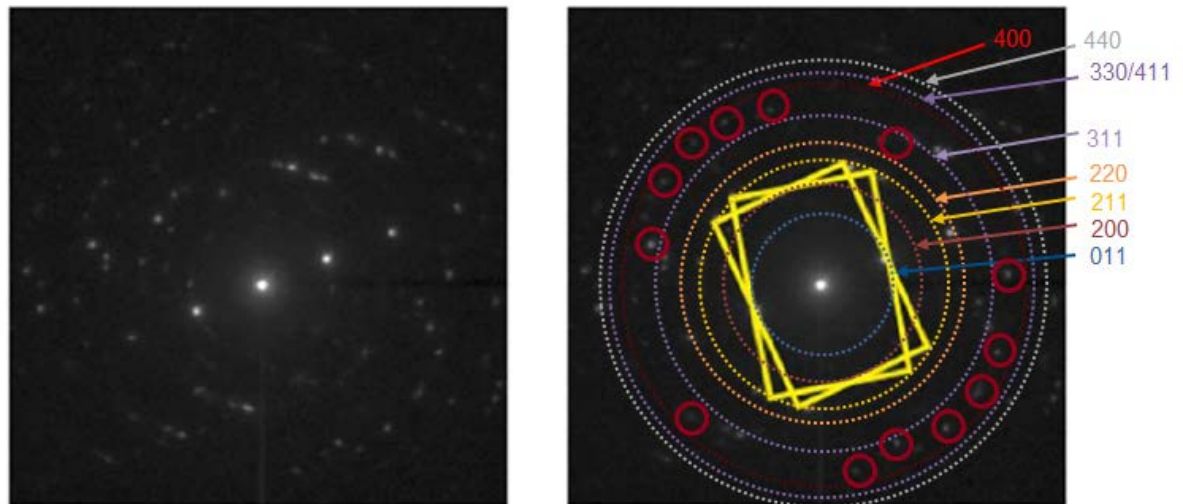


Figure 78: Two crystallites, both in the $(110)_{\text{BCC}}$ orientation, frame 137, rotated by $\sim 12^\circ$ about their common $[110]_{\text{BCC}}$ direction.

Clear spots (red circles) are at locations not consistent with 110_{BCC} orientation

419. Flawed and Unsupported Conclusions on Texture, Variants, and Symmetry Broken Structure. Based on the six examples he shows, and apparently also based on his summary of the other 100 diffraction patterns that he does not show, Dr. Clark makes the sweeping statement that “[t]hese patterns are further confirmation that the FeCo layer is BCC with (110) texture.” (*Id.* at ¶ 153.) He also uses these images as purported examples of showing that the lower FeCo layer is BCC and contains variants from the Kurdjumov-Sachs six-variant system. (*E.g., id.* at ¶ 154, 155. I disagree with both of these statements, which are not supported by Dr. Clark’s microbeam diffraction data, or any other scientifically valid data in his report.

420. In my opinion, Dr. Clark’s assertion that the lower FeCo layer in sample S2MMC has a bcc(110) texture is not supported by any of his microbeam diffraction patterns and any valid and reliable scientific analysis. As explained above, most of the six microbeam diffraction examples do not support the presence of even individual bcc(110) crystals. In addition, these six examples provide no basis for a conclusion that bcc(110) crystals predominate

throughout the lower FeCo layer. For example, Dr. Clark says that he took 1,600 images from this region of the sample, yet he provides images for only six of them. Even if every one of the six samples hand-picked by Dr. Clark was an individual bcc(110) crystal (which is not the case), there is no valid scientific basis for drawing a conclusion about the texture for this entire layer from a sample comprising no more than 0.375 percent of the layer.

421. In addition, as noted above, the presence of crystals with orientations other than (110) shown by Dr. Clark's purported analysis of the 100 other microbeam diffraction images that he apparently took of the lower FeCo layer of sample S0GPPC is inconsistent with the bcc(110) crystals predominating in the FeCo layer and with the lower FeCo layer forming a symmetry broken structure, because it means that the lower FeCo layer has crystals that are not bcc(110) and therefore not part of a six-variant system.

422. As shown earlier, other data, including Dr. Clark's diffraction pattern testing and my own testing, also show that the magnetic layers in Seagate's [REDACTED] write heads contain bcc crystals other than (110), as described above. This is further confirmed, as I discuss below, by the data from Dr. Clark's area fraction analysis, which shows that the majority of crystals are *not* bcc(110) in the FeCo layer.

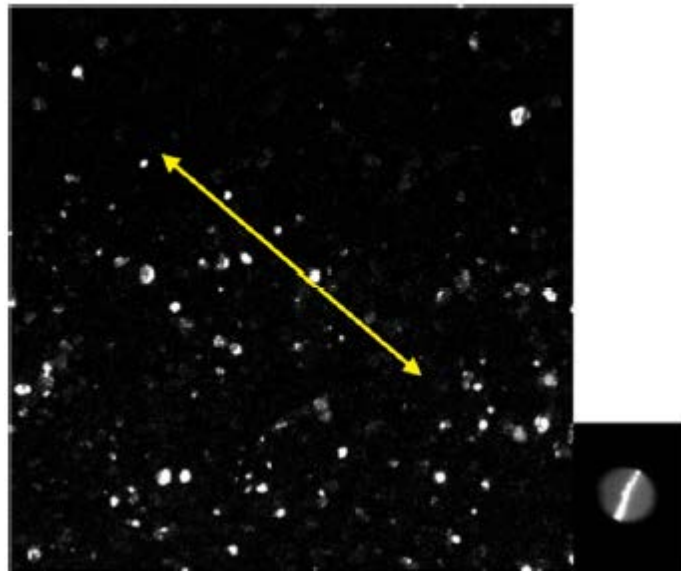
423. In my opinion, Dr. Clark's assertion that the lower FeCo layer in sample S2MMMC contains variants with the orientational relationship for the Kurdjumov-Sachs six-variant system is not supported by any scientifically valid and reliable data or analysis. As noted above, in order to form a six-variant system, the bcc(110) crystals in the overlying layer must be one of six possible variants with particular orientations *relative to* an underlying (111) hexagonal crystal from a (111) textured hexagonal atomic template. Therefore, in order to identify a variant, one must identify not only the overlying bcc(110) crystal, but the underlying (111) hexagonal crystal on which it was grown and determine the orientation of the overlying bcc(110) crystal relative to the underlying (111) hexagonal crystal. Dr. Clark has not shown, or even attempted to show, the presence of any such (111) hexagonal crystals from his microbeam diffraction analysis. None of the microbeam diffraction images he provides corresponds to a (111) hexagonal crystal. Accordingly, there is no data that remotely supports Dr. Clark's assertion that the bcc(110) crystals that he purports to identify for the lower FeCo layer of sample S2MMMC in his microbeam diffraction analysis are one of the six possible variants from a six-variant system and form the symmetry broken structure of the '988 Patent. In addition,

because the evidence clearly establishes the presence of a substantial number of non-(110) crystals in the FeCo layer, it cannot possibly be part of a six-variant system and form a symmetry broken structure.

b. Flawed and Unsupported Conclusions Based on Dark Field Images

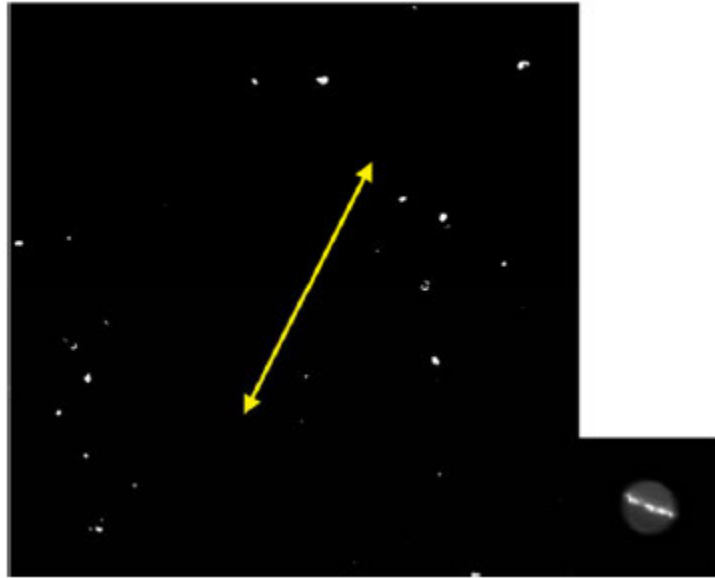
424. I next address Dr. Clark's dark field images. Dr. Clark apparently took these images from sample S2MMMC from the same area of the write head where the microbeam diffraction patterns were taken. (Clark at ¶ 159.)

425. Dr. Clark states that in this area the sample was aligned so that the area in which the images were taken are parallel to the tip of the sample within a rotation of 10 degrees of one another. (*Id.*) Dr. Clark states that he then used a small objective aperture to enclose a segment of the {200} diffraction ring, from which a dark field image in the area of the lower FeCo layer was obtained. (*Id.* at ¶ 160.) He states that the crystallites from this segment of the {200} diffraction ring show up as the bright spots in Figure 82, which I have reproduced below:

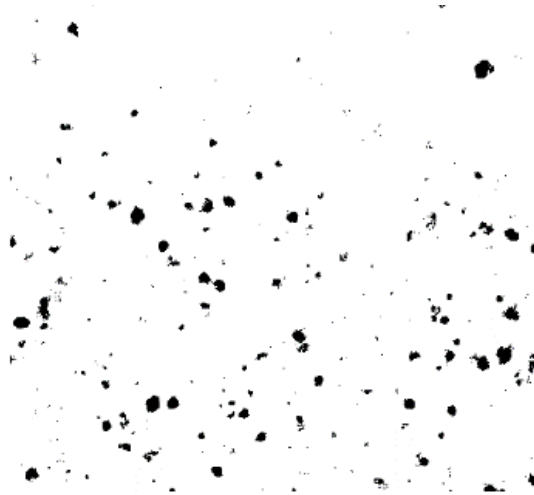


426. Dr. Clark states that the yellow arrow in Figure 82 (shown above) allegedly points in the direction of the objective aperture from the center of the diffraction, so that the bright crystallites allegedly “have their <200> directions aligned parallel to the arrow,” which purportedly is “perpendicular to the long axis of the write head.” (*Id.*) Dr. Clark next states that, in contrast, an image taken at roughly 90 degrees to the position of the yellow arrow in Figure 82

produced an image with significantly fewer illuminated crystallites. (*Id.* at ¶ 161.) He shows this in Figure 83, which I have reproduced below from his report:

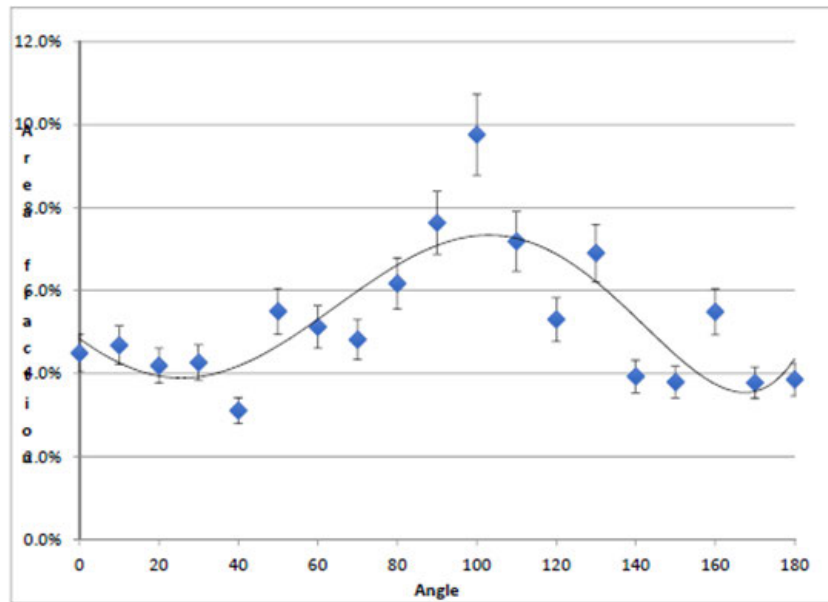


427. Dr. Clark then states that this procedure was repeated at 10-degree intervals around the {200} segment of the diffraction ring in at least a 180-degree rotation, which produced dark field images from this portion of the ring similar to those shown in Figures 54 and 55. (*Id.* at ¶ 162.) To analyze these images, Dr. Clark states that a large area of the dark field image was separated as shown in Figure 84 of his report. (*Id.*) He goes on to say that a “standard stereological computer program,” in this case ImageJ, was used to analyze these images. For each image, he states that a threshold was applied to the isolated area to produce a binary black and white image, as shown in Figure 85 of his report. (*Id.* at ¶ 120.) I have reproduced Figure 85 below:



428. Using the ImageJ software, Dr. Clark states that he sought to measure the fraction of the crystallites that are white, namely, “the area fraction of crystallites that scatter into the objective aperture at that particular position.” (*Id.* at ¶164.) He then added the area fractions for each of the angles he analyzed at 10-degree increments and tabulated them in a table and graphed them in Figure 87. (*Id.* at ¶ 165.) I have reproduced both Table 2 and Figure 87 below—shown side-by-side:

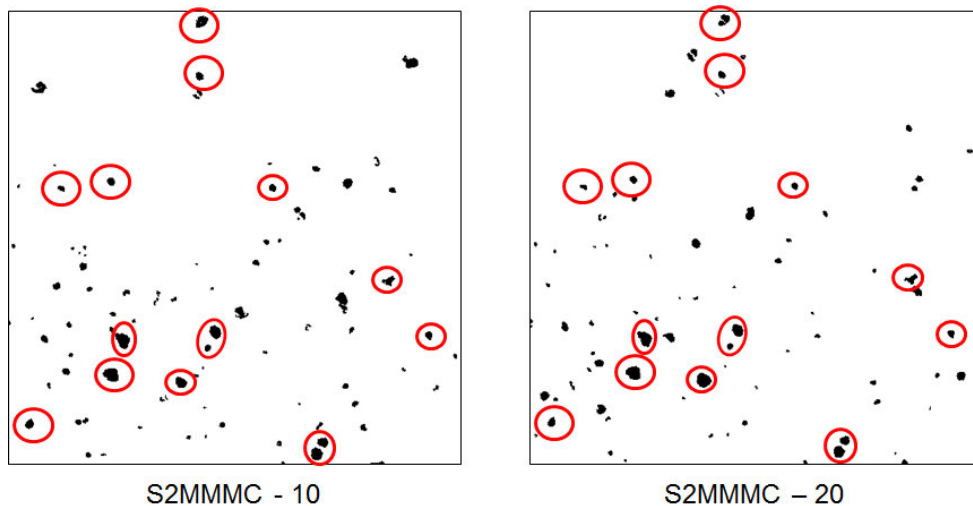
Angle	%Area
0	1.391
10	1.449
20	1.297
30	1.321
40	0.9624
50	1.703
60	1.586
70	1.492
80	1.911
90	2.364
100	3.022
110	2.225
120	1.642
130	2.139
140	1.217
150	1.175
160	1.699
170	1.17
180	1.194



429. I note that Dr. Clark does not provide many details relating to how he conducted his dark field imaging arrived at the data he includes in Table 2 and Figure 87 of this report. In particular, Dr. Clark does not provide information about what threshold he chose to produce his binary black and white images, the specific aperture size he used, how he ensured the aperture

was focused solely on the $\{200\}$ segment, or how he chose his error range, which he has set at 10 percent for each measurement. The results may depend greatly on these parameters, yet no information is provided about them by Dr. Clark.

430. In addition, I note that there are serious issues with Dr. Clark's methodology and his testing that render his data inaccurate. For example, it appears that Dr. Clark counts some of the crystallites twice, which should not occur if the testing was performed correctly. An example of this can be seen below, where the same crystallites appear and are being counted at two different angles:



431. As can be seen above, all of the crystallites circled in red light up at both 10 degrees and 20 degrees. This double-counting, which is present in the majority of the images for each angle, means that Dr. Clark's data is inaccurate and overstates the population of crystallites at the angles where there is double-counting.

432. Similarly, I note that Dr. Clark includes both data for 0 degrees and data for 180 degrees, when one of those measurements should be excluded if he is purporting to show data across a 180-degree range. Furthermore, Dr. Clark collected different data for the crystallites at 0 degrees and 180 degrees. The data at those two points should be the same, because they are symmetrical. But Dr. Clark's chart shows a difference between them. All of these issues raise serious questions regarding the methodology used by Dr. Clark and renders the data unreliable.

433. The goal of Dr. Clark's analysis apparently was to show that there are different amounts of crystallites oriented with their $\langle 200 \rangle$ directions perpendicular to the long axis of the write head in the area of the sample where images were taken. (*Id.* at ¶ 166.) Dr. Clark does not

explicitly state, however, why he chose to focus on these crystallites, as they would include crystals whose orientations are not (110) and have different orientations. This is because, for example, a bcc(100) crystal will create a {200} ring, as discussed above. (*See supra* ¶¶ 388-389.) From this dark field data, Dr. Clark proceeds to make a number of broad and conclusory statements that are unsupported by his data and have no reliable scientific basis.

434. Dr. Clark first repeats a statement from earlier in his report that is unrelated to his dark field image analysis. Dr. Clark simply reasserts that the grain sizes of each are roughly similar with only one or two FeCo grains per NiFe grain for the great majority of the NiFe grains. (Clark at ¶ 167.) As I discuss above, however, there is no reliable and valid scientific basis for Dr. Clark's claim, which is not supported by any reliable and valid data. One cannot draw conclusions about the grain sizes of the entire lower FeCo and especially the NiFe below it from this sample based on any images provided by Dr. Clark (and certainly not from the microbeam diffraction or dark field images). Moreover, even if there were some evidence of grain sizes at particular locations, such incidental images would be insufficient to support broad generalizations about the grain sizes throughout the entire lower FeCo and adjacent NiFe layers.

435. Dr. Clark next makes the sweeping statement that his "dark field analysis, in conjunction with the microbeam diffraction analysis discussed above, shows that the various FeCo grains on top of the various NiFe template layer grains have members of the six-variant system preferentially aligned such that there is an unequal amount of the six variants in the FeCo layer." (*Id.*) Once again, there is no reliable and valid scientific basis for this claim, which also is not supported by any reliable and valid data. Dr. Clark's dark field analysis does not say anything about FeCo grains being "on top of" NiFe grains. Nor does his microbeam diffraction analysis, which does not even attempt to show the orientation of any bcc(110) crystals relative to an underlying NiFe crystal, as discussed above. In fact, as I already have noted, nowhere in Dr. Clark's dark field image analysis, in his microbeam diffraction analysis, or anywhere else in his report, does Dr. Clark show or even attempt to show the specific orientational relationships between any overlying bcc(110) FeCo grains relative to specific underlying (111) hexagonal NiFe grains (such as what is shown in Figure 5 of the '988 Patent), which is required to determine whether a particular FeCo grain can be one of the six possible variants of the '988 Patent. As noted above, in order to form a six-variant system, a bcc(110) crystal in the overlying FeCo layer must be one of six possible variants with a particular orientation *relative to an*

underlying (111) hexagonal crystal from a (111) textured hexagonal atomic template. This means that one must identify not only the overlying bcc(110) crystal, but the underlying (111) hexagonal crystal on which it was grown and the orientation of the overlying bcc(110) crystal relative to the underlying (111) hexagonal crystal. Dr. Clark has not shown, or even attempted to show, the presence of any such (111) hexagonal crystals from his microbeam diffraction or dark field analysis or otherwise. Therefore, in my opinion, his statement has no valid or reliable scientific basis.

436. Moreover, even if Dr. Clark had been able to show that there were bcc(110) crystals in the lower FeCo layer that were oriented over a (111) textured NiFe layer, his dark field data does not support any conclusions about the specific orientations of such crystals relative to the underlying NiFe crystals such that they are one of the only six possible variants allowed by the '988 Patent, or what the relative amounts of specific variants are. Dr. Clark simply shows relative amounts of crystals at particular angles in his sample from his dark field images that have a common $\langle 200 \rangle$ direction, but he has not shown what percentage of these for each angle is a bcc(110) crystal. As noted above, the crystals that will show up having a $\langle 200 \rangle$ direction include crystals not only with (110) orientations but also (100) and potentially other orientations. Therefore, because Dr. Clark has not determined the relative amounts of each, there is no way for him to draw a scientifically reliable and valid conclusion about what the amount of (110) crystals at each angle is.

437. In addition, without showing the orientation of the bcc(110) crystals that are included in his measurements for each angle (of which there are 18 based on his sampling at each 10-degree interval, starting at 0 degrees), Dr. Clark has at most has shown the existence of many orientations—many more than the six possible orientations allowed by the '988 Patent. If these were all “variants” within the meaning of the '988 Patent as Dr. Clark appears to incorrectly assume, this would mean that the lower FeCo layer is not a “symmetry broken structure,” because it would not consist of unequal amounts of the six variants required by the '988 Patent—it would have at least eighteen different “variants.”

438. Dr. Clark goes on to make yet another sweeping and unsupported statement by saying that, “[g]iven the relative grain sizes in the FeCo layer and NiFe template layer, there are no NiFe template grains that have six different overlying grains in the FeCo layer, let alone that each of the six different overlying grains would have equal area and each represent a different

variant from the six-variant system present in the FeCo layer.” (Clark at ¶ 167.) This statement has no factual basis, much less any scientifically reliable and valid underpinnings. It is simply a conclusory assertion. As discussed above several times, Dr. Clark lacks valid data showing the relative grain sizes for these layers across the entire layers, much less the specific relationship and orientation between any two layers, and certainly not anything that remotely allows one to make assessments about variants. As I have noted, Dr. Clark has not shown, and never attempts to show, the orientation of any specific bcc(110) FeCo crystal from the lower FeCo layer of sample S2MMC relative to an underlying (111) hexagonal crystal. Neither his FFT data nor his microbeam diffraction patterns show the presence of even a single NiFe fcc(111) crystal, much less how any such crystals are oriented with respect to any overlying FeCo bcc(110) crystals. Moreover, there certainly is no factual support for drawing broad conclusions about the entire layer of each. As noted repeatedly above, none of the data in Dr. Clark’s report supports any finding regarding the crystal orientations within the NiFe layer, and certainly not the presence of a (111) texture. Similarly, none of the data in Dr. Clark’s report shows the existence of any variant, much less the particular variants required by the ’988 Patent, because Dr. Clark never provides data regarding the relative orientations of any overlying FeCo bcc(110) crystals relative to specific underlying NiFe (111) crystals from a textured atomic template. Accordingly, in my opinion, all of Dr. Clark’s statements and conclusions in paragraph 167 of his report are unsupported by his data and have no reliable scientific basis.

439. Finally, the data from Dr. Clark’s area fraction analysis further confirms in a dramatic way that the FeCo layer analyzed by Dr. Clark cannot possibly be part of a six-variant system and form a symmetry broken structure. Dr. Clark’s analysis shows that in the 180-degree range he analyzes (which should be symmetrical for the remaining 180-degrees for the rest of the sampled area), *fewer than half* of the crystals in the FeCo layer can be bcc(110) crystals. Specifically, in Table 2 of paragraph 165 of his report, Dr. Clark calculates the percentage area of crystallites he has captured, which are from the <200> direction and purport to capture all of the bcc(110) crystals (as I have noted above, he actually is overstating this amount because there are other crystals with different orientations, namely bcc(100) crystals, that he is counting, but we will disregard that for the moment here). When these areas are totaled, they amount to 30.96% of the total area, meaning that the bcc(110) crystals comprise less than half of all of the crystals in the FeCo sample. Because the FeCo layer contains a substantial portion of non-(110)

crystals, it cannot be part of a six-variant system, which can only consist of bcc(110) crystals, and does not form a symmetry broken structure.

c. Other Data Not Considered by Dr. Clark

440. In addition to the flaws in Dr. Clark's analysis and conclusions described above relating to the lower FeCo layer in sample S2MMC, I note that Dr. Clark did not consider other information and data that was or could have been available to him relating to the crystal structure of the lower FeCo layer in sample S2MMC.

441. For example, in his report, Dr. Clark does not refer to any XRD testing he conducted, and he apparently did not consider any XRD data from any source in connection with his analysis of whether the lower FeCo layer in sample S2MMC contains material with a (110) texture. Accordingly, I note that there is no XRD data that would support a conclusion that the lower FeCo layer in the S2MMC sample has a bcc(110) texture.

442. I also note that, in an attempt to show the presence of bcc(110) crystals from a six-variant system in one of the samples discussed in the '988 Patent, the patent uses a pole figure measurement. (*See, e.g., '988 Patent, Fig. 14.*) Dr. Clark did not include any pole figure measurements in his report. Accordingly, I note that there is no pole figure data that would support a conclusion that the lower FeCo layer in the S2MMC sample has only six variants.

d. Conclusion Regarding FeCo Layers

443. In view of all of the flaws in Dr. Clark's analysis that I have described above, and in view of all of the other evidence, it is my opinion that the conclusions drawn by Dr. Clark regarding the crystalline properties of the lower FeCo layer in sample S2MMC lack a reliable factual and scientific basis and are based on the application of flawed and unreliable methodologies. It is also my opinion that none of the evidence I have considered supports the conclusion that the lower or upper FeCo layers in sample S2MMC has a bcc(110) texture or forms a symmetry broken structure, and that in fact the evidence confirms that the lower FeCo layer in sample S2MMC and the FeCo layers in general in Seagate's write-head [REDACTED] designs do *not* have a symmetry broken structure.

3. Sample SBRD8K ([REDACTED] Design)

444. In his report, Dr. Clark states that a similar TEM microbeam diffraction was performed on a region of the lower FeCo layer of sample SBRD8K as was done for samples

SOGPPC and 2MMMC. (Clark at ¶ 194.) In particular, Dr. Clark states that the microbeam diffraction was taken at the area shown by the red square in Figure 105 of his report from a sample that was prepared where the upper FeCo/NiFe layer was removed. (*Id.*) He states that from this area represented by the red square, “1,600 diffraction patterns were obtained by scanning the electron beam incrementally area in the box.” (*Id.*) However, only a handful of these (five, to be exact) are actually included and discussed in his report.

445. Dr. Clark goes on to state that “[b]y defocusing the diffraction pattern image slightly” (as shown in Figure 106), he was able to obtain an enlarged central spot that contains an image of the portion of the sample and that, from this, he was able to confirm that the plan view sample and diffraction pattern were within an alignment of ± 10 degrees. (*Id.* at ¶ 195 and Fig. 106.) In his report, Dr. Clark then provides examples of five diffraction patterns (out of the 1,600 he took) that he says show the presence of bcc(110) crystals, which he indicates by drawing yellow rectangles (and in some cases red rectangles) onto the diffraction pattern. He then goes on to provide conclusions regarding another 100 patterns taken from this area that he purportedly analyzed, although he does not include these images in his report or include his specific analysis of any of them (such as trying to draw the crystals on these images that he does for the five he actually discusses in his report).

446. In the remainder of this section of his report (*see* Clark at ¶¶ 202-210), Dr. Clark describes dark field images that he took from the plan view specimen for sample SBRD8K. He uses these images in an attempt to isolate crystals that have their $\langle 200 \rangle$ directions purportedly aligned perpendicular to the long axis of the write head sample. He then tries to calculate the area fraction of the crystals with these directions at 10-degree increments.

447. From this microbeam diffraction and dark-field testing, Dr. Clark purports to draw broad conclusions about the crystal properties of the lower FeCo layer for sample SBRD8K (he does not analyze the upper layer), the presence of bcc(110) crystals, the distribution of such crystals, their in-plane orientations, and whether they are part of a six-variant system. For the reasons I explain below, it is my opinion that the methodology applied by Dr. Clark to reach his conclusions about the presence of bcc(110) crystals, their relative amounts, and their orientations, and whether they are part of a six-variant system is flawed and unreliable, and that his conclusions are not supported by any valid scientific data. I address separately below the

microbeam diffraction testing and the dark-field testing performed by Dr. Clark and the conclusions he reaches.

a. Flawed and Unsupported Conclusions Based on Microbeam Diffraction Data

448. Flawed and Unsupported Conclusions Regarding the Presence of bcc(110) Crystals. In paragraphs 1196-201 and Figures 107-110 of his report, Dr. Clark explains that individual frames from the set of 1,600 microbeam diffraction images that he captured “may contain diffraction patterns from one, two, or sometimes more separate FeCo crystallites.” (*Id.* at ¶ 196.) He then states that “[t]ypical single crystal patterns for this analysis” are shown in Figure 107 of his report, and that “[t]hese patterns are readily identified and indexed as patterns in the (110)_{BCC} direction.” (*Id.*) He states that this was confirmed by measurement of the ratio of the sides of the rectangles, which were “found to be $5.4:3.8 = 1:\sqrt{2}$, as required.” (*Id.*)

449. Dr. Clark provides a total of five examples of diffraction patterns that allegedly show the presence of individual bcc(110) crystals from the lower FeCo layer of the plan view specimen from sample for sample SBRD8K for the [REDACTED] design. For each of the five images shown in his report, Dr. Clark draws yellow boxes (and in some cases red boxes) (“measured directly in Keynote” software from Apple (*see id.* at ¶ 197)) around the portions of the diffraction pattern that he contends show the presence of a bcc(110) crystal.

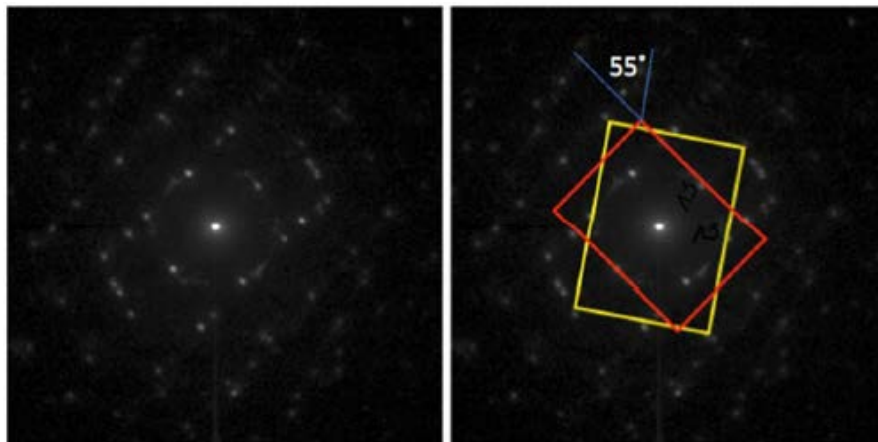
450. Apart from his statement noted above regarding the required ratio of the sides to establish the presence of a bcc(110) crystal, Dr. Clark does not explain or describe the particular methodology he used to draw his yellow and red boxes or to calculate the angles that he includes in the annotations in his report that form the basis for his conclusion. At most, he suggests that the microbeam diffraction patterns “visually identify as standard (110)_{BCC} patterns.” (*Id.* at caption to Fig. 107.) He does not show any indexing of these patterns, however, or describe the basis on which he selected certain spots for his annotations, how he calculated the ratios between the sides of the rectangles he drew, or the method by which he derived his angles (other than nominally for two of his examples). He frequently relies on alleged “spots” that are not clearly discernable, and ignores spots that are inconsistent with his conclusions.

451. In my opinion, Dr. Clark’s methodology for drawing the boxes and calculating the angles purporting to identify individual bcc(110) crystals from the red-box region does not support his conclusion that it shows the presence of a bcc(110) crystal for most of the examples

he discusses in this section of his report. Furthermore, his five examples provide no scientific basis for the broad conclusions he draws about the crystallographic structure of the lower FeCo layer in sample SBRD8K.

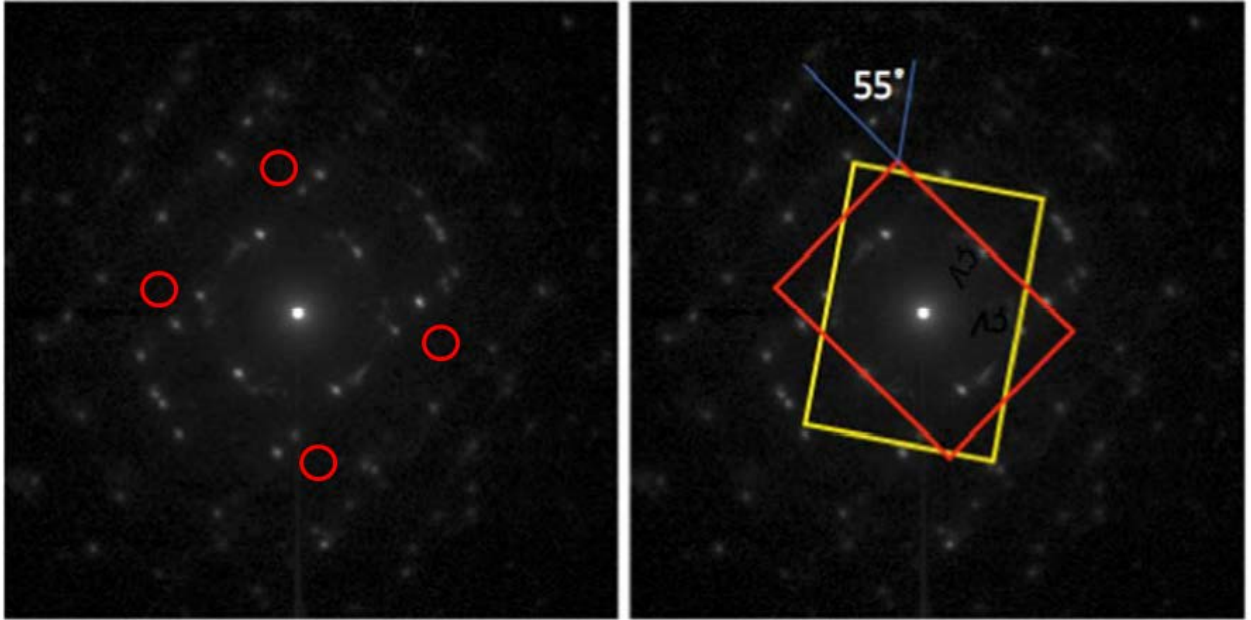
452. To accurately identify the presence of bcc(110) crystals in TEM microbeam diffraction patterns, one needs to clearly identify discernable spots (including the appropriate bright center spot), align those spots with those that are associated with bcc(110) crystals from standard ring diffraction ring patterns, determine whether there are other diffraction spots that are inconsistent with a bcc(110) crystal, and measure the ratio of the two sides of the rectangles to confirm they match the ratio of $1:\sqrt{2}$ for a bcc(110) crystal. To accurately calculate the relative angle between two alleged crystals, one needs to extend either the two longer or two shorter sides of each of the crystals being compared and then accurately measure the angle between them. Because Dr. Clark does not clearly follow this approach, many of his results are flawed, as I explain below.

453. For example, for Figure 108 in his report, Dr. Clark states that “it shows an example diffraction pattern with two crystallites, both in the (110)_{BCC} orientation, but rotated by $\sim 55^\circ$ about their common [110]_{BCC} direction.” (*Id.* at ¶197.) He goes on to say that “[t]his is the separation of two variants in the Kurdjumov-Sachs orientation,” and states that “[t]he measured ratio of the sides of the motif are $1:\sqrt{2}$ as required. (*Id.*) I have reproduced Figure 108 from Dr. Clark’s below:



454. In my opinion, Dr. Clark’s analysis of the pattern in Figure 108 (Frame 1313) is flawed because the spots he has chosen as the basis for his drawing are not clearly discernable. In fact, there are no discernable spots at all for the rectangle he has drawn in red. Therefore, in

my opinion, this pattern does not provide a reliable and valid basis for assessing whether it shows the presence of a bcc(110) crystal. I have noted the spots that Dr. Clark purports to rely on that in my opinion are not clearly discernable with red circles below:

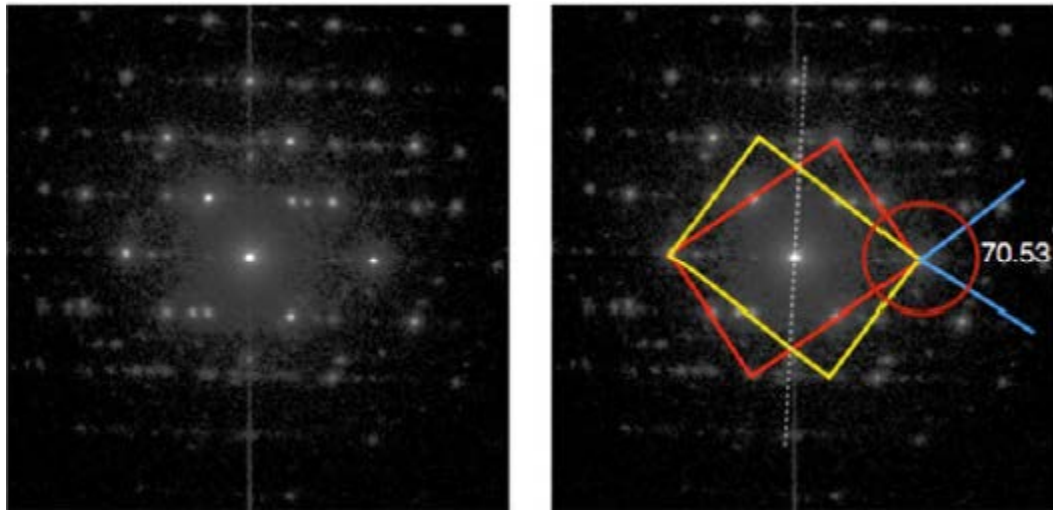


455. I also note that the yellow and red rectangles Dr. Clark has drawn are different sizes, indicating they would come from materials with different lattice spacings.

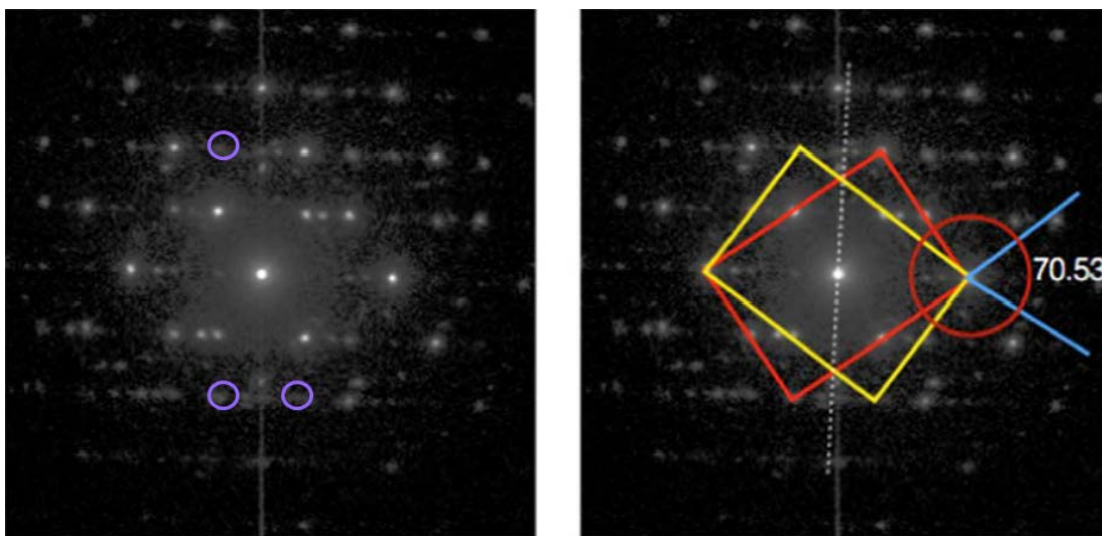
456. I also note that that Dr. Clark uses this Figure 108 as a basis for making the sweeping statement that because the two crystals he has drawn allegedly are offset from one another by an angle of approximately 55 degrees, this shows “the separation of two variants in the Kurdjumov-Sachs orientation.” (Clark at ¶ 197.) This is simply incorrect. As I explained above, one cannot show the existence of a particular variant without showing the orientation of the overlying crystal *relative to* the underlying crystal on which it was grown. As the ’988 Patent makes clear (and as Dr. Clark confirms elsewhere in his report, *see, e.g., id.* at ¶¶ 33-35)), a variant is defined based on the orientational relationship of the “the (110) crystal plane of a bcc-d crystal in comparison to the atomic arrangement of the (111) crystal plane of a hexagonal lattice template crystal.” (’988 Patent at 13:40-43.) Therefore, the relative orientation of the two alleged bcc(110) crystals in the plane cannot be used as a basis for making judgments about whether they are part of the six-variant system required by the ’988 Patent without first showing the orientation of each relative to an underlying (111) hexagonal crystal, which may have a different in-plane orientations. Dr. Clark does not do this. In fact, as I note below, Dr. Clark has

not shown the presence of any underlying (111) hexagonal crystals through his microbeam diffractions patterns.

457. The microbeam diffraction pattern in Figure 109, which purports to show the presence of two bcc(110) crystals in different frames, has similar flaws. I have reproduced Figure 109 from Dr. Clark's report below:



458. In my opinion, Dr. Clark's analysis of the patterns for the two alleged bcc(110) crystals he has drawn in Figure 109 does not allow for his conclusion that it shows the presence of bcc(110) crystals. First, similar to Figure 108, numerous spots that Dr. Clark has chosen in Figure 109 as the basis for his drawings that are not clearly discernable. Therefore, in my opinion, these patterns do not provide a reliable and valid basis for assessing whether they show the presence of bcc(110) crystals. I have noted examples of the spots from Frame 328 that Dr. Clark purports to rely on to draw his two crystals that are not clearly discernable with purple circles below:



459. Finally, I note that that Dr. Clark once again uses this Figure 109 as a basis for making the sweeping statement that because the two crystals he has drawn allegedly are offset from one another by an angle of approximately 70.53 degrees, this shows “the separation of two variants in the Kurdjumov-Sachs orientation.” (Clark at ¶ 155.) This is simply incorrect. For the same reasons I explained for Figure 108 above, one cannot show the existence of a particular variant without showing the orientation of the overlying crystal *relative to* the underlying crystal on which it was grown. Dr. Clark does not do this. In fact, as I note below, Dr. Clark has not shown the presence of any underlying (111) hexagonal crystals through his microbeam diffractions patterns.

460. I have analyzed the patterns in the other figures and provided a table below summarizing my analysis of the eight examples of microbeam diffraction patterns for the lower FeCo layer in sample SBRD8K included in Dr. Clark’s report:

Figure and Frames	Analysis
Figure 107 Frame 1329 (upper) Frame 242 (lower)	Upper image: Some diffraction spots not clearly discernable or are not present at the expected location; no scale bar; the lack of alignment of the corners of the rectangle with nearby spots is significant enough to indicate that this interpretation is not correct Lower image: Some diffraction spots not clearly discernable or are not present at the expected location; no scale bar; the lack of alignment of the corners of the rectangle with nearby spots is significant enough to indicate that this interpretation is not correct
Figure 108 Frame 1313	Some diffraction spots not clearly discernable or are not present at the expected location; rectangles do not have the expected ratio of $1:\sqrt{2}$ for

	bcc(110) crystals; yellow and red rectangles are different sizes as drawn, which if accurate indicates different materials; no scale bar; this interpretation is clearly incorrect
Figure 109 Frame 328	Some diffraction spots not clearly discernable or are not present at the expected location; no scale bar
Figure 110 Frame 1437	Some diffraction spots not clearly discernable or are not present at the expected location; no scale bar; the blue rectangle in particular has no match with any spot data

461. My analysis for these five examples is contained in Exhibit G of my report.

462. Presumably, Dr. Clark chose what he considered to be the best five examples out of the 1,600 images available to him to try to show the presence of bcc(110) crystals in the lower FeCo layer of sample SBRD8K. Yet, as demonstrated above, most of his examples are flawed.

463. In addition to these examples, Dr. Clark states that he analyzed another 100 diffraction patterns taken from this area that were randomly selected out of the 1,600 total diffraction patterns. (Clark at ¶ 200.) He states that he categorized them into four categories as follows:

Category	Results
a) Showed no recognizable pattern	71
b) Showed a single {110} pattern	5
c) Showed multiple {110} patterns	0
d) Showed {110} twins	0
e) Showed a pattern other than {110}	24

464. Dr. Clark does not provide his analysis for any of these other 100 microbeam diffraction patterns that he mentions in his report, and he did not include any of the actual images in Appendix C of his report. Dr. Clark's failure to include these images is inconsistent with the basic scientific practice of showing the data on which you are basing your conclusions. Because Dr. Clark has not provided any of the data on which he allegedly basis his analysis for these 100 other diffraction patterns, it is not possible to assess whether Dr. Clark's categorization of these other 100 images is accurate. To the extent Dr. Clark used the same approach that he did for the five examples for the categorization of the patterns that he does provide in his report, then they will be flawed to the same extent as discussed above.

465. I note that Dr. Clark states in a footnote (*id.* at ¶ 200 n.28) that the numbers are influenced by the initial orientation of the sample in the microscope that may affect the number of $\{110\}_{\text{BCC}}$ patterns that will be observed. He says, however, that this does not affect his opinions, including his view that “the FeCo layer is predominantly $(110)_{\text{BCC}}$.” (*Id.*) Once again, Dr. Clark does not provide any details on how these images were created or provide the images themselves. Accordingly, it is not possible to assess his approach. However, to the extent he purports to rely on this data at all, as noted below, it is inconsistent with his conclusion about the texture of the lower FeCo layer in sample SBRD8K.

466. I note, for example, that according to Dr. Clark, 95 percent of these additional 100 crystals did not have a recognizable pattern or one that was clearly not $\text{bcc}(110)$. The alleged presence of these other unrecognizable crystals and those with other orientations is plainly inconsistent with the $\text{bcc}(110)$ crystals predominating in the FeCo layer and with the lower FeCo layer forming a symmetry broken structure, because it means that the lower FeCo layer has crystals that are not $\text{bcc}(110)$ and therefore not part of a six-variant system. (*E.g.*, ’988 Patent at 12:66-13:2 (“this invention deals with a structure to achieve uniaxial magnetocrystalline orientation via the use of the (110) texture of body centered cubic (BCC) or body centered cubic derivative crystal thin film structures.”).)

467. Furthermore, there is clear evidence in the patterns that he does provide for orientations other than $\text{bcc } 110$, as shown below. In order for the pattern to show only (110) crystals, all of the spots would have to lie upon the yellow rings that I have added in the image shown below on the right. Specifically, I added the set of rings that would appear from a $\text{bcc}(110)$ textured sample, and I aligned the innermost yellow ring, which is 110 , with the spots lying in the middle of the long side of Dr. Clark’s yellow rectangle. As shown below, many of the spots do not lie on the yellow rings I have added. Thus, there must be grain orientations that are not associated with a 110 texture in the layer. I have performed similar analyses (shown in Exhibit G), and other of Dr. Clark’s examples also have numerous spots inconsistent with a $\text{bcc } 110$ texture.

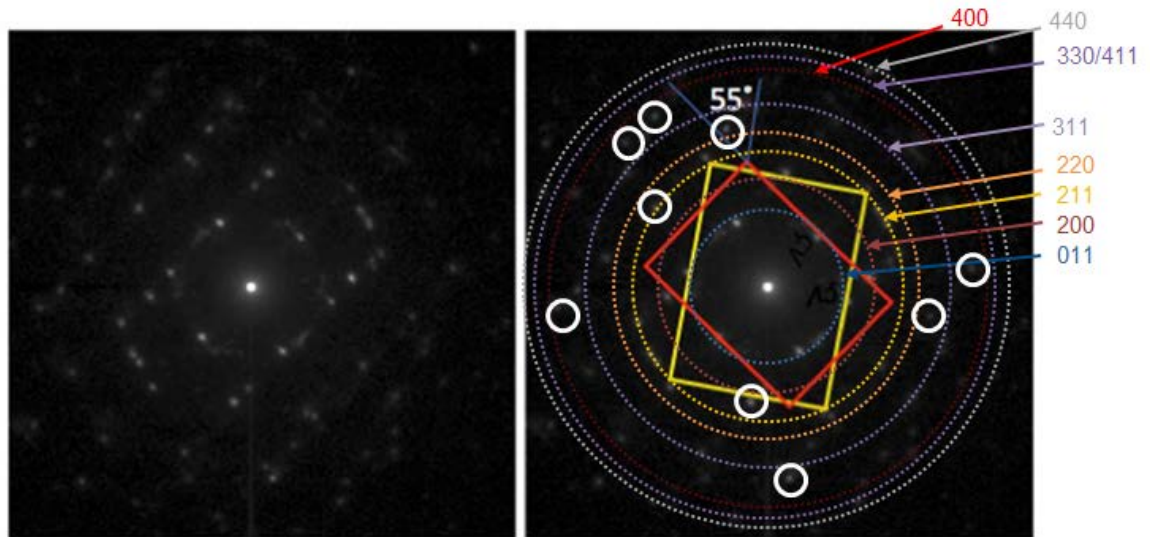


Figure 108: Two crystallites, both in the $(110)_{\text{BCC}}$ orientation, frame 1313, rotated by $\sim 55^\circ$ about their common $[110]_{\text{BCC}}$ direction.

Clear spots (white circles) are at locations not consistent with 110_{BCC} orientation

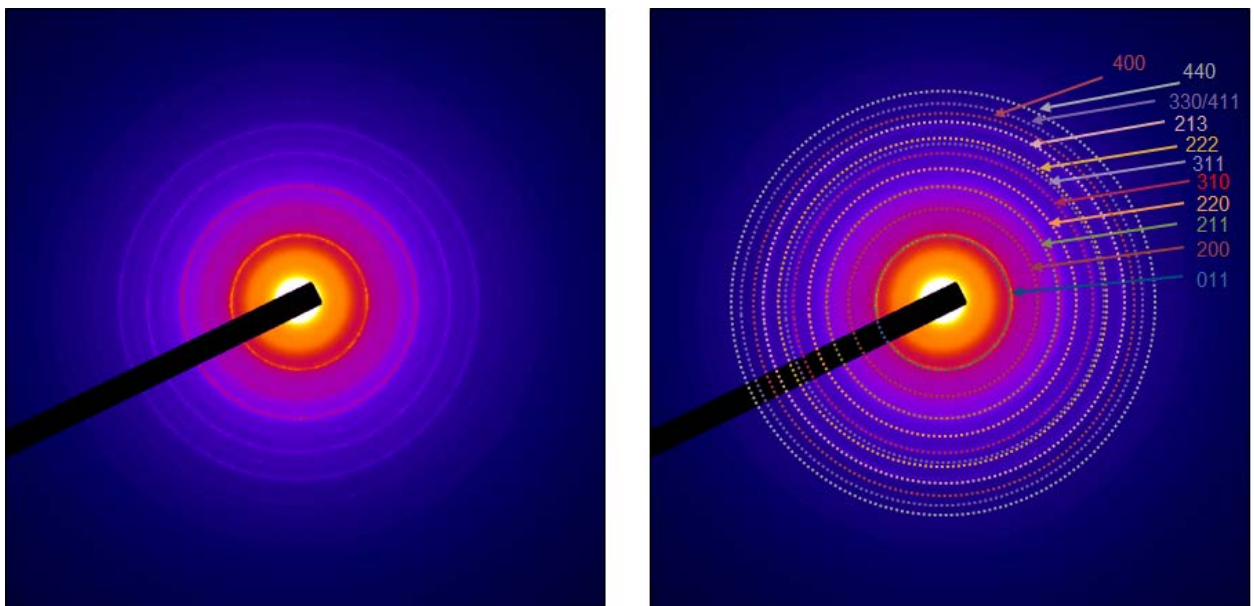
468. Flawed and Unsupported Conclusions on Texture, Variants, and Symmetry Broken Structure. Based on the five examples he shows, and apparently also based on his summary of the other 100 diffraction patterns that he does not show, Dr. Clark makes the sweeping statement that “[t]hese patterns are further confirmation that the FeCo layer is BCC with (110) texture.” (*Id.* at ¶ 196.) He also uses these images as purported examples of showing that the lower FeCo layer is BCC and contains variants from the Kurdjumov-Sachs six-variant system. (*E.g., id.* at ¶ 197, 198.) I disagree with both of these statements, which are not supported by Dr. Clark’s microbeam diffraction data, or any other scientifically valid data in his report.

469. In my opinion, Dr. Clark’s assertion that the lower FeCo layer in sample SBRD8K has a $\text{bcc}(110)$ texture is not supported by any of his microbeam diffraction patterns and any valid and reliable scientific analysis. As explained above, most of the five microbeam diffraction examples do not support the presence of even individual $\text{bcc}(110)$ crystals. In addition, these five examples provide no basis for a conclusion that $\text{bcc}(110)$ crystals predominate throughout the lower FeCo layer, as is required to show texture. For example, Dr. Clark says that he took 1,600 images from this region of the sample, yet he provides images for only five of them. Even if every one of the five samples hand-picked by Dr. Clark was an individual $\text{bcc}(110)$ crystal (which is not the case), there is no valid scientific basis for drawing a

conclusion about the texture for this entire layer from a sample comprising no more than 0.31 percent of the layer.

470. In addition, as noted above, the presence of crystals with orientations other than (110) shown by Dr. Clark's purported analysis of the 100 other microbeam diffraction images that he apparently took of the lower FeCo layer of sample SBRD8K is inconsistent with the bcc(110) crystals predominating in the FeCo layer and with the lower FeCo layer forming a symmetry broken structure, because it means that the lower FeCo layer has crystals that are not bcc(110) and therefore not part of a six-variant system.

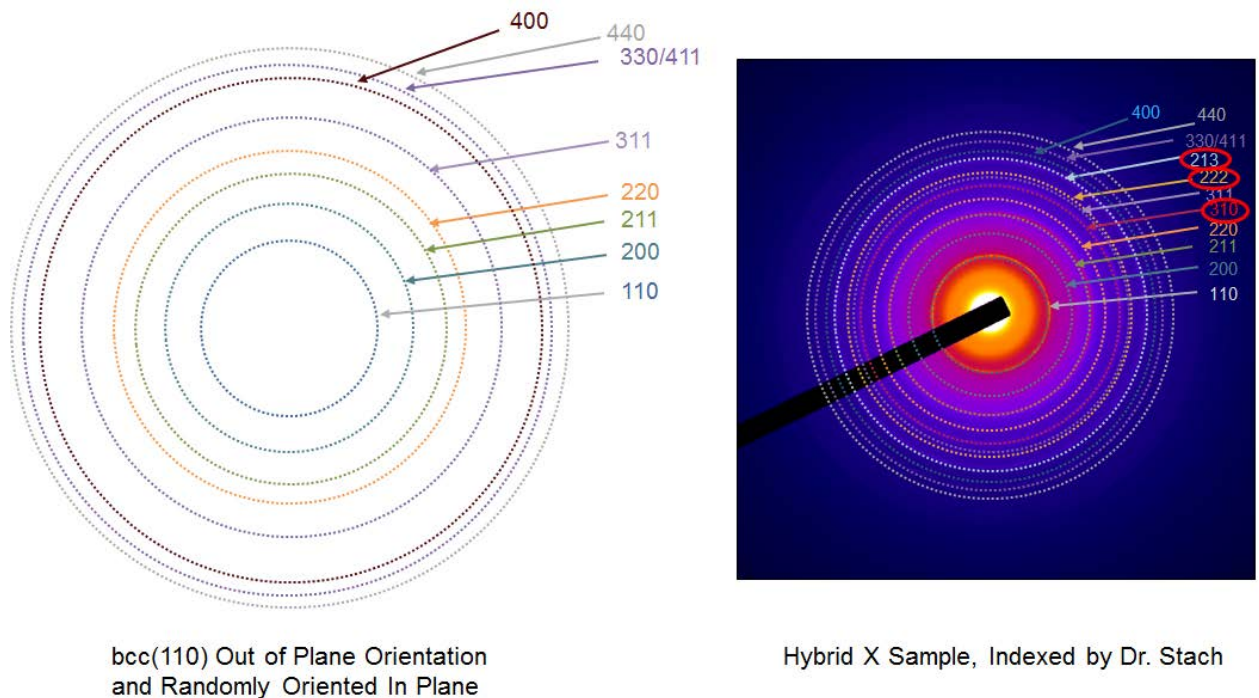
471. Finally, other data, including my own testing, also show that the magnetic layers in Seagate's [REDACTED] write heads contain bcc crystals other than (110). In particular, I took diffraction ring patterns of samples of Seagate's [REDACTED] write heads. (See attached Exhibit D to my report.) I indexed the ring patterns, which I have reproduced below:



472. This data shows that there are orientations other than (110). In particular, there is strong intensity from the 310 ring, and weaker intensity from both the 22 and 213 rings is also present. The fact that there is strong diffraction from the {310} family of planes means that there are grains oriented along the $\langle 100 \rangle$, $\langle 013 \rangle$, and/or $\langle 113 \rangle$ orientations. This can be shown by the fact that the 310 spot appears in the bcc standard diffraction patterns for the $\langle 100 \rangle$, $\langle 013 \rangle$, and $\langle 113 \rangle$ zone axes. Most likely they are $\langle 100 \rangle$ oriented, as that orientation has a

relatively low energy surface, second only to $\{110\}$. (See, e.g., L. Vitos, A.V. Ruban, H.L. Skriver, and J. Kollár, “The Surface Energy of Metals,” Surface Science 411 (1998), Table 5.)

473. To demonstrate this more clearly, I have set forth below on the left a simulated diffraction ring pattern that would appear for a material that had only (110) grains, and on the right the actual diffraction pattern for the sample that I indexed. As can be seen below, the 310 , 222 , and 213 rings are present in the data in the ring pattern on the right, which should *not* be present if the material had only (110) grains (which is the ring pattern shown on the left):



474. This is further confirmed, as I discuss below, by the data from Dr. Clark’s area fraction analysis, which shows that the majority of crystals are *not* bcc(110) in the FeCo layer. Therefore, in my opinion, Dr. Clark does not have a valid scientific basis for concluding that the FeCo layer is (110) textured.

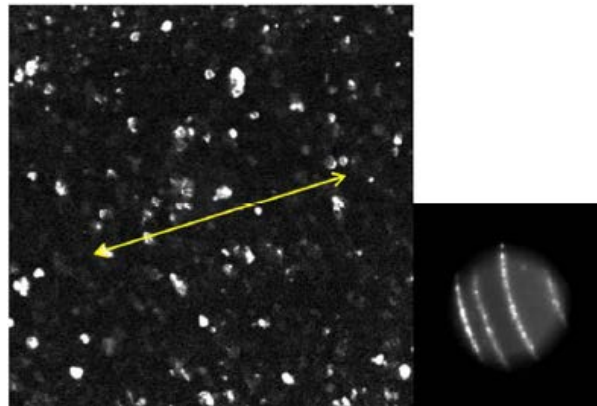
475. In my opinion, Dr. Clark’s assertion that the lower FeCo layer in sample SBRD8K contains variants with the orientational relationship for the Kurdjumov-Sachs six-variant system is not supported by any scientifically valid and reliable data or analysis. As noted above, in order to form a six-variant system, the bcc(110) crystals in the overlying layer must be one of six possible variants with particular orientations *relative to* an underlying (111) hexagonal crystal from a (111) textured hexagonal atomic template. Therefore, in order to identify a

variant, one must identify not only the overlying bcc(110) crystal, but the underlying (111) hexagonal crystal on which it was grown and determine the orientation of the overlying bcc(110) crystal relative to the underlying (111) hexagonal crystal. Dr. Clark has not shown, or even attempted to show, the presence of any such (111) hexagonal crystals from his microbeam diffraction analysis. None of the microbeam diffraction images he provides corresponds to a (111) hexagonal crystal. Accordingly, there is no data that remotely supports Dr. Clark's assertion that the bcc(110) crystals that he purports to identify for the lower FeCo layer of sample SBRD8K in his microbeam diffraction analysis are one of the six possible variants from a six-variant system and form the symmetry broken structure of the '988 Patent.

b. Flawed and Unsupported Conclusions Based on Dark Field Images

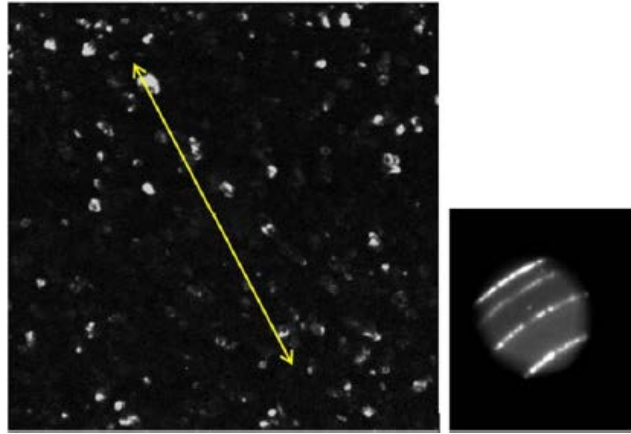
476. I next address Dr. Clark's dark field images. Dr. Clark apparently took these images from sample SBRD8K from the same area of the write head where the microbeam diffraction patterns were taken. (Clark at ¶ 202.)

477. Dr. Clark states that in this area the sample was aligned so that the area in which the images were taken are parallel to the tip of the sample within a rotation of 10 degrees of one another. (*Id.*) Dr. Clark states that he then used a small objective aperture to enclose a segment of the {200} diffraction ring, from which a dark field image in the area of the lower FeCo layer was obtained. (*Id.* at ¶ 203.) He states that the crystallites from this segment of the {200} diffraction ring show up as the bright spots in Figure 112, which I have reproduced below:



478. Dr. Clark states that the yellow arrow in Figure 112 (shown above) allegedly points in the direction of the objective aperture from the center of the diffraction, so that the bright crystallites allegedly “have their <200> directions aligned parallel to the arrow,” which purportedly is “perpendicular to the long axis of the write head.” (*Id.*) Dr. Clark next states that,

in contrast, an image taken at roughly 90 degrees to the position of the yellow arrow in Figure 82 produced an image with significantly fewer illuminated crystallites. (*Id.* at ¶ 204.) He shows this in Figure 113, which I have reproduced below from his report:



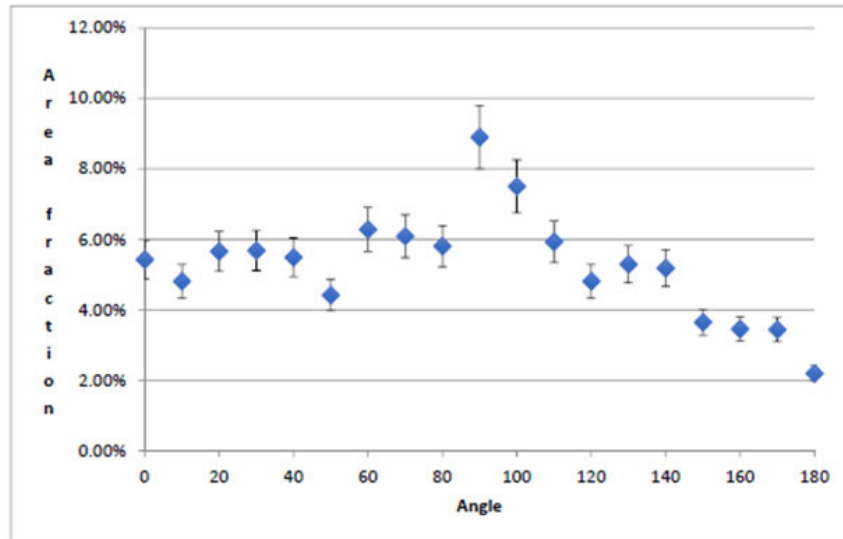
479. Dr. Clark then states that this procedure was repeated at 10-degree intervals around the {200} segment of the diffraction ring in at least a 180-degree rotation, which produced dark field images from this portion of the ring similar to those shown in Figures 54 and 55. (*Id.* at ¶ 205.) To analyze these images, Dr. Clark states that a large area of the dark field image was separated as shown in Figure 114 of his report. (*Id.*) He goes on to say that a “standard stereological computer program,” in this case ImageJ, was used to analyze these images. For each image, he states that a threshold was applied to the isolated area to produce a binary black and white image, as shown in Figure 115 of his report. (*Id.* at ¶ 206.) I have reproduced Figure 115 below:



480. Using the ImageJ software, Dr. Clark states that he sought to measure the fraction of the crystallites that are white, namely, “the area fraction of crystallites that scatter into the

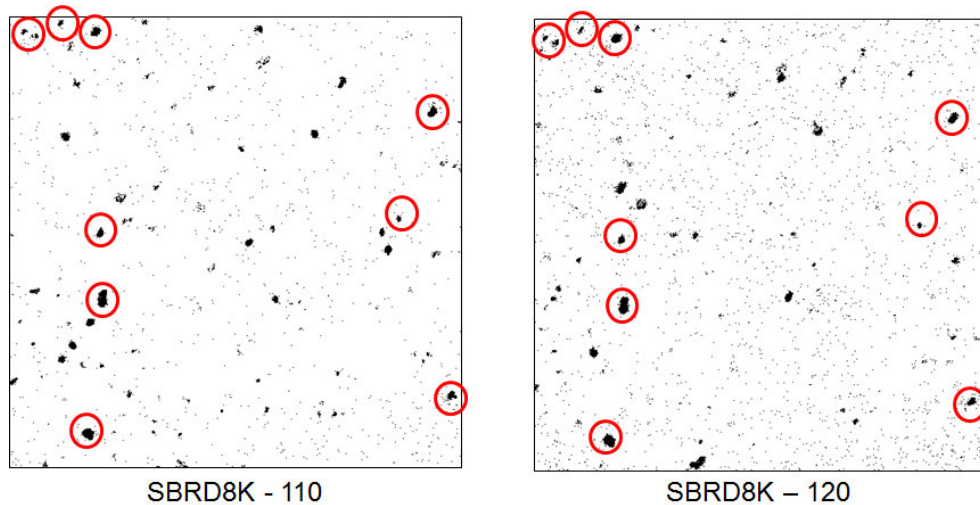
objective aperture at that particular position.” (*Id.* at ¶ 207.) He then added the area fractions for each of the angles he analyzed at 10-degree increments and tabulated them in Table 3 and graphed them in Figure 117. (*Id.* at ¶ 208.) I have reproduced both Table 3 and Figure 117 below—shown side-by-side:

Angle	%Area
0	1.994
10	1.769
20	2.08
30	2.089
40	2.018
50	1.624
60	2.308
70	2.238
80	2.134
90	3.271
100	2.758
110	2.18
120	1.769
130	1.947
140	1.905
150	1.341
160	1.27
170	1.264
180	0.807



481. I note that Dr. Clark does not provide many details relating to how he conducted his dark field imaging arrived at the data he includes in Table 3 and Figure 117 of this report. In particular, Dr. Clark does not provide information about what threshold he chose to produce his binary black and white images, the specific aperture size he used, how he ensured the aperture was focused solely on the {200} segment, or how he chose his error range, which he has set at 10 percent for each measurement. The results may depend greatly on these parameters, yet no information is provided about them by Dr. Clark.

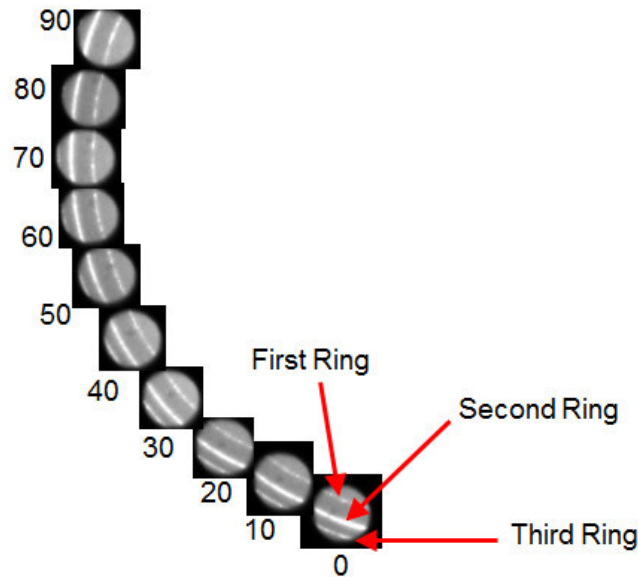
482. In addition, I note that there are serious issues with Dr. Clark’s methodology and his testing that render his data inaccurate. For example, it appears that Dr. Clark counts some of the crystallites twice, which should not occur if the testing was performed correctly. An example of this can be seen below, where the same crystallites appear and are being counted at two different angles:



483. As can be seen above, all of the crystallites circled in red light up at both 110 degrees and 120 degrees. This double-counting, which is present in the majority of the images for each angle, means that Dr. Clark's data is inaccurate and overstates the population of crystallites at the angles where there is double-counting.

484. Similarly, I note that Dr. Clark includes both data for 0 degrees and data for 180 degrees, when one of those measurements should be excluded if he is purporting to show data across a 180-degree range. Furthermore, the data collected by Dr. Clark at these two angles are substantially different. They should be the same if the testing was done properly. The fact that they are substantially different raised further questions about Dr. Clark's testing methodology.

485. I also note that Dr. Clark appears to be capturing data from rings other than the 200 ring, as can be seen in Figures 112 and 113 of his report, both of which show multiple rings within the aperture. I also reviewed the apertures in Appendix C of Dr. Clark's report, and many of them show multiple separate rings, with several of them showing three separate rings, as shown below. I have arranged the apertures in order, and next to each other, to make it more apparent that they capture multiple rings:



486. All of these issues raise serious questions regarding the methodology used by Dr. Clark and renders the data unreliable.

487. The goal of Dr. Clark's analysis apparently was to show that there are different amounts of crystallites oriented with their $\langle 200 \rangle$ directions perpendicular to the long axis of the write head in the area of the sample where images were taken. (*Id.* at ¶ 209.) Dr. Clark does not explicitly state, however, why he chose to focus on these crystallites, as they would include crystals whose orientations are not (110) and have different orientations. This is because, for example, a bcc(100) crystal will create a $\{200\}$ ring, as discussed above. From this dark field data, Dr. Clark proceeds to make a number of broad and conclusory statements that are unsupported by his data and have no reliable scientific basis.

488. Dr. Clark first repeats a statement from earlier in his report that is unrelated to his dark field image analysis. Dr. Clark simply reasserts that the grain sizes of each are roughly similar with only one or two FeCo grains per NiFe grain for the great majority of the NiFe grains. (*Id.* at ¶ 210.) As I discuss above, however, there is no reliable and valid scientific basis for Dr. Clark's claim, which is not supported by any reliable and valid data. One cannot draw conclusions about the grain sizes of the entire lower FeCo and especially the NiFe below it from this sample based on any images provided by Dr. Clark (and certainly not from the microbeam diffraction or dark field images). Moreover, even if there were some evidence of grain sizes at particular locations, such incidental images would be insufficient to support broad generalizations about the grain sizes throughout the entire lower FeCo and adjacent NiFe layers.

489. Dr. Clark next makes the sweeping statement that his “dark field analysis, in conjunction with the microbeam diffraction analysis discussed above, shows that the various FeCo grains on top of the various NiFe template layer grains have members of the six-variant system preferentially aligned such that there is an unequal amount of the six variants in the FeCo layer.” (*Id.*) Once again, there is no reliable and valid scientific basis for this claim, which also is not supported by any reliable and valid data. Dr. Clark’s dark field analysis does not say anything about FeCo grains being “on top of” NiFe grains. Nor does his microbeam diffraction analysis, which does not even attempt to show the orientation of any bcc(110) crystals relative to an underlying NiFe crystal, as discussed above. In fact, as I already have noted, nowhere in Dr. Clark’s dark field image analysis, in his microbeam diffraction analysis, or anywhere else in his report, does Dr. Clark show or even attempt to show the specific orientational relationships between any overlying bcc(110) FeCo grains relative to specific underlying (111) hexagonal NiFe grains (such as what is shown in Figure 5 of the ’988 Patent), which is required to determine whether a particular FeCo grain can be one of the six possible variants of the ’988 Patent. As noted above, in order to form a six-variant system, a bcc(110) crystal in the overlying FeCo layer must be one of six possible variants with a particular orientation *relative to an* underlying (111) hexagonal crystal from a (111) textured hexagonal atomic template. This means that one must identify not only the overlying bcc(110) crystal, but the underlying (111) hexagonal crystal on which it was grown and the orientation of the overlying bcc(110) crystal relative to the underlying (111) hexagonal crystal. Dr. Clark has not shown, nor even attempted to show, the presence of any such (111) hexagonal crystals from his microbeam diffraction or dark field analysis or otherwise. Therefore, in my opinion, his statement has no valid or reliable scientific basis.

490. Moreover, even if Dr. Clark had been able to show that there were bcc(110) crystals in the lower FeCo layer that were oriented over a (111) textured NiFe layer, his dark field data does not support any conclusions about the specific orientations of such crystals relative to the underlying NiFe crystals such that they are one of the only six possible variants allowed by the ’988 Patent, or what the relative amounts of specific variants are. Dr. Clark simply shows relative amounts of crystals at particular angles in his sample from his dark field images that have a common $\langle 200 \rangle$ direction, but he has not shown what percentage of these for each angle is a bcc(110) crystal. As noted above, the crystals that will show up having a $\langle 200 \rangle$

direction include crystals not only with (110) orientations but also (100) and potentially other orientations. Therefore, because Dr. Clark has not determined the relative amounts of each, there is no way for him to draw a scientifically reliable and valid conclusion about what the amount of (110) crystals at each angle is.

491. In addition, without showing the orientation of the bcc(110) crystals that are included in his measurements for each angle (of which there are 18 based on his sampling at each 10-degree interval, starting at 0 degrees), Dr. Clark has at most has shown the existence of many orientations—many more than the six possible orientations allowed by the '988 Patent. If these were all “variants” within the meaning of the '988 Patent as Dr. Clark appears to incorrectly assume, this would mean that the lower FeCo layer is not a “symmetry broken structure,” because it would not consist of unequal amounts of the six variants required by the '988 Patent—it would have at least eighteen different “variants.”

492. Dr. Clark goes on to make yet another sweeping and unsupported statement by saying that, “[g]iven the relative grain sizes in the FeCo layer and NiFe template layer, there are no NiFe template grains that have six different overlying grains in the FeCo layer, let alone that each of the six different overlying grains would have equal area and each represent a different variant from the six-variant system present in the FeCo layer.” (Clark at ¶ 210.) This statement has no factual basis, much less any scientifically reliable and valid underpinnings. It is simply a conclusory assertion. As discussed above several times, Dr. Clark lacks valid data showing the relative grain sizes for these layers across the entire layers, much less the specific relationship and orientation between any two layers, and certainly not anything that remotely allows one to make assessments about variants. As I have noted, Dr. Clark has not shown, and never attempts to show, the orientation of any specific bcc(110) FeCo crystal from the lower FeCo layer of sample SBRD8K relative to an underlying (111) hexagonal crystal. Neither his FFT data nor his microbeam diffraction patterns show the presence of even a single NiFe fcc(111) crystal, much less how any such crystals are oriented with respect to any overlying FeCo bcc(110) crystals. Moreover, there certainly is no factual support for drawing broad conclusions about the entire layer of each. As noted repeatedly above, none of the data in Dr. Clark’s report supports any finding regarding the crystal orientations within the NiFe layer, and certainly not the presence of a (111) texture. Similarly, none of the data in Dr. Clark’s report shows the existence of any variant, much less the particular variants required by the '988 Patent, because Dr. Clark never

provides data regarding the relative orientations of any overlying FeCo bcc(110) crystals relative to specific underlying NiFe (111) crystals from a textured atomic template. Accordingly, in my opinion, all of Dr. Clark's statements and conclusions in paragraph 210 of his report are unsupported by his data and have no reliable scientific basis.

493. Finally, the data from Dr. Clark's area fraction analysis further confirms in a dramatic way that the FeCo layer analyzed by Dr. Clark cannot possibly be part of a six-variant system and form a symmetry broken structure. Dr. Clark's analysis shows that in the 180-degree range he analyzes (which should be symmetrical for the remaining 180-degrees for the rest of the sampled area), *fewer than half* of the crystals in the FeCo layer can be bcc(110) crystals. Specifically, in Table 3 of paragraph 208 of his report, Dr. Clark calculates the percentage area of crystallites he has captured, which are from the <200> direction and purport to capture all of the bcc(110) crystals (as I have noted above, he actually is overstating this amount because there are other crystals with different orientations, namely bcc(100) crystals, that he is counting, but we will disregard that for the moment here). When these areas are totaled, they amount to 36.77% of the total area, meaning that the bcc(110) crystals comprise less than half of all of the crystals in the FeCo sample. Because the FeCo layer contains a substantial portion of non-(110) crystals, it cannot be part of a six-variant system, which can only consist of bcc(110) crystals, and does not form a symmetry broken structure.

b. Other Data Not Considered by Dr. Clark

494. In addition to the flaws in Dr. Clark's analysis and conclusions described above relating to the lower FeCo layer in sample SBRD8K, I note that Dr. Clark did not consider other information and data that was or could have been available to him relating to the crystal structure of the lower FeCo layer in sample SBRD8K.

495. For example, in his report, Dr. Clark does not refer to any XRD testing he conducted, and he apparently did not consider any XRD data from any source in connection with his analysis of whether the lower FeCo layer in sample SBRD8K contains material with a (110) texture. Accordingly, I note that there is no XRD data that would support a conclusion that the lower FeCo layer in the SBRD8K sample has a bcc(110) texture.

496. I also note that, in an attempt to show the presence of bcc(110) crystals from a six-variant system in one of the samples discussed in the '988 Patent, the patent uses a pole figure measurement. (*See, e.g., '988 Patent, Fig. 14.*) Dr. Clark did not include any pole figure

measurements in his report. Accordingly, I note that there is no pole figure data that would support a conclusion that the lower FeCo layer in the SBRD8K sample has only six variants.

c. Conclusion Regarding FeCo Layers

497. In view of all of the flaws in Dr. Clark's analysis that I have described above, and in view of all of the evidence, it is my opinion that the conclusions drawn by Dr. Clark regarding the crystalline properties of the lower FeCo layer in sample SBRD8K lack a reliable factual and scientific basis and are based on the application of flawed and unreliable methodologies. It is also my opinion that none of the evidence I have considered supports the conclusion that the lower or upper FeCo layers in sample SBRD8K has a bcc(110) texture or forms a symmetry broken structure, and that in fact the evidence confirms that the lower FeCo layer in sample SBRD8K and the FeCo layers in general in Seagate's write-head [REDACTED] designs do *not* have a symmetry broken structure.

IX. SUMMARY

498. Based on all of the materials I have considered, it is my opinion that the test methods and measurements conducted by Dr. Clark that he relies on to form his opinions are not reliable. In addition, in my opinion, Dr. Clark applied many of the test methods in a flawed, unscientific, and unreliable manner, and that the conclusions he draws from his tests regarding the crystallographic properties of the NiFe and FeCo layers in the samples he tested for Seagate's [REDACTED] write-head designs are not supported by sufficient and scientifically reliable data.

499. In my opinion, the testing results and data from Dr. Clark's report, along with the data from the testing that I conducted, do not show either the presence of a "layer providing a (111) textured hexagonal atomic template" or a layer forming a "symmetry broken structure."

A. No Evidence of (111) Textured Hexagonal Atomic Template

500. There is no reliable, scientifically valid basis for a conclusion that the NiFe layers in Seagate's [REDACTED] designs are a (111) textured hexagonal atomic template. In particular:

- (i) The handful of FFT images that Dr. Clark relies on to show individual examples of the presence of fcc crystals either indicate no crystalline structure whatsoever or are inconsistent with the presence of fcc crystals in the NiFe layers. The

images clearly do not match the standard diffraction patterns for an fcc crystal. Thus, Dr. Clark's reliance on these FFT images is flawed and unreliable.

(ii) Even if Dr. Clark had been able to show a few examples of some fcc crystals in the NiFe layers (which he did not), there is no evidence that any such crystals have a (111) orientation. None of the six individual FFTs Dr. Clark chose to rely on (or any of the other FFTs in his Appendix) show a (111) orientation relative to the substrate.

(iii) Even if Dr. Clark had shown some examples of fcc(111) crystals in the NiFe layers of the samples he tested (which he did not), he has failed to show that such crystals would predominate throughout the entire NiFe layers to form a (111) textured atomic template. His sample sizes of 1% or less provide no reliable basis for drawing conclusions about the entire layers.

(v) The microbeam diffraction images taken by Dr. Clark for the FeCo layers show no evidence of any underlying fcc(111) hexagonal crystals in the NiFe layers, and Dr. Clark does not contend that they do. The absence of any evidence of hexagonal NiFe crystals in these microbeam diffraction patterns further undermines, and is inconsistent with, any conclusion that the NiFe layers have a (111) texture.

(vi) Similarly, the ring diffraction patterns for the [REDACTED] samples fail to show the existence of any fcc(111) crystals, which also undermines, and is inconsistent with, any conclusion that the NiFe layers have a (111) texture.

(vii) Dr. Clark did not conduct any XRD testing that showed the presence of any fcc(111) crystals.

501. In view of the flaws in Dr. Clark's testing, and in view of all of the evidence, it is my opinion that the conclusions drawn by Dr. Clark regarding the crystalline properties of the NiFe layers in the samples for the [REDACTED] write-head designs that he tested lack a reliable factual and scientific basis and are based on the application of flawed and unreliable methodologies. In my opinion, none of the evidence supports the conclusion that any of the NiFe layers in Seagate's [REDACTED] write-head designs has an fcc(111) texture and is a (111) textured hexagonal atomic template. This is not surprising, because [REDACTED] [REDACTED] are unlikely to form any crystal structure, much less have a (111) texture.

B. No Evidence of Six-Variant System and Symmetry Broken Structure

502. There is no reliable, scientifically valid basis for a conclusion that the FeCo layers in Seagate's [REDACTED] designs form a six-variant system and a symmetry broken structure. In particular:

(i) Dr. Clark has failed to show the existence of any variants from a six-variant system. In order to form a six-variant system and a symmetry broken structure, the bcc(110) crystals in the overlying layer must be one of six possible variants with particular orientations *relative to* an underlying (111) hexagonal crystal from a (111) textured hexagonal atomic template. Therefore, to identify a variant, one must identify not only the overlying bcc(110) crystal, but also the underlying (111) hexagonal crystal on which it was grown and determine the orientation of the overlying bcc(110) crystal relative to the underlying (111) hexagonal crystal. Dr. Clark has not shown the presence of any such underlying (111) hexagonal crystals anywhere in his report, or any orientations of relative to such underlying (111) hexagonal crystals.

(ii) In addition, there is overwhelming evidence that the orientations of the bcc crystals in the FeCo layers tested by Dr. Clark and which he contends form a symmetry broken structure include crystals that are *not* bcc(110) crystals. This is shown by:

- Spot patterns in Dr. Clark's microbeam diffraction patterns that are inconsistent with a (110) orientation, meaning that the FeCo layers have bcc crystals that are not (110) oriented;
- Dr. Clark's own analysis that a significant percentage of the microbeam diffraction patterns he randomly selected and categorize showed crystals that were *not* recognizable as (110) oriented crystals (*i.e.*, 27%, 86%, and 95% of the three groups of 100 images he analyzed were *not* recognizable as (110) oriented crystals);
- The ring diffraction patterns that Dr. Clark obtained (and those that I obtained from my own testing) conclusively show the presence of non-(110) crystals in the FeCo layers, such as crystals that are (100) oriented; and
- The area fraction analysis performed by Dr. Clark indicates that the *majority* of crystals in the FeCo layers he analyzed are *not* (110) crystals. The crystallites he identified as (110) make up no more than 31%, 32%, or 37%,

respectively, of the three FeCo layers he tested, according to Dr. Clark's own data.

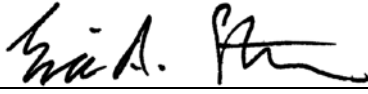
503. The presence of these non-(110) crystals is inconsistent with the bcc(110) crystals predominating in the FeCo layer and thus with the FeCo layers forming a symmetry broken structure. Non-(110) crystals cannot form a six-variant system. Because these layers have substantial numbers of crystals that are not part of a six-variant system, they do not form a symmetry broken structure.

504. Dr. Clark's attempt to find individual examples of bcc(110) crystals in his microbeam analysis is also seriously flawed and fails to provide more than a few examples of the presence of bcc(110) crystals. Many of those same examples include spots consistent with (100) orientations.

505. Dr. Clark's dark-field image analysis is seriously flawed and provides no support for showing an accurate distribution of bcc(110) crystals in the FeCo layers he tested. For his testing, Dr. Clark focused on a diffraction ring (the one with a $\langle 200 \rangle$ direction) that includes bcc crystals that are *not* (110) oriented (and also is based on unreliable data as a result of errors in the testing and double-counting of data, which I have noted above). To the extent the data is reliable, however, it shows (as noted above) that a substantial portion of the FeCo layers are crystals that are *not* bcc(110), and therefore cannot form a six-variant system and a symmetry broken structure.

506. In view of the substantial flaws in Dr. Clark's testing and his analysis that I have described above, and in view of all of the evidence, it is my opinion that the conclusions drawn by Dr. Clark regarding the crystalline properties of the FeCo layers in samples for the [REDACTED] write-head designs he tested lack a reliable factual and scientific basis and are based on the application of flawed and unreliable methodologies. In my opinion, none of the evidence supports the conclusion that any of the FeCo layers in Seagate's [REDACTED] write-head designs consist of crystals that are predominantly (110) oriented and are variants from a six-variant system. Rather, the evidence in my opinion consistently fails to show the existence of variants from a six-variant system in these layers, and conclusively shows the presence of a substantial portion of non-(110) crystals. The substantial presence of these non-(110) crystals is inconsistent with the bcc(110) crystals predominating in the FeCo layer and with the FeCo layers forming a symmetry broken structure, because such evidence confirms that the FeCo layers have

crystals that are not part of a six-variant system and that the FeCo layers in Seagate's write heads therefore do not form a symmetry broken structure.

Signed: _____
Eric Stach, Ph.D.

Dated: July 16, 2018

EXHIBIT A

CURRICULUM VITAE

Eric A. Stach
Department of Materials Science and Engineering
Laboratory for Research on the Structure of Matter
Singh Center for Nanotechnology
University of Pennsylvania
3123 Walnut Street
Philadelphia, PA 19104
stach@seas.upenn.edu

Employment

Department of Materials Science and Engineering, University of Pennsylvania
Professor, 2017 – present

Chief Technology Officer and Co-founder, Hummingbird Scientific, 2004 to present

- Nanotechnology firm which develops and sells advanced scientific instrumentation for nanoscale manipulation and characterization

Electron Microscopy Group, Center for Functional Nanomaterials, Brookhaven National Laboratory

Group Leader

Scientist, 2010 to 2017

- In charge of a ~\$2.25M direct/year research effort at a Department of Energy National User Facility
- Manage a group of 10 staff, post-doctoral and student researchers, as well as oversee the activity of 100–125 external users per year
- Research focus on catalytic nanomaterials for energy conversion, solid-state materials for energy storage, earth-abundant materials for solar energy, the fundamentals of nanoscale crystal growth and the development of novel experimental methods for *in situ* and *operando* characterization
- Special Assistant for *Operando* Initiative, Coordinating the “Operando Initiative” portfolio at Brookhaven, one of the Laboratory’s six Critical Outcomes. 2015–2017

Department of Materials Science and Engineering, Stony Brook University
Adjunct Professor, 2015 to 2018

School of Materials Engineering, Purdue University
Adjunct Professor, 2010 to 2016

Professor, Appointed 2010

Associate Professor (with tenure), 2007 to 2010

Associate Professor (without tenure), 2005 to 2007

- Procured and managed the outcomes of a ~\$1M/year research portfolio, including supervision of graduate and post-doctoral researchers
- Taught classes at the undergraduate and graduate level on electrical, optical and magnetic properties of materials, materials processing and advanced materials characterization

Program Leader, Metals Program, 2003 to 2004

Materials Sciences Division, Lawrence Berkeley National Laboratory

- Directed the Division's Metals Program, focusing on correlated experimental and theoretical studies of the fundamental mechanisms of mechanical deformation.

Materials Staff Scientist, 1998 to 2002

National Center for Electron Microscopy, Lawrence Berkeley National Laboratory

- Directed the Center's efforts in the development of *in-situ* transmission electron microscopy techniques.

Education

Doctor of Philosophy in Materials Science and Engineering – 1998

University of Virginia, Charlottesville, VA

Dissertation: *In-situ transmission electron microscopy studies of dislocation / defect interactions in SiGe / Si heterostructures.*

Dissertation Advisor: Robert Hull, Presently at the Department of Materials Science and Engineering, Rensselaer Polytechnic Institute

Co-advisor: Rudolf M. Tromp, IBM Watson Research Center

Masters of Business Administration – 2018

State University of New York, Stony Brook, NY

Masters of Science in Materials Science and Engineering – 1994

University of Washington, Seattle, WA

Thesis: *Mechanisms for thermal stress relaxation in a model metallic film / ceramic substrate system.*

Bachelor of Science in Engineering – 1992

Mechanical Engineering and Materials Science

Duke University, Durham, NC

Honors and Awards

Fellow, American Physical Society, Class of 2017

Fellow, Microscopy Society of America, Class of 2013

Microscopy Society of America's Eli F. Burton (Young Scientist) Award – 2009

University Faculty Scholar, Purdue University – 2009–2010

Reinhardt Schumann, Jr. Undergraduate Teaching Award, School of Materials Engineering – 2009

Purdue College of Engineering “Early Career Research Excellence Award” – 2007

Outstanding Performance Award – Lawrence Berkeley National Laboratory – 2001.

Winner – Best Poster (Physical Sciences) – Microscopy and Microanalysis Meeting – 2000.

Winner – Micrograph Competition – Microscopy and Microanalysis Meeting – 2000.

IBM Cooperative Fellowship, 1997 – IBM Mentor: Rudolf M. Tromp

Graduate Student Award (Silver Medal) – Materials Research Society Spring Meeting – 1997.

TEACHING

UNIVERSITY OF PENNSYLVANIA

SEMESTER	COURSE NUMBER	TITLE	EVALUATION (OUT OF 4.0) Instructor/class
Fall 2017	MSE 610	Transmission Electron Microscopy And Crystalline Imperfections	3.8 / 3.4

PURDUE UNIVERSITY – 2005 – 2010

SEMESTER	COURSE NUMBER	TITLE	EVALUATION (OUT OF 5.0) Instructor/class
Spring 2010	MSE 640	Transmission Electron Microscopy and Crystalline Imperfections	4.9 / 4.8
Fall 2009	MSE 697	Advanced Transmission Electron Microscopy	4.9 / 4.6
Fall 2009	MSE 582	Transmission Electron Microscopy Skills	4.9 / 4.9
Spring 2009	MSE 40	Transmission Electron Microscopy and Crystalline Imperfections	4.8 / 4.4
Spring 2009	MSE 270	Atomistic Materials Science	4.5 / 3.9
Fall 2008	MSE 370	Electrical, Optical & Magnetic Properties of	4.3 / 4.0

		Materials	
Spring 2008	MSE 640	Transmission Electron Microscopy and Crystalline Imperfections	4.9 / 4.4
Spring 2008	MSE 270	Atomistic Materials Science	4.3 / 4.0
Fall 2007	MSE 548	Deposition Processing	4.2 / 4.2
Spring 2007	MSE 640	Transmission Electron Microscopy and Crystalline Imperfections	5.0 / 4.9
Fall 2007	MSE 370	Electrical, Optical & Magnetic Properties of Materials	4.9 / 4.3
Fall 2007	MSE 335	Materials Characterization Laboratory	4.8 / 4.0
Spring 2006	MSE 640	Transmission Electron Microscopy and Crystalline Imperfections	5.0 / 4.8
Fall 2006	MSE 370	Electrical, Optical & Magnetic Properties of Materials	4.9 / 4.3
Fall 2006	MSE 582	Transmission Electron Microscopy Skills	4.3 / 4.3
Spring 2005	MSE 640	Transmission Electron Microscopy and Crystalline Imperfections	4.9 / 4.3
Average:			4.7 / 4.4

FUNDED PROGRAMS AND PROPOSALS

At The University of Pennsylvania:

Principal Investigator, MRI: Acquisition of a Dual Beam Focused Ion Beam / Scanning Electron Microscope for Research and Education, National Science Foundation, \$799,000, 2018

Principal Investigator, Quantifying the Coarsening Kinetics of Supported Metal Nanoparticles Using Time-resolved Electron Microscopy, Data Analytics and Simulations”, National Science Foundation, \$539,832

Co-Principal Investigator, “Integrated Mesoscale Architectures for Sustainable Catalysis”, Department of Energy, \$638,900

At Brookhaven:

Co-Principal Investigator, Center for Mesoscale Transport Properties, Energy Frontier Research Center, approx. \$20M to Stony Brook University, responsible for \$125,000/yr., 2014–2018

Principal Investigator, Laboratory Directed Research and Development, “Correlative microscopy, spectroscopy, and diffraction with a micro-reactor”, \$567,900 total funds, 2014–2016

At Purdue:

Principal Investigator, “Honda Research Collaboration”, \$105,000, 2010.

Principal Investigator, “Honda Research Collaboration”, \$110,000, 2009.

Co-Principal Investigator, DOE Energy Frontier Research Center “Institute for Atomically-Efficient Chemical Transformations”, \$18M total funds, responsible for \$430,000, 2009–2011

Principal Investigator, “GOALI: Quantifying growth mechanisms in semiconductor nanowires using real time transmission electron microscopy”, Electronic and Photonic Materials Program, Division of Materials Research, NSF. FY2009–2011, \$700,000 total funds to Purdue.

Principal Investigator, “Improving the growth of large-scale nanotube synthesis via heterogeneous modeling”, P.C. Krause, Inc., \$51,000, 2008–2009

Principal Investigator, “Investigate the mechanical behavior of composite rubbers at the nanoscale”, Sandia National Laboratory, \$50,000, 2008–2009.

Co-investigator, “Center for the prediction of reliability, integrity and survivability of microsystems”, DOE NNSA, approx. \$18M, 2008–2013.

Co-investigator, “Nanoscale optical antenna array for controlled, massively parallel manufacturing of nanowire devices”, DARPA, \$4,325,000 2008 – 2012.

Co-investigator, ““Nano-Tungsten for ITER Diverter Plate”, Materials Modification, Inc., \$250,000 (responsible for \$125,000), 2008–2010

Co-investigator, “Low temperature, lead-free nanosolder for microelectronics”, NSF STTR Phase I, \$68,400, 2007–2008.

Principal Investigator, “Understanding the development of chirality during the growth of carbon nanotubes”, Short Term Innovative Research program, Army Research Office, FY2007–2008. \$50,000 to Purdue

Co-investigator, “GOALI: Nanoparticle-enabled printing of large-area electronic hierarchical systems”, Civil, Mechanical and Manufacturing Innovation, National Science Foundation, FY2007–2009, \$490,000 to Purdue.

Principal Investigator, “Quantifying growth mechanisms in semiconductor nanowires using real time transmission electron microscopy”, Electronic Materials Program, Division of Materials Research, NSF. FY2007–2009. \$580,000 total funds to Purdue.

Co-investigator, “Chirality and Growth Mechanisms of Carbon Nanotubes using *In-Situ* TEM”, Air Force Research Laboratory – “Laboratory Director’s Funds”, FY 2006. \$55,000 total award, \$50,000 to Purdue

Co-investigator, “Low-cost substrates for high-performance nanorod array LEDs”, DOE Solid-State Lighting Initiative, Core Technologies, FY 2006 – 2009, approx. \$900,000 total award

Principal investigator – “Measurement of elastic strain in quantum dots”, NIST, FY2006, \$24,500.

Co-investigator – “Development of a quantitative nanoindenter for in-situ transmission electron microscopy” – DOE Phase II SBIR to the Hysitron Corporation, FY2006. \$750,000 total funds, \$20k to Purdue. Project awarded an R&D 100 award and SBIR Tibbetts Award in 2006.

Principal investigator – “Understanding the development of chirality during the growth of carbon nanotubes” – Purdue Research Foundation, FY 2005–2006, \$ 13,800.

At Lawrence Berkeley National Laboratory

Program Leader – Metals Program, Materials Sciences Division. A multi-investigator program funded by the DOE, FY2004 – 2005. \$595,000 / yr. total funds.

Principal Investigator – DOE funded program in “Experimental Nanomechanics”, FY 2003 – 2004. \$60,000/yr.

Principal Investigator – LBNL funded “Laboratory Directed Research and Development” Project “A MEMS ‘Test Kit’ for Structure – Mechanical Property Relationships at the Nanoscale”, FY 2003. \$85,000 total funds.

Co-investigator – DOE funded “Transmission Electron Aberration-corrected Microscope (TEAM) – A cooperative proposal for a national project to develop the next generation electron microscope” FY 2003–2008. Total funds approx. \$25,000,000 over 5 years. Specific responsibilities included column integration and site stability for the final instrument.

Co-investigator – DOE funded “Center for Synthesis and Processing of Carbon-Based Nanostructured Materials”. FY 2001–2004. \$27,500/yr.

PROFESSIONAL SERVICE

External Service

Secretary, Board of Directors, Materials Research Society, 2017–2019

Selected to Department of Energy Oppenheimer Science and Energy Leadership Program, 2017

BESAC Subcommittee Community Workshop – BES 40th Anniversary Program, January, 2018

Panel Chair, “Workshop on Next Generation Energy Storage”, Department of Energy Basic Energy Sciences Basic Research Needs Workshop, Gaithersburg, MD, March, 2017

Member, Stony Brook University Department of Materials Science and Chemical Engineering Advisory Board, 2016 to present.

Member, Center for Nanoscale Materials, Ultrafast Electron Microscopy Committee, 2017 – present.

Member, External Advisory Board, NSF Science and Technology Center Science and Technology Center on Real-Time Functional Imaging (“STROBE”), 2017 to present.

Member, External Advisory Board, NSF Center on Data-Enabled Science and Engineering of Atomic Structure, North Carolina State University, 2016 to present

Plenary presentation, “Workshop on Basic Research Needs for Innovation and Discovery of Transformative Experimental Tools: Solving Grand Challenges in the Energy Sciences”, Department of Energy Basic Energy Sciences Basic Research Needs Workshop, Gaithersburg, MD, June, 2016.

Panel Chair, Committee of Visitors (COV) for the Materials Sciences and Engineering (MSE) Division in the Department of Energy’s (DOE) Office of Basic Energy Sciences (BES), 2015

Member, Board of Directors, Materials Research Society, 2013–2015.

Member, Canadian Centre for Electron Microscopy Advisory Committee, McMaster University, 2014 to present.

Plenary presentation, “Future Directions of Electron Scattering and Diffraction”, Department of Energy Basic Energy Sciences Basic Research Needs Workshop Gaithersburg, MD, February, 2014.

Member, National User Facility Organization Steering Committee, 2008–2009.

User’s Executive Committee, National Center for Electron Microscopy, Chair, 2007 to 2009, Past-Chair, 2010.

Member, Steering Committee, Electron Microscopy Center, Argonne National Laboratory, 2005 to 2010

Member, IEEE’s Technical Committee on Nanomaterials, 2007 to 2010.

Invited Contributor, “Future Science Needs and Opportunities for Electron Scattering”, Department of Energy Basic Energy Sciences Basic Research Needs Workshop, Gaithersburg, MD, March, 2007.

Steering Committee member – ORNL SHaRE microscopy user facility. FY2001–2003.

Member & Short Course Organizer, Education Committee, Microscopy Society of America, 2005 to 2008

Member, Electron Diffraction Subcommittee, International Centre for Diffraction Data – 2003–2005.

Editorships

Editorial Board, Nature Scientific Data, 2016 – present.

Principal Editor, Journal of Materials Research, 2012 – 2016.

Associate Editor, Nanomaterials, Nanoscale Research Letters, 2006 – 2008.

Editorial Board, Nanoscale Research Letters, 2005 – 2008.

Workshop Organization

Co-chair, “Big, Smart and Deep Data”, Microscopy and Microanalysis 2017, St. Louis, August, 2017

International Scientific Advisory Committee, “Seventh Workshop on Nucleation and Growth Mechanisms of Single Wall Carbon Nanotubes”, 2017

Session Chair, “In situ and environmental microscopy of material reactions and processes”, International Microscopy Congress, 2014.

Co-organizer, “Characterization of Energy Materials In-Situ and Operando”, Fall 2013 Materials Research Society Meeting.

Organizing Committee, JCESR Grand Challenge Science and Characterization Workshop, May 2013.

Co-organizer, “Frontiers of in-situ transmission electron microscopy”, NIST, Gaithersburg, MD, April 2013.

Co-organizer, “Watching atoms move: from structures to dynamics to mesoscale processes” AAAS 2013 Annual Meeting

International Scientific Advisory Committee, “Sixth Workshop on Nucleation and Growth Mechanisms of Single Wall Carbon Nanotubes”

Meeting Co-chair, Fall 2012 Materials Research Society Meeting.

Co-organizer, “Carbon nanotubes and related materials”, American Physical Society “March Meeting”, Spring 2012

Co-organizer, “Electron Microscopy in Gases and Liquids”, Microscopy and Microanalysis Meeting, 2012

Symposium Chair, “In-situ Electron Microscopy”, Frontiers of Electron Microscopy in Materials Science, Fall 2011.

Co-organizer, “In-situ Electron Microscopy”, Microscopy and Microanalysis, 2009

Co-organizer, User’s Meeting, Molecular Foundry / National Center for Electron Microscopy, November, 2008.

Co-organizer, “Harnessing the growth of quantum dots: from fundamentals to applications”, Fall 2006 Materials Research Society Meeting.

Co-organizer, “Visualizing and measuring mechanical behavior”, Microscopy and Microanalysis, 2006.

Co-organizer, “Mechanisms of Deformation in Brittle Materials”, Fall 2005 Materials Research Society Meeting.

Co-organizer, “Advances in In-situ Electron Microscopy: Techniques and Applications”, Microscopy and Microanalysis, 2005.

Co-organizer, “Focused Ion Beam Microscopy”, Scanning 2005.

Co-organizer, “Imaging Atomic-scale Mechanics, Chemistry and Structure with Electron Microscopy”, Fall 2004 Materials Research Society Meeting.

Co-organizer, “Focused Ion Beam Microscopy”, Scanning 2004.

Organizer, “Focused Ion Beam Microscopy”, Scanning 2003.

Co-organizer, “Problem Solving with *In-situ* Electron Microscopy”, Microscopy and Microanalysis 2002 Meeting.

Co-organizer, “Current Issues in Heteroepitaxial Growth: Stress Relaxation and Self-assembly” Fall 2001 Materials Research Society Meeting.

Co-organizer, “EM at the Frontier”, Naval Research Lab, Stennis Space Center, November 2000.

Review Service

Proposal Review Committee – ORNL SHaRE microscopy user facility. FY1999–2010.

Reviewer for scientific journals: Science, Nature, Nature Nanotechnology, Nature Materials, Nature Communications, Nano Letters, Physical Review Letters, Physical Review B, Applied Physics Letters, Journal of the American Chemical Society, ACS Nano, Ultramicroscopy, Acta Materialia, Chemistry of Materials, Journal of Applied Physics, Scripta Materialia, Microscopy and Microanalysis, Journal of Materials Research, ACS Applied Materials and Interfaces, Materials Today, Journal of Microscopy, Scanning, Journal of Electron Microscopy, Journal of Materials Science, Scientific Reports, Journal of Physical Chemistry, Journal of Nanoscience and Nanotechnology, Nanoscale, Journal of Biomedical Materials Research, Materials Research Society Proceedings, Department of Energy – Basic Energy Sciences (regular and SBIR), National Science Foundation (regular and panel reviews), Keck Foundation, Center for Integrated Nanotechnologies (BES–user facility at Sandia National Laboratory), Austrian Science Fund, Kentucky Science and Engineering Foundation, American Chemical Society (Petroleum Research Fund), and many more ...

Service And synergistic activities

At the University of Pennsylvania

Alternate, Faculty Personnel Committee, School of Engineering and Applied Science, 2018 to present

Committee Chair, Faculty Search Committee, Department of Materials Science and Engineering, 2018

At Purdue University

Director, Purdue Electron Microscopy Consortium, Purdue University, 2008 – 2010

Director, School of Materials Engineering’s Microstructural Analysis Facility, 2008 – 2010

Scientific Director, Electron Microscopy Center, Birck Nanotechnology Center, Purdue University, 2006 – 2010

Member, Faculty Search Committee, School of Materials Engineering, 2009 – 2010
Member, College of Engineering Strategic Plan Committee, 2009.
Member, Higher Learning Commission Accreditation Review Committee, 2007 – 2010
Member, Internal Advisory Committee, Birck Nanotechnology Center, 2009 – 2010
Member, Senior Faculty Search Committee, School of Materials Engineering, 2008 – 2009
Co-Chair, Birck Nanotechnology Center Policies & Procedures Committee, 2006 – 2009
Member, Undergraduate Education Committee, School of Materials Engineering, 2006 – 2010
Member, College Research Committee, College of Engineering, 2005 – 2007
Member, Advanced Materials for Manufacturing Sub-Committee, Advanced Materials and Manufacturing Cluster Hire Search Committee, 2005.
Mentor, Fall 2005 MGMT 691W “Projects in Entrepreneurship” class project, Purdue University School of Management,
Mentor, Spring 2005 MGMT 691W “Projects in Entrepreneurship” class project, Purdue University School of Management,
Faculty Mentor, Midwest Crossroads Alliance for Graduate Education and Professoriate, Purdue University, 2005 – 2010

Industrial EMPloyment

J. H. Fletcher and Company, Huntington, WV – Summers of 1988 – 1992
Design Engineer: Design of coal mining machinery utilizing both Finite Element Analysis and Computer Aided Design. Assisted in development of several new machine prototypes and gained extensive experience in mechanical component and systems design.

Society Memberships

Materials Research Society
Microscopy Society of America
American Physical Society
American Association for the Advancement of Science
Union of Concerned Scientists

PUBLICATIONS

[Web of Science](#): ~ 23,500 citations, h-index of 56, m-index of 2.6;

[Google Scholar](#): ~ 31,500 citations, h-index of 69, i10-index of 245.

Books, Book Chapters, and Editorships:

- B1. Co-editor, with Thomas Walther, Rafal Dunin-Borkowski and Jean-Luc Rouviere, Focus Issue: Aberration Corrected Transmission Electron Microscopy, Journal of Materials Research, Journal of Materials Research, Vol. **32**, Issue 5, 2017.
- B2. Co-editor, with Scott Mixture, Bryan Huey and Vanessa K. Peterson, Focus Issue: In-situ and operando characterization of materials, Journal of Materials Research, Vol. **30**, Issue 3, 2015
- B3. Co-editor with Paulo Ferreira and Kazutaka Mitsuishi, "In-situ Transmission Electron Microscopy", Materials Research Society Bulletin, Vol. 33, Issue 2, 2008.
- B4. *In situ nanoindentation in a transmission electron microscope*, Andrew Minor, Eric A. Stach and J.W. Morris, Jr., in Dislocations in Solids, vol. 13, ed. by F.R.N. Nabarro and J.P. Hirth.
- B5. Electron Microscopy of Molecular and Atom-Scale Mechanical Behavior, Chemistry and Structure; edited by D. Martin, D.A. Muller, E.A. Stach, P. Midgley, Proceedings of the Materials Research Society, Volume 839, 2005.
- B6. Current Issues in Heteroepitaxial Growth -- Stress Relaxation and Self Assembly; edited by E.A. Stach, E. Chason, R. Hull and S.M. Bader, Proceedings of the Materials Research Society, Volume 696, 2002. Principal editor.
- B7. Guest Editor – "Problem Solving using *In-situ* Transmission Electron Microscopy", Microscopy and Microanalysis, Volume 7(6), November / December 2001.
- B8. *Strain accommodation and relief in SiGe / Si heteroepitaxy*, book chapter by R. Hull and E.A. Stach in Thin Films: Heteroepitaxial Systems volume 15 of Directions in Condensed Matter Physics, edited by A. W. Liu and M. B. Santo, World Scientific Publishing Co., Inc., Rivers Edge, NJ, 1999.

Invited Review / Opinion Articles

- IR1. *Current status and future directions for in situ transmission electron microscopy*; Mitra L. Taheri, Eric A. Stach, Ilke Arslan, P. A. Crozier, Bernd C. Kabius, Thomas LaGrange, Andrew M. Minor, Seiji Takeda, Mihaela Tanase, Jakob B. Wagner, Renu Sharma Ultramicroscopy 170 (2016) 86–95.
- IR2. *Comparative in operando studies in heterogeneous catalysis: Atomic and electronic structural features in the hydrogenation of ethylene over supported Pd and Pt catalysts*, U. Jung, A. Elsen, Y. Li, J. G. Smith, M. W. Small, E. A. Stach, A. I. Frenkel, R. G. Nuzzo, ACS Catalysis (Perspective), **5**, 1539–1551, 2015.

- IR3. *Critical review: Effects of complex interactions on structure and dynamics of supported metal catalysts*, A.I. Frenkel, M.W. Cason, A. Elsen, U. Jung, M.W. Small, R.G. Nuzzo, F.D. Vila, J.J. Rehr, E.A. Stach, and J.C. Yang, *J. Vac. Sci. Tech A*, **32** (2), 020801, 2014.
- JVST A Top 10 Most Cited Articles Published in 2014
- IR4. *Electron tomography: seeing atoms in three dimensions*, Ilke Arslan and Eric A. Stach, *Nature Mat.*, **11**, 911, 2012.
- IR5. *Real time transmission electron microscopy*, Eric A. Stach, *Materials Today*, Special Microscopy Issue, 51–58, December 2008.
- IR6. *Further considerations on high-cycle fatigue of micron-scale polycrystalline silicon*, D.H. Alsem, C.L. Muhlstein, E.A. Stach and R.O. Ritchie, *Scripta Materialia*, **59**, 931–935, 2008.
- IR7. *Nanotubes reveal their true strength*, Eric Stach, *Nature Nanotechnology*, **3**(10), 586–587, 2008.
- IR8. *Visualizing the behavior of dislocations – seeing is believing*, Ian M. Robertson, Paulo J. Ferreira, Gerhard Dehm, Robert Hull and Eric A. Stach, *Materials Research Society Bulletin*, **33**, 122–131, 2008.
- IR9. *Mechanisms for fatigue of micron-scale silicon structural films*, D.H. Alsem, O.N. Pierron, E.A. Stach, C.L. Muhlstein and R.O. Ritchie, *Advanced Engineering Materials*, **9**(1–2), 15–30, 2007.
- IR10. *In situ nanoindentation in the TEM*, O.L. Warren, Z. Shan; S.A.S. Asif, E.A. Stach, J.W. Morris, Jr., and A.M. Minor, *Materials Today*, **10**(4), 59–60, 2007.
- IR11. *Dislocations in semiconductors*, E.A. Stach and R. Hull, review article in Encyclopedia of Materials: Science and Technology, ed. K.H.J. Jurgen Bushow, R.W. Cahn, M.C. Flemings, B. Ilshner, E.J. Kramer and S. Mahajan, Pergamon Press, Amsterdam, 2001.
- IR12. *Equilibrium and metastable strained layer semiconductor heterostructures*, R. Hull and E.A. Stach; *Current Opinion in Solid State and Materials Science*, **1**(1), 21–8, 1996.

Refereed Journal Articles:

- J1. *Anatomy of a Visible Light Activated Photocatalyst for Water Splitting*, S.P. Phivilay, C. Roberts, A. Gamalski, E.A. Stach, S. Zhang, L. Nguyen, Y. Tang, A. Xiong, A. Puretzky, F. Tao, K. Domen, I. Wachs, in press at *ACS Catalysis*.
- J2. *Highly Active Subnanometer Rh Clusters Derived from Rh-doped SrTiO₃ for CO₂ Reduction*, Binhang Yan, Qiyuan Wu, Jiajie Cen, Janis Timoshenko, Anatoly I. Frenkel, Dong Su, Xianyin Chen, John B. Parise, E. A. Stach, A. Orlov and J.G. Chen in press at *Applied Catalysis B: Environmental*.

- J3. *Molecular structure and sour gas surface chemistry of supported K₂O/WO₃/Al₂O₃ catalysts*, Minghui Zhu, Bin Li, Jih-Mirn Jehng, Lohit Sharma, Julian Taborda, Lihua Zhang, Eric Stach, Israel E. Wachs, Zili Wu, and Jonas Baltrusaitis, *Applied Catalysis B: Environmental*, 232, pp.146–154.
- J4. *Segregation induced order–disorder transition in Cu (Au) surface alloys*, Zou, Lianfeng, Wissam A. Saidi, Yinkai Lei, Zhenyu Liu, Jonathan Li, Liang Li, Qing Zhu, D.N. Zakharov, E.A. Stach, J.C. Yang, G. Zhuo, *Acta Materialia*, 154, 220–227, 2018
- J5. *Identifying Dynamic Structural Changes of Active Sites in Pt–Ni Bimetallic Catalysts Using Multimodal Approaches*, Deyu Liu, Yuanyuan Li, Matthew Kottwitz, Binhang Yan, Siyu Yao, Andrew Gamalski, Daniel Grolimund, Olga V. Safonova, Maarten Nachtegaal, Jingguang G. Chen, Eric A. Stach, Ralph G. Nuzzo, and Anatoly I. Frenkel, *ACS Catal.*, 8, 4120–4131, 2018.
- J6. *Structural and Electrochemical Characteristics of Ca-Doped “Flower– like” Li₄Ti₅O₁₂ Motifs as High-Rate Anode Materials for Lithium-Ion Batteries*, Lei Wang, Yiman Zhang, Haoyue Guo, Jing Li, Eric A. Stach, Xiao Tong, Esther S. Takeuchi, Kenneth J. Takeuchi, Ping Liu, Amy C. Marschilok, and Stanislaus S. Wong, *Chemistry of Materials*, DOI: 10.1021/acs.chemmater.7b03847, 2018
- J7. *Evolution and stabilization of subnanometric metal species in confined space by in situ TEM*, Lichen Liu, Dmitri N. Zakharov, Raul Arenal, Patricia Concepcion, Eric A. Stach and Avelino Corma, *Nat. Comm.*, DOI: 10.1038/s41467-018-03012-6, 2018.
- J8. *Atomically Visualizing Elemental Segregation Induced Surface Alloying and Restructuring*, Lianfeng Zou, Jonathan Li, Dmitri N. Zakharov, Wissam A. Saidi, Eric A. Stach, and Guangwen Zhou. *J. Phys. Chem. Lett.*, 8(24), p.6035–6040 2018.
- J9. *Dislocation nucleation facilitated by atomic segregation*, Lianfeng Zuo, Chaoming, Yang, Yinkai Lei, Dmitri Zakharov, Joerg M.K. Wiezorek, Dong SU, Qiyue Yin, Jonathan Li, Zhenyu Liu, Eric A. Stach, Judith C. Yange, Liang Qi, Guofeng Wang, Guangwen Zhou, *Nature Mat.*, 17(1), p.56–63, 2017.
- J10. *Strain coupling of conversion-type Fe₃O₄ thin film for lithium ion batteries*, Sooyeon Hwang, Qingping Meng, Ping-Fan Chen, Kim Kisslinger, Yimei Zhu, Eric A. Stach, Ying-Hao Chu, and Dong Su, *Ange. Chemie. Int. Ed.*, 56(27), 7813–7816, 2017.
- J11. *Two-Dimensional Holey Nanoarchitectures Created by Confined Self-Assembly of Nanoparticles via Block Copolymers: From Synthesis to Energy Storage Property*, Lele Peng, Zhiwei Fang, Jing Li, Lei Wang, Andrew M. Bruck, Yue Zhu, Zhang, Yiman, Kenneth J. Takeuchi, Amy C. Marschilok, Eric A Stach, Esther S. Takeuchi, and Guihua Yu, *ACS Nano* 12(1), p.820–828, 2018.
- J12. *Enhanced carbon dioxide electroreduction to carbon monoxide over defect-rich plasma-activated silver catalysts*, Hemma Mistry, Yong-Wook Choi, Alexander Bagger,

- Fabian Scholten, Cecile Bonifacio, Ilya Sinev, Nuria J Divins, Ioannis Zegkinoglou, Hyo Sang Jeon, Kim Kisslinger, Eric A Stach, Judith C Yang, Jan Rossmeisl, Beatriz Roldan Cuenya, Ange. *Chemie. Int. Ed.*, **29**(38), 11552–11556, 2018.
- J13. *In situ atomic-scale imaging of the metal/oxide interfacial transformation*, Lianfeng Zou, Jonathan Li, Dmitri Zakharov, Eric A. Stach, and Guangwen Zhou, *Nature Comm.* **8**, 307, 2017.
- J14. *Near real time ETEM streaming video analysis*, Y Lin, D Zakharov, R Megret, S Yoo, E Stach, Scientific Data Summit (NYSDS), 2017 New York, 1–4
- J15. *Experimental Study of the Detection Limit in Dual-Gate Biosensors Using Ultra-Thin Silicon Transistors* Ting Wu, Abdullah Alharbi, Kae-Dyi You, Kim Kisslinger, Eric Stach, and Davood Shahrjerdi, *ACS Nano*, **11**, 7, 7142–7147, 2017.
- J16. *Signature of Metallic Behavior in the Metal–Organic Frameworks $M_3(\text{hexaiminobenzene}_2$ ($M = \text{Ni}, \text{Cu}$))*, Jinhu Dou, Lei Sun, Li Yicong, Christopher Hendon, Ju Li, Sheraz Gul, Junko Yano, Eric Stach and Mircea Dinca, *J. Am. Chem. Soc.*, **139**(39), 13608–1361, 2017.
- J17. *Multimodal Study of the Speciations and Activities of Supported Pd Catalysts During the Hydrogenation of Ethylene*, Shen Zhao, Yuanyuan Li, Deyu Liu, Jing Liu, Yao–Min Liu, Dmitri N. Zakharov, Qiyuan Wu, Alexander Orlov, Andrew A. Gewirth, Eric A. Stach, Ralph G. Nuzzo, and Anatoly I. Frenkel, *The Journal of Physical Chemistry C*, DOI: 10.1021/acs.jpcc.7b06270
- J18. *A Tunable 3D Nanostructured Conductive Gel Framework Electrode for High-Performance Lithium Ion Batteries*, Ye She, Jun Zhang, Andrea M. Bruck, Yiman Zhang, Jing Li, Eric A. Stach, Kenneth J. Takeuchi, Amy C. Marschilok, Esther S. Takeuchi, and Guihua Yu., *Advanced Materials* 10.1002/adma.201603922, 2017.
- J19. *Dynamic restructuring drives catalytic activity on nanoporous gold–silver alloy catalysts*, Branko Zugic, Lucun Wang, Christian Heine, Dmitri N. Zakharov, Barbara A.J. Lechner, Eric A. Stach, Juergen Beiner, Miquel Salmeron, Robert J. Madix and Cynthia M. Friend, *Nat. Mat.*, **16**, 558–562, 2017.
- J20. *Atomic level cleaning of poly-methyl-methacrylate residues from the graphene surface using radiolized water at high temperatures*, Ahmad Ehteshamul Islam, Dmitri N. Zakharov, Jennifer Carpena–Nuñez, Ming–Siao Hsiao, Lawrence F. Drummy, Eric A. Stach, and Benji Maruyama, *Appl. Phys. Lett.*, **111**, 103101 (2017).
- J21. *Making Li–Metal Electrodes Rechargeable by Controlling the Direction of Dendrite Growth*, Jian Xie, Yadong, Le Xin, Yuzi Liu, Qi Liu, Fan Yang, and Eric A. Stach, *Nature Energy*, **2**, 17083, 2017.
- J22. *Aberration–Corrected Electron Beam Lithography at the One Nanometer Length Scale*, Vitor R. Manfrinato, Aaron Stein, Lihua Zhang, Chang–Yong Nam, Kevin G.

Yager, Eric A. Stach and Charles T. Black, *Nano Letters*, 17, 4562–4567, 2017 doi: 10.1021/acs.nanolett.7b005

- Featured Cover Article

- J23. *Nanoscale structural oscillations in perovskite oxides induced by oxygen evolution*; Binghong Han, Kelsey A. Stoerzinger, Vasiliki Tileli, Andrew D. Gamalski, Eric A. Stach, Yang Shao-Horn, *Nature Mat.*, **16**, 121–126, 2017.
- J24. *Atomic insight into the layered/spinel phase transformation in charged $\text{LiNi}_{0.80}\text{Co}_{0.15}\text{Al}_{0.05}\text{O}_2$ cathode particles*, Hanlei Zhang, Khim Karki, Yiqing Huang, M. Stanley Whittingham, Eric A. Stach, Guangwen Zhou, *J. Phys. Chem. C*, **121**, 1421–1430, 2017.
- J25. *Inter-granular cracking as a major cause of long-term capacity fading of layered cathodes*, Hao Liu, Mark Wolf, Khim Karki, Young-Sang Yu, Eric A. Stach, Jordi Cabana, Karena W. Chapman, and Peter J. Chupas, *Nano Letters* 17, 3452–3457 (2017).
- J26. *Energy Dispersive X-ray Diffraction (EDXRD) of $\text{Li}_{1.1}\text{V}_3\text{O}_8$ Electrochemical Cell*, Qing Zhang, Andrea M. Bruck, David C. Bock, Jing Li, Eric A. Stach, Esther S. Takeuchi, Kenneth J. Takeuchi, and Amy C. Marschilok, *MRS Advances* 2, 401–406, 2017 doi: 10.1557/adv.2017.54
- J27. *Visualization of structural evolution and phase distribution of a lithium vanadium oxide ($\text{Li}_{1.1}\text{V}_3\text{O}_8$) electrode via an operando and in situ energy dispersive X-ray diffraction technique*, Qing Zhang, Andrea M. Bruck, David C. Bock, Jing Li, Varun Sarbada, Robert Hull, Eric A. Stach, Kenneth J. Takeuchi, Esther S. Takeuchi, and Amy C. Marschilok, *Physical Chemistry Chemical Physics* 19, no. 21 (2017): 14160–14169.
- J28. *Glucose sensing using dual-gated BioFETs with 5nm-thick silicon body*, Ting Wu, Ali Afzali, Kae-Dyi You, Kim Kisslinger, Eric Stach, and Davood Shahrjerdi. In *Device Research Conference (DRC), 2017 75th Annual*, pp. 1–2. IEEE, 2017.
- J29. *A Tunable 3D Nanostructured Conductive Gel Framework Electrode for High-Performance Lithium Ion Batteries*, Ye Shi, Jun Zhang, Andrea M. Bruck, Yiman Zhang, Jing Li, Eric A. Stach, Kenneth J. Takeuchi, Amy C. Marschilok, Esther S. Takeuchi, and Guihua Yu, *Advanced Materials*, 2017.
- J30. *Length-dependent melting behavior of Sn nanowires*, Qiyue Yin, Fan Gao, Jirui Wang, Zhiyong Gu, Eric A. Stach, and Guangwen Zhou, *J. Mater. Res.*, 1–9, 2017.
- J31. *Plasmonic Titanium Nitride Nanostructures via Nitridation of Nanopatterned Titanium Dioxide*, Urcan Guler, Dmitry Zemlyanov, Jongbum Kim, Zhuoxian Wang, Rohith Chandrasekar, Xiangeng Meng, Eric Stach, Alexander V. Kildishev, Vladimir M. Shalaev, and Alexandra Boltasseva. *Advanced Optical Materials* 5, (2017).

- J32. *Importance of Low Dimensional CeO_x Nanostructures in $\text{Pt/CeO}_x\text{-TiO}_2$ Catalysts for the Water–Gas Shift Reaction*, Luo, Si, Laura Barrio, Thuy–Duong Nguyen–Phan, Dimitriy Vovchok, Aaron C. Johnston–Peck, Wenqian Xu, Eric A. Stach, José A. Rodriguez, and Sanjaya D. Senanayake. *The Journal of Physical Chemistry C* 121, 6635–6642, (2017)
- J33. *Investigation of Structural Evolution of $\text{Li}_{1.1}\text{V}_3\text{O}_8$ by In Situ X–ray Diffraction and Density Functional Theory Calculations*, Zhang, Qing, Alexander B. Brady, Christopher J. Pelliccione, David C. Bock, Andrea M. Bruck, Jing Li, Varun Sarbada, Robert Hull, E.A. Stach, K.J. Takeuchi, K.J. and E.S. Takeuchi, *Chemistry of Materials*, 29(5), pp.2364–2373, 2017
- J34. *Lithium Vanadium Oxide ($\text{Li}_{1.1}\text{V}_3\text{O}_8$) Coated with Amorphous Lithium Phosphorous Oxynitride (LiPON): Role of Material Morphology and Interfacial Structure on Resulting Electrochemistry*, Qing Zhang, Andrew K. Kercher, Gabriel M. Veith, Varun Sarbada, Alexander B. Brady, Jing Li, Eric A. Stach, Robert Hull, K.J. Takeuchi, E.S. Takeuchi, and N.J. Dudney, *Journal of The Electrochemical Society*, 164, A1503–A1513, 2017.
- J35. *Correlating Preparative Approaches with Electrochemical Performance of $\text{Fe}_3\text{O}_4\text{-MWNT}$ Composites Used as Anodes in Li–Ion Batteries*, Lei Wang, Yue Ru Li, Jing Li, Shihui Zou, Eric A. Stach, Kenneth J. Takeuchi, Esther S. Takeuchi, Amy C. Marschilok, and Stanislaus S. Wong. *ECS Journal of Solid State Science and Technology* 6, M3122–M3131, 2017.
- J36. *High–pressure vapor–phase hydrodeoxygenation of lignin–derived oxygenates to hydrocarbons by a PtMo bimetallic catalyst: Product selectivity, reaction pathway, and structural characterization*, Sara L. Yohe, Harshavardhan J. Choudhari, Dhairya D. Mehta, Paul J. Dietrich, Michael D. Detwiler, Cem M. Akatay, Eric A. Stach, Jeffrey T. Miller, W. Nicholas Delgass, Rakesh Agrawal and Fabio H. Ribeiro, *Journal of Catalysis* 344, 535–552, 2016.
- J37. *Interrogation of bimetallic particle oxidation in three dimensions at the nanoscale*, Lili Han, Qingping Meng, Deli Wang, Yimei Zhu, Jie Wang, Xiwen Du, Eric A. Stach, and Huolin Xin, *Nature Communications*, 7, 13335, 2016
- J38. *Charge transport in CdTe solar cells revealed by conductive tomographic atomic force microscopy*, Justin Luria, Yasemin Kutes, Andrew Moore, Lihua Zhang, Eric A. Stach and Bryan D. Huey, *Nat. Energy*, 1, 16150, 2016.
- J39. *Polyvinylpyrrolidone–Induced Anisotropic Growth of Gold Nanoprisms in Plasmon–Driven Synthesis*, Yueming Zhai, Joseph S. DuChene, Yi–Chung Wang, Jingjing Qiu, Aaron C. Johnston–Peck, Bo You, Benedetto DiCiaccio, Kun Qian, Evan W. Zhao, Frances Ooi, Dehong Hu, Dong Su, Eric A. Stach, Zihua Zhu, and Wei David Wei, *Nature Mat.*, 15, 889–895, 2016.

- J40. *Highly selective plasma-activated copper catalysts for carbon dioxide reduction to ethylene*, Hemma Mistry, Ana Sofia Varela, Cecile Bonifacio, Ioannis Zegkinoglou, Ilia Sinev, Yong-Wook Choi, Kim Kisslinger, Eric Stach, Judith Yang, Peter Strasser, and Beatriz Roldan Cuenya, *Nature Comm.*, **7**, 12123, 2016.
- J41. *Visualizing non-equilibrium lithiation of spinel oxide via in situ transmission electron microscopy*, Kai He, Sen Zhang, Jing Li, Xiqian Yu, Qingping Meng, Yizhou Zhu, Enyuan Hu, Hongseok Yun, Xiao-Qing Yang, Yimei Zhu, Hong Gan, Yifei Mo, Eric A. Stach, Christopher B. Murray, and Dong Su, *Nat. Comm.*, **7**, 11411, 2016.
- J42. *Real-Time Imaging of Self-Organization and Mechanical Competition in Carbon Nanotube Forest Growth*, Viswanath Balakrishnan, Mostafa Bedewy, Eric R. Meshot, Sebastian W. Pattinson, Erik S. Polsen, Fabrice Laye, Dmitri N. Zakharov, Eric A. Stach, and A. John Hart, *ACS Nano*, **10**, 11496–11504, 2016
- J43. *Atomic Resolution in Situ Imaging of a Double-Bilayer Multistep Growth Mode in Gallium Nitride Nanowires*, A.D. Gamalski, J. Tersoff and E.A. Stach, *Nano Letters*, **16**, 2283–8, 2016.
- J44. *High-Energy Surface and Volume Plasmons in Nanopatterned Sub-10 nm Aluminum Nanostructures*, Richard G. Hobbs, Vitor R. Manfrinato, Yujia Yang, Sarah A. Goodman, Lihua Zhang, Eric A. Stach and Karl K. Berggren, *Nano Lett.*, **16**(7), 4149–4157, 2016
- J45. *Controlling the Formation and Structure of Nanoparticle Superlattices through Surface Ligand Behavior*, Marco AL Cordeiro, Edson R. Leite, and Eric A. Stach, *Langmuir*, **32**, 11606–11614, 2016
- J46. *Reversed Nanoscale Kirkendall Effect in Au-InAs Hybrid Nanoparticles*, Jing Liu, Yorai Amit, Yuanyuan Li, Anna Plonka, Sanjit Ghose, Lihua Zhang, Eric A. Stach, Uri Banin, Anatoly Frenkely, *Chem. Mater.*, **21**, 8032–8043, 2016.
- J47. *Development of a New Generation of Stable, Tunable, and Catalytically Active Nanoparticles Produced by Helium Nanodroplet Deposition Method*, Qiyuan Wu, Claron J. Ridge, Shen Zhao, Dmitri Zakharov, Jiajie Cen, Xiao Tong, Eoghan Connors, Dong Su, Eric A. Stach, C. Michael Lindsay, and Alexander Orlov, *J. Phys. Chem. Lett.*, **7**, 2910–14, 2016.
- J48. *Measurement of the Dewetting, Nucleation, and Deactivation Kinetics of Carbon Nanotube Population Growth by Environmental Transmission Electron Microscopy* M. Bedewy, V. Balakrishnan, E. R. Meshot, D. Zakharov, E. Stach, and A. J. Hart, *Chemistry of Materials*, Vol. 28, No. 11, pp 3804–3813, 2016.
- J49. *Correlating Titania Nanostructured Morphologies with Performance as Anode Materials for Lithium-Ion Batteries*, Crystal S. Lewis, Yue Ru Li, Lei Wang, Jing Li, Eric A. Stach, Kenneth J. Takeuchi, Amy C. Marschilok, Esther S. Takeuchi, and Stanislaus S. Wong. *ACS Sus. Chem. Eng.*, **4**, 6299–6312, 2016.

- J50. *Understanding the Rocksalt-to-Wurtzite phase transformation through microstructural analysis of (Al,Sc)N epitaxial thin films*, Bivas Saha, Sammy Saber, Eric A. Stach, Eric P. Kvam and Timothy D. Sands, Appl. Phys. Lett., **109**, 172102, 2016.
- J51. *Metal-metal chalcogenide molecular precursors to binary, ternary, and quaternary metal chalcogenide electronic devices*, Ruihong Zhang, Seonghyuk Cho, Daw Gen Lim, Xianyi Hu, Eric A. Stach, Carol A. Handwerker, Rakesh Agrawal, Chem. Comm. **52**, 5007, 2016.
- J52. *Nanowire growth kinetics in aberration corrected environmental transmission electron microscopy*, Yi-Chia Chou, F. Panciera, M.C. Reuter, Eric A. Stach and Frances M. Ross, Chem. Comm., **52**, 5686–5689, 2016.
- J53. *High-pressure vapor-phase hydrodeoxygenation of lignin-derived oxygenates to hydrocarbons by a PtMo bimetallic catalyst: Product selectivity, reaction pathway, and structural characterization*, S.L. Yohe, H.J. Choudhari, D.D.Mehta, P.J.Dietrich, M.D. Detwiler, C.M. Akatay, E.A Stach, J.T. Miller, W.N. Delgass, R. Agrawal, and F.H. Ribeiro, J. Catalysis, **344**, pp.535–552, 2016
- J54. *Tuning the activity of oxygen in LiNi_{0.8}Co_{0.15}Al_{0.05}O₂ battery electrodes*, Khim Karki, Yiqing Huang, Sooyeon Hwang, Andrew D. Gamalski, M. Stanley Whittingham, Guangwen Zhou, and Eric A. Stach, ACS Appl. Mater. Interfaces, **8**, 27762–27771, 2016.
- J55. *The effect of the surface composition on Ru-Pt bimetallic catalysts for methanol oxidation*, T.R. Garrick, W. Diao, J.M. Tengco, E.A. Stach, S.D. Senanayake, D.A. Chen, J.R. Monnier and J.W. Weidner, Electrochimica Acta, **195**, 11, 2016.
- J56. *Direct observation of morphological evolution of a catalyst during carbon nanotube forest growth: new insights into growth and growth termination*, Seojeong Jeong, Jaegeun Lee, Hwan-Chul Kim, Jun Yeon Hwang, Bon-Cheol Ku, Dmitri N. Zakharov, Benji Maruyama, Eric A. Stach, Seung Min Kim, Nanoscale, **8**, 2055–2062, 2016
- J57. *Statistical analysis of support thickness and particle size effects in HRTEM imaging of metal nanoparticles*, Stephen D. House, Cecile S. Bonifacio, Ross V. Grieshaber, Long Li, Zhongfan Zhang, Jim Ciston, Eric A. Stach, and Judith C. Yang, Ultramicroscopy **169**, 22–29, 2016.
- J58. *Elucidating the Sole Contribution from Electromagnetic Near-Fields in Plasmon-Enhanced Cu₂O Photocathodes*, Joseph S. DuChene, Benjamin P. Williams, Aaron C. Johnston-Peck, Jingjing Qiu, Mathieu Gomes, Maxime Amilhou, Donald Bejleri, Jiena Weng, Dong Su, Fengwei Huo, Eric A. Stach, Wei David Wei, Adv. Energy Mater., **6**, 1501250, 2016.
- J59. *Unraveling the Hydrogenation of TiO₂ and Graphene Oxide/TiO₂ Composites in Real Time by In Situ Synchrotron X-ray Powder Diffraction and Pair Distribution Function Analysis*, Thuy-Duong Nguyen-Phan, Zongyuan Liu, Si Luo, Andrew D. Gamalski,

- Dimitriy Vovchok, Wenqian Xu, Eric A. Stach, Dmitry E. Polyansky, Etsuko Fujita, José A. Rodriguez, and Sanjaya D. Senanayake, *J. Phys. Chem. C*, **6**, 3472–82, 2016
- J60. *Oxidation-state sensitive imaging of cerium dioxide by atomic-resolution low-angle annular dark field scanning transmission electron microscopy*, Aaron C. Johnston-Peck, Jonathan P. Winterstein, Alan D. Roberts, Joseph S. DuChene, Kun Qian, Brendan C. Sweeny, Wei David Wei, Renu Sharma, Eric A. Stach, and Andrew A. Herzing, *Ultramic.*, **162**, 52–60, 2016.
- J61. *Redox chemistry of a binary transition metal oxide (AB_2O_4): A study of the Cu^{2+}/CuO and Fe^{3+}/FeO interconversions observed upon lithiation in a $CuFe_2O_4$ battery using X-ray absorption spectroscopy*. Christina Cama, Christopher Pelliccione, Alexander B. Brady, Jing Li, Eric Stach, Jiajun Wang, Jun Wang, Esther S. Takeuchi, Kenneth James Takeuchi, and Amy C. Marschilok, *Phys. Chem. Chem. Phys.*, **18**, 16930 –16940, 2016.
- J62. *Sodiation kinetics of metal oxide conversion electrodes: A comparative study with lithiation*, Kai He, Feng Lin, Yizhou Zhu, Xiqian Yu, Jing Li, Ruqian Lin, Dennis Nordlund, Tsu-Chien Weng, Ryan M. Richards, Xiao-Qing Yang, Marca M. Doeff, Eric A. Stach, Yifei Mo, Huolin L. Xin, and Dong Su, *Nano Lett.*, **15**, 5755–5763, 2015.
- J63. *In situ visualization of metallurgical reactions in nanoscale Cu/Sn diffusion couples*, Qiyue Yin, Fan Gao, Zhiyong Gu, Eric A. Stach, and Guangwen Zhou, *Nanoscale*, **7**, 4984–4994, 2015.
- J64. *Striving Toward Noble-Metal-Free Photocatalytic Water Splitting: The Hydrogenated-Graphene- TiO_2 Prototype*, Thuy-Duong Nguyen-Phan, Si Luo, Zongyuan Liu, Andrew D. Gamalski, Jing Tao, Wenqian Xu, Eric A. Stach, Dmitry E. Polyansky, Sanjaya D. Senanayake, Etsuko Fujita, and José A. Rodriguez, *Chem. Mater.*, **27**, 6282–6296, 2015.
- J65. *Operando Characterization of Catalysts through use of a Portable Microreactor*, Shen Zhao, Yuanyuan Li, Eli Stavitski, Ryan Tapper, Stephen Crowley, Marco J. Castaldi, Dmitri N. Zakharov, Ralph G. Nuzzo, Anatoly I. Frenkel, Eric A. Stach, *ChemCatChem*, **7**, 3683–3691, 2015.
- J66. *Probing the active sites for water-gas shift over Pt/molybdenum carbide using multi-walled carbon nanotubes*, Kaiwalya D. Sabnis, M. Cem Akatay, Yanran Cui, Fred G. Sollberger, Eric A. Stach, Jeffrey T. Miller, W. Nicholas Delgass, and Fabio H. Ribeiro, *J. Catal.*, **330**, 442–451, 2015.
- J67. *The Role of Surface Passivation in Controlling Ge Nanowire Faceting*, Andrew D. Gamalski, Jerry Tersoff, Suneel Kodambaka, Dmitri N. Zakharov, Frances M. Ross, and Eric A. Stach, *Nano Letters*, **15**, 8211–8216, 2015.
- J68. *An in situ phosphorus source for the synthesis of Cu_3P and the subsequent conversion to Cu_3PS_4 nanoparticle clusters*, Erik J. Sheets, Wei-Chang Yang, Robert

- B. Balow, Yunjie Wang, Bryce C. Walker, Eric A. Stach, Rakesh Agrawal, J. Mater. Res., **30**, 3710–3716, 2015.
- J69. *Complex structural dynamics of nanocatalysts revealed in operando conditions by correlated imaging and spectroscopy probes*, Y. Li, D. Zakharov, S. Zhao, R. Tappero, U. Jung, A. Elsen, Ph. Baumann, R.G. Nuzzo, E.A. Stach, A.I. Frenkel, Nat. Comm., **6**, 7583, 2015.
- J70. *Synthesis of nanostructures in nanowires using sequential catalyst reactions*, F. Panciera, Y.-C. Chou, M.C. Reuter, D. Zakharov, E.A. Stach, S. Hofmann, S and F.M. Ross, Nat. Mat., **14** (8), 820–825, 2015
- J71. *Development of epitaxial $A_{1-x}Sc_xN$ for artificially structured metal/semiconductor superlattice metamaterials*, Bivas Saha, Sammy Saber, Gururaj Naik, Alexandra Boltasseva, Eric A. Stach, Eric P. Kvam, Timothy D. Sands, physica status solidi (b), **252**, 251–259, 2015.
- J72. *Characterization of V-shaped Defects in 4H-SiC Homoepitaxial Layers*, Fangzhen Wu, Huanhuan Wang, Balaji Raghothamachar, Michael Dudley, Gil Chung, Jie Zhang, Bernd Thomas, Edward K. Sanchez, Stephan G Mueller, and Darren Hansen, J. Elect. Mater., **44**, 1293–1299, 2015
- J73. *Effect of deposition pressure on the microstructure and thermoelectric properties of epitaxial ScN (001) thin films sputtered onto MgO (001) substrates*, Polina Burmistrova, Polina, Dmitri N. Zakharov, Tela Favalaro, Amr Mohammed, Eric A. Stach, Ali Shakouri, and Timothy D. Sands, J. Mater. Res., **30**, 626–634, 2015.
- J74. *Strain and Stability of Ultrathin Ge Layers in Si/Ge/Si Axial Heterojunction Nanowires*, Cheng-Yen Wen, Mark C Reuter, Dong Su, Eric A. Stach, Frances M. Ross, Nano Letters, **15**, 1654–1659, 2015.
- J75. *Superior performance of Ni-W-Ge mixed-metal oxide catalysts for ethanol steam reforming: Synergistic effects of W-and Ni-dopants*, Zongyuan Liu, Wenqian Xu, Siyu Yao, Aaron C Johnson-Peck, Fuzhen Zhao, Piotr Michorczyk, Anna Kubacka, Eric A Stach, Marcos Fernández-García, Sanjaya D Senanayake, José A Rodriguez, J. Cata., **321**, 90–99, 2015.
- J76. *9.0% efficient $Cu_2ZnSn(S,Se)_4$ solar cells from selenized nanoparticle inks*, Caleb K. Miskin, Wei-Chang Yang, Charles J. Hages, Nathaniel J. Carter, C. Joglekar, E.A. Stach, and Rakesh Agrawal, Progress in Photovoltaics: Research and Applications, **23** (5), 654–659, 2015.
- J77. *Real-time Observation of Morphological Transformations in II–VI Semiconducting Nanobelts via Environmental Transmission Electron Microscopy*, R. Agarwal, D. Zakharov, N. Krook, W. Liu, J. Berger, E. Stach, R. Agarwal, Nano Lett, **15**(5), 3303–3308, 2015.

- J78. *Using Real-time Electron Microscopy to Explore the Effects of Transition Metal Composition on the Local Thermal Stability in Charged $\text{Li}_x\text{Ni}_y\text{Mn}_z\text{Co}_{1-y-z}\text{O}_2$ Cathode Materials*, Sooyeon Hwang, Seung Min Kim, Seong-Min Bak, Se Young Kim, Byung Won Cho, Kyung Yoon Chung, Jeong Yong Lee, Eric A. Stach, Wonyoung Chang, Chem. Mater., **27**(11), 3927–3935, 2015.
- J79. *Correlating Size and Composition-Dependent Effects with Magnetic, Mössbauer, and Pair Distribution Function Measurements in a Family of Catalytically Active Ferrite Nanoparticles*, A.L. Tiano, G.C. Papaefthymiou, C.S. Lewis, J. Han, C. Zhang, Q. Li, C. Shi, A.M.M. Abeykoon, S.J.L. Billinge, E. Stach, J. Thomas, K. Guerro, P. Munayco, J. Munayco, R.B. Scorzelli, P. Burnham, A.J. Viescas, S.S. Wong, Chem. Mater., **27**(10), pp 3572–3592, 2015
- J80. *Mechanism and Enhanced Yield of Carbon Nanotube Growth on Stainless Steel by Oxygen-Induced Surface Reconstruction*, Sebastian W. Pattinson, Balakrishnan Viswanath, Dmitri N. Zakharov, Jinjing Li, Eric A. Stach, and A. John Hart, Chem. Mater., **27**, 932–937, 2015.
- J81. *Transitions from Near-Surface to Interior Redox upon Lithiation in Conversion Electrode Materials*, Kai He,* Huolin Xin,* Kejie Zhao, Xiqian Yu, Dennis Nordlund, Tsu-Chien Weng, Jing Li, Yi Jiang, Christopher A. Cadigan, Ryan M. Richards, Marca M. Doeffer, Xiao-Qing Wang, Eric A. Stach, Ju Li, Feng Lin, and Dong Su, Nano Lett., **15**, 1437–1444, 2015.
- J82. *Compositional Inhomogeneity of Multinary Semiconductor Nanoparticles: A Case Study of $\text{Cu}_2\text{ZnSnS}_4$* , Wei-Chang Yang, Caleb K. Miskin, Nathaniel J. Carter, Rakesh Agrawal and Eric A. Stach, Chem. Mater., **26**, 6955–6962, 2015.
- J83. *Graphene-modified nanostructured vanadium pentoxide hybrids with extraordinary electrochemical performance for Li-ion batteries*, Qi Liu, Zhe-Fei Li, Yadong Liu, Hangyu Zhang, Yang Ren, Cheng-Jun Sun, Lia Stanciu, Eric A. Stach and Jian Xie, Nat. Comm., **6**, 6127, 10.1038/ncomms7127, 2015.
- J84. *Hierarchical Heterogeneity at the $\text{CeO}_x\text{-TiO}_2$ Interface: Electronic and Geometric Structural Influence on the Photocatalytic Activity of Oxide on Oxide Nanostructures*, Si Luo, Thuy-Duong Nguyen-Phan, Aaron C. Johnston-Peck, Laura Barrio, Shawn Sallis, Dario A. Arena, Shankhamala Kundu, Wenqian Xu, Louis F. J. Piper, Eric A. Stach, Dmitry E. Polyansky, Etsuko Fujita, José A. Rodriguez, and Sanjaya D. Senanayake, J. Phys. Chem C., **119**, 2669–2679, 2015.
- J85. *Ultrathin europium oxide nanoplatelets: ‘hidden’ parameters and controlled synthesis, unusual crystal structure, and photoluminescence properties*, Damien Hudry, A. M. Abeykoon, Jessica Hoy, Matthew Sfeir, Eric Stach, and James Dickerson, Chemistry of Materials **27**, **965**, 2015.

- J86. *An in situ transmission electron microscopy study of sintering and redispersion phenomena over size-selected metal nanoparticles: environmental effects*, F. Behafarid, S. Pandey, R.E. Diaz, E.A. Stach and B.R. Cuenya, Phys. Chem. Chem. Phys., **16**, 18176–18184, 2014
- J87. *Synthesis of $(\text{CuInS}_2)_{(0.5)}(\text{ZnS})_{(0.5)}$ Alloy Nanocrystals and Their Use for the Fabrication of Solar Cells via Selenization*, B. K. Graeser, C. J. Hages, W. C. Yang, N. J. Carter, C. K. Miskin, E. A. Stach and R. Agrawal, Chem. Mater., **26**, 4060–4063 (2014).
- J88. *Engineering the Activity and Lifetime of Heterogeneous Catalysts for Carbon Nanotube Growth via Substrate Ion Beam Bombardment*, A. E. Islam, P. Nikolaev, P. B. Amama, S. Saber, D. Zakharov, D. Huffman, M. Erford, G. Sargent, S. L. Semiatin, E. A. Stach and B. Maruyama, Nano Lett., **14**, 4997–5003 (2014).
- J89. *Surface-step-induced oscillatory oxide growth*, L. Liang, L. Langli, J. Ciston, W. A. Saidi, E. A. Stach, J. C. Yang and G. Zhou, Phys. Rev. Lett., **113**, 136104 (136105 pp.)–136104 (136105 pp.) (2014).
- J90. *Investigating Local Degradation and Thermal Stability of Charged Nickel-Based Cathode Materials through Real-Time Electron Microscopy*, S. Hwang, S. M. Kim, S.-M. Bak, B.-W. Cho, K. Y. Chung, J. Y. Lee, W. Chang and E. A. Stach, ACS Appl. Mater. & Inter. **6**, 15140–15147 (2014).
- J91. *Investigation of Changes in the Surface Structure of $\text{Li}_x\text{Ni}_{0.8}\text{Co}_{0.15}\text{Al}_{0.05}\text{O}_2$ Cathode Materials Induced by the Initial Charge*, S. Hwang, W. Chang, S. M. Kim, D. Su, D. H. Kim, J. Y. Lee, K. Y. Chung and E. A. Stach, Chem. Mater., **26**, 1084–1092 (2014).
- J92. *Real time observation of ZnO nanostructure formation via the solid-vapor and solid-solid-vapor mechanisms*, B. J. Kim, M. W. Kim, J. S. Jang and E. A. Stach, Nanoscale **6**, 6984–6990 (2014).
- J93. *Au Transport in Catalyst Coarsening and Si Nanowire Formation*, B. J. Kim, J. Tersoff, S. Kodambaka, J. S. Jang, E. A. Stach and F. M. Ross, Nano Lett., **14**, 4554–4559 (2014).
- J94. *Kesterite $\text{Cu}_2\text{ZnSn}(\text{S},\text{Se})_{(4)}$ Absorbers Converted from Metastable, Wurtzite-Derived $\text{Cu}_2\text{ZnSnS}_4$ Nanoparticles*, W. C. Yang, C. K. Miskin, C. J. Hages, E. C. Hanley, C. Handwerker, E. A. Stach and R. Agrawal, Chem. Mater. **26**, 3530–3534 (2014).
- J95. *Prolonged Hot Electron Dynamics in Plasmonic-Metal/Semiconductor Heterostructures with Implications for Solar Photocatalysis*, J. S. DuChene, B. C. Sweeny, A. C. Johnston-Peck, D. Su, E. A. Stach and W. D. Wei, Ange. Chemie Inter. Ed. **53**, 7887–7891 (2014).
- J96. *Adsorbate-Induced Structural Changes in 1–3 nm Platinum Nanoparticles*, Y. Lei, H. Y. Zhao, R. D. Rivas, S. Lee, B. Liu, J. L. Lu, E. Stach, R. E. Winans, K. W. Chapman, J. P.

- Greeley, J. T. Miller, P. J. Chupas and J. W. Elam, *J. Am. Chem. Soc.* **136**, 9320–9326 (2014).
- J97. *Determining the Resolution Limits of Electron-Beam Lithography: Direct Measurement of the Point-Spread Function*, V. R. Manfrinato, J. G. Wen, L. H. Zhang, Y. J. Yang, R. G. Hobbs, B. Baker, D. Su, D. Zakharov, N. J. Zaluzec, D. J. Miller, E. A. Stach and K. K. Berggren, *Nano Lett.*, **14**, 4406–4412 (2014).
- J98. *Correlating Atomic Structure and Transport in Suspended Graphene Nanoribbons*, Z. J. Qi, J. A. Rodriguez-Manzo, A. R. Botello-Mendez, S. J. Hong, E. A. Stach, Y. W. Park, J. C. Charlier, M. Drndic and A. T. C. Johnson, *Nano Lett.*, **14**, 4238–4244 (2014).
- J99. *Surface Plasmon-Driven Water Reduction: Gold Nanoparticle Size Matters*, K. Qian, B. C. Sweeny, A. C. Johnston-Peck, W. X. Niu, J. O. Graham, J. S. DuChene, J. J. Qiu, Y. C. Wang, M. H. Engelhard, D. Su, E. A. Stach and W. D. Wei, *J. Am. Chem. Soc.*, **136**, 9842–9845 (2014).
- J100. *Revealing the Atomic Restructuring of Pt-Co Nanoparticles*, H. L. Xin, S. Alayoglu, R. Z. Tao, A. Genc, C. M. Wang, L. Kovarik, E. A. Stach, L. W. Wang, M. Salmeron, G. A. Somorjai and H. M. Zheng, *Nano Lett.*, **14**, 3203–3207 (2014).
- J101. *Comparative study of the alloying effect on the initial oxidation of Cu-Au(100) and Cu-Pt(100)*, L. L. Luo, Y. H. Kang, J. C. Yang, D. Su, E. A. Stach and G. W. Zhou, *App. Phys. Lett.*, **104** (2014).
- J102. *TiN/(Al,Sc)N metal/dielectric superlattices and multilayers as hyperbolic metamaterials in the visible spectral range*, B. Saha, G. V. Naik, S. Saber, C. Akatay, E. A. Stach, V. M. Shalae, A. Boltasseva and T. D. Sands, *Phys. Rev. B*, **90**, 125420, 2014.
- J103. *Rate-Dependent, Li-Ion Insertion/Deinsertion Behavior of LiFePO₄ Cathodes in Commercial 18650 LiFePO₄ Cells*, Q. Liu, H. He, Z. F. Li, Y. D. Liu, Y. Ren, W. Q. Lu, J. Lu, E. A. Stach and J. Xie, *ACS Appl. Mater. Inter.*, **6**, 3282–3289 (2014).
- J104. *The Structural Evolution of V₂O₅ Nanocrystals during Electrochemical Cycling Studied Using In operando Synchrotron Techniques*, Q. Liu, Y. D. Liu, C. J. Sun, Z. F. Li, Y. Ren, W. Q. Lu, E. A. Stach and J. Xie, *Electrochimica Acta*, **136**, 318–322 (2014).
- J105. *A Manganese-Doped Barium Carbonate Cathode for Alkaline Batteries*, B. Hertzberg, L. Sviridov, E. A. Stach, T. Gupta and D. Steingart, *J. Electrochem. Soc.*, **161**, A835–A840 (2014).
- J106. *Gas mixing system for imaging of nanomaterials under dynamic environments by environmental transmission electron microscopy*, M. C. Akatay, Y. Zvinevich, P. Baumann, F. H. Ribeiro and E. A. Stach, *Rev. Sci. Inst.*, **85**, 033704, 2014.
- J107. *Enhancing the stability of copper chromite catalysts for the selective hydrogenation of furfural using ALD overcoating*, H. B. Zhang, Y. Lei, A. J. Kropf, G. H. Zhang, J. W.

- Elam, J. T. Miller, F. Sollberger, F. Ribeiro, M. C. Akatay, E. A. Stach, J. A. Dumesic and C. L. Marshall, *J. Catal.*, **317**, 284–292 (2014).
- J108. *Water–Gas Shift Reaction on Ni–W–Ce Catalysts: Catalytic Activity and Structural Characterization*, F. Z. Zhao, Z. Y. Liu, W. Q. Xu, S. Y. Yao, A. Kubacka, A. C. Johnston–Peck, S. D. Senanayake, A. Q. Zhang, E. A. Stach, M. Fernandez–Garcia and J. A. Rodriguez, *J. Phys. Chem. C*, **118**, 2528–2538 (2014).
- J109. *Gas–phase epoxidation of propylene in the presence of H₂ and O₂ over small gold ensembles in uncalcined TS–1*, W. S. Lee, M. C. Akatay, E. A. Stach, F. H. Ribeiro and W. N. Delgass, *J. Catal.*, **313**, 104–112 (2014).
- J110. *Pore Structure and Bifunctional Catalyst Activity of Overlayers Applied by Atomic Layer Deposition on Copper Nanoparticles*, A. C. Alba–Rubio, B. J. O’Neill, F. Y. Shi, C. Akatay, C. Canlas, T. Li, R. Winans, J. W. Elam, E. A. Stach, P. M. Voyles and J. A. Dumesic, *ACS Catalysis*, **4**, 1554–1557 (2014).
- J111. *An in situ transmission electron microscopy study of sintering and redispersion phenomena over size–selected metal nanoparticles: environmental effects*, F. Behafarid, S. Pandey, R. E. Diaz, E. A. Stach and B. R. Cuenya, *Physical Chemistry Chemical Physics*, **16**, 18176–18184 (2014).
- J112. *Effect of Co Loading on the Activity and Selectivity of PtCo Aqueous Phase Reforming Catalysts*, P. J. Dietrich, M. C. Akatay, F. G. Sollberger, E. A. Stach, J. T. Miller, W. N. Delgass and F. H. Ribeiro, *ACS Catalysis* **4**, 480–491 (2014).
- J113. *Structural and catalytic differences in the effect of Co and Mo as promoters for Pt–based aqueous phase reforming catalysts*, P. J. Dietrich, F. G. Sollberger, M. C. Akatay, E. A. Stach, W. N. Delgass, J. T. Miller and F. H. Ribeiro, *Applied Catalysis B–Environmental*, **156**, 236–248 (2014).
- J114. *Cu₂ZnSn(S, Se)₄ solar cells from inks of heterogeneous Cu–Zn–Sn–S nanocrystals*, N.J. Carter, W.C. Yang, C.K. Miskin, C.J. Hages, E.A. Stach, and R. Agrawal, *Sol. Energy Mater. Sol. Cells*, **123**, 189–196, 2014
- J115. *A method to determine fault vectors in 4H–SiC from stacking sequences observed on high resolution transmission electron microscopy images*, W. Fangzhen, W. Huanhuan, B. Raghothamachar, M. Dudley, S. G. Mueller, C. Gil, E. K. Sanchez, D. Hansen, M. J. Loboda, Z. Lihua, S. Dong, K. Kisslinger and E. Stach, *J. Appl. Phys.* **116**, 104905–9, 2014.
- J116. *Cobalt Molybdenum Oxynitrides: Synthesis, Structural Characterization, and Catalytic Activity for the Oxygen Reduction Reaction*, Bingfei Cao, Gabriel M. Veith, Rosa D.Rivas, Jue Liu, Eric A. Stach, Radoslav R. Adzic, and Peter G. Khalifah, *Angew. Chem. Int. Ed.*, **125**, 10953–10957, 2013.

- J117. *Control of Metal Nanocrystal Size Reveals Metal–Support Interface Role for Ceria Catalysts*; M. Cargnello, V. Doan–Nguyen, T.R. Gordon, R.E. Diaz, E.A. Stach, R.J. Gorte, P. Fornasiero and C.B. Murray, *Science*, **341**, 771–773, 2013.
- Chosen for ScienceExpress
- J118. *Non–Crystalline–to–Crystalline Transformations in Pt Nanoparticles*; Long Li, Lin–Lin Wang, Duane D. Johnson, Zhongfan Zhang, Sergio Ismael Sanchez, Joo Hyun Kang, Ralph G Nuzzo, Qi Wang, Anatoly I Frenkel, Jie Li, James Ciston, Eric A. Stach, and Judith C Yang, *J. Am. Chem. Soc.*, DOI: 10.1021/ja405497p
- Highlighted as an “Editor’s Choice” in Science Magazine
- J119. *Microstructure of Bimetallic Pt–Pd Catalysts Under Oxidizing Conditions*, Tyne R. Johns, Jason R. Gaudet, Eric J. Peterson, Jeffrey T. Miller, Eric A. Stach, Chang H. Kim, Michael P. Balogh, and Abhaya K. Datye, *ChemCatComm.*, 5: 2636–2645, 2013.
- J120. *Enhanced reaction rate for gas–phase epoxidation of propylene using H₂ and O₂ by Cs promotion of Au/TS–1*, Wen–Sheng Lee, M. Cem Akatay, Eric A. Stach, Fabio H. Riberio, W. Nicholas Delgass, Jr, *J. Catal.*, **308**, 98–113, 2013.
- J121. *Steam Reforming of Ethanol on Ni/CeO₂: Reaction Pathway and Interaction between Ni and the CeO₂ Support*, Wenqian Xu, Zongyuan Liu, Aaron C. Johnston–Peck, Sanjaya D. Senanayake, Gong Zhou, Dario Stacchiola, Eric A. Stach, and José A. Rodriguez, *ACS Catalysis*, **3**, 975, 2013
- J122. *Nature of the Mixed–Oxide Interface in Ceria–Titania Catalysts: Clusters, Chains, and Nanoparticles*; Aaron C. Johnston–Peck, Sanjaya D. Senanayake, José J. Plata, Shankhamala Kundu, Wenqian Xu, Laura Barrio, Jesús Graciani, Javier Fdez. Sanz, Rufino M. Navarro, José L. G. Fierro, Eric A. Stach, and José A. Rodriguez, *J. Phys. Chem. C.*, **117**, 14463, 2013.
- J123. *Revisiting the “In–clustering” question in InGaN through the use of aberration–corrected STEM and low–loss EELS below the knock–on threshold*, K.H. Baloch, A.C. Johnston–Peck, K. Kisslinger, E.A. Stach and S. Gradecak, *Appl. Phys. Lett.*, **102**, 191910, 2013.
- J124. *Structural modification of graphene sheets to create a dense network of edge sites*, Mei–xian Wang, Qi Liu, Zhe–Fei Li, Hong–fang Sun, Eric A. Stach, and Jian Xie, *J. Phys. Chem. Lett.*, **4**, 1484–88, 2013.
- J125. *Resolution limits of electron–beam lithography towards the atomic scale*, Vitor Manfrinato, Lihua Zhang, Dong Su, Huigao Duan, Richard Hobbs, Eric A. Stach and Karl Berggren, *Nano Letters*, **13**, 1555, 2013.
- J126. *Hartree simulations of coupled quantum Hall edge states in corner–overgrown heterostructures*, L. Steinke, P. Cantwell, E. Stach, D. Schuh, A. Fontcuberta i Morral, M. Bichler, G. Abstreiter and M. Grayson, *Phys. Rev. B*, **87**, 165428, 2013.
- J127. *Heterogeneous Catalysts Need Not Be so “Heterogeneous”: Monodisperse Pt*

- Nanocrystals by Combining Shape-Controlled Synthesis and Purification by Colloidal Recrystallization*; Yijin Kang, Meng Li, Yun Cai, Matteo Cargnello, Rosa E. Diaz, Thomas R. Gordon, Noah L. Wieder, Radoslav R. Adzic, Raymond J. Gorte, Eric A. Stach, and Christopher B. Murray, *J. Am. Chem. Soc.*, **135**, 2741–2747, 2013.
- J128. *Hydrogen-Induced Morphotropic Phase Transformation of Single Crystalline Vanadium Dioxide Nanobeams*; Woong-Ki Hong, Jong Bae Park, Jongwon Yoon, Bong-Joong Kim, Jung Inn Sohn, Young Boo Lee, Tae-Sung Bae, Sung-Jin Chang, Yun Suk Huh, Byoungchul Son, Eric A. Stach, Takhee Lee, and Mark E. Welland, *Nano Lett.*, **13**, 1822, 2013.
- J129. *Engineering Catalytic Contacts and Thermal Stability: Gold/Iron Oxide Binary Nanocrystal Superlattices for CO Oxidation*, Yijin Kang, Xingchen Ye, Jun Chen, Liang Qi, Rosa E. Diaz, Vicky Doan-Nguyen, Guozhong Xing, Cherie R. Kagan, Ju Li, Raymond J. Gorte, Eric A. Stach, and Christopher B. Murray, *J. Am. Chem. Soc.*, **135**, 1499–1505, 2013.
- J130. *Design of Pt-Pd binary superlattices exploiting shape-effects and synergistic effects for oxygen reduction reactions*, Yijin Kang, Xingchen Ye, Jun Chen, Yun Cai, Rosa E. Diaz, Radoslav R. Adzic, Eric A. Stach, Christopher B. Murray, *J. Am. Chem. Soc.*, **135**, 42, 2013.
- J131. *Correlating Structural Changes and Gas Evolution during the Thermal Decomposition of Charged $\text{Li}_x\text{Ni}_{0.8}\text{Co}_{0.15}\text{Al}_{0.05}\text{O}_2$ Cathode Materials*; Seong-Min Bak, Kyung-Wan Nam, Wonyoung Chang, Xiqian Yu, Enyuan Hu, Sooyeon Hwang, Eric A. Stach, Kwang-Bum Kim, Kyung Yoon Chung, and Xiao-Qing Yang, *Chem. Mater.*, **25**, 337–351, 2013.
- J132. *Shape-controlled synthesis of Pt nanocrystals: the role of metal carbonyls*; Yijin Kang, Jun Beom Pyo, Xingchen Ye, Rosa E. Diaz, Thomas R. Gordon, Eric A. Stach, and Christopher B. Murray, *ACS Nano*, **7**, 645, 2013.
- J133. *Growth Pathways in Ultralow Temperature Ge Nucleation from Au*; B. J. Kim, C.Y. Wen, J. Tersoff, M. C. Reuter, E. A. Stach and F.M. Ross, *Nano Lett.*, **12**, 5867–5872, 2012.
- J134. *Heterogeneous nanoclusters assembled by PNA-templated double-stranded DNA*, D.Z. Su, A.L. Stadler, M. Gurevich, E. Palma, E. Stach, D. van der Lelie and O. Gang, *Nanoscale*, **4**, 6722, 2012.
- J135. *Step-edge induced oxide growth during the oxidation of Cu surfaces*; Guangwen Zhou, Langli Luo, Liang Li, James Ciston, Eric A. Stach and Judy Yang, *Phys. Rev. Lett.*, **109**, 235502, 2012.
- J136. *Counting Au catalytic sites for the water-gas shift reaction*, M. Shekhar, J. Wang, W.S. Lee, M.C. Akatay, E.A. Stach, W.N. Delgass and F.H. Ribeiro, *J. Catalysis*, **293**, 94–102, 2012.
- J137. *Size-dependent evolution of the atomic vibrational density of states and thermodynamic properties of isolated Fe nanoparticles*; B. Roldan Cuenya, L.K. Ono,

- J.R. Croy, K. Paredis, A. Kara, H. Heinrich, J. Zhao, E.E. Alp, A.T. DelaRiva, A. Dayte, E.A. Stach and W. Keune, *Phys. Rev. B*, **86**, 165406, 2012.
- J138. *Syntheses of Boron Nitride Nanotubes from Borazine and Decaborane Molecular Precursors by Catalytic Chemical Vapor Deposition with a Floating Nickel Catalyst*, S. Chatterjee, M. Kim, D. Zakharov, S.M. Kim, E. Stach, B. Maruyama and L. Sneedon, *Chem. Mater.*, **24**, 2872–79, 2012.
- J139. *Probing the gold active sites in Au/TS-1 for gas-phase epoxidation of propylene in the presence of hydrogen and oxygen*, W.S. Lee, L.-C. Lai, M.C. Akatay, E.A. Stach, F.H. Riberio and W.N. Delgass, *J. Catal.*, 296, 31–42, 2012
- J140. *Understanding the Chemistry of H₂ Production for 1-Propanol Reforming: Pathway and Support Modification Effects*, Rodrigo Lobo, Christopher L. Marshall, Paul J. Dietrich, Fabio H. Ribeiro, Cem Akatay, Eric A. Stach, Anil Mane, Yu Lei, Jeffrey Elam, and Jeffrey T. Miller, *ACS Catalysis*, 2, 2316–26, 2012.
- J141. *Preparation of high-surface-area carbon nanoparticle/graphene composites*, M.X. Wang, Q. Liu, H.F. Sun, E.A. Stach, H.Y. Zhang, L. Stanciu and X. Jie, *Carbon*, **50**, 3845–53, 2012.
- J142. *Silver layer instability in a SnO₂/Ag/SnO₂ trilayer on silicon*, Suk Jun Kim, Eric A. Stach and Carol A. Handwerker, *Thin Solid Films*, **520**, 6189–95, 2012.
- J143. *Estimating the In-Plane Young's Modulus of Polycrystalline Films in MEMS*, P.R. Cantwell, H. Kim, M.M. Schneider, H.H. Hsu, D. Peroulis, E.A. Stach and A.J. Strachan, *J. MEMS*, 21, 840–9, 2012.
- J144. *Controlling the Growth of Si/Ge Nanowires and Heterojunctions Using Silver–Gold Alloy Catalysts*, Yi-Chia Chou, Cheng-Yen Wen, Mark C. Reuter, Dong Su, Eric A. Stach, and Frances M. Ross, *ACS Nano*, **6**, 6407–6415, 2012.
- J145. *Revealing Correlation of Valence State with Nanoporous Structure in Cobalt Catalyst Nanoparticles by In Situ Environmental TEM*, H.L. Xin, E.A. Pach, R.E. Diaz, E.A. Stach, M. Salmeron and H.M. Zheng, *ACS Nano*, **6**, 4241–7, 2012.
- J146. *Size and Support Effects for the Water–Gas Shift Catalysis over Gold Nanoparticles Supported on Model Al₂O₃ and TiO₂*, S. Mayank, W. Jun, W.-S. Lee, W.D. Williams, S.M. Kim, E.A. Stach and F.H. Ribeiro, *J. Am. Chem. Soc.*, **134**, 4700–4708, 2012.
- J147. *Aqueous Phase Glycerol Reforming by PtMo Bimetallic Nano-Particle Catalyst: Product Selectivity and Structural Characterization*, P.J. Dietrich R.J. Lobo-Lapidus, T. Wu, A. Sumer, M.C. Akatay, B.R. Fingland, N. Guo, J.A. Dumesic, C.L. Marshall, E. Stach, J. Jellineck, W.N. Delgass, F.H. Riberio and J.T. Miller, *Topics in Catalysis*, **55**, 53–59, 2012.
- J148. *Highly Active Pt₃Pb and Core-Shell Pt₃Pb–Pt Electrocatalysts for Formic Acid Oxidation*, K. Yijin; Q. Liang; L. Meng, R.E. Diaz, D. Su, R.R. Adzic, E. Stach, J. Li and C.B. Murray, *ACS Nano*, **6**, 2818–2825, 2012.

- J149. *Reproducible preparation of Au/TS-1 with high reaction rate for gas phase epoxidation of propylene*; W.-S. Lee; M.C. Akatay E.A. Stach, F.H. Riberio and W.N. Delgass, J. Catalysis, **287**, 178–189, 2012.
- J150. *Utilizing the thermodynamic nanoparticle size effects for low temperature Pb-free solder*; J.P. Koppes, K.A. Grossklau, A.R. Muza, R.R. Revur, S. Sengupta, A. Rae, E.A. Stach and C.A. Handwerker, Mat. Sci. Eng. B, **177**, 197–204, 2012.
- J151. *Kinetics of congruent vaporization of ZnO islands*; B.J. Kim, R.E. García and E.A. Stach, Phys. Rev. Lett., **107**, 1461010, 2011.
- J152. *Vacancies, twins, and the thermal stability of ultrafine-grained copper*; C. Saldana, A.H. King, E.A. Stach, W.D. Compton and S. Chandrareskar, Appl. Phys. Lett., **99**, 231911, 2011.
- J153. *Crystallization and electrochemical performance of $La_{0.6}Sr_{0.4}Co_{0.2}Fe_{0.8}O_{3-\delta}$ - $Ce_{0.8}Gd_{0.2}O_{1.9}$ thin film cathodes processed by single solution spray pyrolysis*; B.F. Angoua, P.R. Cantwell, E.A. Stach and E. Slamovich, Solid State Ionics, **203**, 62–68, 2011.
- J154. *Truncated Ditetragonal Gold Prisms as Nanofacet Activators of Catalytic Platinum*; F. Lu, Z. Yu, L. Zhang, Y.G. Zhang, X.J. Wang, R.R. Adzic, E.A. Stach and O. Gang, J. Am. Chem. Soc., **133**, 18074–77, 2011.
- J155. *Mechanism of vertical Ge nanowire nucleation on Si (111) during subeutectic annealing and growth*; S.J. Park. S.H. Chung, B.-J. Kim, M.H. Qi, X.F. Xu, E.A. Stach and C. Yang, J. Mater. Res., **26**, 2744–48, 2011.
- J156. *Graphene formation on step-free 4H-SiC(0001)*; M.L. Bolen, R. Colby, E.A. Stach and M. Capano, in press, J. Appl. Phys.
- J157. *Built-in Electric Field Minimization in (In, Ga)N Nanoheterostructures*; Z.W. Liang, I.H. Wildeson, R. Colby, D.A. Ewold, T. Zhang, T.D. Sands, E.A. Stach, B. Benes and R.E. García, Nano Lett., **11**, 4515–19, 2011.
- J158. *Differences in Catalytic Sites for CO Oxidation and Propylene Epoxidation on Au Nanoparticles*; W.S. Lee, R. Zhang, M.C. Akatay, C.D. Baertsch, E.A. Stach, F.H. Ribeiro, and W.N. Delgass, ACS Catalysis, **1**, 1327–1330, 2011.
- J159. *Laser direct write of silicon nanowires*; J.I. Mitchell, S.J. Park, C.A. Watson, P. Srisungsitthisunti, C. Tansarawiput, M.H. Qi, E.A. Stach, C. Yang and X.F. Xu, Opt. Eng., **50**, 104301, 2011.
- J160. *Dislocation pinning effects induced by nano-precipitates during warm laser shock peening: Dislocation dynamic simulation and experiments*; Y. Liao, C. Ye, H. Gao, B.-J. Kim, S. Suslov, E.A. Stach, and G.J. Cheng, J. Appl. Phys. **110**, 023518, 2011.
- J161. *The periodically changing morphology of the nanowire growth interface*; C.-Y. Wen, J. Tersoff, M. C. Reuter, J. H. Park, S. Kodambaka, E. A. Stach and F. M. Ross, Phys. Rev. Lett., **107**, 025503, 2011.

- J162. *Multimodal grain size distribution and high hardness in fine grained tungsten fabricated by spark plasma sintering*, E.-A. Osman, D.V. Quach, M. Efe, P.R. Cantwell, B. Hiem, E.A. Stach, J.R. Groza and J.P. Allain, *Mater. Sci. Eng. A*, **528**, 5670–5677, 2011.
- J163. *Control and characterization of individual grains and grain boundaries in graphene grown by chemical vapour deposition*, Q.K. Yu, L.A. Jauregui, W. Wu, R. Colby, J.F. Tian, Z.H. Su, H.L. Cao, Z.H. Liu, D. Pandey, D.G. Wei, T.F. Chung, P. Peng, N.P. Guisinger, E.A. Stach, J.M. Bao, S.S. Pei and Y.P. Chen, *Nature Mat.*, **10**, 443–449, 2011.
- Featured Cover Article
- J164. *Desorption induced formation of negative nanowires in GaN*, B. J. Kim and E. A. Stach, *J. Cryst. Growth*, **324**, 119–123, 2011.
- J165. *Carbon-based supercapacitors produced by the activation of graphene*, Y. Zhu, S. Murali, M.D. Stoller, K.J. Ganesh, W. Cai, P.J. Ferreira, A. Pirkle, R.M. Wallace, K.A. Cychosz, M. Thommes, D. Su, E.A. Stach and R.S. Ruoff, *Science*, **332**, 1537–1541, 2011.
- Chosen for ScienceExpress
- J166. *Surface functionalized silica as a toolkit for studying aqueous phase palladium adsorption and mineralization on thiol moiety in the absence of external reducing agents*, J.S. Lim, S.-M. Kim, S.Y. Lee, E.A. Stach, J.N. Culver and M.T. Harris, *J. Colloid Interface Sci.*, **356**, 31–36, 2011.
- J167. *Enhancing the catalytic performance of Pt/C catalysts using steam-etched carbon blacks as a catalyst support*, M.X. Wang, F. Xu, Q. Liu, H.F. Sun, R.H. Cheng, H. He, E.A. Stach and J.A. Xie, *Carbon*, **49**, 256–265, 2011.
- J168. *Nanoscale graphite-supported Pt catalysts for oxygen reduction reactions in fuel cells*, Mei-xian Wang, Fan Xu, Hong-fang Sun, Qi Liu, Kateryna Artyushkova, Eric A. Stach, and Jian Xie, *Electrochimica Acta*, **56**, 2566–2573, 2011.
- J169. *Fatigue performance improvement in AISI 4140 steel by dynamic strain aging and dynamic precipitation during warm laser shock peening*, C.H. Ye, S. Suslov, B.J. Kim, E.A. Stach and G. Chang, *Acta Mat.*, **59**, 1014–1025, 2011.
- J170. *Amorphous interface layer in thin graphite films grown on the carbon face of SiC*, R. Colby, M.L. Bohen, M.A. Capano, E.A. Stach, *Appl. Phys. Lett.*, **99**, 101904, 2011.
- J171. *Controlled growth of ordered nanopore arrays with GaN nanorods*, I. Wildeson, D. Ewoldt, R. Colby, E.A. Stach, and T.D. Sands, *Nano Lett.*, **11**, 535–540, 2011.
- J172. *Step-flow kinetics in nanowire growth*, C.-Y. Wen, J. Tersoff, M. C. Reuter, E. A. Stach, and F. M. Ross, *Phys. Rev. Lett.*, **105**, 195502, 2010.
- J173. *Empirical study of Hall bars on few-layer graphene on C-face 4H-SiC*, M.L. Bolen, T. Shen, J.J. Gu, R. Colby, E.A. Stach, P.D. Ye, and M.A. Capano, *J. Elect. Mater.*, **39**, 2969–2701, 2010.

- J174. *Fabrication of 7.2% Efficient CZTSSe Solar Cells Using CZTS Nanocrystals*; Qijie Guo, Grayson M. Ford, Wei-Chang Yang, Bryce C. Walker, Eric A. Stach, Hugh W. Hillhouse, and Rakesh Agrawal, *J. Am. Chem. Soc.* **132**, 17384–17386, 2010.
- J175. *Nanomanipulation of ridges in few-layer epitaxial graphene grown on the carbon-face of 4H-SiC*; G. Prakash, M.L. Bolen, R. Colby, E. A. Stach, M. A. Capano, and R. Reifenger, *New J. Phys.*, **12**, 125009, 2010.
- J176. *Biogenic aqueous-phase palladium crystallization on tobacco mosaic virus without an additional chemical reduction agent*; Jung-Sun Lim, Seung-Min Kim, Sang-Yup Lee, Eric A. Stach, James N. Culver and Michael T. Harris, *Nano Letters* **10**, 3863–3967, 2010.
- J177. *Metallic corner atoms in gold clusters are the dominant active site for rutile supported water-gas shift catalysts*; W. Damion Williams, Mayank Shekhar, Wen-Sheng Lee, Vincent Kispersky, W. Nicholas Delgass, Fabio H. Ribeiro, Seung Min Kim, Eric A. Stach, Jeffrey T. Miller, Lawrence F. Allard Jr., *J. Am. Chem. Soc.*, **132** (40), 14108–14120, 2010.
- J178. *Investigation of carbon corrosion in polymer electrolyte fuel cells using steam etching*; M.X. Wang, Q. Liu, H.F. Sun, N. Ogbeifun, F. Xu, E.A. Stach and J.A. Xie, *Mater. Chem. Phys.*, **123**, 761–766, 2010.
- J179. *Nucleation of highly dense nanoscale precipitates based on warm laser shock peening*; Yiliang Liao, Chang Ye, Bong-Joong Kim, Sergey Suslov, Eric Stach and Gary J. Cheng, *J. Appl. Phys.*, **108**, 063518, 2010.
- J180. *Wear mechanisms and friction parameters for sliding wear of micron-scale polysilicon sidewalls*; D.H. Alsem, R. van der Hulst, E.A. Stach, M.T. Dugger, J.Th.M. De Hosson, and R. O. Ritchie, *Sens. Actuators A: Phys.* **163**, 373–382 (2010).
- J181. *GaN nanostructure design for optimal dislocation filtering*; Zhiwen Liang, Robert Colby, Isaac H. Wildeson, David A. Ewoldt, Timothy D. Sands, Eric A. Stach and R. Edwin Garcia, *J. Appl. Phys.* **108**, 074313, 2010.
- J182. *III-nitride nanopyramid LEDs grown by organometallic vapor phase epitaxy*; Isaac H. Wildeson, Robert Colby, David A. Ewoldt, Zhiwen Liang, Dmitri N. Zakharov, Nestor Zaluzec, R. Edwin Garcia, Eric A. Stach and Timothy D. Sands, *J. Appl. Phys.* **108**, 044303, 2010.
- J183. *Catalyst and catalyst support morphology evolution in single-walled carbon nanotube supergrowth: growth deceleration and termination*; Seung-Min Kim, Cary L. Pint, Placidus B. Amama, Robert H. Hauge, Benji Maruyama and Eric A. Stach, *J. Mater. Res.*, **25**, 1875, 2010.
- Invited Feature Paper – Best Symposium Paper
- J184. *Genesis and evolution of Pt species during atomic layer deposition on oxide supports characterized by in-situ XAFS analysis and Water Gas Shift reaction of model Pt catalysts*; Worajit Setthapun, W. Damion Williams, Seung Min Kim, Hao Feng, Jeffrey W.

- Elam, Federico A. Rabuffetti, Kenneth R. Poeppelmeier, Peter C. Stair, Eric A. Stach, Fabio H. Ribeiro, Jeffrey T. Miller and Christopher L. Marshall, *J. Phys. Chem. C.*, **114**(21), 9758–9771, 2010.
- J185. *The growth and characterization of Si and Ge nanowires grown from reactive metal catalysts*; F. M. Ross, C.-Y. Wen, E. A. Stach, B. A. Wacaser and M. C. Reuter, *Philosophical Magazine*, **90**(20), 2807–2816, 2010.
- J186. *Transmission electron microscopy observation of corrosion behaviors of platinized carbon blacks under thermal and electrochemical conditions*; Z. Y. Liu, J. L. Zhang, P. T. Yu, J. X. Zhang, R. Makharia, K. L. More and E. A. Stach, *Journal of the Electrochemical Society*, **157**(6), B906–913, 2010.
- J187. *Dislocation filtering in GaN nanostructures demonstrated by transmission electron microscopy and numerical analysis*; R. Colby, Z. Liang, I. Wildeson, T. Sands, R.E. García and E.A. Stach, *Nano Letters*, **10**, 1568–1573, 2010.
- J188. *Comment on “Size-Dependent Melting Properties of Small Tin Particles: Nanocalorimetric Measurements”*; J. Koppes, A. Muza, C. Handwerker and E.A. Stach, *Phys. Rev. Lett.*, **104**, 189601, 2010.
- J189. *Acceleration of interparticle sintering by Ag migration in Cu–Ag core–shell nanoparticles*; Suk Jun Kim, Eric A. Stach, and Carol A. Handwerker, *Appl. Phys. Lett.*, **96**, 144101, 2010.
- J190. *Mechanism of dynamic structural reorganization in polyoxometalate catalysts*; Hari Nair, Jeffery T. Miller, Eric A. Stach and Chelsey D. Baertsch, *J. Catalysis*, **270**(1), 40–47, 2010.
- J191. *Formation of Au/Pd alloy nanoparticles on TMV*; Jung-Sun Lim, Seung-Min Kim, Sang Yup Lee, Eric Stach, J. Culver and Michael Harris, *J. Nanomaterials*, 620505, 2010.
- J192. *The effects of cubic stiffness on fatigue characterization resonator performance*; M. Budnitski, M.C. Scates, R.O. Ritchie, E.A. Stach, C.L. Muhlstein and O.N. Pierron, *Sensors and Actuators*, **157**(2), 228–234, 2010.
- J193. *Large scale graphene films synthesized on metals and transferred to insulators for electronic applications*; Helin Cao, Qingkai Yu, Deepak Pandey, Dmitry Zemlyanov, Robert Colby, Isaac Childres, Vladimir Drachev, Eric Stach, Jie Lian, Hao Li, Steven S. Pei and Yong P. Chen, *J. Appl. Phys.*, **107**, 044310, 2010.
- J194. *Influence of alumina type on the evolution and activity of alumina-supported Fe catalysts in single-walled carbon nanotube carpet growth*; Placidus B. Amama, Cary L. Pint, Seung Min Kim, Laura McJilton, Kurt G. Eyink, Eric A. Stach, Robert H. Hauge, Benji Maruyama, *ACS Nano*, **4**(2), 895–904, 2010.
- J195. *Evolution in catalyst morphology leads to carbon nanotube growth termination*; Seung Min Kim, Cary L. Pint, Placidus B. Amama, Dmitri N. Zakharov, Robert H. Hauge, Benji Maruyama, and Eric A. Stach, *J. Phys. Chem. Lett.*, **1**, 918–922, 2010.

- J196. *Structure, growth kinetics and ledge flow during vapor–solid–solid growth of copper–catalyzed silicon nanowires*; C.-Y. Wen, M. C. Reuter, J. Tersoff, E. A. Stach and F. M. Ross, Nano Letters, Nano Lett., **10** (2), 514–519, 2010.
- J197. *Biomagnetic glasses: preparation, characterization and biosensor applications*, Yu-Ho Won, Ho Seong Jang, Seung Min Kim, Millikarunarao Ganesana, Eric Stach, Silvana Andreescu, and Lia Stanciu, Langmuir, **26**(6), 4320–4326, 2010.
- J198. *Quantitative study of Au(III) and Pd(II) ion biosorption on genetically engineered tobacco mosaic virus*; Jung-Sun Lim; Seung-Min Kim; Sang-Yup Lee; Eric A Stach; James N Culver, Michael T. Harris, J. Colloid & Interface Science, **342**, 455–461, 2010.
- J199. *Formation of the ST12 phase in nanocrystalline Ge at ambient pressures*; Suk Jun Kim, Ong Khac Quy, Ling-Shao Chang, Eric A. Stach, Carol A. Handwerker and Alexander Wei, J. Mater. Chem., **20**, 331 – 337, 2010.
- J200. *Cross-sectional transmission electron microscopy of thin graphite films grown by chemical vapor deposition*, Robert Colby, Helin Cao, Qingkai Yu, Steven S. Pei, Eric A. Stach, Yong P. Chen, Diamond and Related Materials, **19**, 143–146, 2010.
- J201. *Formation of compositionally abrupt axial heterojunctions in Si/Ge nanowires*, C.-Y. Wen, M. C. Reuter, J. Bruley, J. Tersoff, S. Kodambaka, E. A. Stach and F. M. Ross, Science, **326**, 1247 2009.
- J202. *Size effects in the phase transition of nanoscale Au–Si eutectic*; B. J. Kim, J. Tersoff, C.Y. Wen, M. C. Reuter, E. A. Stach and F.M. Ross, Phys. Rev. Lett. **103**, 155701, 2009.
- J203. *Preferential growth of single-walled carbon nanotubes with metallic conductivity*, Avetik R. Harutyunyan, Gugang Chen, Elena M. Pigos, Oleg A. Kuznetsov, Tereza Paronyan, Kapila Hewaparakrama, Seung Min Kim, Dmitri Zakharov, Eric A. Stach and Gamini Sumanasekera, Science, **326**, 116, 2009.
- J204. *Nanogap engineering – an investigation of polyethyleneimine to control the growth front morphology of electrochemically deposited gold nanowires*; Manuel DaSilva, Daniel S. Wood, Matthew M. Schneider, Bong-Joong Kim, Eric A. Stach and Timothy D. Sands, Small, **5**(21), 2387–2391, 2009.
- J205. *Fabrication of ZnS nanoparticle chains on a protein template*, S. Padalkar, J. Hulleman, S. M. Kim, T. Tumkur, J.-C. Rochet, E. Stach and L. Stanciu, J. Nanoparticle Res., **11**(8), 2031–2041, 2009.
- J206. *Pseudomorphic stabilization of rocksalt GaN in TiN/GaN multilayers and superlattices*, Vijay Rawat, Dmitri N. Zakharov, Eric A. Stach, and Timothy D. Sands, Phys. Rev. B **80**, 024114, 2009.
- J207. *0.8 V supply voltage deep submicron inversion-mode $In_{0.75}Ga_{0.25}As$ MOSFETs for high-speed low-power logic applications*; Y.Q. Wu, W.K. Wang, O. Koybasi, D.N. Zakharov, E. Stach, S. Nakahara, J.C.M. Hwang, and P.D. Ye, IEEE Elect. Dev. Lett., **30**, 700–702, 2009.

- J208. *An efficient, scalable approach to the rapid reduction of high density layers of surface-supported metal-oxide catalyst with hydrazine vapor*, Cary L. Pint, Seung Min Kim, Eric A. Stach, and Robert H. Hauge, ACS Nano, 3(7)1897–1905, 2009.
- J209. *Stabilizing nanostructured materials by coherent nano-twins and their grain-boundary triple junction drag*, C. Saldana, T. G. Murthy, M. R. Shankar, E. A. Stach and S. Chandrasekar, Applied Physics Letters, **94**, 021910, 2009.
- J210. *The role of water in super growth of single-walled carbon nanotube carpets*, Placidus B. Amama, Cary Pint, Laura McJilton, Seung Min Kim, Eric A. Stach, P. Terry Murray, Robert H. Hauge, and Benji Maruyama, Nano Letters, **9**(1), 44–49, 2009.
- J211. *Kinetics of individual nucleation events observed in nanoscale vapor-liquid-solid growth*, B. J. Kim, J. Tersoff, S. Kodambaka, M. C. Reuter, E. A. Stach and F. M. Ross, Science, **322**, 1070–73, 2008.
- J212. *Nanometer-scale sharpness in corner-overgrown heterostructures*, L. Steinke, P. Cantwell, D. Zakharov, E. Stach, N. J. Zaluzec, A. Fontcuberta i Morral, M. Bichler, G. Abstreiter, and M. Grayson, Appl. Phys. Lett., **93**, 193117, 2008.
- J213. *Micron-scale friction and sliding wear of polycrystalline silicon thin structural films in ambient air*, D.H. Alsem, M.T. Dugger, E.A. Stach and R.O. Ritchie, J. Microelectromechanical Systems, **17**(5), 1144 – 1154, 2008.
- J214. *Double-walled boron nitride nanotubes grown by floating chemical vapor deposition*, M. J. Kim, S. Chatterjee, S. M. Kim, E. A. Stach, M. Bradley, M. Pender, L. Sneddon and B. Maruyama, Nano Letters, **8**(10); 3298–3302, 2008. DOI: 10.1021/nl8016835
- J215. *Development of CuInSe₂ nanocrystal and nanoring inks for low-cost solar cells*, Qijie Guo, Suk Jun Kim, Mahaprasad Kar, William Shafarman, Robert Birkmire, Eric A. Stach, Rakesh Agrawal and Hugh W. Hillhouse, Nano Letters, **8**(9); 2982–2987, 2008. DOI: 10.1021/nl802042g
- J216. *Detection of single atoms and buried defects in three dimensions by aberration-corrected electron microscopy with 0.5 Å information limit*, C. Kisielowski, B. Freitag, M. Bischoff, H. van Lin, S. Lazar, G. Knippels, P. Tiemeijer, M. van der Stam, S. von Harrach, M. Stekelenburg, M. Haider, S. Uhlemann, H. Müller, P. Hartel, B. Kabius, D. Miller, I. Petrov, E. A., T. Donchev, E.A. Kenik, A. Lupini, J. Bentley, S. Pennycook, I.M. Anderson, A.M. Minor, A.K. Schmid, T. Duden, V. Radmilovic, Q. Ramasse, M. Watanabe, R. Erni, E.A. Stach, P. Denes and U. Dahmen, Microsc. Microanal. **14**, 454–462, 2008.
- J217. *Organometallic vapor phase epitaxial growth of GaN on ZrN / AlN / Si substrates*, Mark H. Oliver, Jeremy L. Schroeder, David A. Ewoldt, Isaac H. Wildeson, Vijay Rawat, Robert Colby, Patrick R. Cantwell, Eric A. Stach, and Timothy D. Sands, Appl. Phys. Lett., **93**, 023109, 2008.
- J218. *Protein-templated semiconductor nanoparticle chains*, S. Padalkar, J.D. Hulleman, S.M. Kim, J.C. Rochet, E.A. Stach and L.A. Stanciu, Nanotechnology, **19**(27) 275602,

2008.

- J219. *Molecular beam epitaxy growth of InAs and $\text{In}_{0.8}\text{Ga}_{0.2}\text{As}$ channel materials on GaAs substrate for metal oxide semiconductor field effect transistor applications*; N. Li, E.S. Harmon, D.B. Salzman, D.N. Zakharov, J.H. Jeon, E. Stach, J.M. Woodall, X.W. Wang, T.P. Ma and F. Walker, J. Vac. Sci. Tech. B., **26**(3) 1187–1190, 2008.
- J220. *Effect of post-release sidewall morphology on the mechanical properties of polycrystalline silicon structural films*; D. H. Alsem, S. Timpe, B. L. Boyce, M. T. Dugger, E. A. Stach, K. Komvopoulos and R. O. Ritchie, Sensors and Actuators A, **147**, 553–560, 2008.
- J221. *Large lattice strain in individual grains of deformed nanocrystalline Ni*; Zhiwei Shan, E.A. Stach, J.M.K Wiezorek, D.M. Follstaedt, J.A. Knapp E.A. Stach and S.X. Mao, Applied Physics Letters, **92**, 091917, 2008.
- J222. *Inter- and intra-grain agglomerate fracture in nanocrystalline nickel*; Zhiwei Shan, J.A. Knapp, D.M. Follstaedt, E.A. Stach, J.M.K Wiezorek, and S.X. Mao, Physical Review Letters, **100**, 105502, 2008.
- J223. *Effect of twin plane spacing on the deformation of copper containing a high density of growth twins*; Z.W. Shan, L. Lu, A.M. Minor, E. A. Stach and S. X. Mao, JOM, **60**(9) 71–74, 2008.
- J224. *Peeling force spectroscopy: exposing the adhesive nanomechanics of one-dimensional nanostructures*; M. C. Strus, L. Zalamea, A. Raman, R. B. Pipes, C. V. Nguyen, and E. A. Stach, Nano Lett., **8** (2), 544 –550, 2008.
- J225. *Electrical properties of ZnO nanowire field effect transistors by surface passivation*; Woong-Ki Hong, Bong-Joong Kim, Tae-Wook Kim, Gunho Jo, Sunghoon Song, Soon-Seen Kwon, Ahnsook Yoon, Eric A Stach, and Takhee Lee, Colloids and Surfaces A: Physicochem. Eng. Aspects **313–314**, 378–382, 2008.
- J226. *Directed self-assembly of quantum structures by nanomechanical stamping using probe tips*; Curtis Taylor, Euclides Marega, Eric A Stach, Gregory Salamo, Lindsay Hussey, Martin Muñoz and Ajay Malshe, Nanotechnology **19**, 015301, 2008.
- J227. *Role of molecular surface passivation in electrical transport properties of InAs nanowires*; Qingling Hang, Fudong Wang, Patrick D. Carpenter, Dmitri Zemlyanov, Dmitri Zakharov, Eric A. Stach, William E. Buhro, and David B. Janes, Nano Letters, **8**(1); 49–55, 2008.
- J228. *Nanoscale mechanisms of misfit dislocation propagation in undulated $\text{Si}_{1-x}\text{Ge}_x/\text{Si}(100)$ epitaxial thin films*; Chi-Chin Wu, Robert Hull and Eric A. Stach, Nanotechnology, **18**, 165705, 2007.
- J229. *Realization of highly reproducible ZnO nanowire field effect transistors with n-channel depletion and enhancement modes*; Woong-Ki Hong, Dae-Kue Hwang, Il-Kyu Park, Gunho Jo, Sunghoon Song, Seong-Ju Park, Takhee Lee, Bong-Joong Kim and Eric A. Stach, Applied Physics Letters, **90**(24), 243103, 2007.

- J230. *Dislocation dynamics in nanocrystalline Ni*; Zhiwei Shan, E.A. Stach, J.M.K Wiezorek, D.M. Follstaedt, J.A. Knapp E.A. Stach and S.X. Mao, Physical Review Letters, **98**, 095502, 2007.
- J231. *An electron microscopy study of wear in polysilicon microelectromechanical systems*; D.H. Alsem, E.A. Stach, M.T. Dugger, M. Enachescu and R.O. Ritchie, Thin Solid Films, **515**, 3259, 2007.
- J232. *Alpha-synuclein as a template for the synthesis of metallic nanowires*; Sonal Padalkar, Parijat Deb, Kara Gunzeman, Jean-Christophe Rochet, John Hulleman, Eric A. Stach and Lia Stanciu, Nanotechnology, **18**, 055609, 2007.
- J233. *Very high-cycle fatigue failure in micron-scale polycrystalline silicon films: effects of environment and surface oxide thickness*; D.H. Alsem, R. Timmerman, B.L. Boyce, E.A. Stach, J.T.M. De Hosson and R.O. Ritchie, J. Appl. Phys., **101**, 013515, 2007.
- J234. *Dislocation-grain boundary interactions: a tribute to David Brandon*; Jeff T.M. De Hosson, Wouter A. Soer, Andy M. Minor, Steven Shan, Eric A. Stach, S.A. Syed Asif, Oden L. Warren, J. Mat. Sci., **41**, 7704–7719, 2006.
- J235. *Quantifying the onset of plasticity at the nanoscale*; A.M. Minor, S.A. Syed Asif, Z.W. Shan, E.A. Stach, E. Cyrankowski, T. Wyrobek and O. Warren, Nature Materials, **5**(9) 697–702, 2006.
- J236. *Graphene-based composite materials*; S. Stankovich, D.A. Dikin, G. Dommett, K. M. Kohlhaas, E. Zimney, E.A. Stach, R.D. Piner, S.B.T. Nguyen, and R.S. Ruoff, Nature, **442**, 282–286, 2006. One of Nature’s “Most Downloaded” in 2006.
- J237. *Using EELS to observe composition and electronic structure variations at dislocation cores in GaN*; I. Arslan, A. Bleloch, E. A. Stach, S. Ogut and N. D. Browning, Philosophical Magazine A, December, **86**, 4727–4746, 2006.
- J238. *Size effects in the nanoindentation response of silicon*; Daibin Ge, A. M. Minor, E.A. Stach and J.W. Morris Jr., Phil. Mag. A, **86**, 4069–800, 2006.
- J239. *Vertical single-walled carbon nanotubes grown from porous anodic alumina templates*; Matthew R. Maschmann, Aaron D. Franklin, Placidus B. Amama, Dmitri N. Zakharov, Eric A. Stach, Timothy D. Sands, Timothy S. Fisher, Nanotechnology, **17**, 3925–3929, 2006.
- J240. *Fabrication and characterization of solid-state nanopores using a field emission scanning electron microscope*; H. Chung, S.M. Iqbal, E.A. Stach, A.H. King, N.J. Zaluzec and R. Bashir, Appl. Phys. Lett., **88**, 103109, 2006.
- J241. *Ultrastructural examination of dentin using focused ion-beam cross-sectioning and transmission electron microscopy*; R. K. Nalla, A. E. Porter, C. Daraio, A. M. Minor, V. Radmilovic, E. A. Stach, A. P. Tomsia, and R. O. Ritchie, Micron, **36**, 672–80, 2005.
- J242. *Quantitative characterization of the growth and morphological evolution of bicrystalline aluminum thin films*; D. H. Alsem, E.A. Stach, and J. Th. M. de Hosson, Journal of Materials Science (Letters), **40**(18) 5033–5036, 2005.

- J243. *Faceted and vertically aligned GaN nanorod arrays fabricated without catalysts or lithography*, Parijat Deb, Vijay Rawat, Hyoung Kim, Sangho Kim, Mark Oliver, Mike Marshall, Eric Stach and Timothy Sands, Nano Letters, **5**(9) 1847–51, 2005. Featured in American Chemical Society's Nanofocus review as "Image of the Month".
- J244. *Nanoscale dislocation patterning by ultra-low load indentation*, Curtis R. Taylor, Eric A. Stach, Gregory Salalmo and Ajay P. Malshe, Appl. Phys. Lett. **87**, 073108, 2005.
- J245. *Response to comment on "Grain boundary mediated plasticity in nanocrystalline nickel"*; Zhiwei Shan, E.A. Stach, J.M.K. Wiezorek, J.A. Knapp, D.M. Follstaedt, and S.X. Mao, Science, **308**, 356, 2005.
- J246. *Morphological, spectroscopic and microstructural analysis of femtosecond laser processed lithium niobate*, D.C. Deshpande, A.P. Malshe, E.A. Stach, V.R Radmilovic, D. Alexander, D. Doerr and D. Hirt, J. Appl. Phys., **97**, 074316, 2005.
- J247. *Fatigue failure in thin-film polysilicon is due to sub-critical cracking within the oxide layer*, D.H. Alsem, E.A. Stach, C.L. Muhlstein and R.O. Ritchie, Appl. Phys. Lett., **86**, 041914, 2005.
- J248. *Room temperature dislocation plasticity in silicon*, A.M. Minor, E.T. Lilleodden, M. Jin, E.A. Stach, Daryl Chrzan, and J.W. Morris, Jr., Phil. Mag. A., **85**(2–3), 323–330, 2005.
- J249. *The atomic and electronic structure of mixed dislocations in GaN*, I. Arslan, A. Bleloch, E.A. Stach & N.D. Browning; Phys. Rev. Lett., **94**, 025504, 2005.
- J250. *Dislocation-grain boundary interactions in martensitic steel observed through in situ nanoindentation in a TEM*, T. Ohmura, A.M. Minor, E.A. Stach, and J.W. Morris, Jr., J. Mater. Res., **19**(12), 3626–3632, 2004.
- J251. *Direct observation of stress-induced grain growth during the indentation of ultra-fine grained aluminum*, M. Jin, A.M. Minor, E.A. Stach and J.W. Morris, Jr., Acta Mat. **52**(18) 5381–87, 2004.
- J252. *The effect of solute Mg on grain boundary and dislocation dynamics during nanoindentation of Al-Mg thin films*, W.A. Soer, J.Th.M. De Hosson, A.M. Minor, J.W. Morris, Jr. and E.A. Stach, Acta Materialia, **52**, 5783–90, 2004.
- J253. *Characteristic dimensions and the micro-mechanisms of fracture and fatigue in 'nano' and 'bio' materials*; R.O. Ritchie, J.J. Kruzic, C.L. Muhlstein, R.K. Nalla and E.A. Stach, Inter. J. Fracture **128**, 1–15, 2004
- J254. *A mechanistic understanding of fatigue in polysilicon structural thin-films*; R.O. Ritchie, D.H. Alsem, E.A. Stach and C.L. Muhlstein, Journal of Materials, **56**(11) 192, 2004.
- J255. *Grain boundary mediated plasticity in nanocrystalline nickel*, Z.W. Shan, E.A. Stach, J.M.K. Wiezorek, J.A. Knapp, D.M. Follstaedt and S.X. Mao, Science, **305**, 654–7, 2004.
- J256. *Structural changes of boron carbide under contact loading*; D. Ge, V. Domnich, T. Juliano, Y. Gogotsi and E.A. Stach, Acta Mat. **52**(13), 3921–7, 2004.

- J257. *Direct observations of incipient plasticity during nanoindentation of Al*; A.M. Minor, E.T. Lilleodden, E.A. Stach and J.W. Morris, Jr., J. Mater. Res., **19**(1) 176–82, 2004.
- J258. *Metal delocalization and surface decoration in direct-write nanolithography by electron beam induced deposition*, V. Gopal, E.A. Stach, V.R. Radmilovic, and I.A. Mowat, Appl. Phys. Lett., **85**(1), 49–51, 2004.
- J259. *Rapid prototyping of site-specific nanocontacts by electron and ion beam assisted direct-write nanolithography*, V. Gopal, C. Daraio, S. Jin, P. Yang and E.A. Stach, Nano Letters, **4**(11), 2059–2063, 2004.
- J260. *Using the FIB to characterize nanoparticle materials*; C.R. Perrey, C.B. Carter, J. Michael, P. Kotula, E.A. Stach, and V.R. Radmilovic, J. Microsc., **214**(3) 222–236, 2004.
- J261. *Surface characterization of metal nanoparticles*; X. Phung, J.R. Groza, E.A. Stach, L.N. Williams, Mat. Sci. Eng A, **359**, 261–8, 2003.
- J262. *Formation of a few nanometer wide holes in membranes with a dual beam focused ion beam system*, T. Schenkel, V. Radmilovic, E. A. Stach, S.-J. Park, and A. Persaud, J. Vac. Sci. Technol. B **21**(6), 2720–3, 2003.
- J263. *An off-normal fiber-like texture in thin films on single crystalline substrates*; C. Detavernier, A.S. Özcan, J. Jordan-Sweet, E.A. Stach, J. Tersoff, F.M. Ross, C. Lavoie, Nature, **426**, 641–5, 2003.
- J264. *Nanoscale surface and subsurface defects induced in lithium niobate by a femtosecond laser*, E.A. Stach, V.R. Radmilovic, D.C. Deshpande, A.P. Malshe, D. Alexander, D. Doerr, Appl. Phys. Lett., **83** (21) 4420–2, 2003.
- J265. *In-situ nanoindentation of epitaxial TiN / MgO (100) in a transmission electron microscope*; A.M. Minor, E.A. Stach, J.W. Morris, Jr. and I. Petrov, J. Elect. Mat., **32**(10), 1023–7, 2003.
- J266. *Fatigue problems of the future: high-cycle fatigue failures of silicon MEMS*; C. L. Muhlstein, E. A. Stach, and R. O. Ritchie, J. Eng. Integrity Soc., **14**, 4–12, 2003.
- J267. *Watching GaN nanowires grow*, E.A. Stach, P. Pauzauskie, T. Kuykendall, J. Goldberger and P. Yang, Nano Letters, **3**(6), 867–9, May 2003.
- J268. *On the origin of the orientation ratio in sputtered longitudinal media*; B. G. Demczyk, J. N. Zhou, G. Choe, E.A. Stach, E.C. Nelson and U. Dahmen, J. Appl. Phys., **93**(10) 7393–5, 2003.
- J269. *An in situ transmission electron microscopy study of the thermal stability of near-surface microstructures induced by deep rolling and laser-shock peening*, I. Altenberger, E. A. Stach, G. Y. Liu, R. K. Nalla and R. O. Ritchie, Scripta Mater., **48**, 1593–98, 2003.
- J270. *Nitride mediated epitaxy of CoSi₂ on Si(001)*; R.K.K. Chong, M. Yeadon, W.K. Choi, E.A. Stach and C.B. Boothroyd, Appl. Phys. Lett. **82**(12) 1833–5, 2003.

- J271. *In situ TEM study of the nanoindentation behavior of Al*; A.M. Minor, E.T. Lilleodden, E.A. Stach and J.W. Morris, Jr., J. Elect. Mat., **31** (10), 958–964, 2002.
- J272. *Electromigration in passivated Cu interconnects studied by transmission x-ray microscopy*; G. Schneider, M.A. Meyer, G. Denbeaux, E. Anderson, B. Bates, A. Pearson, C. Knöchel, D. Hambach, E. A. Stach and E. Zschech, J. Vac. Sci. Tech. B, **20** (6), 3089–3094, 2002.
- J273. *Dynamical x-ray microscopic investigations of electromigration of passivated inlaid Cu interconnect structures*; G. Schneider, G. Denbeaux, E. H. Anderson, B. Bates, A. Pearson, M. A. Meyer, E. Zschech, D. Hambach, and E. A. Stach, Appl. Phys. Lett., **81**(14), 2535–2537, 2002.
- J274. *A reaction-layer mechanism for the delayed failure of micron-scale polycrystalline silicon structural films subjected to high-cycle fatigue loading*; C.L. Muhlstein, E.A. Stach, and R.O. Ritchie, Acta Mater., **50**, 3579–3596 2002.
- J275. *Mechanism of fatigue in micron-scale films of polycrystalline silicon for MEMS applications*; C.L. Muhlstein, E.A. Stach, and R.O. Ritchie, Appl. Phys. Lett., **80**(9), 1532–4, 2002. Selected by Nature Physics Editor as a “Research Highlight” for March, 2002.
- J276. *Nitrogen effects on the crystallization kinetics of amorphous TiO_xN_y thin films*; K. Hukari, R. Dannenberg and E.A. Stach, J. Mater. Res. **17**(3), 550–555, 2002.
- J277. *Development of a nanoindenter for in-situ transmission electron microscopy*; E. A. Stach, T. Freeman, A. M. Minor, D. K. Owen, J. Cumings, M. A. Wall, T. Chraska, R. Hull, J.W. Morris, Jr., A. Zettl and U. Dahmen, Microscopy and Microanalysis, **7**(6) 507–517, 2001.
- J278. *Quantitative in-situ nanoindentation of aluminum thin films*; A.M. Minor, J.W. Morris Jr. and E.A. Stach, Appl. Phys. Lett, **79** (11), 1625–27, 2001.
- J279. *Enhancement of dislocation velocities by stress assisted kink nucleation at the native oxide / SiGe interface*; E.A. Stach and R. Hull, Appl. Phys. Lett., **79**(3), 335–7, 2001.
- J280. *Microstructural properties of $(Ba,Sr)TiO_3$ films fabricated from $BaF_2/SrF_2/TiO_2$ amorphous multilayers*; I. Takeuchi, K. Chang and R. P. Sharma, L. Bendersky, H. Chang, X.-D. Xiang, E.A. Stach, and C.-Y. Song, J. Appl. Phys., **90**, 2474–8, 2001.
- J281. *Phenomenological description of grain growth stagnation for nanocrystalline films and powders*; R. Dannenberg, E. A. Stach and J.R. Groza, J. Mater. Res., **16**(4), 1090–5, 2001.
- J282. *A tilting procedure to enhance compositional contrast and reduce residual Bragg contrast in EFTEM imaging of planar interfaces*; K.T. Moore, E.A. Stach, J.M. Howe, D.C. Elbert, D.R. Veblen, Micron, **33**(1), 39–51, 2001.
- J283. *A new mechanism for dislocation blocking in strained layer epitaxial growth*; E. A. Stach, R. Hull, K. W. Schwarz, F. M. Ross and R.M. Tromp, Phys. Rev. Lett. **84**(5), 947, 2000.

- J284. *Structural and chemical characterization of free-standing GaN films separated from sapphire substrates by laser lift-off*; E.A. Stach, M. Kelsch, E.C. Nelson, W.S. Wong, T. Sands and N.W. Cheung, Appl. Phys. Lett., **77** (12) 1819, 2000.
- J285. *In-situ transmission electron microscopy studies of the interaction between dislocations in strained SiGe / Si (001) heterostructures*; E. A. Stach, R. Hull, R. M. Tromp, F. M. Ross and M. C. Reuter, and J. C. Bean, Phil. Mag. A, **80**, 2159, 2000.
- J286. *In-situ TEM observations of normal grain growth in nanocrystalline Ag thin films*; R. Dannenberg, E.A. Stach, J.R. Groza, and B.J. Dresser, Thin Solid Films **379**(1-2) 133-8, 2000.
- J287. *In-situ TEM observations of abnormal grain growth, coarsening and substrate dewetting in nanocrystalline Ag films*; R. Dannenberg, E.A. Stach, J.R. Groza and B.J. Dresser, Thin Solid Films **370** (1-2), 54, 2000.
- J288. *Characterization of twin defects formed during GaAs(111)B MBE growth*; Y. Park, M. Cich, R. Zhao, P. Specht, E.R. Weber, E.A. Stach, and S. Nozaki, J. Vac. Sci and Tech. B, **18** (3), 1566, 2000.
- J289. *Interactions of moving dislocations in semiconductors with point, line and planar defects*; R. Hull, E.A. Stach, R. M. Tromp, F. M. Ross and M. C. Reuter, phys. stat. sol. (a), **171** (1), 133, 1999.
- J290. *Analysis of electron intensity as a function of aperture size in energy-filtered transmission electron microscopy imaging*; K.T. Moore, J.M. Howe, D.R. Veblen, T.M. Murray and E.A. Stach, Ultramicroscopy, **80** (3) 231, 1999.
- J291. *Effect of the surface upon misfit dislocation velocities during the growth and annealing of SiGe / Si (001) heterostructures*; E. A. Stach, R. Hull, R. M. Tromp, M. C. Reuter, M. Copel, F. K. LeGoues, and J. C. Bean, J. Appl. Phys. **83** (4), 1931, 1998.
- J292. *In-situ studies of the interaction of dislocations with point defects during annealing of ion implanted Si / SiGe / Si (001) heterostructures*; E. A. Stach, R. Hull, J. C. Bean, K. S. Jones, and A. Nejim, Microscopy and Microanalysis **4** (3), 294, 1998.
- J293. *Applications of in-situ electron and ion microscopy to the study of electronic materials and devices*; R. Hull, J. Demarest, D. Dunn, Y. Quan and E. A. Stach, Microscopy and Microanalysis **4** (3), 308, 1998.
- J294. *Suppression of boron transient enhanced diffusion in SiGe heterojunction bipolar transistors by carbon incorporation*; L. D. Lanzerotti, J. C. Sturm, E. Stach, R. Hull, T. Buyuklimanli and C. Magee, Appl. Phys. Lett. **70** (23) 3125, 1997.

Invited Oral Conference Presentations:

- I1. *Atomic Resolution Imaging of Organic Materials using Low-Dose Electron Microscopy*, Microscopy Society of America, St. Louis, MO, July 2017.
- I2. *Characterizing Working Catalysts with Correlated Electron and Photon Probes*, Microscopy Society of America, St. Louis, MO, July 2017.

- I3. *Characterizing Working Catalysts with Correlated Electron and Photon Probes*, Cornell Summer School, Ithaca, NY, July 2017.
- I4. *Using Direct Electron Detectors to Quantify Real Time Processes in Materials*, Electron Microscopy with High Time Resolution workshop, Strasbourg, France, May 2017.
- I5. *Characterizing Working Catalysts with Correlated Electron and Photon Probes*, American Chemical Society, San Francisco, CA April 2017.
- I6. *Watching Catalysts Work: Using Environmental TEM to understand nanotube growth*, American Chemical Society, San Francisco, CA April 2017.
- I7. *Characterizing NiPt Bimetallic Catalysts with Correlated Electron and Photon Probes*, Fall Materials Research Society Meeting, Boston, MA, December 2016.
- I8. *Characterizing Working Catalysts with Correlated Electron and Photon Probes; In-Situ and Operando Spectroscopy and Microscopy for Catalysts, Surfaces, & Materials Focus Topic*, 63rd Annual Meeting of the American Vacuum Society, Nashville, TN, November, 2016
- I9. Plenary Presentation, International Committee on Nanostructured Materials, Quebec City, August, 2016. Declined.
- I10. *Operando Characterization: correlating data from multiple probes to understand the function of energy-related nanomaterials*, Workshop on Basic Research Needs for Innovation and Discovery of Transformative Experimental Tools: Solving Grand Challenges in the Energy Sciences, June, 2016
- I11. *Characterizing Working Catalysts with Correlated Electron and Photon Probes*, Symposium VV, Fall 2015 Materials Research Society Meeting, November 2015
- I12. *Transmission electron microscopy in liquids and gases*, Workshop: Theory & Computation for Interface Sciences & Catalysis, Center for Functional Nanomaterials, November, 2015.
- I13. *Using operando probes to link electrons and photons in heterogeneous catalysis*, Frontiers of Electron Microscopy in Materials Science, Lake Tahoe, CA September, 2015
- I14. *Characterizing working catalysts with electron and photon probes*, American Chemical Society Meeting, Boston, MA, August, 2015 (I was invited, but had post-doctoral research Shen Zhao give my talk due to other commitments that arose).
- I15. *Using operando probes to link electrons and photons in heterogeneous catalysis*, Microscopy and Microanalysis Meeting, Portland, OR, August, 2015
- I16. *Using operando probes to link electrons and photons in heterogeneous catalysis*, Advanced Light Source Users Meeting, October, 2015 (Talk given by Skype)

- I17. *Using operando probes to link electrons and photons in heterogeneous catalysis*, Workshop on Electron Microscopy for Biological, Environmental, and Energy Research, Pacific Northwest National Laboratory, July 29 – 30, 2015.
- I18. *Creating a Big Data Ecosystem at Brookhaven National Laboratory*, NSRC Workshop on Big, Deep and Smart Data Analytics in Materials Imaging, Oak Ridge National Laboratory, June, 2015.
- I19. *A New Paradigm for Electron Microscopy: Fast Detectors and Extreme Data Experimentation*, Eric Stach, AAAS Annual Meeting, San Jose, Feb 12, 2015
- I20. *Environmental Transmission Electron Microscopy: The Example of Carbon Nanotubes*, Eric Stach, Advances in In-situ Characterization, Ohio State Materials Week, May 2014
- I21. *Electron microscopy at the Center for Functional Nanomaterials*, Eric Stach, Spring 2014 Polymer Symposium, UMass Amherst, May 2014
- I22. *Environmental Transmission Electron Microscopy: The Example of Carbon Nanotubes*, Eric Stach, Midwest Imaging and Microanalysis Workshop, Notre Dame University, May 2014
- I23. *A Closed Cell Micro-Reactor for Operando X-ray Absorption Spectroscopy and Transmission Electron Microscopy*, Eric A. Stach, Yuanyuan Li, Dmitri Zakharov, Ralph Nuzzo, Anatoly Frenkel, Workshop 3: Exploring the Pivotal Role of Next Generation X-rays in Bridging the Scale-Gaps in Next Generation Energy Materials under Extremes, NSLS-CFN User Meeting, 2014
- I24. *Exploring the Complementarity Between Advanced Electron Microscopy and Soft X-ray Spectromicroscopy*, Eric A. Stach, Yuanyuan Li, Dmitri Zakharov, Ralph Nuzzo, Anatoly Frenkel Workshop 2: Complex Functional Materials: Probing the Meso-Scale Structural Organization and the System Dynamics with Soft X-rays, NSLS-CFN User Meeting, 2014.
- I25. Microscopy and Microanalysis 2013 Meeting, New Instrumentation at the Limits: Characteristics and Applications Symposium, August, 2013.
- I26. *The Role of Nanotube Interactions on Self-Organization and Growth Termination during CNT Carpet Growth*, Eric Andrew Stach, Dmitri Zakharov, Mostafa Bedewy, Eric Meshot, A. John Hart, Nanowire and Nanotubes: Advanced Heterostructures, Doping and Devices Symposium, Fall 2013 MRS Meeting, Boston, MA, December 2013.
- I27. Microscopy and Microanalysis 2013 Meeting, Pre-meeting congress on Environmental Transmission Electron Microscopy, August, 2013.
- I28. International Conference on Electron Microscopy and XXXIV Annual Meeting of the Electron Microscope Society of India, Kolkata, July 3–5, 2013 declined.
- I29. Advanced Catalyst Characterization Workshop at BP, Naperville, June 18–19, 2013.

- I30. 4th International Workshop on Remote Electron Microscopy and In Situ Studies, May 22–24, 2013. Declined.
- I31. 2013 NSLS/CFN Joint Users' Meeting, May 21–23, 2013. Declined.
- I32. *Environmental TEM: What is it good for?*, Beyond Resolution: The Next Revolution in TEM; Key West, Florida, May 1–4, 2013.
- I33. *Real time studies of growth termination via chemo–mechanical coupling*; The Sixth Rice University, Air Force Research Laboratory, and NASA on Nucleation and Growth Mechanisms of Single Wall Carbon Nanotubes, Bandera, TX, April 12–16, 2013.
- I34. *In-situ characterization of the thermal degradation of $\text{LiNi}_{0.8}\text{Co}_{0.15}\text{Al}_{0.05}\text{O}_2$ cathode materials in lithium ion batteries*, In-situ characterization methods in energy research symposium, Spring 2013, Materials Research Society Meeting
- I35. Advanced Energy Materials Session, 2013 Renewable Energy and Energy Efficiency Workshop (Louisville, March 24–26, 2013). Declined.
- I36. TMS 2013, Nanostructured Materials for Lithium Ion Batteries and for Supercapacitors Symposium, March 3–7, 2013. Declined.
- I37. *Inhomogeneity of nanoparticle reduction and oxidation studied via environmental transmission electron microscopy*, Fall 2012 Materials Research Society Meeting, Frontiers of Chemical Imaging: Integrating Electrons, Photons and Ions, November, 2012
- I38. *Environmental TEM in catalysis research*, 244th Annual American Chemical Society Meeting, Spectroscopy and Microscopy in Catalysis: The In Situ Age Philadelphia, PA, August 2012.
- I39. *Environmental TEM in catalysis research*; Advanced Microscopy and Theoretical Calculations, Nagoya, Japan, May, 2012.
- I40. Plenary Lecture. 11th Annual Conference of the Yugoslav Materials Research Society, Herceg Novi, Montenegro, September, 2011. Unable to attend.
- I41. *Environmental Transmission Electron Microscopy (broadly defined)*, Future directions in Electron Optics, Materials and Manufacturing Directorate, Wright Patterson Air Force Research Laboratory, August, 2011.
- I42. *Catalyst morphological evolution during CNT growth*, The Fifth Rice University, Air Force Research Laboratory, and NASA Workshop on Nucleation and Growth Mechanisms of Single Wall Carbon Nanotubes.
- I43. *The effect of gaseous ambients on catalytic nanoparticles and the impact on nanotube chirality selection*, Session A30: Focus Session: Carbon Nanotubes: Chirality–Controlled Growth of Carbon Nanotubes and Nanostructures, American Physical Society Meeting, Portland, Oregon, March 2011.

- I44. *In-situ transmission electron microscopy*, Symposium Tutorial Presentation, Symposium TT: “In Situ X-Ray Synchrotron Radiation Spectroscopies in Energy-Related Materials Science and Heterogeneous Catalysis”, Fall 2010 Materials Research Society Meeting, November, 2010.
- I45. *Update on the Purdue / BNL ETEM work in the CNT Collaboration*, SWNT Collaborators Workshop, Yellow Springs, OH, October, 2010.
- I46. *Understanding the mechanisms of carbon nanotube growth and growth termination*, plenary lecture at Nanomex '10, International and Interdisciplinary Meeting on Nanoscience and Nanotechnology, Cuernavaca, Mexico, November, 2010.
- I47. Declined. “Understanding materials using in-situ microscopy” in Göttingen, Germany on Nov. 10–12, 2010.
- I48. *Environmental TEM: What does aberration correction gain you?*, Midwest Microscopy Society (M3S) Meeting: In-situ TEM, October, 2010.
- I49. *Environmental TEM: What does aberration correction gain you?*, Symposium on Materials Characterization using Advanced Electron Microscopy; Rutgers University, October, 2010.
- I50. Update on the Purdue / BNL ETEM work in the CNT Collaboration, SWNT Collaborators Workshop, Yellow Springs, OH, October, 2010.
- I51. *Declined*, Extended Defects in Semiconductors (EDS2010).
- I52. *Evolution in catalyst morphology leads to carbon nanotube growth termination*, S.M. Kim, C.L. Pint, P. Amama, R.H. Hauge, B. Maruyama, and E.A. Stach, in “Nanostructure Applications in Cross-over Scientific and Technology Fields”, International Materials Research Congress, Cancun, Mexico, August 2010.
- I53. *Characterizing and optimizing the performance of the FEI Titan ETEM*, Microscopy and Microanalysis Meeting, August 2010.
- I54. *Declined*, 11th IUMRS International Conference in Asia (IUMRS-ICA 2010).
- I55. *Stabilizing nanostructured metals via the incorporation of high densities of twins*, International Symposium on Plasticity and its Current Applications, St. Kitts, January 2010.
- I56. *Using in-situ TEM to understand growth termination of water-assisted single-walled carbon nanotube arrays*, Midwest Microscopy Society (M3S) Meeting, August, 2009.
- I57. Declined, Workshop on In-situ Nanomechanics, Indian Institute of Science, August, 2009.
- I58. *Understanding the interplay of mechanisms contributing to termination of water-assisted single-walled carbon nanotube array growth*, “C.L. Pint, S.M. Kim, P. Amama, B. Maruyama, E.A. Stach, and R.H. Hauge, NT '09, Beijing, CN (6–21–2009).

- (a) Selected as an invited presentation from the pool of submitted abstracts
- I59. *Kinetics of individual nucleation events in nanoscale vapor-liquid-solid growth*, “Semiconductor Nanowires”, Materials Research Society Meeting, Spring 2009.
 - I60. *Optimizing our ETEM for controlled nanostructure growth: some substantial successes and several remaining challenges*, FEI Corporation Workshop on Environmental Transmission Electron Microscopy, Eindhoven, The Netherlands, April, 2009.
 - I61. Declined. International Symposium on Plasticity and its Current Applications, January 2009.
 - I62. *Ostwald ripening of Fe on alumina during nanotube growth*, “In-situ Studies Across Spatial and Temporal Length Scales for Nanoscience and Technology”, Materials Research Society Meeting, Fall 2008.
 - I63. *Ostwald ripening of Fe on alumina during nanotube growth*, Advanced Electron Microscopy in Materials Science, ORNL Workshop, November, 2008.
 - I64. *Ostwald ripening of Fe on alumina during nanotube growth*, In-situ Electron Microscopy, AVS 55th International Symposium, October, 2008.
 - I65. *Ostwald ripening of Fe on alumina during nanotube growth*, Yellow Springs Workshop on Nanotube Growth Mechanisms, October, 2008.
 - I66. Declined; Workshop on Aberration-Corrected Microscopy and Spectroscopy for Materials, ORNL, September, 2008.
 - I67. *Expanding in-situ mechanical testing into the “ultrafast” regime*, Ultrafast Electron Microscopy and Ultrafast Science Symposium, Microscopy and Microanalysis Meeting, August, 2008.
 - I68. *Kinetics of individual nucleation events observed in nanoscale vapor-liquid-solid growth*, “Opportunities and Challenges for In-Situ Microscopy, User’s Week 2008, Argonne National Laboratory, May, 2008.
 - I69. *Exploiting quantitative in-situ nanoindentation to investigate the mechanisms of plastic deformation in thin films*, American Ceramic Society Annual Meeting, Daytona, FL, January, 2008
 - I70. Declined. International Symposium on Plasticity and its Current Applications, Keahou Bay January 2008.
 - I71. *Quantitative in-situ nanoindentation of thin films*, Center for Electron Nanoscopy Inauguration, Denmark Technical University, Lyngby, Denmark, December 2007.
 - I72. *Using real time electron microscopy to understand nucleation and growth in semiconducting nanowires and carbon nanotubes*, Quantitative Electron Microscopy for Materials Science, Fall 2007 MRS meeting, Boston, MA, November 2007.

- I73. *Using real time electron microscopy to understand nucleation and growth in semiconducting nanowires and carbon nanotubes*, In-situ Electron Microscopy, AVS 54th International Symposium, October, 2007.
- I74. *Using real time electron microscopy to understand nucleation and growth in semiconducting nanowires and carbon nanotubes*, Frontiers of Electron Microscopy in Materials Science Conference, October, 2007
- I75. Declined, Interamerican Congress of Electron Microscopy 2007, September 2007
- I76. *Using real time microscopy to understand the nucleation of nanotubes and nanowires*, Ninth Annual Conference of the Yugoslav Materials Research Society, Herceg Novi, Montenegro, September, 2007.
- I77. Declined, 2007 ASME Mechanics and Materials Conference, Austin, Texas, June, 2007.
- I78. *Why is ultra-fast imaging needed for in-situ transmission electron microscopy?*, Fast Electron Gun Workshop, Argonne National Laboratory, June 5th, 2007.
- I79. *Using real time electron microscopy to understand nucleation and growth in semiconducting nanowires and carbon nanotubes*, In Situ Studies of Interfacial Reactivity Workshop, User's Week 2007, Argonne National Laboratory, May 10, 2007.
- I80. *Understanding the mechanisms of single walled nanotube growth from "spin-on-catalysts" using real time imaging in the TEM*, E.A. Stach, Seung Min Kim, Mark Pender, Tyson C. Back, Allison Jacques and Benji Maruyama, 2007 Workshop on Nucleation and Growth of Single Wall Carbon Nanotubes.
- I81. *Understanding the onset of plasticity in materials using quantitative in-situ nanoindentation*, E.A. Stach, A.M. Minor, D. Ge, J.W. Morris, Jr., S. Asif, T. Wyrobek and O. Warren, 2007 International Conference on Metallurgical Coatings and Thin Films (ICMCTM), San Diego, April 2007.
- I82. *Size effects on the deformation behavior of silicon*; E.A. Stach, A.M. Minor, D. Ge, J.W. Morris, Jr., S. Asif, T. Wyrobek and O. Warren, Workshop on the Mechanical Behavior of Systems at Small Length Scales, Indian Institute of Science, Bangalore, February, 2007.
- I83. *Observing mechanical behavior and crystal growth at improved time resolution*. E.A. Stach, Workshop on Dynamic Transmission Electron Microscopy, Lawrence Livermore National Laboratory, Livermore, CA Aug 10 & 11, 2006.
- I84. Declined, Extended Defects in Semiconductors, Halle, 2006.
- I85. *Quantitative nanoindentation in-situ to the TEM*, E.A. Stach, A. Minor, Z. Shan, , M. Jin, J.W. Morris, Jr., A. Syed and O. Warren, AVS Prairie Chapter Symposium, June 2006.

- I86. *Characterization of nanomaterials*, Eric Stach, Food Nanotechnology Grand Rounds, Food & Drug Administration, April 25 2006.
- I87. *Quantitative in-situ nanoindentation of silicon*, E.A. Stach, D. Ge, A.M. Minor, J.W. Morris, Jr., S. Asif, T. Wyrobek and O. Warren “In-situ electron microscopy”, Fall 2005 MRS meeting, Boston MA.
- I88. *In-situ nanoindentation: a quantitative technique for understanding nanoscale deformation mechanisms*, E.A. Stach, A. Minor, D. Ge, M. Jin and J.W. Morris, Jr., “Dynamics of Materials Revealed by Electron Microscopy”, Midwest Microscopy and Microanalysis Society, Urbana, Illinois, June 2005.
- I89. Declined, Eighth Annual Conference of the Yugoslav Materials Research Society, Herceg Novi, Montenegro, September, 2005.
- I90. *In-situ transmission electron microscopy studies of the deformation of nanocrystalline metals*, E.A. Stach, A. Minor, D. Ge, M. Jin, J.W. Morris, Jr., Z. Shan, S.X. Mao, J.M.K. Wiezorek, D.M. Follstaedt and J.A. Knapp, China-US Workshop on Advanced Materials, May, 2005.
- I91. *In-situ nanoindentation of ultrananocrystalline diamond and amorphous diamond thin film coating*, E.A. Stach, A.M. Minor, D. Ge, J.W. Morris, Jr., T.A. Friedmann, X. Xiao, O. Auciello, J.A. Carlisle, “Nanostructured diamond and diamond-like materials for micro- and nano-devices”, Spring 2005 MRS meeting, April, 2005.
- I92. *Using the electron microscope to explore reliability in nanostructured materials*, E.A. Stach, D. Ge, M. Jin, A. Minor, J.W. Morris, Jr., V. Gopal, and V. Radmilovic, “Thin Films — Stresses and Mechanical Properties XI”, Spring 2005 MRS meeting, April 2005.
- I93. *In-situ nanoindentation: a novel technique for understanding nanoscale deformation mechanisms*, The 10th International Symposium on Advanced Physical Fields, National Institute for Materials Science, Tsukuba, Japan, March 2005
- I94. *Using the electron microscope to explore reliability in microelectromechanical systems and nanostructured materials*, E.A. Stach, V. Gopal, M. Jin, D.H. Alsem, M.J. Williamson, A. Minor, V. Radmilovic, C.L. Muhlstein, J.W. Morris, Jr., and R.O. Ritchie, Microscopy and Microanalysis, Savannah, Georgia, August, 2004.
- I95. *In-situ nanoindentation – a unique probe of deformation response in materials*, E.A. Stach, A.M. Minor, E.T. Lilleodden, M. Jin, D. Chrzan, J.W. Morris, Jr., T.A. Friedmann, X. Xiao, O.H. Auciello, and J.A. Carlisle, Microscopy and Microanalysis Meeting, San Antonio, TX, August 2003.
- I96. *In-situ TEM studies of nanoindentation: a novel method for quantitatively exploring thin film mechanical behavior*, E.A. Stach, A.M. Minor, E.T. Lilleodden, M. Jin and J.W. Morris, Jr., American Society for Mechanical Engineering, Scottsdale, AZ, June 2003.

- I97. *Quantitative in-situ nanoindentation: a novel method for exploring thin film mechanical behavior*; E.A. Stach, A.M. Minor, E.T. Lilleodden, M. Jin and J.W. Morris, Jr., American Physical Society Meeting, Texas, March 2003.
- I98. *In-situ transmission electron microscopy studies of grain growth in thin films during simultaneous heating and electrical bias*; E.A. Stach, X. Phung, L. Stanciu, J.R. Groza, K. Hukari, "Materials Processing Under the Influence of Electrical and Magnetic Fields" TMS Annual Meeting, San Diego, CA, March 2003.
- I99. *Quantitative determination of the kinetics of nanope growth in GaN*; E.A. Stach, W.S. Wong and M. Kneissl, 4th Symposium on Non-Stoichiometric III-V Compounds, Asilomar, CA, October 2002.
- I100. *Quantitative in-situ nanoindentation: a novel method for exploring thin film mechanical behavior*; E.A. Stach, A. Minor, E.T. Lilleodden and J.W. Morris, Jr., XI International Materials Research Congress, Cancún, Mexico, August 2002.
- I101. *Transmission electron microscopy in thin film mechanical property research*, E.A. Stach, Chama River Workshop on Thin Film Mechanical Properties, Cuba, New Mexico, August 2002.
- I102. *Fatigue of thin-film silicon-based MEMS materials: experiments, mechanisms and durability*; C. Muhlstein, E.A. Stach (presenting) and R.O. Ritchie, at "MEMS and Nanotechnology" Symposium, 14th U.S. National Congress of Theoretical and Applied Mechanics, Blacksburg, VA, June 2002.
- I103. *On the suppression of premature fatigue failure in thin-film polycrystalline silicon for MEMS*; C. Muhlstein, E.A. Stach (presenting) and R.O. Ritchie, at "Mechanics of Thin Films and Other Small Structures" Symposium, Fourteenth U.S. National Congress of Theoretical and Applied Mechanics, Blacksburg, VA, June 2002.
- I104. *Thermochemical decomposition in GaN: Laser lift-off and novel defect formation*, E.A. Stach, T. Sands, Y. Cho and W.S. Wong, "Defect and Impurity-Engineered Semiconductors and Devices, III", Materials Research Society Meeting, San Francisco, CA, April 2002.
- I105. *In-situ TEM: a tool for quantitative observations of deformation behavior in thin films and nanostructured materials*; E.A. Stach, DOE Workshop on New Materials Science Enabled by *In-situ* Microscopies, Half Moon Bay, CA, January 2001.
- I106. *In-situ transmission electron microscopy studies of dislocations in metallic thin films*; E.A. Stach, A. M. Minor, J. W. Morris, Jr., J. A. Floro, S. Seel and C. V. Thompson, International Conference on Materials for Advanced Technologies – "Thin Films: Stress, Strain and Structure – Property Relationships" Symposium, IUMRS Meeting, Singapore, July 2001.

- I107. *In-situ transmission electron microscopy studies of dislocations in metallic thin films*; E.A. Stach, A. Minor, J.W. Morris, Jr., J.A. Floro, S.C. Seel and C.V. Thompson “Dislocations and Deformation Mechanisms in Thin Films and Small Structures”, Spring 2001 Materials Research Society meeting, San Francisco, CA, April 2001.
- I108. *In-situ transmission electron microscopy studies of defect formation and dislocation interactions in semiconductor materials*; E.A. Stach, R. Hull, R.M. Tromp, K. Schwarz, F.M. Ross, C.F. Kisielowski, T. Sands and W.S. Wong, International Conference on Extended Defects in Semiconductors, Sussex, England, July 2000.
- I109. *In-situ microscopy in an aberration-free microscope*; Summer Workshop on Aberration Correction in Electron Microscopy, Argonne National Laboratory, Argonne, IL, July 2000.
- I110. *In-situ transmission electron microscopy studies of dislocations in thin film systems*; E.A. Stach, R. Hull, R.M. Tromp, F.M. Ross, K.W. Schwarz, M.C. Reuter, and W.D. Nix, Fall 1999 Materials Research Society Meeting, Boston, MA, December 1999.

Departmental Seminars

At Materials Science Departments unless otherwise noted

- 1998: National Center for Electron Microscopy, Lawrence Berkeley National Laboratory
- 1999: Sandia National Laboratories, Livermore
- 2000: Xerox Palo Alto Research Center; Lucent Bell Laboratories; University of California at Berkeley
- 2001: Sandia National Laboratories, Albuquerque; Northern California Society for Microscopy; University of Illinois at Urbana-Champaign; University of Virginia; Cornell University
- 2002: IBM Almaden Research Laboratory; Palo Alto Research Center, Incorporated; The Advanced Light Source, Lawrence Berkeley National Laboratory; University of Washington; Stanford University; University of Colorado at Boulder; Brown University
- 2003: University of California, Los Angeles; Department of Mechanical Engineering, University of Nevada, Reno; Department of Mechanical Engineering, University of Arkansas; Department of Physics, University of California, Berkeley; IBM Almaden Research Laboratory; Sandia National Laboratories, Albuquerque; Hysitron Corporation; Zyvex Corporation

2004: Argonne National Laboratory; Purdue University; University of Florida; University of Maryland, University of California at Berkeley; Sandia National Laboratories, Albuquerque; Department of Mechanical Engineering, Princeton University; Palo Alto Research Center, Incorporated

2005: Case Western Reserve University; Tohoku University; Argonne National Laboratory; Ohio State University; Department of Chemical Engineering, University of Louisville; University of Michigan; GE Global Research

2006: Harvard University

2007: University of Virginia

2008: Department of Mechanical Engineering, University of Pittsburgh; Department of Mechanical Engineering, Michigan Technological University; Center for Nano and Molecular Science and Technology, University of Texas, Austin; Northwestern University

2009: Center for Nanoscale Science and Technology, National Institute of Standards and Technology; Center for Functional Nanomaterials, Brookhaven National Laboratory

2010: University of Illinois at Urbana–Champaign; Ohio State University; Nanoscale Research and Engineering Center, Columbia University; Rensselaer Polytechnic Institute

2011: Cornell University; University of Pennsylvania; Massachusetts Institute of Technology's Center for Excitonics

2012: IBM T.J. Watson Research Center, Physical Sciences Seminar; Discovery Lecture, Center for Nanophase Materials Science, Oak Ridge National Laboratory

2013: Brown University, Joint Materials and Mechanics Group Seminar; Stevens Institute of Technology, Department of Materials Science and Engineering; Princeton Research Institute for the Science of Materials; University of Connecticut

2014: Brown University

2015: University of Pittsburgh

2016: University of Florida; Notre Dame University (Skype); University of Pennsylvania; Center for Nanoscale Science and Technology, National Institute of Standards and Technology; Massachusetts Institute of Technology

2017: BASF Corporation, Heterogeneous Catalysis Research Center; Rowland Institute, Harvard University, Dartmouth College, Duke University

EXHIBIT B

List of Materials Considered by Eric Stach

Initial Expert Report of Dr. William Alan Thomas Clark

Appendix C to Initial Expert Report of Dr. William Alan Thomas Clark

Initial Expert Report of Dr. Kevin Coffey

U.S. Patent No. 7,128,988

U.S. Patent No. 6,248,416

Markman Order (Dkt. No. 78)

Seagate's First Supplemental Response to LMS's Interrogatory No. 10

KK Fung, *Identification and Determination of Crystal Structures and Orientations by Electron Diffraction* (Jan. 2001), available at:
<http://personal.cityu.edu.hk/~appkchu/AP5301/Electron%20Diffraction%20-%20Paper.pdf>

D. Lambeth et al., *Magnetic Media Performance: Control Methods for Crystalline Texture and Orientation*, Mat. Res. Soc. Symp. Proc., Vol. 517, p. 185 (1998)

B. Futltz and J. Howe, *Transmission Electron Microscopy and Diffractometry of Materials* (2013)

J.W. Edington, *Practical Electron Microscopy in Materials Science* (1976)

D.B. Williams and C.B. Carter, *Transmission Electron Microscopy*, Springer (2009)

Milton Ohring, *Materials Science of Thin Films* (1990)

L. Vitos, A.V. Ruban, H.L. Skriver, and J. Kollár, "The Surface Energy of Metals," *Surface Science* (1998)

EXHIBIT C

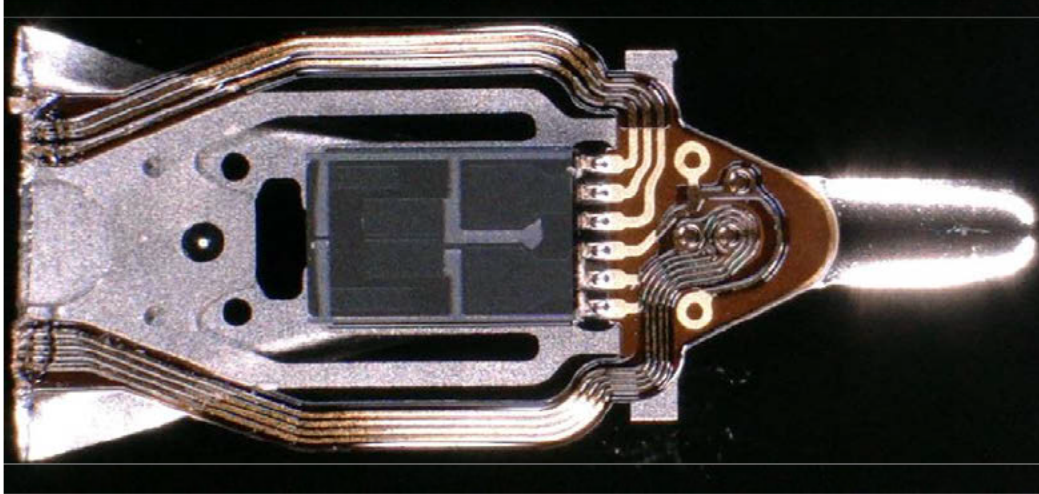
Explanation of Sample Preparation of Seagate [REDACTED] Drive

1. I directed EAG Laboratories (“EAG”) at 810 Kifer Road, Sunnyvale, CA 94086 to prepare samples of write poles from HDDs manufactured by Seagate and sold within the United States by online retailers (*i.e.*, Staples, NewEgg). More particularly, I directed Udit Sharma at EAG to prepare a plan-view sample of a write pole from a Seagate Constellation ES.2 2 TB 3.5” HDD model ST32000645SS. The Seagate model ST32000645SS HDD has the internal product name Mantaray and includes an [REDACTED] write pole configuration.

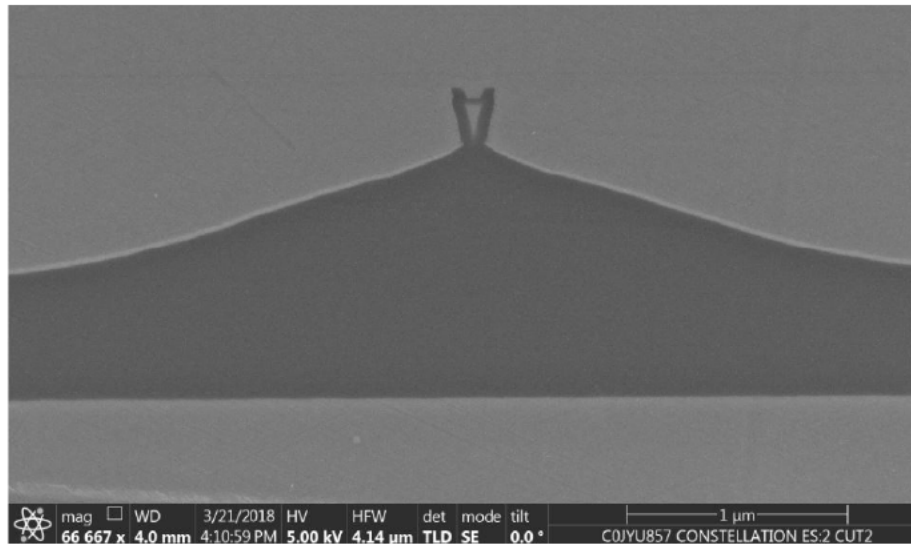
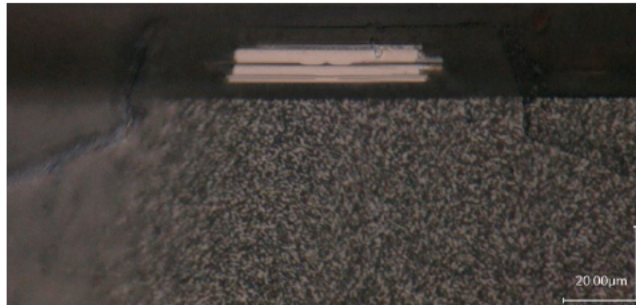
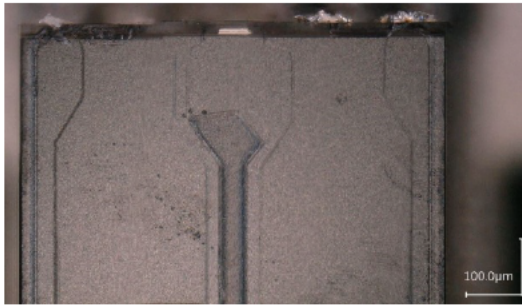
2. At my direction, the HDD was disassembled by EAG. Below is an image of the ST32000645SS HDD, which contains the [REDACTED] write pole.

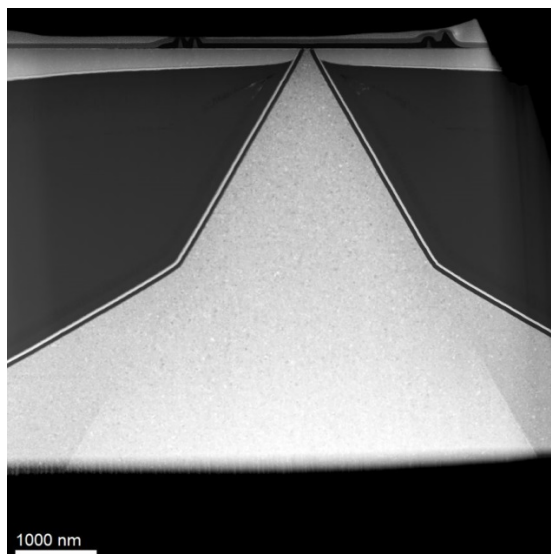
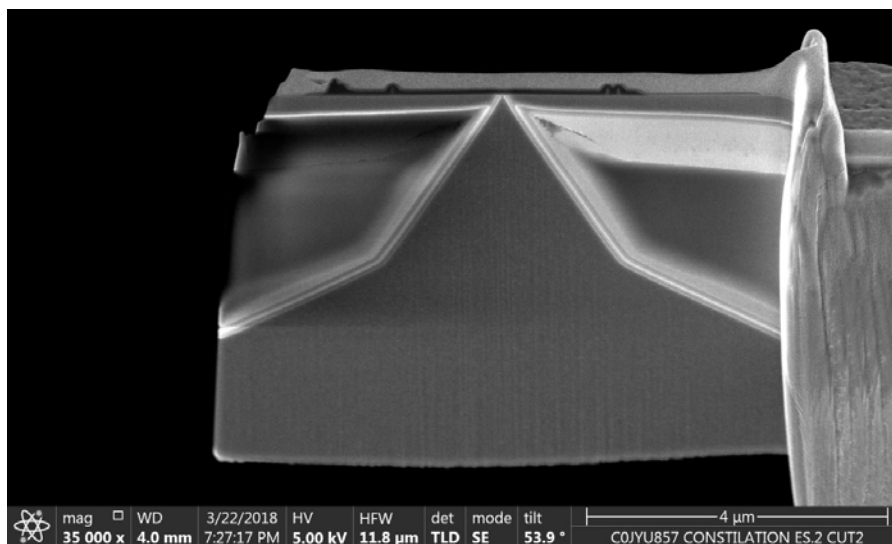
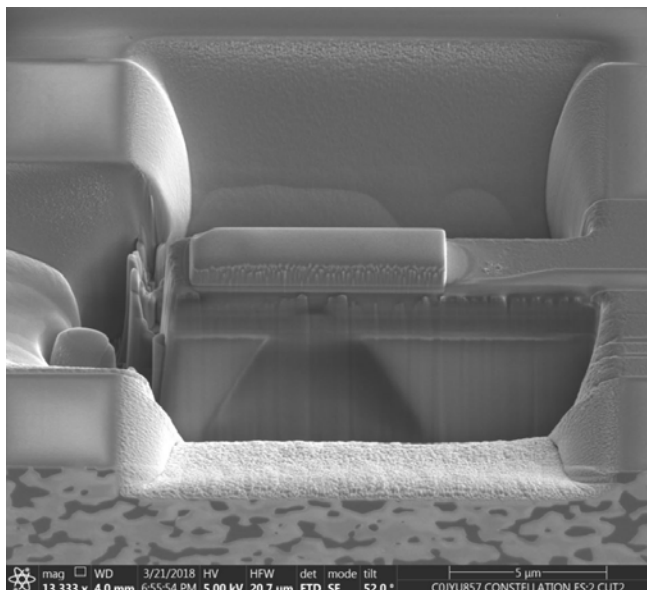


3. At my direction a slider from the HDD was extracted. Below is an image of a portion of the HGA from the ST32000645SS HDD.

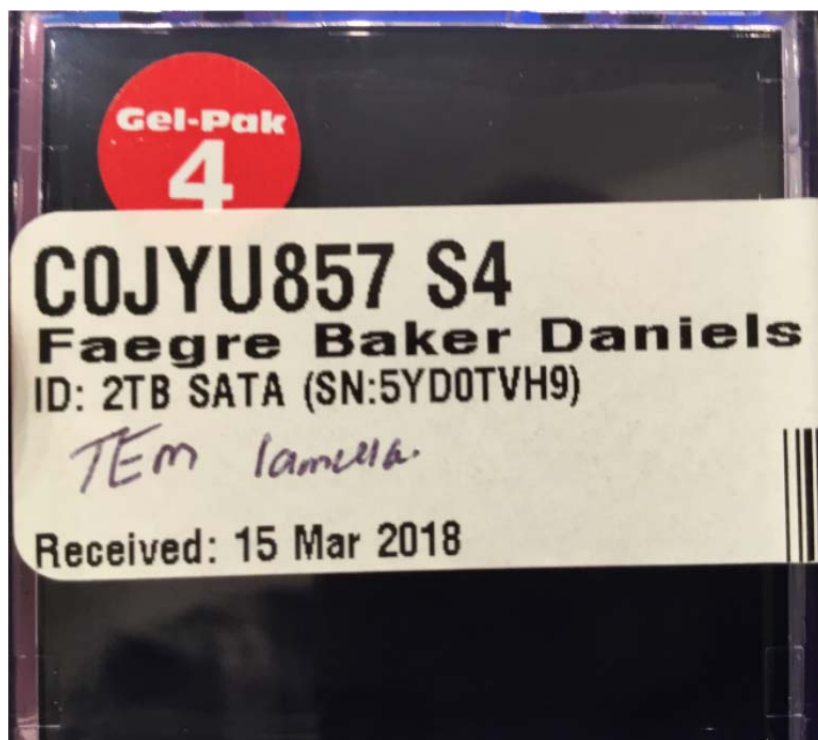
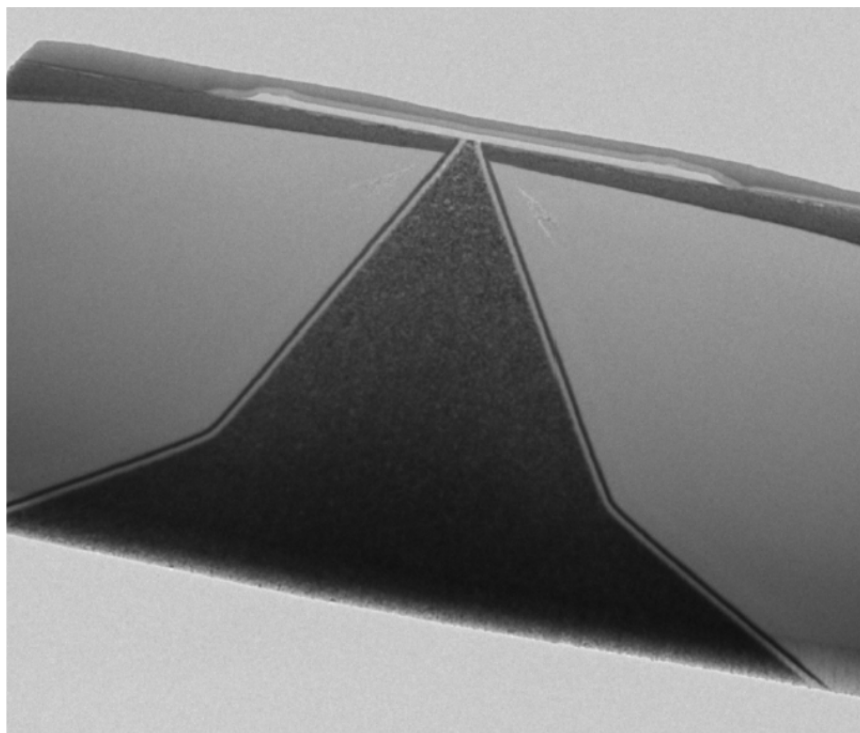


4. EAG used a focused ion beam to isolate the area of interest of the write pole from the rest of the slider to create a lamella. Below are images of the slider from the ST32000645SS HDD and its [REDACTED] write pole.





5. The lamella was mounted to a TEM grid and shipped to my office in gel packs. Below is an image I took of the sample prepared by EAG.



6. After receiving the sample, I obtained TEM images and diffraction patterns using a Japan Electron Optics Limited (JEOL) F200 instrument, located at the Singh Center for Nanotechnology at the University of Pennsylvania. The instrument is equipped with an ultrabright cold field emission source and a three condenser lens system which allows plane parallel (Kohler) illumination so that I could obtain diffraction patterns from specific areas of the sample. The diffraction patterns were obtained at 500 mm camera length, so as to allow capture of a full range of diffraction rings from the sample. Images were specifically obtained in the ‘plan view’ orientation, as this orientation allows a statistically valid measure of whether or not the sample has significant texture in the growth direction. Diffraction patterns were “false colored” using Gatan’s Digital Micrograph Software.

7. I obtained both bright field and annular dark field images of the plan view of the samples. I further obtained diffraction patterns of both samples, and indexed the rings from the diffraction patterns.

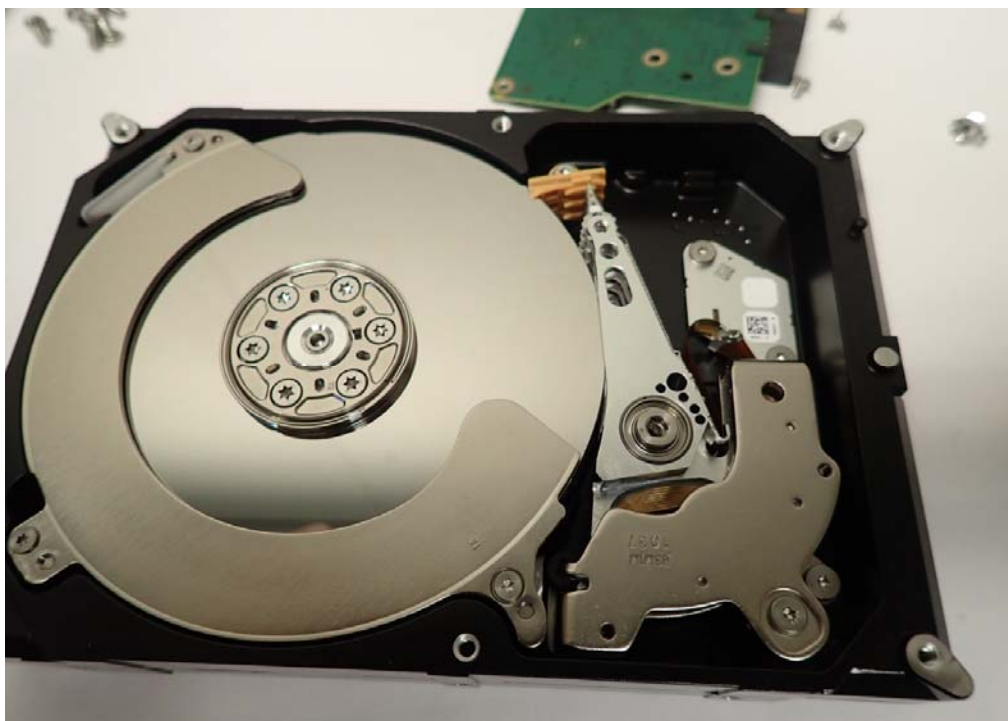
EXHIBIT D

Explanation of Sample Preparation of Seagate [REDACTED] Drive

1. I directed EAG Laboratories (“EAG”) at 810 Kifer Road, Sunnyvale, CA 94086 to prepare samples of write poles from HDDs manufactured by Seagate and sold within the United States by online retailers (*i.e.*, Staples, NewEgg). More particularly, I directed Udit Sharma at EAG to prepare a plan-view sample of a write pole from a Seagate Barracuda Green 2 TB 3.5” model ST2000DL001. The Seagate model ST2000DL001 HDD has the internal product name Bogart and includes a [REDACTED] write pole configuration.

2. At my direction, the HDD was disassembled by EAG. Below is an image of the ST2000DL001 HDD, which contains the [REDACTED] write pole.

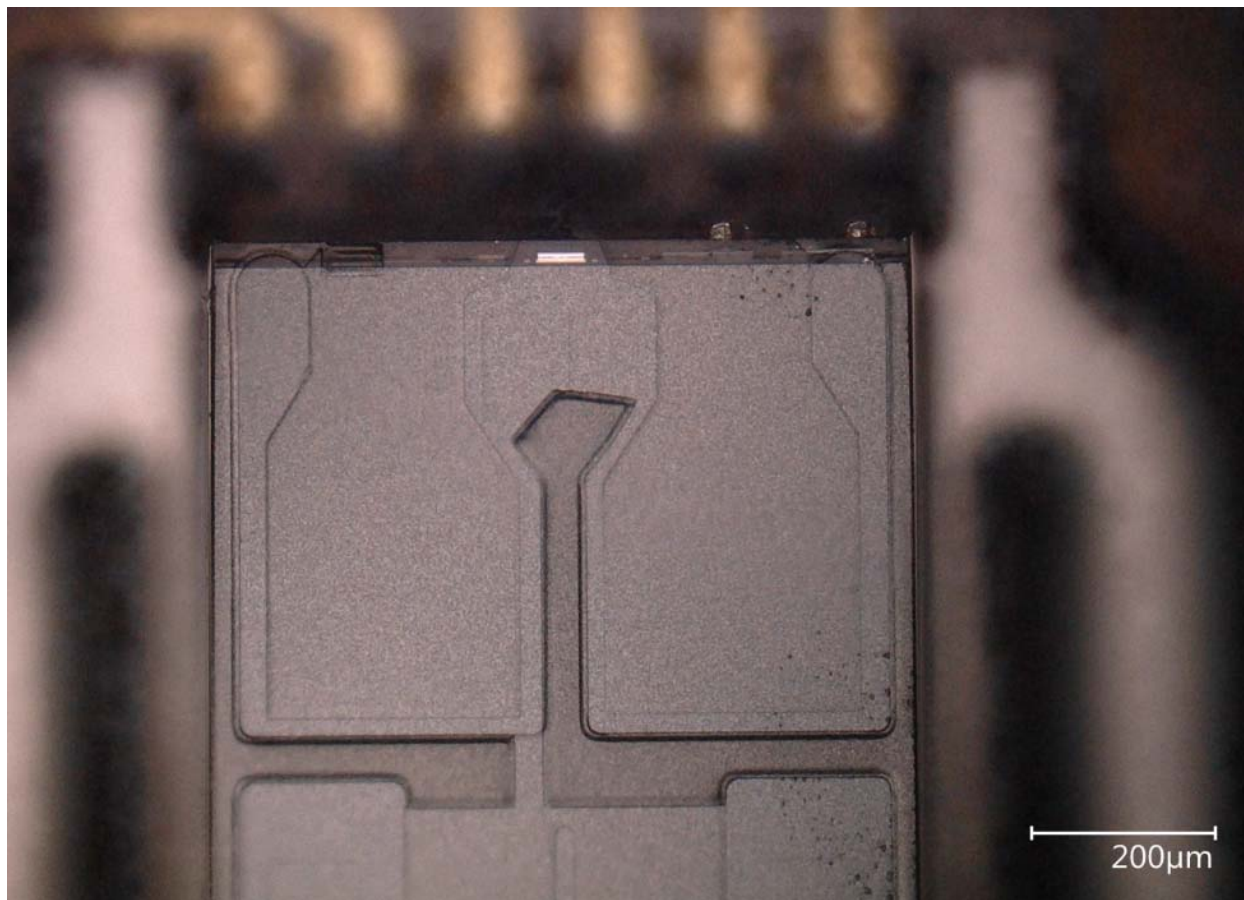




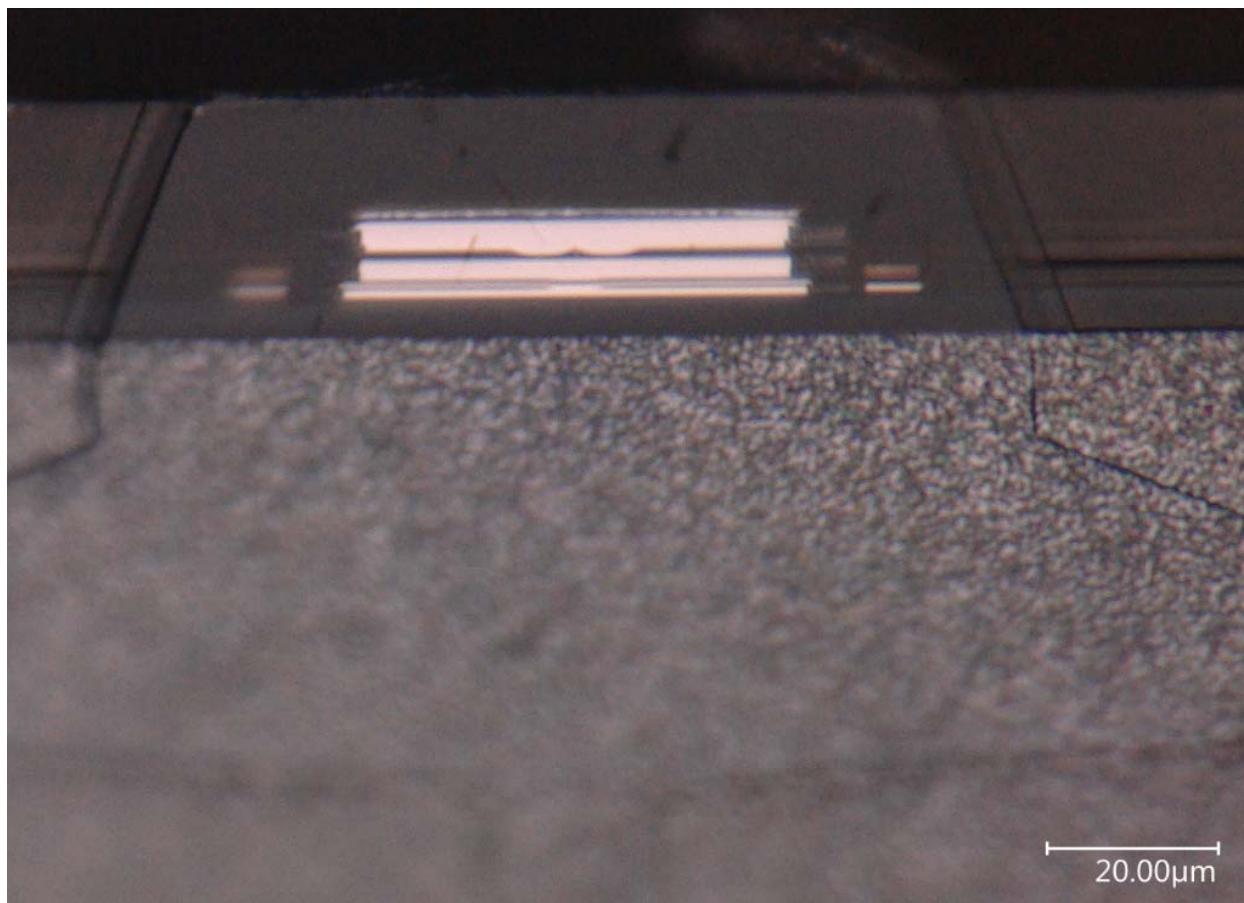
3. At my direction a slider from the HDD was extracted. Below is an image of HGAs on the arm, and then removed from the ST2000DL001 HDD.



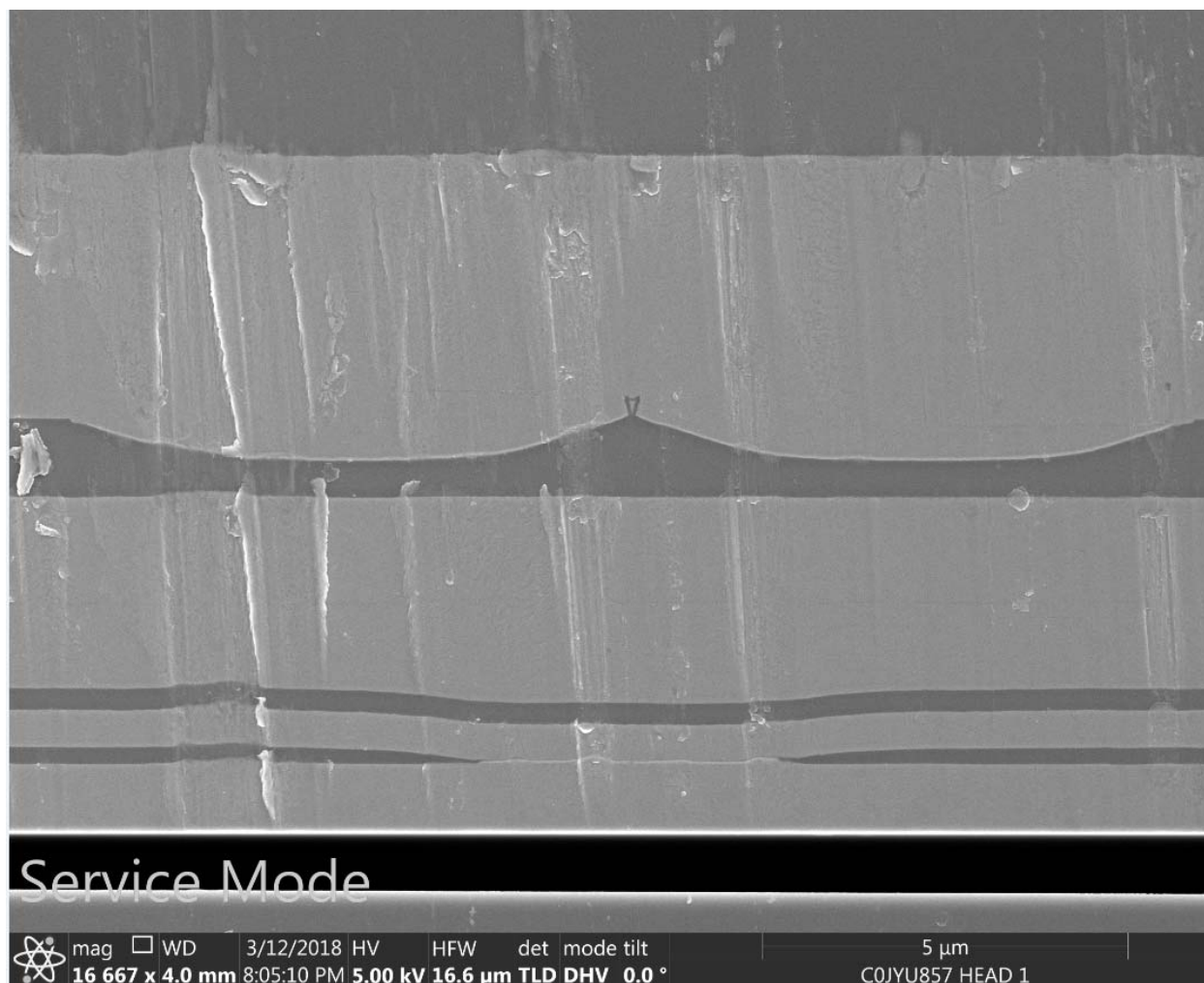
4. Below is an image of the slider portion of the HGA. The read/write head is contained entirely within the small white slit at the top center of the image.

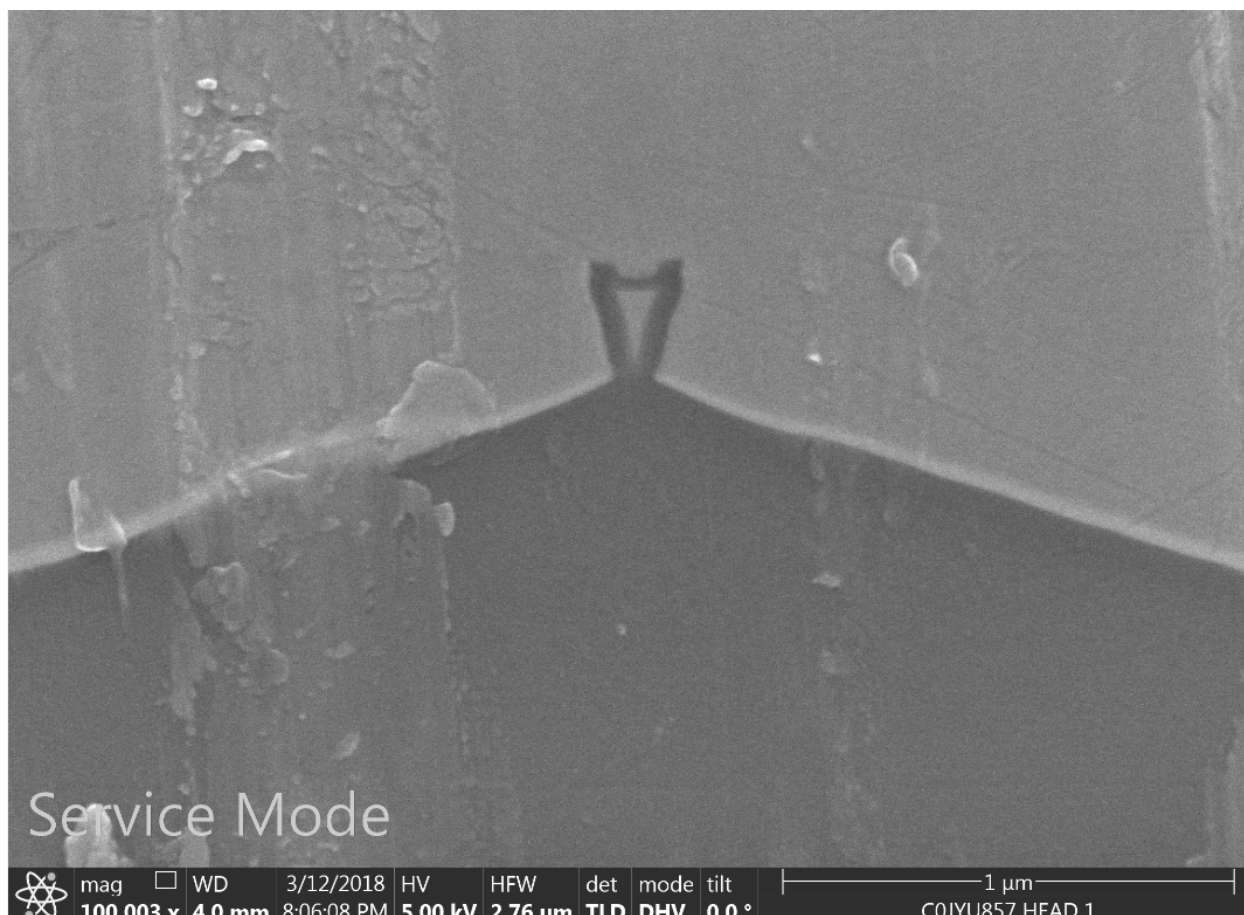


5. EAG created a further zoomed in picture of the above slider, and write head below:



6. EAG used a focused ion beam to isolate the area of interest of the write pole from the rest of the slider to create a lamella. Below are images of the slider from the S ST2000DL001 HDD and its [REDACTED] write pole.

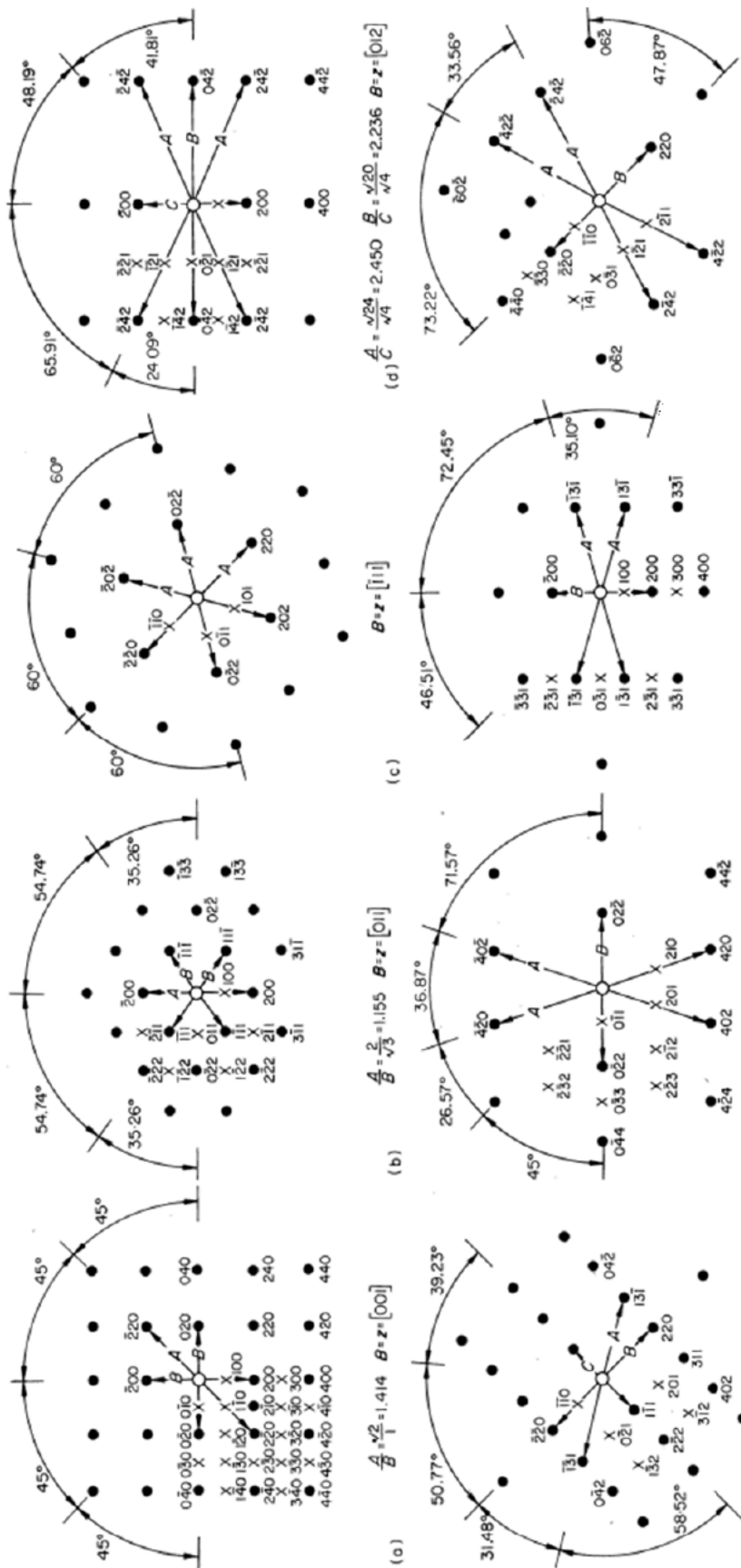




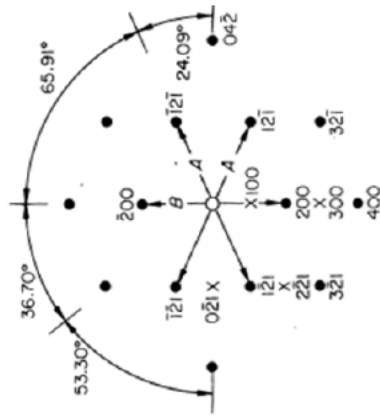
7. The lamella was mounted to a TEM grid and shipped to my office in gel packs. After receiving the sample, I obtained TEM images and diffraction patterns using a Japan Electron Optics Limited (JEOL) F200 instrument, located at the Singh Center for Nanotechnology at the University of Pennsylvania. The instrument is equipped with an ultrabright cold field emission source and a three condenser lens system which allows plane parallel (Kohler) illumination so that I could obtain diffraction patterns from specific areas of the sample. The diffraction patterns were obtained at 500 mm camera length, so as to allow capture of a full range of diffraction rings from the sample. Images were specifically obtained in the ‘plan view’ orientation, as this orientation allows a statistically valid measure of whether or not the sample has significant texture in the growth direction. Diffraction patterns were “false colored” using Gatan’s Digital Micrograph Software.

8. I obtained both bright field and annular dark field images of the plan view of the samples. I further obtained diffraction patterns of both samples, and indexed the rings from the diffraction patterns.

EXHIBIT E

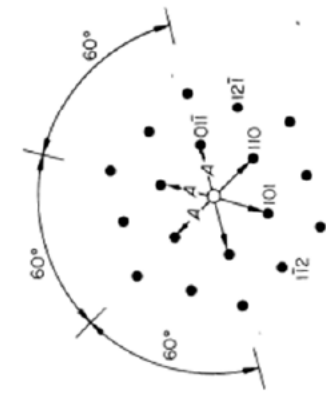


FCC STANDARD DIFFRACTION PATTERNS



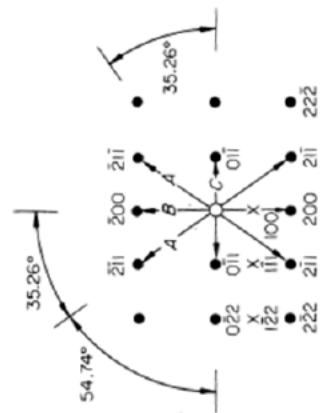
$$\frac{A}{B} = \frac{\sqrt{4}}{\sqrt{2}} = 1.414 \quad B = z = [001]$$

(a)



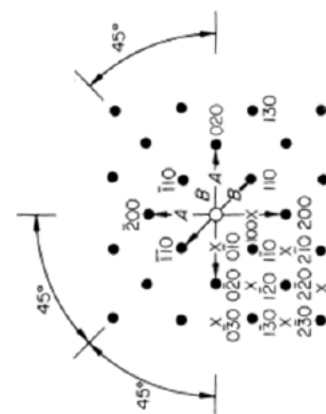
$$\frac{A}{C} = \frac{\sqrt{6}}{\sqrt{2}} = 1.732 \quad B = z = [111]$$

(b)



$$\frac{A}{C} = \frac{\sqrt{6}}{\sqrt{2}} = 1.732 \quad B = z = [111]$$

(c)



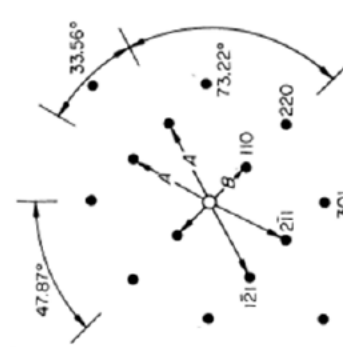
$$\frac{A}{B} = \frac{\sqrt{4}}{\sqrt{2}} = 1.414 \quad B = z = [001]$$

(d)



$$\frac{A}{B} = \frac{\sqrt{4}}{\sqrt{2}} = 1.414 \quad B = z = [001]$$

(e)



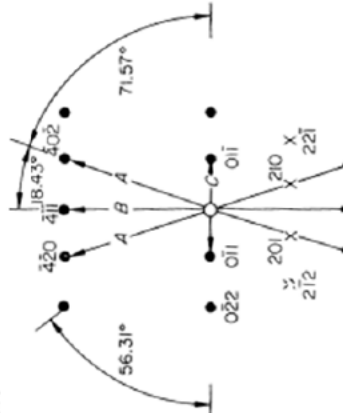
$$\frac{A}{B} = \frac{\sqrt{6}}{\sqrt{4}} = 1.225 \quad B = z = [012]$$

(f)



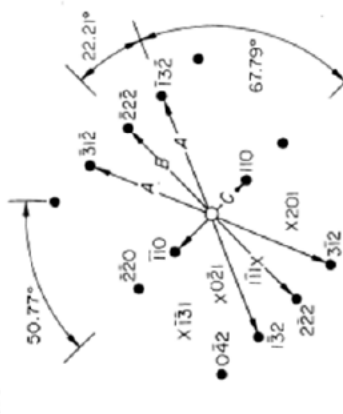
$$\frac{A}{C} = \frac{\sqrt{14}}{\sqrt{4}} = 1.871 \quad B = z = [013]$$

(g)



$$\frac{A}{C} = \frac{\sqrt{20}}{\sqrt{2}} = 3.162 \quad B = z = [222]$$

(h)



$$\frac{A}{C} = \frac{\sqrt{14}}{\sqrt{2}} = 2.646 \quad B = z = [112]$$

(i)



$$\frac{A}{B} = \frac{\sqrt{6}}{\sqrt{2}} = 1.732 \quad B = z = [113]$$

(j)

$$\frac{A}{B} = \frac{\sqrt{6}}{\sqrt{2}} = 1.732 \quad B = z = [113]$$

(k)

$$\frac{A}{C} = \frac{\sqrt{14}}{\sqrt{4}} = 1.871 \quad B = z = [013]$$

(l)

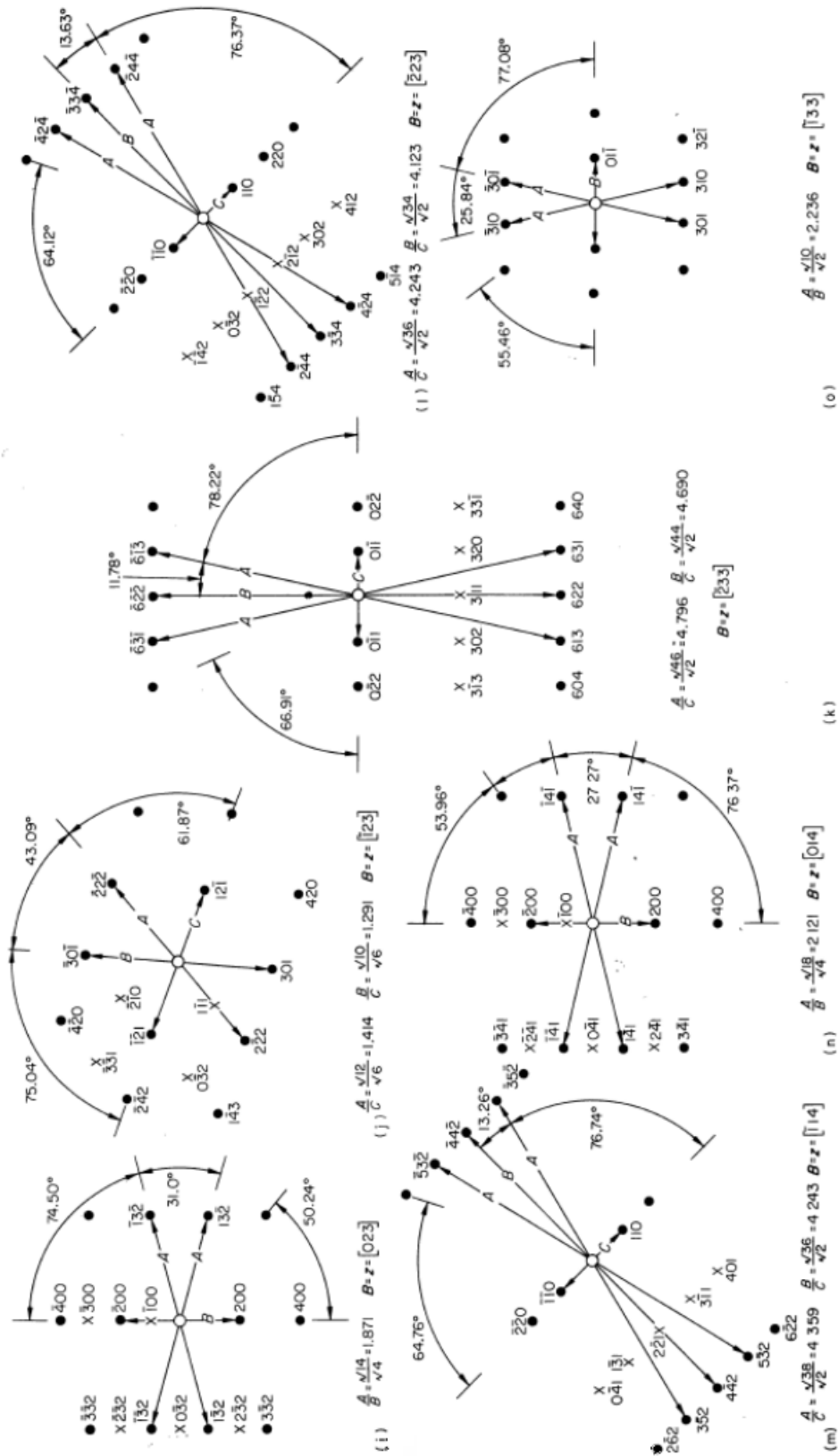
$$\frac{A}{C} = \frac{\sqrt{20}}{\sqrt{2}} = 3.162 \quad B = z = [222]$$

(m)

$$\frac{A}{C} = \frac{\sqrt{14}}{\sqrt{2}} = 2.646 \quad B = z = [112]$$

(n)

BCC STANDARD DIFFRACTION PATTERNS



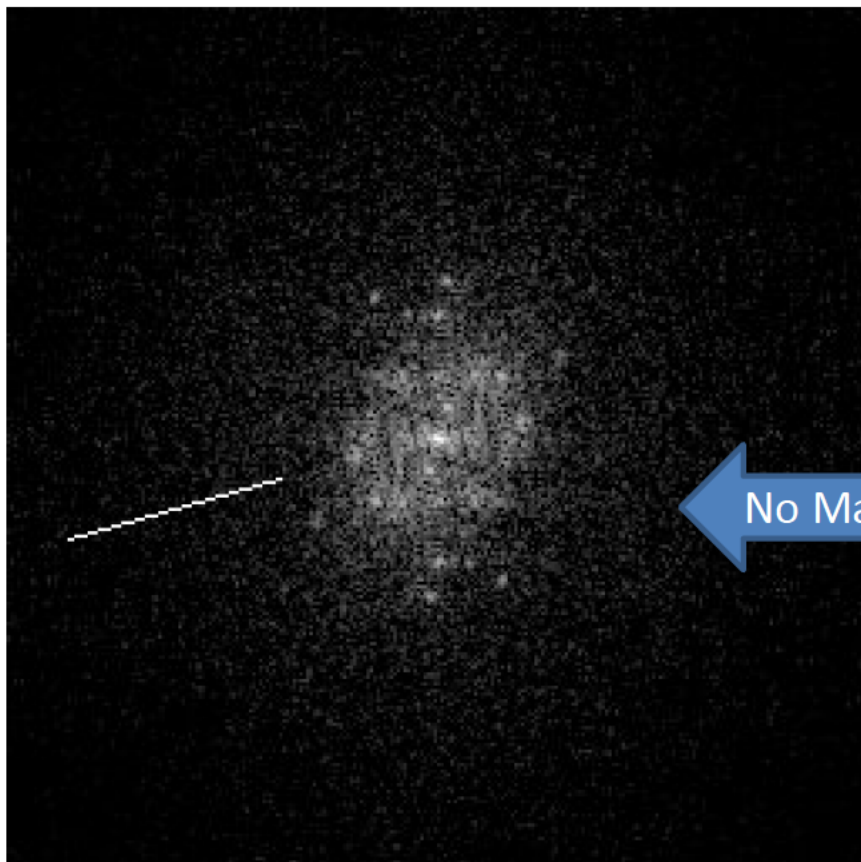
BCC STANDARD DIFFRACTION PATTERNS

EXHIBIT F

FFT Diffraction Patterns in Dr. Clark's Appendix C

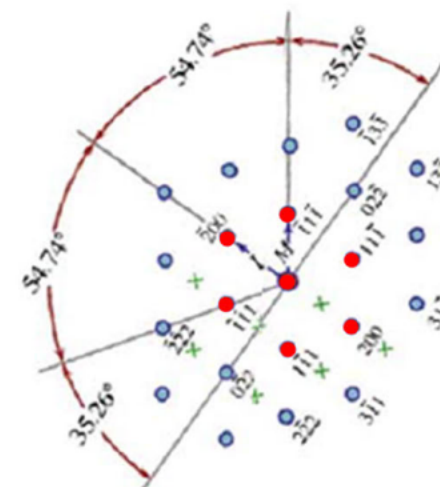
Sample	Position	Filename	No. of Points	No. of FFT's per point	Total No. of FFT's per file	Total No. of FFT's per Layer
S0GPPC	Upper	Middle1	4	3	12	42
		Middle2	3	3	9	
		Middle3	3	3	9	
		Middle4	3	3	9	
		Middle5	1	3	3	
	Lower	Frameright1	7	2	14	54
		Frameright2	7	2	14	
		Frameright3	5	2	10	
		Frameright4	5	2	10	
		Frameright5	3	2	6	
S2MMMC	Upper	18.10.05 CCD Acquire	1	3	3	3
	Lower	18.08.14 CCD Acquire	4	3	12	12
SBRD8K	Lower	18.21.37 CCD Acquire	4	3	12	12

Sample S0GPPC - Framerright1T FFT

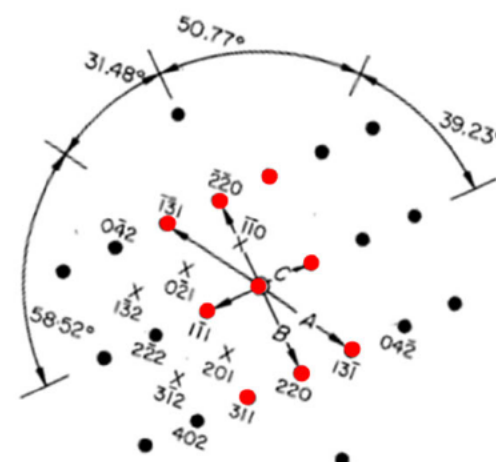


Framerright1T

No Match

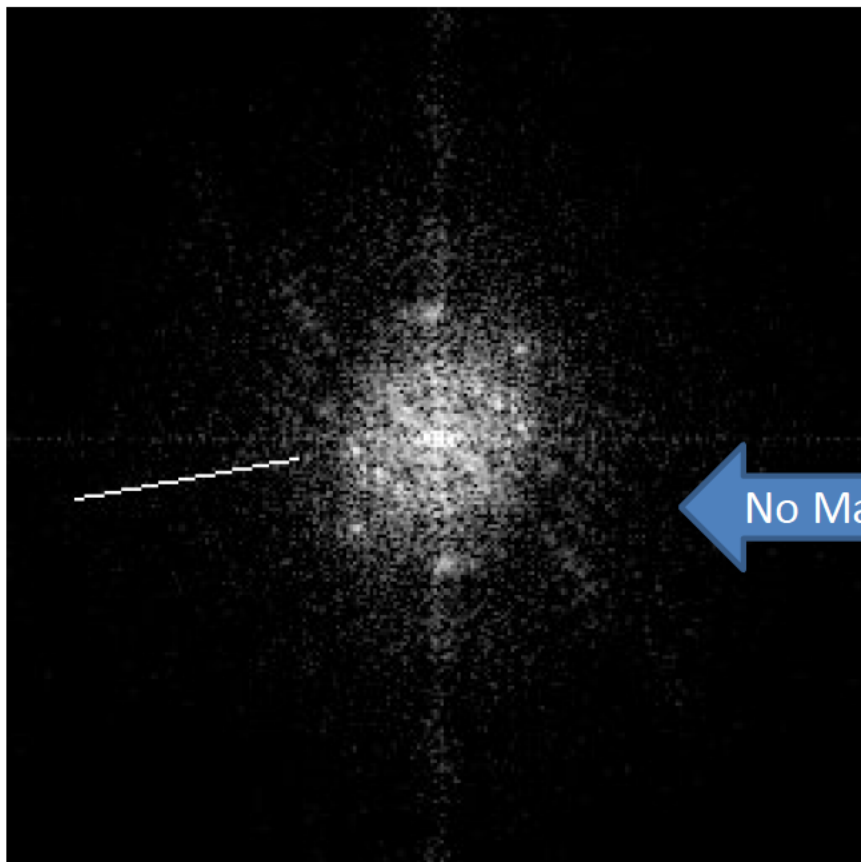


Standard Diffraction Pattern for {110}Fcc



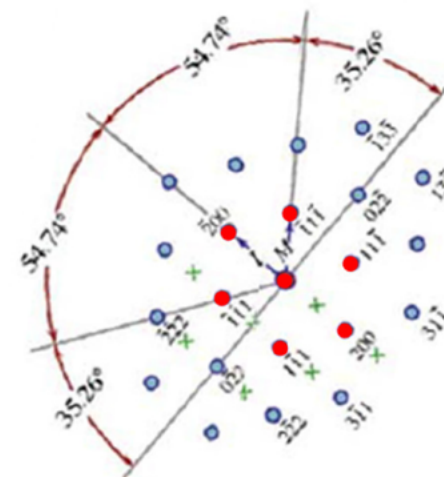
Standard Diffraction Pattern for {112}Fcc

Sample S0GPPC - Framerright2T FFT

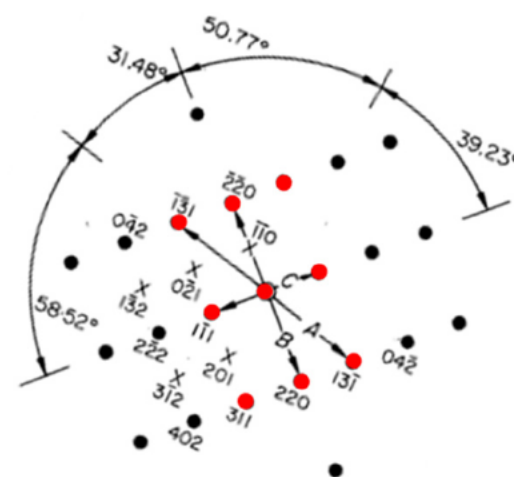


Framerright2T

No Match

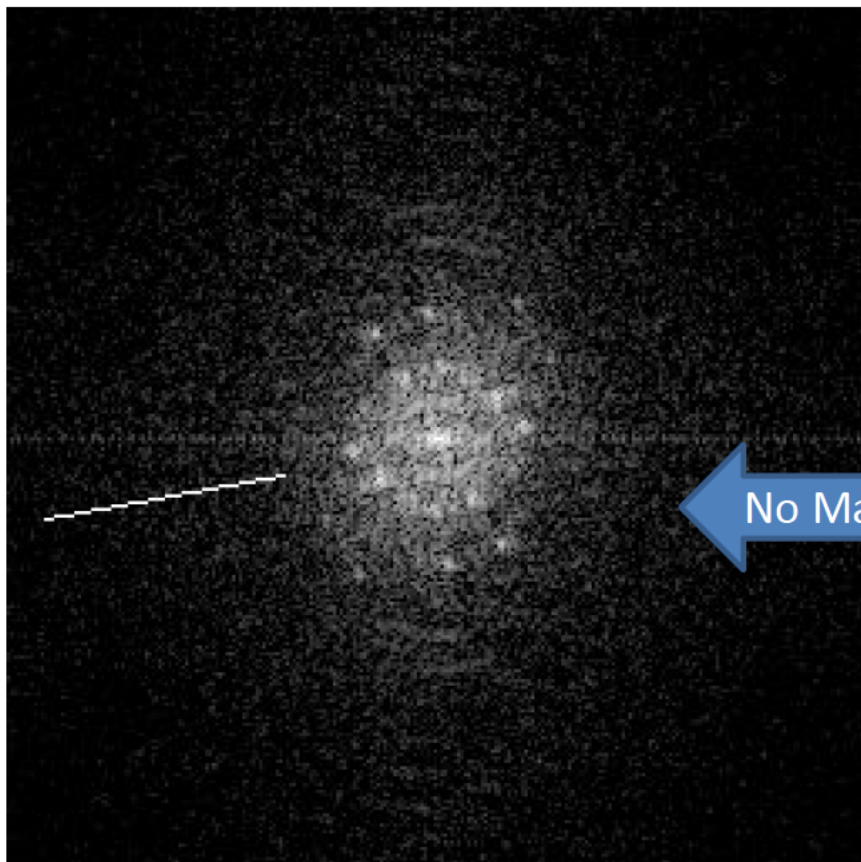


Standard Diffraction Pattern for {110}Fcc



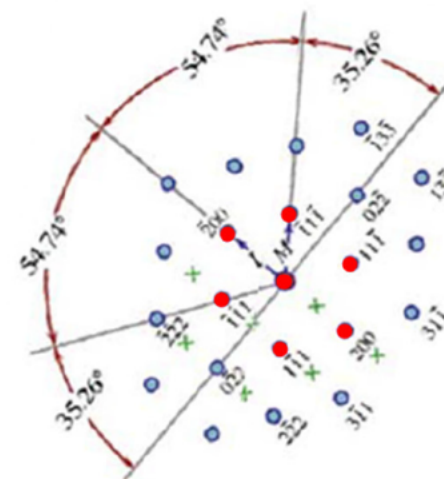
Standard Diffraction Pattern for {112}Fcc

Sample S0GPPC - Framerright3T FFT

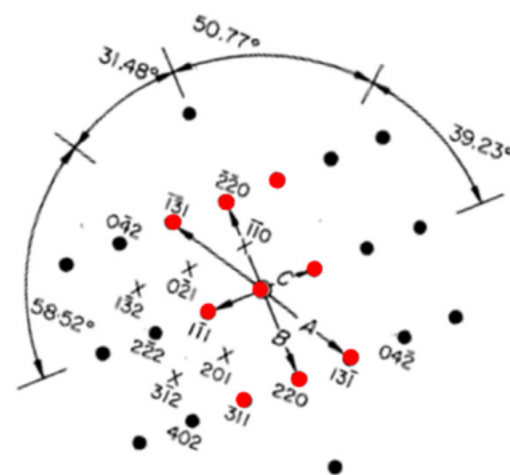


Framerright3T

No Match

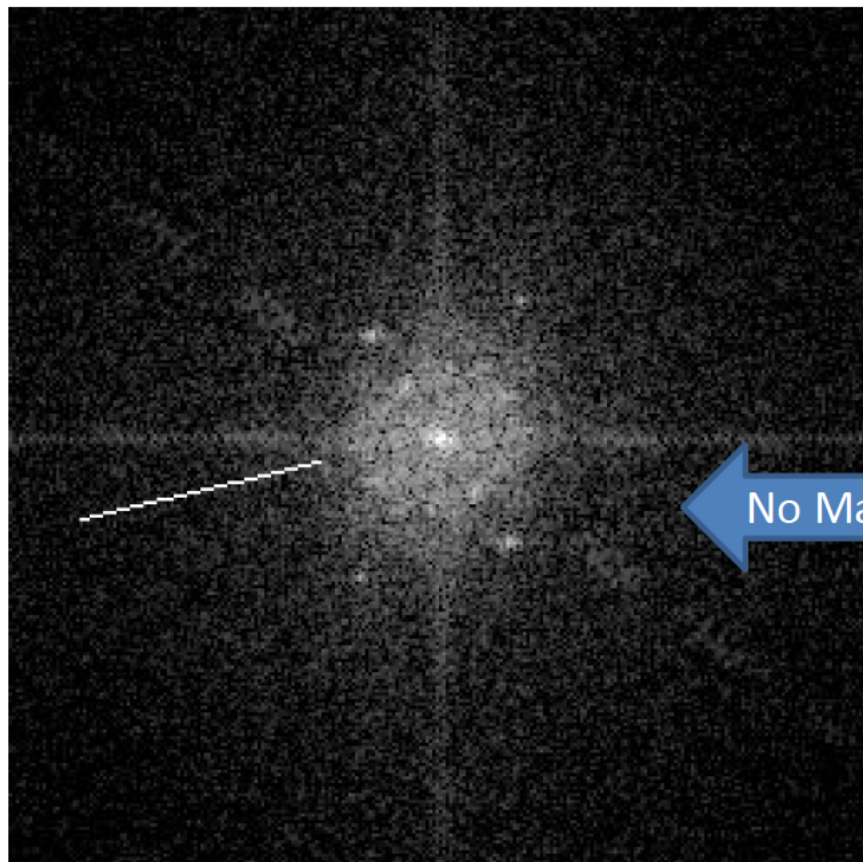


Standard Diffraction Pattern for {110}Fcc



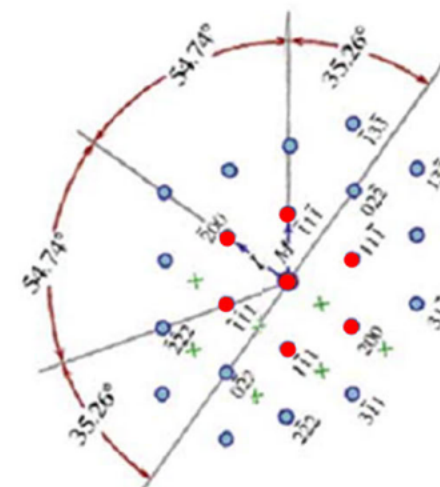
Standard Diffraction Pattern for {112}Fcc

Sample S0GPPC - Framerright4T FFT

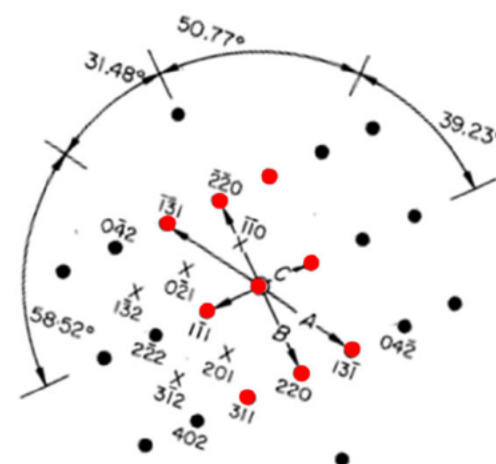


Frameright4T

No Match

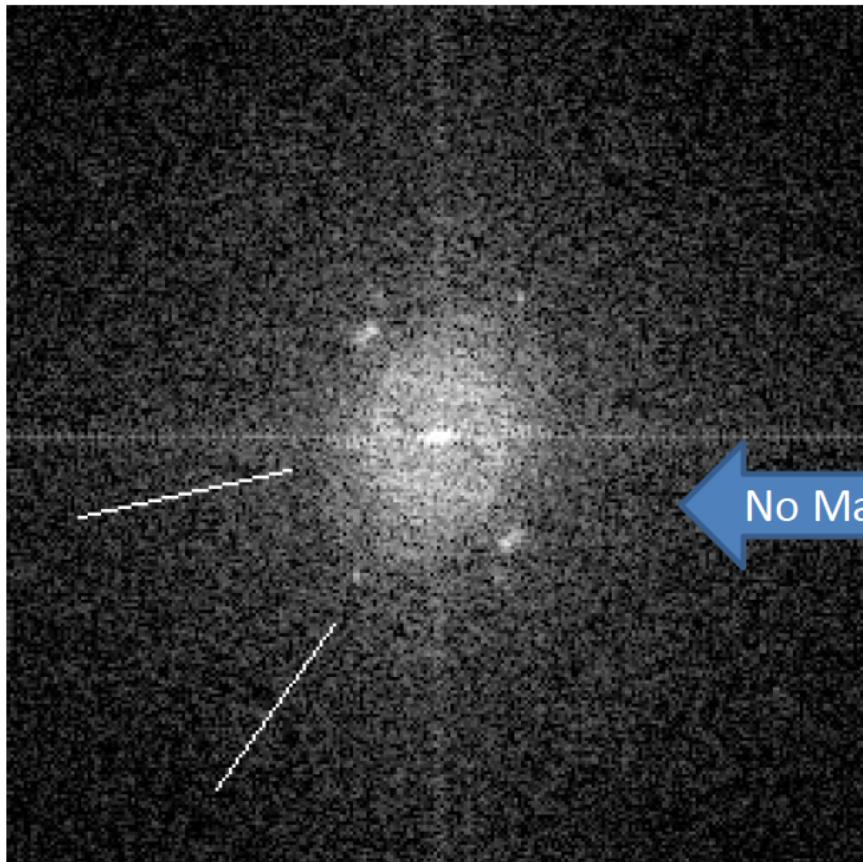


Standard Diffraction Pattern for {110}Fcc



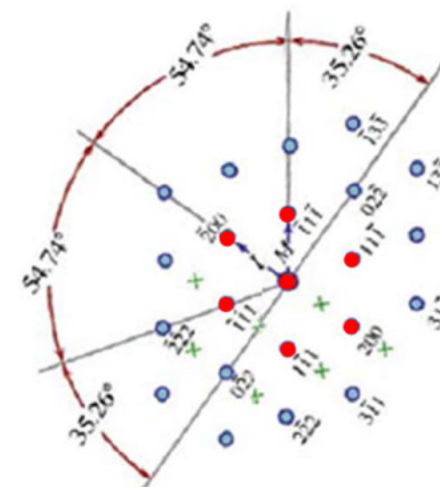
Standard Diffraction Pattern for {112}Fcc

Sample S0GPPC - Framerright5T FFT

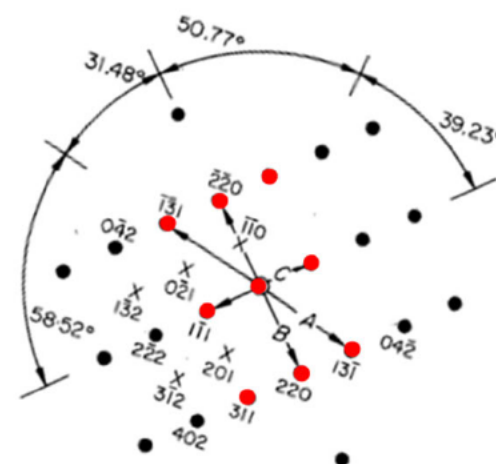


Frameright5T

No Match

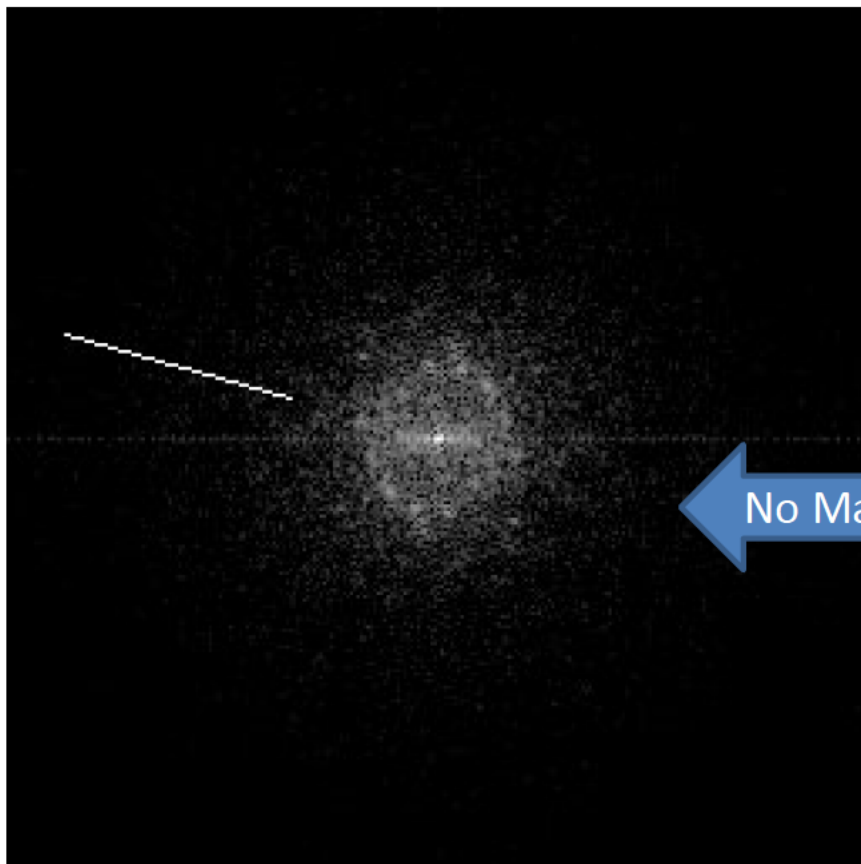


Standard Diffraction Pattern for {110}Fcc



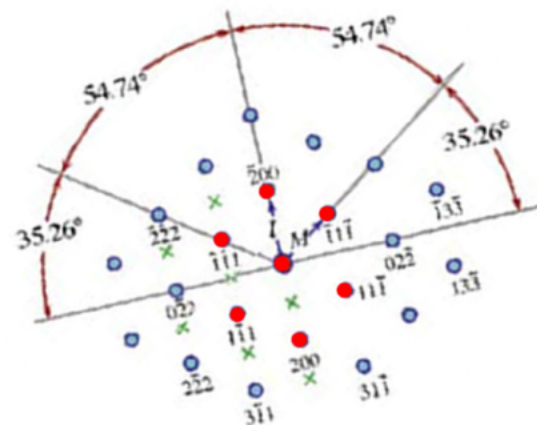
Standard Diffraction Pattern for {112}Fcc

Sample S0GPPC - Framerright6T FFT

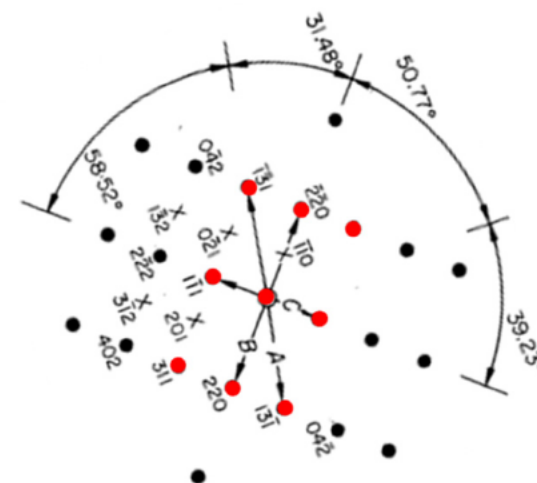


Framerright6T

No Match

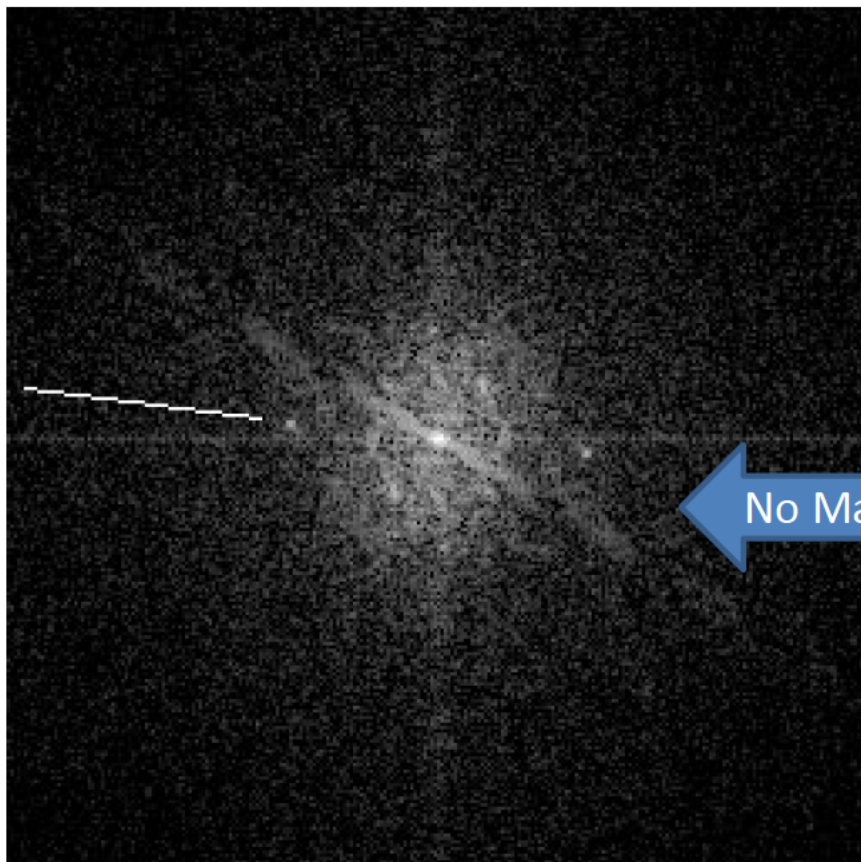


Standard Diffraction Pattern for {110}Fcc



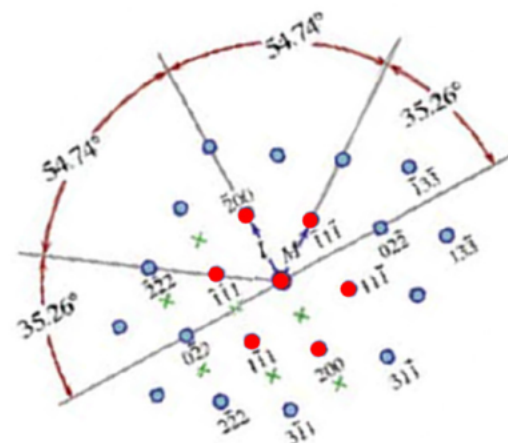
Standard Diffraction Pattern for {112}Fcc

Sample S0GPPC - Framerright7T FFT

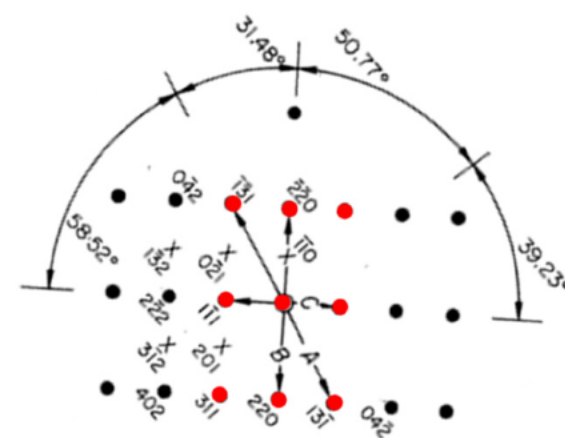


Framerright7T

No Match

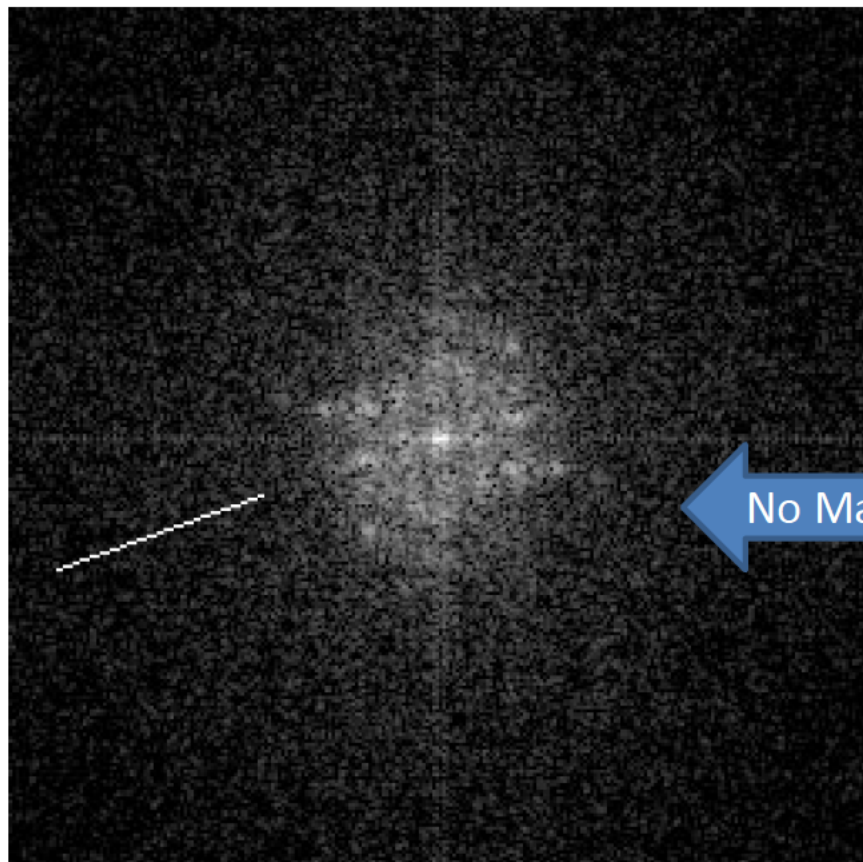


Standard Diffraction Pattern for {110}Fcc



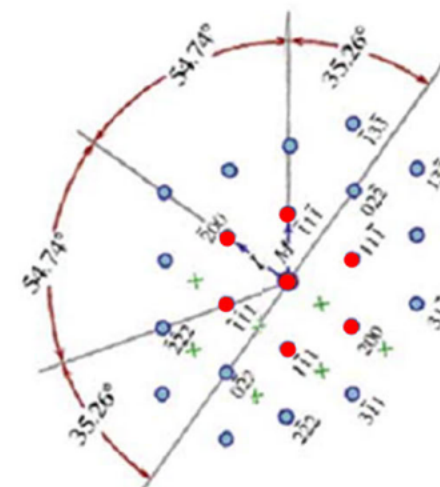
Standard Diffraction Pattern for {112}Fcc

Sample S0GPPC - Framerright21T FFT

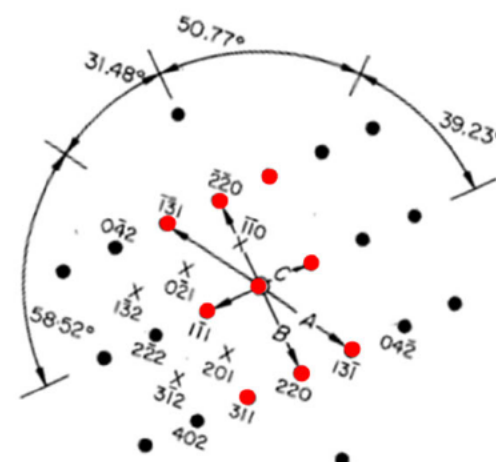


Framerright21T

No Match

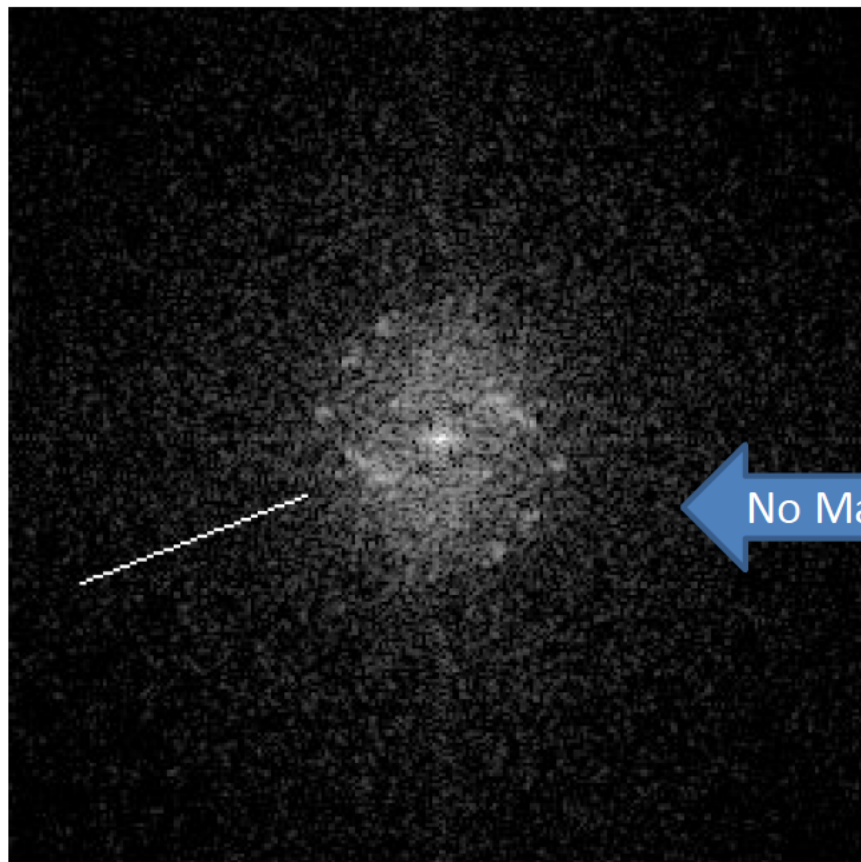


Standard Diffraction Pattern for {110}Fcc



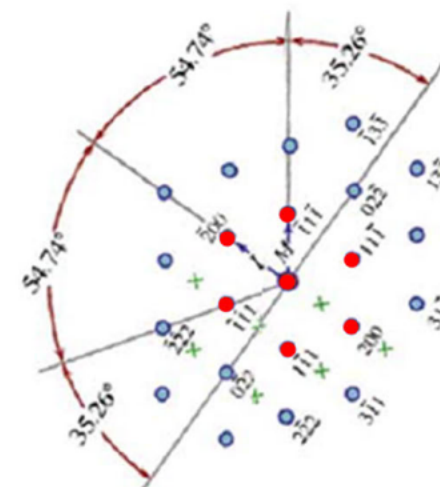
Standard Diffraction Pattern for {112}Fcc

Sample S0GPPC - Framerright22T FFT

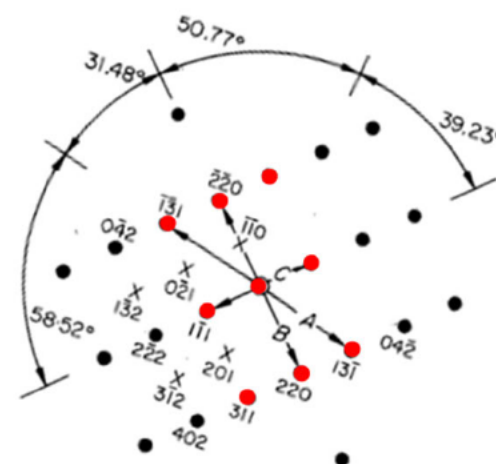


Framerright22T

No Match

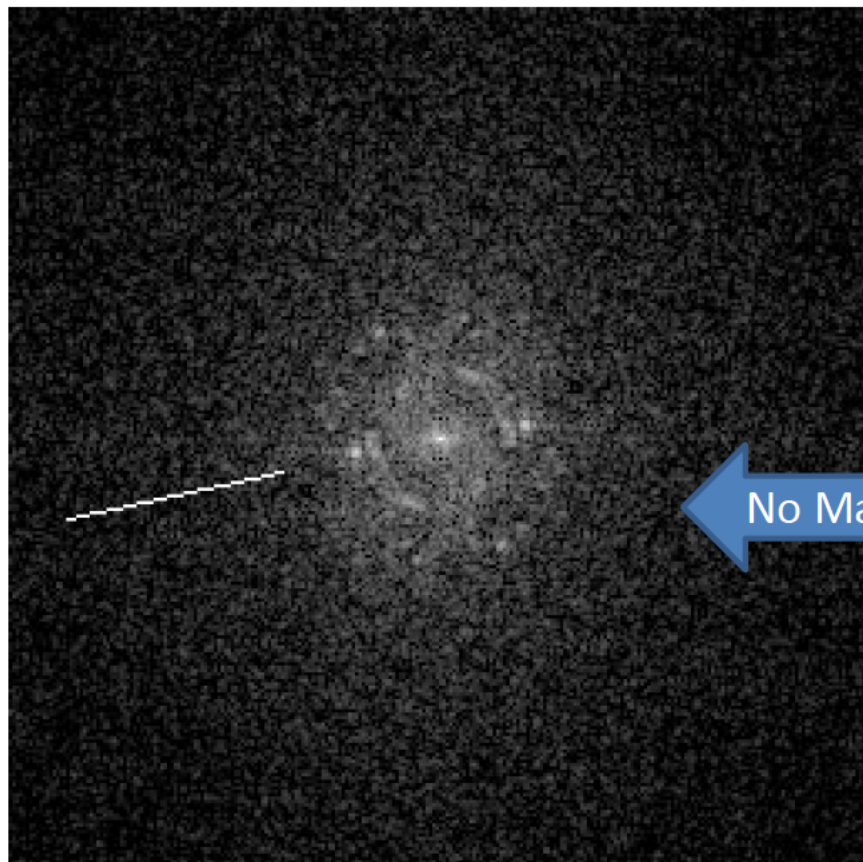


Standard Diffraction Pattern for {110}Fcc



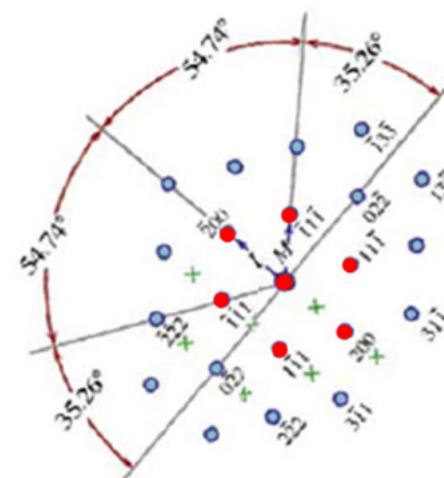
Standard Diffraction Pattern for {112}Fcc

Sample S0GPPC - Framerright23T FFT

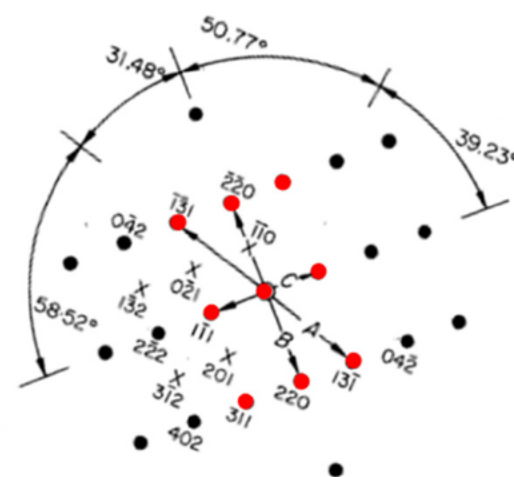


Framerright23T

No Match



Standard Diffraction Pattern for {110}Fcc



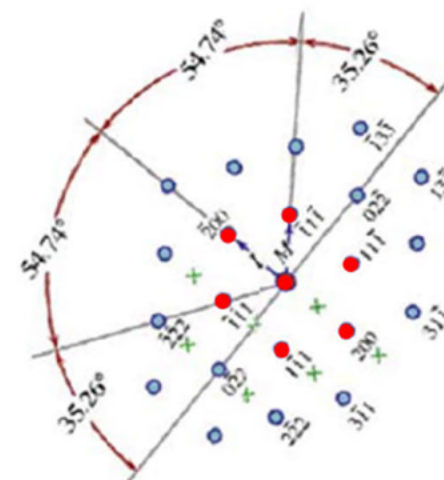
Standard Diffraction Pattern for {112}Fcc

Sample S0GPPC - Framerright24T FFT

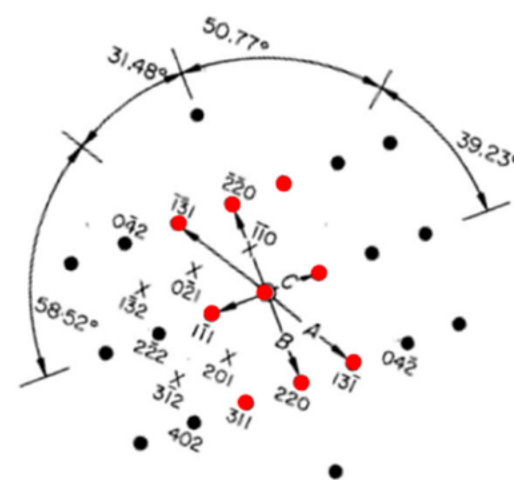


Framerright24T

No Match

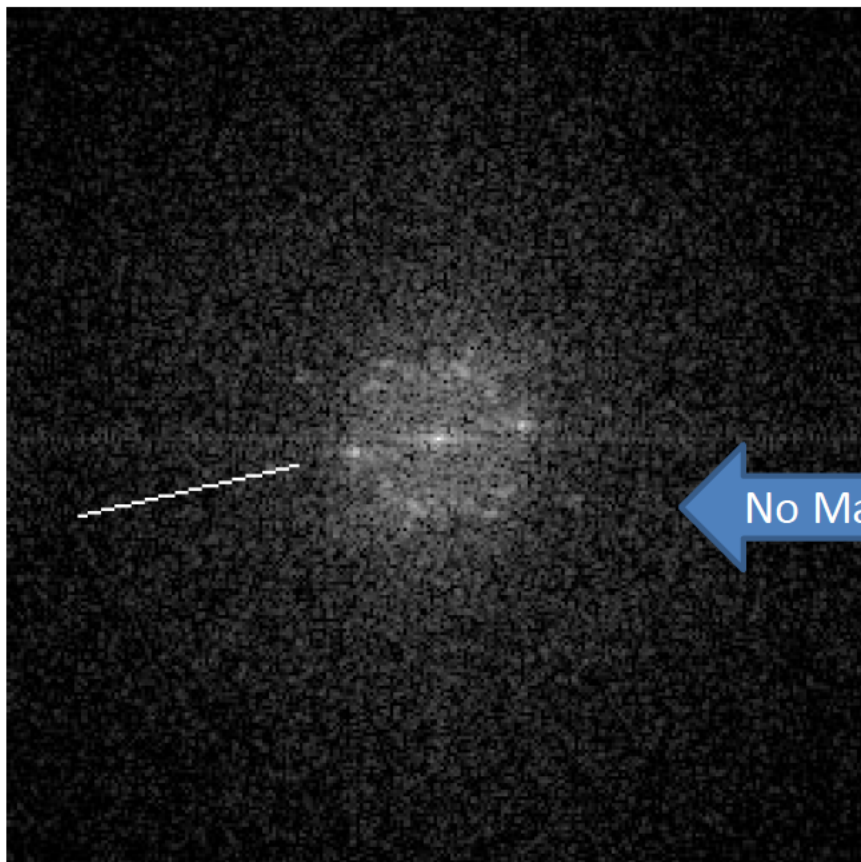


Standard Diffraction Pattern for {110}Fcc



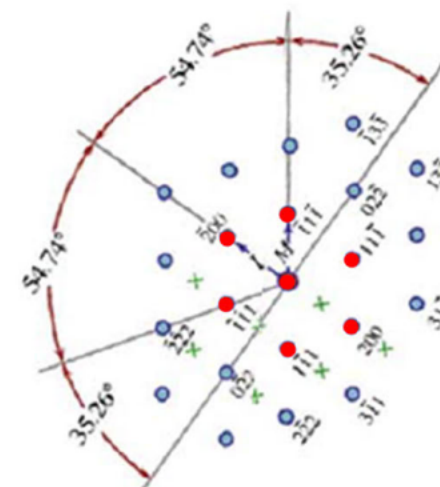
Standard Diffraction Pattern for {112}Fcc

Sample S0GPPC - Framerright25T FFT

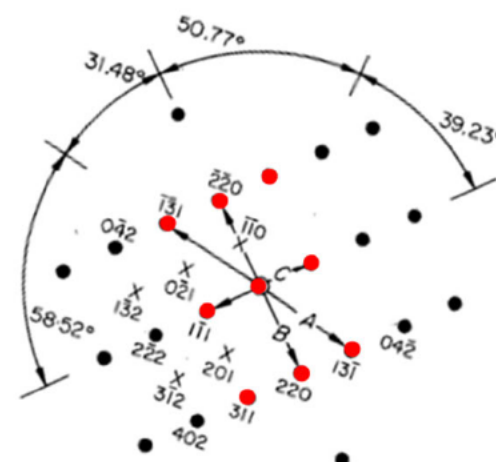


Framerright25T

No Match

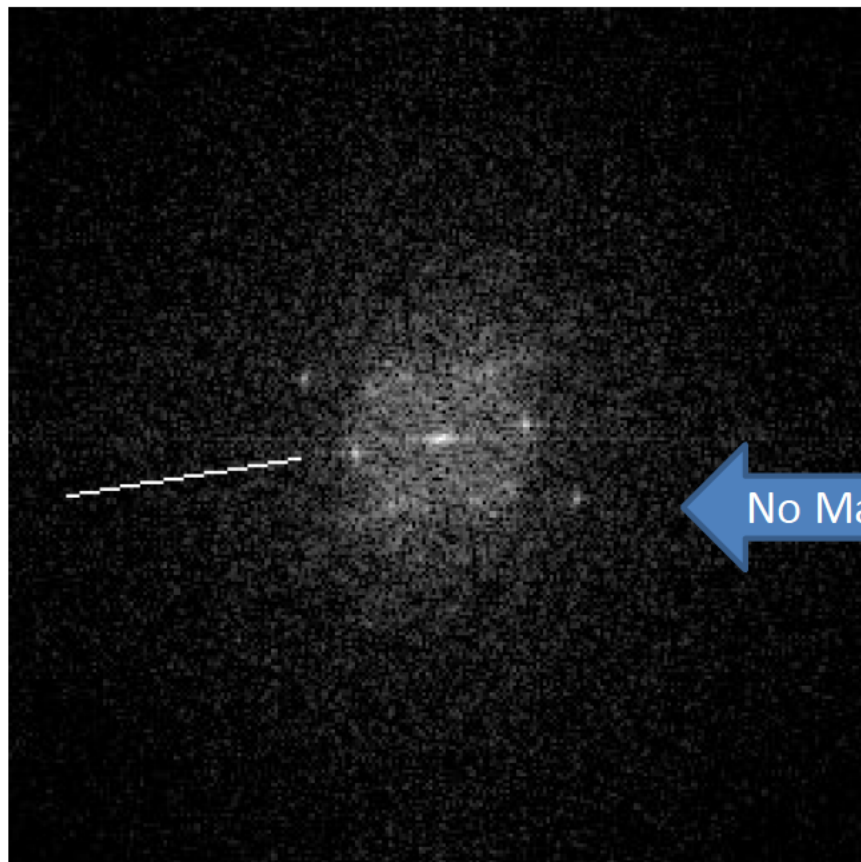


Standard Diffraction Pattern for $\{110\}$ Fcc



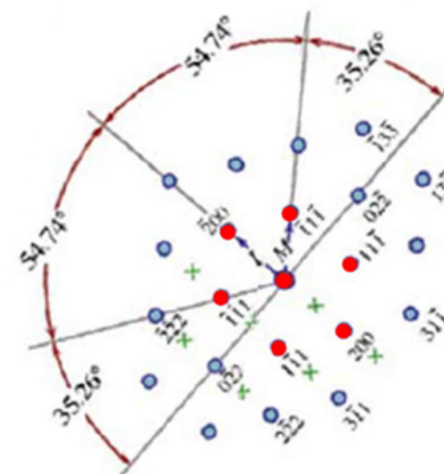
Standard Diffraction Pattern for $\{112\}$ Fcc

Sample S0GPPC - Frameright26T FFT

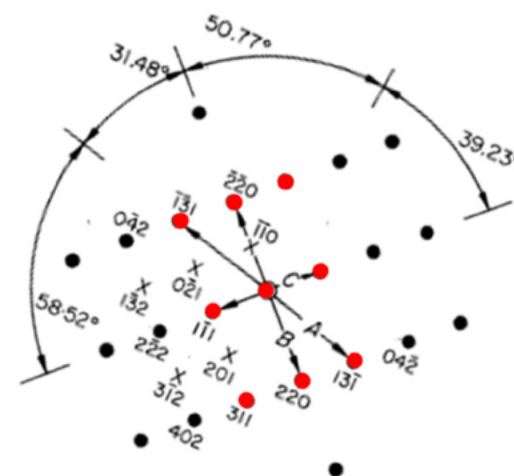


Frameright26T

No Match

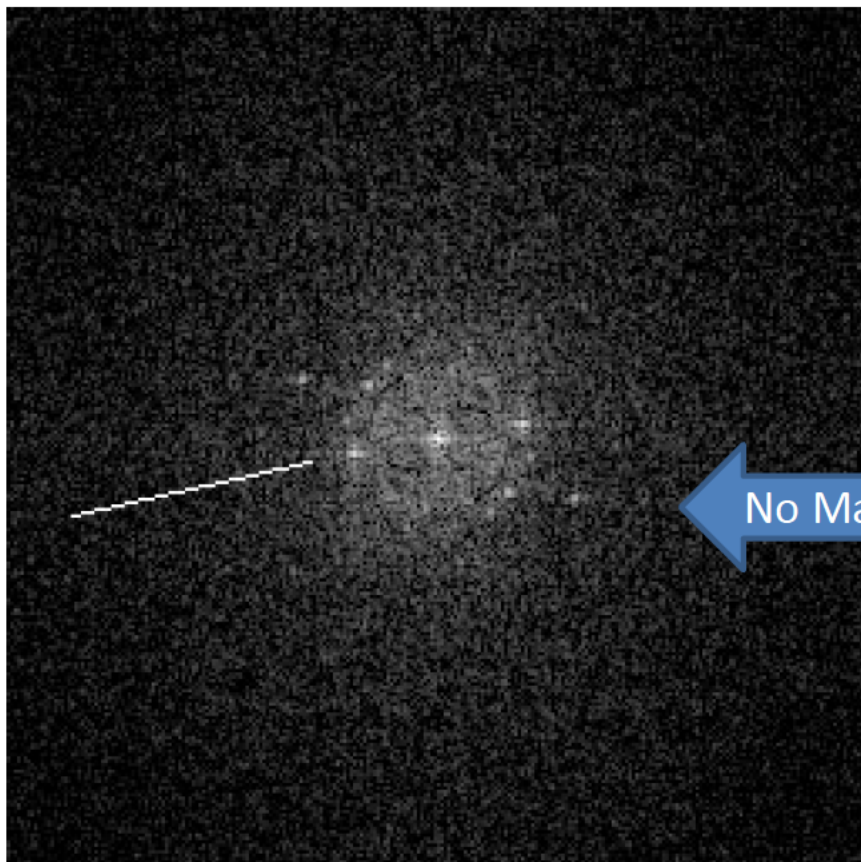


Standard Diffraction Pattern for {110}Fcc



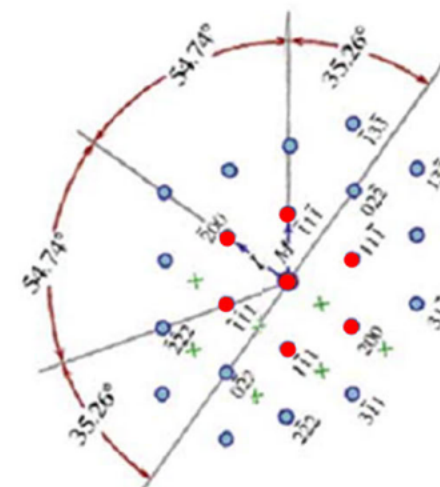
Standard Diffraction Pattern for {112}Fcc

Sample S0GPPC - Framerright27T FFT

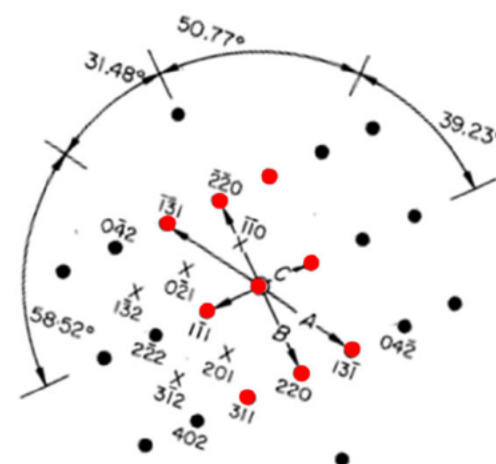


Framerright27T

No Match



Standard Diffraction Pattern for {110}Fcc



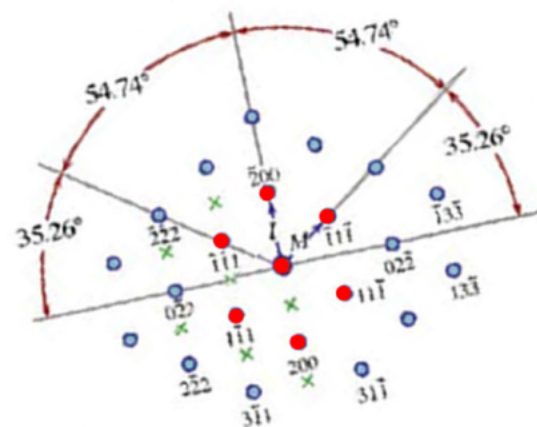
Standard Diffraction Pattern for {112}Fcc

Sample S0GPPC - Framerright31T FFT

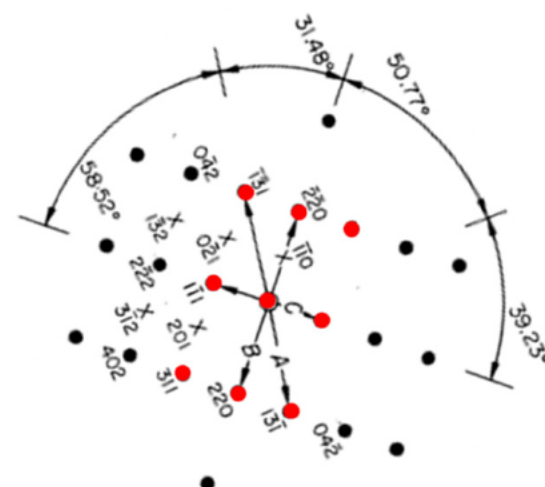


Framerright31T

No Match

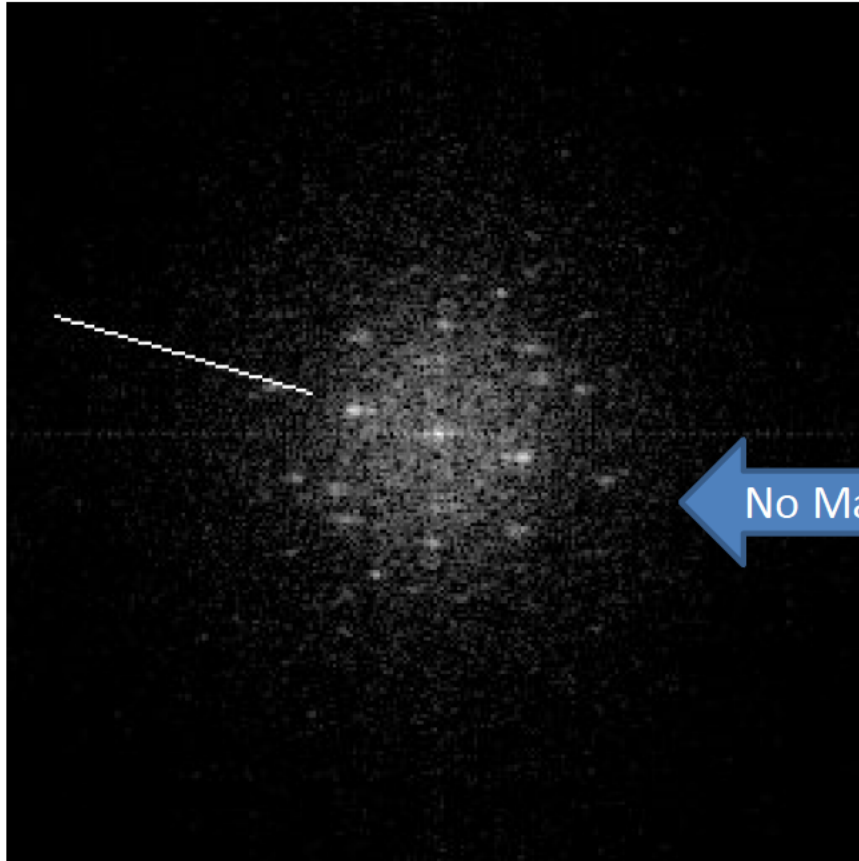


Standard Diffraction Pattern for {110}Fcc



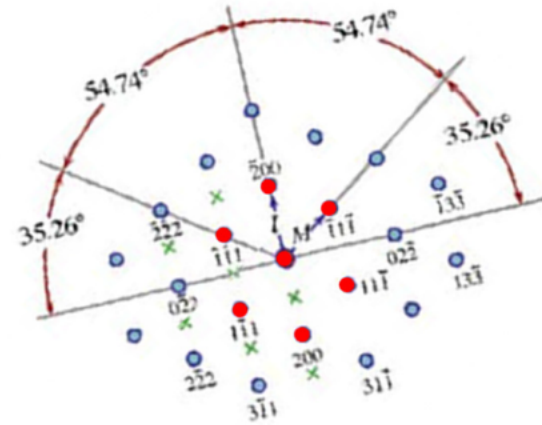
Standard Diffraction Pattern for {112}Fcc

Sample S0GPPC - Frameright32T FFT

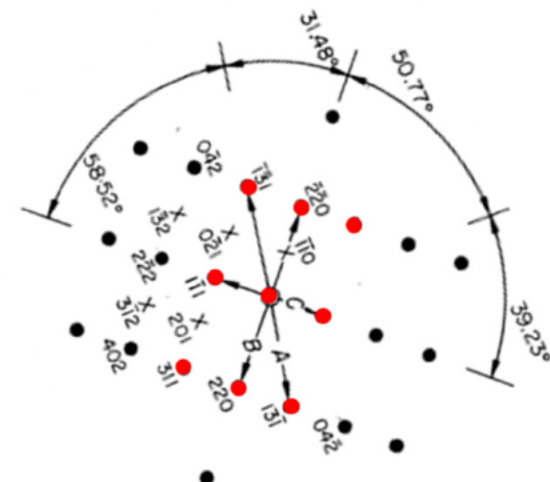


Frameright32T

No Match



Standard Diffraction Pattern for {110}Fcc



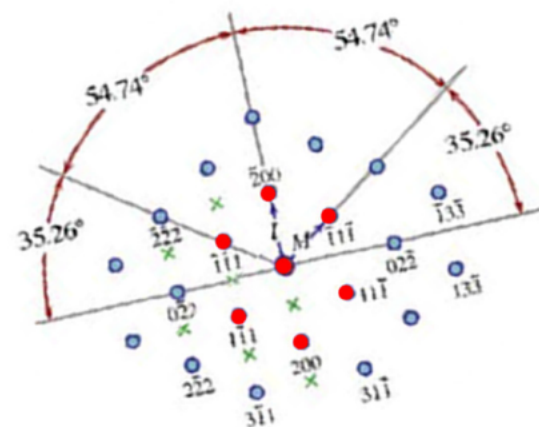
Standard Diffraction Pattern for {112}Fcc

Sample S0GPPC - Framerright33T FFT

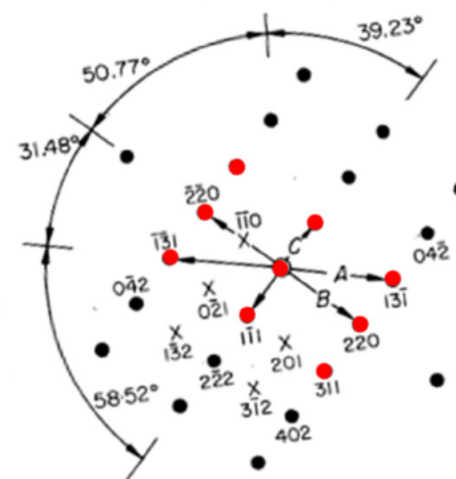


Framerright33T

No Match

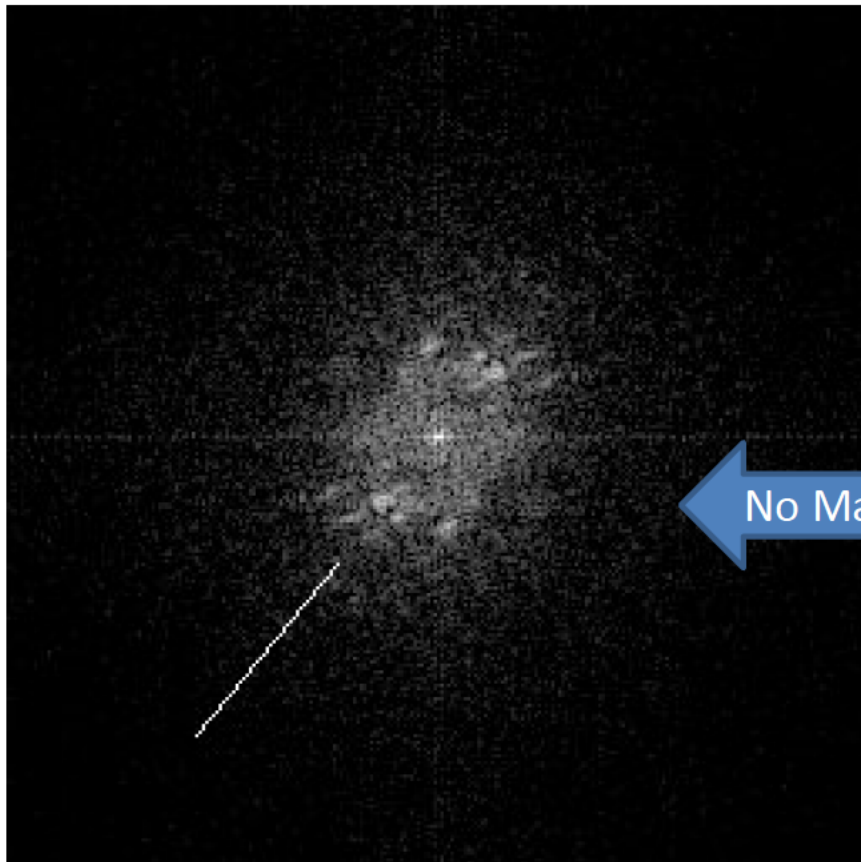


Standard Diffraction Pattern for {110}Fcc



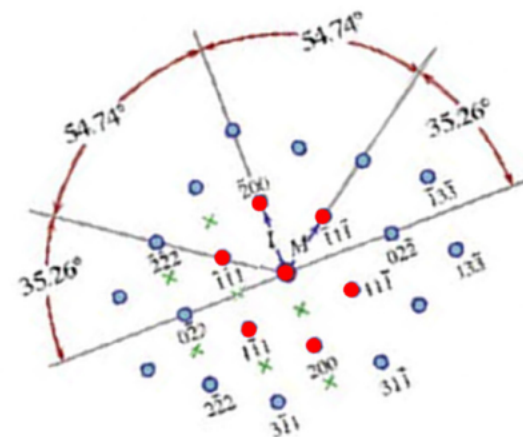
Standard Diffraction Pattern for {112}Fcc

Sample S0GPPC - Frameright34T FFT

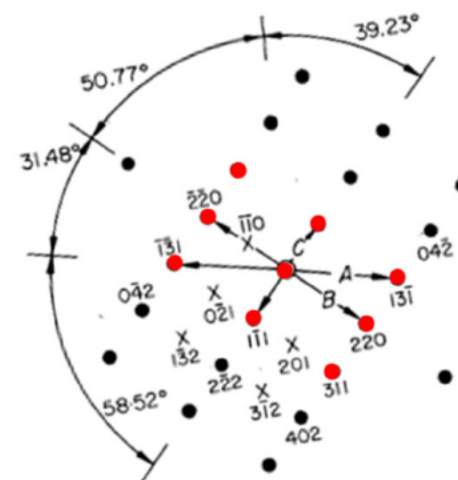


Frameright34T

No Match

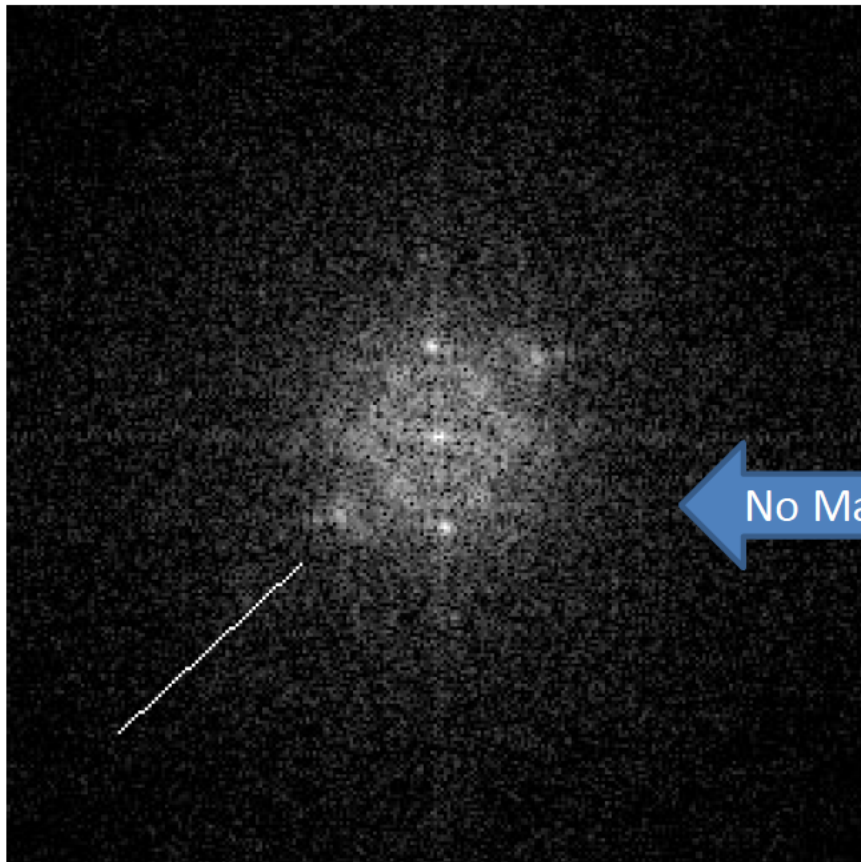


Standard Diffraction Pattern for {110}Fcc



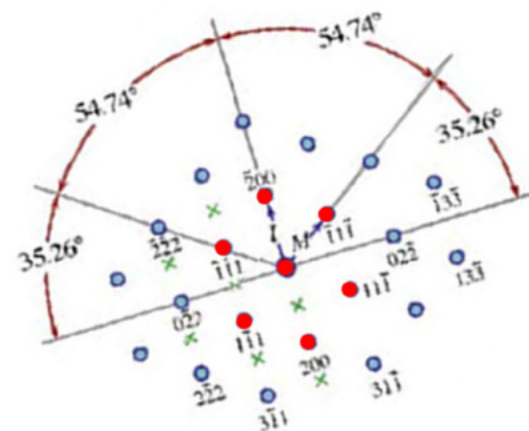
Standard Diffraction Pattern for {112}Fcc

Sample S0GPPC - Frameright35T FFT

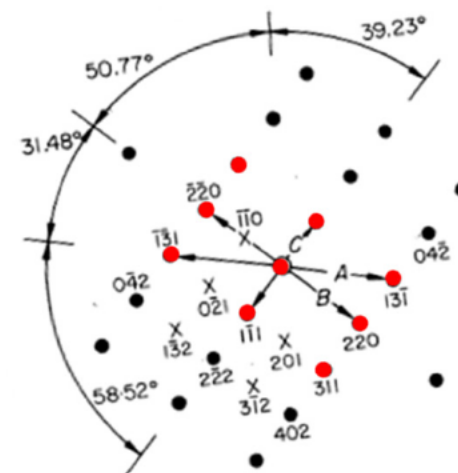


Frameright35T

No Match

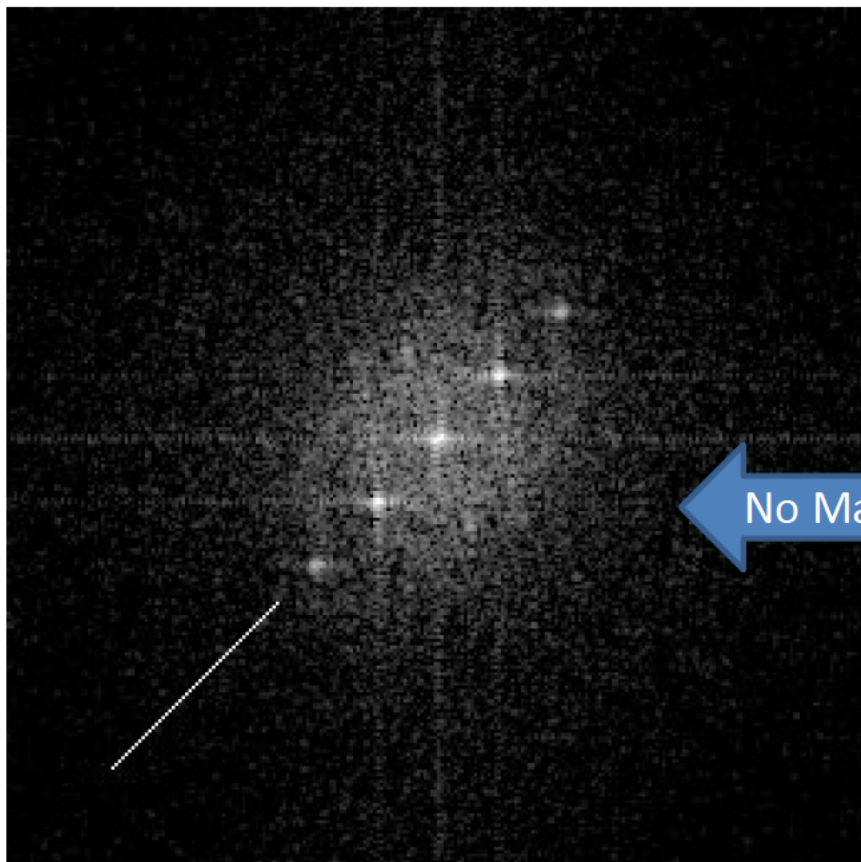


Standard Diffraction Pattern for {110}Fcc



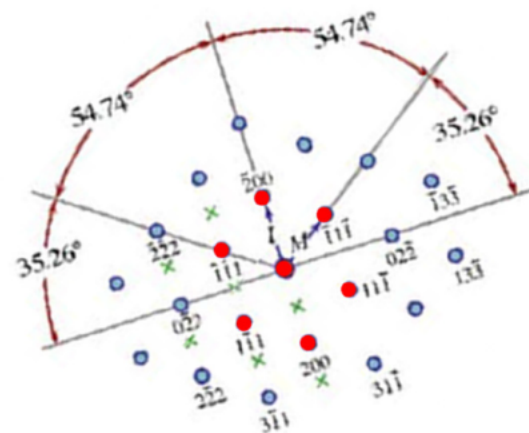
Standard Diffraction Pattern for {112}Fcc

Sample S0GPPC - Framerright41T FFT

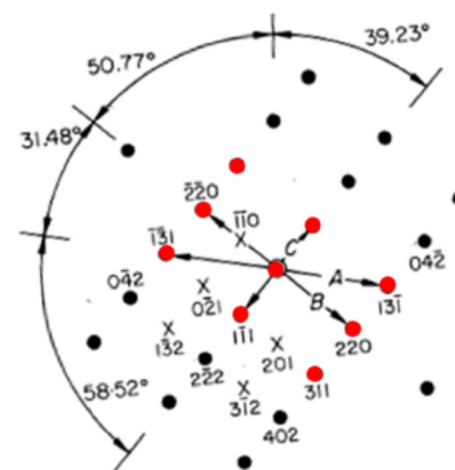


Framerright41T

No Match

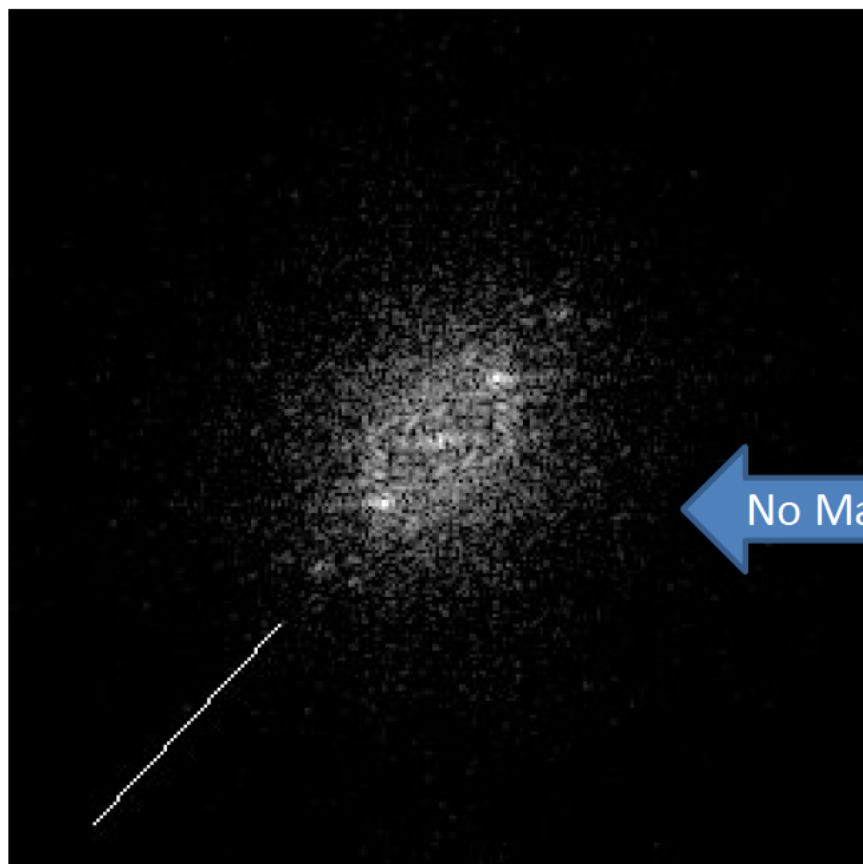


Standard Diffraction Pattern for {110}Fcc



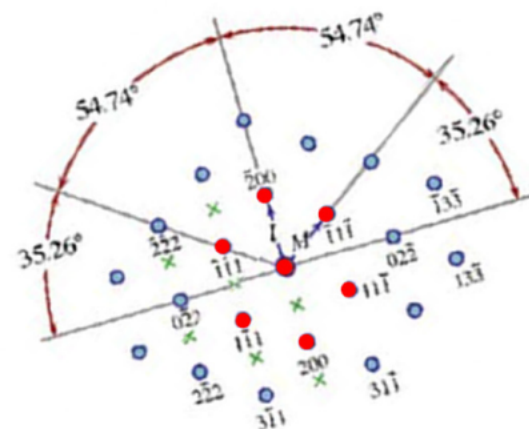
Standard Diffraction Pattern for {112}Fcc

Sample S0GPPC - Framerright42T FFT

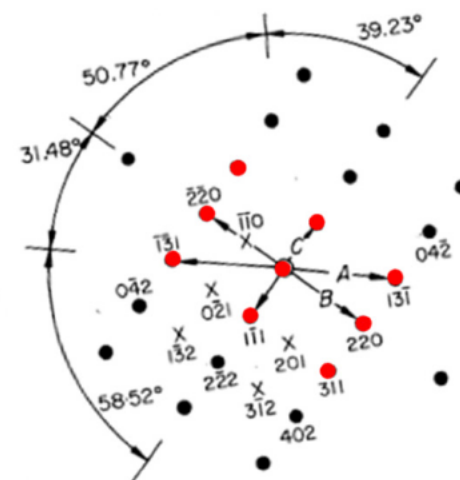


Framerright42T

No Match

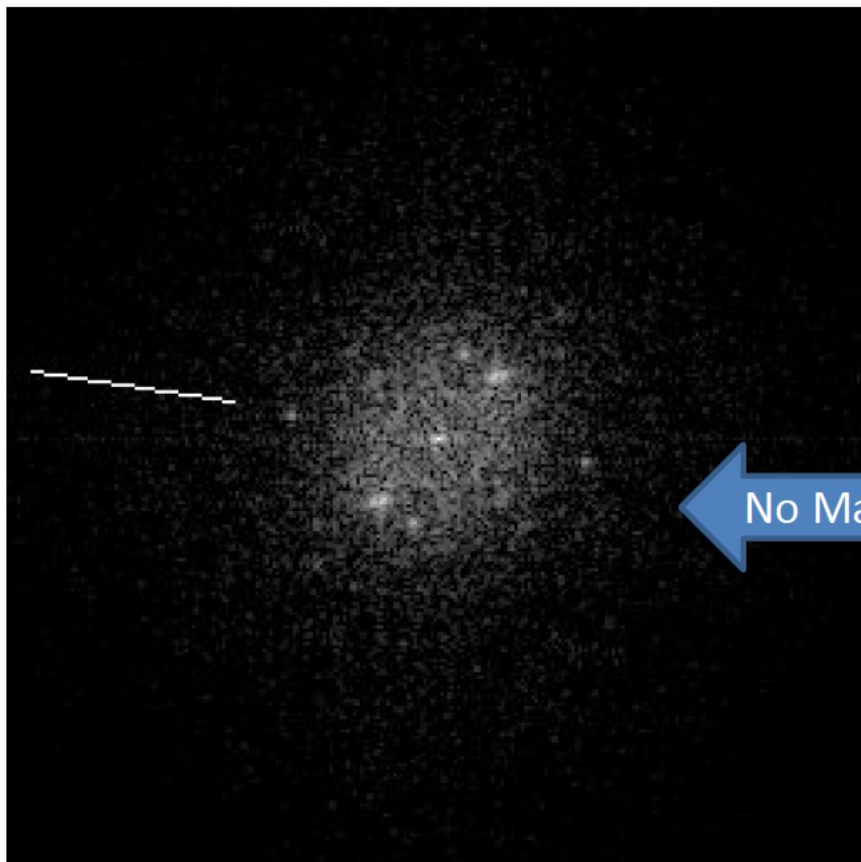


Standard Diffraction Pattern for {110}Fcc



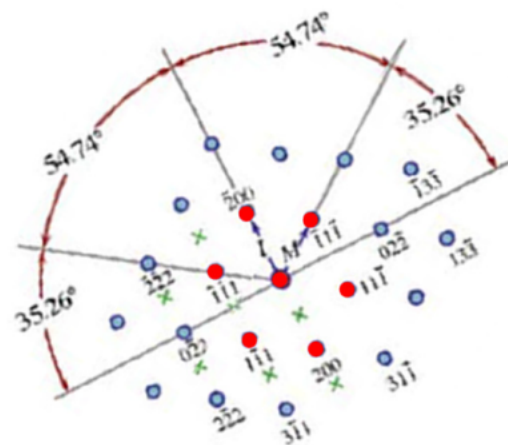
Standard Diffraction Pattern for {112}Fcc

Sample S0GPPC - Framerright43T FFT

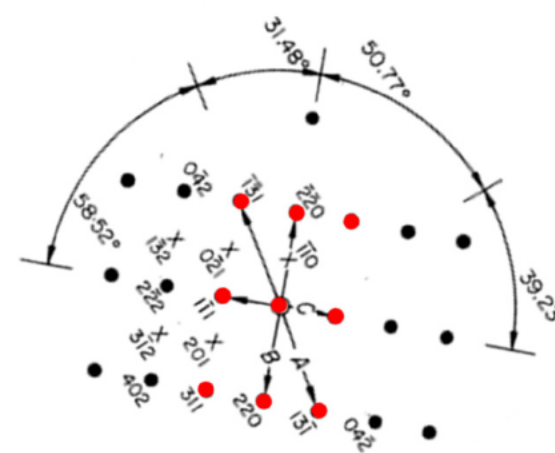


Framerright43T

No Match

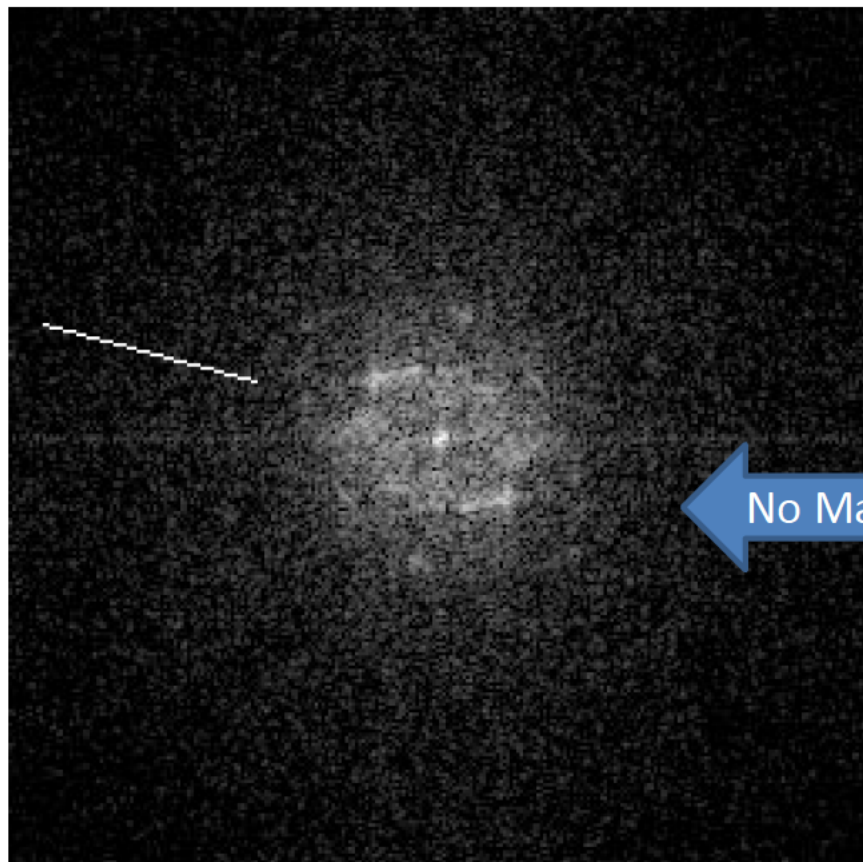


Standard Diffraction Pattern for {110}Fcc



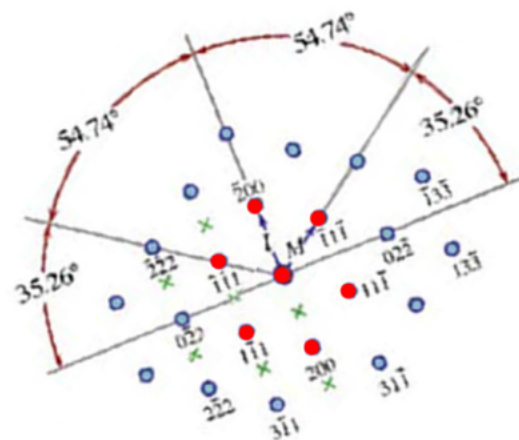
Standard Diffraction Pattern for {112}Fcc

Sample S0GPPC - Frameright44T FFT

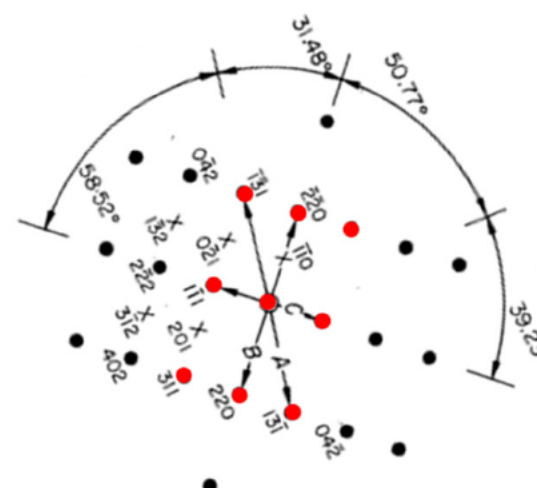


Frameright44T

No Match

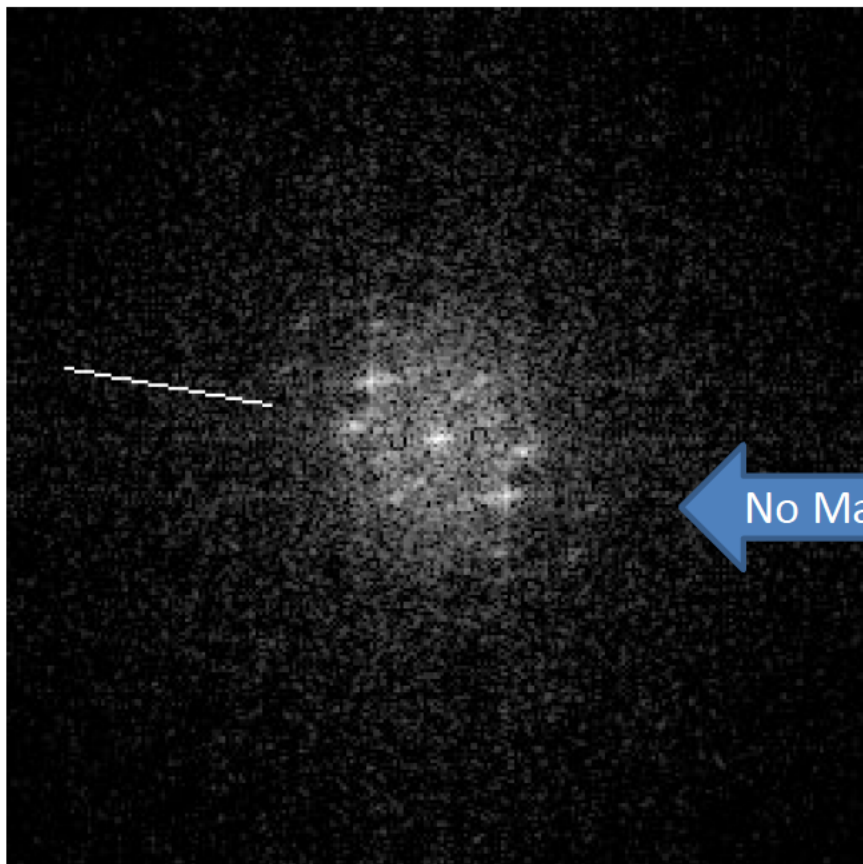


Standard Diffraction Pattern for {110}Fcc



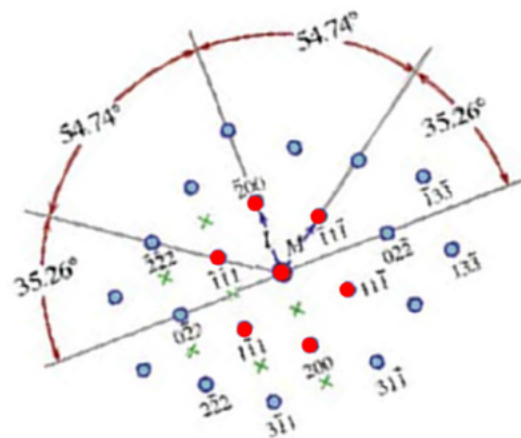
Standard Diffraction Pattern for {112}Fcc

Sample S0GPPC - Frameright45T FFT

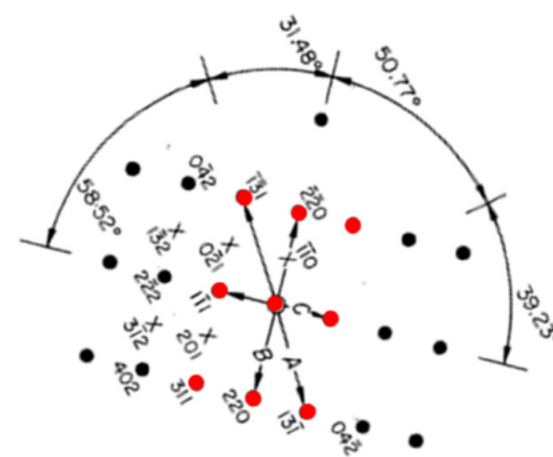


Frameright45T

No Match

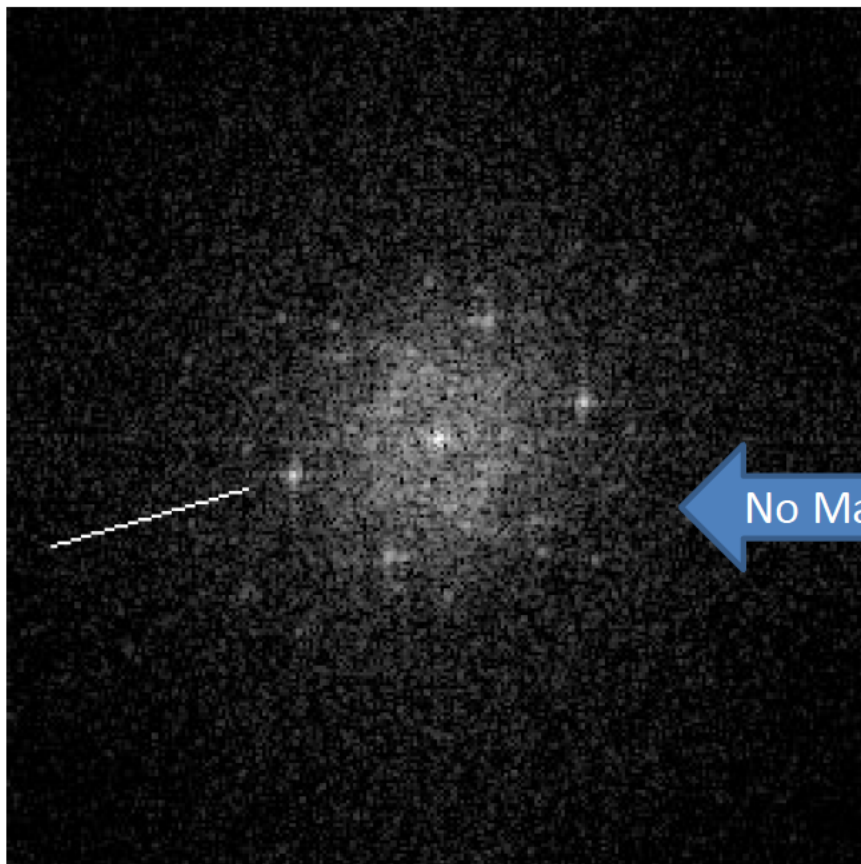


Standard Diffraction Pattern for {110}Fcc



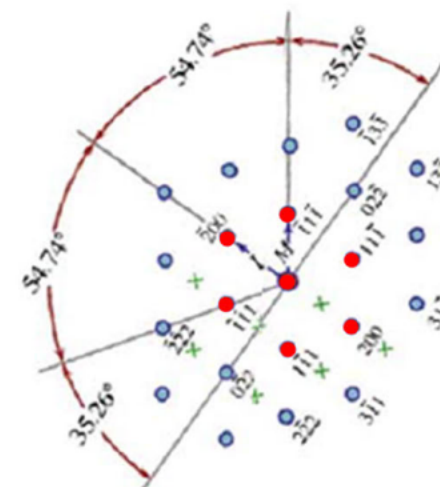
Standard Diffraction Pattern for {112}Fcc

Sample S0GPPC - Framerright51T FFT

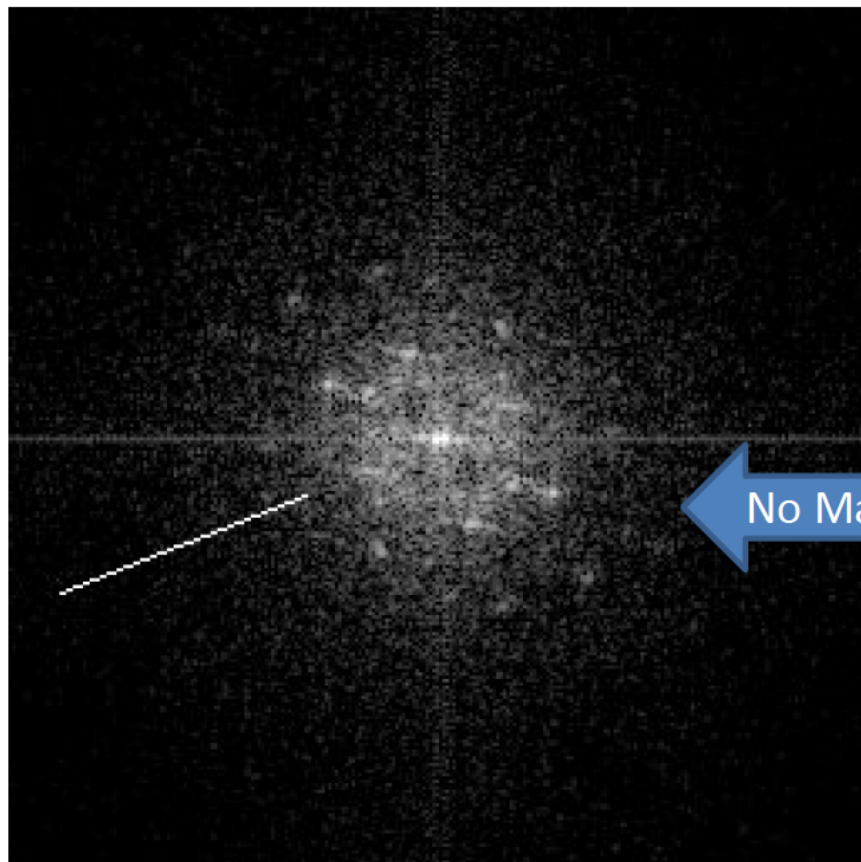


Framerright51T

No Match

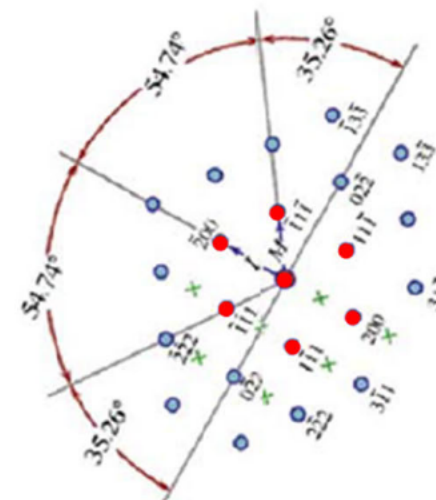


Sample S0GPPC - Framerright52T FFT

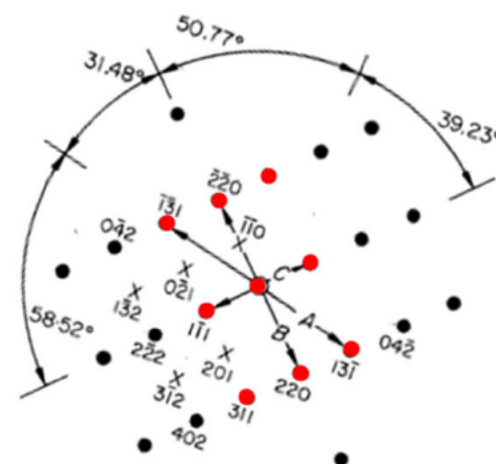


Framerright52T

No Match

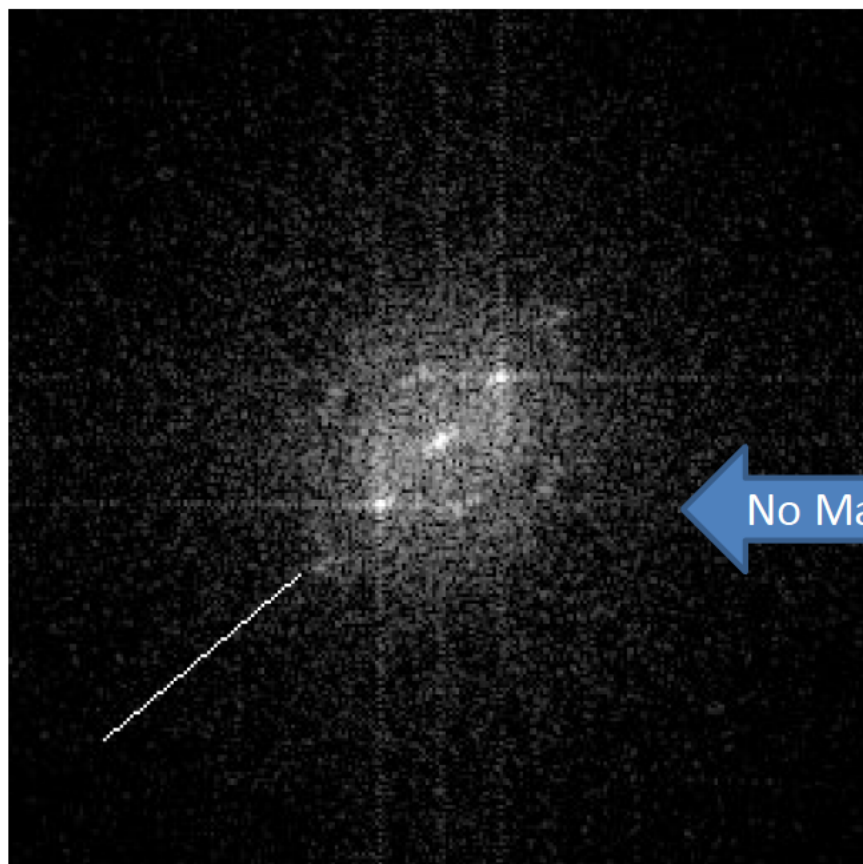


Standard Diffraction Pattern for {110}Fcc



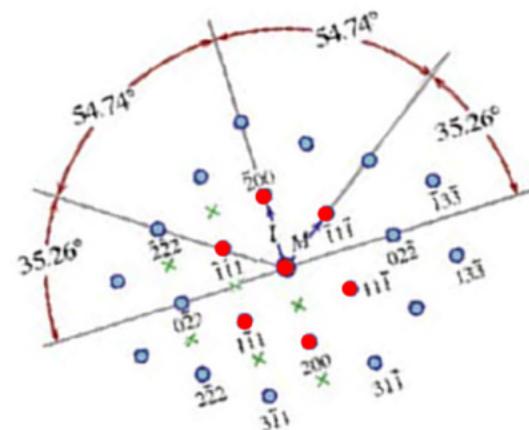
Standard Diffraction Pattern for {112}Fcc

Sample S0GPPC - Framerright53T FFT

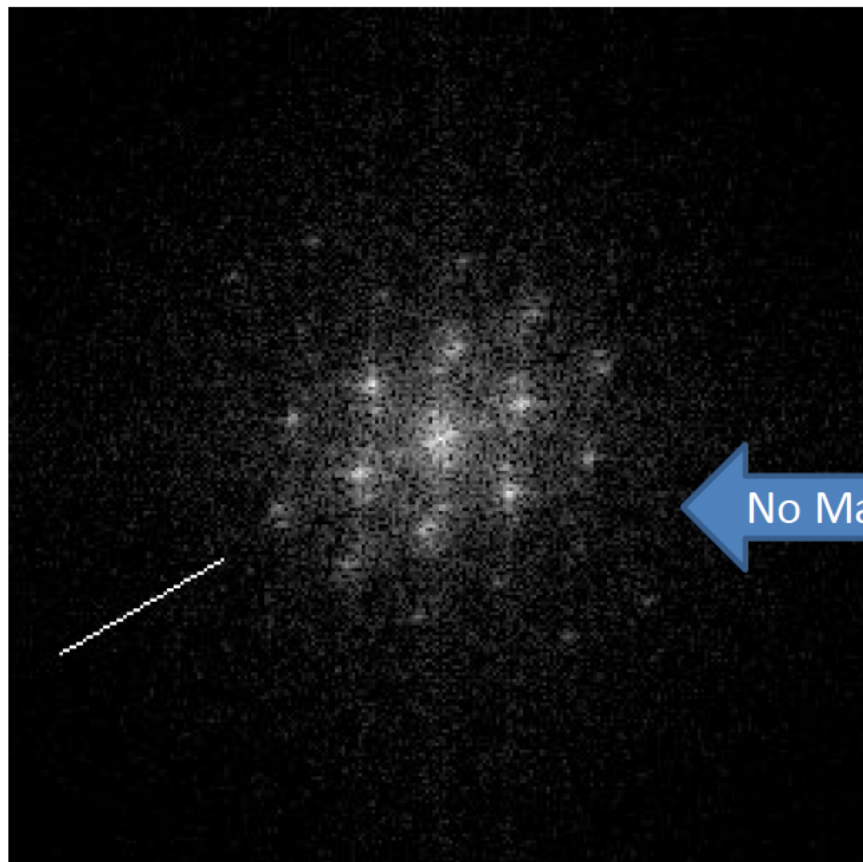


Framerright53T

No Match

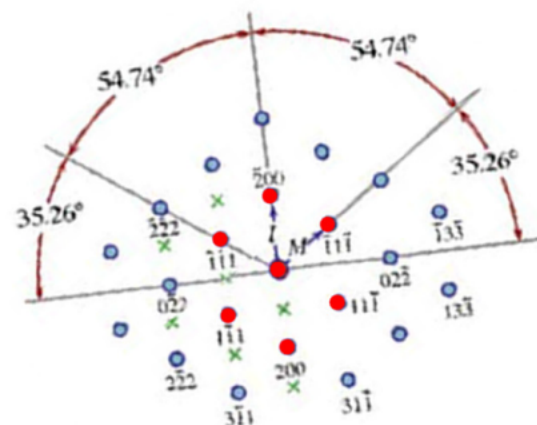


Sample S0GPPC - Middle11T FFT

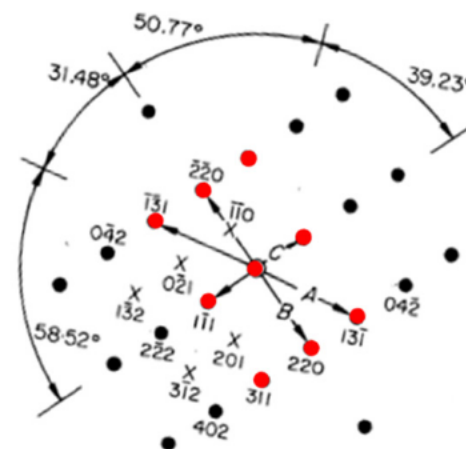


Middle11T

No Match

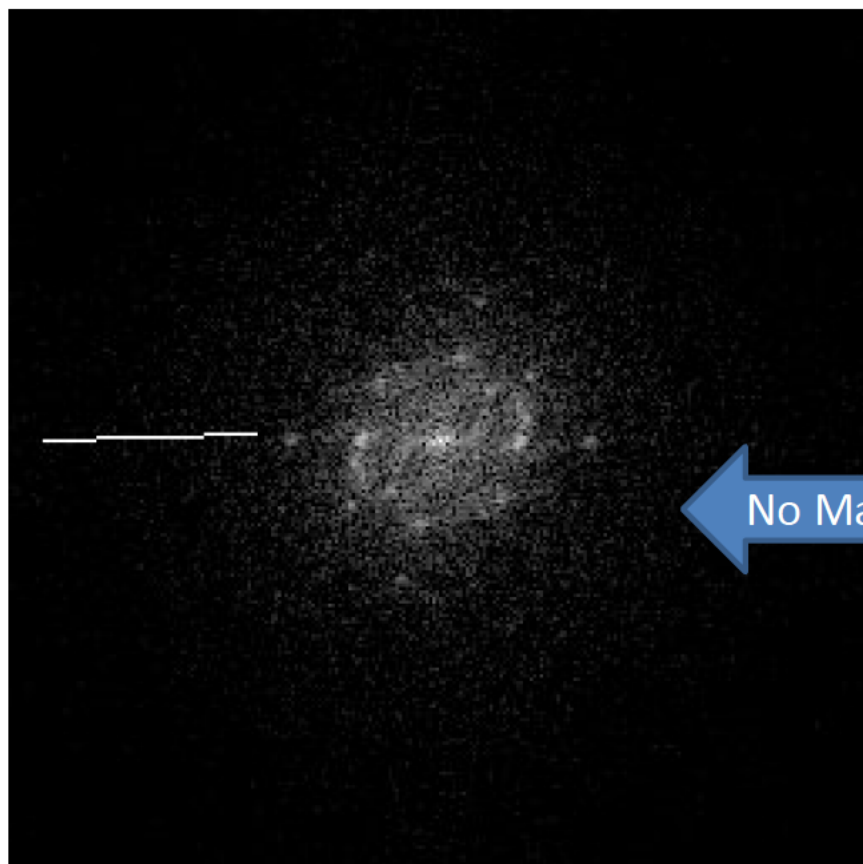


Standard Diffraction Pattern for {110}Fcc



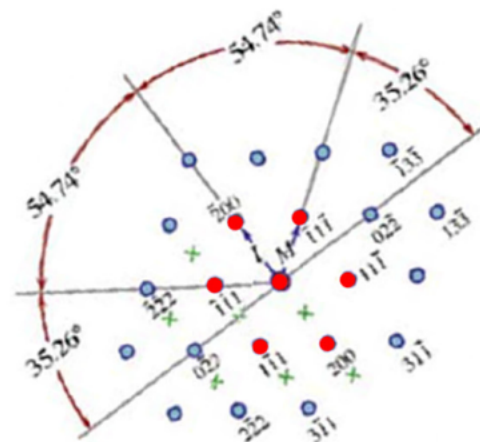
Standard Diffraction Pattern for {112}Fcc

Sample S0GPPC - Middle12T FFT

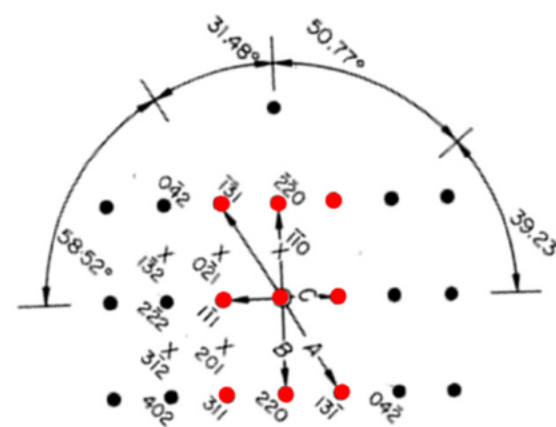


Middle12T

No Match

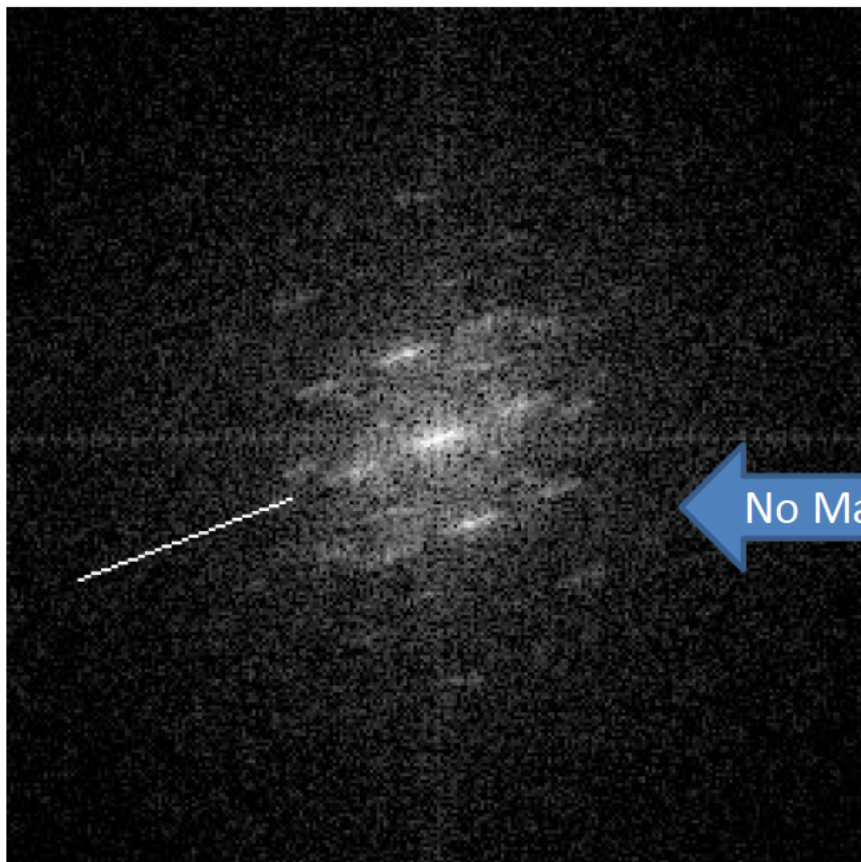


Standard Diffraction Pattern for {110}Fcc



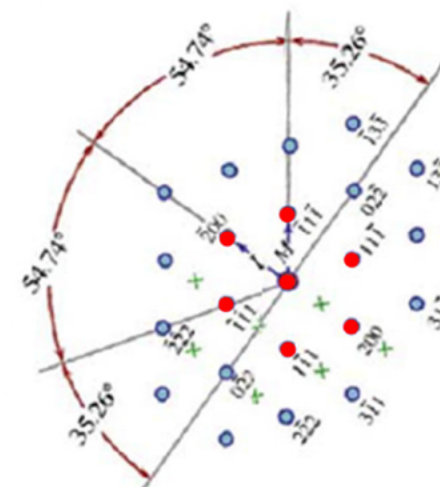
Standard Diffraction Pattern for {112}Fcc

Sample S0GPPC - Middle13T FFT

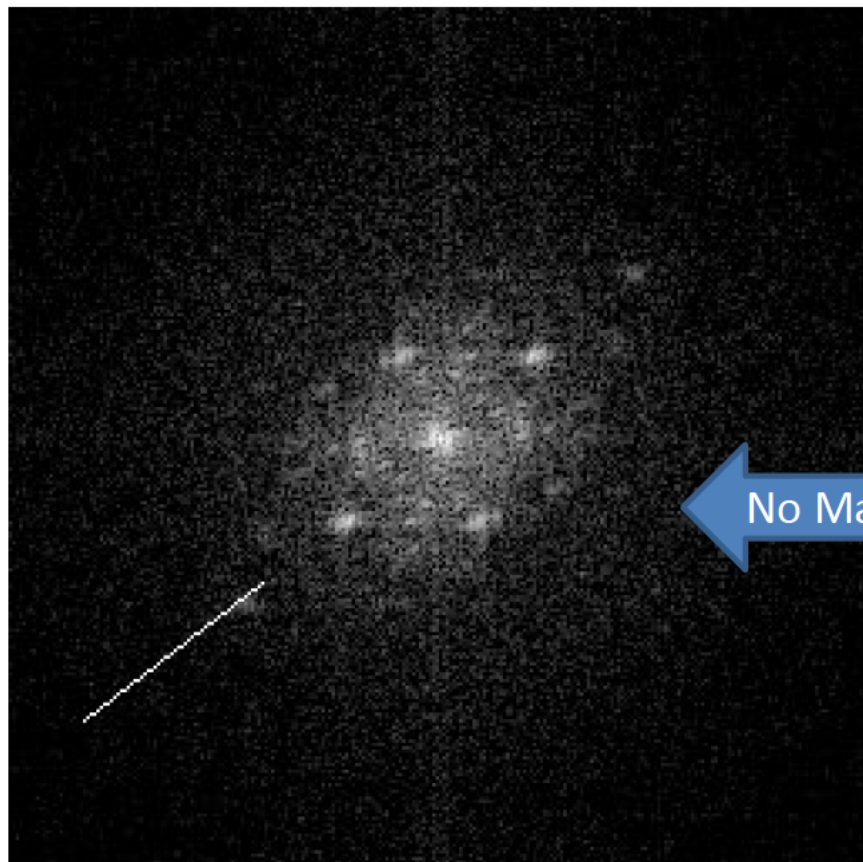


Middle13T

No Match

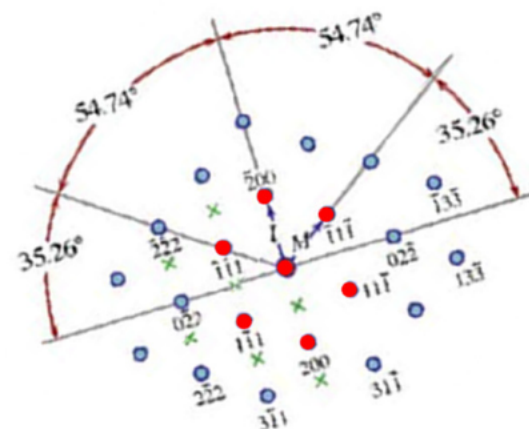


Sample S0GPPC - Middle14T FFT

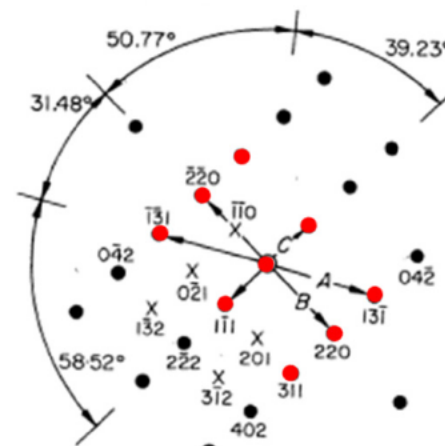


Middle14T

No Match

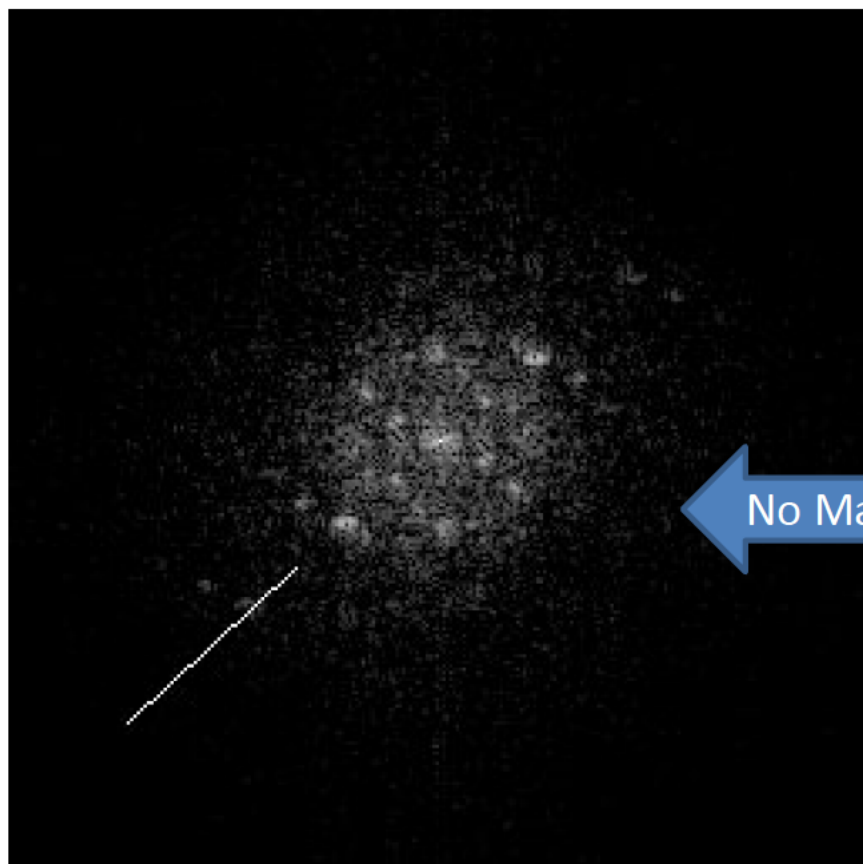


Standard Diffraction Pattern for {110}Fcc



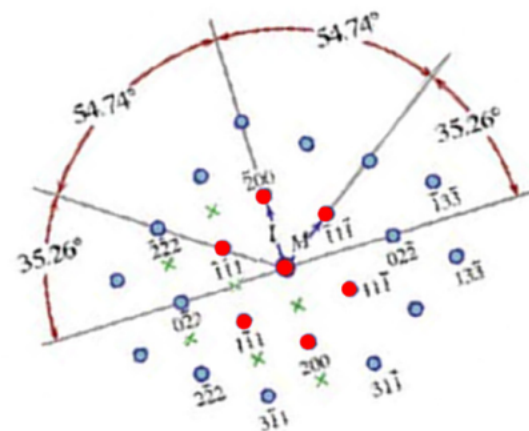
Standard Diffraction Pattern for {112}Fcc

Sample S0GPPC - Middle21T FFT

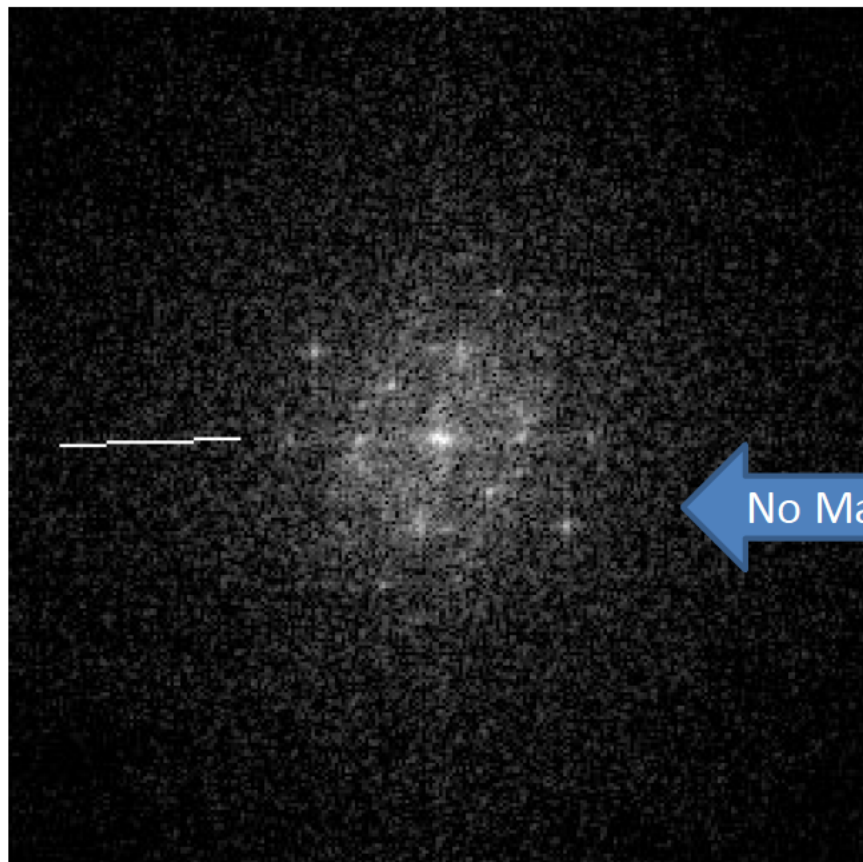


Middle21T

No Match

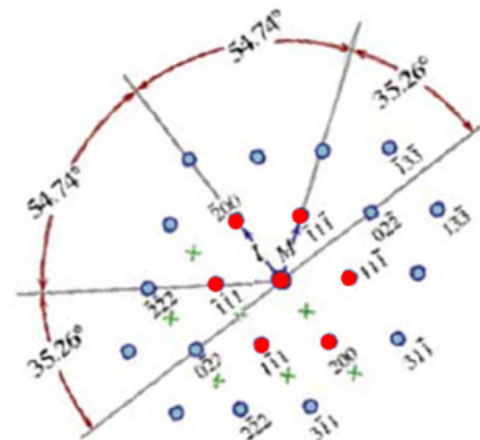


Sample S0GPPC - Middle22T FFT

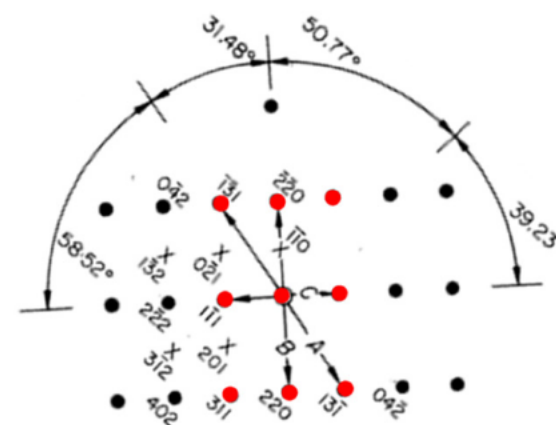


Middle22T

No Match

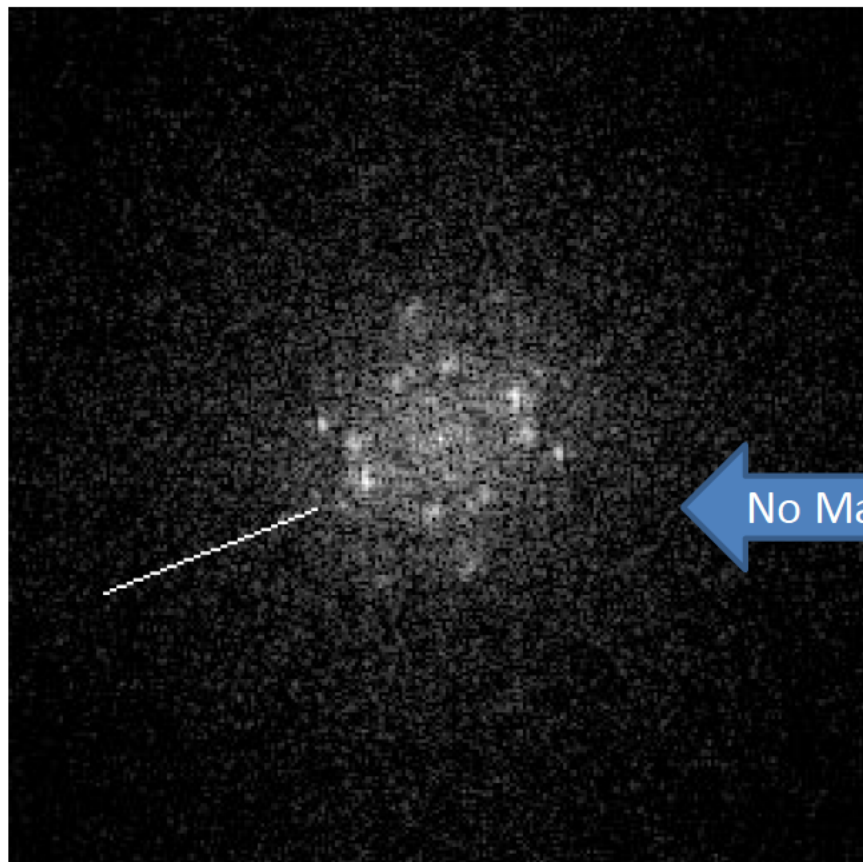


Standard Diffraction Pattern for {110}Fcc



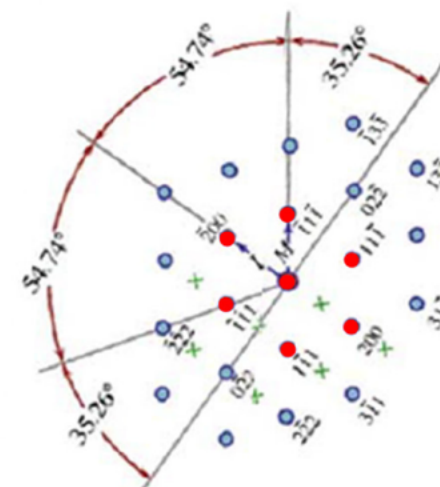
Standard Diffraction Pattern for {112}Fcc

Sample S0GPPC - Middle23T FFT

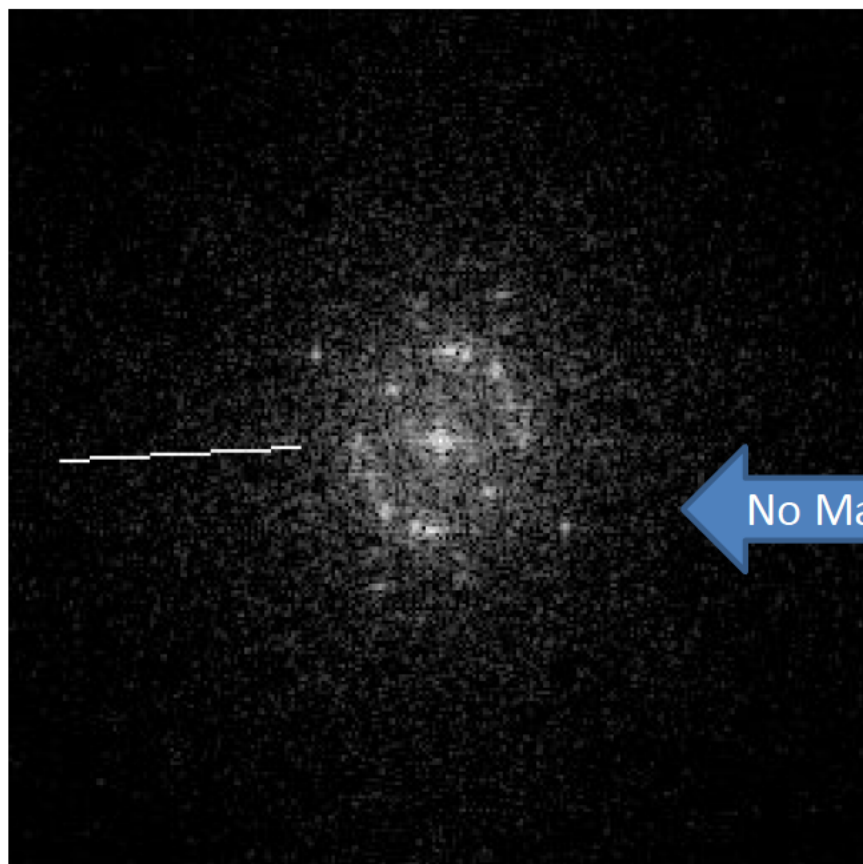


Middle23T

No Match

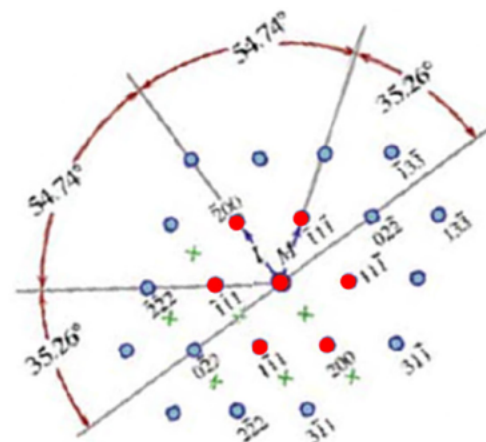


Sample S0GPPC - MiddleNi31T FFT

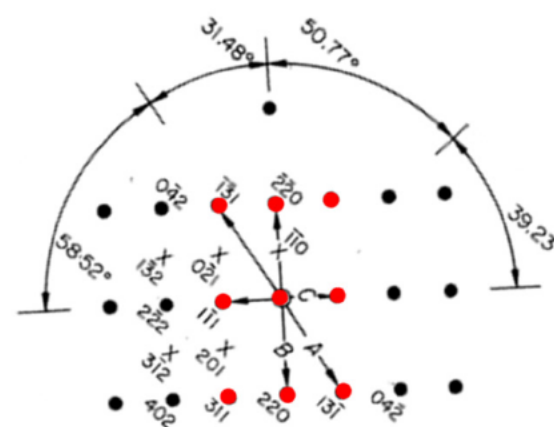


MiddleNi31T

No Match

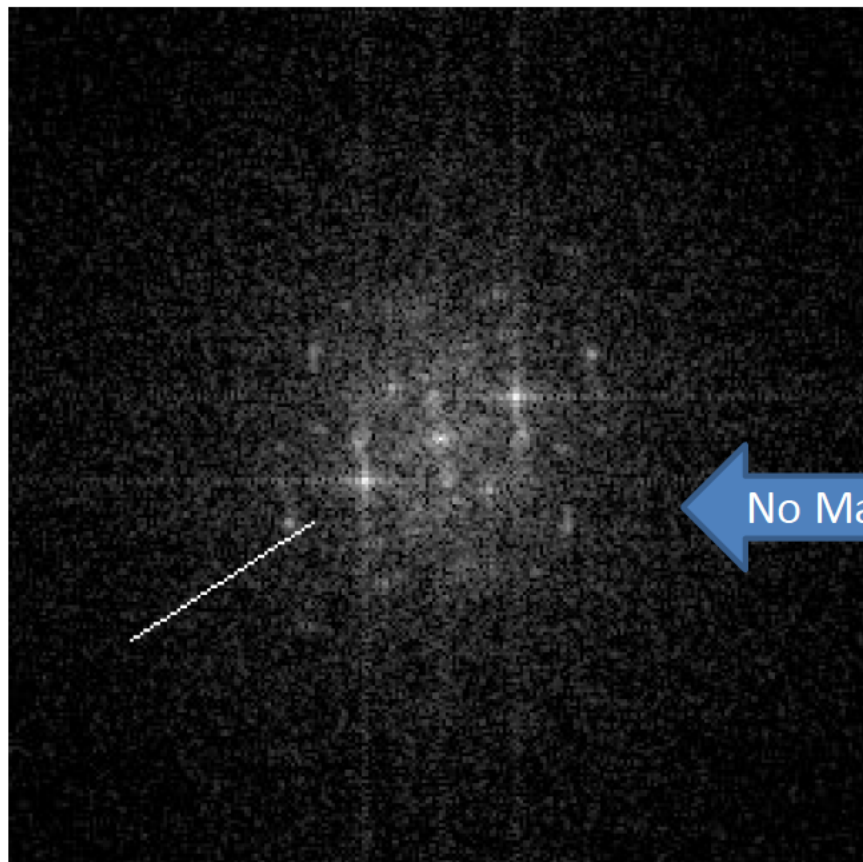


Standard Diffraction Pattern for {110}Fcc



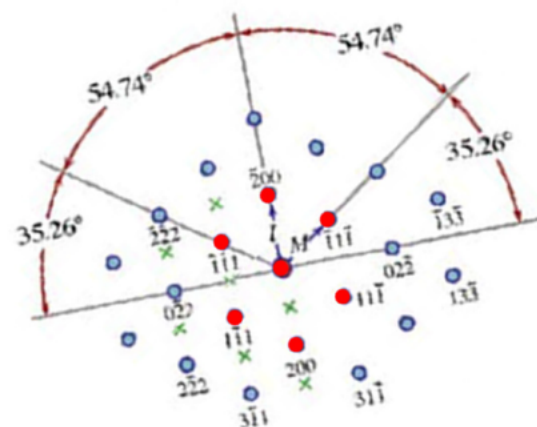
Standard Diffraction Pattern for {112}Fcc

Sample S0GPPC - MiddleNi32T FFT

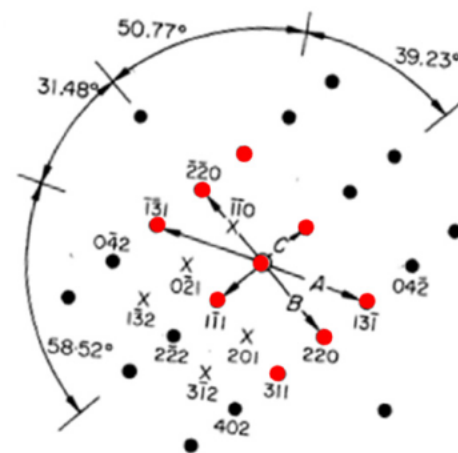


MiddleNi32T

No Match

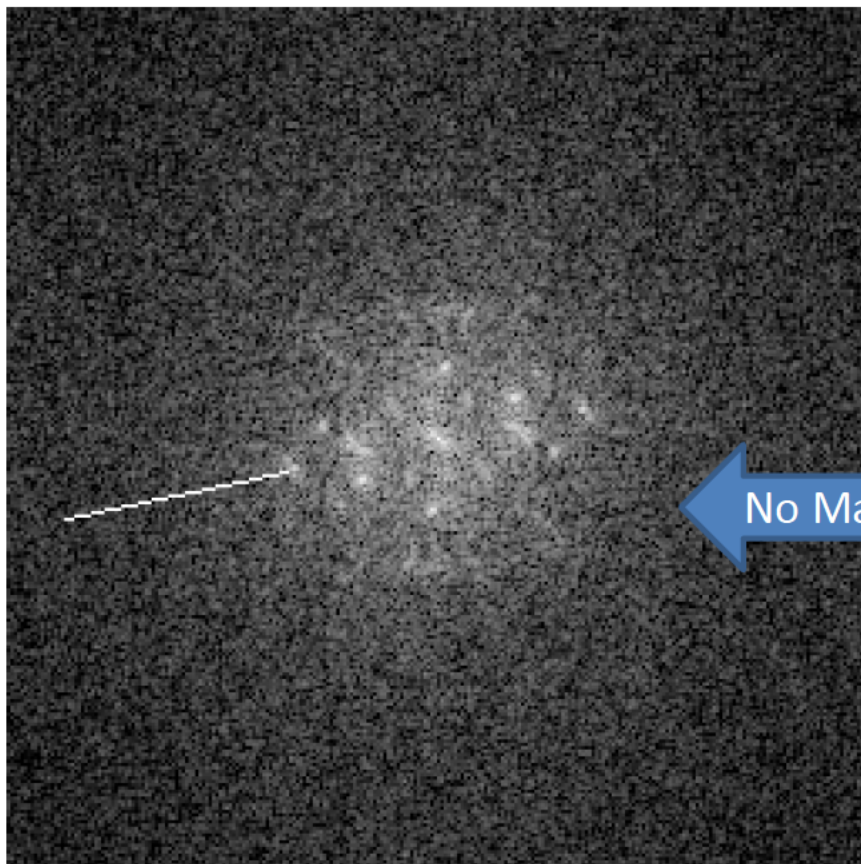


Standard Diffraction Pattern for {110}Fcc



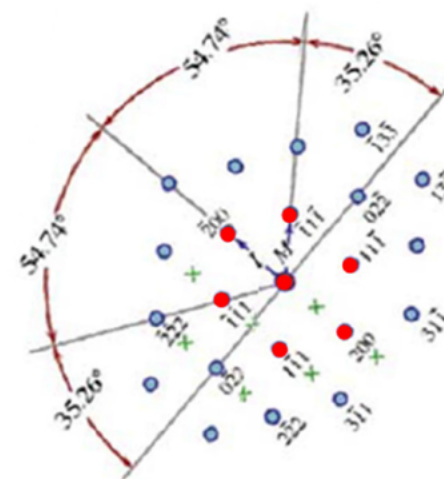
Standard Diffraction Pattern for {112}Fcc

Sample S0GPPC - MiddleNi33T FFT

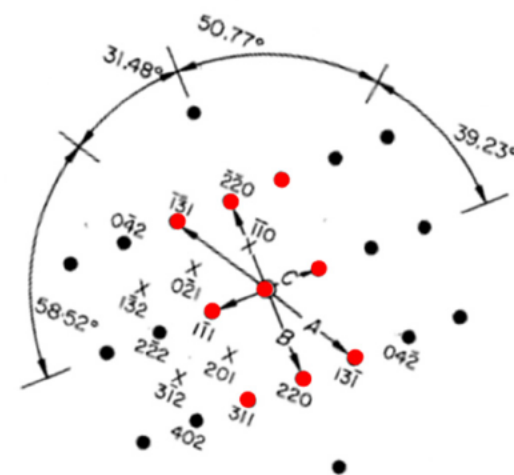


MiddleNi33T

No Match



Standard Diffraction Pattern for {110}Fcc



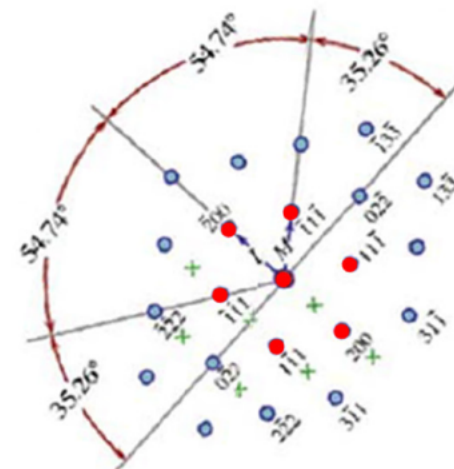
Standard Diffraction Pattern for {112}Fcc

Sample S0GPPC - MiddleNi41T FFT

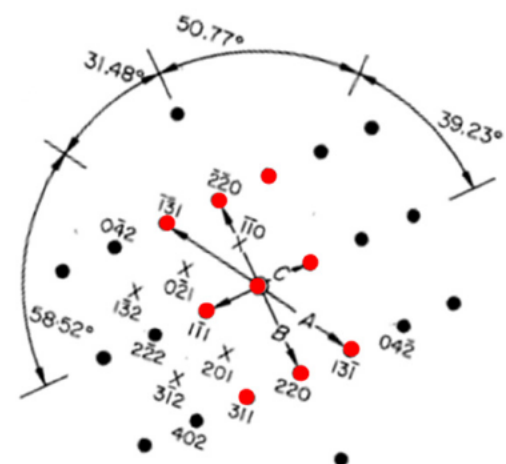


MiddleNi41T

No Match

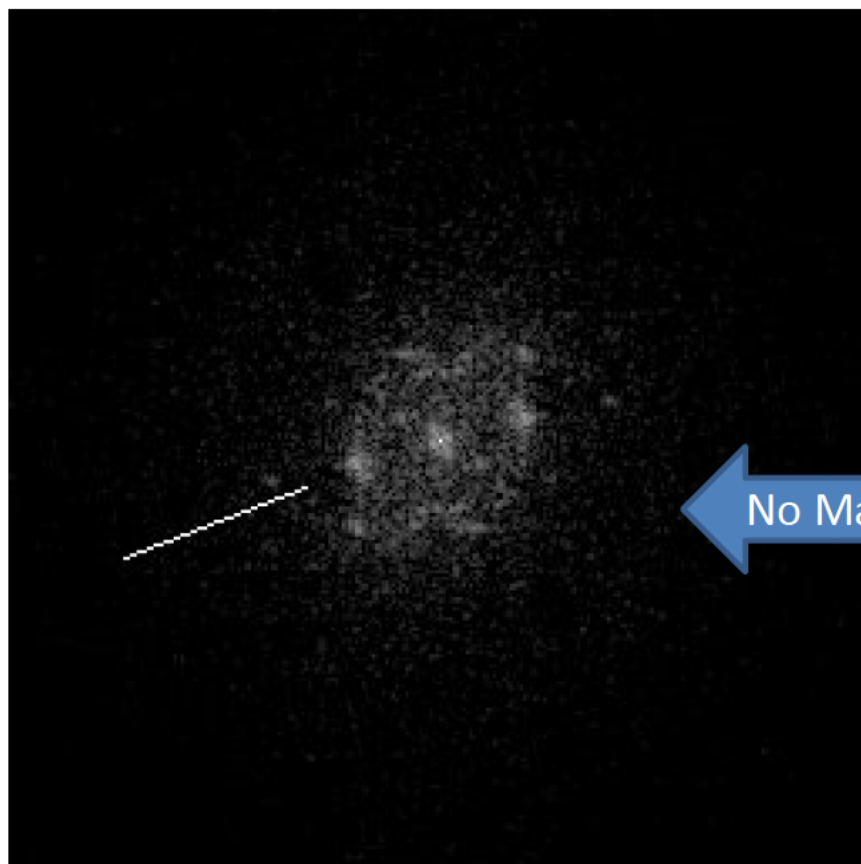


Standard Diffraction Pattern for {110}Fcc



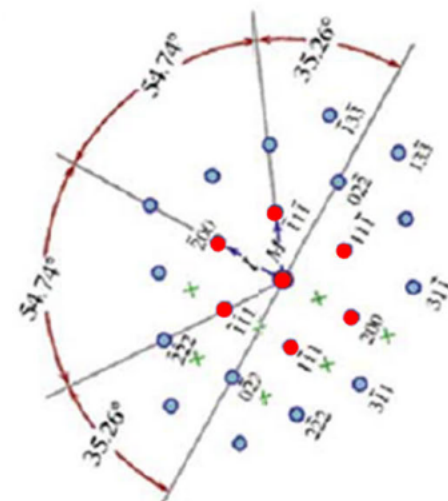
Standard Diffraction Pattern for {112}Fcc

Sample S0GPPC - MiddleNi42T FFT

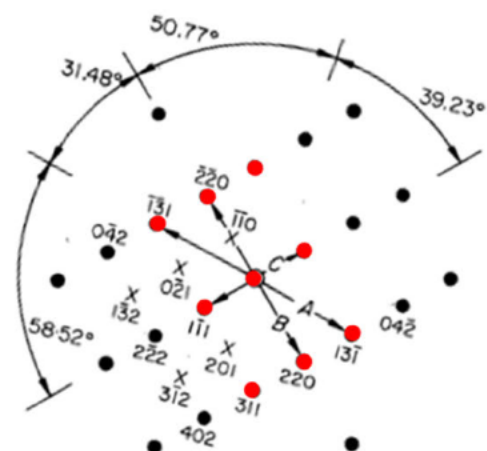


MiddleNi42T

No Match

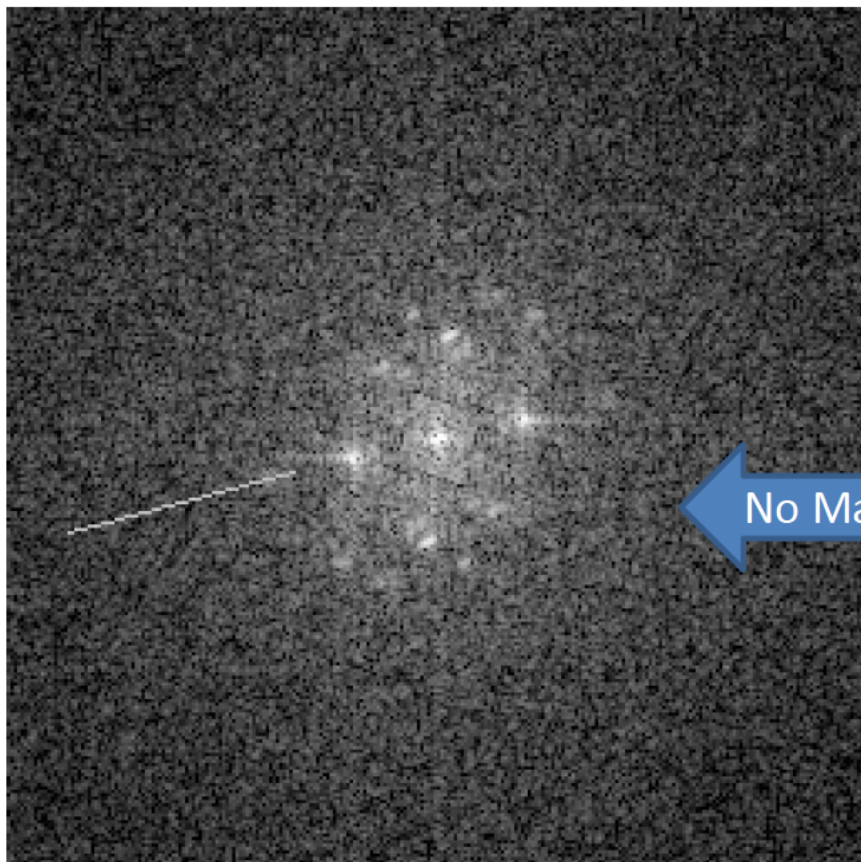


Standard Diffraction Pattern for {110}Fcc



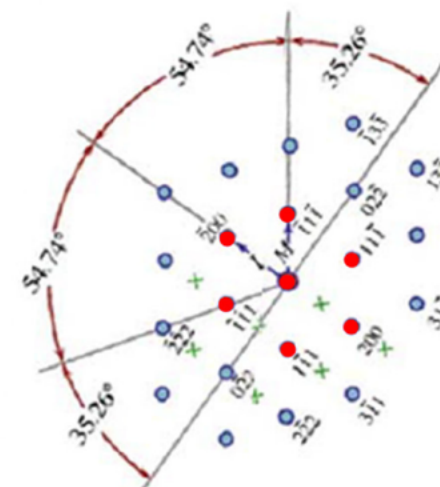
Standard Diffraction Pattern for {112}Fcc

Sample S0GPPC - MiddleNi43T FFT

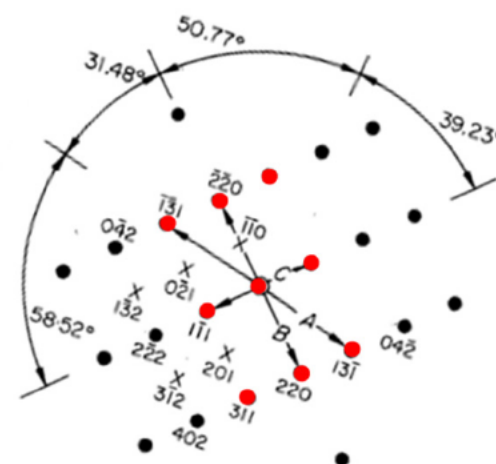


MiddleNi43T

No Match

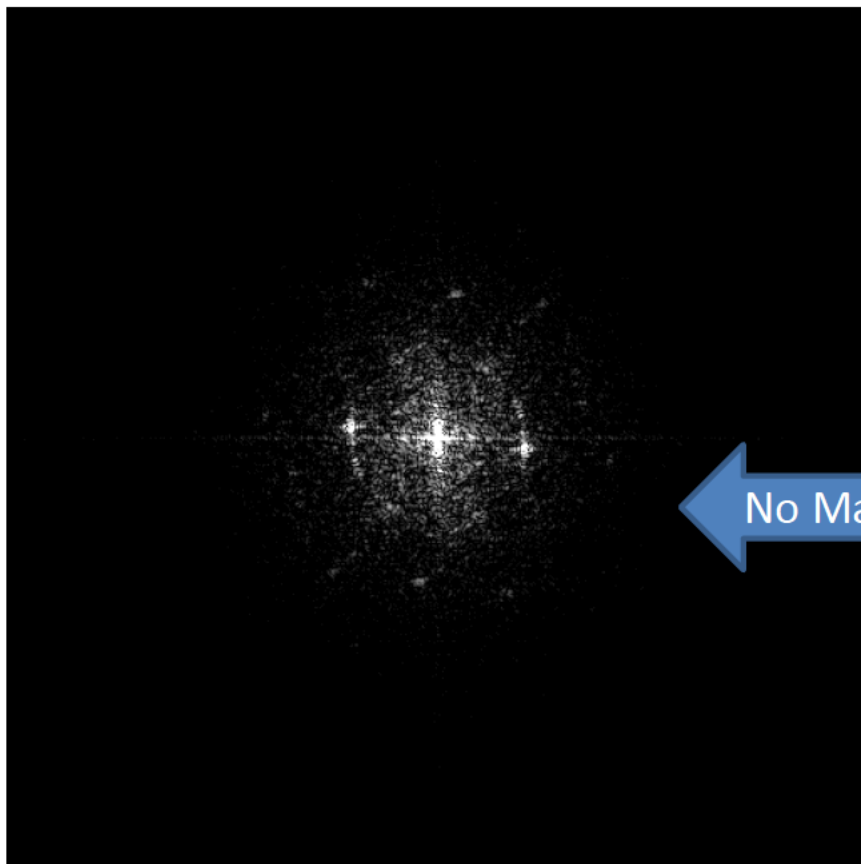


Standard Diffraction Pattern for {110}Fcc



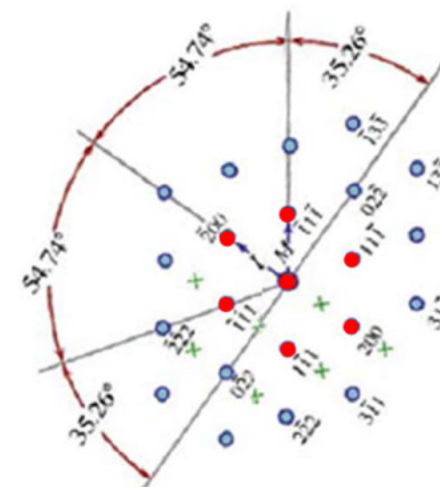
Standard Diffraction Pattern for {112}Fcc

Sample S2MMC - 18.08.14 CCD Acquire 1T FFT

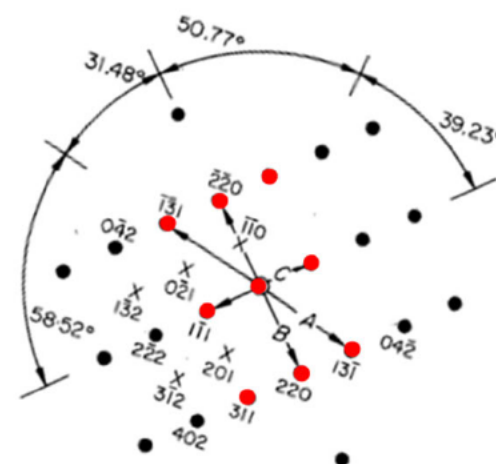


18.08.14 CCD Acquire 1T

No Match

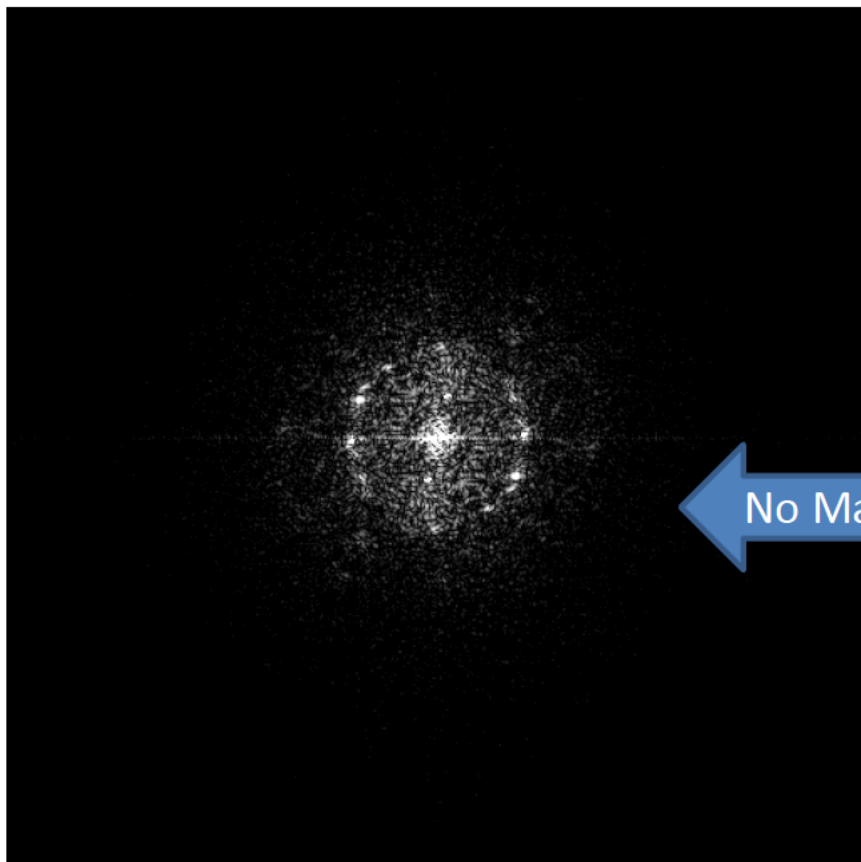


Standard Diffraction Pattern for {110}Fcc



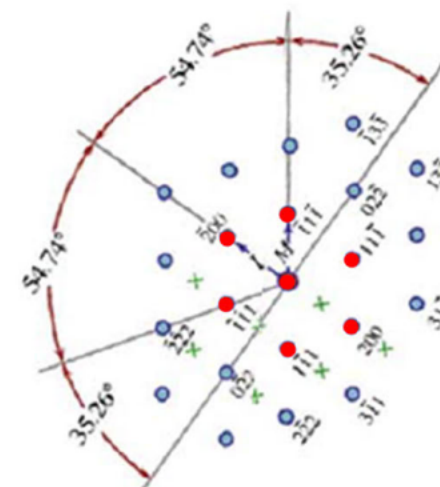
Standard Diffraction Pattern for {112}Fcc

Sample S2MMC - 18.08.14 CCD Acquire 2T FFT



18.08.14 CCD Acquire 2T

No Match

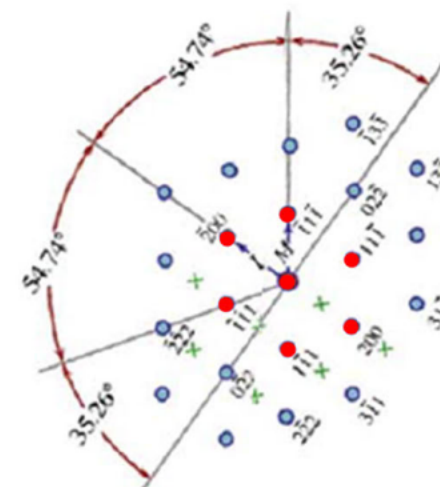


Sample S2MMC - 18.08.14 CCD Acquire 3T FFT

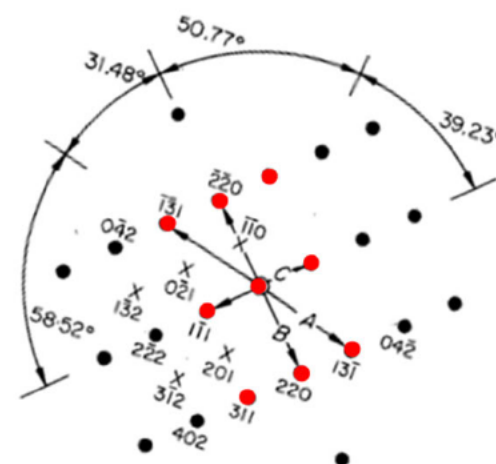


18.08.14 CCD Acquire 3T

No Match

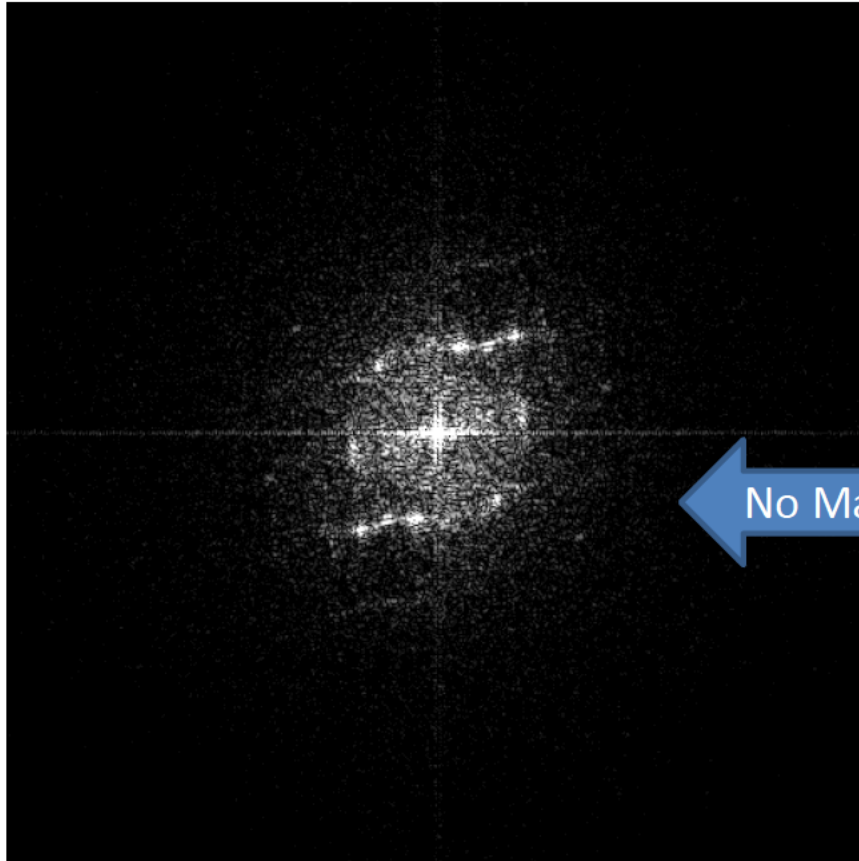


Standard Diffraction Pattern for {110}Fcc



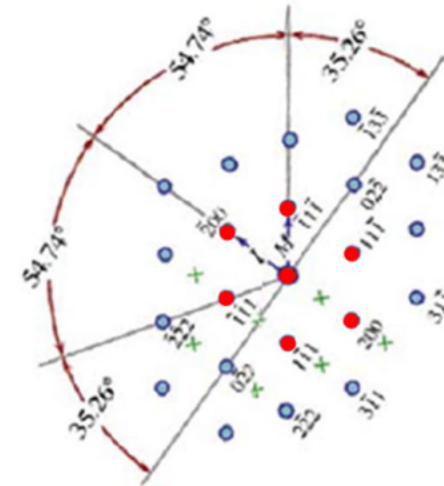
Standard Diffraction Pattern for {112}Fcc

Sample S2MMC - 18.08.14 CCD Acquire 4T FFT

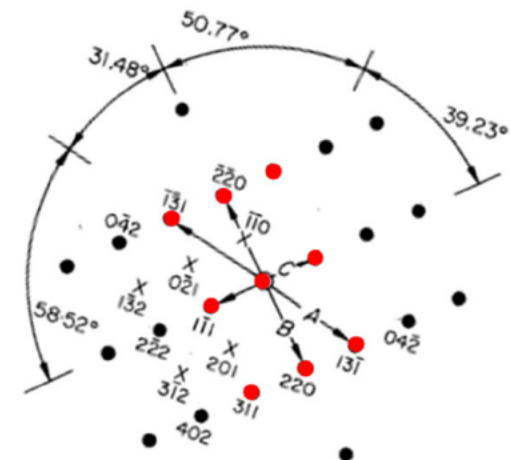


18.08.14 CCD Acquire 4T

No Match

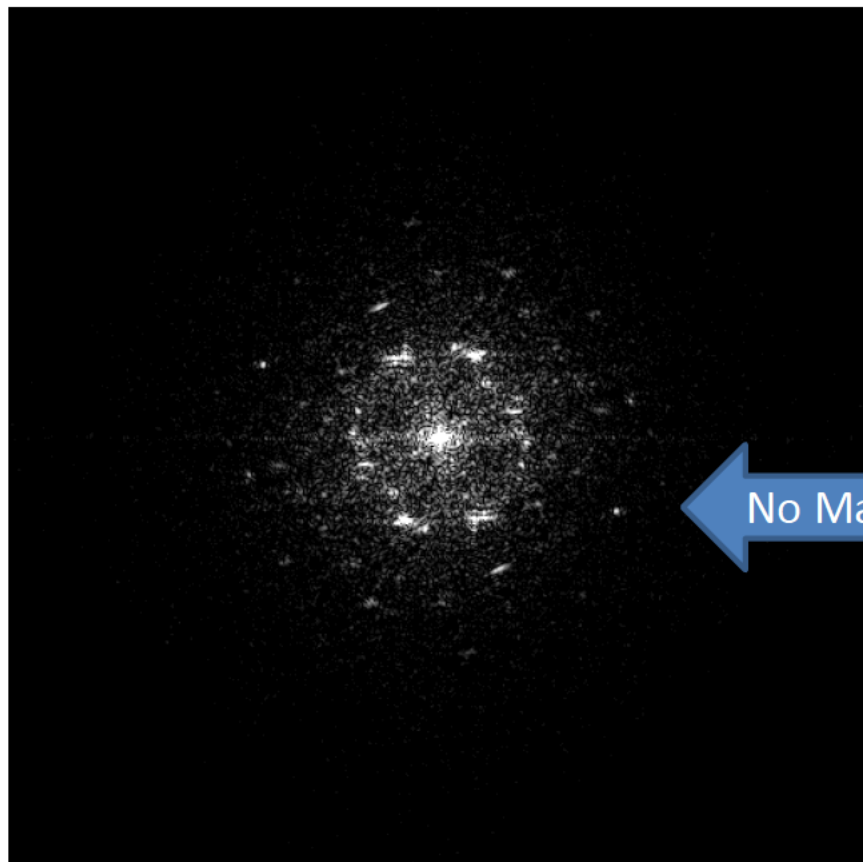


Standard Diffraction Pattern for {110}Fcc



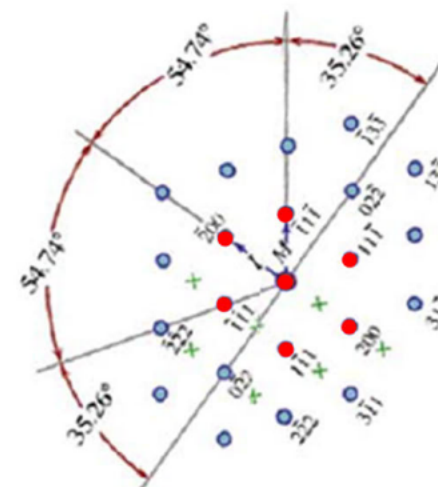
Standard Diffraction Pattern for {112}Fcc

Sample S2MMC - 18.10.05 CCD Acquire 1T FFT

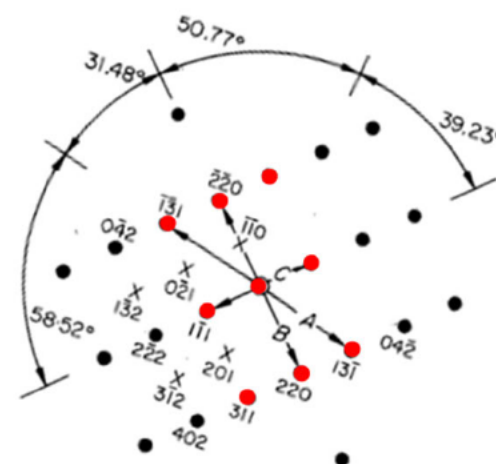


18.10.05 CCD Acquire 1T

No Match

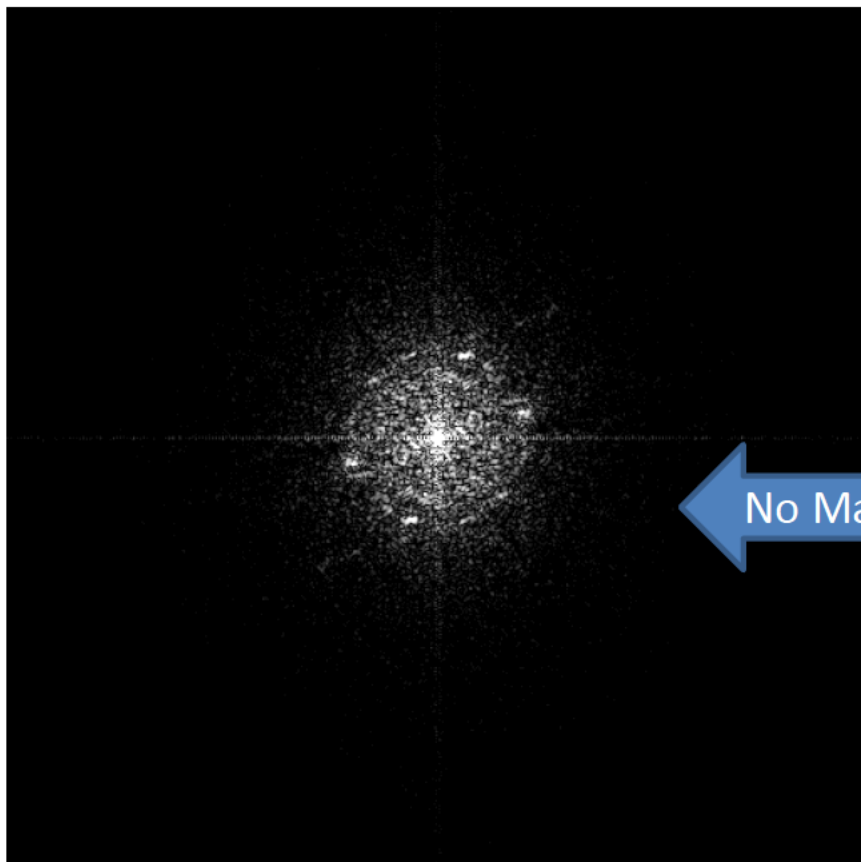


Standard Diffraction Pattern for {110}Fcc



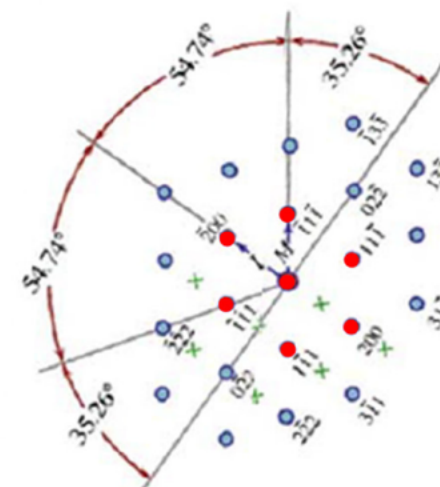
Standard Diffraction Pattern for {112}Fcc

Sample SBR8DK - 18.21.37 CCD Acquire 1T FFT

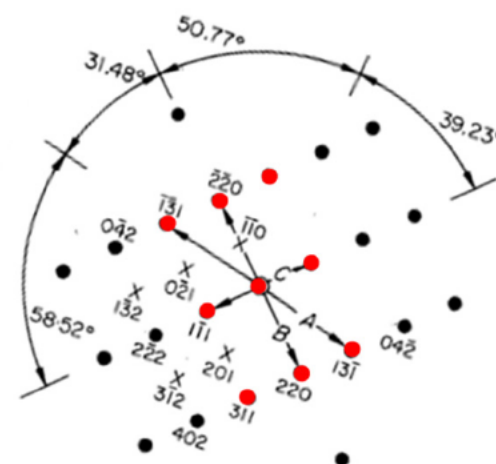


18.21.37 CCD Acquire 1T

No Match

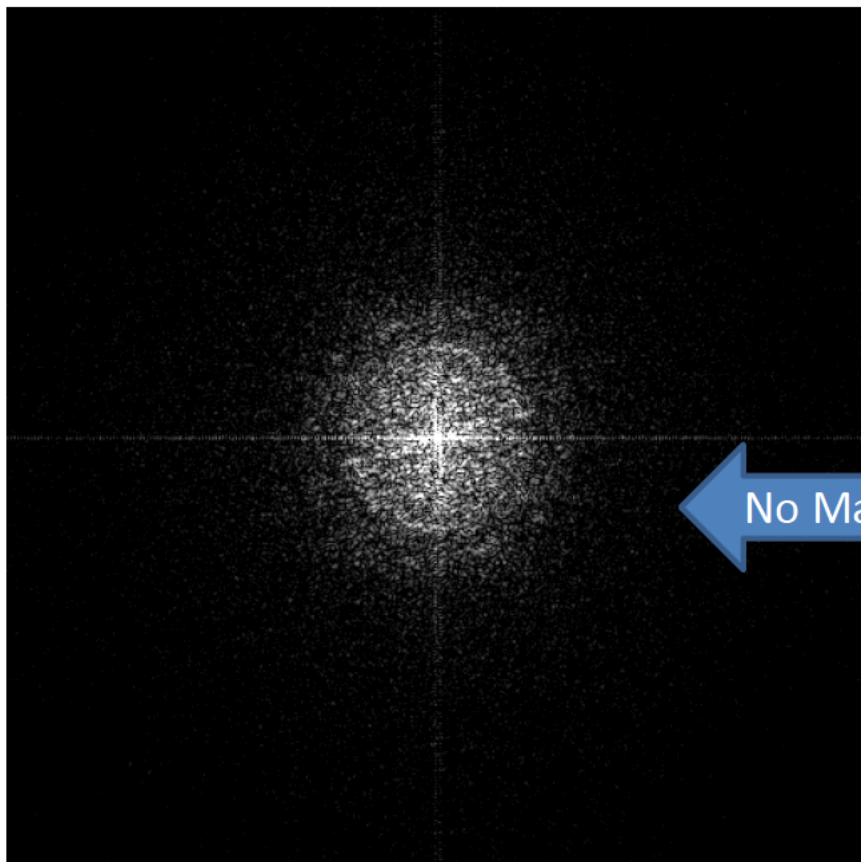


Standard Diffraction Pattern for {110}Fcc



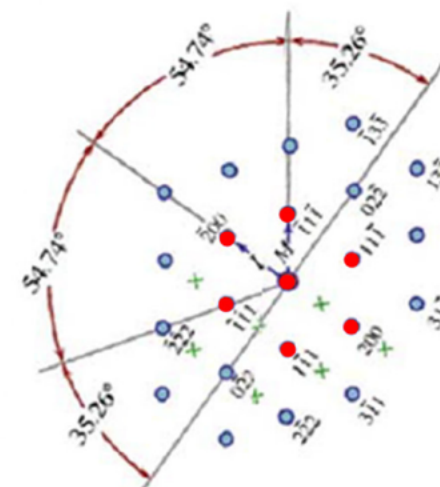
Standard Diffraction Pattern for {112}Fcc

Sample SBR8DK - 18.21.37 CCD Acquire 2T FFT

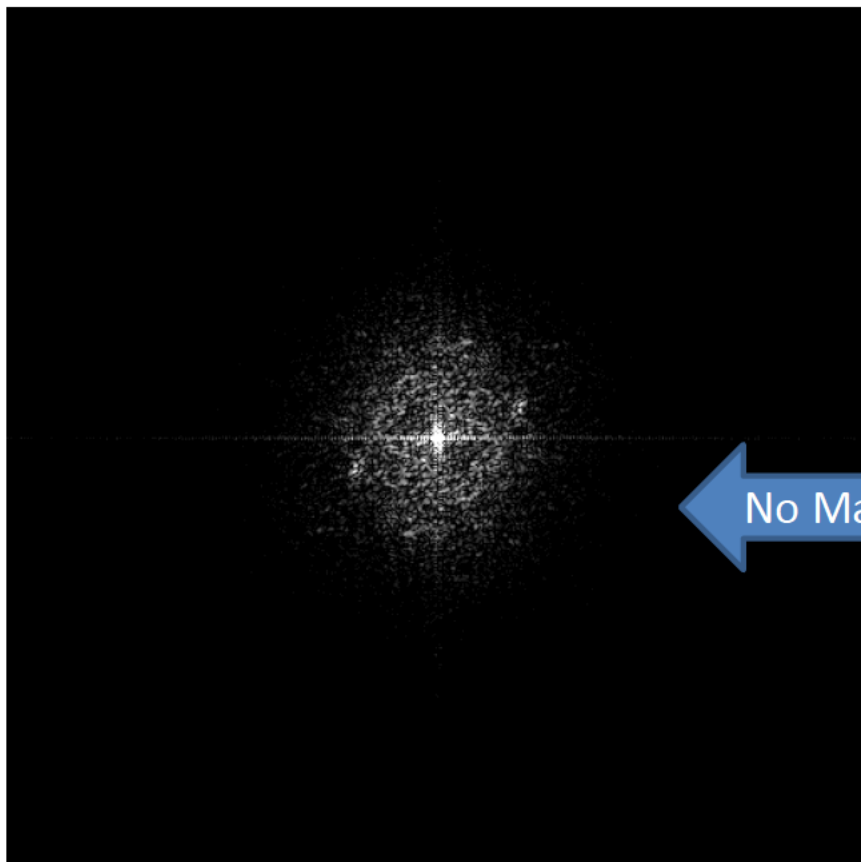


18.21.37 CCD Acquire 2T

No Match

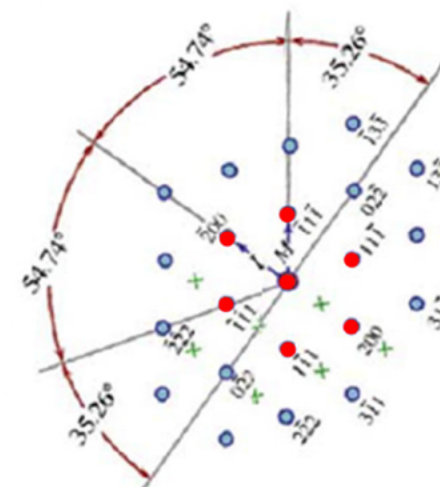


Sample SBR8DK - 18.21.37 CCD Acquire 3T FFT

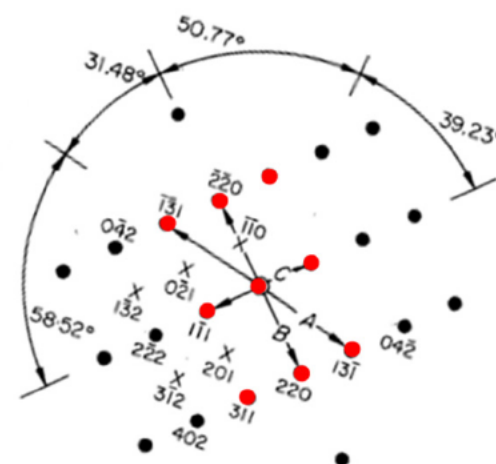


18.21.37 CCD Acquire 3T

No Match

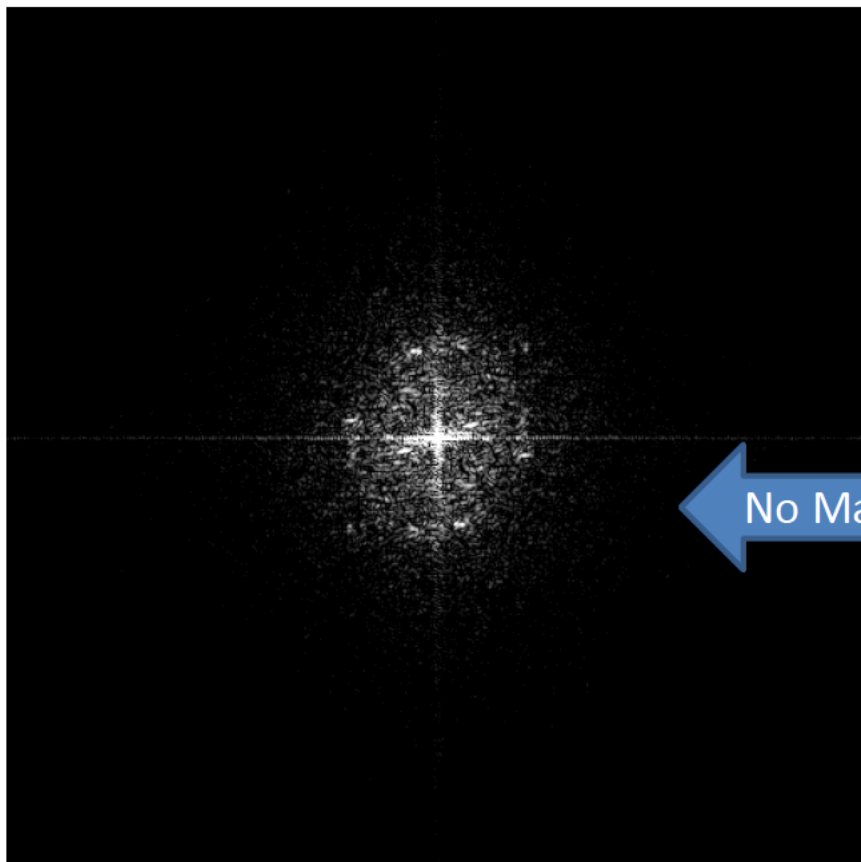


Standard Diffraction Pattern for {110}Fcc



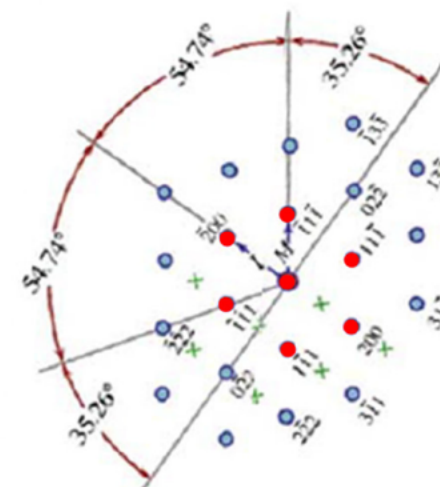
Standard Diffraction Pattern for {112}Fcc

Sample SBR8DK - 18.21.37 CCD Acquire 4T FFT

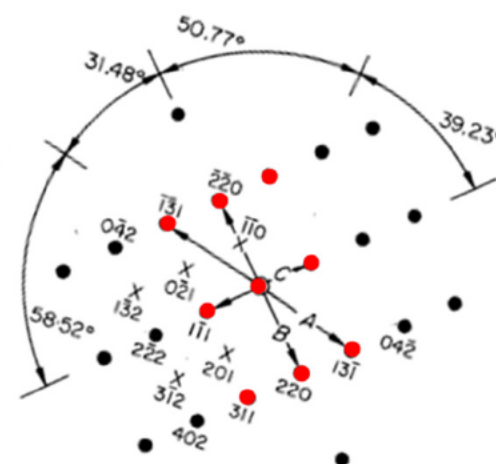


18.21.37 CCD Acquire 4T

No Match



Standard Diffraction Pattern for {110}Fcc

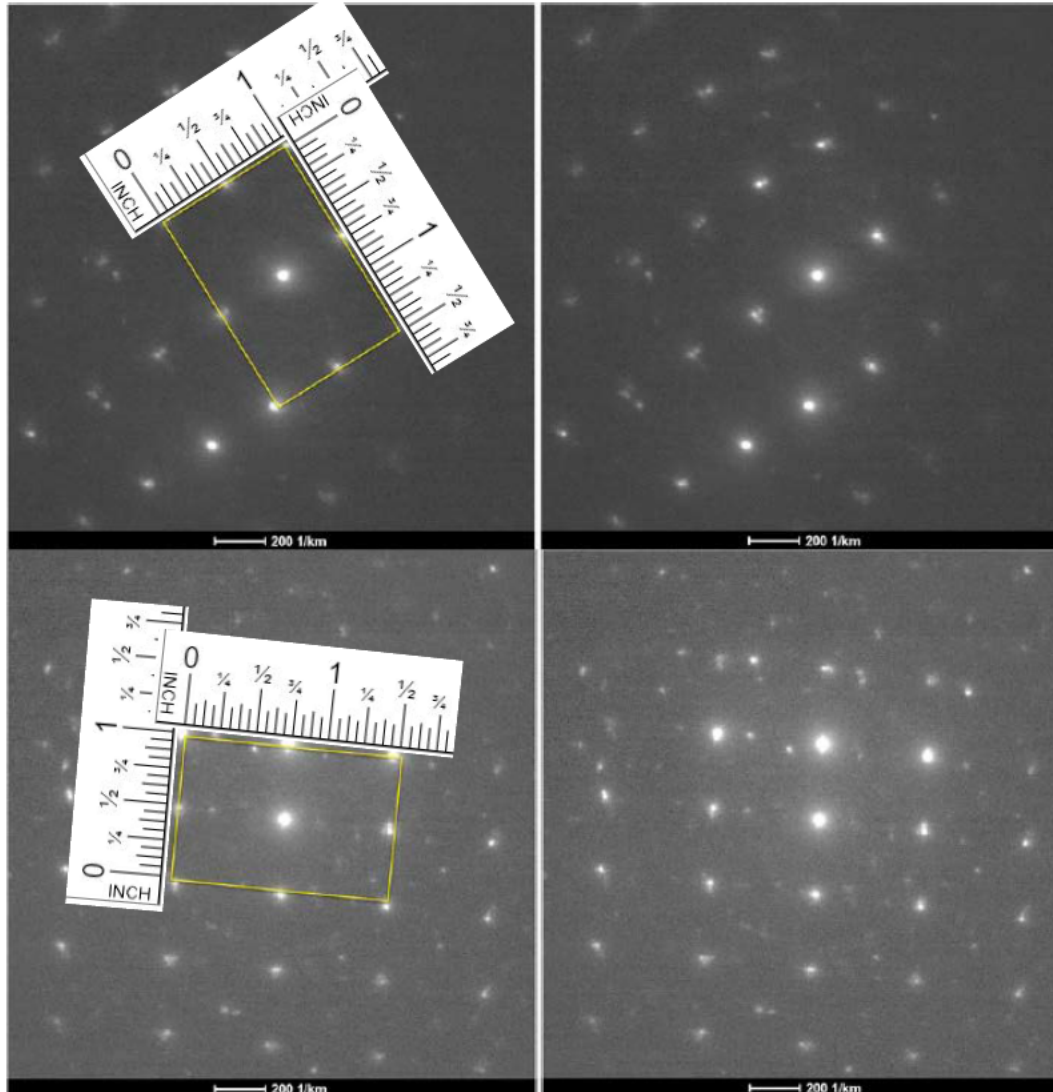


Standard Diffraction Pattern for {112}Fcc

EXHIBIT G

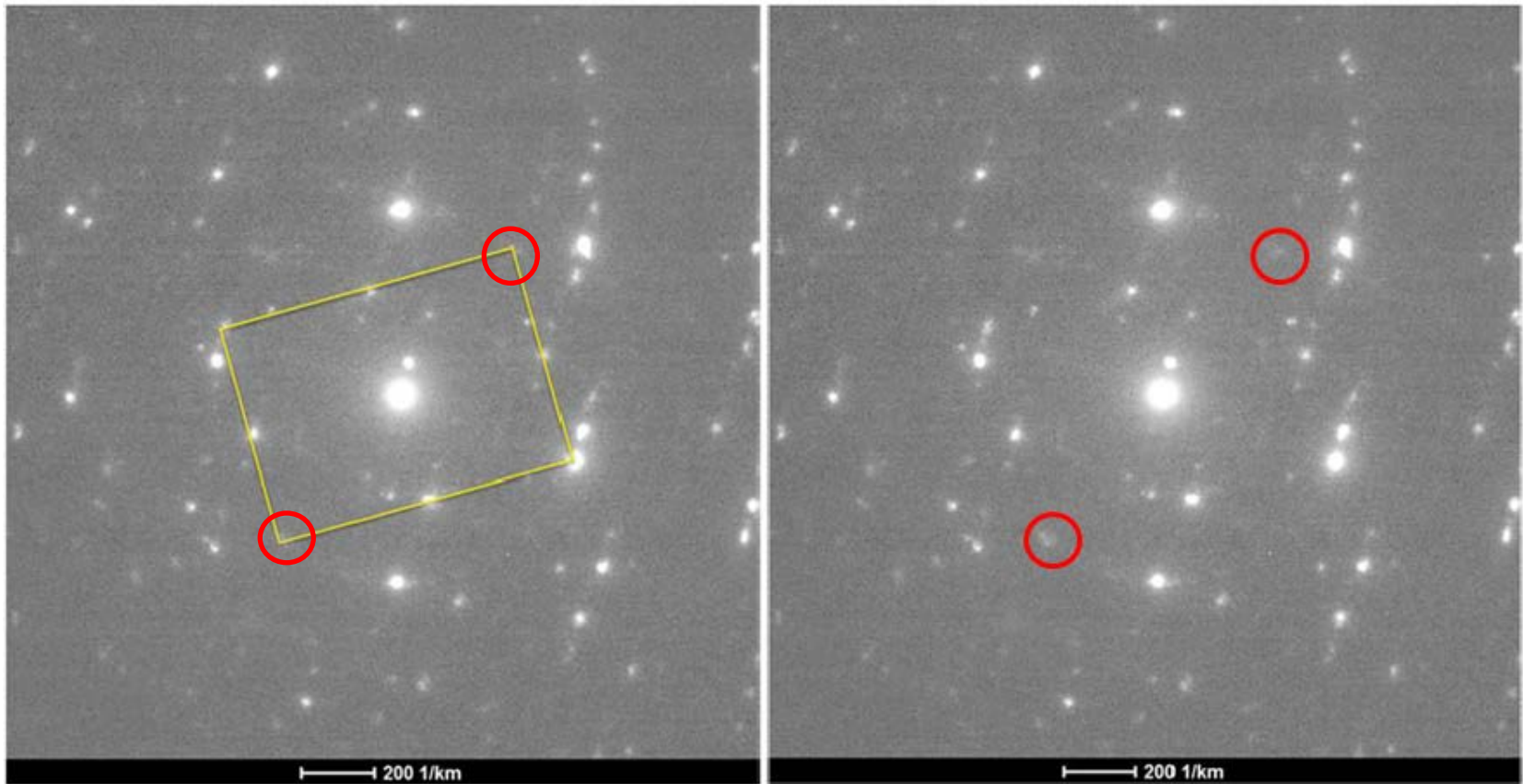
SOGPPC - Figure 47

Ratio = 1:1.5



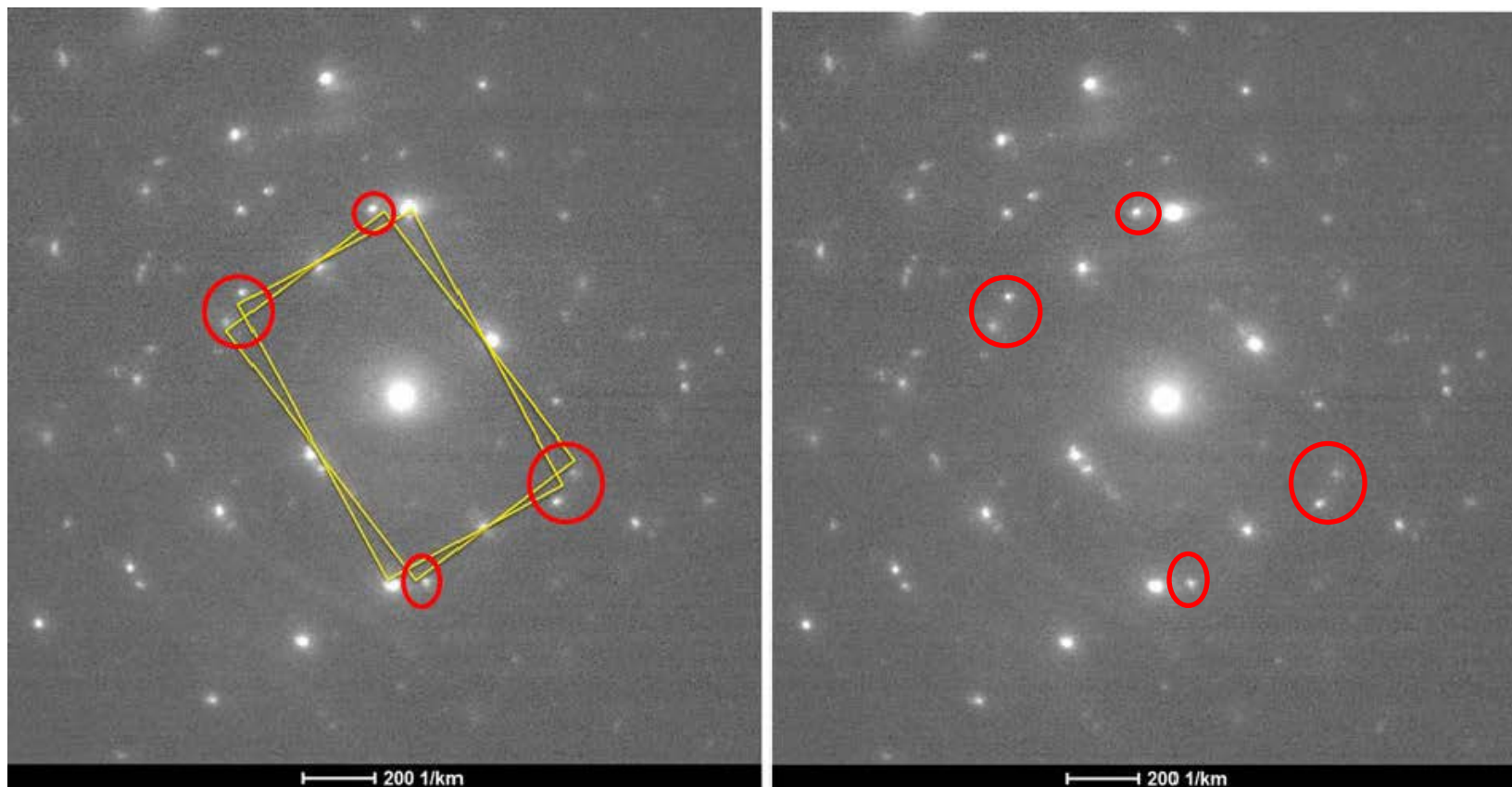
Ratio = 1:1.5

S0GPPC - Figure 48



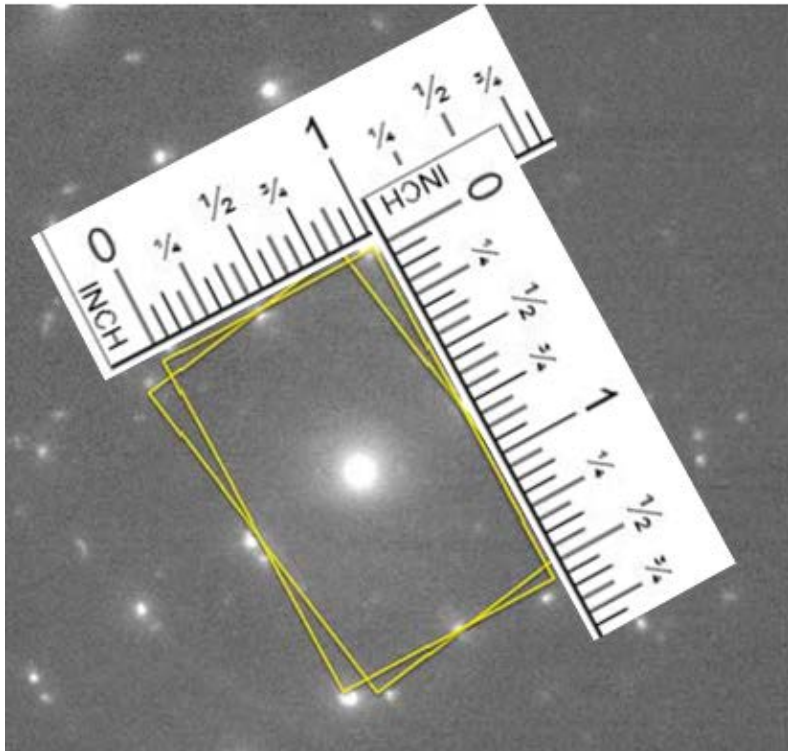
Red circles added by Dr. Stach to indicate spots that are weak, not clearly discernable or not present.

S0GPPC - Figure 49

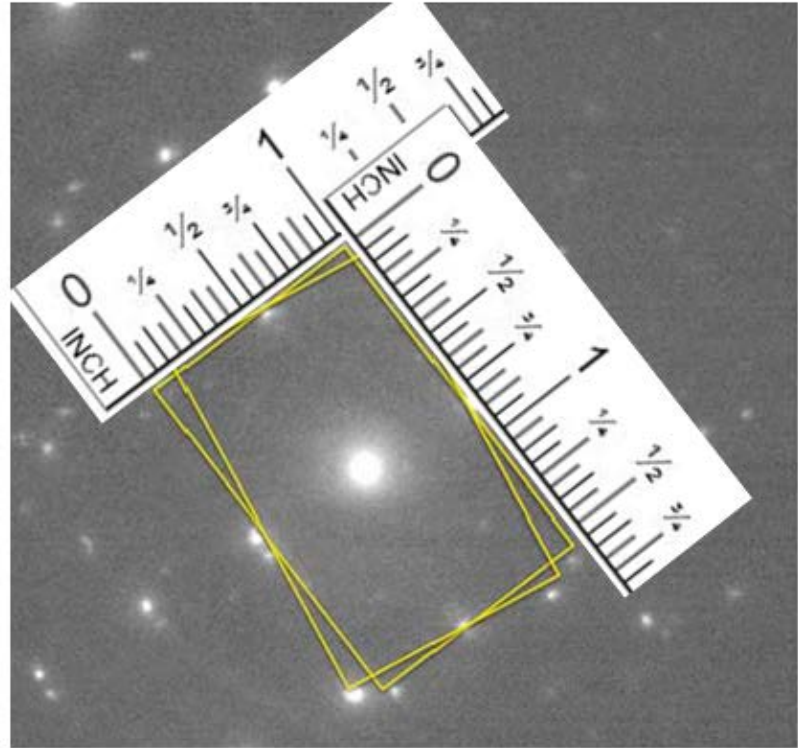


Red circles added by Dr. Stach to indicate spots that are not clearly discernable or not present. The lack of alignment with the box corners and nearby spots are significant enough to indicate that this interpretation is incorrect.

S0GPPC - Figure 49

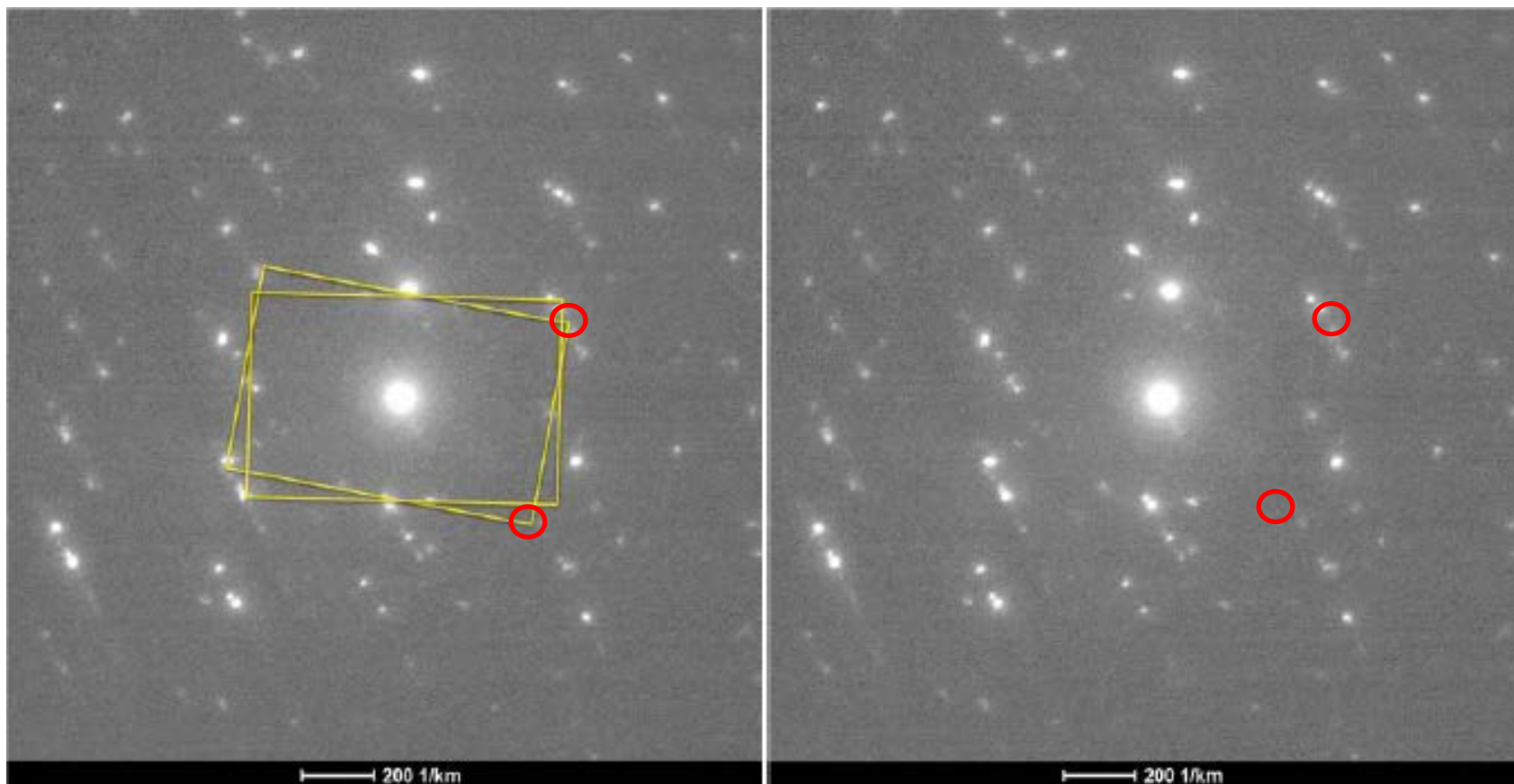


Ratio = 1:1.5625



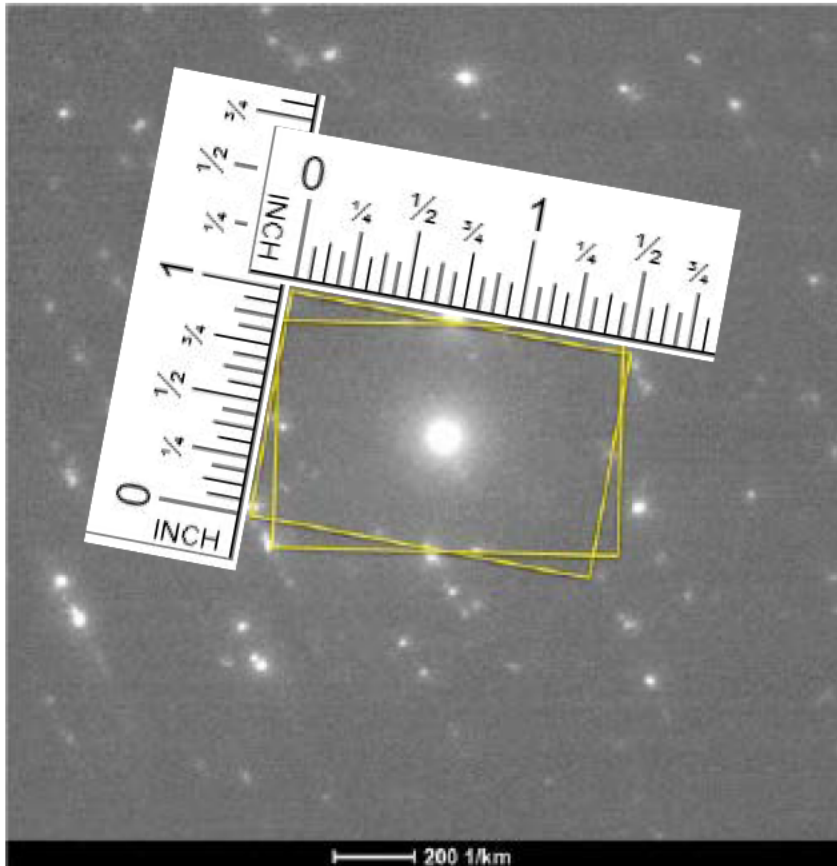
Ratio = 1:1.5625

S0GPPC - Figure 50

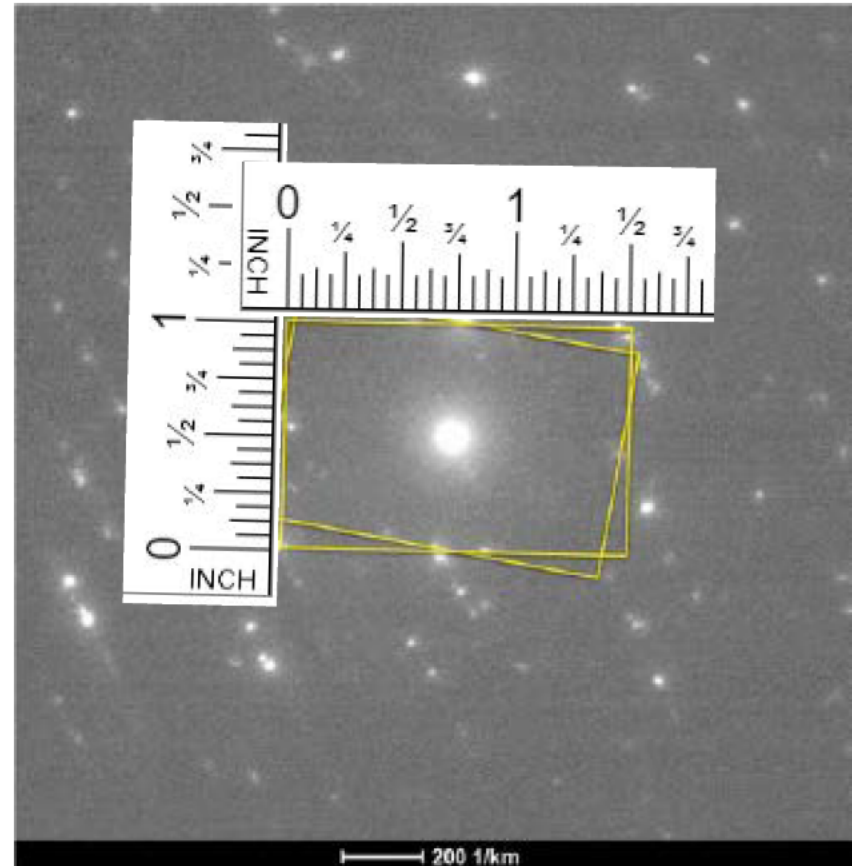


Red circles added by Dr. Stach to indicate spots that are not clearly discernable or not present. The lack of alignment with the box corners and nearby spots are significant enough to indicate that this interpretation is incorrect.

SOGPPC - Figure 50



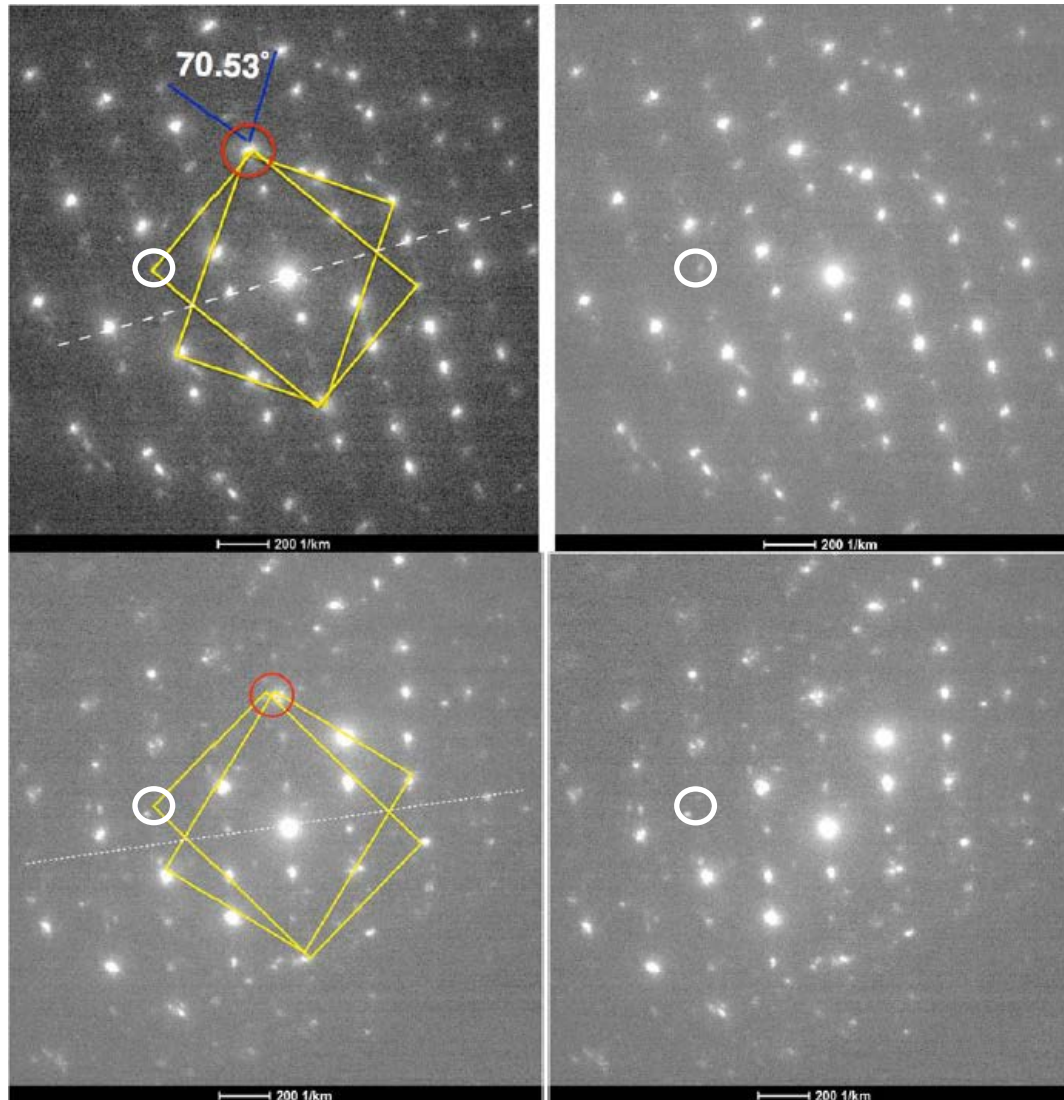
Ratio = 1:1.5



Ratio = 1:1.5

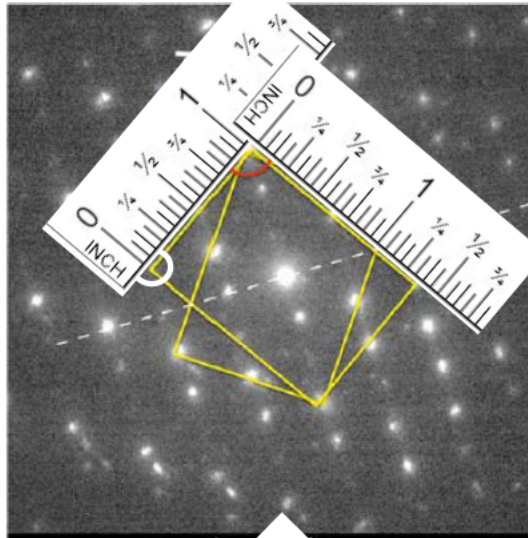
S0GPPC - Figure 51

- White rings inserted by Dr. Stach to show missing or not clearly discernable spots
- Red rings in original image
- The lack of alignment with the box corners and nearby spots are significant enough to indicate that this interpretation is incorrect.

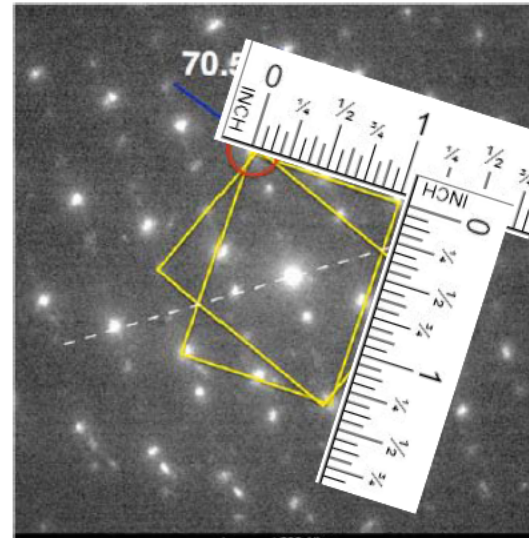


SOGPPC - Figure 51

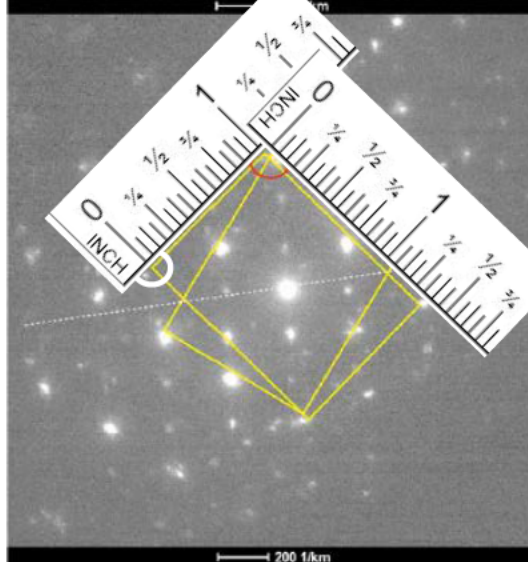
Ratio = 1.5:1



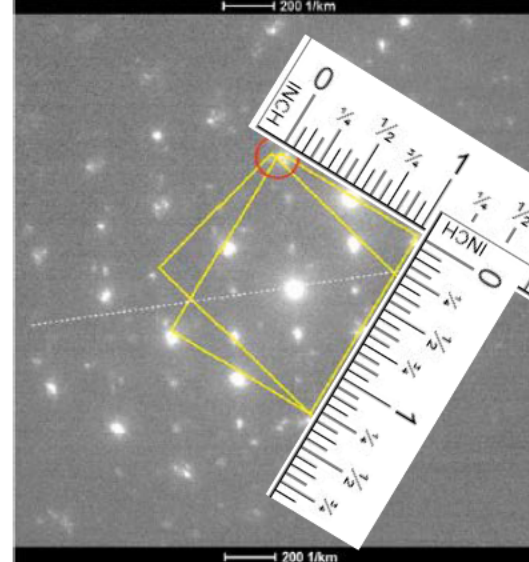
Ratio 1.375:1



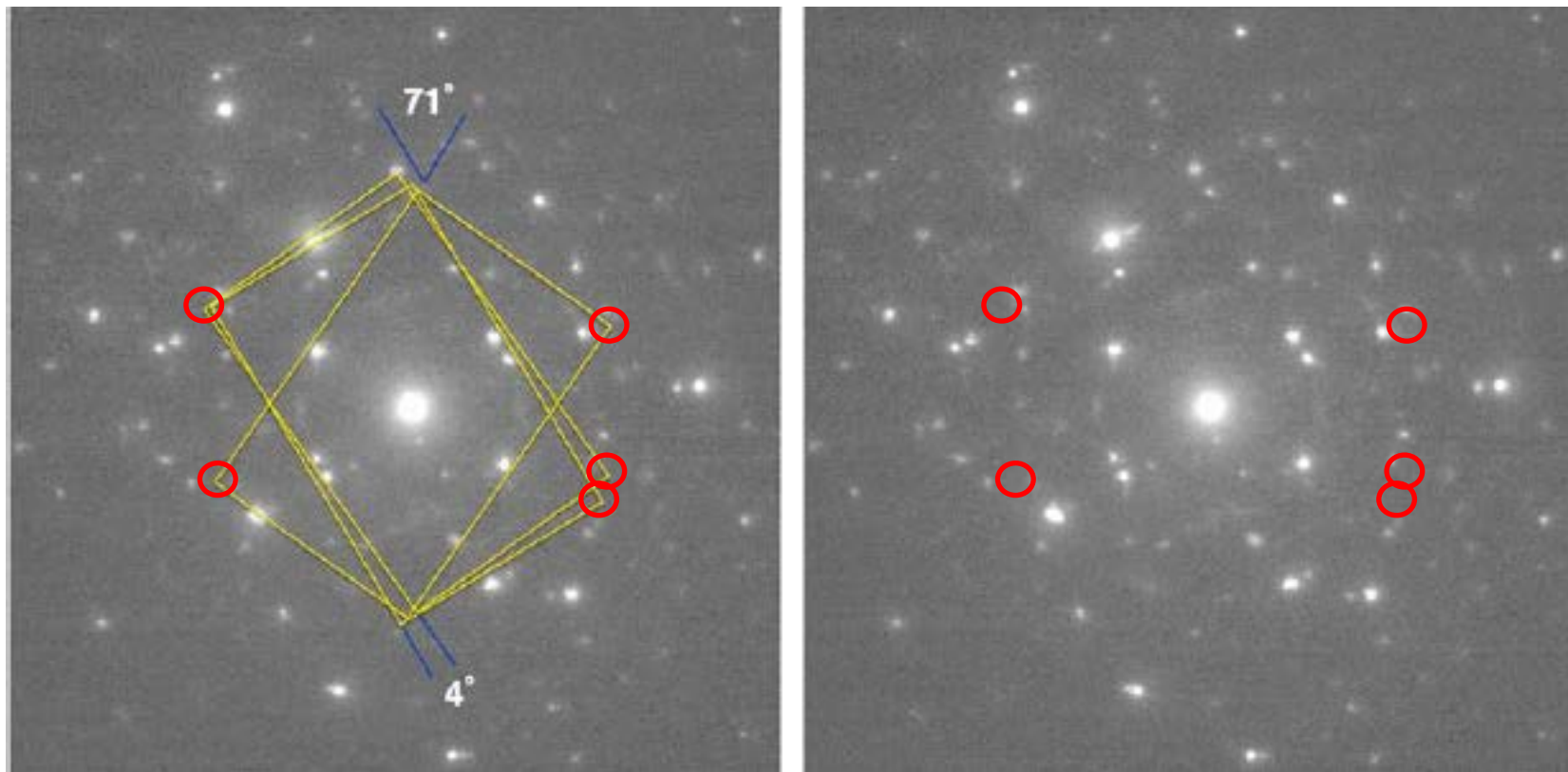
Ratio = 1.375:1



Ratio = 1.313:1

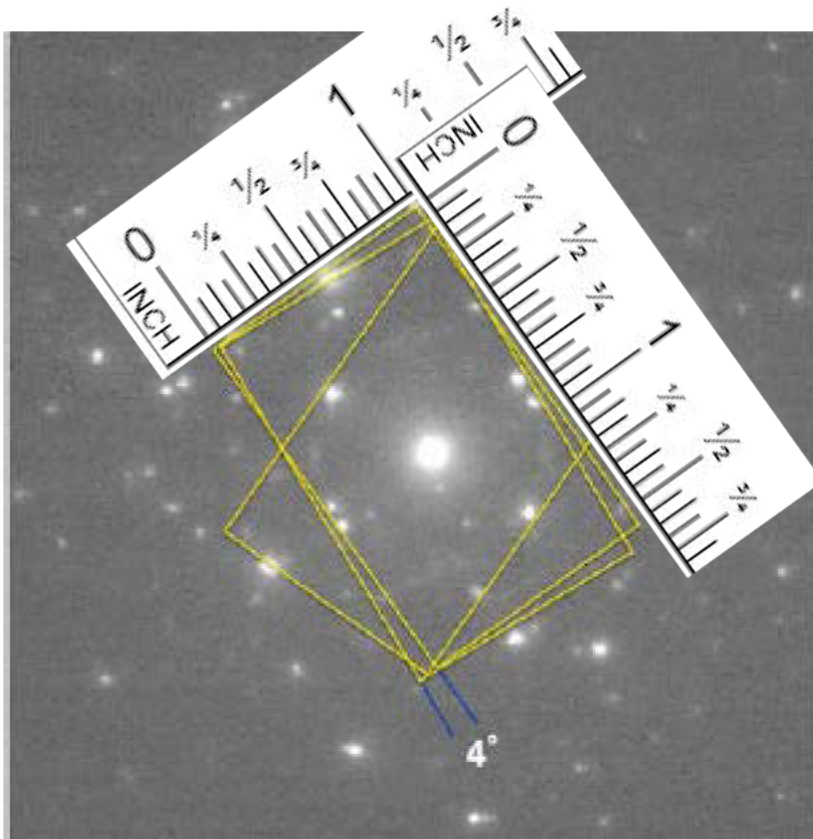


S0GPPC - Figure 52

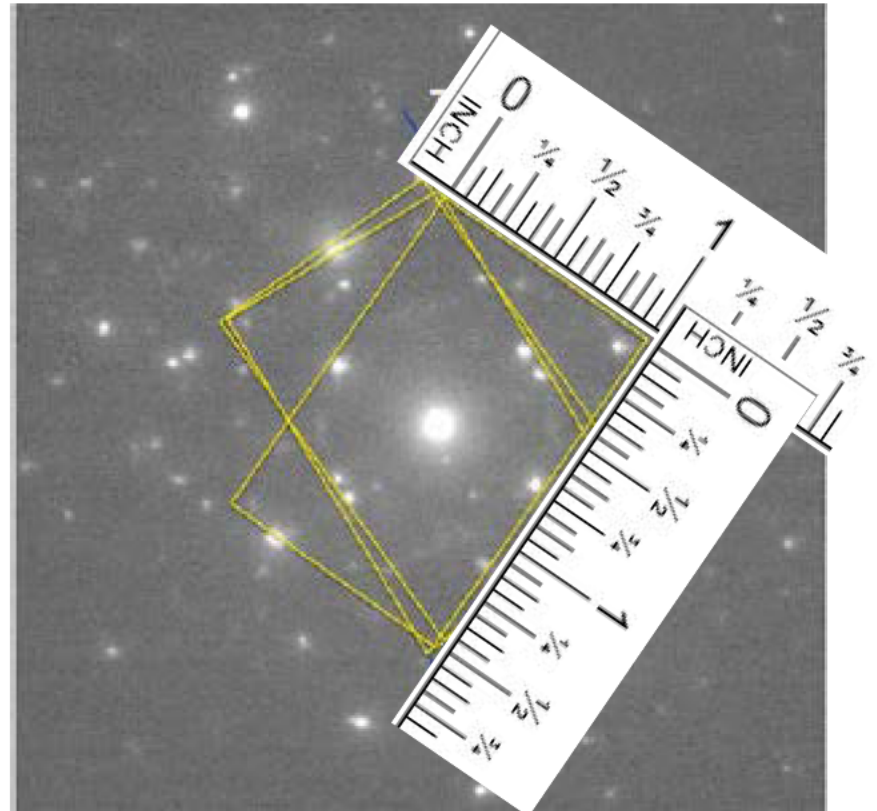


Red circles added by Dr. Stach to indicate spots that are not clearly discernable or not present. The lack of alignment with the box corners and nearby spots are significant enough to indicate that this interpretation is incorrect.

S0GPPC - Figure 52



Ratio = 1.563:1

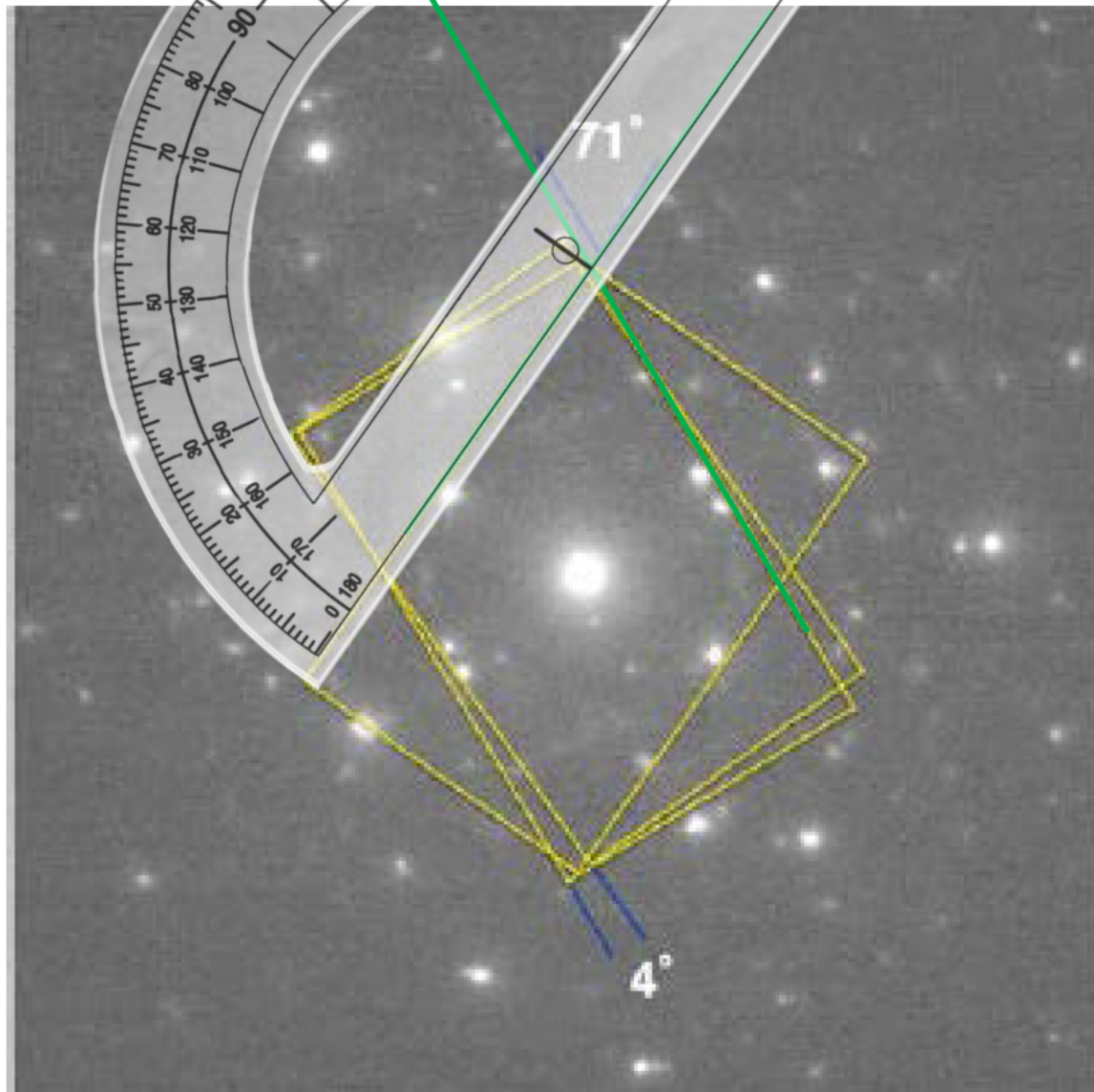


Ratio = 1.5:1

SOGPPC

66 degrees

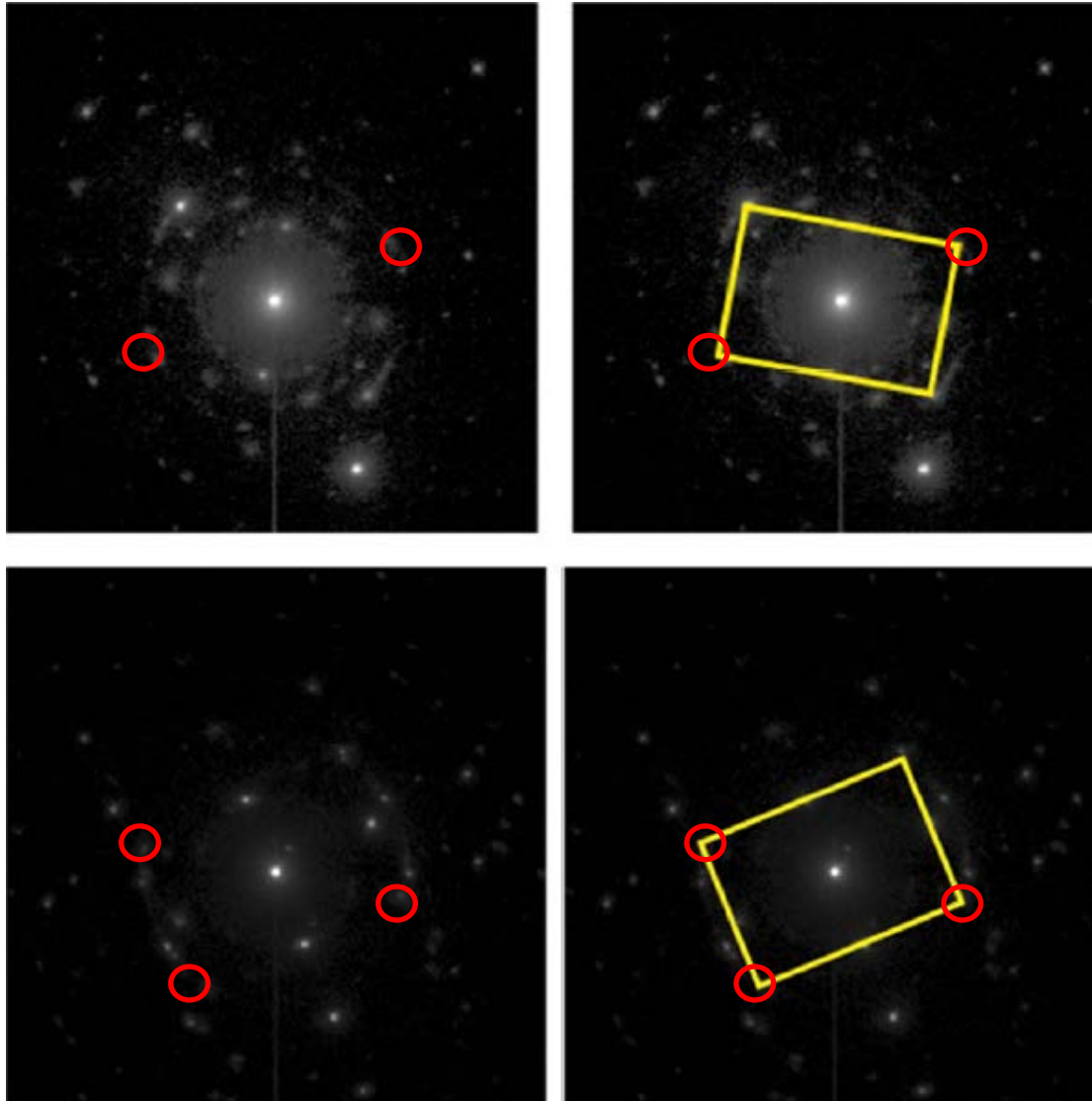
Fig. 52



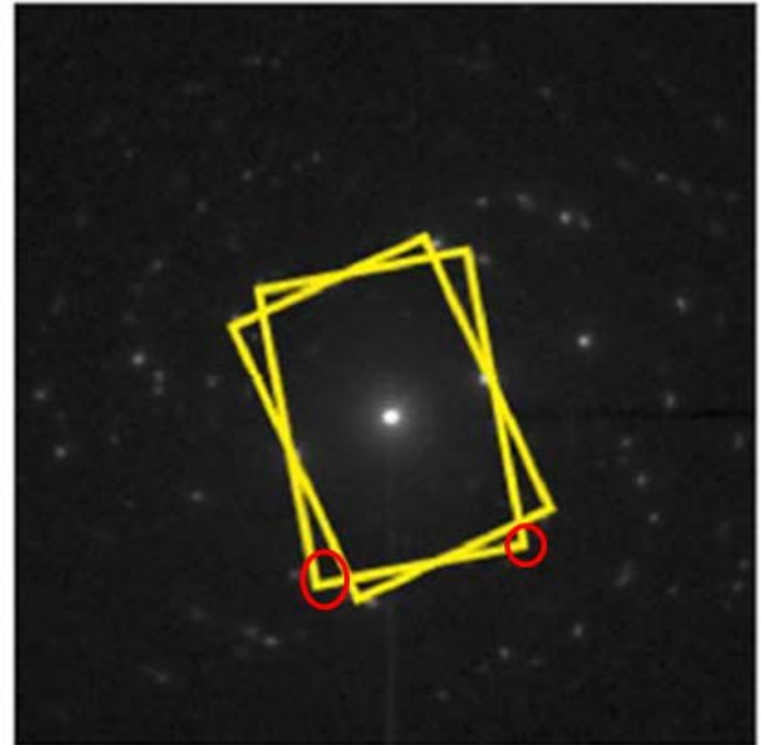
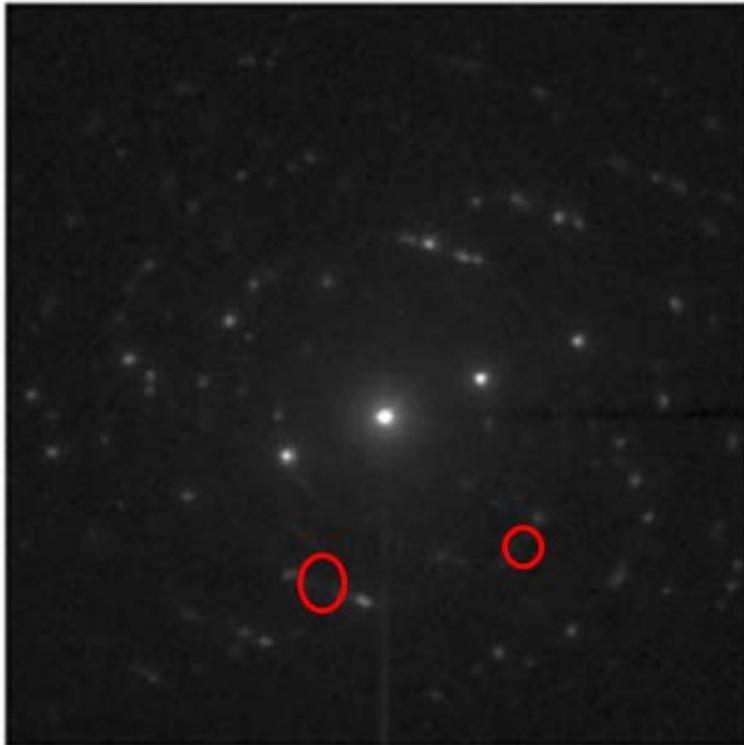
- Green lines and protractor added by Dr. Stach

S2MMMC - Figure 77

Red circles
added by Dr.
Stach to indicate
spots that are
not clearly
discernable or
not present.

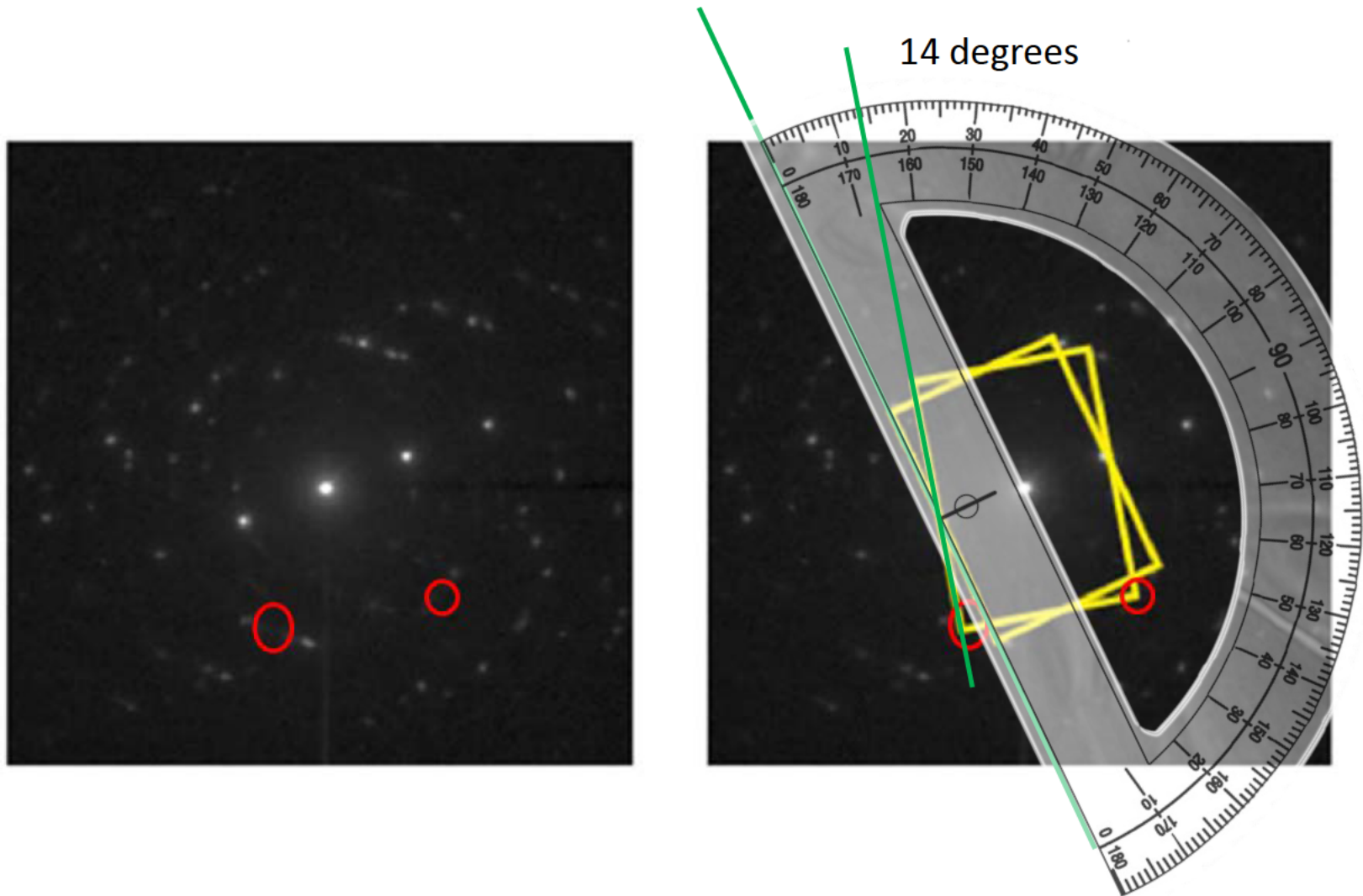


S2MMMC - Figure 78



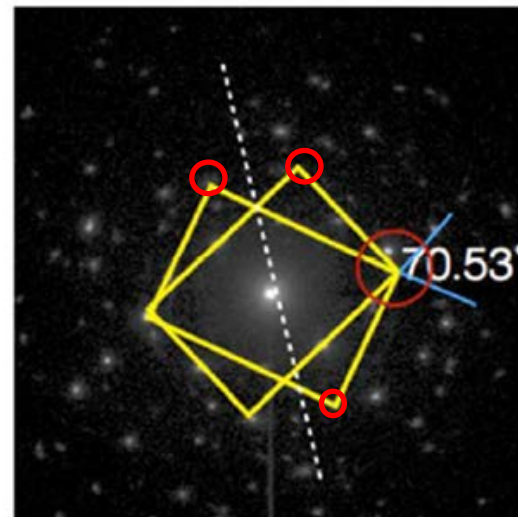
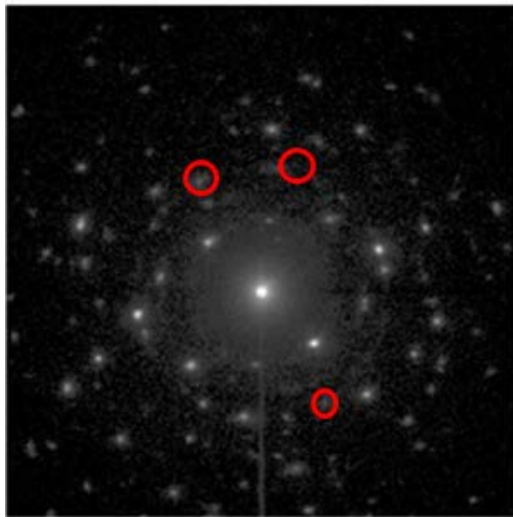
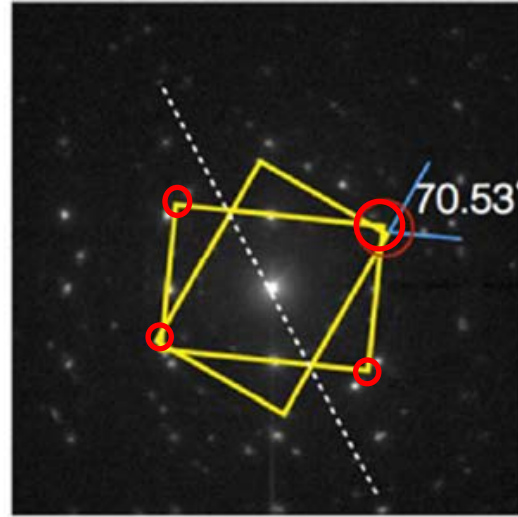
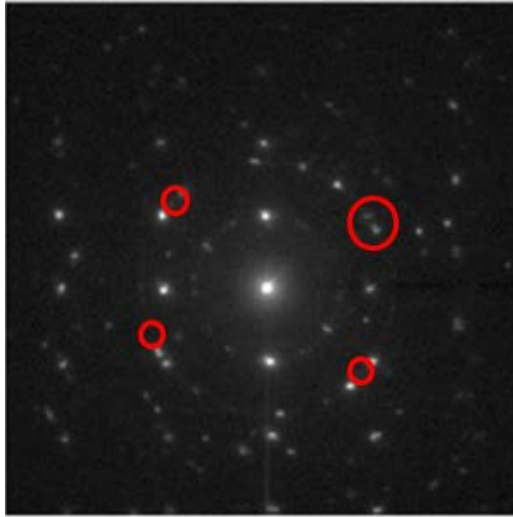
Red circles added by Dr. Stach to indicate spots that are not clearly discernable or not present. This interpretation is clearly incorrect.

S2MMMC - Figure 78

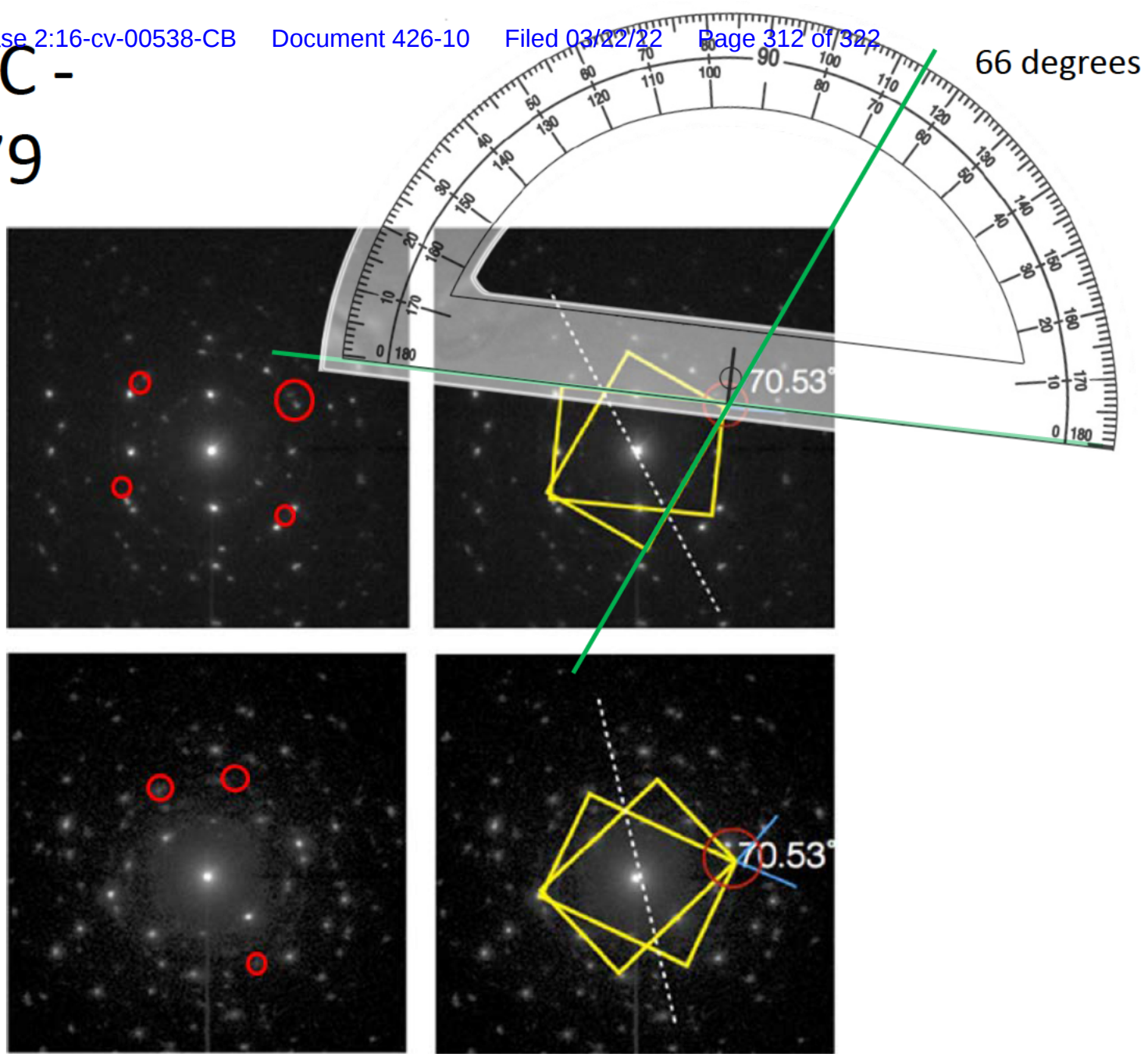


S2MMMC - Figure 79

Red circles
added by Dr.
Stach to indicate
spots that are
not clearly
discernable or
not present.

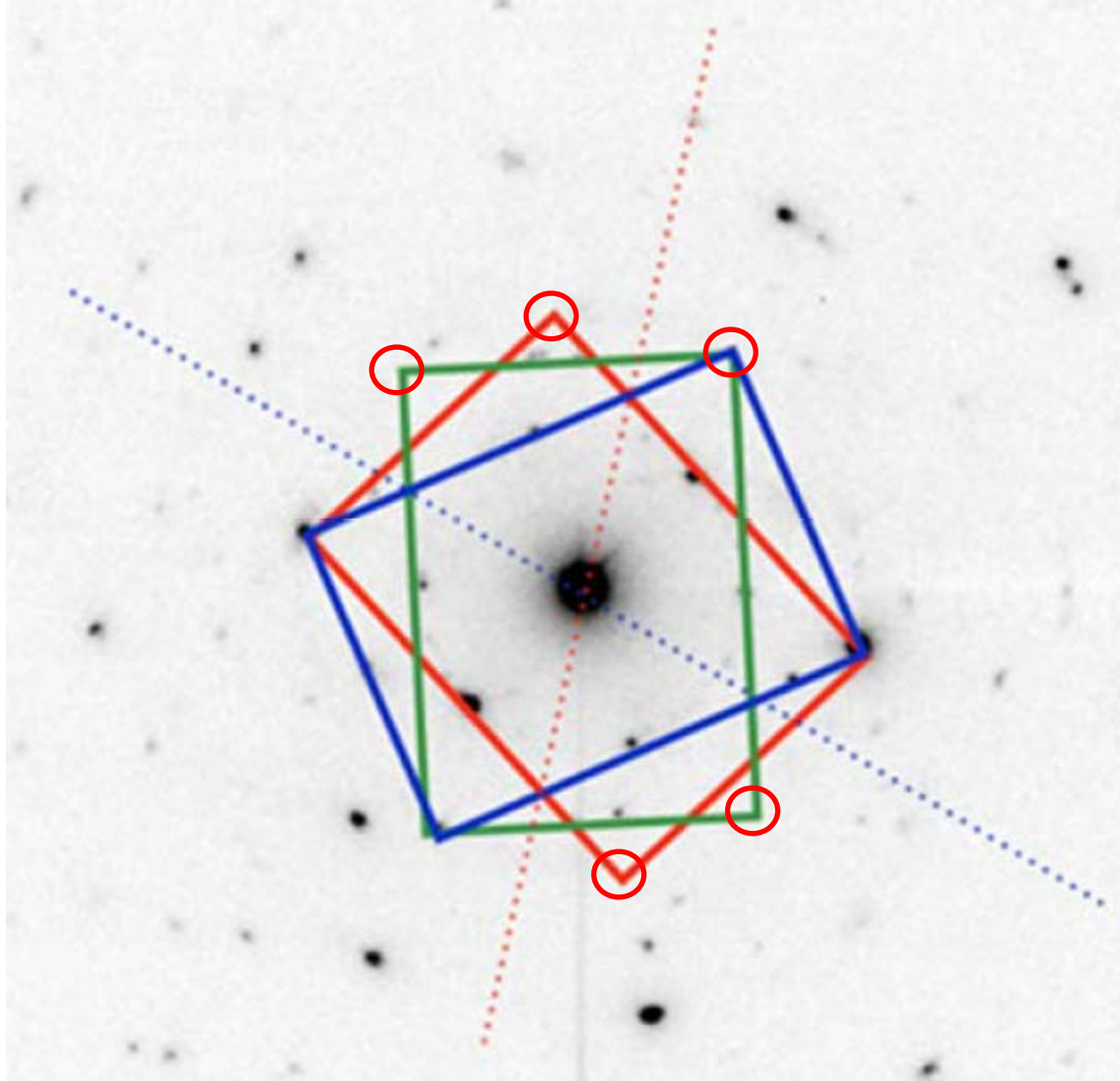


S2MMMC - Figure 79



S2MMC - Figure 80

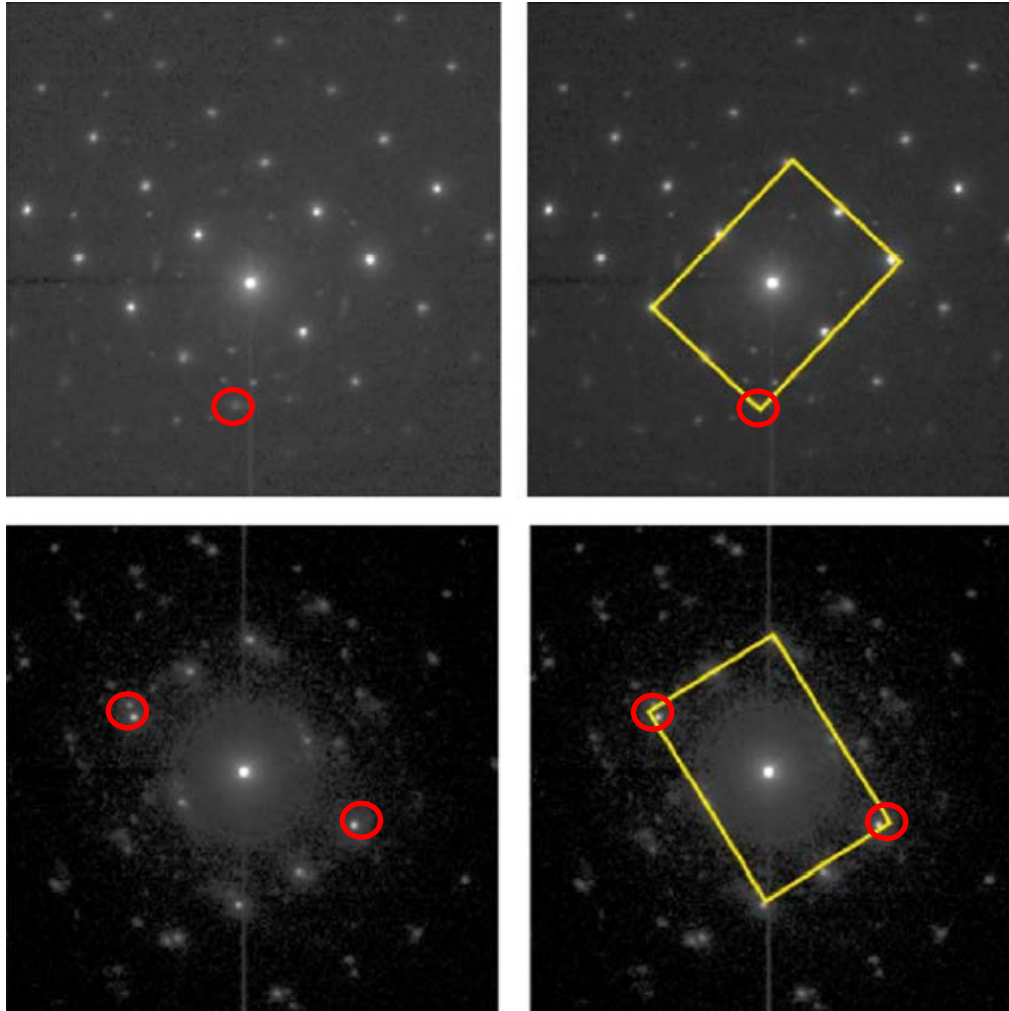
Red circles
added by Dr.
Stach to
indicate spots
that are not
clearly
discernable or
not present.



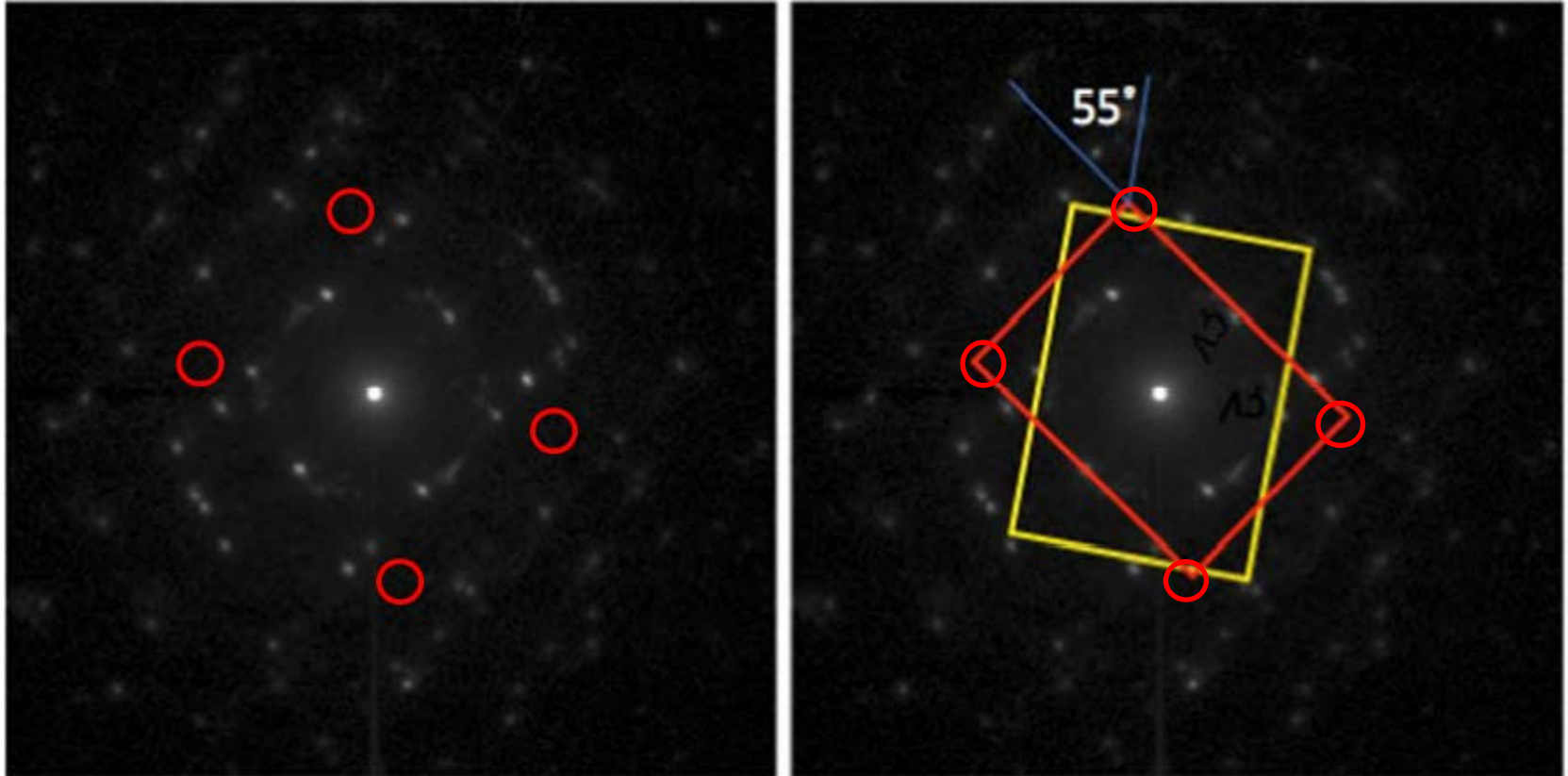
SBR8DK - Figure 107

Red circles added by Dr. Stach to indicate spots that are not clearly discernable or not present.

The lack of alignment with the box corners and nearby spots are significant enough to indicate that this interpretation is incorrect.

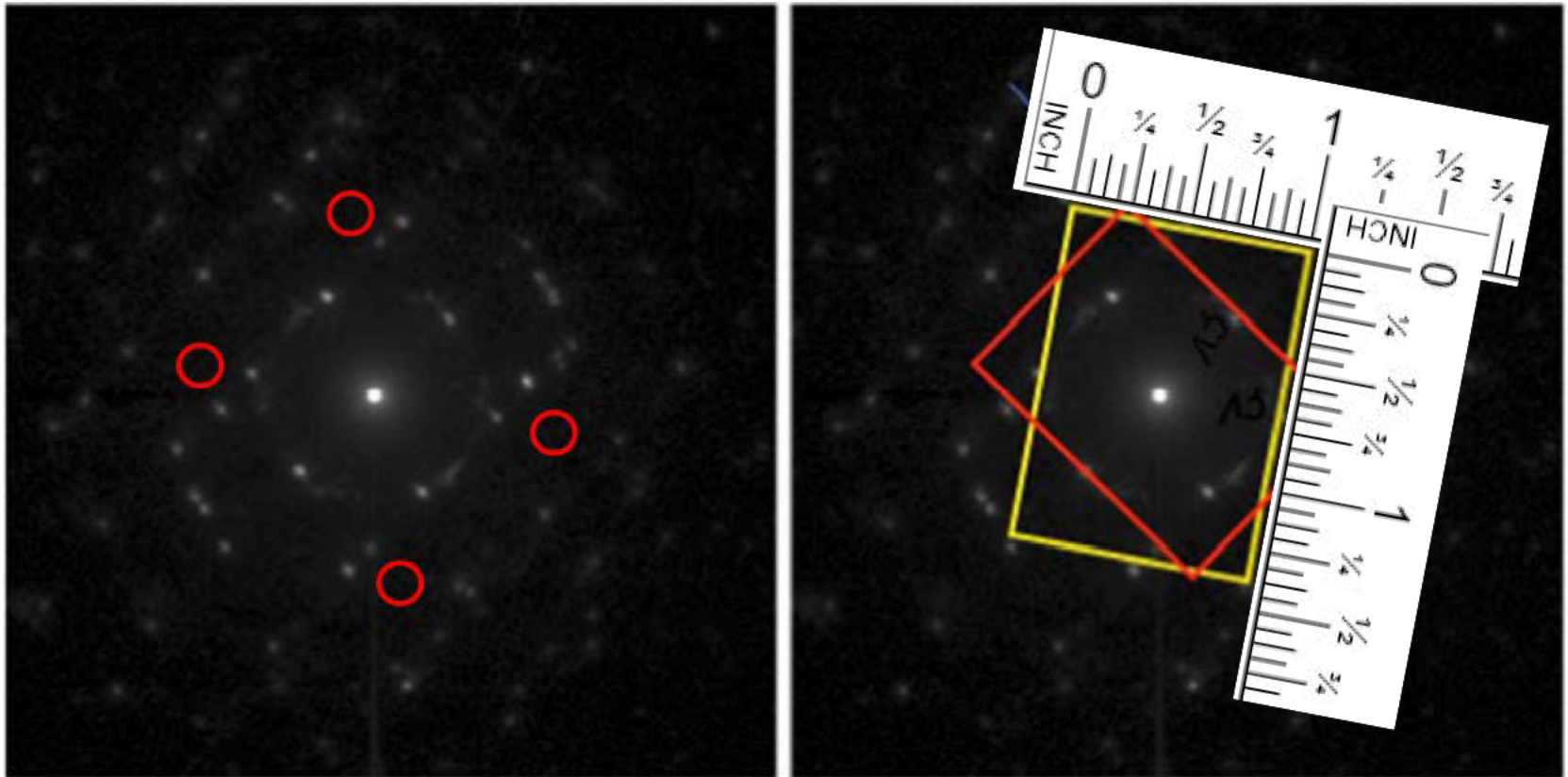


SBR8DK - Figure 108



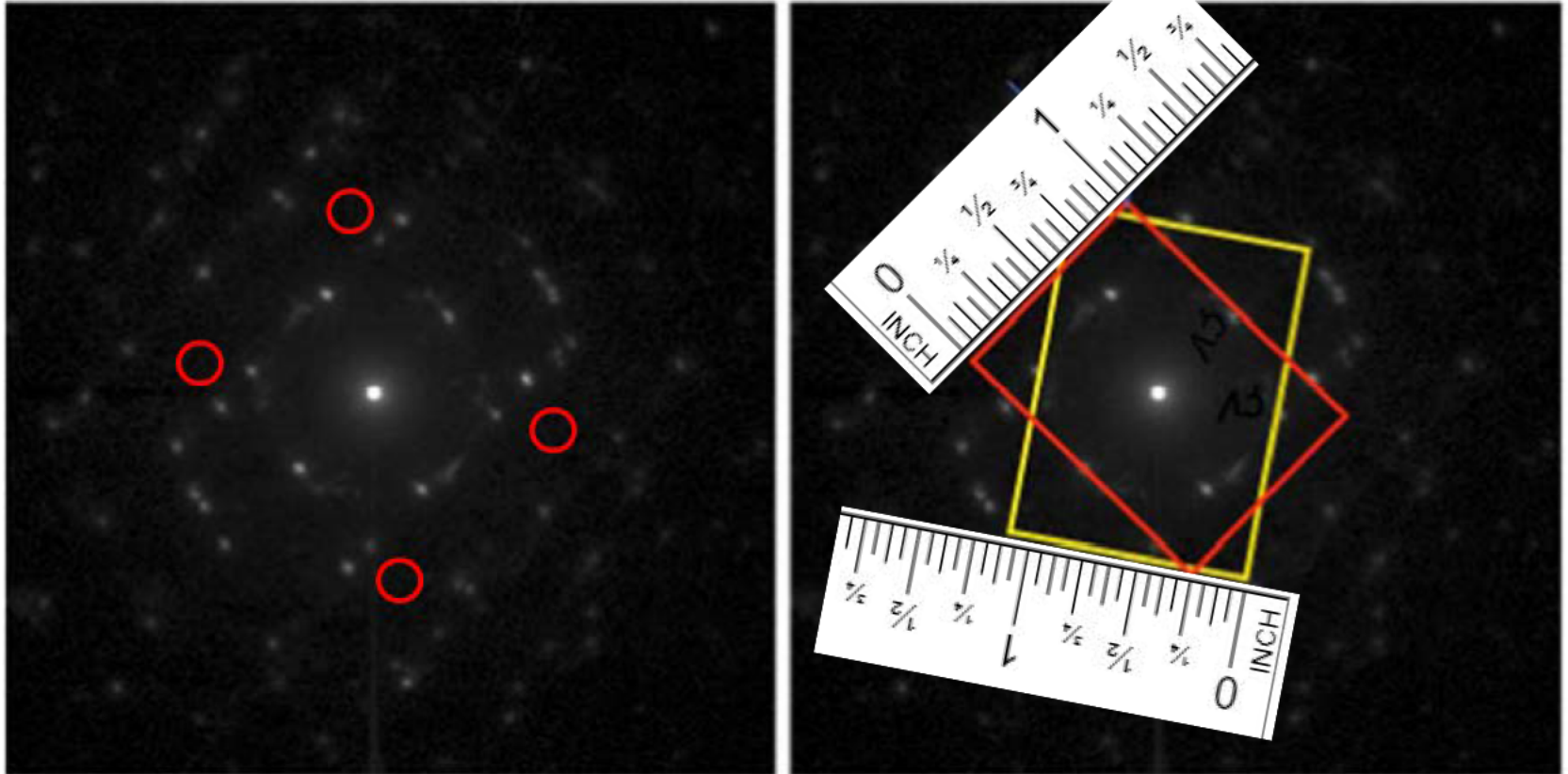
Red circles added by Dr. Stach to indicate spots that are not clearly discernable or not present. This interpretation is clearly incorrect.

SBR8DK - Figure 108



Ratio = 1:1.375

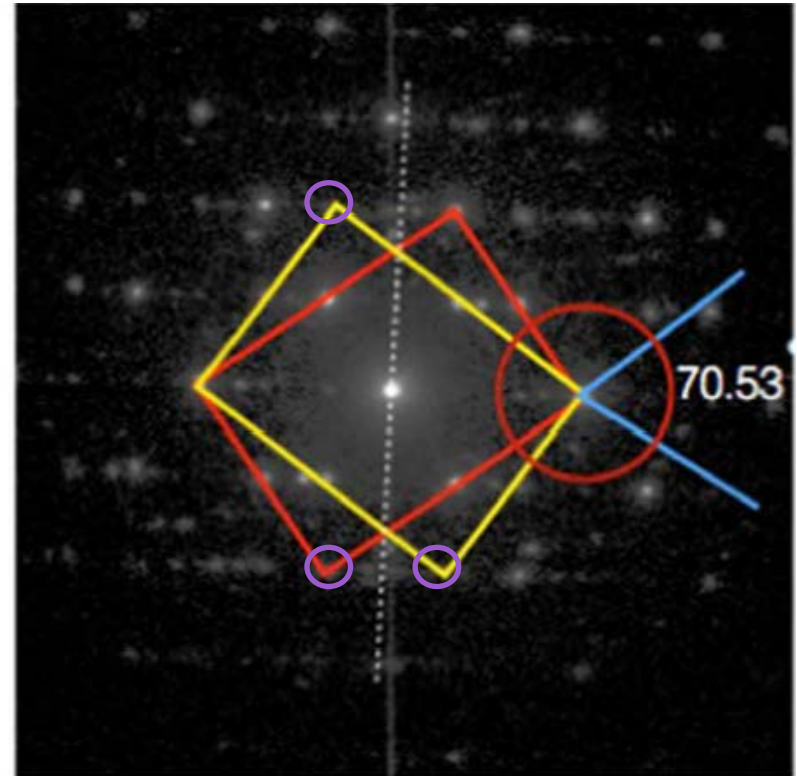
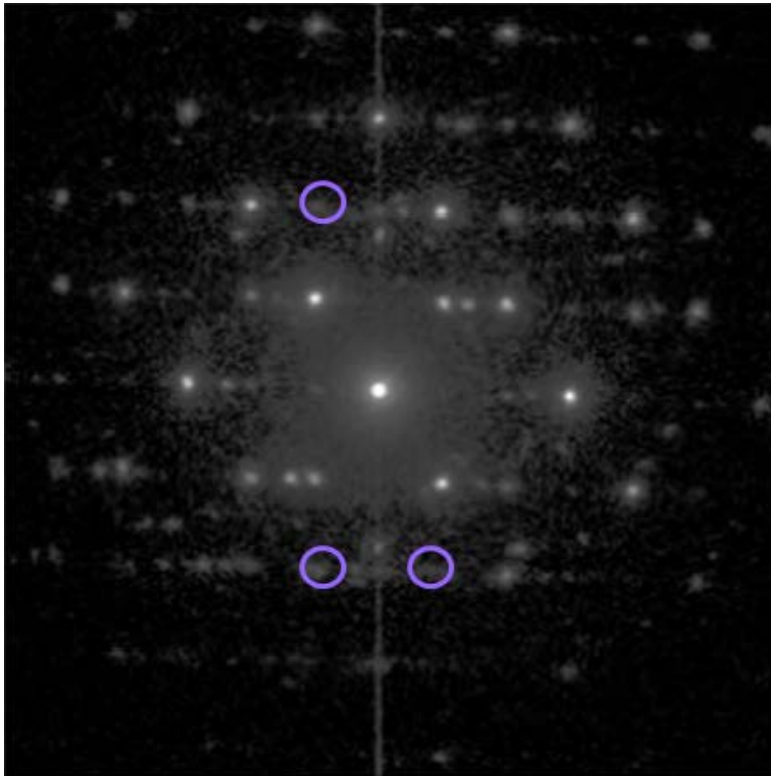
SBR8DK - Figure 108



Short side of red rectangle = 1 inch

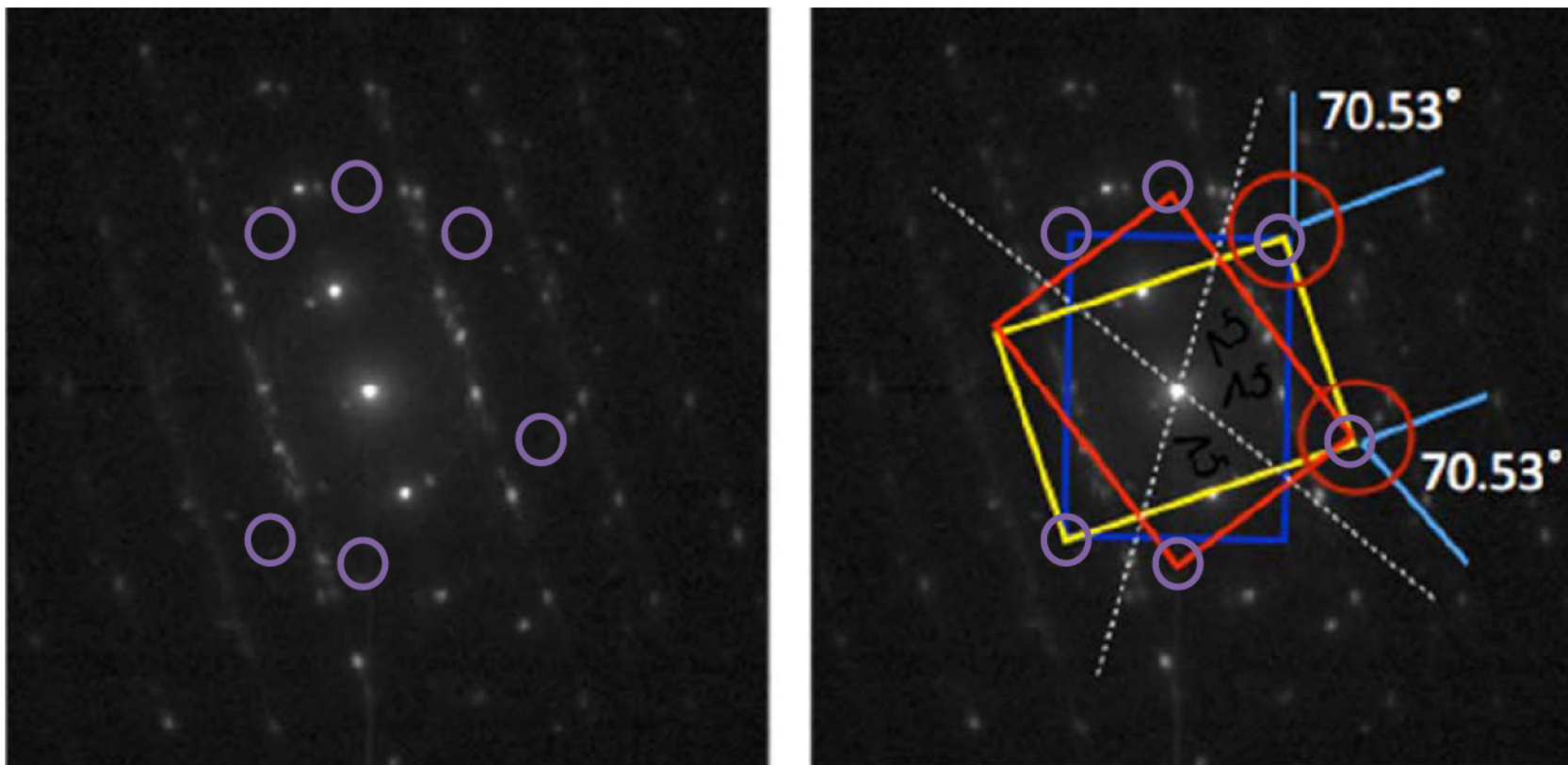
Short side of yellow rectangle = 1.12 inches

SBR8DK - Figure 109



Purple circles added by Dr. Stach to indicate spots that are weak, not clearly discernable or not present.

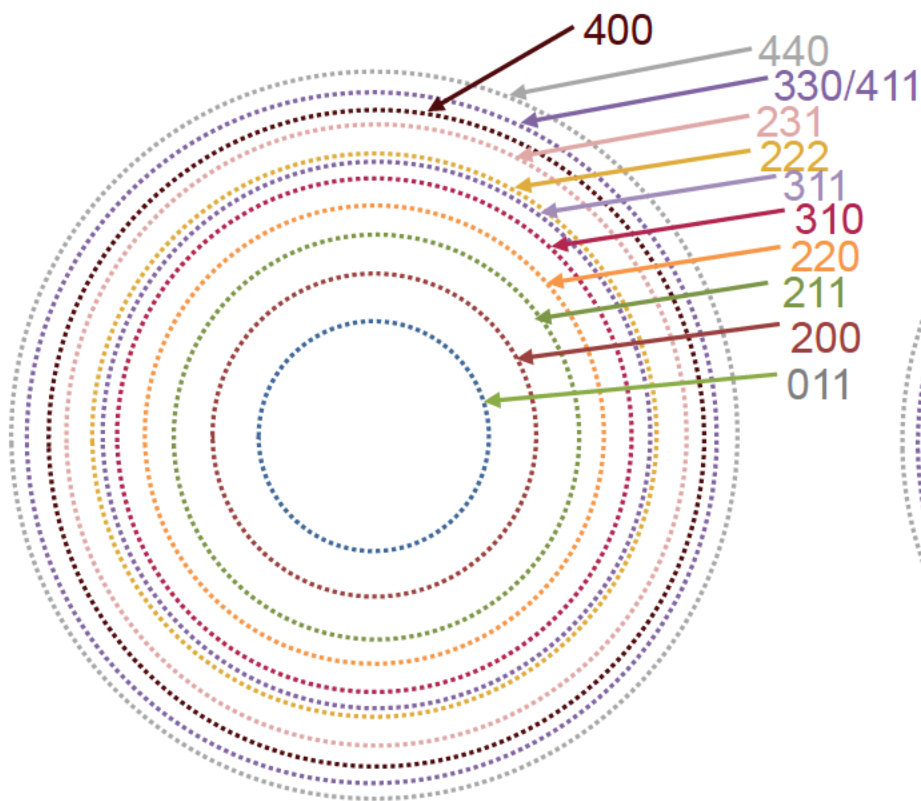
SBR8DK - Figure 110



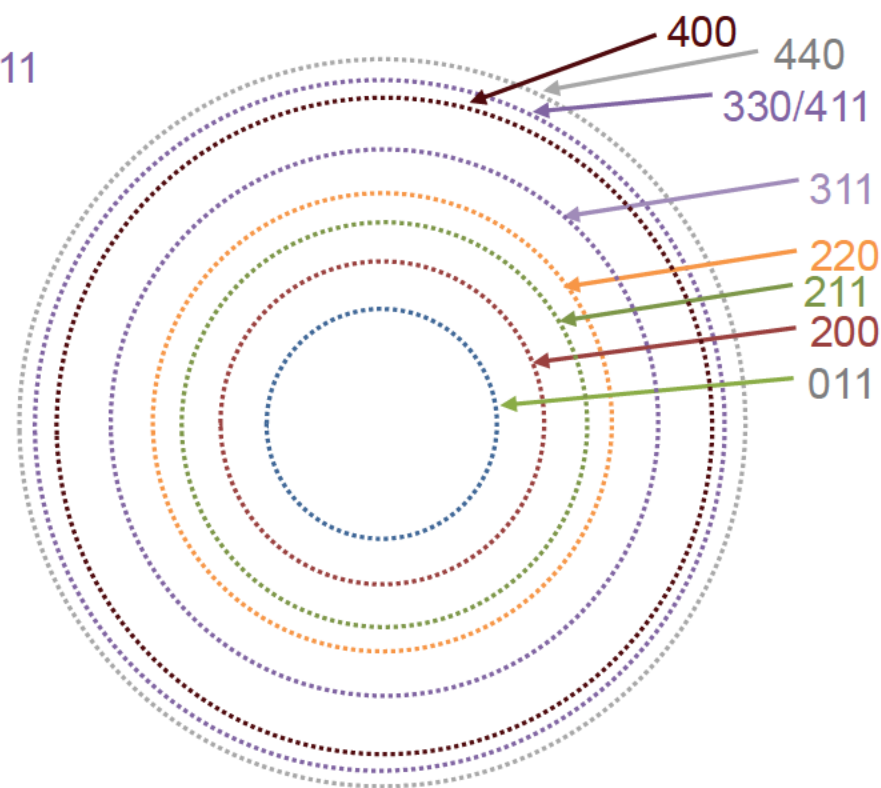
Purple circles added by Dr. Stach to indicate spots that are not clearly discernable or not present. The blue box in particular has no match with any spot data.

EXHIBIT H

Simulated bcc Diffraction Rings

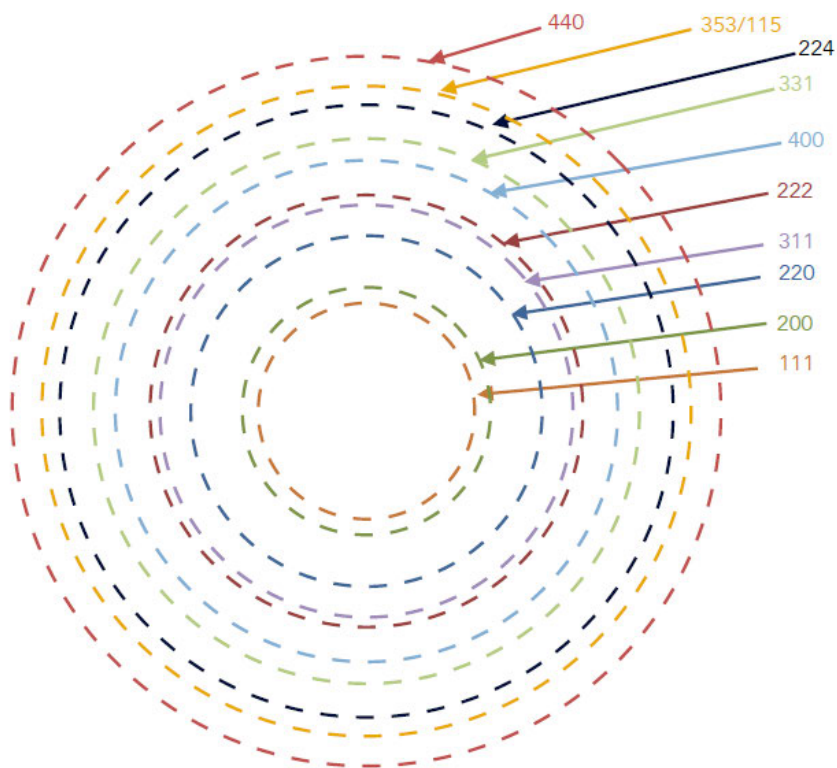


bcc Randomly Oriented (Out of Plane and In Plane)

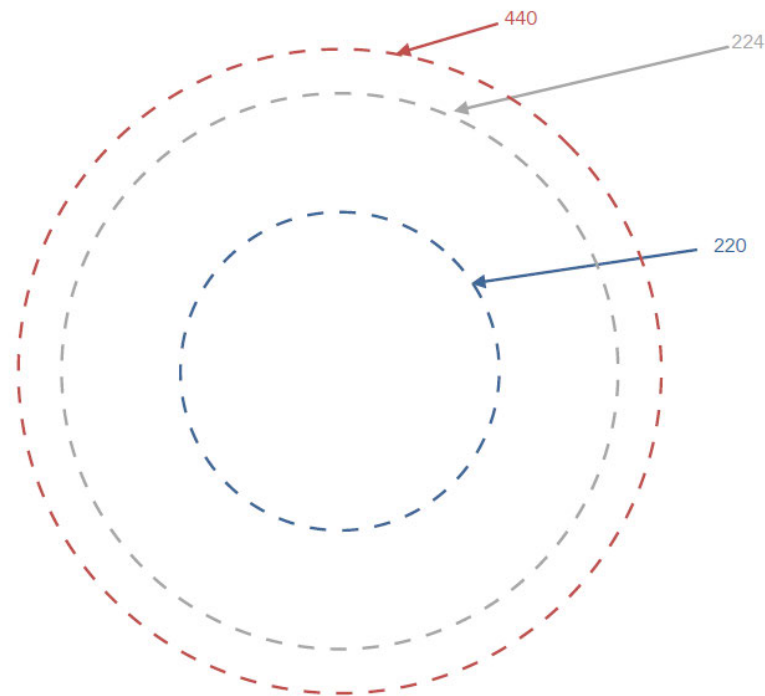


bcc(110) Orientation Out of Plane and Randomly Oriented In Plane

Simulated fcc Diffraction Rings



fcc Randomly Oriented (Out of Plane and In Plane)



fcc(111) Orientation Out of Plane
and Randomly Oriented In Plane